JOINT EUROPEAN TORUS

JET

JET JOINT UNDERTAKING

PROGRESS REPORT 1991

Volume I

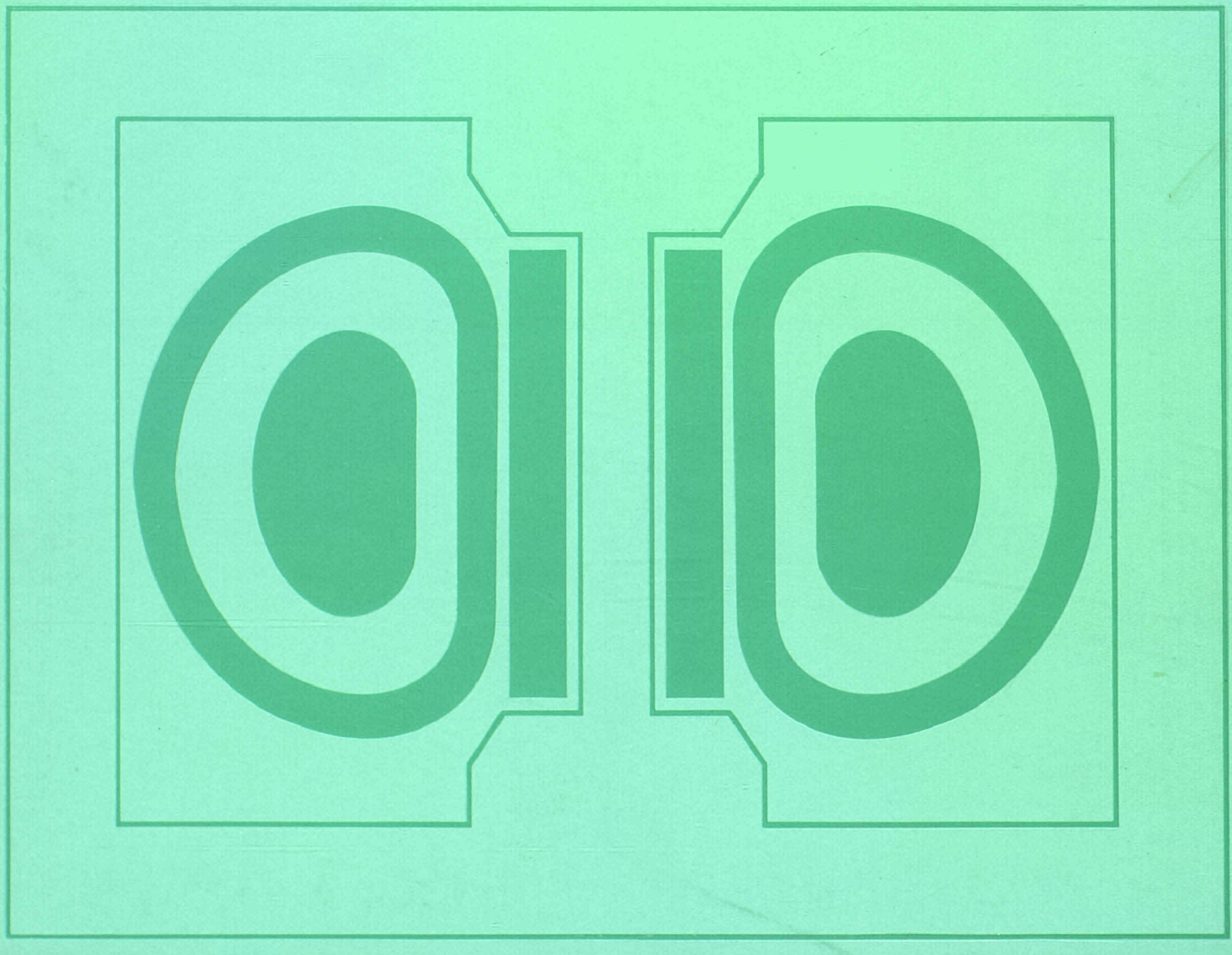

9

EUR 14434 EN
EUR-JET-PR9

JET JOINT UNDERTAKING

PROGRESS REPORT 1991
Volume I

April 1992

This document is intended for information only
and should not be used as a technical reference.

EUR14434 EN (EUR-JET-PR9) April 1992.
Editorial work on this report was carried out by B.E.Keen.
The preparation for publication was undertaken by JET
Publications Group, JET Joint Undertaking, Abingdon, UK.

Catalogue number : CD-NB-14434-EN-C for the Report EUR 14434 Volumes I and II

Printed in England

Contents

Volume I

Volume II

Reprints of JET Papers

Foreword

This is the ninth JET Progress Report, which provides an overview summary and puts into context the scientific and technical advances made on JET during 1991. In addition, the Report is supplemented by appendices of contributions (in Preprint form) of the more important JET articles published during the year (in Volume II of this Report).

This Report provides a more detailed account of JETs scientific and technical progress than that contained in the JET Annual Report. It is aimed not only at specialists and experts engaged in nuclear fusion and plasma physics, but also at a more general scientific community. To meet these general aims, the Report contains a brief summary of the background to the Project, and describes the basic objectives of JET and the principal design aspects of the machine. In addition, the Project Team structure is included as it is within this structure that the activities and responsibilities for machine operation are carried out and the scientific programme is executed.

1991 was another very successful year for the Project. By the end of the year, JET had completed Phase III of the planned operation programme on Full Power Optimization studies. The stage had been reached where two of the main objectives set out in the original JET design had been fulfilled (that is demonstrating effective heating methods in near reactor conditions, and the scaling of plasma behaviour as parameters approached the reactor range). The pursuit of the other major objectives - of studying plasma wall interactions in near reactor conditions and studying alpha-particle production, confinement and consequent plasma heating - were well advanced. A major step forward was the first experiment involving tritium in the JET machine, which produced in excess of 1.7MW of fusion power, during the Preliminary Tritium Experiment (PTE).

During early 1991, the machine was already in a scheduled shutdown. This shutdown had started in November 1990, and the main tasks were to repair and strengthen the mechanical supports for in-vessel wall protection tiles and to install target plates at the top and bottom of the vessel, for use during single and double-null X-point configurations.

In 1990, operation had been disrupted and somewhat limited due to damage to wall protection tiles. During the shutdown from November 1990 to April 1991, remedial action was taken. Critical welds were systematically strengthened, cantilevered mountings were eliminated and weak mechanical supports were modified and stiffened. These actions which involved a considerable work on a large number of components were remarkably successful insofar as no further damage to tile support mechanisms were observed during the 1991 campaign.

The main task of the shutdown was installation of the X-point target plates. Each target plate consists of 48 inconel sectors firmly attached to the vacuum vessel. These sectors provide a dimensionally accurate base for fixing the tiles, and were aligned with an absolute accuracy of ±1.5mm. To allow a comparative assessment of carbon and beryllium as a target materials, carbon fibre composite (CFC) tiles were fitted at the top target plate, and beryllium tiles at the bottom.

A disadvantage of beryllium as a target plate material is its low melting temperature making it prone to surface damage and irregularities. The beryllium target plate tiles were carefully machined to eliminate leading edges, which would be nearly normal to magnetic field lines and therefore receive high power density. This work was successful, as melting at leading edges was not observed during the 1991 campaign. However, this tile shaping resulted in a considerable reduction in effective area of the target plates.

When machine operation resumed in June 1991, only beryllium target plate tiles had been specially shaped. The carbon target plate tiles, although well aligned, had their leading edges exposed to high power fluxes. Operation soon revealed that carbon plate performance was indeed limited by local hot-spots at leading edges. This was a phenomenon not observed with the specially shaped beryllium tiles. Therefore, it was decided in Summer 1991 to machine the

carbon target plate tiles in a similar fashion, to allow a meaningful comparison of the two materials. Machining was completed and the tiles installed during September.

During 1991, a number of new systems were brought into operation and improved machine performance. In particular, the Reactive Power Compensation system (to reduce reactive power consumption), was integrated rapidly into routine operation. The system operated reliably and demonstrated its usefulness in keeping JET power consumption within limits of contracts with the Electricity Companies.

Other new facilities included: improvements in poloidal field circuit to permit X-point operation at higher currents and to allow operation as an AC tokamak; upgrading in energy of the second neutral injector to 140keV; use of the ICRF heating system as a phased array for fast wave current drive studies; an extended gas introduction system for radiative divertor studies; and an improved Plasma Fault Protection System which, allowed softer termination of the plasma on indication of an approaching disruption.

The experimental programme restarted in June 1991. Operation was aimed mainly towards:

(i) exploiting new facilities, such as the X-point targets, improvements in the poloidal field circuit, enhancements to heating systems and new diagnostics;
(ii) advancing understanding in several key areas of tokamak physics, such as energy and particle transport, impurity production and transport, magnetic topology and H-mode physics;
(iii) improving fusion performance;
(iv) addressing issues relevant to the Pumped Divertor and to Next Step devices (including a preliminary tritium experiment).

During 1991, the machine operated for 157 days, considerably more than in 1990, and approached the sum of the 1989 and 1990 operational periods. The number of pulses in 1991 was 3493 (compared with 2500 in 1990), bringing the total number to 27023. The percentage of commissioning pulses in 1991 (about 20%) was roughly the same as in 1990.

To avoid damage to in-vessel components before the PTE, plasma currents were limited in 1991 to the smallest values compatible with programme requirements. This is reflected in the plasma current distribution, where the higher plasma currents (>3MA) make up only 51.0% of the total (compared with 65.5% in 1990). Nevertheless, the percentage of low plasma current pulses was much reduced.

Investigation of the performance of diverted plasmas utilizing the newly installed toroidal X-point targets was a central activity throughout the campaign. With beryllium tiles at the lower target and CFC tiles at the upper target, a careful study of the relative merits of the two materials was undertaken. In addition, two designs of CFC tile were examined and allowed the limitations arising from heating of tile edges to be studied. The principal aims of the target assessment were: to establish the power handling capabilities of different target materials and of different target designs; to investigate the causes of limitations in the power handling capabilities; and to study the influence of different target materials on bulk plasma performance.

The targets performed broadly as expected. The improved tile design yielded about a factor 2 improvement in power handling capability. Comparisons of H-mode performance using CFC and Be targets showed that the two materials gave similar results at moderate to high densities, but that the CFC targets permitted considerably better fusion yield to be achieved in the relatively low density hot-ion H-modes. Significantly, it was found that reliable H-modes could be achieved using the Be targets even after extensive (deliberate) surface melting. While the performance in all H-mode plasmas was limited ultimately by impurity influxes, since neither target was actively cooled, a significant improvement in power handling capability was observed at high density. As a result, extensive gas puffing was used successfully to reduce power loading on the targets and thereby delay impurity influxes.

Plasma performance was extended in several ways. Uprating the shaping amplifier from 40 to 50kA permitted improved X-point configurations at 3 and 4MA, and 5MA double-null X-point plasmas to be established for the first time. Extensive experiments were performed at plasma currents in the range 3-4.5MA, over a wide range of plasma densities and at combined heating powers up to 25MW. In many cases, performance was limited by impurity influxes, though this could be influenced by varying the X-point to target distance, by judicious use of gas-puffing and by exploiting both X-point targets. The highest stored energy of 12.7MJ was obtained in a 4MA plasma with 21MW heating power. A most significant result was that, at high densities, fusion yield was independent of type of heating (NB or ICRF). Furthermore, no significant difference in performance between sawteething and sawtooth-free discharges was observed, indicating that sawteeth do not play a major role in confinement properties of these plasmas.

Considerable efforts were made to increase the fusion yield of plasmas in preparation for the PTE. Single-null and

double-null plasmas were investigated using both NB and ICRF heating. Studies focussed on hot-ion and H-mode plasmas in the range 3-4MA, as experience had shown that, in the present configuration, these plasmas produced the highest neutron yield and offered the best prospects for further development to higher performance. Optimization of 3MA/2.8T discharges yielded the highest neutron yield obtained of $4.3 \times 10^{16} s^{-1}$, corresponding to a fusion product $n_D(0)\tau_E T_i(0) = 9.2 \times 10^{20} m^{-3} keVs$ and $Q_{DT}=1.14$.

The design of Next Step devices is based upon the exploitation of a variety of current drive schemes. Two principal techniques for bulk current drive have been explored in JET: lower hybrid current drive (LHCD) and bootstrap current. While the LHCD system has been employed in a variety of experiments, including a 1 minute duration limiter pulse, the emphasis in recent experiments was on optimization of synergistic effects between ICRF and LHCD to optimize current drive efficiency and the demonstration of 100% current drive at the highest current. Studies have shown that synergistic effects are optimized in plasmas with low electron density and peaked density and temperature profiles. Under these conditions, high current drive efficiencies were achieved and 100% current drive attained at currents up to 1.5MA.

In many JET H-modes, bootstrap current fractions of 25% are typical. Previously, no attempt had been made to optimize this figure nor to address the issue of whether significant bootstrap current could be obtained in ICRF heated plasmas with no central particle source. In low current (1-1.5MA) ICRF heated H-mode plasmas bootstrap current fractions of up to 70% were achieved and sawteeth were stabilized, presumably as a result of current profile broadening. In addition, these plasmas exhibited high thermal energy confinement.

Operation of the tokamak as an AC device offers an alternative route to quasi-continuous operation without the overheads entailed in external current drive systems. The feasibility of such a scheme has previously been demonstrated on small tokamaks at currents up to 4kA. Recent changes in the poloidal field circuit permitted this to be investigated at significantly higher current, up to 2MA. Reliable operation and additional heating of a two-cycle plasma was established at 2MA and plasma parameters were very similar in the two cycles. Although it was not possible to demonstrate a smooth transition between the two cycles with zero dwell time, dwell times as small as 50ms and as long as 6s were achieved without difficulty. Extensive studies were also made of the optimum control of the current ramp-down for successful termination of the first cycle and initiation of the second.

Control of the heat and particle flux to the first wall and of the resultant impurity influxes to the plasma is one of the most important problems currently facing the development of fusion as a viable energy source. The new phase of JET starting in early 1992, based on the installation of a Pumped Divertor, is designed to address this problem and to develop techniques for its satisfactory resolution. Therefore, a programme of research was undertaken to investigate the performance of the present divertor configuration in JET to obtain baseline data for comparison with the predictions of simulation code calculations. In addition, detailed observations of divertor parameters are being used to validate numerical simulations of Pumped Divertor operation.

The second half of 1991 was dominated by work relevant to the preparation, execution and aftermath of the Preliminary Tritium Experiment. The physics, technical and safety aspects of this experiment required a project wide effort and coordination involving all JET Divisions. Two Task Forces were set up for the experiment. The Physics Task Force was charged with the selection and optimisation of the type of tritium discharge, the choice of method of tritium injection and, preparation of simulation codes and diagnostics. The Technology Task Force was responsible for design, construction and commissioning of new systems for the introduction of tritium and recovery of tritiated exhaust gases; preparation of safety reports and documentation to obtain necessary authorisations from UK Safety Authorities, from AEA and the JET Council; and for installation and commissioning of radiological protection instrumentation required for the experiment. Additional tasks included procurement of tritium and provision for its safe storage, setting up an emergency desk in the Control Room, definition and execution of emergency exercises and extensive staff training in tritium hazards and operation of tritium systems.

The introduction of a significant fraction of tritium into a tokamak plasma for the first time is the most significant accomplishment of the recent experimental programme. This experiment was noteworthy not only for the production of over 1.7MW of fusion power, but for several substantial technical achievements: the establishment of procedures for the monitoring and tracking of tritium in a tokamak environment; the demonstration of reliable techniques for the handling of tritium and its introduction into the tokamak; and the first tritium neutral beam injection. Significant scientific

information was also obtained in a number of areas: validation of simulation codes used to extrapolate from D-D to D-T performance; investigation of the transport of tritium in a tokamak plasma; and the study of removal of tritium from the tokamak first wall and ancillary systems.

The target plasma for this experiment was a hot ion H-mode in the single-null configuration at 3MA/2.8T. To minimize activation of the vessel, optimization of this discharge was performed in deuterium. In the two full power pulses to which the final experiment was limited, tritium was introduced using tritium fuel in two of the sixteen NB sources, resulting in a central tritium concentration of ~10%. The performance of the discharges lay in the middle of the range of the hot ion modes produced during the optimization experiment, having an actual Q_{DT}=0.15 and a projected Q_{DT}=0.5 for an optimized mixture. The peak fusion power achieved was 1.7MW, with an integrated fusion energy of 2MJ. Overall, the experiment has produced invaluable scientific and technical data for the preparation of the full D-T phase of JET planned for 1996.

The future of JET was assured, when, at its meeting on 19 December 1991, the Council of Ministers adopted Decisions concerning the Euratom Fusion Programme in the period to the end of 1994 and a modification to the JET Statutes, which prolonged its statutory lifetime by four years until 21st December 1996. The extension will allow JET to implement the new Pumped Divertor Phase of operation, the objective of which is to establish the effective control of plasma impurities in operating conditions close to those of the Next Step. This programme of studies will be pursued before the final phase of full D-T operations in JET.

Present achievements show that the main objectives of JET are being actively addressed and substantial progress is being made. During 1991, a large proportion of JETs effort was devoted to preparation for the new pumped divertor phase of operations. Intensive design and procurement activities were continued to ensure timely delivery of the many components of the pumped divertor and related modifications to be installed during the 1992/93 shutdown. In addition, preparations for the full D-T phase of operations have continued. JET has completed installation of all the main components of the active gas handling system in readiness for the system's commissioning programme.

JET is also providing important input into the collaboration on the International Thermonuclear Experimental Reactor (ITER) Project. The ITER Conceptual Design Activities (CDA) were completed in December 1990. The four ITER partners, Europe, USA, Japan and the Russian Federation, have now negotiated an agreement on the Engineering Design Activity (EDA), and the draft agreement has been submitted to Governments for ratification. Under this agreement, the parties will jointly conduct activities to establish engineering design and construction planning for a device capable of controlled ignition and extended burn. When the agreement is signed, the ITER Council will appoint a Director with responsibility for directing and coordinating activities. A joint central team located at three co-centres (San Diego, USA; Garching, Germany; and Naka, Japan) will be established to assist the Director. The supporting physics and technology programmes and some design work will be undertaken by the Partners under Task Agreements. The JET programme is expected to make unique and essential contributions to the ITER EDA.

In spite of severe budgeting constraints, JET has made impressive advances. However, the Project must continue to achieve economies where possible during the coming years to ensure successful completion of the programme. It has already had to restrict the scope of the programme, to reduce staffing levels and to intensify economies in operational expenditure. In spite of these cuts, JET must continue along the path towards simulating the operation of a fusion reactor and providing fundamental results in preparation for the Next Step device. JET's exceptional achievements reflect the continuous cooperation and assistance received from the Associated Laboratories and from the Commission of the European Communities. I am confident that with such dedication of the staff and the support and guidance of the JET Council, JET Scientific Council and the JET Executive Committee, the Project will meet the challenges ahead and will continue to contribute substantially to crucial information to ensure that fusion will be an important source of energy for future generations.

Dr P-H Rebut
Director
April 1992

Introduction, Background and Report Summary

Introduction

JET Progress Reports are aimed both at specialists in plasma physics and nuclear fusion research and at the more general scientific community. This contrasts with the JET Annual Reports, which provide overview descriptions of the scientific, technical and administrative status of the JET programme, and is directed to the average member of the public.

To meet these general aims, the Progress Report contains a brief summary of the background to the Project, describes the basic objectives of JET and sets out the principal design aspects of the machine. In addition, the Project Team structure is detailed, since it is within this framework that machine activities and responsibilities are organized and the scientific programme is executed.

The main part of the 1991 Report provides overview summaries of scientific and technical advances made during the year, supplemented by appendices of detailed contributions (in preprint form) of the more important JET scientific and technical articles produced during the year. The final part of the Report briefly sets out developments underway to further improve JET's performance and plans for future experiments through to its foreseen completion.

Background

Objectives of JET

The Joint European Torus (JET) is the largest single project of the nuclear fusion research programme of the European Atomic Energy Community (EURATOM). The project was designed with the essential objectives of obtaining and studying plasma in conditions and with dimensions approaching those needed in a fusion reactor. These studies are aimed at defining the parameters, the size and working conditions of a tokamak reactor. The realisation of this objective involves four main areas of work:

(i) the scaling of plasma behaviour as parameters approach the reactor range;
(ii) the plasma-wall interaction in these conditions;
(iii) the study of plasma heating; and
(iv) the study of alpha-particle production, confinement and consequent plasma heating.

Two of the key technological issues in the subsequent development of a fusion reactor are faced for the first time in JET. These are the use of tritium and the application of remote maintenance and repair techniques. The physics basis of the post-JET programme will be greatly strengthened if other fusion experiments currently in progress are successful. The way should then be clear to concentrate on the engineering and technical problems involved in progressing from an advanced experimental device like JET to a prototype power reactor.

Basic JET Design

To meet these overall aims, the basic JET apparatus was designed as a large tokamak device with overall dimensions of about 15m in diameter and 12m in height. A diagram of the apparatus is shown in Fig.1 and its principal parameters are given in Table I. At the heart of the machine, there is a toroidal vacuum vessel of major radius 2.96m having a D-shaped cross-section 2.5m wide by 4.2m high. During operation of the machine, a small quantity of gas (hydrogen, deuterium or tritium) is introduced into the vacuum chamber and is heated by passing a large current through the gas. Originally, the machine was designed to carry 4.8MA, but has already been modified to achieve 7MA. This current is produced by transformer action using the massive eight-limbed magnetic circuit, which dominates the apparatus

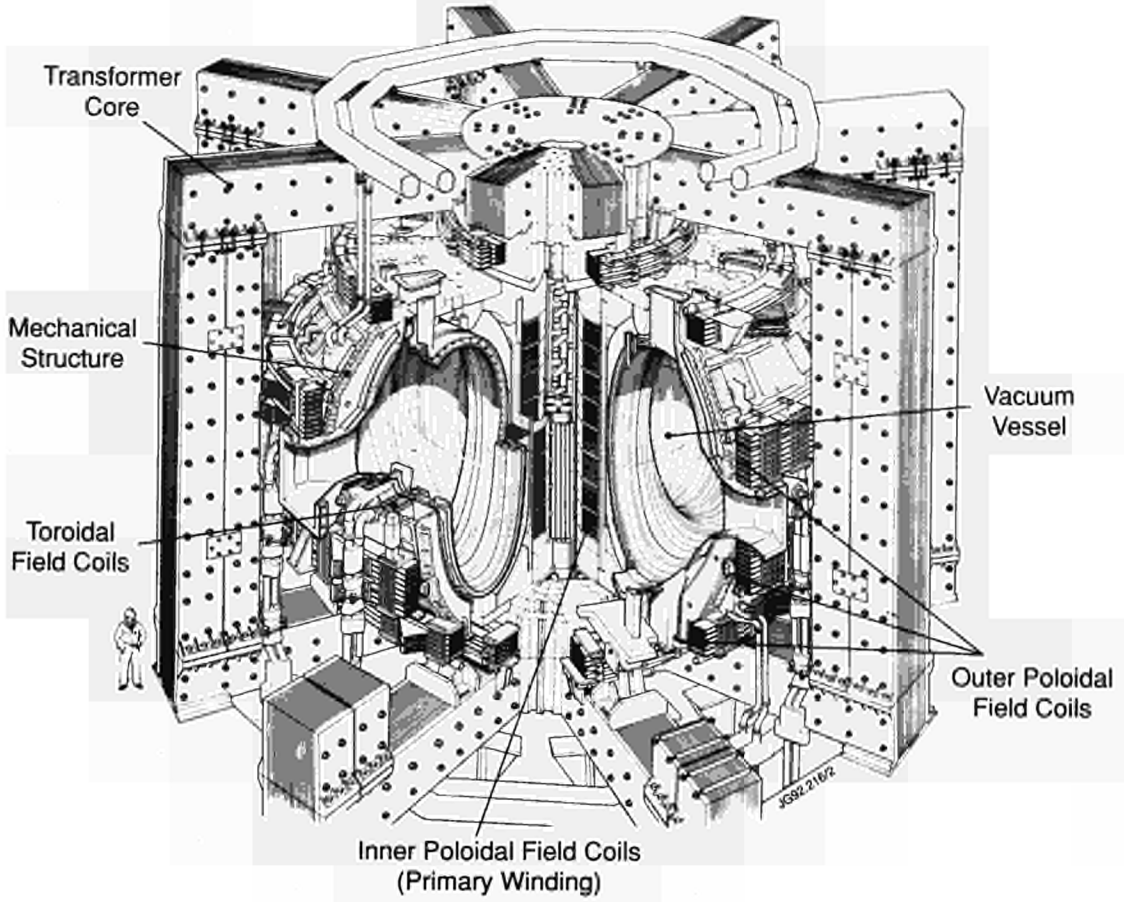

Fig.1: Diagram of the JET Tokamak.

Table I
Principal Parameters

Parameter	*Value*
Plasma minor radius (horizontal), a	1.25m
Plasma minor radius (vertical), b	2.10m
Plasma major radius, R_0	2.96m
Plasma aspect ratio, R_0/a	2.37
Plasma elongation ratio, ε=b/a	1.68
Flat top pulse length	60s
Toroidal magnetic field (plasma centre)	3.45T
Plasma current, D-shaped plasma	7.0MA
Volts-seconds available	54Vs
Toroidal field peak power	380MW
Poloidal field peak power	300MW
Additional heating power (into torus)	~50MW
Weight of vacuum vessel	108t
Weight of toroidal field coils	364t
Weight of iron core	2800t

(see Fig.1). A set of coils around the centre limb of the magnetic circuit forms the primary winding of the transformer with the plasma acting as the single turn secondary. Additional heating of the plasma is provided by the propagation and absorbtion high power radio frequency waves in the plasma and by the injection of beams of energetic neutral atoms into the torus.

The plasma is confined away from the walls of the vacuum vessel by a complex system of magnetic fields, in which the main component, the toroidal field, is provided by 32 D-shaped coils surrounding the vacuum vessel. This field, coupled with that produced by the current flowing through the plasma, forms the basic magnetic field for the tokamak confinement system, which provides a full design field at the plasma centre of 3.45T. The poloidal coils, positioned around the outside of the vacuum vessel, shape and position the plasma in operation.

Initial experiments have been undertaken using hydrogen and deuterium plasmas, but in the later stages of the

operation, it is planned to operate with deuterium-tritium plasmas, so that fusion reactions can occur to produce significant a-particle heating in the plasma.

In order to reach conditions close to those relevant to a fusion reactor, a plasma density of $\sim 10^{20} m^{-3}$ at a temperature of 10-20keV would be needed. Even with a current of up to 7MA in JET, this would be inadequate to provide the temperature required using ohmic heating alone. Consequently, additional heating is required and two main systems are being used at JET, as follows:

- Injection into the plasma of highly energetic neutral atoms (Neutral Injection Heating);
- Coupling of high power electromagnetic radiation to the plasma (Radio Frequency (RF) Heating).

Project Team Structure

The Project structure adopted, for management purposes, is divided into four Departments (see Table II):

- Machine and Development Department;
- Experimental and Theory Department;
- Heating and Operations Department;
- Administration Department.

In addition, some scientific and technical duties are carried out within the Directorate and in the Coordinating Staff Unit.

The main duties of the Administration Department have been described in previous JET Annual Reports. This Report concentrates on progress made in the scientific and technical areas during 1991. To aid this description, the functions of these Departments are described below.

Machine and Development Department

The Machine and Development Department is responsible for the performance capacity of the machine as well as equipment for the active phase, together with enhancements directly related to it (excluding heating) and the integration of any new elements on to the machine. In addition, the Department is responsible for machine services. The Department contains three Divisions:

(a) *Magnet and Power Supplies Division* is responsible for the design, construction, installation, operation and maintenance of the tokamak electromagnetic system and of plasma control. The area of responsibility encompasses the toroidal, poloidal and divertor magnets,

Table II
JET Departmental and Divisional Structure

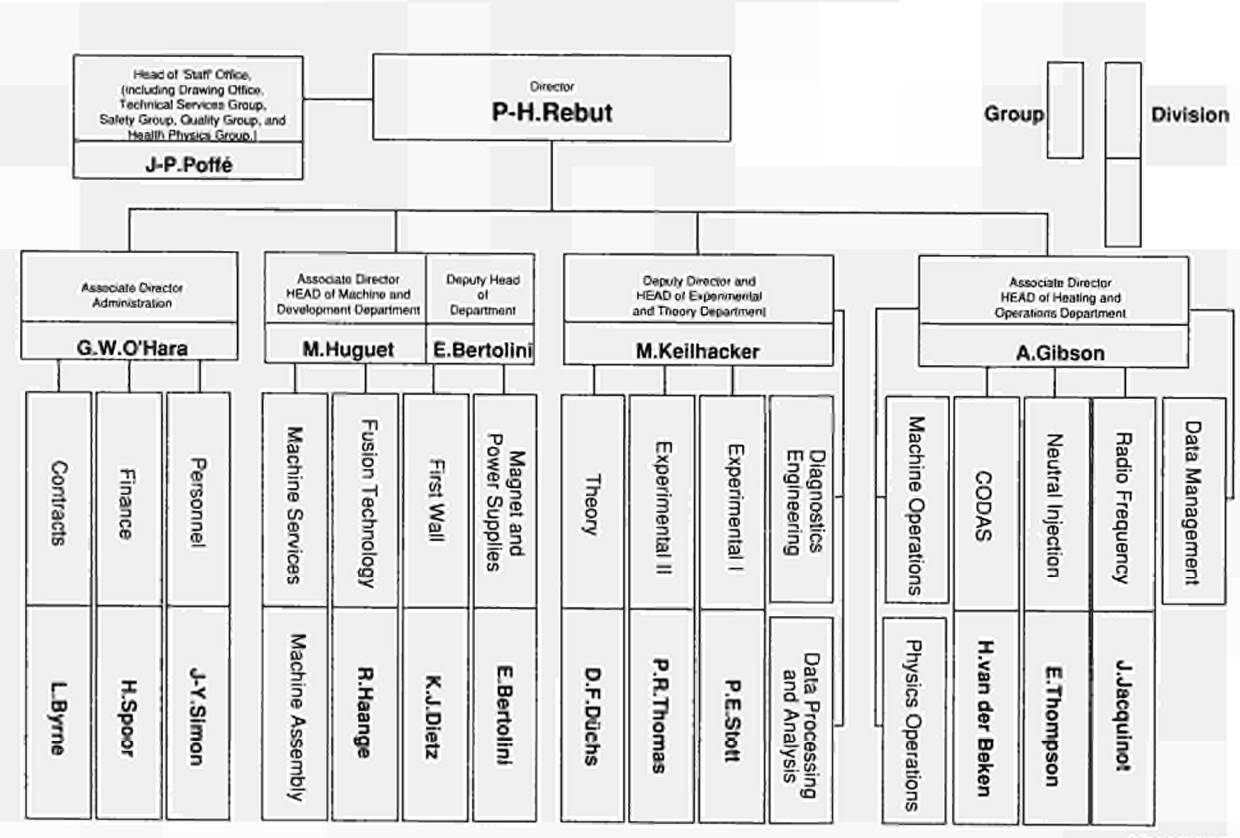

JG92.36/10

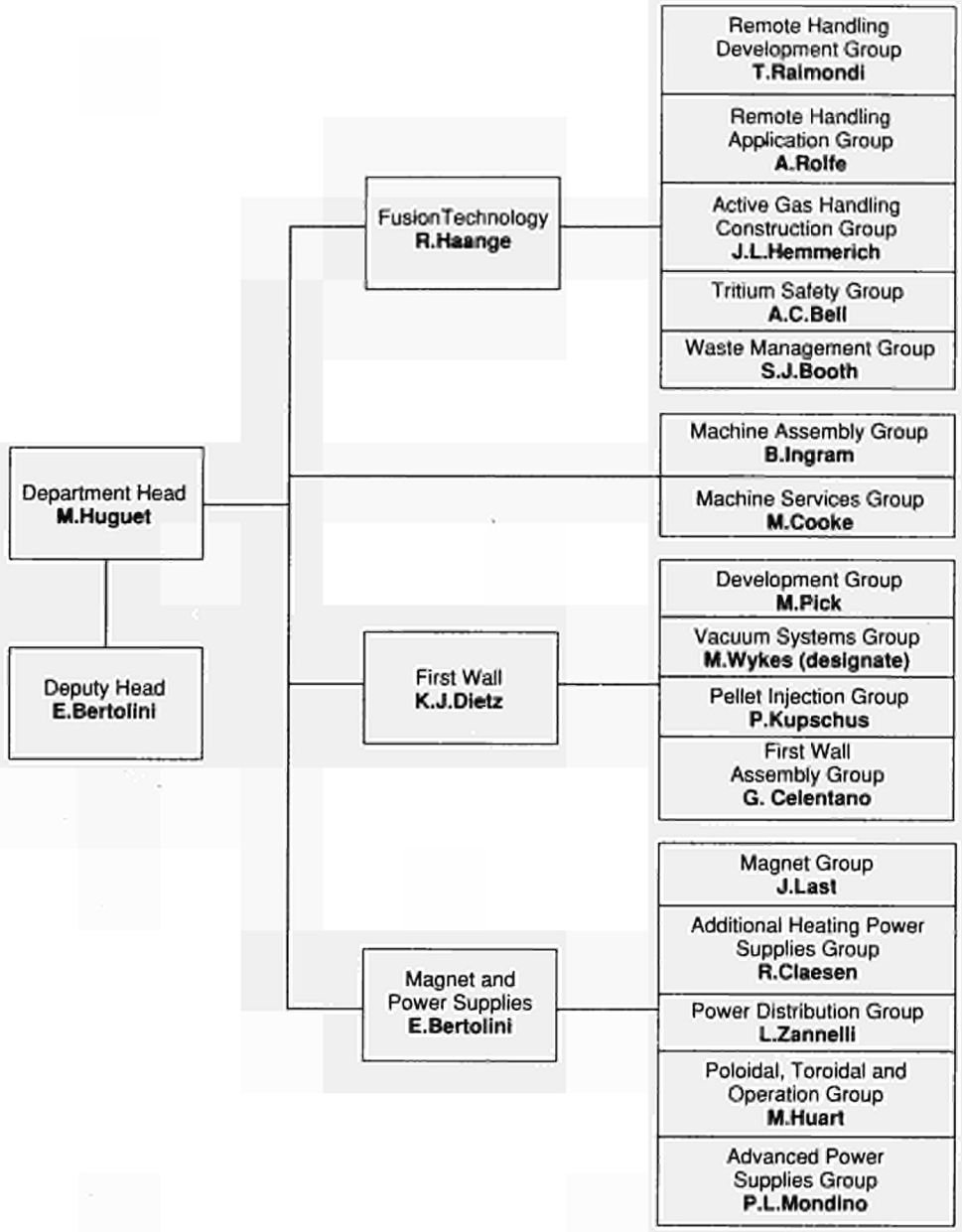

Fig.2: Machine and Development Department, Group Structure (December 1991)

mechanical structure, methods for controlling plasma position and shape and all power supply equipment needed for magnets, plasma control, additional heating and auxiliaries;

(b) *First Wall Division*, which is responsible for the vital area of plasma wall interactions. Its main tasks include the provision and maintenance inside the vacuum vessel of conditions leading to high quality plasma discharges. The Division develops, designs, procures and installs the first wall systems and its components, such as limiters, wall protections and internal pumping devices. The area of responsibility encompasses the vacuum vessel as a whole, together with its associated systems, such as pumping, bakeout and gas introduction;

(c) *Fusion Technology Division*, which is responsible for the design and development of remote handling methods and tools to cope with the requirements of the JET device, and for maintenance, inspection and repairs. Tasks also include the design and construction of facilities for handling tritium.

The Structure of the Machine and Development Department to Group Leader level is shown in Fig.2 and the list of staff within the Department is shown in Fig.3.

MACHINE AND DEVELOPMENT DEPARTMENT
Head of Department: M. Huguet
Deputy Head of Department: E. Bertolini

D. Carre
Mrs. H. Marriot
B. Ingram
S. McLaughlin
C. Sborchia
R.A.S. Smith

MAGNET AND POWER SUPPLIES DIVISION
Head: E. Bertolini

P. Barabaschi
P. Bertoldi
T. Bonicelli
D. Chiron
R. Claesen
E. Daly
N. Dolgetta
P. Doyle
H. T. Fielding
C. Folco
M. Garibba
J. Goff
D. Halliwell
M. Huart
F. Jensen
J. R. Last
H. McBrian
J. McKivett
V. Marchese
G. Marcon
L. Mears
P. Mondino
G. Murphy
Mrs. J. Nolan
P. Noll
R. Ostrom
P. Presle
A. Santagiustina
G. Sannazzaro
S. Shaw
R. Suter
M. Tabellini
A. Tesini
S. Turley
J. van Veen
C. R. Wilson
G. C. Wilson
L. Zannelli

FUSION TECHNOLOGY DIVISION
Head: R. Haange

A. C. Bell
G. Benali
S. J. Booth
P. Brown
T. Businaro
C. J. Caldwell-Nichols
Mrs. J. Campbell
P. Chuilon
R. Cusack
F. Delvart
L. Galbiati
A. Galetsas
J. Gowman
J. L. Hemmerich
M. Irving
Mrs. M. E. Jones
L. P. D. F. Jones
J. F. Jaeger
J. F. Junger
A. Konstantellos
R. Lässer
M. Laveyry
Miss. J. Lech
A. Loving
J. Lupo
J. Mart
P. Milverton
G. Newbert
A. Nowak
S. Puppin
T. Raimondi
K. D. Walker
M. Wykes

FIRST WALL DIVISION
Head: K. J. Dietz

W. P. Bailey
S. Bryan
H. Buttgereit
G. Celentano
Mrs. D. Cranmer
E. Deksnis
C. Froger
M. Gadeberg
D. Holland
Mrs. I. Hyde
G. Israel
H. Jensen
P. Kupschus
E. Martin
B. Macklin
A. Miller
J. Orchard
A. Peacock
R. Pearce
M. Pick
L. Rossi
S. Scott
T. Szabo
R. Thomas
M. Watson
T. Winkel

Fig.3: Project Team Staff in the Machine and Development Department (December 1991)

Experimental and Theory Department

The main functions of the Department relate to the measurement and validation of plasma parameters and to the theory of tokamak physics. The main tasks are:

- to conceive and define a set of coherent measurements;
- to be responsible for the construction of necessary diagnostics;
- to be responsible for the operation of the diagnostics and the quality of measurements and the definition of the plasma parameters;
- to follow the theory of tokamak physics;
- to play a major role in interpretation of data.

The Department contains two Groups (Diagnostics Engineering Group and Data Processing and Analysis Group) and three Divisions:

(a) *Experimental Division 1 (ED1)*, which is responsible for specification, procurement and operation of about half the JET diagnostic systems. ED1 undertakes electrical measurements, electron temperature measurements, surface and limiter physics and neutron diagnostics;

(b) *Experimental Division 2 (ED2)*, which is responsible for specification, procurement and operation of the other half of the JET diagnostic systems. ED2 undertakes all spectroscopic diagnostics, bolometry, interferometry, the soft X-ray array and neutral particle analysis;

(c) *Theory Division*, which is responsible for prediction by computer simulation of JET performance, interpretation of JET data and the application of analytic plasma theory to gain an understanding of JET physics.

The structure of the Experimental and Theory Department to Group Leader level is shown in Fig.4 and the list of staff in the Department is shown in Fig.5.

Heating and Operations Department

Heating and Operations Department is responsible for heating the plasma, the organisation of experimental data, and the day-to-day operation of the machine. The main functions of the Department are:

- heating the plasma and analysis of its effects;

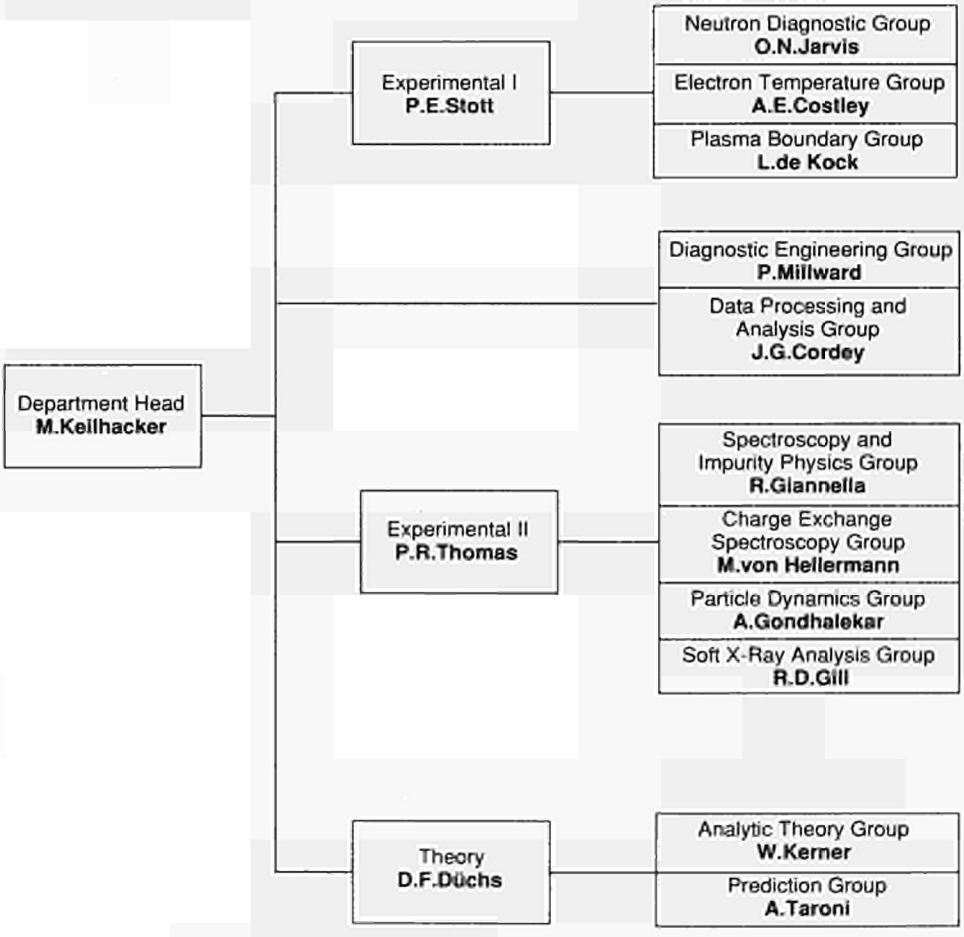

Fig.4: Experimental and Theory Department, Group Structure (December 1991)

EXPERIMENTAL AND THEORY DEPARTMENT

Head of Department: M. Keilhacker

B. Balet
M. Barnes
K. Blackler
J. Christiansen
J. G. Cordey
C. J. Hancock
J. Hoekzema
J. P. Jéral
P. Millward
D. O'Brien
R. Oord
J. Reid
P. J. Roberts
Miss K. Slavin
Mrs. P. Stubberfield
K. Thomsen
Mrs. R. Thormaehlen
A. Tiscornia
E. van der Goot
G. Vlases
D. Ward
J. Wesson
C. H. Wilson
D. Wilson

EXPERIMENTAL DIVISION I

Head: P. E. Stott

S. Ali-Arshad
Miss. N. Avery
D. Bartlett
B. W. Brown
D. Campbell
S. Clement
E. Clipsham
J. P. Coad
A. E. Costley
J. Ehrenberg
L. de Kock
J. Fessey
C. Gowers
Mrs. M. Harper
P. J. Harbour
M. Hone
I. Hurdle
O. N. Jarvis
B. Laundy
M. Loughlin
F. B. Marcus
G. Matthews
G. Neill
C. Nicholson
P. Nielsen
H. Oosterbeek
R. Prentice
G. Sadler
B. Schunke
A. C. C. Sips
A. Stevens
D. Summers
P. van Belle
J. Vince

EXPERIMENTAL DIVISION II

Head: P. R. Thomas

B. Alper
Mrs. K. Bell
G. Braithwaite
J. L. Bonnerue
S. Corti
G. B. Denne-Hinnov
A. Edwards
Mrs. A. Flowers
R. Giannella
R. Gill
A. Gondhalekar
N. Gottardi
D. Halton
L. D. Horton
H. Jäckel
G. Janeschitz
R. König
G. Magyar
J. L. Martin
P. Morgan
H. Morsi
R. Reichle
J. O'Rourke
J. Ryan
D. Pasini
M. Stamp
S. A. Staunton-Lambert
M. von Hellermann
B. Viaccoz

THEORY DIVISION

Head: D. F. Düchs

W. Core
Mrs. S. Costar
L. G. Eriksson
A. Galway
Mrs. S. Hutchinson
B. Keegan
W. Kerner
F. Porcelli
H. C. Sack
R. Simonini
E. Springmann
A. Taroni
F. Tibone
W. Zwingmann

Fig 5: Project Team Staff in Experimental and Theory Department (December 1991)

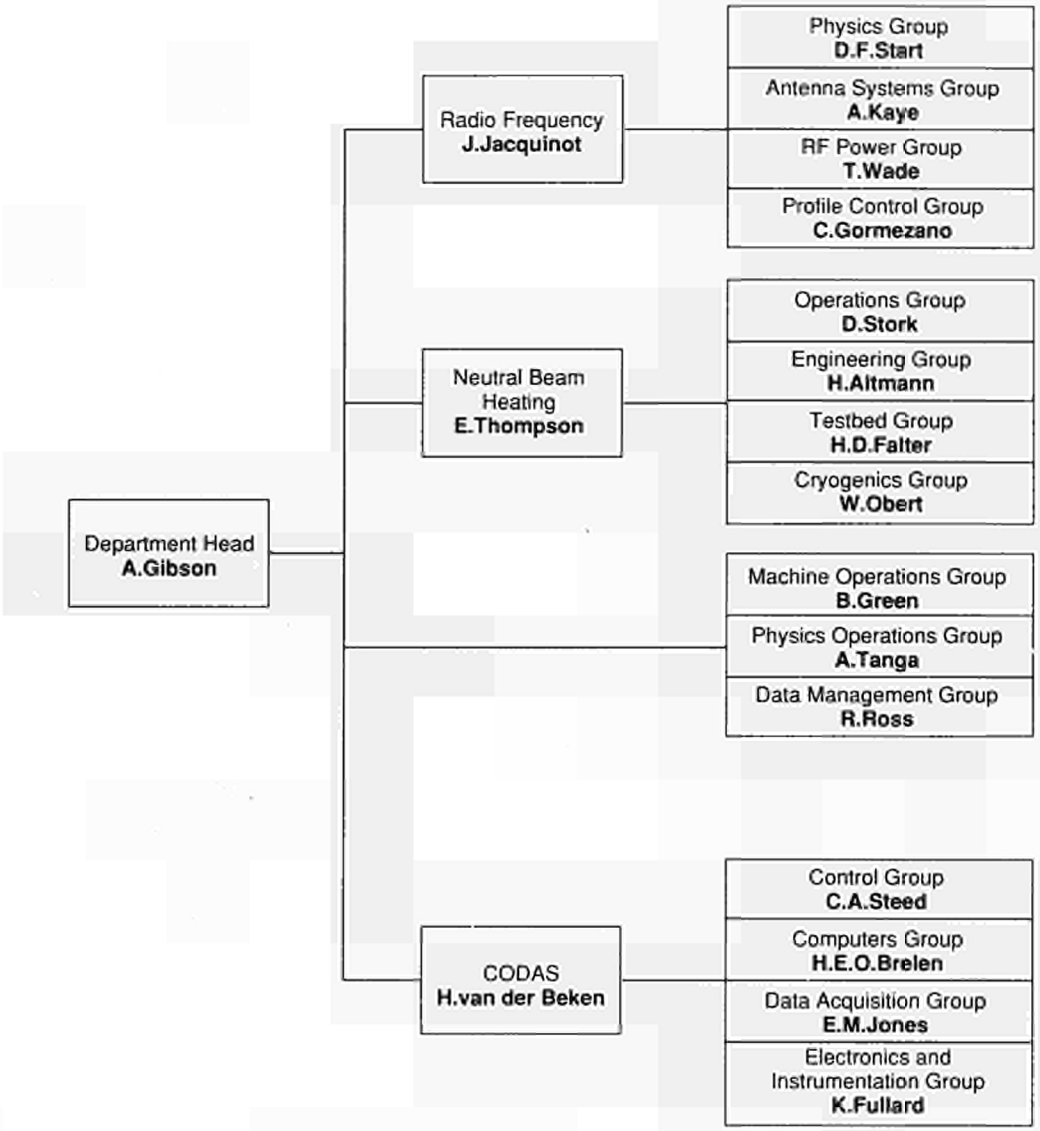

Fig.6: Heating and Operations Department, Group Structure (December 1991)

- centralising the interpretation of experimental results and investigating their coherence;
- organising data acquisition and computers;
- preparing and co-ordinating operation of the machine across the different Departments.

The Department is composed of three groups (Machine Operations Group, Physics Operation Group, and Data Management Group) and three Divisions:

(a) *Control and Data Acquisition System Division (CODAS)*, which is responsible for the implementation, upgrading and operation of computer-based control and data acquisition systems for JET;

(b) *Neutral Beam Heating Division*, which is responsible for construction, installation, commissioning and operation of the neutral injection system, including development towards full power operation. It also participates in studies of physics of neutral beam heating;

(c) *Radio Frequency Heating Division*, which is responsible for the design, construction, commissioning and operating the RF heating system during the different stages of its development to full power. The Division also participates in studies of the physics of RF heating.

The structure of the Heating and Theory Department to Group Leader level is shown in Fig.6, and the list of staff in the Department is shown in Fig.7.

In addition, all Divisions are involved in:

- execution of the experimental programme;
- interpretation of results in collaboration with other appropriate Divisions and Departments;
- making proposals for future experiments.

PLASMA HEATING AND OPERATIONS DEPARTMENT

Head of Department: A. Gibson

K. Adams
M. J. Bolton
A. Conway
D. Cook
S. Cooper
T. Dale
P. Gaze
B. Green
N. Green
R. Greenfield
C. Hookham
J. How
M. Hughes
M. Johnson
P. J. Lomas
Mrs. P. Longworth
C. Lowry
M. Macrae
R. C. Meadows
B. S. Regan
R. Rigley
Mrs. J. Roberts
R. T. Ross
P. Rutter
G. Saibene
Miss. D. Samuel
R. Sartori
P. Smeulders
W. Smith
F. W. Taker
A. Tanga
K. A. Taylor
B. Tubbing
M. Walker
M. Wallwork
J. M. Watt
B. Workman

NEUTRAL BEAM HEATING DIVISION

Head: E. Thompson

H. Altmann
A. Bickley
A. Browne
C. D. Challis
D. Cooper
J. F. Davies
G. Deschamps
A. Dines
H. P. L. de Esch
D. Ewers
H. Falter
Mrs. S. Humphreys
D. Hurford
J. Z. Jensen
T. T. C. Jones
F. Long
J. G. Lundqvist
D. Martin
P. Massmann
C. Mayaux
Mrs. D. Noyes
W. Obert
S. Papastergiou
A. J. Parfitt
D. Raisbeck
D. Stork
L. Svensson
J. Waterhouse

RADIO FREQUENCY HEATING DIVISION

Head: J. Jacquinot

V. Bhatnagar
S. C. Booth
G. Bosia
M. Brandon
H. Brinkschulte
M. Brusati
M. Bures
Miss. M. Casson
G. Cottrell
P. Crawley
T. Dobbing
D. T. Edwards
A. Franklin
P. Finberg
M. Gammelin
B. Glossop
C. Gormezano
R. Horn
G. Jessop
A. Kaye
M. Lennholm
P. Murry
M. Pain
J. Plancoulaine
F. Rimini
P. Schild
M. Schmid
Ms. V. Shaw
A. Sibley
D. Start
C. Steele
T. Wade
C. Walker

CONTROL AND DATA ACQUISITION SYSTEMS DIVISION

Head: H. van der Beken

M. B. Baronian
Mrs. A. M. Bellido
M. J. M. Botman
H. E. O. Brelen
W. J. Brewerton
T. Budd
P. J. Card
J. J. Davis
S. Dmitrenko
S. E. Dorling
K. Fullard
E. M. Jones
F. J. Junique
G. J. Kelly
N. G. Kidd
J. G. Krom
D. S. Nassi
C. Perry
C. A. Steed
C. Terella
G. Wolfers
I. D. Young

Fig.7: Project Team Staff in Plasma Heating and Operations Department (December 1991)

Directorate

Within the Directorate are one scientific and one technical group, (Scientific Assistants to the Director and Technical Assistant to the Director (including Publications Group)), whose main tasks are as follows:

- Scientific Assistants to the Director, who assist and advise the Director on scientific aspects of JET operation and future development;
- Technical Assistant to the Director, who assists and advises the Director on organizational and technical

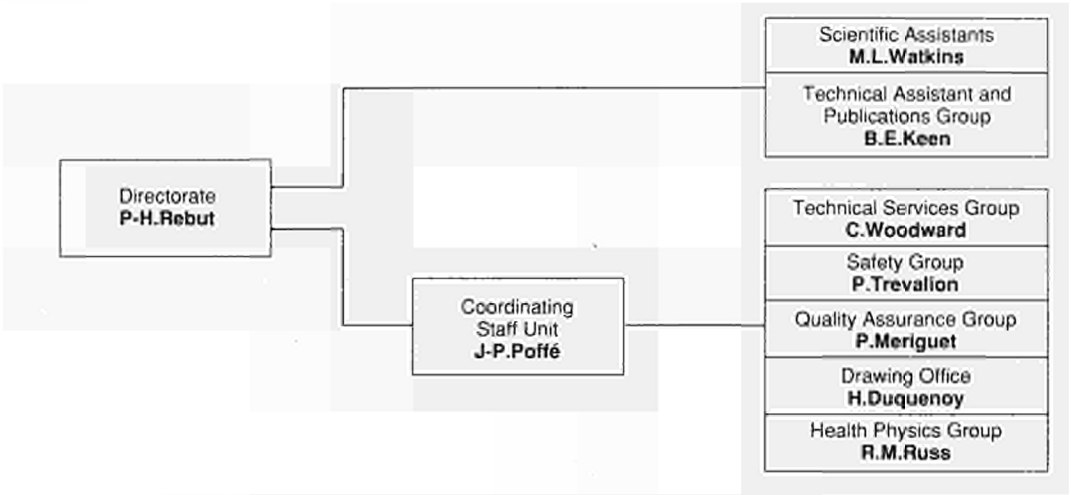

Fig.8: Directorate and Coordinating Staff Unit, Group Structure (December 1991)

DIRECTORATE AND COORDINATING STAFF UNIT

Director: Dr. P-H. Rebut

DIRECTORATE

Mrs. S-J. Ashwood
Mrs. G. Blankenback
D. Boucher
Mrs. M. Deitrich
M. Drew
D. Gambier
Miss. C. Hampson
M. Hugon
B. E. Keen
J. McMahon
J. H. C. Maple
S. Morris
K. Musgrave
T. O'Hanlon
Mrs. C. Simmons
Ms. M. Straub
Mrs. J. Talbot
M. L. Watkins
Miss. C. Weaver
M. Woollard

COORDINATING STAFF UNIT

Head: J-P. Poffé

Ms. L. Ashby
M. Axton
P. Barker
J. Banham
P. Burton
C. Callaghan
D. Campling
G. Dalle-Carbonare
N. Davies
H. Duquenoy
A. Gibson
A. Girard
J. A. Green
M. Guillet
A. D. Haigh
Mrs. E. Harries
F. Hurd
H. D. Jones
R. Litchfield
Miss. K. Luker
P. Meriguet
J. McDonald
H. Panissie
B. Patel
Mrs. J. Reid
R. M. Russ
K. Sandland
P. Schofield
M. Scotcher
P. Trevalion
C. Woodward

Fig.9: Project Team Staff in Directorate and Coordinating Staff Unit (December 1991)

matters related to JET operation. He also acts as JET Publications Officer, and is Leader of the Publications Group.

Coordinating Staff Unit

The Coordinating Staff Unit is responsible for the provision of engineering services to the Project and for the implementation of specific coordinating tasks at the Project level.

It comprises five Groups:

- Technical Services Group;
- Safety Group;
- Drawing Office;
- Quality Group;
- Health Physics and Safety Group

The structure of the Directorate and Coordinating Staff Unit to Group Leader level is shown in Fig.8 and the list of staff in these areas is shown in Fig.9.

Report Summary

The first section of this Report provides a brief introduction and background information relevant to the Report. The second and third sections set out an overview of progress on JET during 1991 and with a survey of scientific and technical achievements during 1991 sets these advances in their general context. This summary is specifically cross-referenced to reports and articles prepared and presented by JET staff during 1991. The more important of these articles, which are of general interest, are reproduced as appendices to this Report.

The fourth section is devoted to future plans and certain developments which might enable enhancements of the machine to further improve its overall performance. Some attention has been devoted to methods of surmounting certain limitations and these are detailed in this section.

The Appendices contain a list of work topics which have been carried out under Task Agreements with various Association Laboratories, and selected articles prepared by JET authors are reproduced in detail, providing some details of the activities and achievements made on JET during 1991. In addition, a full list is included of all Articles, Reports and Conference papers published by JET authors in 1991.

Technical Achievements during 1991

Introduction

From November 1990 to April 1991, the machine was in a scheduled shutdown in order to carry out a number of main tasks as follows:

- repair and reinforcement of mechanical supports for in-vessel wall protection tiles to improve accurate tile placement and to provide a system more resilient to disruptions;
- installation of new X-Point Target Plates: Tiles carefully shaped to protect each edge (Carbon - top; Beryllium - bottom) to improve overall power loading capability during single and double-null X-point configurations, and to compare carbon with beryllium;
- both NB systems brought up to 140keV D operation ($P_{NB} \approx 15.5$MW);
- modifications to power supplies systems; including poloidal shaping amplifier upgrade to 50kA; and introduction of reactive power compensation system;
- X-point gas introduction system installed;
- subsequently design, construct and commission new systems for the introduction and recovery of tritium for the preliminary tritium experiment (P.T.E.)

Machine operation took place from May to September, except for an incident in May when arcing occurred on the poloidal field coils and had to be remedied. This took about three weeks. A further interuption took place due to a leak occuring in the bellows on one of the lights on the In-Vessel Inspection System (IVIS). This coincided with an outage of the high voltage power grid for planned maintenance. In addition, the September shutdown was used to install redesigned carbon target plate tiles. Machine operation started again in late September and continued to end of the year.

The following sections detail the technical achievements made during this period.

Torus Systems

The activities during 1991 were shared between carrying out maintenance and installation work during the shutdown (which started at the end of 1990 and continued during the first half of 1991) the provision of services (vacuum system, wall conditioning, gas introduction and pellet injection) for subsequent machine operation; activities related to the design, procurement and installation of components for the New Phase on the Pumped Divertor; and the commissioning of the high-speed pellet Prototype Launcher, preparation of its installation in the Torus Hall and the continued development of the high-speed multiple pellet launcher.

At the beginning of the period, responsibilities for design, procurement and installation of wall components were divided between two new groups (First Wall Installation Group and First Wall Development Group) which replace the Limiter and Divertor Group. In the light of the required effort for the Pumped Divertor Phase, additional manpower was allocated to these activities.

In-Vessel Components

Two shutdowns took place during 1991. The first scheduled shutdown started in November 1990 and ended in April 1991. The principal objectives were to install new continuous upper and lower X-point target plates and to strengthen wall components, especially the wall protection. Due to previous usage of beryllium, the work was carried out in full pressurized suits and was based on two-shift working for six days per week. About 23 weeks were required (5200 man-hours), which were spent in the torus or in the adjacent work area.

A second shutdown which was unscheduled took place in September and lasted four weeks. Due to a leak in a bellows which could be repaired only from the inside of the machine,

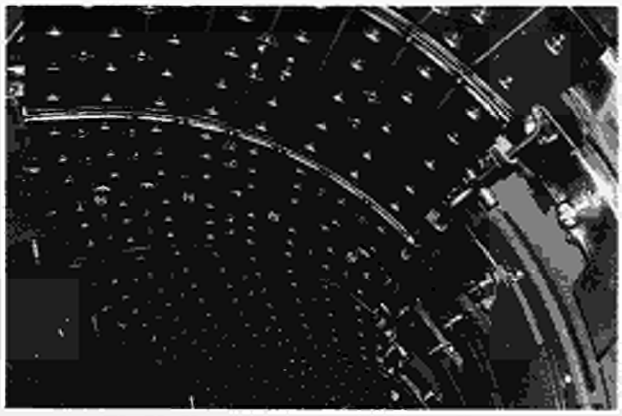

Fig.10: Upper target plate after installation.

the vessel had to be cooled down, vented and entrance effected before the bellows could be exchanged. This shut-down was used as well to install modified wall protection tiles.

Among the new wall elements which were introduced into the vessel during the scheduled shutdown were the toroidally continuous X-point target plates, at the top and the bottom of the vacuum vessel. They replaced the provisional target plates which consisted of toroidally spaced energy dumps initially devised as wall protection. The new X-point target plates are each made up of 48 cylindrical segments attached to the rigid sectors of the machine covering the top and bottom over a poloidal arc of 1 m length. Fig.10 shows the upper target plate after installation. The accuracy of the mechanical alignment between two adjacent sectors was better than ± 1 mm. The active areas of the lower plates were covered with beryllium tiles whilst the upper plates were covered with carbon fibre reinforced graphite.

The beryllium tile assemblies were designed in such a way as to optimize the power handling capability of the system, whilst reducing the probability of producing "hot spots" leading to carbon or beryllium "blooms". The power handling capability was carefully analyzed taking into account the expected plasma configurations and field line angles. The design required the machining of each tile so that its surface was tangential to the toroidal shape of the plasma, as opposed to the cylindrical shape of the dump plates themselves. This ensures a more even power loading of the tiles. An additional slope was machined onto all tiles at dump plate segment edges to allow for steps from sector to sector of up to 2mm. This allowed for the maximum expected manufacturing and installation tolerances of the torus and dump plate segments. In order to shield all possible edges from exposure to the plasma, additional machining was required on the edges of adjacent tiles as well as the areas around the fixation holes on the top of the tiles. The final design was such that localised surface melting was expected to occur on sloped faces of the tiles for 20 MW of conducted power after 0.5 s.

The graphite fibre tiles were initially not shaped in this intricate way, but had flat surfaces which were slightly raised in some areas to compensate for the cylindrical shape of the target plate segments. During the operational period, carbon "blooms" ocurred at low incident power and re-shaping was required. In this case, the difference in the power loading of the inner and outer strike zone was taken into account allowing for a greater overall performance of the dump plates. The original graphite tiles on the upper target plate were replaced by modified tiles during the September shutdown.

A detailed assessment of the actual performance of the dump plate tiles was performed during the experimental campaign. The graphite and the beryllium target tiles responded similarly to the plasma and it was found that there was an onset of a bloom in both cases at a conducted energy of about 8MJ for 16MW of input power in general agreement with expected behaviour.

Problems experienced with the wall protection during the 1990 operations were caused by "halo" currents. The wall components were designed to withstand eddy current forces but they were not strong enough to cope with the forces created by the interaction between wall transferred "halo" currents and the toroidal field. A series of component failures and damage to in vessel components occurred. The damage included mainly bellows protection plates which had been pulled off the wall, arcing at first wall component connection bolts, bent tile carrier rails and bent tile backing plates.

Progress was achieved in understanding the occurrence and effects of halo currents in the JET vessel. A detailed analysis of damage, its location and distribution, as well as an analysis of damage which had occurred during previous operational periods, improved knowledge of the nature and magnitude of plasma "halo" induced currents in first wall components. During the scheduled shutdown, strategically located and instrumented tiles to measure these currents were installed in the vessel. Together with the resulting measurements, analysis provided important information required to design the new pumped divertor components which consequently required partially a re-design.

Based on this understanding of "halo" current effects, remedial action was taken during the shutdown to reinforce

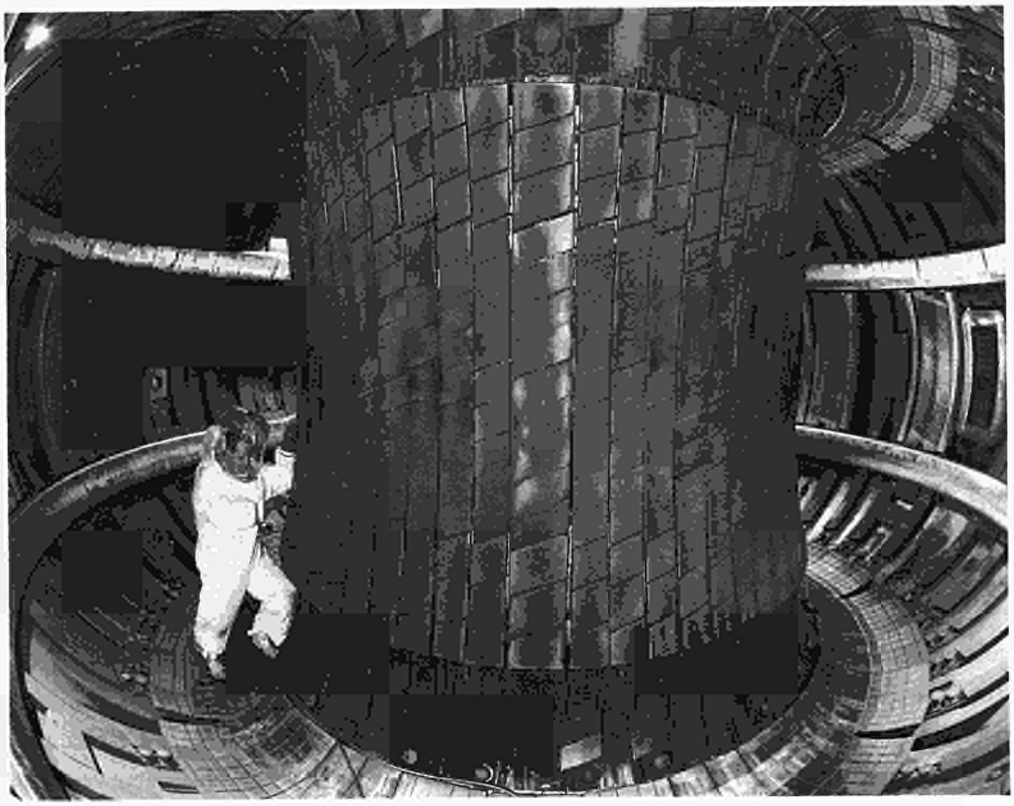

Fig.11: Inside of the vacuum vessel before operations in 1991.

the wall protection in the affected areas. Welds were strengthened, fasteners improved, weak mechanical supports were modified and cantilevered supports were eliminated. Operational experience during the subsequent operational period proved that these modifications were successful. No further wall damage was observed.

Fig.11 shows the inside of the vacuum vessel before operations resumed in 1991. The upper and lower X-point target plates are the main new features in this picture. Adjacent are mushroom shaped wall protection tiles. These are made of carbon fibre material and designed to take the forces resulting from "halo" currents. Some are instrumented. The plasma facing material of the belt limiters was also changed, with beryllium on the upper belt and graphite on the lower one.

Development of In-Vessel Components for the Pumped Divertor

In parallel to tasks carried out in relation to the shutdown, large effort was devoted to the design, procurement and preparation for the installation of pumped divertor components during 1992/1993. Fig.12 shows a three dimensional view of intended major divertor components.

The upper X-point target plate will be retained and will allow for double null discharges, albeit at reduced power. In

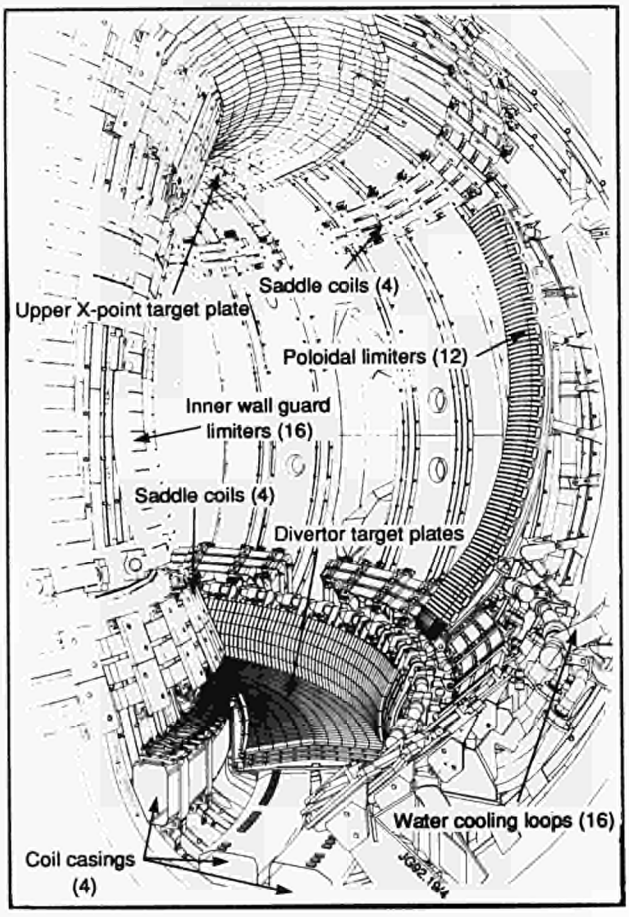

Fig.12: View of the major divertor components for the New Phase of JET.

addition, it serves as an energy dump for discharges, which terminate in a vertical instability with upwards movement. The material facing the plasma can be either beryllium or carbon fibre reinforced graphite.

Eight saddle coils, four at the lower and four at the upper part of the vessel will create radial magnetic fields to counteract MHD instabilities and to prevent locked modes. The coils are bakeable up to 500°C, each has three windings and can carry currents ≤ 25 kA-turns at voltages ≤ 8 kV and at frequencies up to 10 kHz.

Sixteen inner wall guard limiters, evenly distributed toroidally, protect the vessel against damage due to radial disruptions and are also designed to take "halo" current forces due to vertical instabilities with downward plasma movements. The plasma facing material is fibre reinforced graphite.

The divertor target plate is toroidally closed and is located at the bottom of the vessel. It consists in the initial configuration of radiatively cooled beryllium blocks capable of handling 20 MW of conducted power for 4 s with the surface temperature remaining below 1000°C. At a later stage, an actively cooled system is envisaged which would allow for prolonged pulse operation at 40 MW conducted to the target plates with the aim to achieve stationary plasma conditions. A total of sixteen water cooling loops, supply the target plates and incorporate bellows and electrically insulating breaks. The latter are designed for stand-off voltages of several kV, internal operating pressure and bakeable up to 400°C.

Four coil casings made of inconel surround the divertor coils. They will be used as a container during the vacuum impregnation of the coils and act later as the leak tight enclosure around the epoxy resin covering the coils. The inside of the coil casings will be pumped to avoid pressure build-up during operation under neutron irradiation.

Twelve poloidal limiters will be installed at the outside of the vessel adjacent to RF antennae. Their main task is to protect the RF antennae from the plasma. The bottom part is in the interaction area with "halo currents" and is able to withstand forces of 5 tonnes each. The plasma facing material can be either beryllium or graphite.

The procurement of in-vessel components for the pumped divertor, which are required at the beginning of the 1992/1993 shutdown, is well under way. All contracts have been placed and progress in the manufacturing of the components is satisfactory, but sustained effort will be required to maintain the time schedule. Further design and development work will still be necessary for components to be installed early in 1993.

In addition to the equipment shown in Fig.12, there are further elements which are under design and procurement and which form an essential part of the pumped divertor. This main ones are: fibre graphite protection tiles for the saddle coils and the divertor target plate; mushroom tiles adjacent to the upper X-point target plate; thermal shields to protect the coil casings from thermal radiation from the vessel and to avoid differential expansion between coil and casing; diagnostics to measure target plate temperatures, "halo" currents and voltages across electrical breaks; and in-vessel gas introduction pipework with 24 introduction points at the level of the target plates.

Installation of In-Vessel Components for the Pumped Divertor

In parallel with the design and procurement of the components for the pumped divertor, the organisation and preparation of installation inside the vacuum vessel due to start in March 1992, was a major task. The preceding tritium operation during the preliminary tritium experiment together with the wall conditioning with beryllium evaporation requires work must start in full pressurized suits. Therefore, all inner wall components will be stripped off at the earliest stage and removed and the vessel will be decontaminated. Then, minimal personal protection will be required for the installation of the divertor. This will allow an increase in the number of personnel working in the vessel and will enhance their efficiency. Decontamination methods are presently being studied.

The amount of work to be carried out inside the vessel and the requirement to minimize installation time demanded optimization of working conditions inside the vessel (beryllium, tritium, radiation and limited space). This necessitated setting up dedicated organisation for in vessel work and led to the definition of suitable working methods, the development of special procedures, and the design and procurement of specialized jigs and tools.

The definition of procedures for handling components, through the ports and inside the vessel, has required considerable effort. In addition to using the articulated boom and the TARM for the introduction of components into the vessel and the boom for positioning components at the wall, a specially designed toroidal travelling crane, designed for a safe working load of 1.3 tonnes, will be installed inside the vessel. A series of bosses will be

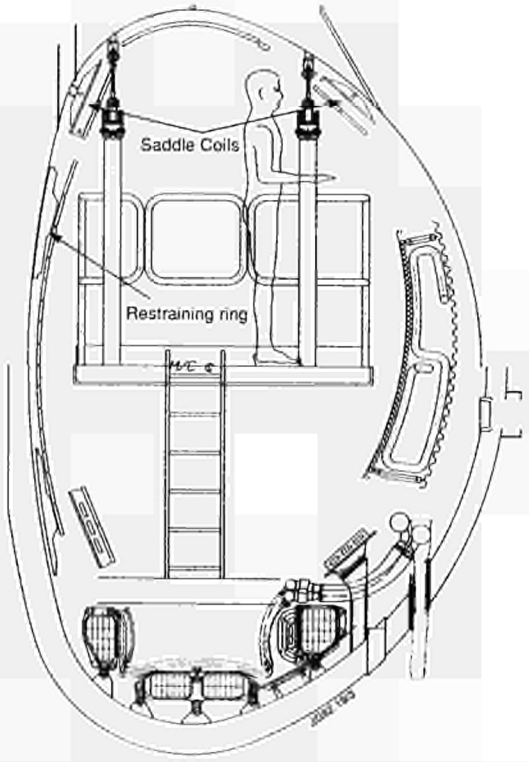

Fig.13: Sketch of inside of vessel during installation of component in the New Phase.

welded to the top of the vessel and stay inside as part of the wall. They will initially support temporary lifting gear required during the building of the divertor coils and subsequently will be used for the crane and a mobile platform required for the installation of other components. A sketch of the inside of the vessel during installation is shown in Fig.13 with the travelling crane and the suspended platform installed.

The toroidal geometry and the inaccuracies in the construction of the vacuum vessel (locally up to 12mm deviation from the theoretical dimensions) make it difficult to install the divertor system to the required level of accuracy (better than ± 0.5mm). Therefore, special fixtures and jigs were developed and will be used to set the position of each component as closely at possible to the magnetic configuration of the machine using external datum points as reference.

Vacuum System

The vacuum system worked reliably and machine availability was not limited. However, problems were experienced with control equipment, which were mainly traced to computer error in the local control units or to unreliable electrical connectors. Due to the age of equipment, it becomes increasingly difficult to obtain spare parts.

Only five leaks occurred during the 1991 operational campaign and all but one could be repaired without venting the vessel or impairing the operation. However, one large leak (of 2×10^4 mbarℓs^{-1}) led to the unscheduled shutdown in September. This occurred in a bellows and the vessel rose to atmospheric pressure at wall temperatures of 300°C. This resulted in oxidation of inner surfaces and soaked up air in the porous graphite elements (several tonnes in weight) inside the vessel. The bellows was only accessible from the inside the vacuum vessel. The vessel had to be cooled down, opened and the bellows exchanged. Subsequent vessel conditioning required a prolonged effort. After baking to 300°C and leak check glow discharge cleaning was carried our for 87 hours in deuterium and 54 hours in helium. Following a beryllium evaporation the vessel was ready for plasma operation.

Instrumentation

The residual gas analyzers (RGA) currently used to measure partial pressures inside the vacuum vessel is not compatible with the radiation levels expected during the main D-T plasma phase of JET. This is mainly due to the existence of radiation sensitive components, such as semiconductors in the vicinity of the quadrupole head located at the torus. There was no alternative available which would fulfil requirements. Therefore, a prototype radiation resistant RGA was developed following a collaborative design phase with industry and delivery took place at the end of 1990.

The new RGA combines radiation hard vacuum tube based electronics at the quadrupole head, with semiconductor based electronics placed away from high levels of radiation. The two sections are designed to operate approximately 100 m apart connected by electrical cables. A block diagram of the set-up is shown in Fig.14.

A programme of testing and further development of this RGA was carried out throughout 1991. This started with tests on a small vacuum system outside of the Torus Hall and was continued with the measuring head being placed in the

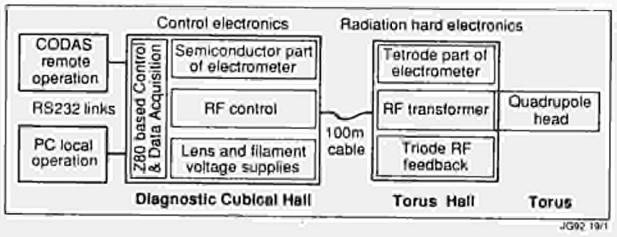

Fig.14: Block diagram of new residual gas analyser (RGA).

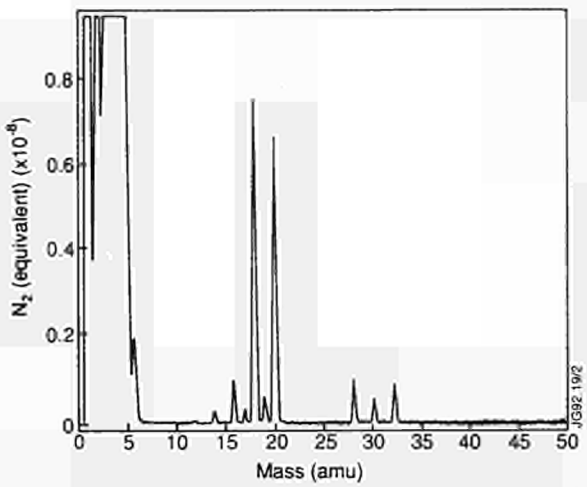

Fig.15: Plot of output from new residual gas analyser.

torus vacuum. Good results were obtained. It is planned that five radiation hard RGAs will be installed in the divertor shutdown so that further experience can be obtained with them prior to the main D-T phase.

A typical scan of the torus vacuum during operation using the new RGA is given in Fig.15, which shows good resolution and peak definition. The masses in the range 12 to 32 result mainly from deuterated species of methane, water and acetylene.

Gas Introduction

The piezo-driven gas inlet valves used as part of the gas introduction system were redesigned to meet the flow requirements for the future divertor configuration. The valves operate by the action of a clamped piezo crystal contracting and pulling open a seal on an orifice. In the new design, the piezo crystal stack was doubled in length to provide a larger stroke and hence a larger opening. Delivery was taken of three of the new valves and their performance was analyzed. The three valves had very similar flow characteristics, and was an improvement on the old valves which had widely differing characteristics. A deuterium flow rate of 100 mbℓs^{-1} into a vacuum, was measured with a reservoir pressure of approximately 500mbar. The previous design of this valve required pressures up to three times higher to achieve this flow rate. The new design piezo valve will now be used in the divertor gas introduction system.

Gas Collection

The preparation of the preliminary tritium experiment (PTE) involved the vacuum system in that all tritium injected into the vessel and the neutral injection box (NIB) had to be removed from the torus through the vacuum system before it could go to storage in uranium beds. Therefore, the vacuum system had to be modified, a gas collection system had to be introduced and measuring systems had to be added.

The design and installation of hardware for tritium has been an on-going effort since 1990. The equipment to be designed and installed within the responsibility of the Vacuum Group was the gas collection and measuring system consisting of modifications to the cold finger, new connecting pipework, some additional valves, the residual gas analyser system for monitoring leaks, the sample bottle arrangement, the connecting line to the tritium storage system, and the necessary control and measurement equipment for the operation of the gas collection.

A diagram of the vacuum system including the gas collection is shown in Fig.16. The exhaust gases from the Torus and the NIBs are pumped via turbomolecular pumps (TO1 - TO7) located in the Torus Hall and roots/rotary pump combinations (R1, R2) located in the West Wing of the Torus Hall. There is a vacuum connection (backing crown) between the torus and the West Wing. The torus and the NIBs can be isolated separately from the roots/rotary combinations by individual all metal valves (V5, V6). During the PTE both metal valves to the fore pumping systems were closed, sealed and locked and the pumping carried out by a small cryo pump (cold finger) connected to the torus or the NIBs by valves V2 and V3. Prior to tritium retrieval all the exhaust gases from both systems, Torus and NIBs were collected on the cold finger.

After one plasma pulse, the gas from the torus was collected for 10 minutes in the backing crown and consecutively sampled using the sample bottles, checked for tritium content (IC1) and for possible fore vacuum air leaks (residual gas analyser MS) before being pumped onto the cold finger at LHe temperature. As soon as 4barℓ had been collected from the system the isolation valve V1 to the cold finger was closed and the cold finger warmed up so that hydrogen isotopes could be transferred to the 345ℓ reservoir for further processing. The 4 barℓ limit was intended to keep the reservoir pressure below 15mbar avoiding a possible explosive mixture in the event of an air leak. After this the cold finger was re-cooled in preparation for a new batch. This operation took ~1.5 - 2 hours.

During the times that the cold finger was collecting the torus gas the NIBs were being pumped by their own cryopumps which were regenerated overnight and the gas pumped in the same manner and under the same restrictions as described for the torus gas collection system.

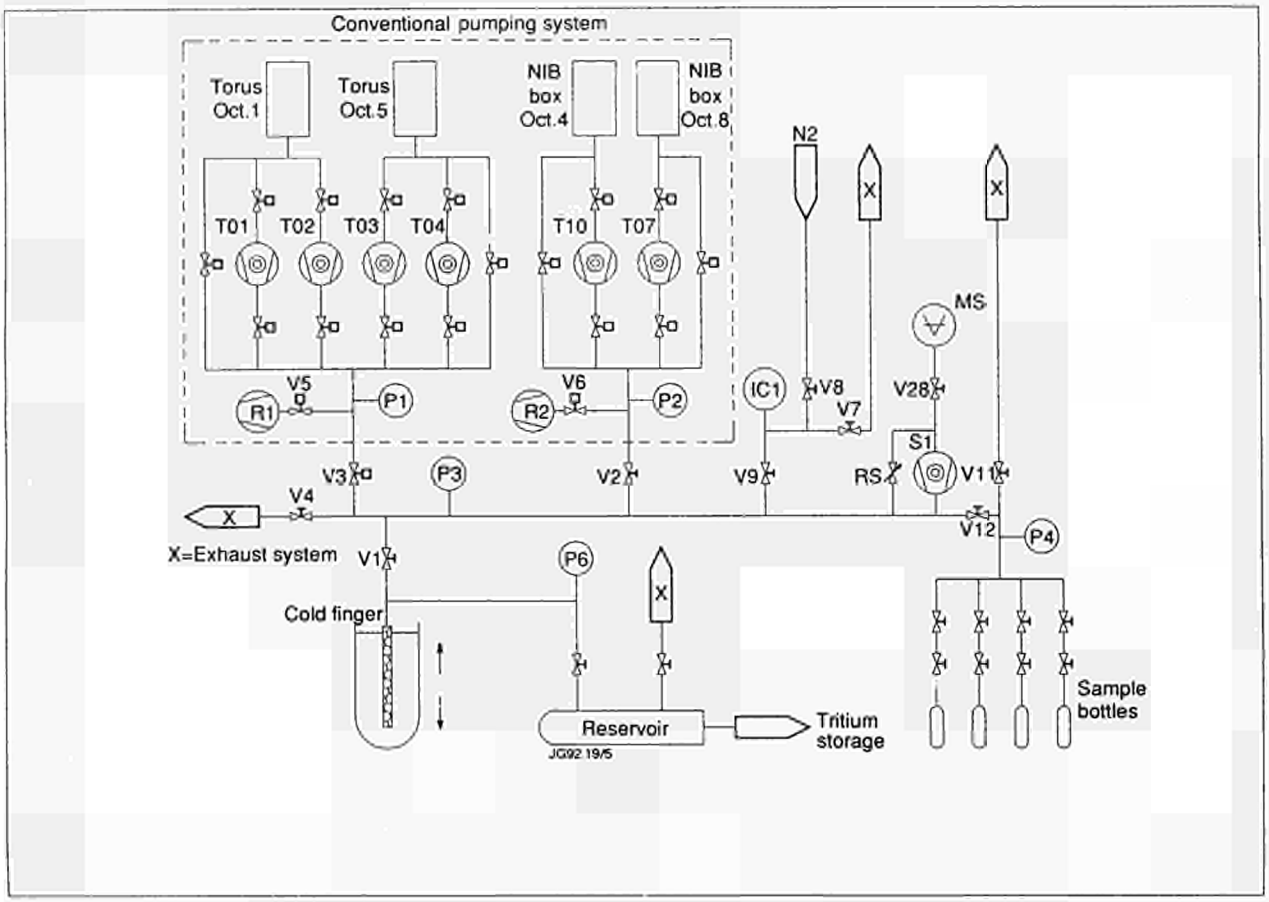

Fig.16: Pumping and measuring system for preliminary tritium experiment (PTE).

Vessel supports

Additional supports for the vacuum vessel were required to counteract forces on the vacuum vessel which occur during disruptions. The present supports were installed in 1987 and were designed to follow thermal expansion of the vessel during baking cycles. The movable links, however, which should allow for thermal decoupling were seizing in some cases during heating and cooling cycles of the vacuum vessel. During the shutdown in September, the clearance between the movable and fixed parts of the supports was increased to avoid this problem.

The consequence of this modification was that now the locking at operating temperatures could not always be achieved reliably. This required an additional mechanical locking by bolts when the operating temperature was reached. Although the present supports fulfil the requirements during the operational periods, access to the torus hall is required, first to unlock and later to lock the supports again when the operational temperature of the vessel is changed.

This situation is not tolerable for the later tritium operation because access to the Torus Hall will no longer be possible. Therefore a detailed analysis of the behaviour of the supports was made, taking into account the operational experience including forces and their direction occurring during disruptions. Based on that analysis, modifications and a partial redesign will be required to achieve reliable operation of the supports. It is expected that this will be carried out during the 1992/1993 shutdown.

Pellet Injection

This section summarises the present JET multi-pellet injector, its operation and work on its upgrading by implementation of a single-pellet two-stage gun for higher pellet speed capability. A more elaborate description of the design of a launcher extending the two-stage gun principle towards multi-pellets, potentially higher velocities and compatibility with the D-T phase will be described later, as well as details of the pellet centrifuge now under procurement.

Collaborative effort under the Pellet Agreement with the United States Department of Energy (USDoE) continued. This relates to work on the three-barrel, repetitive, pneumatic, single-stage gun launcher with pellets of 2.7, 4 and 6 mm sizes and speeds around 1.3 kms^{-1}, constructed by Oak Ridge National Laboratory (ORNL) and mounted on the JET pellet injector box (PIB) interface. The attendance at JET of US personnel was somewhat lower than the four

man-years per year foreseen under the Agreement. Negotiations for a prolongation of the Pellet Agreement have so far not been successful. Experimental work under the Agreement will therefore cease at the end of the current 1991/92 Campaign, though joint evaluation of JET data will continue to the end of 1992. The ORNL Launcher will be decommissioned in 1992 and returned to the US where its implementation on another tokamak experiment is being considered. During the Preliminary Tritium Experiment (PTE), the pellet injector was valved off. However, immediately following the PTE, the injector resumed operation. A careful assessment of the possible amount of exposure of the ORNL launcher to tritium was jointly carried out and showed that, with certain conditions maintained, the level will not impede the re-installation of the launcher on another experiment.

The pellet injector was extensively used in a number of experiments for various purposes of density profile shaping and fuelling. The following highlights may be mentioned:

- The combination of the Pellet Enhanced Performance (PEP) mode (previously also found in JET limiter discharges) with the H-mode by injecting 4 mm pellets into 3 to 4MA X-point discharges [1], was further investigated. The aim was better documentation and more detailed data to reveal the cause of its (transient) plasma performance improvement with respect to energy confinement. In these experiments, the central electron and temperatures were close to each other and were ~ 15 keV predominantly by central ICRF deposition. A record neutron rate from D-D reactions of $1.8 \times 10^{16} s^{-1}$ was found for PEP shots with predominant neutral injection heating at relatively high densities and modest central ion temperature of ~7keV.
- A number of attempts were made to study PEP modes generated by the injection of 6mm pellets into 4MA discharges. Contrary to results in 1990, the density peaked over the full radial plasma profile, rather than just the central core as in the 4 mm pellet case, (see Fig 17). Since the 6 mm pellet particle content was three times higher than that of the 4mm pellet, these discharges were dense, and, therefore, relatively cold. Their density and the density gradients decay on a characteristic timescale of about 1s, as was the case with the earlier 4mm shots. Therefore, even disregarding losses, they will require higher power than the available 10-15MW to heat to high thermo-nuclear performance in the time frame of about 1s, (typically T_i does not exceed 5 keV). A possible improvement in confinement properties of these plasmas is not as evident as in the 4mm cases, and the assessment needs laborious transport calculations. These are now being further evaluated.

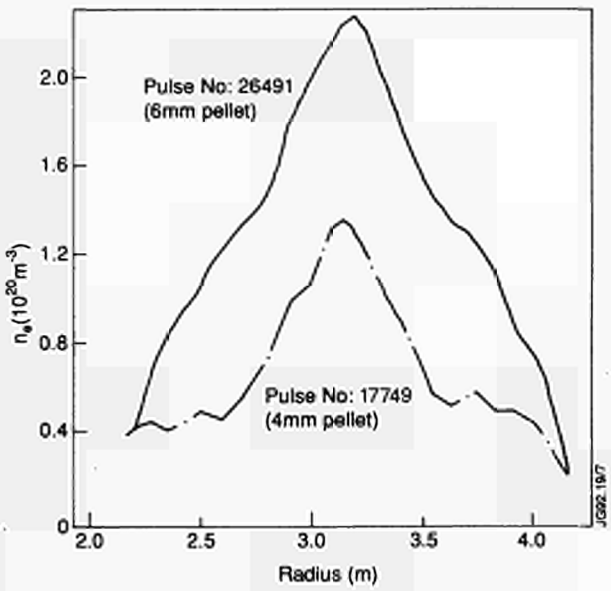

Fig.17: Density peaked over the full radial plasma profile with a 6mm pellet, rather than just the central core as in the 4 mm pellet case

Power Supplies and Magnet Systems

The JET electromagnetic system is made up of toroidal and poloidal coils with their mechanical structure, the purpose of which is to establish, maintain and control the tokamak magnetic configuration (see Fig.18). It includes the toroidal coils, the poloidal coil P1, acting as primary winding of the tokamak transformer and coils P2, P3 and P4, to control plasma radial position, vertical position and shape. To perform these functions, the coils must be energised by suitable DC power supplies, whose voltages and currents are controlled in real-time by the plasma position and current control system (PPCC). Additional DC power supplies energize the neutral beam (NB) injectors, the ion cyclotron radio frequency (ICRF) heating system and the lower hybrid current drive (LHCD) system.

The total installed DC power required by JET exceeds 1500MVA with a delivered power peak above 1000MW and an energy content per pulse up to 10,000MJ. More than half of the power and of the energy is taken directly from the UK National Grid at 400kV and the rest is provided by two vertical shaft flywheel generators.

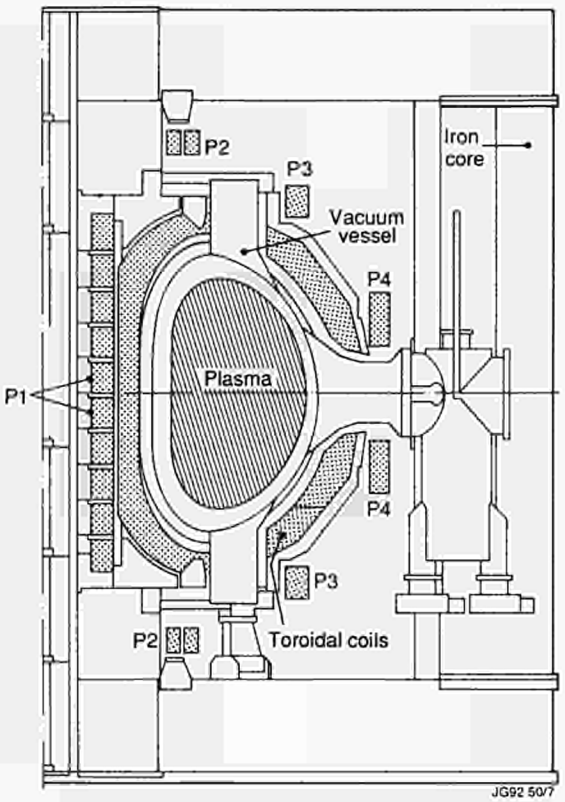

Fig.18: Cross section of JET showing toroidal and poloidal coils

Consequently, a major feature of the JET power supply scheme is the 400kV - 33kV distribution system. Auxiliary power is supplied by the 20MVA, 11kV/3.3kV/415V distribution system.

JET development, an essential part of the scientific programme towards enhanced plasma performance, calls for continuous modifications and upgrading of the electromagnetic system, of the plasma control and of the additional heating power supplies.

The main objectives during 1991 were to complete the development of the tokamak, the additional heating and the lower hybrid system power supplies and to progress further with the large contracts of major components of the multi-coil divertor (i.e. four poloidal coils and the associated power supplies), the fast radial field amplifiers for improving the stabilisation of highly elongated plasmas and the disruption feedback amplifiers for MHD instability control. Extensive analytical and computer studies were also carried out, to assess the feasibility and stability of the required divertor configurations.

The electromagnetic system comprises the toroidal and poloidal coils with their associated mechanical structure and the power supplies to energise the coils.

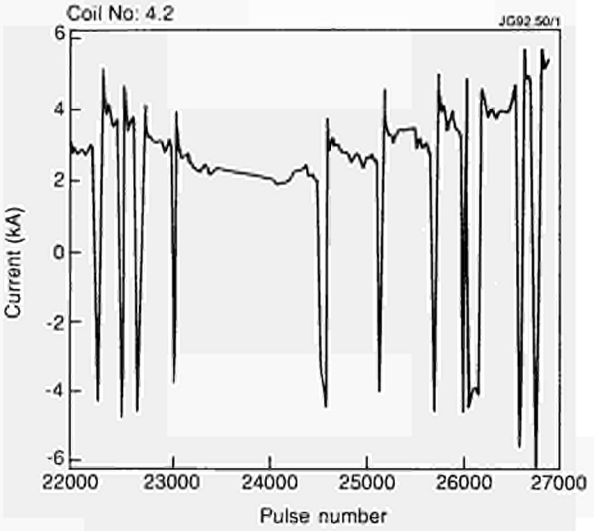

Fig.19: Peak fault current in the TF Coil 4.2 during 1990 and 1991

Magnet System

The magnetic system remained unchanged in its functions during 1991.

Toroidal Coils

An Additional Faulty Coil

During 1990, an interturn fault was detected in TF Coil 4.2. This fault has had no effect on operation and has been monitored since discovery to detect any deterioration. This was carried out by measuring the fault ampere-turns during a standardised TF coil pulse and was made each day. Fig.19 shows the peak fault current throughout 1990 and 1991. The peak fault current increased after each TF polarity reversal but then settled. This behaviour is not understood. The overall trend showed a slight increase towards the end of 1991, due to frequent polarity changes.

No faults were detected in the other TF coils. These have been monitored similarly during operation and also by measurements at the coil terminals during shutdowns. These measurements included:

i) Impedance of each coil as a function of frequency (20 Hz to 50 kHz);
ii) Impedance of each coil turn at selected frequencies (DC, 0.1, 1 and 10 kHz);
iii) Frequency response tests using a spectrum analyser (25 kHz to 2 MHz).

This operation is intended to examine the effect of magnetic field ripple on the plasma confinement. TF Coil 4.2 will be changed during the 1992 shutdown. A spare TF coil is being prepared for insertion into Octant No.4.

Operation with 16 TF Coils

Preparations were made for a toroidal field ripple experiment in which only alternate toroidal coils will be energised. The TF coils are already connected as two alternate sets, an 'odd' set and an 'even' set, so an alternate set can be selected by simply changing busbar links. It was decided to prepare the 'odd' set as the in-vessel field line geometry of these coils gave reduced chance of damaging internal diagnostics.

Use of the 'odd' set means that the faulty coil would not be energised but that fault currents opposing the field changes would be induced in it. These currents give an outward force on the faulty coil. Faulty currents of ~3kA and an outward force of about two tonnes are indicated. Existing instrumentation has been modified to cause a trip if the outward force exceeds an acceptable level of five tonnes.

The shape of the TF coils is optimised so that magnetic forces only cause tensile stresses in the coil (i.e. no bending stresses). This shape is only optimum for 32 coils. When sixteen coils are used, shear stresses due to bending occur. To limit the shear stress to 7MPa, the coil current cannot exceed 60kA (compared with 67kA for 32 coil operation).

Poloidal Coils

Increased Shaping Current to 50kA

The acceptable shaping current in coils P2 and P3 was increased from 40kA to 50kA to allow the application of stronger shaping fields to the plasma. Before the shaping current could be increased, a new stress analysis of these coils was made. The acceptance level for stresses were as follows:

Tensile or compressive stress in Coil P2 (Cu)	100MPa
Tensile of compressive stress in Coil P3 (Cu)	60MPa
Shear stress in insulation	15MPa

The analysis showed that Coil P2 was strong enough for operation at 50kA but that operating restrictions had to be placed on Coil P3. Stresses in coil P3 are a function of the current in Coil P3; the ampere-turns in Coil P4; the temperature rise of Coil P3 and the plasma current, in decreasing order of importance.

Therefore, the currents in the coils had to be adjusted to keep within safe stresses, by setting protection levels depending on the proposed experiment. In addition, the strength of the coil mounted busbars was reviewed and some extra supports were added.

Magnet Power Supplies

The Magnet Power Supplies are divided into two systems; the Toroidal Field Power Supplies for the establishment of the toroidal field (TF) confining the plasma ring, and the Poloidal Field Power Supplies for the establishment and sustainment of the current in the plasma ring and for the control of the position of the plasma ring. The Toroidal Field Power Supplies consist of a flywheel-generator-diode rectifier, rated 67kA DC, 9.0kV no-load voltage, 2600MJ energy and two transformer-thyristor rectifiers supplied from the 33kV distribution.

The Poloidal Field Power Supplies consist of a flywheel-generator-diode rectifier (similar to the toroidal field supplies), a DC switching network and a transformer-thyristor PVFA 5-6, rated 2.8kV DC no-load voltage, 35kA DC. This establishes and sustains current, up to 7MA, in the plasma ring. In addition, the Poloidal Field Power Supplies include the amplifiers to control the position of the plasma ring: PRFA 1-2 + PRFA 3-4 rated ± 5.2kV DC (no-load), ± 3kA DC, for the control of the vertical position, PVFA 3-4 and PVFB, rated 12kV at 1kA, 4.7kV at 6kA, 2.3kV at 25kA for the control of the radial position and PVFA 1, rated 1.4kV DC (no-load), 40kA DC for the control of the plasma shape.

AC Plug Braking for the Flywheel Generators

Two motor operated change-over isolators (11kV, 1250A) for the 8.8MW pony motors were installed in December 1990. The isolators consist of a six pole change-over, operated from a single motor drive. These undertake two functions; change-over the motor supply from 11kV (direct) for motoring, to 5.5kV (reverse) for braking; and isolate the 11/5.5kV step-down transformer when the braking mode is not used.

The switchgear was commissioned successfully with the pony motors and the generators in February 1991. The switchgear was then used extensively for speed cycling the generators prior to re-start of operation. Throughout these cycles and subsequent operation, the equipment performed faultlessly (680 cycles). Inspection of the sacrificial contacts fitted to the poles (required to break the pony motor remanent current during change-over) revealed no undue wear. This new switchgear replaced two sets of three motorised 11kV, 850A on-load switches, which had been in operation since 1985. During this time, there had been a number of mechanical faults (failure of spring guides, failure of pole supporting arm, etc).

PVFA1-2 Conversion to Four Quadrant

As part of a demonstration of AC plasma operation, a four quadrant power supply for the plasma radial position stabilisation was required. Each unit, PVFA1 and PVFA2, consists of two sub-units (rated 1.4kV DC no-load voltage, 20kA DC load current), which can be configured in parallel (reference configuration) or in series. PVFA1 normally supplies current to the shaping field circuit (single unit operation of PVFA 1-2 system).

The conversion of the PVFA 1-2 to four quadrants was completed in January 1991. In this configuration, the rating is ± 2.4kV no-load voltage and 19kA load current, with a circulating current set at 500A.

The configuration was commissioned on an inductive dummy load (9mH, 9mΩ) in local control during February 1991 and in remote control during April 1991. The full swing of the load current is ± 19kA. Measurement of the voltage loop bandwidth (at low current) gave 200Hz at -3dB. With PVFA 1-2 connected as a "vertical field" power supply (coils P4), JET successfully demonstrated AC operation at large plasma current (± 2MA) in July 1991.

PVFA 1-2 Conversion to 50kA

PVFA 1 normally supplies current to the shaping field circuit (single unit operation of PVFA 1-2 system) up to a nominal value of 40kA DC (35kA DC originally). To increase the plasma current in the double-null configuration, while keeping the X-point within the vacuum vessel, required larger shaping field currents. The 1991 experimental programme needed a maximum shaping field current of 50kA DC, which exceeded the capability of a single unit. Furthermore, the voltage capability of a single unit would be insufficient in view of the increased voltage drop due to commutation. Therefore, it was proposed to connect the two units PVFA 1 and PVFA 2 in their reference configuration directly in parallel without additional DC chokes but with active control of the current balance between the two units. The study was started in February and the implementation was completed. The configuration was commissioned on the coils in June up to 50kA DC.

Plasma Control

A.C. Operation

The plasma position and current control system (PPCC) was enhanced to permit operation of JET with reversal of the plasma current during the pulse. For this mode of operation, the PFX amplifier was disconnected from P1 coil and the four quadrant shaping amplifier PVFA1, 2 (anti-parallel configuration) was connected to the P4 vertical field coil. It was possible to produce weakly elongated limiter plasmas at ± 2MA and a short dwell time of typically 0.25s between successive pulses.

Improvement in Control of Disruptions

Despite attempts to improve vertical stabilisation, disruptions frequently led to loss of vertical position and, consequently, to larger vertical plasma displacements (up to about 1m). The associated vertical force acting on the vessel is large at high plasma current and when large shaping currents are applied, such as in single or double-null configurations. The vertical instability produces potentially dangerous forces at in-vessel elements such as protection tiles.

The systems for plasma current and shape control (PPCC and RPSC) have been modified to reduce the PFX current in the P1 coil and the PSFA current flowing through the shaping coils as quickly as possible when a disruption precursor, in the form of a locked helical mode, is detected by the plasma fault protection system (PFPS). In most cases, the delay between the locked mode signal and the disruption (typically, several 100ms) permits a substantial reduction of the PFX/PSFA currents. In turn, the destabilising force at the plasma is greatly reduced at the time of the disruption and the vertical position is much better maintained than without this current reduction. As a result, the vertical force on the vessel could be reduced by a factor x10 in most disruptions.

Improvement of Vertical Stabilisation

The local control circuit of the poloidal radial field amplifier (PRFA) was modified to extend the -3 dB bandwidth of the amplifier from 100 to 300Hz. Consequently, it was possible to stabilise quiescent plasmas with a larger degree of "open loop instability" than previously. In particular, it was possible to increase substantially the gap between the wall and the X-points of magnetic limiter configurations, typically up to about 0.3m.

It has been suspected that the vertical stabilisation could be improved by using, for feedback, the rate of change of the current moment $M = I_p \times Z_p$ with respect to the equatorial plane rather than the rate of change of the poloidal flux difference between locations Z = 1.7m at R = 3m which was applied previously (flux extrapolation from saddle loop locations at the vessel). For this reason, the current moment method was implemented in PPCC and tested up to the

stabilisation limit by ramping up the shaping currents in 2MA plasmas. These tests and subsequent experience indicated that the current moment method does not give a significant increase of the stabilisation range in comparison with that obtained with the flux propagation method. Nevertheless, the new method is now in current use. The conceptual advantage of the current moment method lies in the fact that the method is independent of the plasma shape changes and of externally generated magnetic fields. This feature may be more important for future divertor operation.

The disruption behavior of the modified vertical stabilisation was tested with deliberately generated disruptions of strongly elongated plasmas and with different feedback parameters. These tests showed that both, the increase of the PRFA bandwidth (small amplitude) and the use of the current moment method, did not noticably improve the disruption performance. The stabilisation system usually saturated during the disruption and the vertical position was lost. Particularly vulnerable are up/down asymmetric "single null" plasmas with high current. The detailed mechanism of the destabilisation is not clear at present and will be the subject of further analysis.

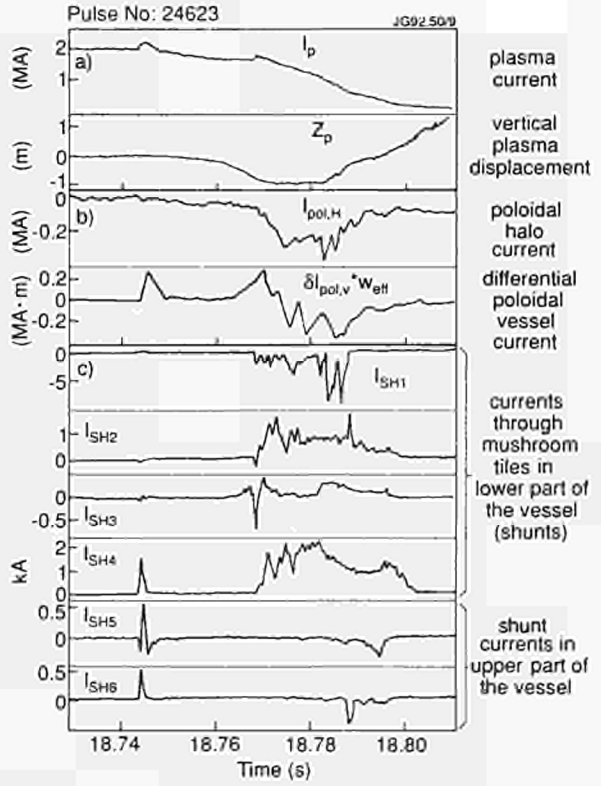

Fig.20: current evolution during a disruption (Pulse No: 24623):
(a) plasma current and vertical displacement;
(b) halo current and poloidal vessel current effective width;
(c) currents through shunt resistors (SH)

X-Point Sweeping

The Study Contract with National Grid on sweeping has been completed. From the technical viewpoint, sweeping could be possible, at 2Hz, up to 20MW peak-to-peak and, at 4Hz, up to 50MW. No torsional oscillations on the turbo-generators of the Didcot Power Station should be induced in these operating conditions. A formal request will be sent to National Grid and to National Power Companies to obtain their approval for sweeping.

Electromagnetic Analysis

2D Code: The 2D direct equilibrium code has been further developed for interactive use with a PC or a work-station. With this code, it is possible to generate, to modify and to display JET equilibria in a very short time. The code has been checked against the PROTEUS code and gives the same equilibria. Ultimately, this tool is intended to be used during plasma operation to establish in a convenient way the desired control parameters such as reference waveforms.

3D Code: A 3D static magnetic code has been written and adapted for practical use in JET, to examine, for example, the non-axisymmetric fields caused by the iron magnetic circuit or by the TF coils. The code has been written with the objective that it should be expandable for dynamic analysis, in particular to assess the eddy currents in the mechanical shell and their effect on the vertical stabilisation of the pumped divertor plasma.

Evidence of Halo Currents

Large amplitude vertical displacements, as often occur in disruptions, produce currents outside the confined plasma region. These "halo" currents flow along lines of force through plasma facing elements to and from the vessel. In JET, these have previously been deduced from differential measurements of the toroidal magnetic field at the top and bottom inside the vessel and from the top/bottom poloidal voltage difference along 2m long vessel segments. These currents can reach up to about 20% of the plasma current. These limit the vertical plasma displacement and, therefore, to some extent, the maximum force acting on the vessel during a vertical instability. However, these currents are of concern for the plasma facing elements due to the magnetic forces caused by the currents passing through them.

In 1991, direct measurements of halo currents were implemented by means of shunts inside six supports and toroidal locations. An example of the evolution of currents during the disruption of a 2MA double-null plasma is shown

in Fig.20. The analysis shows that the magnitude of the locally measured currents is consistent with the global halo current measurements when one takes into account the projected area of the tiles seen along the lines of force. Furthermore, these measurements indicate that there are significant and erratic differences between currents at the same poloidal position but different toroidal position. This indicates that the current flow at in-vessel elements can be temporarily larger than expected from a toroidally uniform current distribution.

Additional Heating Power Supplies

Radio Frequency (ICRF) Power Supplies

During the year, several modifications were carried out to these power supplies. The most important changes were the increase of the reapplication time; suppression of precharging before the pulse and during reapplications; and the implementation of a more sophisticated timer circuit.

During operation, it was found that the design value of 5ms for the reapplication time was too short. If the high frequency power was re-applied after 5ms, the arc would strike again. To remedy this, the reapplication time was increased to 20ms while the high frequency power was not re-applied as a step but as a ramp. Following increase of the re-application time to 20ms, the filtering inductor could not be precharged any more as the power supply for the precharging was not strong enough. However, since the high frequency power and hence the DC load current was re-applied as a ramp, the thyristor regulator was fast enough to keep the voltage within its limits.

Another important change was the implementation of a more "intelligent" pulse - pause timer circuit. Originally, the pause time was independent of the pulse time. This was changed to a one-to-thirty pause timer. These modifications were first tested during the shutdown with the RF generators connected to a dummy load.

Lower Hybrid (LHCD) Power Supplies

Two power supplies have been operated with their klystrons on the machine. As a result, some minor changes were made to the power supplies to improve their response. The remaining four power supplies were tested on dummy load and all, except one, have been operated with the klystrons as loads. The klystrons were connected to their dummy loads during these tests.

All protecting crowbars for the klystrons have been tested to full voltage. During the year, the klystrons were operated on the machine for pulses up to two minutes duration. However, the power supplies were only designed for pulses up to a maximum of 20s. To implement this, a complete reevaluation of the components of the power supplies was carried out. The resulting curve, giving the maximum allowed current versus time, was programmed in the system (see Fig.21). The system was fully tested and used for pulse durations of up to two minutes. This feature has now been implemented in all the other power supplies and is an integral part of their operation.

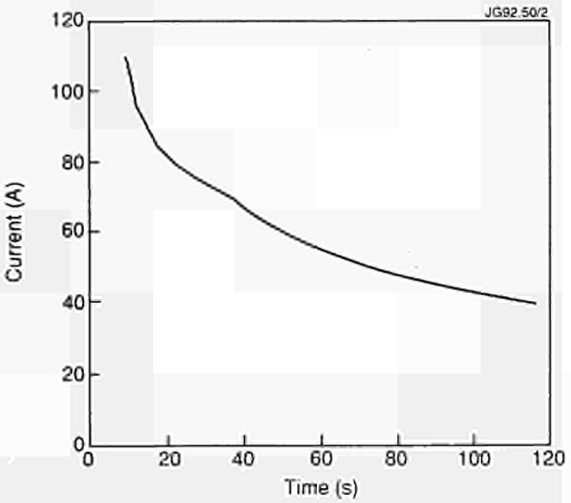

Fig.21: Maximum allowed DC power supply current versus time for four klystrons

Neutral Beam Power Supplies

During the 1991 shutdown, the Octant No.8 power supplies were converted for operation at 140kV. In addition, changes were undertaken to improve reliability further. At the end of the shutdown, all NB power supplies were tested ready for operation at 140kV.

Two of the injectors were chosen as the tritium fuelling source for the Preliminary Tritium Experiment (PTE), one protection system, module No.4, was re-converted back to 85kV in September. A second protection system, module No.5, was also re-converted back to 85kV for operation with two high current injectors. These reconversions were fully tested on dummy load and then used with the injectors as load. For the successful PTE, all the NB power supplies had to perform correctly for the two shots in synchronous operation. As a preliminary test, the two tritium injectors were tested in two asynchronous shots. On the first one, one of the power supplies failed. The fault was repaired with minimum delay. For the two synchronous tritium shots, all power supplies performed correctly.

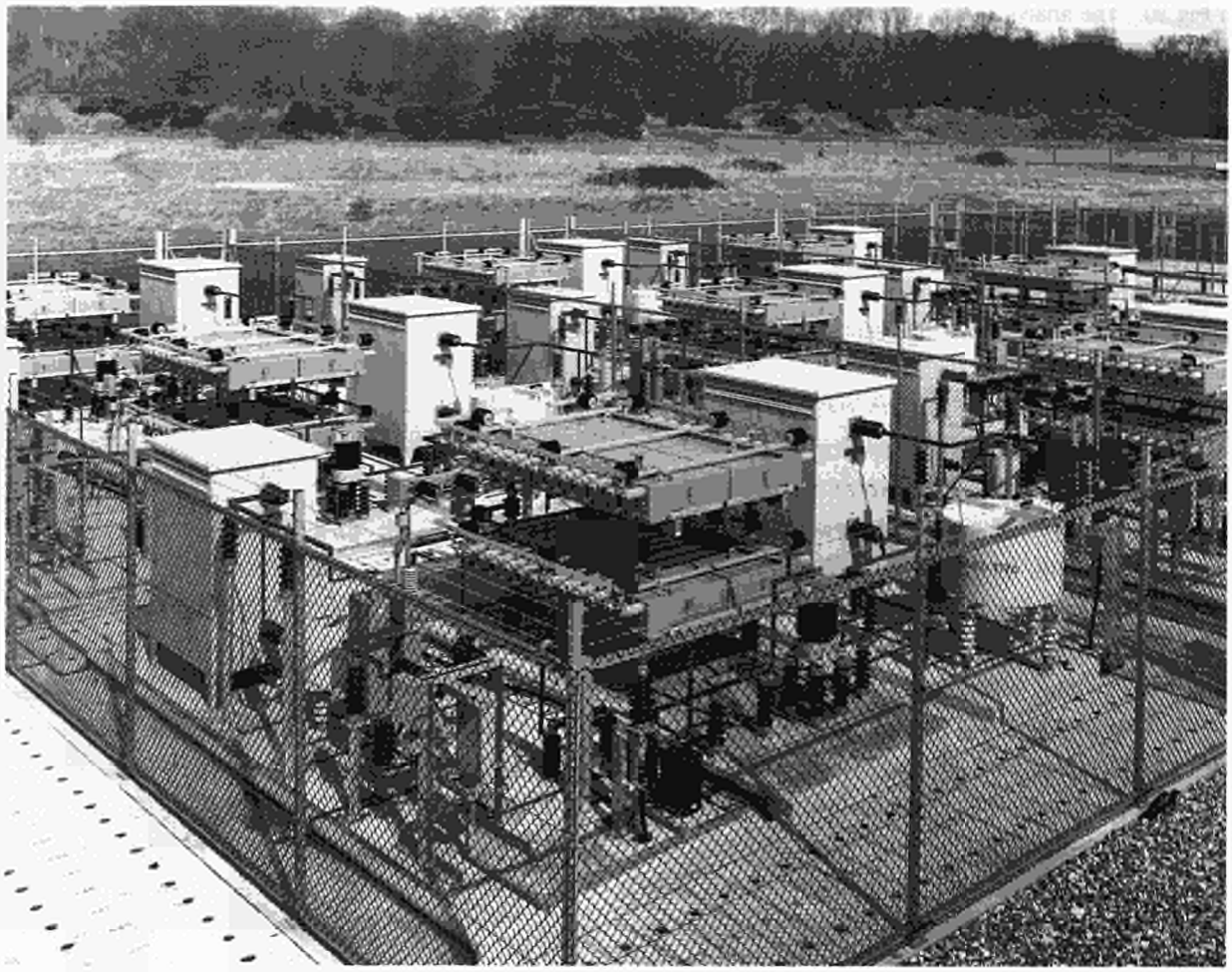

Fig.22: The outdoor area of the Reactive Power Compensation System showing the three 50MVAr Units installed initially

Neutral Beam Testbed Power Supplies

During 1991, the power supplies in the NB Testbed were operated on a routine basis. Due to the heavy load on the Testbed, only repairs due to power faults were carried out; it was not possible to perform any preventive maintenance except the bare minimum routine maintenance. This resulted in the Testbed being off-line only for emergency repairs and calibration at times not planned.

The JET Power Distribution System

The 33kV Distribution System

New 33kV feeders were installed and commissioned for the Disruption Feedback Amplifier System (including the 33kV splitter cubicle), for the Gyrotron of the alpha-particle diagnostic (supplied by a 33kV/600V, 2MA transformer) and for the bi-directional 33kV - 11kV, 30MA transformer.

The 30MVA bi-directional transformer will be available to supply additional Heating Test-beds and other loads for commissioning purposes, when either these 400kV or the 132kV, HV transmission lines will be under maintenance.

Service, Construction and Installation Work

These activities cover a variety of jobs throughout the project, which included:

(a) Detailed design of civil work and cable/busbars routing for Fast Radial Field Amplifier (FRFA) and for Divertor Power Supplies;

(b) Design and installation work for the Active Gas Handling (AGHS), and for the Preliminary Tritium Experiment system including traywork, trunking and cabling for instrumentation;

(c) Cable installation for CODAS, Diagnostics, First Wall, Radio Frequency Heating and Machine Services;

(d) Extension of the 415V distribution throughout site.

Reactive Power Compensation

The completion tests were concluded by mid-November 1990, and acceptance tests were performed after the 1991

shutdown. A standard pulse was used: the TF coils were supplied with 60kA by the generator and by the two static units; during the current flat-top, the delay angle of the static units was moved from near zero to 60 degrees for a few seconds, to take maximum reactive power from the 400kV Grid. A view of the outdoor area of the system is shown in Fig.22.

The feedback control with hysteresis, proposed by JET, worked correctly and allowed switching on and off of the compensation units, respectively, at two different preset values of the voltage drop with reference to the busbar voltage measured at a predetermined time before the pulse. The behaviour of the system, with two compensation units connected to the same busbar, was tested. Again, the two units were switched on and off when the different preset values of the voltage drop were reached; the busbar voltage waveform is shown in Fig.23. The pulse was repeated and the results were reproducible. The asyncronous operation of a vacuum switch was reproduced: the measured voltage waveform was compared with the simulated one and found to be very similar. The snubber circuit allowed the suppression of high frequency (4-5KHz) harmonics, present on the busbar voltage, during the standard pulse flat-top. The total harmonic distortion (THD) of the busbar voltage decreased from 5.6% to 4.8%; the compensation units were then added to the standard pulse and the THD dropped further to 2.5%; the distortion of the 400kV voltage, at the point of supply, remained basically unchanged between 0.4 - 0.8% and it was only marginally affected by the JET pulse. The experience gained supports the choice of the vacuum switch, as the active element of the system.

Electricity Supply

Since the privatisation of the Electricity Supply Industry in the UK, the supply of electricity to JET relies on three Contracts:

(a) The Contract with Southern Electric (first signed in 1990 and renewed annually) provides up to 20MA of continuous AC power at 11kV, for the auxilliary loads. JET required ~4x107 units in 1991, 27% more than in 1990, at a total cost of 1.95MECU. The global cost for units would be reduced (by 10%), if the rates charged by SEB (the State owned company and JET's previous supplier) were applied. There is a trend (1989 - 1991) indicating a steady increase of electric power required by JET due to the extension of the auxiliary network for the loads;

(b) The Contract with National Grid signed in 1991 covers the usage of the 400kV Grid for JET DC pulsed loads. Each new operating scenario must be assessed by National Grid, to make sure the contractual limits are not exceeded, effecting both the National Power Contractors. An example is the study performed to define the parameters for the X-point sweeping in the new divertor magnetic configuration;

(c) The Contract with National Power, covers the supply of electricity through the 400kV Grid. This Contract is still proceeding by means of a Letter of Intent, since there is still an important clause under negotiation.

Maintenance, Operation and Other Studies

Maintenance and operation of the Power Supplies was a major activity during the year, since the machine is either used for experiments or it is out of service for maintenance or modifications. As more and more power supplies are still being installed the operation and the maintenance of the power supplies will become even more important in the future.

Maintenance

To help in the maintenance of the different Power Supplies an electronic maintenance team, an electrical maintenance team (MEC) and a mechanical maintenance team (GEC) form part of the Division. In addition to undertaking maintenance, these teams are also involved in operation and undertake installations during operational periods. The

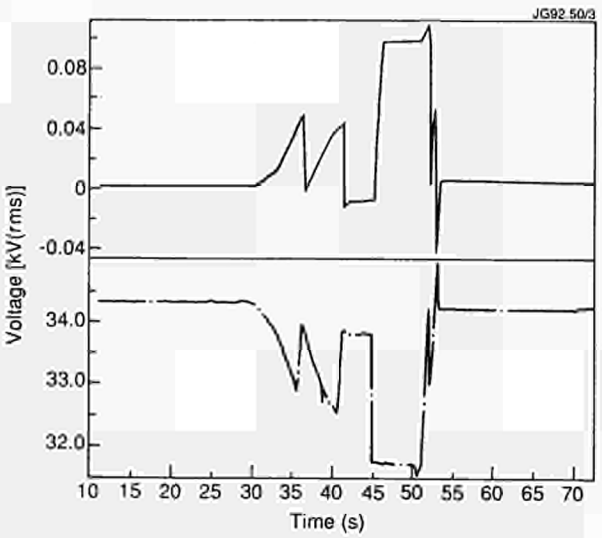

Fig.23: Waveform of the busbar voltage (rms value) during a pulse with two compensation units

electronic maintenance team is also responsible for fault finding and repair of the electronic cards which are used in the different power supplies. During maintenance days and in shutdown periods, the mechanical components of the machine and of the coils are systematically checked, especially the poloidal and the toroidal busbar connections. A bad contact in the connections on one of these busbars could cause severe damage due to he high current.

The high voltage DC rectifiers installed outdoors require regular maintenance especially during winter, when dirt in the air combined with the ever present humidity can cause problems on isolators. Regular cleaning of these insulators, mainly on the 60kV Lower Hybrid power supply system, is carried out to prevent arcing.

Operational downtime in the poloidal and toroidal power supplies was reduced due to improved rectification of faults as these occurred and a reduction in the overall number of faults. There were no significant problems with the flywheel generators during the year and the machines continued to run without vibration problems and improved conditions with respect to oil loss from the main bearings. A new test facility was installed in the pneumatic workshop to allow off-line testing of these switches and it is expected that this will bring a further reduction in downtime caused by switch failure. Operational failures in the thyristor amplifier areas have been confined mainly to fuse failure or equipment temperature problems in hot weather both of which are associated with component ageing. These problems are being overcome by an ongoing programme of component replacement.

Neutral Beam Heating System

The major focus of the work carried out on the Neutral Beam (NB) heating system during 1991 was related to the Preliminary Tritium Experiment (PTE) for which neutral beam injection was used, not only to heat the plasma using fourteen beams of deuterium, but also to inject the tritium fuel using two tritium beams. Details of this successful experiment are described in the section on the Preliminary Tritium Experiment. This was also the first occasion that multi-ampere energetic tritium beams had been produced at the megawatt power level and was a considerable technical achievement. Further, it demonstrated the importance and flexibility of the JET NB system, which had already been used to inject multi-megawatt beams of H, D, ^{3}He and ^{4}He.

Due to the requirement to maximise the tritium fuelling of the plasma, two of the JET Positive Ion Injectors (PINIs) (consisting of a plasma generator and ion accelerator) were used in their four-grid 80kV configuration. At this beam energy, the maximum conversion efficiency of the primary tritium ion beam to energetic neutral atoms was ~72%.

Production of Tritium Neutral Beams

Overview

The proposal to use PINIs for tritium injection during the PTE was investigated in early 1991. Preliminary studies showed that this approach to the introduction of tritium offered certain advantages over gas puffing:

i) the tritium fuel would have a known deposition profile which, dependent only on the plasma density, could be peaked in the plasma centre;
ii) the total amount of tritium introduced into the torus would be minimised;
iii) development, testing, installation and commissioning would have minimal impact upon tokamak operation.

The required PINI and associated development was carried out on the NB Testbed. Manufacture of the necessary apparatus and upgrading of the beamline was performed by the NB Engineering Group and necessary control and interlock systems were designed, built and commissioned by the NB Operations Group. The newly formed NB Cryo Group developed *"fast"* regeneration scenarios for the regeneration of the injector cryo-pumps when loaded with a D-T mixture.

Further details are covered in the section on Technical Aspects of the Preliminary Tritium Experiment (PTE).

General Activities

In addition to the successful contribution to the preliminary tritium experiment (PTE), significant progress has been achieved in other activities which are summarised:

Testbed

No further experimental work has been carried out to enhance the performance of the hypervapotron high heat flux elements described in the 1990 Progress Report. However, a theoretical finite element model has been developed, which incorporates turbulent and nucleate boiling heat transfer. As shown in Fig.24, good agreement is obtained with the measured surface temperature of the hypervapotron as a function of incident thermal flux. The only fitted parameter is a 33% increase in the turbulent heat transfer of

a smooth walled pipe, having the same hydraulic diameter as the gap between the *"teeth"* of the vapotron structure with a coolant velocity in this region equal to that of the main flow. This work shows that, contrary to original explanations of the hypervapotron cooling principle, the heat transfer improves with coolant flow velocity and the heat removal by turbulent flow in the grooves between fins, is more dominant than the ejection of steam from this region.

Experimental developments on water-cooled high heat transfer elements have been devoted to further tests on swirl tubes for NET. In addition, tests for ENEA have been undertaken, using the cooled panels envisaged for a proposed *"drive-in"* target neutron source.

Tests of the power handling capability of the inertial beryllium tiles, to be used for the JET Mk I Pumped Divertor, have resulted in the optimization of the castellations necessary to prevent cracking resulting from excessive thermal stresses. It has been demonstrated that with 6mm castellations, the tiles can withstand > 20MWm^{-2} peak power density for a 3s modulated beam (100ms - on, 150ms - off). This simulates the sweeping of the X-point of the pumped divertor.

In addition to the work on isotope exchange for the PTE, considerable experimental time has been devoted to studies of implantation and isotope exchange of energetic beam implanted species in the testbed beam calorimeter. The results appear to be inconsistent with existing theories and modelling work is in progress in an attempted to identify the physical processes involved.

Engineering Activities

Work planned for the shutdown in the early part of 1991 was completed satisfactorily. Major activities including the installation of one set of improved full energy ion dumps, box scrapers and remote PINI steering mechanisms. These have been in operation and demonstrated the expected improvement in performance. The second set of these components will be installed in the 1992/93 shutdown, together with the Mark II duct scraper and protection assemblies, which have been delivered.

The various manufacturing contracts for major components for the pumped divertor, cryo-pump and its water cooled entrance baffle and the high heat flux elements for the Mark II target plates, have been placed and are underway.

Operations Activities

The flexibility and versatility of both injection systems, used throughout the 1991 experimental programme, have been

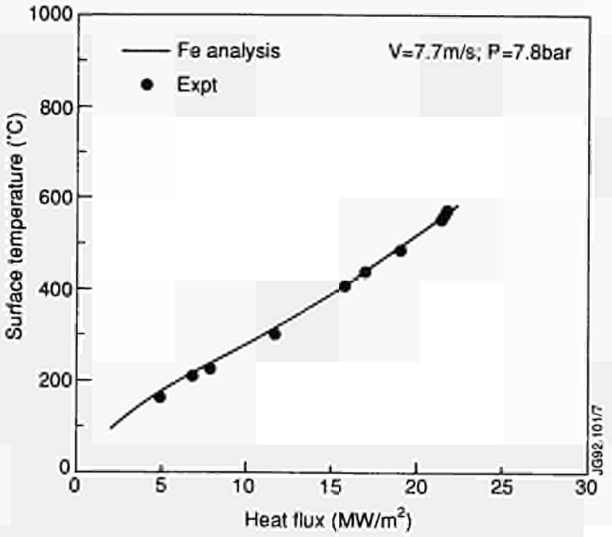

Fig.24: Comparison between calculated and measured performance of hypervapotron high heat flux element.

significantly extended in a number of ways. This can be illustrated by dividing the operation during 1991 into the following phases which covered differing requirements of the JET experimental programme.

Phase I

The complete sixteen PINI system was commissioned and operated up to 140kV in deuterium. Reliable operation was obtained at full voltage and up to 15MW power was routinely injected into the plasma (i.e. 7.5MW per injector). This phase covered operations during May-July 1991.

Phase II

Both injectors were converted to operation with ^{3}He beams. For the Octant No.4 injector, this involved re-establishing the operation achieved in 1990 and was extended to higher extraction voltage (125kV was the limit for the 1990 operations). For the Octant No.8 injector, ^{3}He operation was commissioned for the first time and successfully operated up to 145kV extraction voltage. Routine operation was established on both injectors and extensive characterisation of the beamline operation was carried out. At the end of this phase (which will be returned to early in 1992), injected powers of up to 13.5MW at extraction voltages of 135-145kV were achieved. This phase covered operations in July and August 1991.

Phase III

In this phase, the injectors were first converted back to deuterium operation and the components loaded with ^{3}He were degassed using D° beams. This phase covered opera-

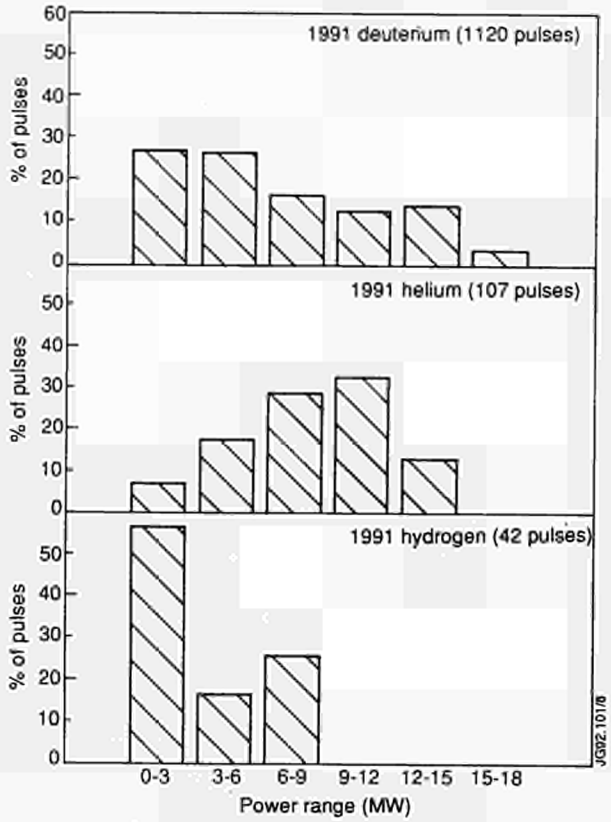

Fig.25: Distribution of injected power for the various beam species used throughout 1991.

tions in late-August 1991 and much new information was obtained which is detailed below.

Phase IV

The injector at Octant No.8 was converted to the configuration required by the Preliminary Tritium Experiment (PTE). This is described later in this report. After the tritium phase, operations were resumed in the deuterium configuration of Phase IV for November until December.

Phase V

During this phase (mid-December 1991), the injectors were successfully and quickly converted to hydrogen operation. The system was operated with 12 PINIs at 120kV extraction voltage and the four grid PINIs at 70-75kV. The maximum power injected in this configuration was 8.2MW with the highest total energy being 6.7MW for 4.5s. The comparatively modest power reflects the low conversion efficiency of positive ions to neutral atoms at high values of keV per nucleon.

An overview of the power distribution for injected pulses in D°, ^{3}He° and H° operation is shown in Fig.25. Due to the high reliability maintained throughout 1991, the distribution of power reflects the demands of the experimenal programme and not a shortfall in performance.

Operation of the Injectors in ^{3}He

During helium injector operation, the beamline pressure is minimised by the use of a layer of argon 'frost' introduced onto the LHe cooled cryo-panel surfaces. The technique was developed [1] on the Octant No. 4 injector during 1990. Considerable effort was invested in the optimization of this technique during the 1991 operation. The cryo-sorption of helium on argon frost maintained sufficiently low pressures over a limited but useful range of helium gas flows.

The neutral power transmission to the torus was determined from water calorimetric measurements using the beamline calorimeter to intercept the beam. The downstream losses during injection into the tokamak (when the calorimeter is moved out of the beam) were estimated to be ~ 20% of that previously measured on the calorimeter. This estimate was validated from data using the scraper and duct liner thermocouples over a number of shots. The PINIs were operated with a relatively low gas flow to reduce the gas load on the cryopumps and the re-ionised power in the duct. No separate neutraliser gas-feed was used, and a ^{3}He flow of 24mbℓs^{-1} was provided to the PINI only which yielded a neutral target thickness of 60% of the maximum target. Even with this reduced gas flow, the neutral power from one injector is still 6.7MW at 150keV energy.

The maximum energy for beam operation in ^{3}He is limited by the 30A current limit from the HV power supplies. At 30A, the perveance matched voltage for ^{3}He is 155kV. Compared to deuterium, operation of the PINIs in helium proved to be generally more difficult. The progress in improving voltage hold-off during source conditioning was also slower in helium. In helium operation, it was more critical to adjust the relative rise times of the HV and extracted current (via the PINI arc notching circuit) to avoid repetitive breakdown from overshoots in the extracted current. However, reliable operation was achieved on all PINIs at at *least* 140kV. This is a considerable improvement over the 125kV limit reached in 1990. In addition, several of the best conditioned PINIs were successfully operated up to the 155kV limit.

This system was successful in achieving full long pulse high power He^3 injection. Up to 13MW of ^{3}He° was injected into JET, with minimal neutron production and consequential activation of the torus.

Reversion to Operation with Deuterium.

When returning to deuterium operation, the helium particles implanted into the copper dumps and scrapers were released by the impinging beam. Argon frosting was not used in D_2 operation and the pumping speed of the injector turbomolecular pump was insufficient to maintain the pressure of the desorbed He^3 below the limit required for injection into the tokamak which is determined by re-ionization in the input duct to the torus. Therefore a series of pulses dedicated to removal of implanted He^3 was developed to minimise the time required to change from ^3He to D_2 injection.

Cryogenics Activities

The increased importance of the role of cryogenics in the experimental programme resulted in the creation of a Cryo Group. The responsibilities of this group include the following ares:

- maintaining continuous operation of the cryo-plant;
- supplying all cryogens to the JET site;
- execution of planned upgrades to the liquid helium (LHe) and liquid nitrogen (LN) systems and integration into existing plant;
- enhancement of cryo-distribution system;
- cryogenic engineering of LHCD and pumped divertor cryo-pumps;
- technical support/maintenance of large NB and PI cryo-pumps.

The planned upgrades of the liquid helium and liquid nitrogen systems are necessary not only to supply the new users (Active Gas Handling, LHCD and Pumped Divertor cryo-pumps, etc.) but also the increased demands imposed by D-T (and ^3He) operation which require the NB cryo-pumps to be regenerated on a daily (as opposed to weekly) basis.

Throughout the year, reliable operation of the cryo-plant was maintained and part of the new liquid Helium distribution system was brought into operation. Preparatory work for the major additions and extensions to the cryo-plant to be implemented during the 1992/93 shutdown was well under-way.

References

[1] P Massmann, A J Bickley, J F Davies, G.H Deschamps, H P L de Esch, H D Falter, R S Hemsworth and T T C Jones. Proc 16th Symp. on Fusion Technology (SOFT), (1990), p463.

ICRF Heating and Lower Hybrid Current Drive Systems

The purpose of the large Ion Cyclotron Resonance Frequency (ICRF) heating and Lower Hybrid (LH) current drive systems are quite different :

- The ICRF heating system is for high power localised heating of the JET plasma and has been used since 1985. The system is also used for current drive studies which are in their initial stage. The corresponding localisation depends mainly on the value of the magnetic field and is insensitive to parameters such as density and temperature. The wide frequency band (23 to 57MHz) allows variation in the position of heating of the ion species which is resonant with the wave : hydrogen, deuterium or helium. The maximum design power is 24MW in the plasma, of which 22MW haas been coupled so far [1];
- The LHCD (Lower Hybrid Current Drive) system (12MW at 3.7 GHz) can drive a significant fraction of the plasma current by direct acceleration of the plasma electrons. It can be used to stabilize sawtooth oscillations, thereby increasing the central electron temperature. This is the main tool for controlling the plasma current profile. A prototype system consisting of two launching units (LOP built by JET, and LOC build by CEA Cadarache, France) fed by a total klystron power of 4MW was installed in 1990. Initial physics experiments have shown that up to 1.5MA of non-inductive plasma current have been produced in combination with ICRF heating (these results will be discussed in a later part of the report). Up to 2.5MW have been coupled to the plasma, corresponding to 3MW klystron power;

Both radio-frequency (RF) systems have been instrumental in achieving long pulse plasma operation of up to one minute flat-top duration, by providing a high temperature, low resistivity plasma to limit resistive flux consumption from the Ohmic transformer and in part by direct current drive. A one minute long pulse has been achieved at I_p = 2MA, B_T = 1.9T, with 50s LH pulse at 1MW (only six klystrons out of eight were operated due to power supply limitations) and three successive 20s 3 MW pulses of ICRF at 28 MHz H minority, using two generators in monopole phasing at each step. The combined application of two RF systems provided 230MJ of energy out of a total of 280MJ in the plasma , which included the Ohmic contribution, and

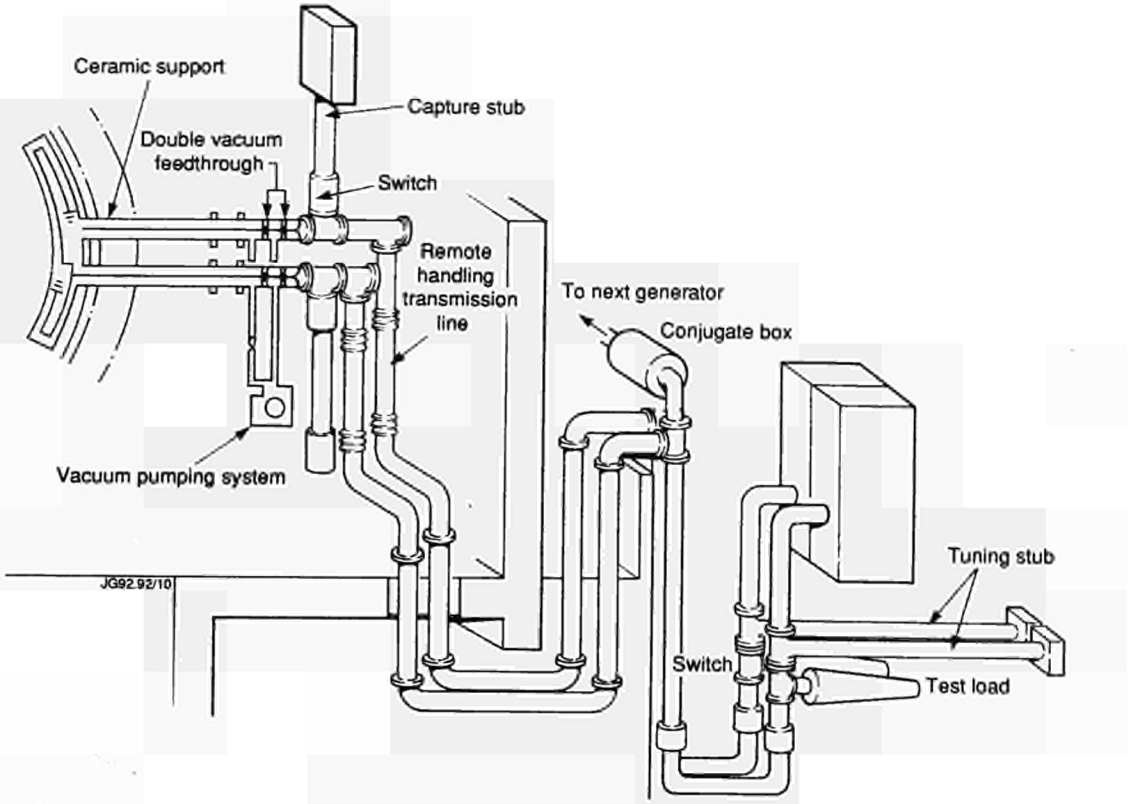

Fig.26: Diagram of the ICRF System;

reduced by about 40 % the flux consumption. Both the ICRF coupling resistance and the LH reflected power were maintained approximately constant throughout the pulse, indicating steady coupling conditions with no impurity influxes associated with antenna and launcher operation [2].

Technical Achievements with ICRF System

The upgraded ICRF heating system consists of eight tandem amplifier-antenna systems. Table III summaries the main characteristics of the RF system used in 1991. The system has been significantly modified since its initial operation. a diagram of its main components is shown in Fig 26.

The upgrade of each of the eight generators from 3 to 4MW was completed and 32 MW 20s pulses were delivered in a steady matched (VSWR 1:1.5) test load. A maximum power of 22MW for 1.75 s was launched into the plasma (within 5% of the theoretical limit), after taking losses and reflection in the system into account.

During long pulse operation, up to 30MJ per antenna have been launched into the plasma without indication of impurity release specific to ICRH edge effects. A side view of Octant No. 3 antenna after long pulse operation as seen from a CCD camera routinely observed in the Control Room, is shown in Fig 27. The heating of the screen has remained below the lowest detectable level.

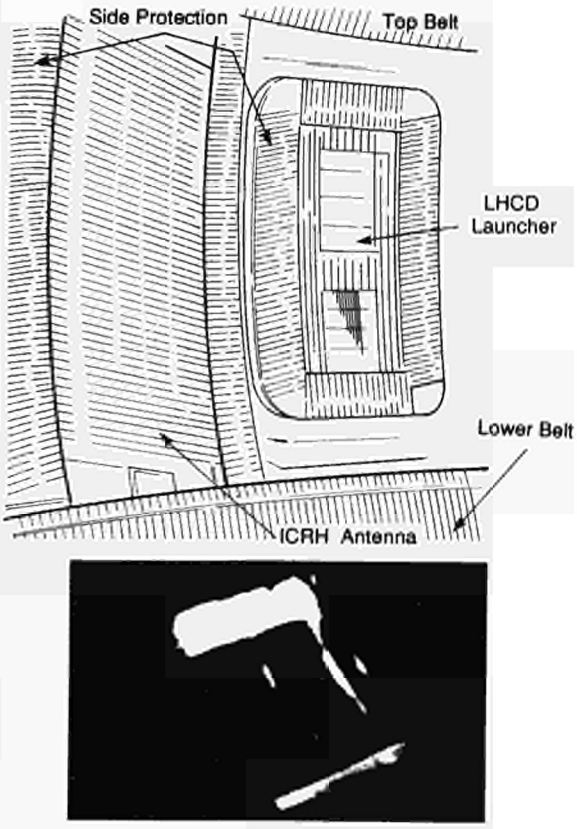

Fig.27: View of one ICRF antenna seen in the control room from a CCD camera at t=44.1s during a one minute long pulse. The light emitting parts are the upper and lower belt limiters and side protections of ICRF antenna and of LHCD launcher.

Table III
Nominal Characteristics of the ICRF Plant

Frequency Range	23 to 57 MHz
8 Generators	4 MW output per generator module (20s)
8 Antennae	• Beryllium bars (15°inclination) • Two adjacent loops operated with either Monopole phasing (0,0) or dipole phasing (0,π), or a phased array (0-π) • Getter pumps on vacuum transmission lines
16 Transmission lines (Generator to antenna)	Each line 84 m long rated at 50kV peak (ϕ ~ 230mm, 30Ω)
Feedback loops for	• Plasma position for constant coupling resistance • RF power level or antennae RF current • Phase between the antennae • Frequency (Δf ~ 1 MHz) for matching • Motorised tuning stub for matching • Tetrode screen dissipation (acting on anode voltage)

This performance was achieved in the limiter configuration. The evolution of experiments has entailed the use of different plasma configurations such as double and single-null X-points with possibly a large distance between the last closed magnetic surface and the antenna. In addition, the antenna impedance does not present a constant load, resulting in stringent conditions for delivering the heating power.

Control and protection circuitry has been developed to handle naturally occurring transient antenna breakdowns, incoherent energy cross-coupling between antennas and rapidly varying plasma loads during L to H-mode transitions, and monster sawtooth crash [3]. Fig 28 shows a schematic diagram of the control and matching system for each ICRF amplifier (there are 16 in the JET ICRH plant).

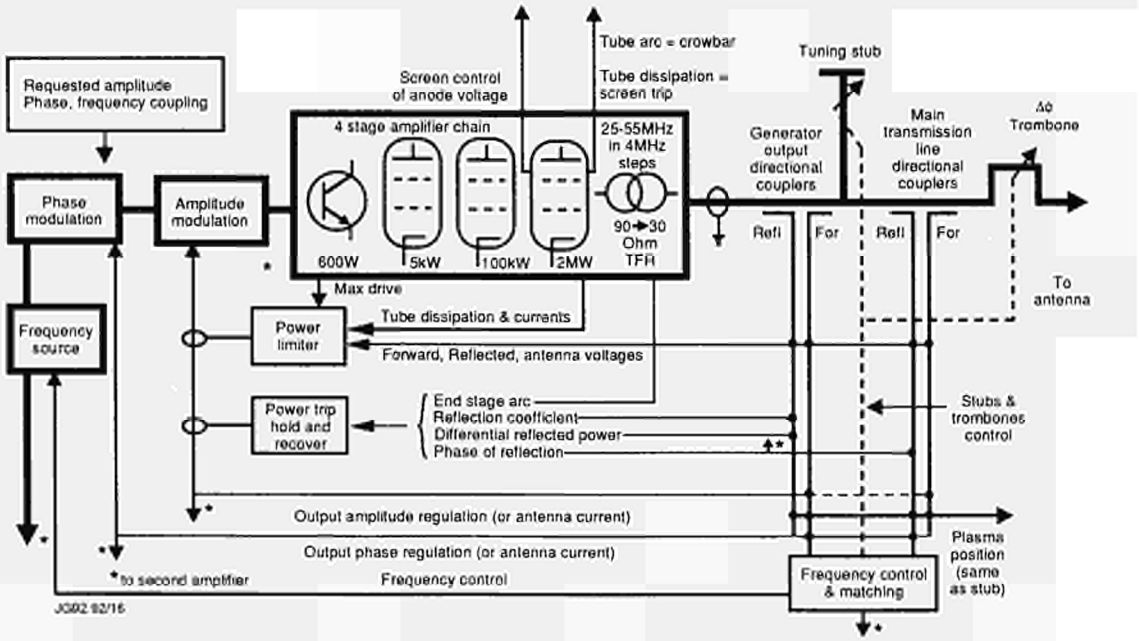

Fig.28: Schematic diagram of the control and matching system for each ICRF amplifier.

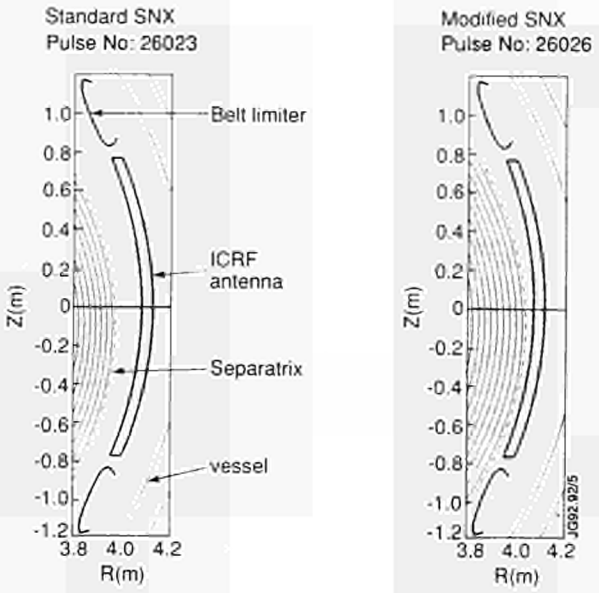

Fig.29: Standard single-null X-point configuration for hot-ion mode studies with NBI only compared with modified single null X-point configuration for combined NBI and ICRF operation.

An amplitude and phase modulated frequency source drives the 2MW amplifier chain. The output is connected via matching circuits to a coaxial transmission line feeding the antenna. Signals from the RF directional couplers on the transmission line provide most of the system monitoring and control. The object is to sustain the RF power as close as possible to the requested level during a pulse, irrespective of the variations and transients in plasma loading of the antenna. The phase of the directional coupler signal is used to obtain a match between the generator and antenna by varying the tuning stub and frequency or electrical length of the line. The plasma position can also be varied by a feedback loop to hold the antenna coupling resistance at the requested value.

If any of the transmission line or tetrode parameters are exceeded, the power output is limited automatically to that value. Arcs in the antenna or generator cause a RF power trip for ~20 ms before reapplication. If the number of trips exceeds a preset maximum value or if an arc in the tetrode causes a crowbar to fire, the RF pulse is terminated prematurely.

This improved control system has permitted the ICRF plant to operate with some of the plasma configurations (in particular tilted single null plasmas), frequently used with high power Neutral Beam Injection (NBI), which were not suitable until recently for ICRF heating. The reason was the large separation between plasma and ICRF antennae, which, together with the poloidal assymetry of the plasma-antenna distance, implied low loading resistance. During 1991, a significant amount of ICRF power was coupled in these configurations. In particular, 8MW of ICRF power was coupled to the single-null X-point (SNX) configuration. The last closed flux surface of a standard SNX plasma was at least 15 cm from the antennae at the vessel midplane with additional large poloidal asymmetries of the flux surfaces as shown in Fig.29. A slightly modified configuration was used in conjunction with the coupling resistance-radial plasma position feedback to give a coupling resistance in the 3Ω range at a typical plasma-antenna distance of 4cm. The poloidal asymmetry of the plasma-antenna distance was also reduced. At this power input, H-modes were readily obtained.

Control of ICRF plant in High Performance Discharges

The hot-ion mode discharge provides good central confinement in addition to H-mode enhancement. Due to centrally peaked power deposition by ICRF heating, hot-ion mode discharges can be optimised with combined NB and ICRF heating, by depositing the RF power in the region where the confinement is enhanced. In a short series of experiments (~6 shots), it was found that NB power could be exchanged for RF power (at a few MW), whilst maintaining or even increasing the reactivity. Addition of the RF power results in an important gain, 20-30%, in the reactivity rate, as shown in Fig 30. This feature arises from the increase in T_e in these

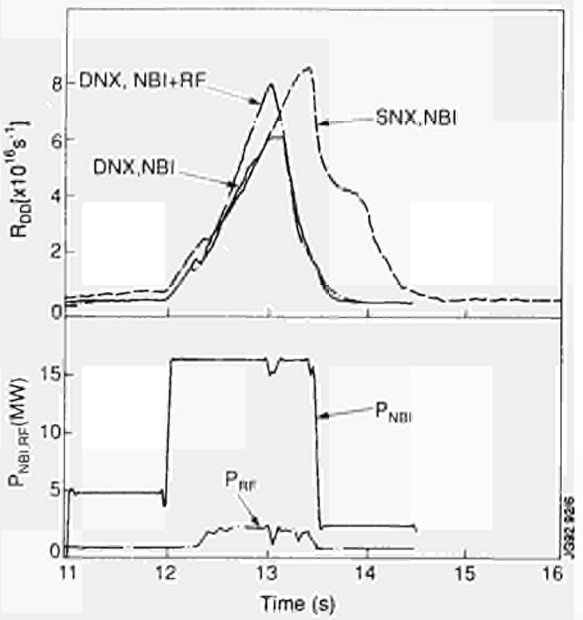

Fig.30: Time behaviour of the D-D reactivity for NBI only and combined NBI and ICRF hot ion modes. Addition of a few MW of ICRF increases the reactivity rate.

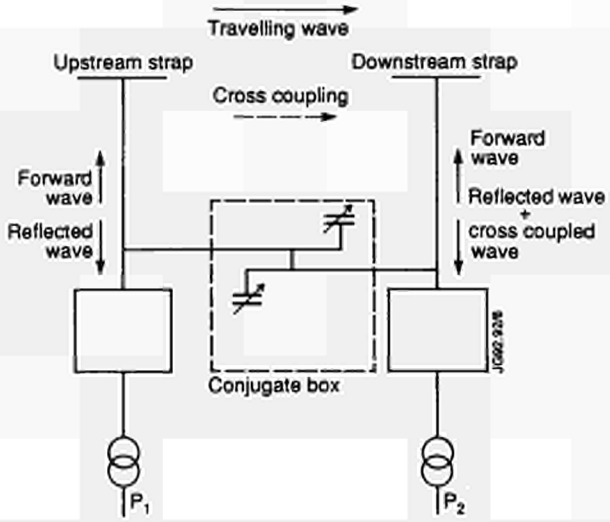

Fig.31: Principle of ICRF operation during phased operation. Cross-coupled power results in unbalanced input power. The conjugate box will allow the cross-coupled power to be recirculated and to maintain maximum input power.

cases δT_e–0.5-2 keV, which increases the slowing down time of the beam ions. High values of the fusion yield, R_{DD} = 7-8 x 10^{16} s^{-1}, were achieved reliably and reproducibly and the performance was limited by the influx of impurities after ~1s of the high power heating. The achieved R_{DD} values (8.2 x$10^{16}s^{-1}$) was amongst the highest values obtained in optimised SNX with NB heating alone.

A DNX configuration well adapted to the antenna shape was developed for 4MA plasmas. High power ICRF heating in combination with NBI was successfully applied and high quality H-modes with record stored energies were obtained. In this configuration, a coupling resistance higher than 4Ω was obtained. During the H-mode, the plasma-antenna distance was <2 cm. With combined NBI and ICRF heating, the same distance was typically ~ 2 cm larger and the corresponding coupling resistance did not exceed ~ 3.5 Ω.

Fast Wave Current Drive Experiments

For experiments such as current drive experiments, a relative phasing of the antenna conductor currents is required to allow a significant directivity of the wave to be achieved. Coupling between antenna conductors, which contributes to the required spectrum, poses delicate technical problems. Cross-coupled power from one conductor to the other must be maintained equal for proper control of the $k_{//}$ spectrum as a consequence of the phase lead, results in asymmetric coupling resistance, and requires the power output from the generators to be unbalanced as shown in Fig 31 [4]. In the dotted box, a longer term solution, called the conjugate box which recirculates the cross-coupled power and allow operation with low plasma loading resistance, is indicated. This technique has been developed in collaboration with ORNL, USA, and will be described in another section of this report. The new algorithmn, allowing the phase and amplitude of the wave to be controlled, is indicated in Fig 32. This system operates independently of the matching described above. Power up to 14 MW with 90° phasing has been achieved as shown in Fig 33.

Technical Achievements with the LHCD System

The prototype launcher [5, 6], which comprises one third of the full system, was installed in 1990. Its characteristics

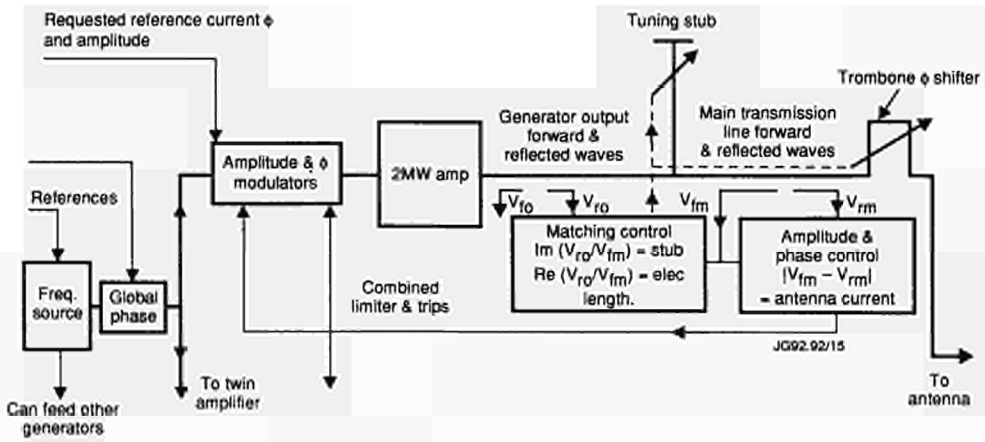

Fig. 32: New algorithm for the ICRF plant control allowing the phase and amplitude to be controlled.

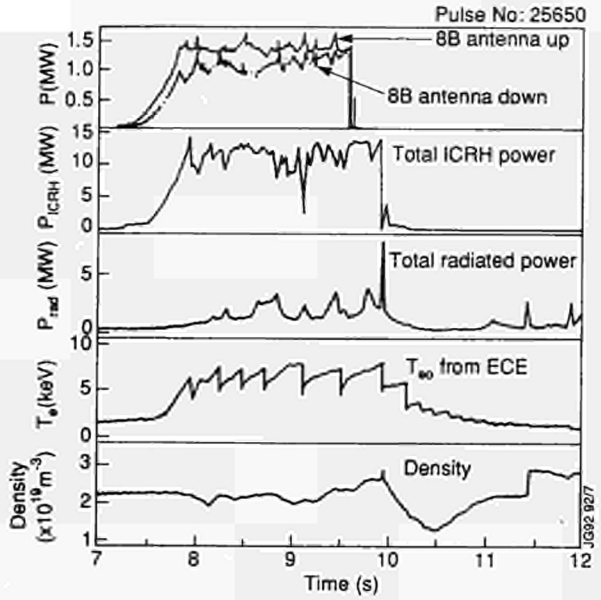

Fig.33: Time history of signals during ICRF minority current drive experiments. The imbalance between power from top and bottom Antenna No. 8B results from the required 90° phasing and is indicative of the cross-coupled power.

Table IV
LHCD System Parameters

Generator	**Prototype system**
Frequency	3.7GHz
Number of klystrons	8
Power (generator)	
10s pulse	4.8MW
20s pulse	4MW
Duty cycle	1/30
Efficiency	42%
Phase control	10 degrees
Maximum VSWR	1.8
Length of transmission line	40m
Estimated insertion losses	1dB
Launcher	
Number of waveguides (16 multijunctions)	128
Waveguide material	Stainless Steel and Copper
Coating	Copper + Carbon
Maximum temperature	350 C
Total weight	10tonnes
Stroke	210mm
Response	12mm/15 ms

are given in Table IV and a sketch of its main components are shown in Fig 34. Circulators allow the klystrons to operate at high power, while the power reflected by the plasma can reach 8%. High power switches and dummy loads permit commissioning of the klystrons at their maximum power. The hybrid junctions located in the Torus Hall direct the main part of the reflected power towards the dummy loads also located in the Torus Hall. During vacuum conditioning, or when the matching conditions are poor, the power reflected by the plasma is 50%, most going to the dummy loads in the Torus Hall.

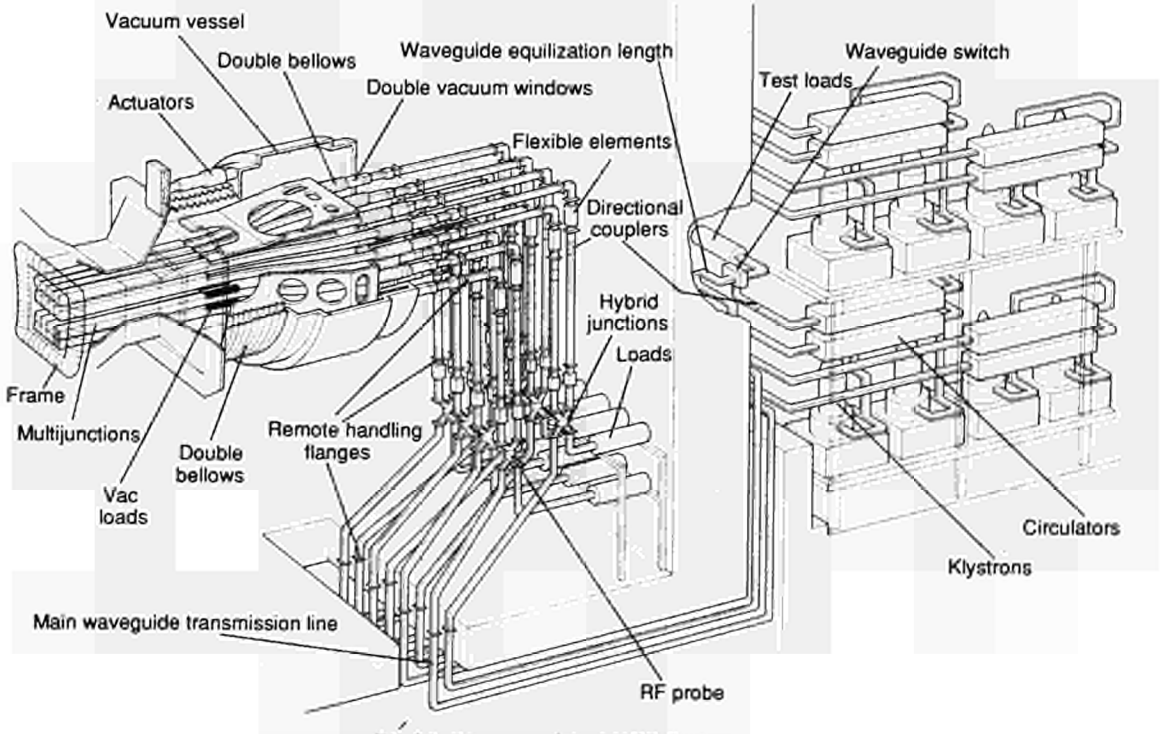

Fig.34: Diagram of the LHCD System.

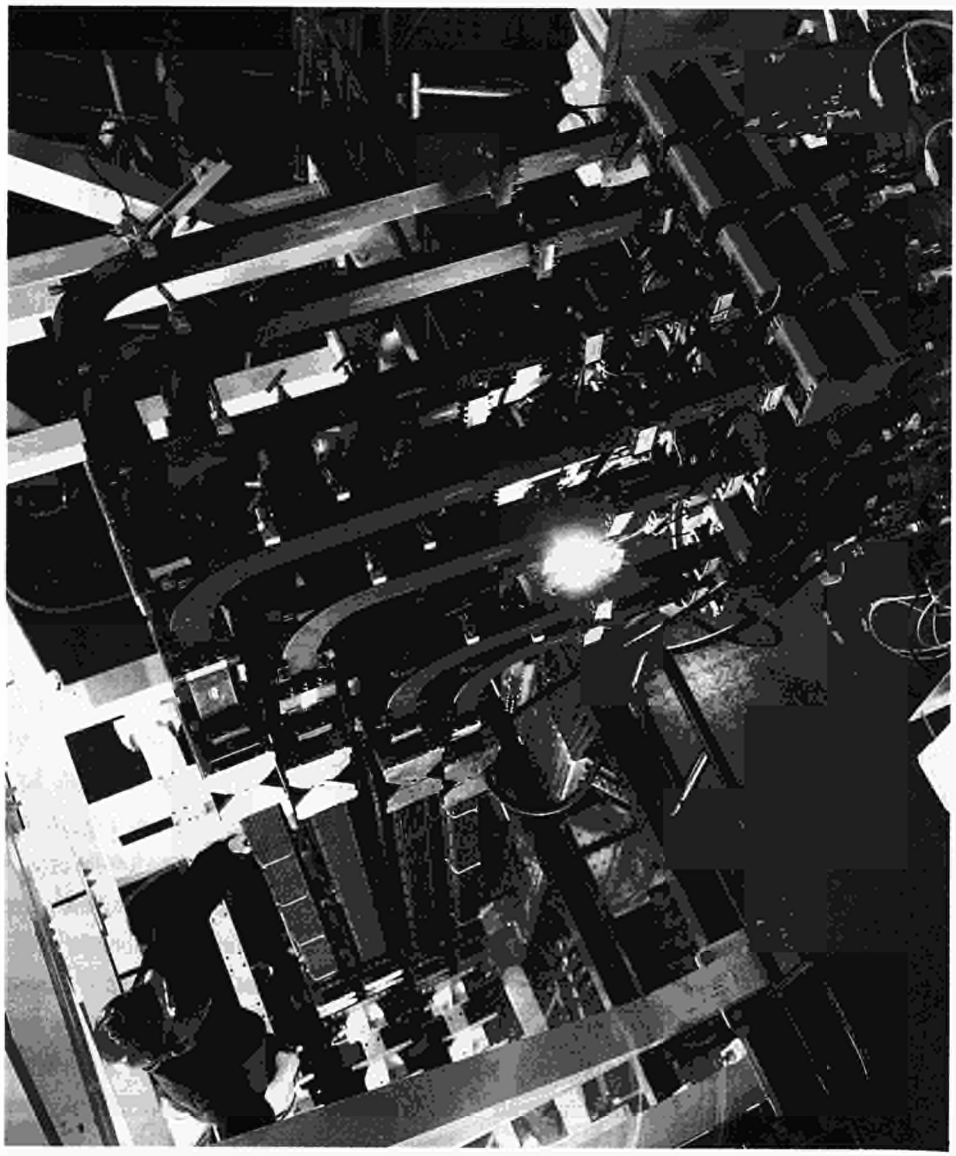

Fig.35: View of the LHCD end plate, of the vacuum windows together with their ancillary and protective systems and of the splitting waveguide network in the Torus Hall.

Therefore, these loads limit the power which can be used during vacuum conditioning or during poor plasma matching. A view of the LHCD system in the Torus Hall is shown in Fig 35.

During the initial campaign in 1990, some problems were encountered in the trip system (one window was broken), in the baking system (the LH vessel temperature was limited to 250°C) and in the position control system, which was not reliable. A thorough inspection of the vacuum part of the launcher has shown that there was no damage to the structure, including the inner hanger, due to the plasma thermal load or due to disruption induced stresses. Debris such as carbon flakes and droplets of metal coming from other components were removed from the end part of the waveguides.

Remedial action has been taken, on the following:

- installation of light detectors at the vacuum windows;
- new algorithmn for the trip system avoiding detection of false breakdowns;
- replacement of the lip of the vacuum vessel end plate allowing the vacuum vessel to be much more robust during thermal stresses;
- replacement of the thermal insulation on the vacuum vessel together with a new power control allowing baking temperatures up to 380° C to be achieved;
- installation of a new safety system using adjustable legs between torus and the LH vessel;
- replacement of a new servo-valve of the position control system insensitive to magnetic interference.

The main achievements with the LHCD system were :

- with LHCD only, a plasma current of 0.4MA was driven with no residual inductive voltage [7];

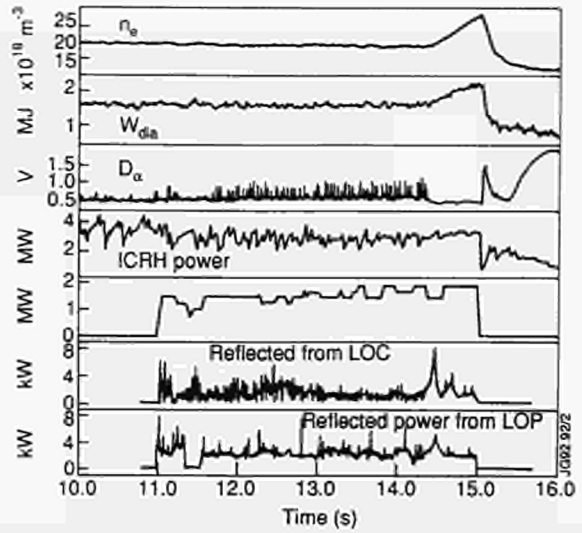

Fig.36: Reflectivity of LHCD modules during an ELM-free H-mode. ELMs induce spikes in the reflection coefficient. A transition in reflectivity is noted when the ELM-free period starts but the matching remains good.

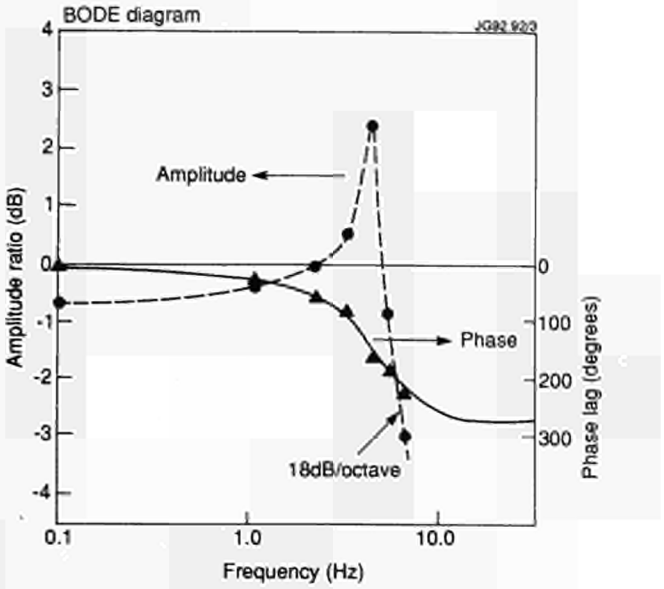

Fig.37: Bode diagram of the LHCD launcher for conditions near the stability limit,with input of 2mm peak-to-peak sinusoidal waveform. The resonance at 4.5Hz is close to theoretical calculations.

- the fully driven current rose to 1.5MA when a hot electron target plasma was used heated with ICRF in monopole phasing configuration;
- the current drive efficiency, nRI/P, exceeding $0.4x10^{10}m^{-2}AW^{-1}$, which is unsurpassed [8];
- the observation of synergistic effects between ICRF and LH, where part of the ICRF fast wave is damped on fast electrons produced by Lower Hybrid waves [9, 10];
- triggering an H-mode in combination with ICRF heating.

Power handling of the LH system has been improved but still requires a significant amount of conditioning time with plasma. A set of more powerful dummy loads have been installed in the Torus Hall for the L0P prototype to improve the conditioning in vacuum and to allow operation in poorly matched conditions. Up to 1.7MW for 1s out of a maximum 2.4MW have been delivered to the L0P launcher and 1MW has been coupled for 50s during the long pulse operation. Up to 2.2MW for 8s and 2.5MW for 1s have been coupled to the plasma in a large variety of plasma conditions.

Power handling depends strongly upon matching conditions and high power conditioning can only be carried out when plasma loading is such that the power reflected back does not exceed ~10 %. Due to an error of 5mm in the poloidal location of the two prototype launchers within L0, the poloidal location of the launcher must be well defined within ±0.5mm and this depends upon the respective location of the LHCD launcher and the ICRF antenna and upon the poloidal shape of the plasma [11].

Operation with low reflection coefficient has been found for a variety of plasmas, including ELM-free H-modes in double-null configurations. An example of the coupling in such conditions is indicated in Fig 36 showing that the coupling can be maintained at a low level (~3%) even during the ELM-free phase but not during the giant ELM's.

The required accuracy in locating the launcher to a precise poloidal location has been achieved by improving the hydraulic system which was fully commissioned during this year. Particular effort was applied to improving the cleanliness of the system, which incorporates about 150m of large bore tube (50 mm in diameter) and has a volume of about 250 litres. The fluid has been changed to a water based fluid (95% water and 5% diethanolamine). The main improvements resulted from a change in servo-valve specification, and accepting a reduction in frequency response in order to improve reliability. The system now operates reliably with a resolution in position of 0.3 mm (without integral terms in the loop) and a closed loop frequency response of 4 Hz. A typical Bode diagram of the closed loop performance is shown in Fig 37, with a velocity gain of about $20s^{-1}$ and large differential term in the loop. The frequency response is limited by the flexible hoses in the loop and could be increased significantly if required.

The sensitivity of the servo-valves to magnetic field has been measured. The original high performance valve could tolerate about 0.01T. The replacement valve has an iron body and cap and is immune to about 0.2T. This enables location of the valve close to the port; it is presently about 2m, outside the port.

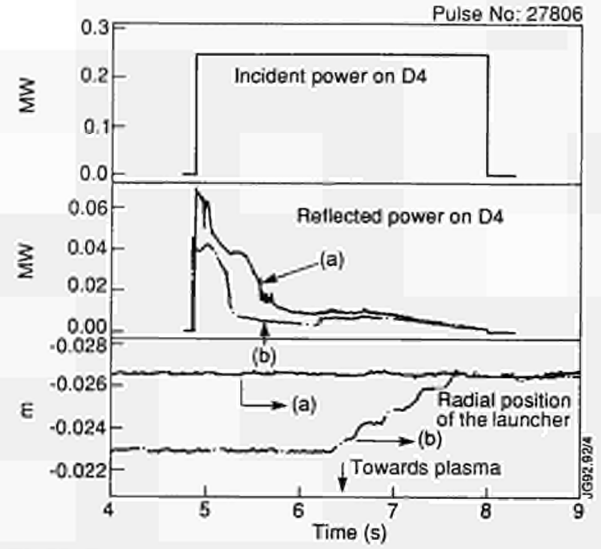

Fig.38: Time history of reflected power on D4 modules during controlled launcher movements with preset waveforms. The launcher is flush with the ICRF antenna at a position of -0.024m. The position can be held within ±0.3mm.

The security of the system against various failures has been extensively analysed and has resulted in imposition of a velocity limit of about $0.1ms^{-1}$ on controlled movement and an asymptotic velocity of $0.3ms^{-1}$ on total loss of pressure. The former is achieved with a series flow regulating valve and the latter with orifice plates on the offset cylinder ports. Mechanical sprung buffers will safely arrest the launcher from the asymptotic velocity. Pressure relief valves limit the maximum acceleration to $4ms^{-2}$.

This system has been used under CODAS control to move the launcher during pulses. A typical case is shown in Fig 38; the series PLC processing the waveform introduces a 0.3s staircase on the ramp-up and ramp-down and limits the frequency response under CODAS control, at present.

References

[1] J. Jacquinot and the JET team, in Controlled Fusion and Plasma Physics (Proc 18th Eur. Conf., Berlin, 1991) **33**, No. 13 (1991) 1657.

[2] M. Bures, M. et al. Plasma Phys. and Contr. Fusion **33**, No. 8 (1991) 937.

[3] T. Wade et al, Proc. 14th IEEE Symp. on Fusion Eng., (San Diego, USA) (1991).

[4] G. Bosia, et al. Proc. IAEA Tech. Comm. Meeting on Fast Wave Current Drive in Reactor Scale Tokamaks, Arles, France (1991), to be published.

[5] C. Gormezano et al. Proc. 12th Symp. on Fusion. Eng., (Monterey, USA) (1987).

[6] M. Pain et al. Proc. 13th Symp. on Fusion Eng. (Knoxville USA (1989))

[7] C. Gormezano, et al. Proc. IAEA Tech. Com. Meeting on Fast Wave Current Drive in Reactor Scale Tokamaks, Arles 1991, to be published.

[8] C. Gormezano, Fusion Eng. and Design **14**, 99 (1991)

[9] C. Gormezano et al in Proceedings 18th Eur. Conf. Cont. Fusion and Plasma., Berlin, Germany (1991) III, 389.

[10] D. Moreau and C. Gormezano in Controlled Fusion and Plasma Physics (Proc. 18th Eur. Conf., Berlin, Germany 1991) Vol 33, No. 13.

[11] C. Gormezano et al, 32nd APS Meeting, (Cincinatti, USA) (1990) (JET-IR(90)07).

Remote Handling and Waste Management

During 1991, the Remote Handling and Waste Management Group's manpower were heavily committed to shutdown activities and to preparation, execution and clean-up associated with the preliminary tritium experiment (PTE). Main progress in these areas is detailed below.

Remote Handling

Maintenance and repair of the tokamak and auxiliary systems in the Torus Hall during the D-T phase of JET will only be possible remotely, (ie controlled from outside the JET biological shield). Development of the remote handling equipment and procedures for maintenance tasks is carried out by the Remote Handling Groups in Fusion Technology Division. The manpower of these groups is also heavily involved in shutdown activities where remote handling equipment is being deployed, albeit hitherto in hands-on or semi-automatic mode. Whilst the use of remote handling equipment during JET shutdowns provides an excellent testing ground for the effectiveness and reliability of equipment, it also means that as a consequence of the associated manpower effort, only limited effort has been available for development of full remote handling procedures. Therefore, it is now envisaged that the remote handling for the D-T phase will concentrate on a few essential ex-vessel and in-vessel operations, including gaining remote entry into the vacuum vessel using the telescopic articulated remote mast (TARM) and the articulated boom with special end effectors or the MASCOT IV manipulators. The latter would allow, to a certain extent, to carry out non-planned activities inside and outside the vacuum vessel.

Special Tools

Work on refinement of the existing special tools, notably the welding trolley, the circular port cutters and the sleeve welders has been ongoing. The modifications include features for improved remote handleability and also ruggedisation.

About 15 new cutting, welding and alignment tools have been defined for the installation and remote handling of the new Pumped Divertor system. Two new types of welding tool have so far been fully designed and delivered. The remainder are being progressively designed and manufactured. Design and proving trials of new tile handling tools for the pumped divertor, poloidal limiters, guard limiters and RF antennae have been taking place. Final design and manufacture of these will take place in 1992.

Control Systems

Work has proceeded well on the design and manufacture of the new remote handling hand control terminal. This device will provide the man-machine-interface for all remote handling equipment, except manipulator, and can be used as a portable device or as a part of the remote handling control room equipment. The prototype hand control terminal has been delivered and acceptance tested. The first application program to be installed is that for control of the TARM.

The new UNIX based overall control system has been defined and a definition of the communication system and network messages has been issued.

The TARM interface cubicle which will connect the TARM and its services to the remote handling control room equipment has been specified and will be procured in 1992.

New articulated boom end-effectors for handling the Pumped Divertor components have defined. A series of new end-effectors for the installation of the Lower Hybrid system and Divertor modules have been designed and tenders for manufacture have been called for. A new end-effector for installation of the poloidal and inner wall guard limiters has been designed and procurement is planned for early 1992.

Articulated Boom

Subsequent to its use in the 1990/91 shutdown, the articulated boom underwent extensive stripdown and maintenance. No problems or unexpected wear in any of the components was found. Detailed improvements have been made to boom end-stops, camera arm drives and joint gaiters. Also some modifications to improve maintainability of the drives have been incorporated. As part of the continued preparation for use in the remote phase, the boom video system has been commissioned. In order to prepare the boom for operation during the Pumped Divertor phase a new boom addition has been designed and an order placed for its manufacture. This will comprise three links and two joints as compared to one joint in the existing boom addition. With the new addition the boom will approximately be one metre longer than at present and will have an additional articulation to provide more manoeuvrability within the more constrained in-vessel environment. To cater for the increase torsion loading imposed by the new Lower Hybrid system design, an upgrade to the torque capacity of the A6 drive has been required. A new drive system has been designed to provide both more torque and to alleviate the severe crowding problem within the A6 flange of the cables and service connectors doe end-effectors. This upgrade will be procured in early 1992. To accommodate the new torsion requirement at A6 and to improve the end-effector/boom mechanical interface, the A6 interface module is also being modified.

To control the new boom configuration and to provide a more maintainable control system, a new Local Boom Controller is being developed. The hardware selected is a proprietary system of modular units which will be assembled and tested in-house. The software has been fully specified by the boom operators and the code is now being developed and tested in-house. It is anticipated that the system should be fully commissioned and operating by the end of the 1992/93 shutdown.

The Mascot IV manipulator unit, together with TV drive arms was installed on the boom and operated through the port of the vessel mockup in the Assembly Hall. Pre-operational tests were carried out on the boom, confirming the static repeatability of 2mm. Modifications to facilitate emergency retrieval interventions have been initiated.

Telescopic Articulated Remote Mast (TARM)

During 1991, the TARM has been installed on the main 150 tonne crane on three occasions for various types of testing. The main crane has been modified and strengthened to accommodate the test findings and the work has culminated in a fully load tested TARM/crane combination certified for use in the 1992/93 shutdown for A2 antennae installation. Fig.39 shows the TARM connected to the main crane with its horizontal telescoping section extended and MASCOT IV manipulator fitted. Work to fully commission the elec-

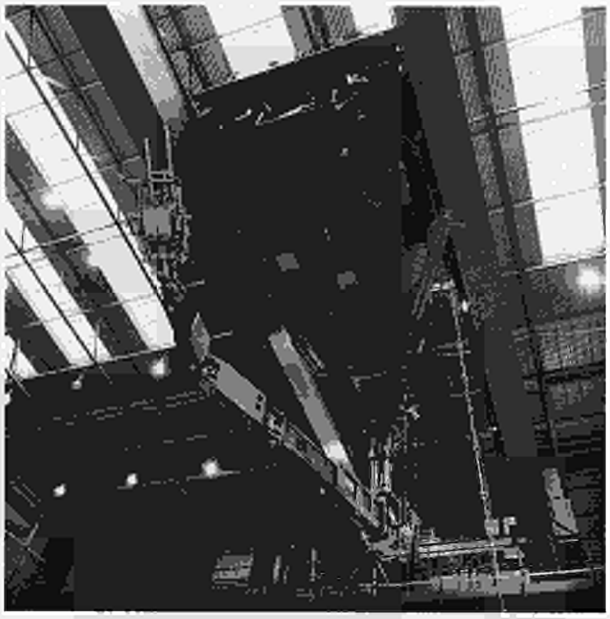

Fig.39: The TARM connected to the main crane with its horizontal telescoping section extended and MASCOT IV manipulator fitted.

trical and control system of the TARM on the crane will be undertaken in 1992. The TARM gas, hydraulic, welding and cutting tool services have been progressively commissioned. The will continue into 1992.

MASCOT

Within the framework of an Article 14 Study Contract with the Ecole Polytechnique of Lausanne, Switzerland, advances have been made in the control system of the MASCOT IV manipulator. Tests have shown that by adopting a frequency control method the heat losses of the motors can be reduced by about 20%. Studies with a view to replacing the AC motors with more efficient brushless DC types have been initiated.

Computer algorithms were improved under a Fellowship granted by the EC Teleman Programme. In particular, the "constraint" algorithm is now working satisfactorily and can be adapted to any cartesian or angular degrees of freedom as required. The combination of such algorithms with teach and repeat and weight compensation is also possible.

In-Vessel Inspection System (IVIS)

The in-vessel inspection system (IVIS) has continued to be of great value in JET operation. Development work to improve the quality of image and reliability is ongoing. The viewing tube developed in association with ENEA, Italy, in which the glass cylinder in replaced by a flat sapphire window has made good progress and testing at operating temperature and in vacuum has started. IVIS has been shown to be so important to JET operations, that is has now been decided to enhance the system for use during the D-T phase.

Extensive gamma radiation testing of miniature CCD cameras has been successfully undertaken. The miniature cameras have been proven in remote handling task mock-up tests to be extremely valuable viewing aids and so three types of cameras were tested for total dose limits when exposed to the dose rates expected within the torus during an active phase.

Waste Management

The responsibilities of the Waste Management Group established in 1990 have considerably increased in 1991 and the manpower has been increased to achieve this work. Its responsibilities include the provision of the infrastructure in JET for waste handling (radwastes as well as beryllium-contaminated wastes) and the provision and maintenance of respiratory protection systems and equipment. Following the preliminary tritium experiment, the 1992/93 shutdown be the first time that JET has had to deal with considerable quantities of tritium-contaminated components and materials, when these are removed from the vacuum vessel.

During the first part of the year, the Waste Management Group was involved in the operation of facilities for shutdown related work. These included the Torus Access Cabin (TAC), the Beryllium Handling Facility (BHF), the Suit Cleaning Facility and the PVC Workshop in K7. At the same time the packaging and disposal of beryllium contaminated and active waste arisings was carried out. In the case of low level solid radwastes, the finalisation of both a quality assurance programme and waste management procedures to meet the requirements for disposal at the Drigg Repository was an ongoing activity for much of the year.

The Group was subsequently involved in the planning for the first tritium experiment and the planning of facilities and procedures for the Divertor Shutdown, commencing in early 1992, where many of the operations will be affected by tritium as well as beryllium and induced activity. The main emphasis on the management of tritiated wastes concerned the Divertor Shutdown, but procedures and equipment were prepared to handle water leaks in case of an incident.

Specific tasks covered in the period included:

Waste Handling Facility

During the initial four month period in the 1992 shutdown, a considerable volume of active components and associated

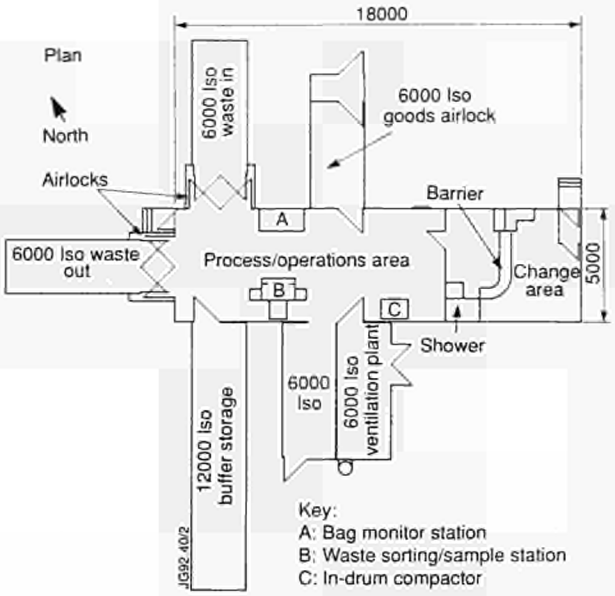

Fig.40: Layout of new Waste Handling Facility.

Fig.41: View inside the Beryllium Handling Facilities in the Assembly Hall.

contaminated secondary wastes will be produced. The materials will be contaminated with tritium as well as beryllium and activation products. A new Waste Handling Facility has been designed (see Fig.40) and is being constructed for commissioning before the start of the shutdown. The facility will be used to carry out the sorting, packaging, analysis and preparation for disposal of the materials and wastes.

Torus Access Systems

A number of modifications have been made to the Torus Access Cabin (TAC) and associated systems, in preparation for the 1992 shutdown. A structural extension to increase the size of the operations area and improve the facilities for personnel changing and movement of components and materials was completed. The ventilation system for the torus and TAC have been extensively modified to take account of the presence of tritium in the vacuum vessel. Enhancements have also been carried out on the breathing air system and the electrical and communications systems.

Beryllium Handling Facility

A number of enhancements have been made to the Beryllium Handling Facility (BHF) to allow materials contaminated with tritium to be handled. These include an improved, tritium compatible ventilation system, an improved drainage system that will be connected directly into the active drain for the Assembly Hall in 1992, improved decontamination facilities and a new access and change area. Fig.41 shows a view inside the BHF in the Assembly Hall which is extensively used for maintenance and repair work of Be-contaminated components.

Suit Cleaning Facility

In line with the preparations in other areas for handling materials that may be contaminated with tritium, the suit cleaning facility has had modifications to the ventilation system. An ultrasonic cleaning bath has been installed for decontamination of respirator components and small parts associated with the pressurised suits.

PVC Workshop

The workshop has been in operation throughout the year producing isolators and tented enclosures for beryllium and tritium related tasks. Isolators used for the introduction of tritium during the first tritium experiment were fabricated in the workshop.

Waste Management Operations

Housekeeping wastes, potentially contaminated with beryllium, have been disposed of throughout the year to a licenced landfill site. An additional 80m^3 of potentially low level radwaste were reclassified as beryllium waste for landfill disposal, following analysis which demonstrated that it was free of activity. The QA programme and Waste Management Procedures for the disposal of low level wastes have now been accepted by the relevant authorities. This clears the way for radwaste disposal to the Drigg repository. Waste Management Operations at JET have been audited by Harwell and found to be acceptable. An initial consignment of

radwaste has been dispatched to Harwell for disposal at Drigg. As part of the QA requirements, Area Waste Officers have been nominated in each Division in JET.

Methods have been established for the packaging of wastes and components arising during the 1992 shutdown. Requirements for waste sorting and sampling, particularly for tritium have also been studied. A bowser for the transport of tritiated aqueous wastes has been designed and is currently under construction for delivery early in 1992. The temporary storage facility for tritiated water was commissioned during the year. The new JET site active drainage system, was also commissioned in 1991.

Control and Data Acquistion (CODAS)

The JET Control and Data Acquisition System, CODAS, is based on a network of minicomputers. It is the only way to operate JET and it allows centralised control, monitoring and data acquisition. The various components of JET have been logically grouped into subsystems, such as Vacuum, Toroidal Field, Lower Hybrid additional heating, etc. Each subsystem is controlled and monitored by one dedicated computer interfaced to the machine and its diagnostics through CAMAC instrumentation and EUROCARD-based signal conditioning. Embedded front-end intelligence is implemented through CAMAC-based microprocessors for real-time applications. The actions of the various computers are coordinated by a supervisory software running in the Machine Console computer. This supervisory function includes the countdown sequence for each plasma discharge. The present allocation and configuration of all CODAS computers is given in Table V, while Tables VI and VII provide other quantitative data. Figures 42 and 43 illustrate the evolution of the JET data acquisition over recent years.

During 1991, CODAS Division has continued its role of expanding and improving operational support to the operation of JET. In addition, a large amount of effort was devoted to the design and prototyping of the CODAS upgrade to be implemented during the 1992 Shutdown. These points will be expanded under the headings Operational Support and CODAS Upgrade in the following sections.

Operational Support

Networks

There has been an increased exploitation of computer networking through the year. The pilot network which was completed last year has been expanded to cover the whole site. It has been named JETNet. Connection points were installed in every laboratory and office on the JET site, over 900 connections in total. Co-axial cables were used within buildings to form 97 local segments. Fibre-optic cables join the 15 buildings together in a pattern that allows the network-server computers to be placed together in the central computer room, for ease of maintenance. The network signals are buffered at various points by battery-supported repeaters so that network traffic is localized where possible and so that local faults do not propagate throughout the network.

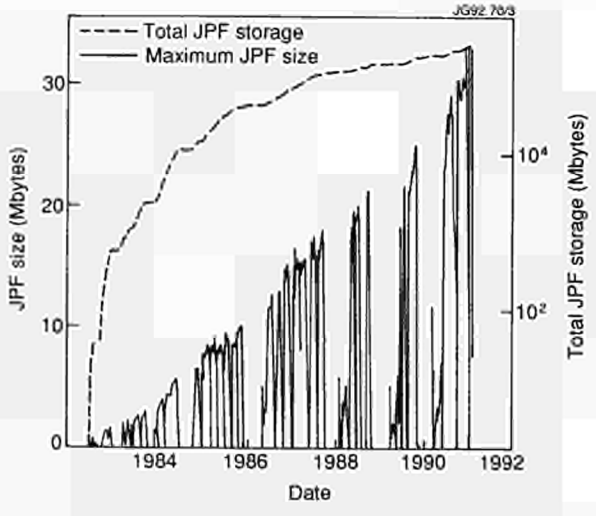

Fig.42: Evolution of JPF size and volume over the period 1983 - 1992.

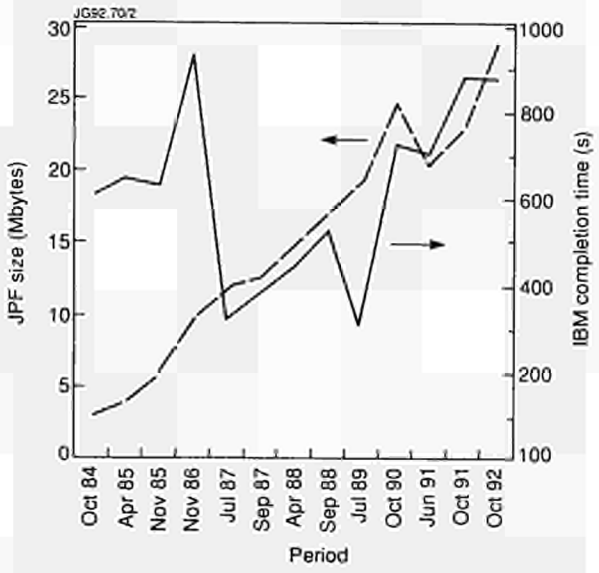

Fig.43: Evolution of JPF size and collection time over the period 1983 - 1992.

Table V
CODAS Computer Configuration at the end of 1991

Sub-System	Usage	Model	Memory (MByte)	Disks(MByte)	
AH*	NI Additional Heating (Oct 8)	ND110CX	3.5	1x70	1x450
AN*	Analysis and Storage	ND560	4.0	1x70	1x140 2x450
CB	Message Switcher B	ND110CX	4.0	1x70	2x140
CP	Cables Database	ND530	6.0	1x70	1x450
DA*	On-line diagnostic	ND520	4.0	1x70	1x140
DB*	On-line diagnostic	ND520	4.0	1x70	1x140
DC*	On-line diagnostic	ND520	4.0	1x70	1x140
DD*	On-line diagnostic	ND530	4.0	1x70	1x140
DE*	On-line diagnostic	ND520	4.0	1x70	1x140
DF*	On-line diagnostic	ND520	6.0	1x70	1x140
DG*	On-line diagnostic	ND520	4.0	1x70	1x140
DH	Diagnostic Commissioning	ND550	6.0	1x70	1x450
EC*	Experiment Console	ND570CX	6.0	1x70	1x140
EL	Electronics	ND110CX	2.0	1x70	1x140
GS*	General Services	ND110CX	2.5	1x70	1x140
XC*	Pellet Test Bed	ND110CX	4.0	2x70	1x140
LH	Lower Hybrid	ND110CX	3.5	1x70	1x140
MC*	Machine Console	ND110CX	2.5	1x70	1x140
PF*	Poloidal Field	ND110CX	3.0	1x70	1x140
PL*	Pellet Launcher	ND110CX	2.5	1x70	1x140
PM*	Pulse Management	ND550	7.0	1x70	1x140 1x450
RB*	Radio Frequency Test Bed	ND110CX	2.25	1x70	1x450
RF*	Radio Frequency	ND100	3.0	1x70	1x140
RH	Remote Handling	ND110CX	2.5	1x70	1x140
SA*	Message switching & JPFCollection	ND110CX	4.0	1x70	1x140
SB	Standby-System/Backup	ND110CX	4.0	2x70	1x450
SS*	Safety & Access	ND110CX	3.0	2x70	1x140
TB*	NI Test Bed	ND120CX	4.0	1x70	1x450
TF*	Toroidal Field	ND110CX	2.5	1x70	1x450
TR	Tritium	ND110CX	2.5	1x70	1x140
TR	Test	ND520	4.0	1x70	2x450
XX	Ethernet Gateway	ND110CX	2.5	2x45	
VC*	Vacuum	ND110CX	4.5	1x70	1x140
YB	Integration	ND530	6.0	1x70	1x450
YC*	NI Additional Heating (Oct 4)	ND110CX	3.5	1x70	1x450
YD	Sc Dpt Development	ND570CX	6.0	1x70	1x450
YE	CODAS System Development	ND520	6.0	1x70	1x450

* *Indicates on-line computers used for operation and testbed*

The network operating system, Vines, was selected to run in all JETNet's servers. E-mail services have been established under Vines between users of all the types of computers in use at JET, including IBM mainframe, Unix , PCs and Apple Macintosh. The users send messages to a named person without the need to know which type of computer the recipient is using.

Documentation

The rationalization of all CODAS hardware documentation into a single database, Electra, has been largly completed. The system is comprehensive, with over 50 screen layouts. A user can check, from any JETNet terminal, the specification, stocks, modification-state of any electronic item. The structure of all CAMAC serial highways, cubicles or subracks

Table VI
Quantitative Information on CODAS Installation

Item	End 1990	End 1991
CODAS Interface Cubicle	157	165
CAMAC Crates	248	255
CAMAC Modules	3,289	3,195
Eurocard Modules (Signal Conditioning and Power Supplies)	7,951	8,180
CAMAC Serial Loop (Fibre Optic)	25	25
On-line Computers	24	24
Off line and Commissioning Computers	14	13
Size of JPF	29	33
Number of diagnostics on-line with CODAS	35	42
Number of diagnostics under commissioning with CODAS	4	2

Table VII
Review of CODAS Electronics Stock Holding
(installed, pre-procurement, loaned and spares)

		End 90	End 91
1.	CAMAC system modules	911	908
2.	CAMAC digital I/O modules	900	910
3.	Timing system (CAMAC & Eurocard)	1,371	1,430
4.	CAMAC analogue I/O modules	1389	1,352
5.	CAMAC display modules	410	406
6.	CAMAC auxiliary controllers	153	151
7.	CAMAC powered crates	284	280
8.	U-port adaptor	205	215
9.	CISS modules	1,040	977
10.	CCTV	694	690
11.	Cubicle frames	345	354
12.	Console devices (not CAMAC)	693	648
13.	Power supply modules	2,071	2,097
14.	Intercom, Public Address, Computer terminal network	651	731
15.	Pool instruments	1,046	1,003
16.	Analogue I/O in Eurocard	2,829	2,863
17.	Digital I/O in Eurocard	4,901	4,975
18.	Eurocard sub-racks	1,045	1,024
19.	JETNet active devices	new	187
20.	VME modules	new	5
		20,938	21,206
	In crease		1.3%

can be displayed as tables or as AutoCAD drawings where these exist. 4000 such drawings are accessible.

Electra has been expanded to record the progress of current jobs, mainly CODAS interface system enchancements. At each stage of the work, an entry is made by those involved. Electra's scheduler then adjusts the predicted completion date.

New Cubicles

The interface electronics between the JET plant and CODAS has grown only slightly. This is due to a balance between the installation of six new cubicles for various diagnostics and the removal of other cubicles.

Enhancements

A total of 158 fully documented improvements were made to existing systems, together with 253 recorded maintenance interventions. There have been minor changes to other site-wide services provided by CODAS, including the computer-terminal, intercom, public address and instruments pool but, in general, these services are in a steady state.

Module Developments

New electronic design facilities have been used to develop a Serial Highway Driver, coded VHD1, for the planned UNIX computers. This design is now in production. Various other Versa Module Eurocard (VME) developments are at the design stage, the principal aim being to provide cheaper and more effective designs than could be provided in the older CAMAC standard. The new designs will be used in new control and diagnostic systems to be installed during the Divertor Shutdown. Fewer hardware designs are needed than in CAMAC systems because more use of microprocessors and field-programmable integrated circuits means that quite different functions can be achieved by firmware changes only.

Timing system improvements

Sychronization of all CODAS precision timing signals has been improved by using a single central frequency reference, which is distributed on fibre-optic cables. Correct operation is now confirmed by a range of frequency comparator modules.

Future Module Developments

The move to UNIX computers will have only a secondary effect on the interface electronics following the decision to

leave the CAMAC equipment in place. It is necessary only to fit the newly developed VHD1 cards to the UNIX computer and the JET plant is effectively re-connected.

The VME developments would allow most functions now implemented in CAMAC to be duplicated, but at lower cost, and with better performace. The designs to be implemented will be selected mainly by the need to find economical solutions for new JET diagnostics, which are predicted to need a three-fold increase in data collection capacity.

Feedback and Real-time Systems

Front-end feedback systems have continued to expand either by modifying existing control loops to adapt them to the operation or by providing additional facilities. The following are two typical examples:

a) The plasma fault protection system has been expanded to provide improved protection against disruption. It uses the Mode Lock signal which is a disruption precursor to request "soft" pulse termination. An algorithm has been added for control of the plasma current rise by real time actions on the Thyristor Make Switches of the Poloidal Field circuit. Other algorithms monitor abnormal C and Be light signals and ramp down the additional heating when programmable thresholds are exceeded;

b) The Plasma Position and Current Control has been modified to cope with the AC operation experiment and to reduce quickly the plasma elongation when a mode lock is detected. This allows better control of the vertical stability reducing the effects of a disruption with a mode lock precursor.

Similar changes have been made to the Plasma Density Validation, Plasma Density Feedback and Plasma Termination Network to adapt them to new operational demands.

Level I Software

This is the top layer of the CODAS software which allows convenient and safe operation of JET. It has been expanded by the inclusion of additional algorithms such as calculation of the voltage and current waveforms of the Toroidal Field Static Units and Flywheel Generator Convertor to obtain the required Toroidal Field profile and checks on I^2t limits and stress levels.

CODAS Upgrade

Policy

As mentioned in 1990 Progress Report, it had been decided to move CODAS to a UNIX environment to maintain its services in the best possible way until the end of 1996. The structure of the system will be similar. The CAMAC interface will be retained and the Man Machine Interface (MMI) will be upgraded to use Windows. The changeover will be implemented during the 1992/93 Shutdown period.

Present Status

Operating System and Basic Libraries

In the early phase of the preparation to the move of CODAS, the primitives used in SINTRAN, the Norsk Data operating system, and the content of the basic libraries were reviewed to identify the necessary changes taking into account the cost of retrofit on the application software. At present all changes have been made and the libraries have been released with a minimum of changes to the user image.

CAMAC Interface

The existing control of the CAMAC loops had been implemented through a set of two complex boards hosted in the Norsk Data computer and a CAMAC driver software included in SINTRAN. The required functions have been transferred to a VME board based on a MOTOROLA 68030 microprocessor and a custom daughter board. This implementation makes the CAMAC driver hardware independent of the host computer and available to other institutions. The software driver has been developed and tested on the development computers and the performance obtained matches the JET requirements. Production of all units required for the CODAS upgrade will proceed soon.

Plant Access

The existing access to input/output channels is based on a layer of software called "JET Drivers" allowing application software to perform access by name without knowing the details and idiosyncrasies of the connection to CAMAC. To minimise the costs of retrofit to application software all the functionalities of the JET Drivers have been ported to UNIX and this software, has been fully commissioned. Significant savings in porting effort were obtained by using a preprocessor converting the existing code written in NPL (Nord Programming Language - Structured assembler for Norsk Data machines) into C and making final changes by hand.

CODAS Software Tools

Most CODAS software tools have been ported to UNIX. This ranges from the software distribution and up dated

procedures to database support through the microprocessor support and on-line test tools.

CODAS Packages

CODAS makes extensive use of common software packages which are used in all subsystems in addition to software specific to some subsystems. The following packages have been ported and passed successfully the initial test phase:

- GAP — General Acquisition Program which gathers all JET data.
- MIMIC — Displays schematic representation of the plant and provides basic interactive points.
- ALARM — Monitors and reports alarms.
- COUNTDOWN — Coordinate pre- and post- pulse activities of all JET subsystems.
- Touch Panel — Provides basis for operator actions from consoles.
- RUT — Provides a large part of sequencing and other similar tasks which are defined in ASCII files. These files are all re-usable under UNIX.
- Waveform — Allows definition, modification and management of all real time waveforms used during JET pulses.

Man Machine Interface

The new Man Machine Interface (MMI) will be based on X-window which allows a user to interact conveniently with various tasks on the same screen. After the required familiarisation and consultation, MOTIF was selected as the Graphic User Interface standard. The common solution used in control systems is to use a Workstation to support the Man Machine Interface. The availability of X-terminals led JET to consider the possibility of using such terminals supported by MMI computers as an alternative to Workstations. After analysis and tests it was shown that a medium size MMI computer could support about six X-terminals. The final decision was based on a financial comparison which showed that using X-terminals and MMI computers were cheaper than using Workstations. The financial information was obtained from Full Tender Action.

Network

Network technology is still evolving quickly and JET considered various configurations. The selected design is based on ETHERNET multi-segments connected through bridges. In the case of JET, it leads to an efficient network which is easy to manage. A schematic representation is shown on Fig. 44. The procurement of the network component was the object of a Full Tender Action.

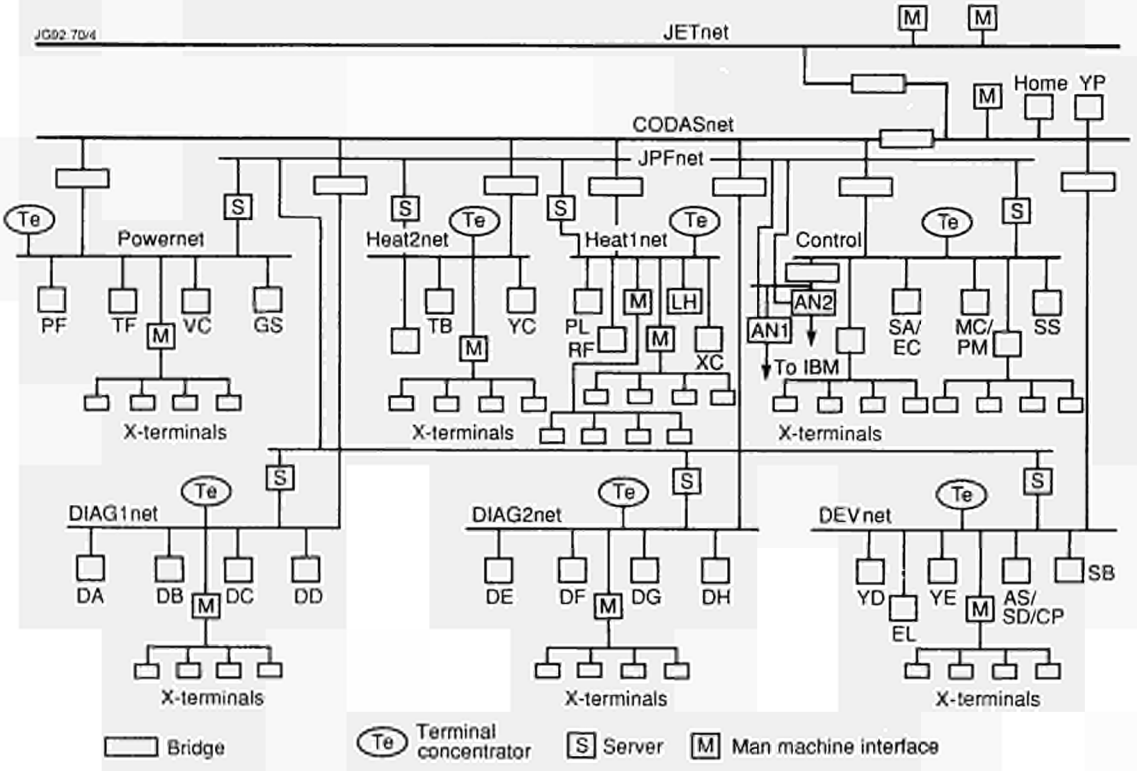

Fig.44: Schematic of CODAS Computer Network (CODAS Net).

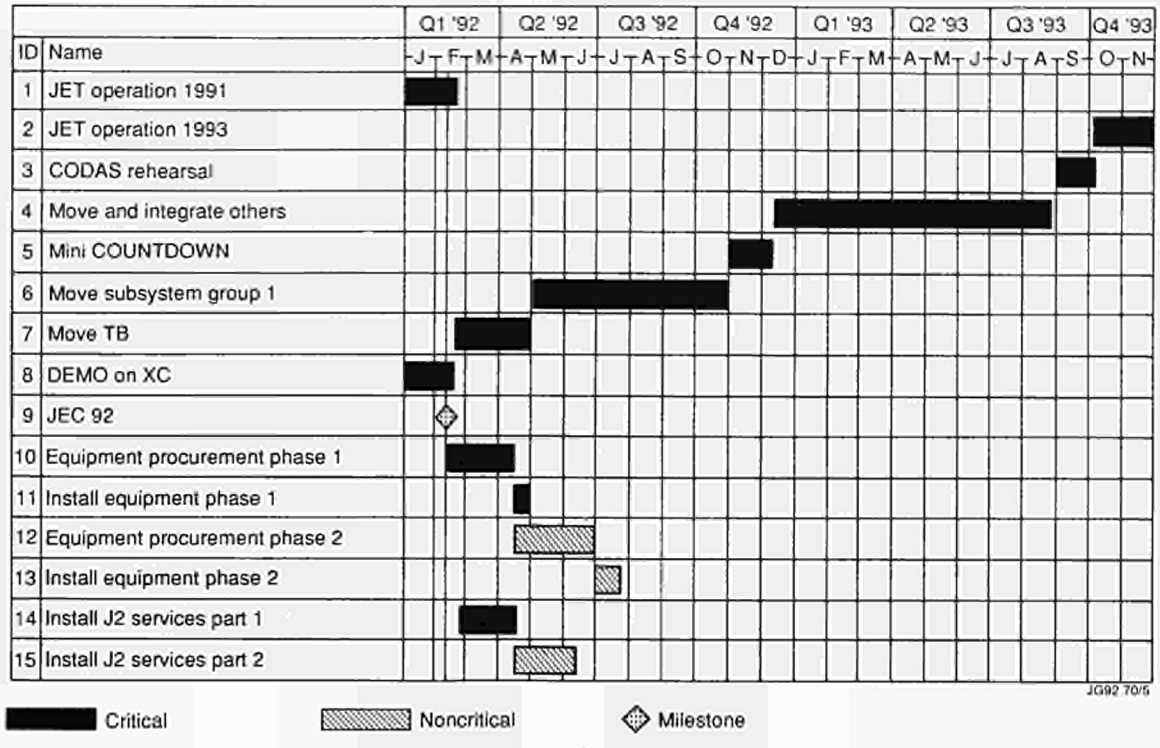

Fig.45: Current planning of UNIX System.

Pellet Test Bed Integration

In addition to the CODAS software packages and tools, the software specific to the Pellet Testbed activities has been ported to UNIX. The system integration is complete and the commissioning was successful ending with launching of pellets using control and data acquisition working under UNIX. As anticipated the overall system behaviour must be analysed and the system tuned before proceeding to move other CODAS subsystems and services.

Current Planning

The summary of the current planning is shown in Fig. 45. After acceptance of the Pellet Launcher Testbed subsystem, the Neutral Beam Test Bed subsystem will be moved to UNIX. As this facility will be operating during the Shutdown, it will exercise the new system extensively allowing the identification of possible problems. Then a number of subsystems will be moved and run together allowing tests of the normal sequences of the JET Countdown (pre-pulse, pulse, post-pulse) and the subsystem synchronisation and co-ordination through a series of dry runs. After this, the other subsystems will be moved and integrated into CODAS operation, leading to a full and formal CODAS rehearsal before starting JET recommissioning and operation. During the initial phase of the Shutdown, some old computers will be retained and used either to maintain some essential services like Access Control or to allow commissioning of the new elements of the machine (eg Divertor power supplies). It is anticipated that a subset of all components required for the CODAS upgrade will be installed by the middle of April 1992 and the installation should be completed by the middle of June 1992.

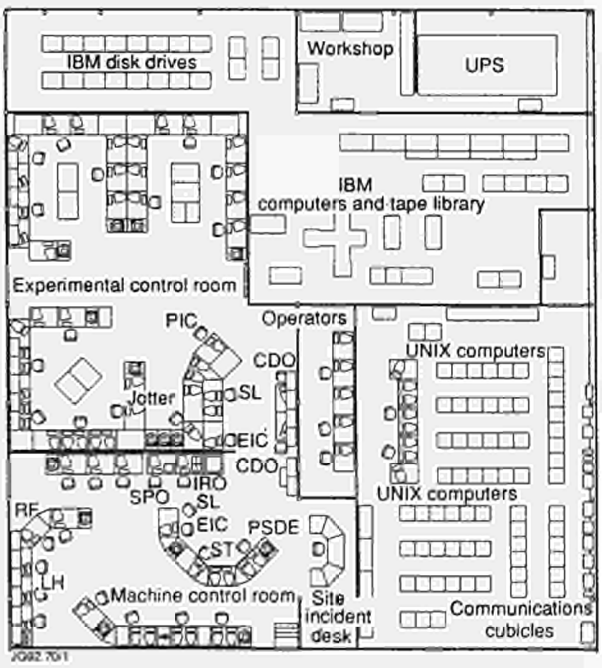

Fig.46: Layout of UNIX and IBM computers in J2 Building.

Control and Computer Rooms

Replacement of the CAMAC based consoles by X-terminals and deployment of new computers will require complete re-arrangement of the control and computer rooms. In addition, the overall layout of the J2 building will be modified to accommodate the relocation of the JET IBM mainframe from Harwell to JET. This relocation will not only bring significant savings but it will also remove the communication bottleneck created by the existing British Telecom links. The new layouts are shown in Fig. 46.

JET Data Management

The JET Data Management Group is responsible for the provision of a Mainframe Computing Service for scientific and engineering computing. This includes provision of appropriate software and hardware systems. The Group is also responsible for the management of JET data and for organisation and control of routine data processing.

The computing service is based on an IBM 3090 three-way processor mainframe with two vector facilities. There are 90GBytes of disc storage and a further 240GBytes of IBM mass storage. The JET Mainframe Data Processing Centre is housed at UKAEA Harwell Laboratory, and operated under contract by a team from that Laboratory.

The JET Computing Centre has been operating since June 1987 and the computing load has grown significantly since. To maintain good interactive response and accommodate an increasing load of background batch work, the central computer was upgraded in February 1990 from an IBM 3090/200E to an IBM 3090/300J with three processors, two vector facilities and 196 MBytes of memory (64MB central and 128MB expanded). This has almost double the processing capacity. The upgrade has permitted a significant growth in all areas of the mainframe computing workload, most critically in the intershot processing, the CAD work from the JET Drawing Office and interactive (TSO) work. These improvements have significantly enhanced the Project's Design and Data Processing capabilities.

The Data Management Group provides the contract between the users, operators and system programmers, through the Help Desk Service, backed up by specialists in the Group. This ensures the smooth running of the system. The data communications between the JET site system and the Computer Centre are mainly the responsibility of CODAS Division and these have operated reliably.

One link is dedicated to the transmission of the raw JET data files (JPFs) from the NORD system to the IBM. The increasing sophistication of JET measurements and analysis techniques have lead to a growth in the JPF size which is now about 30 to 35 MBytes per shot. Various optimizations have been made in order to keep the data collection and transmission time within eight minutes from the end of the pulse. The running of the extended intershot analysis has also been further refined and the first set of plots are returned to the control room within a further two minutes. The whole intershot analysis is completed in eight minutes from receipt of JPF. All the JPFs (currently in excess of 240 MBytes) are stored in compressed form on the IBM Mass Store, and a further 70 GBytes of analysed data from the intershot and other analysis work is also stored on the IBM system, within the PPF on-line data base.

The Central Physics File (CPF), stored and used under the SAS environment, forms a complete higher level data selection and storage system. A subset of all data is extracted at time points of interest, determined by the Timeslice program and the interactive timeslice editor, TED, and stored in the SAS databases. These data are the basis for extended statistical analysis, and the source for other extracts such as the TRANSPORT bank. This system is fully automated, and used by many physicists in the Project.

In addition, the Group provides support for the increasing numbers of Personal Computers (PCs) on site (over 350) which are used both as stand-alone work-stations and terminals to the IBM and NORD computers, and for the Applemac Systems introduced for work processing (~ 60 systems).

The development and evolution of a prototype network incorporating PCs, MACs, Unix work-stations and connections to the IBM mainframe has been completed with the CODAS Division. Work is now in progress to extend these network services, Electronic Mail, File Servers, Access to shared printers and the main frame, to other JET users.

Diagnostic Systems

The status of JET's operating diagnostic systems at the end of 1991 is summarized in Table VIII and their general layout in the machine is shown in Fig.47. The staged introduction of the diagnostic systems onto JET has proceeded from the start of JET operation in June 1983. The present status is that 43 systems are in routine operation on the machine. A further 21 systems are in preparation or in the design stage

Table VIII
Status of JET Diagnostic Systems, December 1991
Operational Diagnostics

System	Diagnostic	Purpose	Association	Automation
KB1	Bolometer array	Time and space resolved total radiated power	IPP Garching	A
KB2X	X-point bolometer	Time and space resolved power from X-point region	JET and IPP Garching	A
KC1	Magnetic diagnostics	Plasma current, loop volts, plasma position, shape of flux surfaces, diamagnetic loop, fast MHD	JET	A
KE3	Lidar Thomson scattering	T_e and n_e profiles	JET and Stuttgart University	A
KE5	q-profile Thomson scattering	Measurement of q-profile	JET	SA
KF1	High energy neutral particle analyser	Ion energy distribution up to 3.5MeV	Purchased from Ioffe St Petersburg	SA
KG1	Multichannel far infrared interferometer	$\int n_e ds$ on six vertical chords and two horizontal chords	CEA Fontenay-aux-Roses	SA
KG3	Microwave reflectometer	n_e profiles and fluctuations	JET and FOM Rijnhuizen	A
KG4	Polarimeter	$\int n_e B_p ds$ on six vertical chords	JET and CEA Fontenay-aux-Roses	SA
KH1	Hard X-ray monitors	Runaway electrons and disruptions	JET	A
KH2	X-ray pulse height spectrometer	Monitor of T_e, impurities, LH fast electrons	JET	SA
KJ1*	Soft X-ray diode arrays	MHD instabilities and location of rational surfaces	IPP Garching	SA
KJ2*	Toroidal soft X-rays	Toroidal mode numbers	JET	SA
KK1	Electron cyclotron emission spatial scan	$T_e(r,t)$ with scan time of a few milliseconds	NPL, UKAEA Culham and JET	A
KK2	Electron cyclotron emission fast system	$T_e(r,t)$ on microsecond time scale	FOM Rijnhuizen	A
KK3	Electron cyclotron emission heterodyne	$T_e(r,t)$ with high spatial resolution	JET	SA
KL1*	Limiter viewing	Monitor hot spots on limiter, walls, RF antennae, divertor target tiles	JET	A
KL3	Surface temperature	Surface temperature of target tiles	JET	M
KM1	2.4MeV neutron spectrometer	Neutron spectra in D-D discharges, ion temperatures and energy distributions	UKAEA Harwell	SA
KM3	2.4MeV time-of-flight neutron spectrometer		NEBESD Studsvik	A
KM7	Time-resolved neutron yield monitor	Triton burning studies	JET and UKAEA Harwell	A
KN1	Time-resolved neutron yield monitor	Time resolved neutron flux	UKAEA Harwell	A
KN2	Neutron activation	Absolute fluxes of neutrons	UKAEA Harwell	SA
KN3*	Neutron yield profile measuring system	Space and time resolved profile of neutron flux	UKAEA Harwell	A
KN4	Delayed neutron activation	Absolute fluxes of neutrons	Mol	A
KR2	Active phase NPA	Ion distribution function, $T_i(r)$	ENEA Frascati	A
KS1	Active phase spectroscopy	Impurity behaviour in active conditions	IPP Garching	SA
KS2*	Spatial scan X-ray crystal spectroscopy	Space and time resolved impurity profiles	IPP Garching	SA
KS3	H-alpha and visible light monitors	Ionisation rate, Z_{eff}, impurity fluxes from wall and limiter	JET	SA
KS4	Charge exchange recombination spectroscopy (using heating beam)	Fully ionized light impurity concentration, $T_i(r)$, rotation velocities	JET	SA
KS5	Active Balmer α spectroscopy	T_D, n_D and $Z_{eff}(r)$	JET	SA
KS6*	Bragg rotor X-ray spectrometer	Monitor of low and medium Z impurity radiation	UKAEA Culham	SA
KS7*	Poloidal rotation	Multichannel spectroscopic measurement of poloidal rotation	UKAEA Culham	M
KT1*	VUV spectroscopy spatial scan	Time and space resolved impurity densities	CEA Fontenay-aux-Roses	A
KT2*	VUV broardband spectroscopy	Impurity survey	UKAEA Culham	A
KT3	Active phase CX spectroscopy	Fully ionized light impurity concentration, $T_i(r)$, rotation velocities	JET	SA
KT4*	Grazing incidence + visible spectroscopy	Impurity survey	UKAEA Culham	A
KX1	High resolution X-ray crystal spectroscopy	Central ion temperature, rotation and Ni concentration	ENEA Frascati	A
KY2	Surface probe fast transfer system	Plasma wall and limiter interactions including release of hydrogen isotope recycling	UKAEA Culham	Automated, but not usually operated unattended
KY3*	Plasma boundary probes	Vertical probe drives for reciprocating Langmuir and surface collector probes	JET, UKAEA Culham and IPP Garching	
KY4	Fixed Langmuir probes (X-point belt limiter)	Edge parameters	JET	SA
KZ3*	Laser injected trace elements	Particle transport, T_i, impurity behaviour	JET	M
Ky1	Gamma-rays	Fast ion distribution	JET	M

* Not compatible with tritium A=Automatic; SA=Semi-automatic; M=Manual

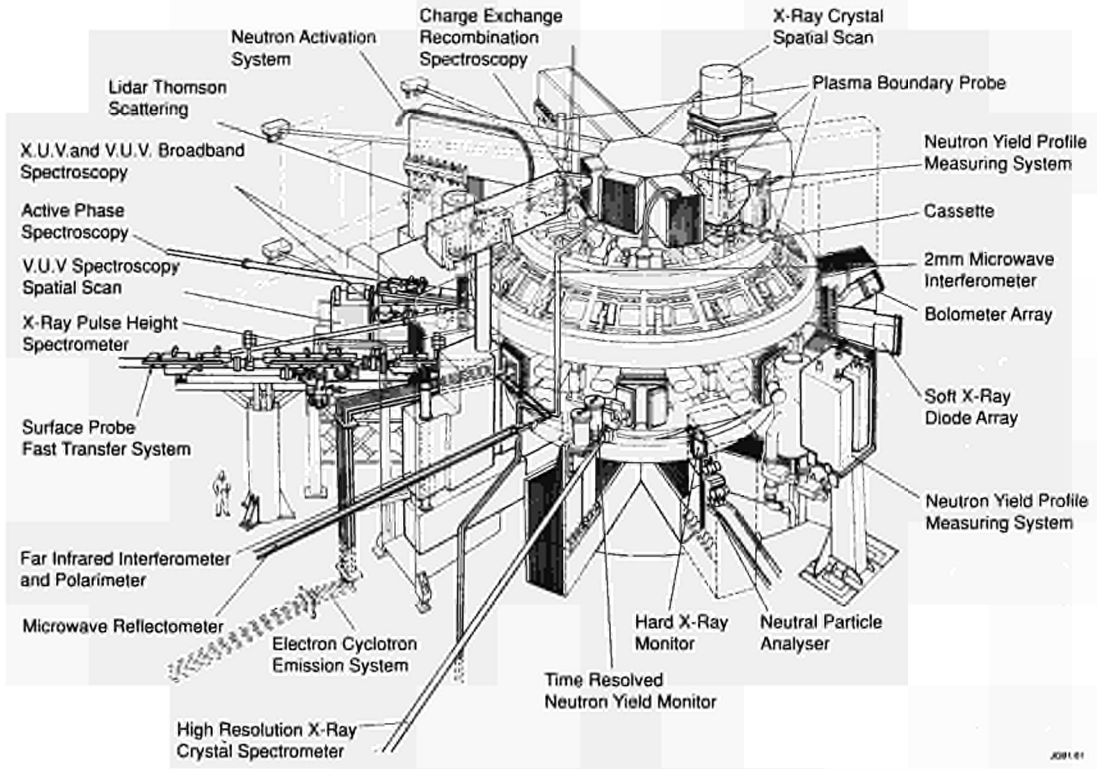

Fig. 47: General layout of diagnostics in the JET machine.

for operation in the New Phase of JET or in the active D-T phase. Table IX sets out a list of additional diagnostics under construction for the D-T phase of operation. Those for use on the Pumped Divertor will be discussed further in the section on the New Phase of JET. Operational experience has been good and most of the systems are now operating automatically with minimal manual supervision. The resulting measurements are of a high quality in terms of accuracy and reliability, and provide essential information on plasma behaviour in JET. Further details on specific diagnostics systems are given below.

Magnetics

The basic system of flux and poloidal field measurements has worked reliably during this year. The special set of tangential and normal coils at the lower divertor was reconnected so that boundary identification codes (XLOC, EFIT) could be used in single-null and double-null configurations. Extensive use was made of the high frequency response ceramic coils at the outer midplane for studies of ELM precursors and fishbone oscillations.

The real time triggering facility was extended to a specialised ELM trigger and a sophisticated trigger for

Table IX
Additional Diagnostics under Construction

System	Diagnostic	Purpose	Association	Status
KE4	Fast ion and alpha-particle diagnostic	Space and time resolved velocity distribution	JET	Under construction
KE7	Lidar Thomson scattering	Higher spatial resolution, n_e and T_e in plasma edge	JET	Being tested
KJ3	Compact soft X-ray cameras	MHD instabilities, plasma shape	JET	Design
KJ4	Compact soft X-ray camera	Toroidal mode number determination	JET	Design
KM2	14MeV neutron spectrometer	Neutron spectra in D-T discharges, ion temperatures and energy distributions	UKAEA Harwell	In installation
KM5	14MeV time-of-flight neutron spectrometer		SERC Gothenberg	In installation
KT3D	Active phase visible and UV spectroscopy	Light impurity concentrations, $T_i(r)$ in divertor and centre	JET	Design
KB4	In-vessel bolometer array	Time and space resolved radiated power	JET	Design

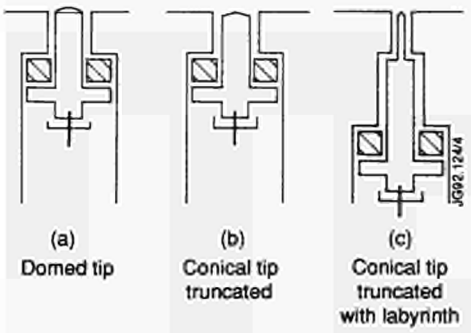

Fig. 48: Designs of tips used in the Langmuir probes of the divertor target.

MHD oscillations to provide amplitude levels for different n-modes. The trigger signals were distributed via the real time trigger network to other diagnostics. The studies of the compensation of error fields as measured by the diamagnetic loops has continued. It is now clear that the fault in TF Coil No: 4.2 is significant so that satisfactory compensation can only be achieved at a particular time during the pulse and that a new compensation needs to be carried out for every individual toroidal field (TF) waveform until the investigation of systematic fault compensation is completed. The second loop is far away from the faulty coil and has a much higher coupling to the poloidal circuit. In particular, when coil P4 is used with a high number of turns and push/pull mode for upper/lower large errors occur. Further errors are introduced in both loops by the change in shape of the TF coils when energized. Concentrated efforts can eliminate all errors to much better than 0.5 MJ stored energy.

For the pumped divertor phase, the flux surfaces in the divertor region need to be defined accurately to correlate measurements in the SOL of the core with those in the divertor. Therefore, two poloidal sets of 11 tangential and 11 normal pick-up coils will be mounted in the divertor structure. Just under the divertor module, 11 saddle loops will measure the flux near the poloidal position of the pick-up coils. The loops span about 90° in toroidal direction and are mounted on the divertor coil casings. In additon, the tangential coils are designed to measure MHD fluctuations with moderate frequency response.

It proved necessary to supplement the original set of flux loops and pick-up coils by new coils close to the new plasma boundary to make the magnetic equilibrium codes more accurate. Two sets of seven extra coils are planned on the poloidal limiters and several other coils at strategic positions. These coils are based on a ceramic coil carrier and have a frequency response to 0.5MHz. They are supplemented by a toroidal set of 16 coils to allow a detailed analysis of high frequency, high m and, n MHD modes.

Plasma Boundary Probes

The number of single element Langmuir probes in the vessel of JET has been increased from 23 to 46 during the 1991 campaign. Two poloidal arrays were built in the carbon upper (12 probes) and in the Beryllium lower (16 probes) divertor targets as well as in the belt limiters (10 probes), ICRF (4 probes) and LH (4 probes) antennae protection tiles. Single element probes in the upper (C) and lower (Be) targets were originally designed to offer a well defined collector area. (see Fig 48(a): domed tip probe). This design has worked well but probes in high heat load areas were progressively destroyed. Additionally, the probes in this campaign showed, in many cases, very large saturation currents I_{sat}, exceeding the capacity of the power supplies. Several steps were taken to improve the situation. Firstly, a new switched mode high current power supply was successfully employed (feeding a number of probes in parallel). Secondly, probes in the Be target were changed to a smaller collecting area in order to bring the heat load down and reduce the maximum total current - (see Fig. 48(b), conical tip probe). In the carbon target, where all tiles were replaced the probe design was changed to reduce the surface area even further and also include a labyrinth to shield the insulators from carbon deposits (see Fig. 48(c)). The new probe surfaces are more prone to errors due to misalignment particularly in the carbon target and the effective surface areas had to be reassessed.

However, the probe performance, with respect to heavy erosion due to extreme heat load, has not improved significantly. Nevertheless, a great deal of useful information has been obtained, both on the hardware and on the software side, from the operations of the divertor probes in plasmas conditions similar to those envisaged for the pumped divertor. This information is being used on the design for the probes in the targets of the pumped divertor.

The basic set of Langmuir probes in the divertor target is designed to give plasma parameters of the configurations which are swept across the target. Two sets of 11 probes are located near the positions of the magnetic measurements. The probes have a body of larger cross-section than the collection area in order to form a heat sink. They fit into holders located between the target elements. In order to cope with divertor plasmas with ELMy H-modes and possible stationary plasma configurations, an array of triple probes

has been proposed giving a time resolved measurement of plasma parameters at 45 poloidal positions simultaneously.

The long stroke (25 cm) fast scanning probe has operated according to expectation. About 100 diverted discharges with additional heating were explored and the long stroke has made it possible to reach the last closed flux surface (LCFS) in diverted discharges in almost all cases. The probe body made from 4D CFC and the carbon electrodes have survived without damage. Control of the depth of the stroke by means of timed gas pulses was very reproducible and easy to achieve. An example of the movements is shown in Fig. 49 with different depth during different phases of the discharge. This probe will also be used during the pumped divertor phase and will supplement measurements taken by the active Li-beam diagnostic which is at the same poloidal position.

Both the Fast Transfer System and Plasma Boundary Probe system on Octant No: 1 have been used to expose collector probes. Among the subjects studied are the efficiency of the beryllium evaporation and the nature of the escaping fast He ions from the core. Particularly important was the exposure of a stationary probe during the preliminary tritium experiment (PTE) from which the tritium coverage of the first wall could be deduced. The Surface Analysis Station has been mothballed during this year due to a shortage of staff effort. However, analysis continued on a contract basis. The Plasma Boundary Probe System will be retained for the pumped divertor phase.

Following a Workshop on Diagnostics for the Pumped Divertor for JET, preliminary studies have been started on several methods to measure erosion/deposition on the target plate on a shot-by-shot basis. The net erosion of the target material in the strike zones is one of the most uncertain elements in the design of the divertor plates. The methods under investigation are: remote monitoring of local radioactive isotope content; ellipsometry; interference fringes and speckle interferometry.

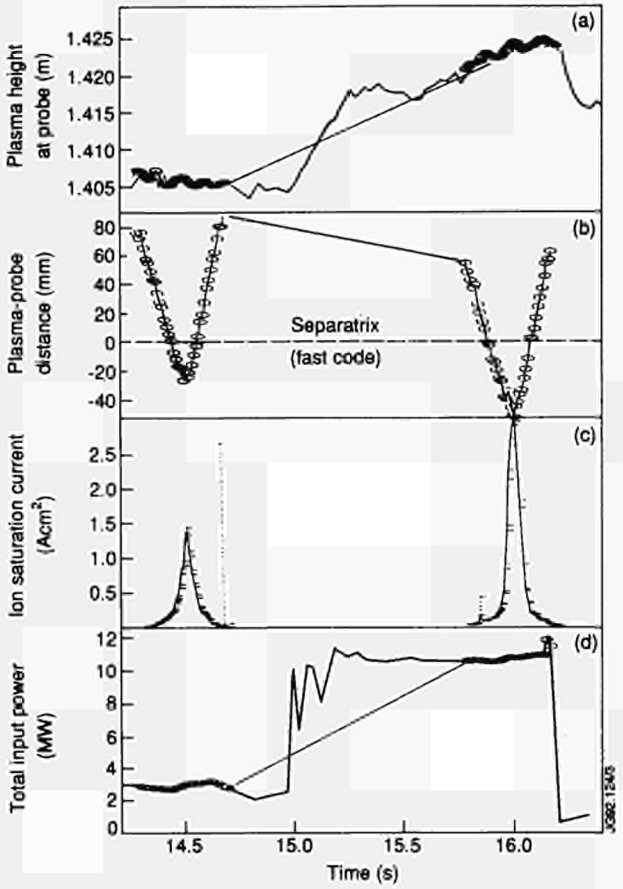

Fig. 49: Data obtained with the fast moving probe during a 3MA/ 2.8T discharge, heated with NBI up to 12MW (curved) during the ohmic phase (14.5 s) and the H-mode phase (16.0 s). According to the magnetic equilibrium code FAST, the probe was crossing the separatrix by 27 and 52 mm, respectively (curve b), and the particle fluxes (Acm^{-2}) are shown in graph (c). The boundary plasma position at the time of the measurements is shown in (a) with respect to the equatorial plane of the machine.

Limiter Observations

CCD cameras equipped with filter carousels (CI, CII, CIII, OII, BeI, BeII, and H_α/D_α) have been extensively used to observe general discharge behaviour and more importantly to assess the loading of the Carbon and Beryllium targets.

Camera observations of the new X-point targets shows that both upper and lower targets had been well aligned and poloidal contours of impurity influxes and hydrogen recycling have been obtained from the video images. These poloidal contours are thought to be representative of the overall interaction with the target neglecting the few hot spots. The profiles, calibrated in photon flux, have been made generally available.

In the course of the PTE experiment, substantial neutron interference on the CCD camera was evident to such an extent that during the period of maximum neutron yield complete picture saturation occurred.

The first experiments with an automatic aperture adjusted camera were successfully concluded. This technique extends the dynamic range of the camera significantly but is not yet suitable for immediate assessment of data as is required for operations. The Peltier cooled prototype of the Cd-Hg-Te IR array with 32 x 32 pixels has produced preliminary results of temperature measurements of the

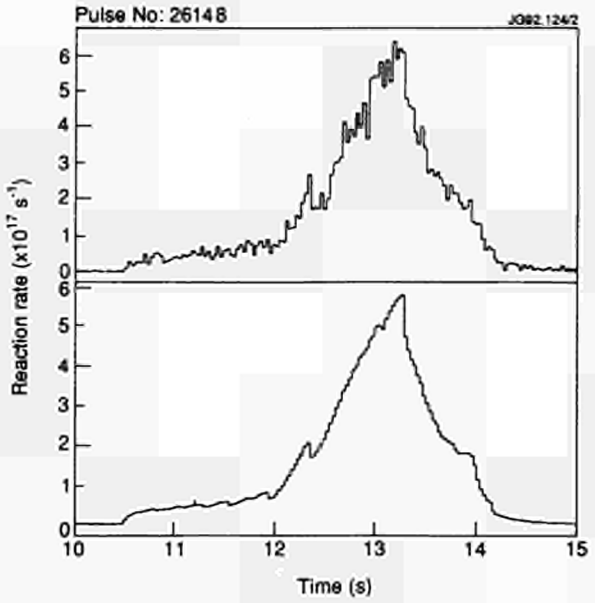

Fig. 50:Time-traces from silicon diode (upper) and from fission chambers (lower) for the D-T discharge Pulse No: 26148

Carbon target. The device has reliably operated on the machine since Autumn 1991. A high resolution cooled IR array and improved CCD/CID cameras are under investigation for use during the pumped divertor phase.

In-Vessel Pressure Gauges

Pressure gauges, used in 1990 and damaged by an air leak during operation were replaced in 1991 by a new set of four. However, electrical short circuits probably by contact between the conductor of beaded in-vessel cables and the vessel earth, possibly caused by material expansion at the operating temperature of 600°K, prevented operation. This fault was symptomatic with all gauges and it was therefore decided that a complete different type of cables (mineral insulated) would be used in the future. For the pump divertor phase the design of the pressure gauges was reviewed and changes will be made (all electrodes on an integral ceramic plate rather than insulation by separate ceramic rings only) so that electrical short-circuits can be eliminated and that the mechanical strength is improved. Three sets of five gauges, seperated 90° toroidally, will be mounted under the target structure, with short tubes connecting them to the surface of the target.

Active Lithium Beam Edge Diagnostic

A feasibility study of a Li-beam diagnostic for JET was successfully completed. It is proposed to inject a neutral Li-beam at 50keV from the top of the machine. Estimates of beam divergence and intensity in relation to the photon collection efficiency of the telescope system indicate a spatial resolution of 5 mm as compared to a density gradient length of 20mm and a time resolution for density profiles of about 1 ms. Based on this study the decision was taken to build this diagnostic.

Neutron Flux Measurements

The strength of the 2.5 MeV neutron emission from JET plasmas formed with deuterium fuel is measured with pairs of fission chambers positioned near three of the main horizontal ports of the machine. Each pair comprises a ^{235}U chamber for low neutron yields and a ^{238}U chamber for high yields. The two discharges of the main Preliminary Tritium Experiment, Pulse Nos: 26147 and 26148, were initially formed in deuterium but were heated with 14 Positive Ion Neutral Injectors (PINI's) injecting deuterium and 2 PINI's injecting tritium. In these discharges, the 14 MeV neutron emission was about 30 times the strength of the 2.5 MeV neutron emission, with a peak intensity of 6 x $10^{17}s^{-1}$ (1.7 MW). These discharges provided the first opportunity to test the fission chambers with 14 MeV neutrons. In particular, the ^{235}U fission chambers were operated close to the limit of their associated electronic equipment; this was not the case for the ^{238}U fission chambers as these are 6000 times less sensitive. The fission chambers were calibrated retrospectively against activation measurements, as described below.

Since the fission chambers cannot discriminate between 2.5 and 14 MeV neutrons, the 14 MeV neutron emission had to be recorded separately using several silicon diodes positioned strategically to cover the anticipated intensity range. These diodes [1] provide an effective energy threshold of about 8MeV; these were calibrated against activation measurements prior to the main discharges.

Fig.50 shows time-traces of the neutron emission for Pulse No: 26148 as recorded with the least sensitive of the silicon diodes and with the ^{235}U fission chambers. Detailed neutron transport calculations have predicted that the ^{235}U fission chambers should be only slightly more efficient (x 1.09) for 14MeV neutrons than for 2.5MeV neutrons. However, the ^{238}U fission chambers should be 2.05 times more efficient when recording fission events (i.e. in counting mode). These figures were confirmed experimentally. For count-rates in excess of 1MHz, the neutron emission must be deduced from the average ionization level instead of by analyzing individual pulses. Rather surprisingly, the ^{238}U fission chambers when operated in this way (i.e. in current mode) show the same increase in efficiency as the ^{235}U

fission chambers, indicating that the recorded current is mostly generated by gamma-radiation from neutron capture events in the leak shield surrounding the chamber. In principle, the combination of the ^{235}U fission chambers (in counting or current mode) and of the ^{238}U fission chambers (in counting mode) can be exploited directly to obtain the ratio of 14 to 2.5 MeV neutron emission strengths for the range of ratios between 0.1 and 3.

Activation Measurements

The fission chambers and silicon diodes must be calibrated through measurements of induced radioactivity in suitable materials. The preferred method for measuring the 2.5 MeV neutron emission is delayed-neutron counting from thorium samples placed inside the vacuum vessel for the duration of a single discharge. The delayed-neutron detectors have been accurately calibrated through measurements in a standard neutron spectrum at the BR1 Research Reactor, in Belgium. For 14 MeV neutrons, the preferred method employs small samples of silicon, exploiting the $^{28}Si(n,p)^{28}Al$ reaction, for which the effective reaction threshold is about 5 MeV. The special attraction of both materials, thorium and silicon, lies in their short decay half-lives which permit the samples to be recycled between discharges. Cross-calibration with longer-lived activities using standard dosimetry materials is important for the silicon reaction, since the silicon reaction cross-sections are not well known. Such measurements have shown that the silicon cross-sections adopted in this work are indeed compatible with the accepted cross-sections for the $^{63}Cu(n,2n)^{62}Cu$ reaction, resolving a reported discrepancy [2].

The delayed-neutron method has not been independently standardized for use with 14 MeV neutrons. However, data on the contributing delayed-neutron precursors have now been obtained from a careful study of the literature [3], so that the efficiency of the technique for 14 MeV neutron emission can be established from first principles. The estimated accuracy of the delayed-neutron measurement technique for D-T plasmas is ± 15%. When applied to the two tritium discharges, the delayed neutron counting method provided yields of 14 MeV neutrons that were only 4% below those obtained using the conventional activation methods. Using this result, the delayed-neutron method can now be used for accurate (±7%) measurements of the D-T neutron yields during the final phase of JET operations. This technique is attractive because of its simplicity and wide dynamic range.

Activation measurements are converted into neutron yields through the mediation of extensive neutron transport calculations using ray-tracing in addition to the conventional Monte Carlo approach [4]. These calculations should be highly accurate provided the essential features of the tokamak are correctly modelled. The task of modelling the machine is greatly simplified by use of irradiation positions inside the vacuum vessel, such that the irradiated material has a view of the plasma that is unobstructed by vacuum vessel walls or other plasma facing components. An overall accuracy of ±7% is claimed. Combining the experimental and computational results permitted the fusion performance of the two main tritium discharges to be calculated to an accuracy of±7% (see Scientific Aspects of PTE).

Neutron Spectrometry

The time-of-flight 2.5 MeV neutron spectrometer was rebuilt during the 1990/91 shutdown. The new spectrometer incorporates much of the equipment delivered as part of the 14 MeV neutron spectrometer intended for use during the

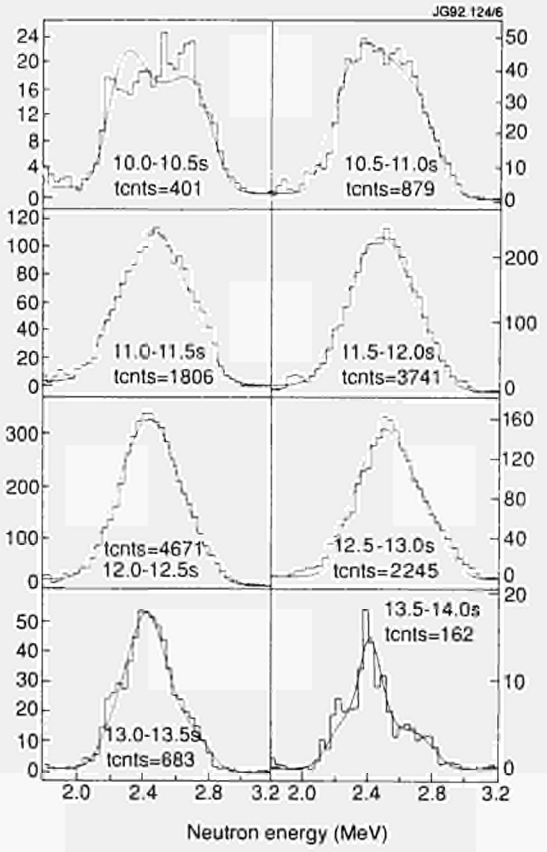

Fig. 51: A series of neutron energy spectra obtained with the time-of-flight spectrometer showing how the spectrum shape for a deuterium beam-heated discharge varies with time after heating is applied. Analysis of such discharges allows determination of the time dependence of axial plasma temperature despite strong interference from beam-plasma neutron emission.

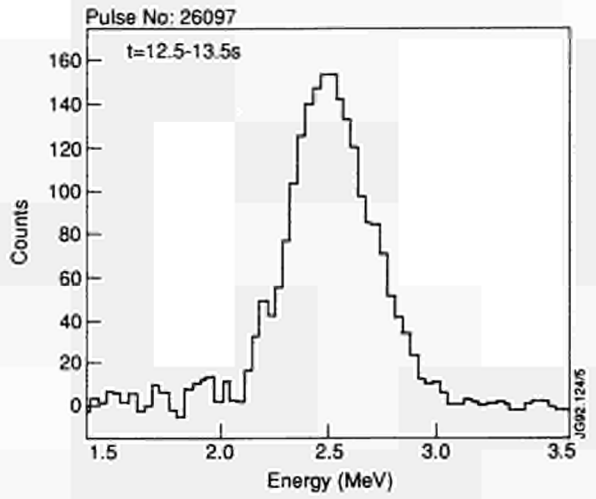

Fig.52: Showing the neutron energy spectrum in the region of 2.5 MeV for a discharge during which one PINI was fuelled with a 1% admixture of tritium. The 2.5 and 14 MeV neutron fluxes were of comparable strength but the selection criteria set on the detector electronics were such as to effectively exclude contamination from the 14MeV neutrons. For the 100% admixture discharges, the detector signal rates were excessive so that the electronics saturated.

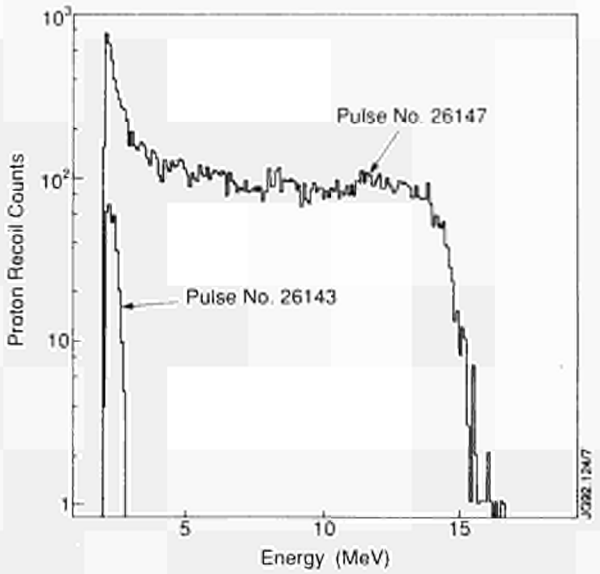

Fig.53: Proton recoil spectra measured with the liquid scintillator neutron spectrometer for D-D Pulse No: 26143 and D-T Pulse No: 26147. Mono-energetic neutrons produce flat proton recoil energy spectra. The change in neutron energy and forty-fold increase in intensity can be seen. The neutron spectra can be recovered by differentiating the proton spectra.

final D-T phase of JET operations. It retains the energy resolution of the former spectrometer (120keV) but has about 6 times greater detection efficiency. This increase is critical because it permits high quality neutron energy spectra to be acquired on a time-scale of down to 200ms (for the highest intensity D-D discharges), compared with 1s previously. Since JET rarely sustains high neutron emission strengths for as long as one second, the improvement is obvious. The time evolution of the neutron energy spectra can now be studied, as illustrated in Fig.51. The first example shows the spectrum due to beam injection into a cold plasma (beam-plasma reaction dominated); the subsequent spectra are obtained as the plasma is heated to its peak temperature so that the thermal reaction contribution becomes important. Finally, an impurity influx takes place and the beam power is reduced, so that the separate thermal and beam-plasma contributions are seen. By taking advantage of such sequences of spectra, the maximum plasma temperature attained can be estimated, whereas analysis of the single high-temperature spectrum on its own can only provide an upper limit on the peak temperature.

It had been hoped that the time-of-flight neutron spectrometer would provide a measurement of the 2.5 MeV neutron yield in the presence of a much stronger flux of 14MeV neutrons, so that the deuteron to triton fuelling density ratio could be deduced. Such spectra were successfully recorded when 1% of tritium was used in the deuterium gas feed to the "tritium" PINI's. The resulting energy spectrum, Fig.52, is little affected by the 14 MeV neutrons, despite their comparable intensities. However, during the full tritium experiment, the radiation background in the Roof Laboratory was far too high for satisfactory operation of the instrument. The floor loading limit in the Roof Laboratory precludes the addition of sufficient extra shielding to permit this diagnostic to operate during full D-T discharges.

A simple (moderate energy resolution) liquid scintillator neutron spectrometer was placed above the time-of-flight spectrometer during the tritium experiment. The resulting proton recoil pulse-height spectrum is shown in Fig.53, which is compared with the spectrum obtained with 2.5MeV neutrons during an earlier discharge of the same type but lacking in tritium injection. The considerable increase in neutron flux and change from 2.5 to 14MeV neutrons are obvious. Neutron energy spectra can be recovered from the proton recoil spectra by the simple differentiation.

Neutron Emission Profiles

During the 1990/91 shutdown, the pulse-processing and data-acquisition system of the neutron profile monitor was effectively doubled so that 2.5 and 14 MeV neutron measurements could be made independently. The motivation for this upgrade was originally to permit the burn-up of the 1MeV tritons emitted during high yield deuterium discharges to be studied, but proved most opportune for the

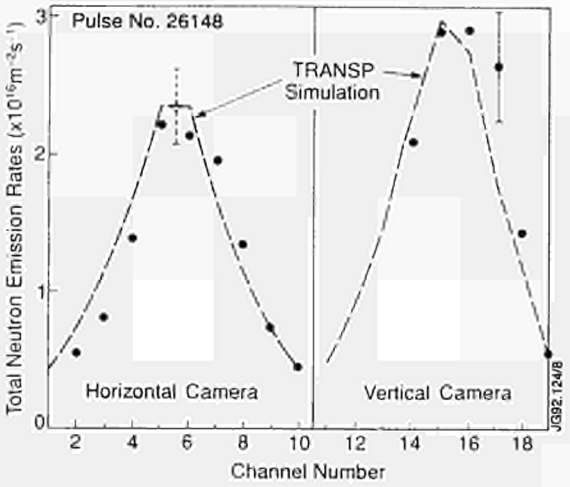

Fig. 54: Comparing the line-integrated neutron emission measured with the neutron profile monitor at peak emission rate for D-T Pulse No: 26148 with predictions of the TRANSP simulation code. The overall agreement is satisfactory.

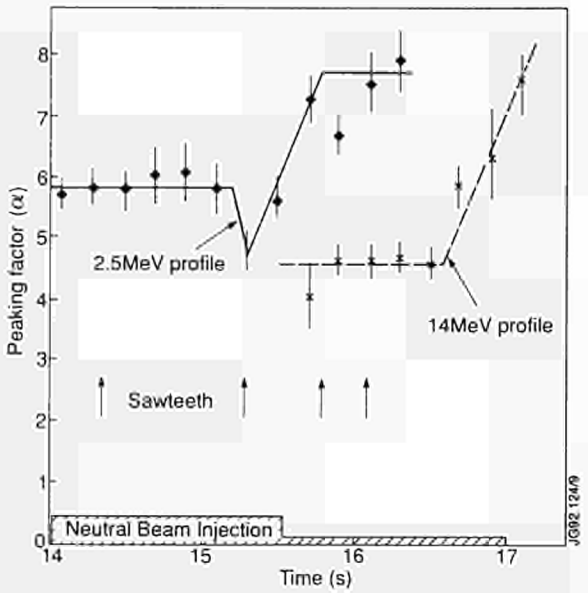

Fig. 55: Profile peaking factors for 2.5 and 14MeV neutrons obtained with the neutron profile monitor for a discharge with 12 MW NBI. The effective slowing down time for 1.01MeV tritons is about 1.4s for times between 14.5 and 16.5s.

study of the discharges of the Preliminary Tritium Experiment. The instrument performed well for the 1% discharges, for which separate 2.5 and 14MeV neutron emission profiles were obtained and the 2.5 and 14MeV counting rates were of similar magnitude. For the 100% discharges, the collimation channels were reduced in aperture with suitable collimator inserts to prevent the electronics from being overloaded. The results were satisfactory, considering that the profile monitor was required to operate so close to the limit of its capability. The present type of detector (liquid scintillator) is unsuitable for power levels in excess of 2MW.

Fig.54 compares the line-integrated neutron measurements obtained at the peak of the 100% tritium Pulse No: 26148 with the prediction from the code TRANSP. Through iteration on some of the plasma parameters, the total neutron emission from TRANSP has been adjusted to agree with the neutron emission strength measured with the fission chambers. The total emission obtained by integration over the experimental profiles was adjusted in a similar manner. The relative displacement of the two sets of profiles is attributed to the approximate nature of the calculation of flux surface positions used in TRANSP. Analysis of the 1% discharges will be more challenging as, for these, both 2.5 and 14 MeV neutron profiles have been determined.

Triton Burnup Studies

The 14 MeV neutron emission from the burnup of tritons produced in D-D fusion reactions has been extensively studied in recent years. The results are found to agree well with the predictions of standard theory for normal discharges but anomalous losses are apparent for discharges in which the triton slowing down time is long (up to 2s); these losses have previously been attributed either to triton diffusion, with diffusion coefficients of about $0.1 m^2 s^{-1}$, or to charge-exchange effects. However, the availability of 14MeV neutron emissivity profiles has shown that the triton diffusion coefficient must be much smaller than $0.1 m^2 s^{-1}$ and may be compatible with the classical value. This is illustrated in Fig 55, which shows the behaviour of the radial profile peaking factors for 2.5 and 14 MeV neutrons for a NBI-heated discharge after the NBI heating is suddenly reduced (at 15.5s). The 14 MeV profile follows closely the peaking of the 2.5 MeV profile which occurs at beam switch-off, but only after a time corresponding to that required for the 1 MeV tritons to slow down to their peak reactivity at about 200 keV. There is also no broadening of the 14 MeV profile with time. This discharge has an unusually long triton slowing down time and was run prior to the enhancement of the data-acquisition system so that the 14 MeV neutron profile could not be studied during the main period of beam heating. This restriction has now been removed. Now, the 14 MeV profile is very broad, almost flat, immediately following beam switch-on but that it rapidly adopts a very similar profile to that of the 2.5 MeV neutrons; the only additional feature is that whilst both profiles flatten at a sawtooth crash, the 14 MeV profile recovers much more slowly - showing that the displaced tritons remain on the flux surfaces to which they are moved and that the profile only recovers because of the production of new tritons.

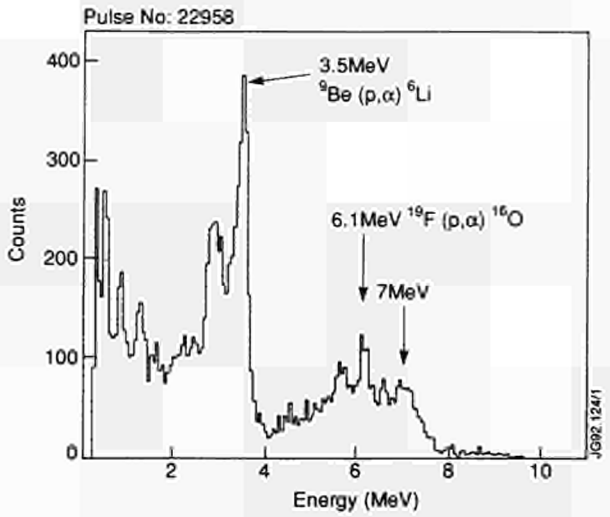

Fig. 56: Showing the gamma-ray energy spectrum obtained with a NaI(Tl) scintillation detector positioned above the time-of-flight neutron spectrometer. The spectrum shows the presence of flourine, caused by a leak in a vacuum seal between the vacuum vessel and a region containing SF6.

Gamma-ray Measurements

The study of gamma-ray emission from the plasma depends upon the presence of an appreciable component of fast ions with sufficient energy to produce observable numbers of fusion or nuclear reactions with fuel and impurity ions. The observation of identifiable gamma-ray lines provides information on the fast ion density/energy distribution and also on the impurity ion density. As reported previously [5], observation of the 16 MeV gamma-rays from 3He-D fusion reactions produced by high-power ICRF heating has shown that 140kW of fusion energy, mostly in the form of fast charged particles, has been generated. These studies have not been pursued recently because of the contamination of the desired signal with gamma-rays from nuclear reactions between the ^{3}He ions and beryllium impurity ions. The Preliminary Tritium Experiment offered the first opportunity for measuring the 16 MeV gamma-rays from the mirror reaction ^{3}H-D, which was expected to be a strong signal considering the record fusion power of 1.8MW. However, no 16 MeV gamma-rays were observed. Even more surprising was the failure to observe the 4.4 MeV gamma-rays from α-^{9}Be reactions induced by the 400 kW of 3.5 MeV alpha particles. The most probable explanation is that the experimental arrangement was far from ideal, as there was no dedicated line-of-sight available and no local radiation sheilding was provided against the very high level of the neutron-induced gamma-radiation background in the Roof Laboratory experienced with these D-T discharges.

In spite of the negative results reported above, some interesting observations of plasma impurities have been made. For example, gamma-radiation from flourine was observed (Fig.56); this proved to be associated with a leaking vacuum seal which permit SF6 to enter the plasma. In addition, the 7s half-life decay of ^{16}N has been observed, resulting from the activation of ^{16}O. Such results demonstrate the power of this diagnostic, which could be appreciably enhanced if a dedicated line-of-sight were available

Electron Cyclotron Emission (ECE) System

The three instruments in the ECE measurement system, the Michelson interferometer, the grating polychromator and the heterodyne radiometer, continue to provide electron temperature data on almost all JET pulses. Although the Michelson interferometer has only moderate spatial and temporal resolution (~15 cm and ~15 ms, respectively), it provides several hundred absolutely calibrated temperature profiles on all plasma pulses with toroidal field above 1.5 T. These temperature profiles are used routinely to cross-calibrate the temperatures measured by the fast, multi-channel instruments (a 12-channel grating polychromator and a 44-channel heterodyne radiometer), which are difficult to calibrate with black-body sources. This permits a detailed study of the time evolution of the absolute electron temperature at many fixed radii in the plasma, with both good spatial resolution (~ 6cm for the polychromator and ~3cm for the radiometer) and temporal resolution ~10ms.

The absolute response of the complete Michelson/waveguide/antenna system was re-measured during the shutdown in early 1991 using the beryllium compatible high-temperature black-body source mounted in front of the antenna, in the vacuum vessel. Subsequent comparisons with the plasma electron temperatures measured by the LIDAR Thomson scattering diagnostic continue to show agreement within the estimated absolute uncertainty of ±10%.

The polychromator time resolution is limited by its detector speed and by signal-to-noise ratio considerations. However, the radiometer, has been limited by the speed of the data acquisition and the signal electronics. As part of a collaboration with the Massachusetts Institute of Technology, USA, a fast stand-alone data acquisition has been constructed for the radiometer to allow the study of high frequency fluctuations in the ECE signals caused by ballooning modes in high beta plasmas. The new acquisition

system allows sampling of up to 128,000 data points for each of eight radiometer channels at rates up to 1 MHz. With very large signal bandwidths, the signal-to-noise ratio of the measurement is limited by the photon statistical noise inherent to black-body radiation. Therefore, small temperature fluctuations may not be visible in the data from a single channel, so software is being developed to perform a correlation analysis on the data from a number of channels. This should considerably enhance the capability of detecting coherent fluctuations which have a radial extent covering two or more channels. Fig.57 is an example of this technique. It shows the result of applying the software to data from 36 radiometer channels on a discharge exhibiting some low m-number MHD activity. The cross-coherence between each pair of radiometer channels has been calculated, and the resulting two dimensional grid plotted as contours with major radius on both axes.

The codes developed by CNR-Milan, Italy, for the simulation of non-thermal ECE spectra have been applied to the interpretation of spectra measured during LHCD experiments. Using data from the fast electron bremsstrahlung (FEB) camera to constrain the spatial localization and parallel energy of the fast electrons, and estimating the suprathermal density from the measured non-inductive plasma current, it has been possible to iterate on the perpendicular temperature to obtain ECE spectra which fit those measured. An example for a pulse with full LH current drive (375 kA from 2 MW LH power) is shown in Fig.58. In this case the FEB camera indicates that the current channel is peaked on axis ($r < 0.6$ m) and the mean parallel energy is ~115keV. The model ECE spectra fit the measurements when a perpendicular temperature of 23keV and density of 1.4×10^{-3} of the bulk plasma are used.

Microwave Transmission Interferometry and Reflectometry

Difficulties were experienced on many JET pulses with the operation of the single channel microwave transmission interferometer due to cut-off and refraction effects arising from high values of the electron density. It will not be possible to use the system during the pumped divertor phase of JET operation due to its vertical line-of-sight and so, in July 1991, it was decided to stop operating the system. The far-infrared multichannel interferometer operated reliably throughout the year and so the loss of measurement capability was not serious.

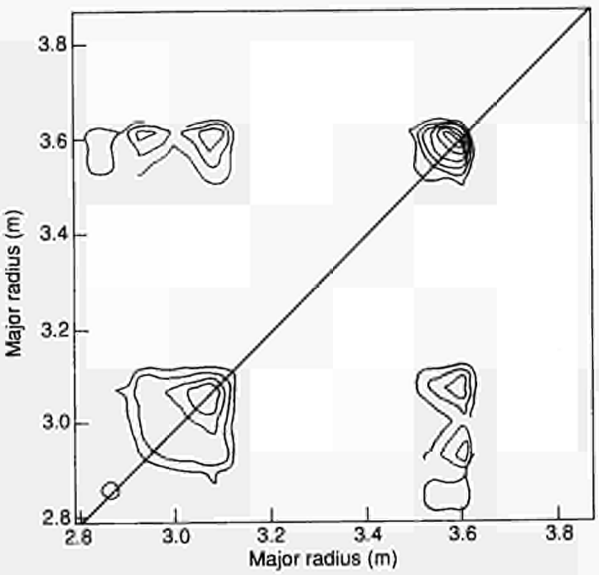

Fig. 57 Example of cross-coherence (>0.4) between pairs of the ECE heterodyne radiometer channels on a discharge exhibiting low m,n number MHD activity. The plot shows that the modes are localized at R ~ 3.06m (q=1) and R ~ 3.56m (q=2) and that there is significant coupling between them.

The multichannel reflectometer probes the JET plasma along a major radius in the mid-plane with electromagnetic radiation propagating in the ordinary mode through the plasma. The instrument has twelve channels covering the frequency range 18.6 - 80 GHz and so potentially can probe electron densities in the range 4×10^{18} - $8 \times 10^{19} m^{-3}$. In practice, the attenuation in the transmission system at the highest frequency is too high to permit routine operation and so the highest density probed is normally $7 \times 10^{19} m^{-3}$. The instrument can be operated with the source frequencies periodically swept, to measure the electron density profile, or with the probing frequencies fixed to measure relative fast movements of the different density layers.

Further improvements were made to the instrument during 1991. More sensitive fringe counters with a resolution of 0.01 fringe were developed and fitted by the FOM Laboratory, Netherlands. Use of these units improves the accuracy of the phase measurements and, in particular, the reference measurements made to the inner wall of the torus, which are used in deriving density profiles. The intermediate frequency amplifiers, which amplify the signals derived directly from the detectors, were adjusted individually to provide optimum gain for each channel and, therefore, the maximum possible dynamic range. Parts of the electronic circuits have been modified to allow the simultaneous recording of fringe counter data and signals derived from the homodyne section of the detection system. Thus, it is now possible

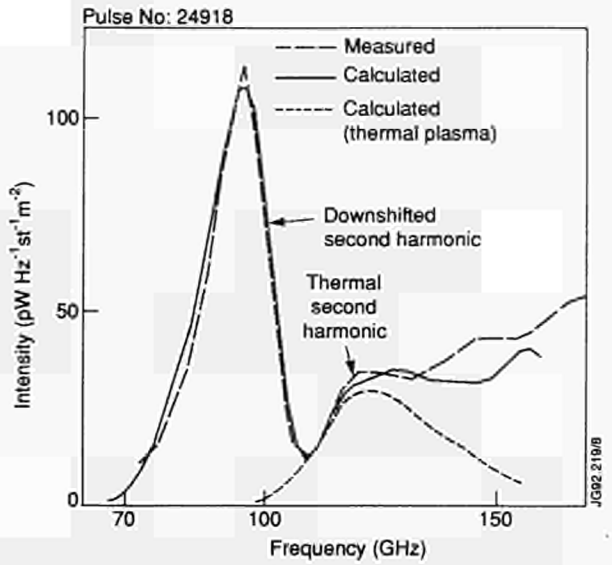

Fig. 58: Measured and calculated ECE spectra with LHCD. The suprathermal populations are modelled with a perpendicular temperature of 23keV and density of 1.4×10^{-3} of the bulk value. The calculated thermal spectrum corresponding to the bulk plasma temperature is shown for comparison.

to study density fluctuations at the same time as measuring the density profile.

Analysis techniques have been further developed in which only the change in phase between sample times on the fringe counters are utilized. This technique makes the detection of erroneous fringe jumps, and therefore their elimination, much easier. New software is also being developed to detect fringe jumps through the use of bit masks and to use the evolution of the fixed frequency signals, recorded between sweeps, to carry out consistency

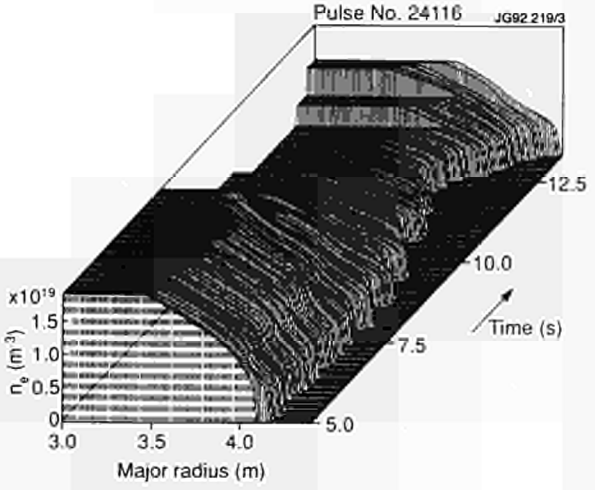

Fig. 59: Edge density profiles measured with the multichannel reflectometer on a pulse in which the density is decreased and then increased by gas puffing.

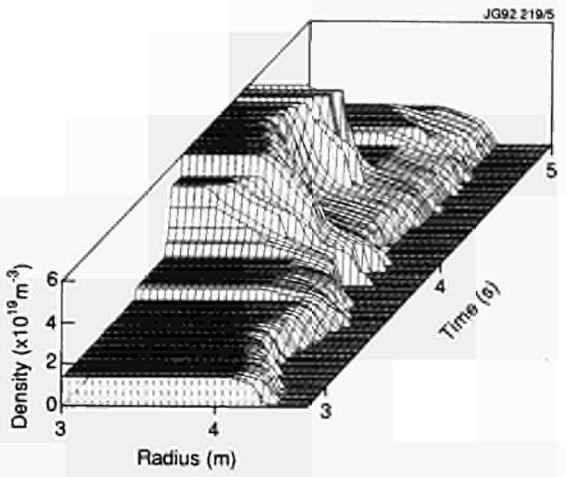

Fig. 60: Edge density profiles measured with multichannel reflectometer on a pulse in with a pellet injected at t = 3.8s.

checks on the changes observed in the electron density profiles, which arebeen derived from the swept frequency data.

These improvements have meant that as many as 400 density profiles of the outer region of the plasma are now frequently obtained on individual JET pulses. An example of measured profiles is shown in Fig.59. Good agreement is generally found with density profiles measured with the LIDAR diagnostic. The reflectometer profiles complement those obtained with the transmission interferometer and with probes. They are used in a wide range of studies, particularly studies of edge related phenomena. Dramatic changes in the profiles are observed (Fig.60) as a result of pellet injection, although the time response of the system is not adequate to make measurements during the injection process itself. Data recorded on plasma fluctuation have been used in studies of ELM's. The power spectra of the measured fluctuations show enhanced levels over the frequency band 5 - 100kHz during an ELM (Fig.61).

The work on correlation reflectometry has continued. A full-wave 1-D model of a radial viewing correlation reflectometer has been developed. In the model, density fluctuations are simulated by a set of wavelets of finite spatial extent. The radial position, amplitude, correlation length and wavenumber of the fluctuations can be varied. For random fluctuations distributed throughout the plasma, the model predicts that significant coherence would be measured, even for large interlayer separations, due to the effect of the common propagation region. However, under ohmic and H mode conditions very low levels of coherence are observed even for small (< 4mm) interlayer separations.

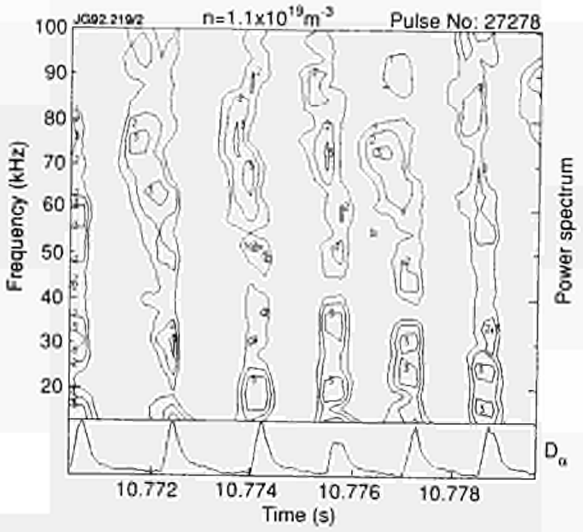

Fig.61: Contour plot of power spectrum of fluctuating reflectometer signal for the channel probing n_e = 1.1x10^{19}m^{-3}, with ELMs present. The D_α signal is shown for comparison. The fluctuation level is enhanced at the time of the ELMs.

A possible explanation for the discrepancy is that experimentally at least two dimensions are important whereas in the model only one is considered. Further work on the modelling is in progress.

Towards the end of the year a toroidal correlation reflectometer was assembled. The device utilizes one channel (29 or 34GHz) of the multichannel system and a second reflectometer operating at the same frequency on one of the ECE viewing antennas but separated toroidally by 155mm. The probing radiation is in the ordinary mode. Preliminary results suggest that under ohmic conditions the correlation level between the reflectometers is low but under H-mode and L-mode conditions the coherence is significant. Also, the cross-phase increases with frequency suggesting that the observed density perturbations are propagating toroidally. Further measurements and analysis are in progress.

Measurements have been obtained with the simple 'comb' reflectometer which operates at 27, 40, 60 and 90 GHz in the ordinary mode and probes the upper X-point region. The maximum frequency in reflection is determined by observing the level of fluctuations - these are substantially enhanced for those channels in reflection - and thereby an estimate of the density in the X-point region is determined. A typical result is shown in Fig.62. In general, the results look promising although under some conditions enhanced fluctuations are observed even when the density cannot be sufficient for the channels to be in reflection.

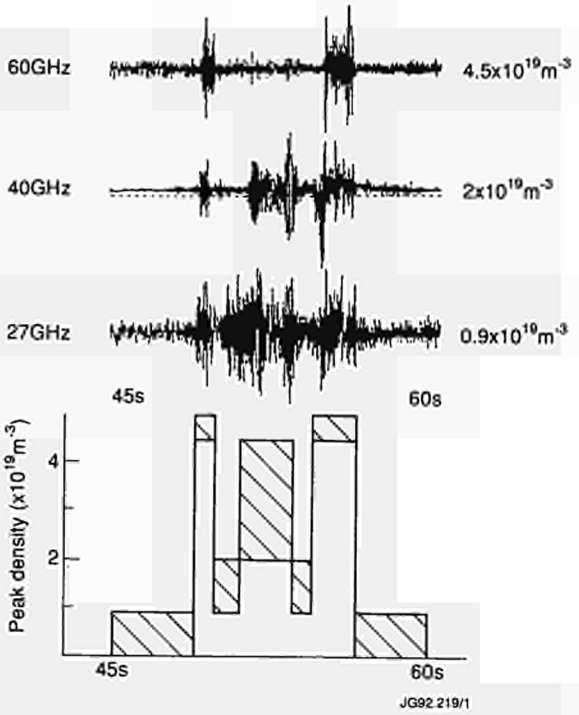

Fig. 62: Typical data obtained with a simple 'comb' type reflectometer probing the X-point region. The deduced time history of the peak density in the line-of-sight is also shown.

Thomson Scattering

The work on the main Thomson scattering systems has concentrated in three areas:

i) routine operation of the existing (up to ~ 1Hz) LIDAR system (full profile R = 2. 1 - 4.5 m);

ii) commissioning of the higher spatial resolution LIDAR system (radial extent ~ 75 cm);

iii) operation of the original laser of the single point scattering system for: (a) laser ablation measurements, and (b) q-profile scattering system commissioning.

In addition, a new LIDAR scattering system for the divertor region has been designed.

The main LIDAR scattering system has operated throughout the year with high reliability, producing full profiles of electron temperature, density and pressure for most pulses. An improvement in the long term reliability of the density calibration has been achieved by carrying out in-site window cleaning of the inside of the vacuum windows. The large collection windows are protected by mechanical shutters from the build up of deposits during glow cleaning and beryllium evaporation. However, a gradual build up of a coating slowly reduces transmission during long periods (months) of plasma operation. With the present mode of operation, this produces a gradual change in density as measured by the LIDAR system. This can be clearly seen on

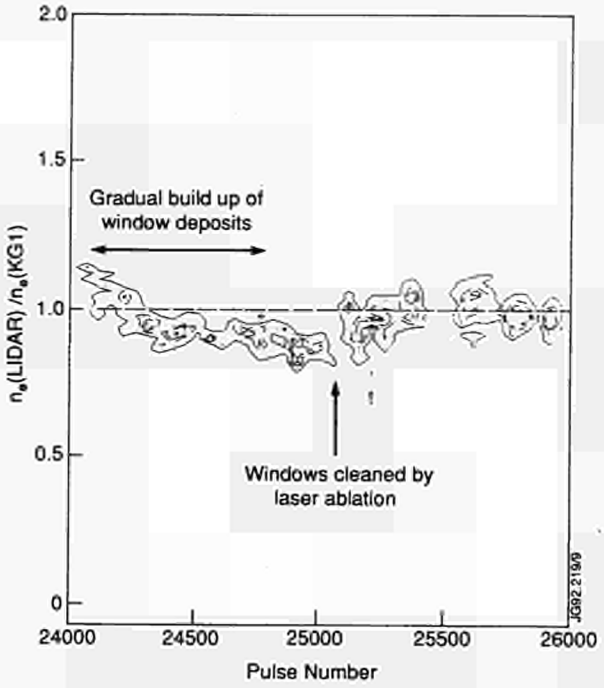

Fig. 63: Comparison of line integral density data measured with the multichannel interferometer and the LIDAR system showing the effect of the build-up of deposits from plasma operation and their removal by laser ablation. The grid cell size is 0.02 x 50 discharges and the contour lines are drawn at 7, 10, 13, 16 and 19 observations per cell.

the comparison of the LIDAR and interferometer density measurements, (see Fig.63). The LIDAR window monitoring system shows that the coating is chromatically neutral, a fact confirmed by a T_e comparison with ECE measurements, which shows no effect. The windows can now be periodically cleaned by laser ablation of the internal surface coating. The LIDAR laser is remotely steered to a point on one of the collection windows and a series of nine pulses, each of a few joules energy is fired, cleaning a 10cm^2 area. A computer program automatically points the laser to all areas of the collection windows. In this way, the whole window area can be cleaned in one or two commissioning shifts. The improvement is clearly seen in the density comparison data.

Despite recent set-backs, the goal of increasing the repetition rate of the LIDAR measurements has continued and a contract has been placed for the development of a 4Hz ruby laser. If this is fully successful it may also be possible to upgrade the existing laser to the same performance. This would allow LIDAR measurements at 8Hz when the laser beams are combined along the same path.

The new streak camera based detection system for the higher resolution channel of the LIDAR diagnostic has been commissioned. Scattered light received by the upper collection mirror on the concrete tower in the Torus Hall is separated from the main LIDAR collection path in the Roof Laboratory and relayed to the new three channel filter dispersion system. Three images of the scattering volume, each 2 - 3 mm in diameter and each covering a different wavelength range, are formed on the streak camera photocathode by an aspheric lens. The channel spectral widths have been chosen to give a lower temperature range than for the main LIDAR system. The camera streaks these images vertically across the anode screen at ~8 mm/ns giving a 5ns record (see Fig.64(a)). This allows a 75 cm segment of the outer plasma diameter to be observed. The combination of laser pulse width and streak camera temporal resolution gives ~5 cm for the spatial resolution of T_e and n_e along the plasma path, (Fig.64(b)). This shows the very steep gradients that can appear in the density profile during pellet injection.

The original Single Point Thomson Scattering laser has continued to be used as a source for laser ablation experiments. In addition, it has been used as the source for the continued attempts to measure the q profile by Thomson scattering. With the original fixed Fabry-Perot etalon, it

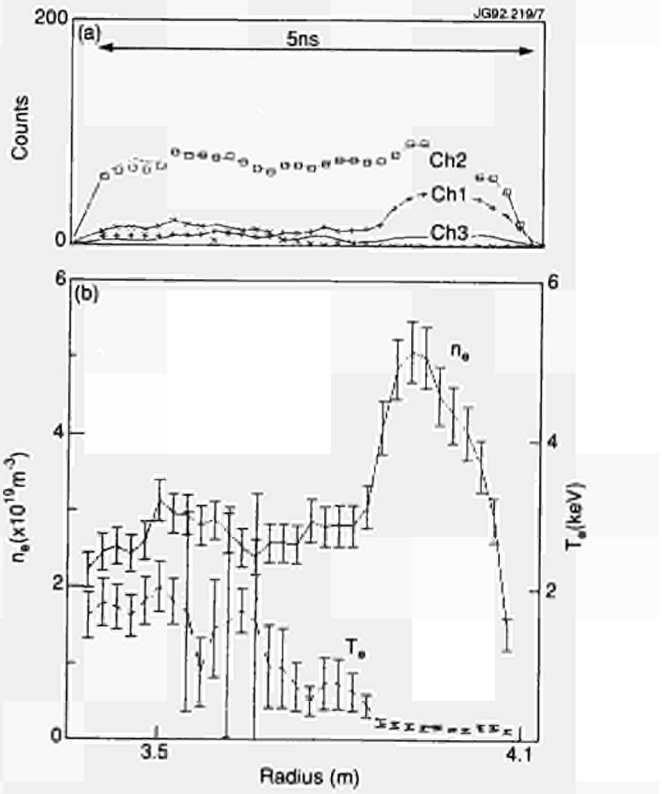

Fig. 64: Preliminary results from the Higher Resolution LIDAR system: (a) digitized streak camera signals in the three channels (continuous lines) plus the computed best fit spectral data (symbols); (b) the computed T_e and n_e profiles showing steep n_e gradient just after the pellet injection.

would have been possible to make measurements only at a specific total magnetic field. Therefore, the system was modified with an adjustable scanning Fabry-Perot system to allow measurements independent of the toroidal field.

Unavoidably, the q-profile measurement involves a very small solid angle of collection and so the scattered signal is very small. Attempts at measurements have been concentrated on discharges with pellet injection and consequently high density. In spite of this, it has not been possible to observe a resonant field enhancement. This experiment is a collaborative effort with the UKAEA, Culham Laboratory, who provided the new Fabry-Perot system.

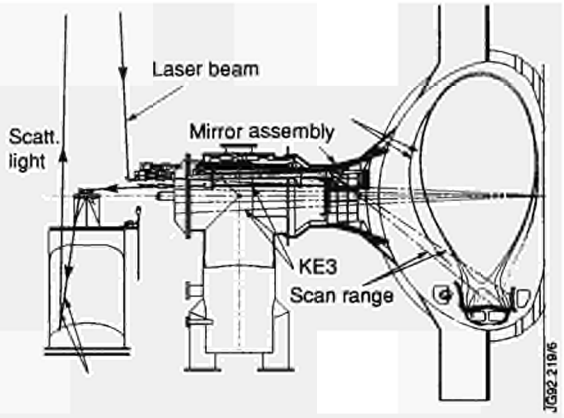

Fig. 65: Schematic of the Thomson scattering system being prepared for the measurements in the pumped divertor region.

Fast Ion and Alpha Particle Diagnostic

During 1991, all the technical systems for the initial phase of operation of this system were installed and commissioning started. The in-vessel components, including steerable launch and receive mirrors, were installed during the shutdown. The installation of the launch and receive waveguides was completed with special attention being paid to the alignment. Care was taken to ensure that the alignment was precise and insensitive to thermal expansion. Quasi-optical universal polarizers for launch and receive channels were constructed and tested, and found to perform adequately. The protection and preliminary control systems, and detection and data acqusition systems were constructed.

During the year, a collaborative agreement with the USDoE was established. Under the terms of the agreement, the DoE is loaning JET a 140 GHz, 60 kW, CW gyrotron, which operates in the TE_{03} mode and high voltage power supplies. While lower in power than the gyrotron that will eventually be used on the system (400kW), this gyrotron should be sufficient for the planned preliminary measurements. In addition, specialist staff from the Lawrence Livermore National Laboratory and the Massachusetts Institute of Technology, USA, have spent time at JET assisting with the commissioning of the system and preparation for the plasma measurements.

Supporting theoretical and numerical work has continued. Predictive and analysis codes have been further developed. In particular, the parameter range in which relativistic dielectric effects can be calculated reliably has been extended. A relativistic ray tracing code for use in regimes previously inaccessible to such codes has been developed.

A relativistic treatment of the dielectric effects is now considered indispensable for extraordinary (X) mode scattering: the latter may yield a considerably better signal to noise ratio than ordinary O-mode scattering. One problem with X-mode scattering is the increased refraction of the beams relative to O-mode. However, relativistic ray-tracing does, predict that the refraction of X-mode beams is noticeably less than that predicted with cold plasma ray-tracing.

Electron Density and Temperature Diagnostics for the Pumped Divertor

A dedicated set of diagnostics for measuring electron density and temperature in the pumped divertor plasma is being prepared. It consists of a LIDAR Thomson scattering system and an integrated microwave system.

Access to the divertor region through vertical ports will be extemely limited and so the LIDAR Thomson scattering system will probe the plasma through a main horizontal port (Octant 5) via an in-vessel mirror (Fig.65). However, this line-of-sight will have a particular advantage. Predictive codes show that the magnetic flux contours will follow approximately straight lines from the X-point region to the target plates and so the LIDAR system will measure approximately along a line of constant flux. Measurement along such a line will be useful in the assessment and optimisation of the performance of the pumped divertor. The established advantages of LIDAR, in particular the ability to discriminate against plasma background radiation because of the short sampling time, will be available.

The lasers and the detectors will be located in the Roof Laboratory. The in-vessel mirror assembly will be removable so that during service periods and shutdowns the articulated boom can access the vessel. The mirrors will be adjustable remotely through wobble stick drives fitted to the door of Octant No: 5. The drives will engage automatically when the door is closed.

The laser beam and collection optics will be scannable in a radial direction so that the divertor plasma can be followed as the divertor position is swept. Accurate beam steering will be employed so that the beam can be directed through a 10 mm gap in the target plates. This will reduce the stray light and should enable measurements to be made close to the target plates.

Close to the target plates, the plasma parameters may change on scale lengths of ≤1 cm. Therefore, it is desirable to have a very short laser pulse and very fast detectors so that the spatial resolution is high. With the restricted access a practical limit on the spatial resolution is ~5cm. The existing 300ps ruby laser combined with a streak camera has already achieved such a resolution. The laser pulse will be provided by the main LIDAR lasers and directed into the divertor region when a measurement is required. Under some circumstances, it should be possible to make measurements in the scrape-off layer. In this case, the laser beam will be almost tangential to the flux surface and so the spatial resolution in the radial direction will be determined mainly by the diameter of the laser beam, which will be ~10 mm.

The integrated microwave system will contain a two-frequency interferometer for measuring the electron density, a multi-channel 'comb' type fixed frequency reflectometer for measuring the peak density, and a system for measuring the electron cyclotron absorption (ECA) from which the electron density-temperature product will be determined. All three systems will share the waveguides used to transmit radiation to and from the plasma, as well as the antennas located in the divertor assembly itself. This means that not only will the measurements be made along the same sightlines, but the number of components in the region of the divertor where access is very restricted will be minimised. It is planned to install three sets of waveguides to give three different sightlines through the divertor plasma.

Since the transmission waveguide will be oversized, long and have a considerable number of bends, it is not feasible to use conventional swept frequency reflectometry which relies on a reflection-free propagation path. However, it should be possible to use multi-channel fixed frequency 'comb' type instrument. For the pumped divertor, a number of fixed frequencies in the range 60 GHz to 90 GHz (in the ordinary mode polarization) will be used to determine peak densities in the range 4×10^{19} m^{-3} to 1×10^{20} m^{-3}.

The imperfect characteristics of the transmission waveguide also constrain the interferometer to operate in a fixed frequency mode. However, by using sources at two different frequencies, and heterodyne detection with the local oscillators phase locked to the sources which probe the plasma, it is possible to distinguish between a rising and falling line integral density and to compensate for spurious phase shifts caused by mechanical movements of the antennae. With probe frequencies of 130 GHz and 170 GHz, it should be possible to measure line integral densities in the range predicted for the divertor plasma, with an accuracy of a few percent.

It is not possible to measure electron cyclotron emission from the divertor plasma, since it would be swamped by the much more intense emission, at the same frequencies, from the plasma core. However, for the electron density and temperature values expected for the divertor plasma, the electron cyclotron absorption (ECA) should be in a measurable range: typically between 10% and 90% for second harmonic extraordinary mode radiation. The only sources which have sufficient power for this diagnostic emit radiation with a long coherence length, and it is therefore necessary to overcome the problem of standing waves in the transmission waveguide which would corrupt the required measurements of the returning microwave power. The solution currently under investigation is to use a rapidly frequency swept source and heterodyne detection using the same source as local oscillator. By adjusting the length of the reference arm through which the local oscillator radiation passes to be about the same as the plasma arm (~100m), the beat frequency in the heterodyne detector can be adjusted to a suitable value. Standing waves due to multiple reflections within the transmission waveguide should have a longer propagation path, hence a different beat frequency, and could be eliminated by filtering the beat signal. A large scale mock-up to demonstrate this principle and to develop various aspects of the hardware is currently under construction. It is anticipated that it will be possible to measure the profile of the $n_e T_e$ product in the range 25 to 500 x 10^{19} m^{-3} keV at most values of toroidal field, with an accuracy of ~ ± 10%.

Neutral Particle Analysis

MeV energy protons and α-particles

A new high energy neutral particle analyzer (NPA) instrument, purchased from the A.F. Ioffe Physical-Technical Institute, St. Petersburg, Russia, was installed on JET during 1991. The NPA, consisting of eight energy channels with common mass selection, measures fluxes of hydrogen, deuterium, tritium, helium-3 and helium-4 atoms and their energy spectra in the range 0.5≤ E (MeV) ≤ 3.5. MeV ions

in the plasma arise from hydrogen and helium minority ICRF heating, or from fusion reactions. These ions then neutralize by charge exchange with low energy atoms in the plasma, or by recombination, forming MeV atoms which exit the plasma. The low energy atoms in the plasma are from injected neutral beams, or from recycling.

The NPA is installed vertically at the top of the torus with its line-of-sight intersecting Octant No:4 deuterium and helium beams at the plasma centre. The NPA registration efficiency for MeV atoms is 0.5 - 0.75, and given mainly by stripping in the carbon foil. The NPA detectors, consisting of 3cm² 8μm thick (Cs + Tl) scintillators optically coupled to photomultipliers, have a detection efficiency for fast ions of ~100%, but much smaller for neutrons. The measured contrast between detection efficiency for ions and for neutrons is $\approx 10^5$ for the low energy channels, and $\approx 10^8$ for the higher energy channels, for 2.45MeV D-D fusion neutrons. Measurements made during the Preliminary Tritium Experiment showed practically the same contrast for 14 MeV D-T fusion neutrons.

The performance of the instrument has exceed initial expectations in respect of discrimination against neutron noise and magnitude of high energy atomic flux measured. The instrument has been applied in elucidating ICRF minority heating physics; in questions of high energy ion loss due to MHD activity and to static field fluctuations; and in aspects of ion neutralization processes and atomic cross-sections. In He^3 minority ICRF heating experiments, detection of MeV energy He^3 by double charge-exchange on injected He^4 beams has been demonstrated. Time resolved measurements were undertaken of fusion a-particle energy spectra in the MeV range. A team from the Ioffe Institute worked at JET for installation, testing and initial exploitation of the instrument. This collaboration has progressed efficiently and fruitfully.

Low Energy NPA

The time-of-flight NPA instrument, located at the bottom of Octant No: 1, with a vertical line-of-sight crossing the torus mid-plane at R = 3.1m, has been deployed for measurements of energy spectra of flux of H, D, T, ^{3}He, and ^{4}He atoms emitted from the plasma, in the energy range $0.5 \leq E\,(keV) \leq 200$, from which energy spectra of ions in the plasma can be deduced. This facility has been used routinely to make inferences about plasma behaviour, relative concentrations of different ions in the plasma, and physics of NBI and ICRF heating.

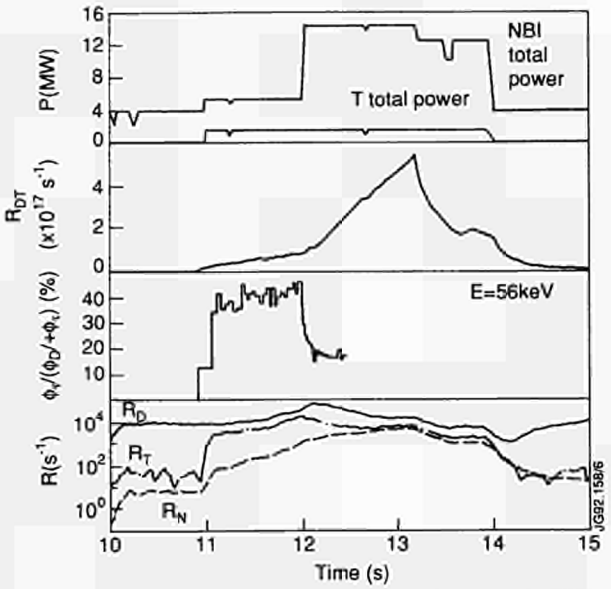

Fig.66: Evolution of deuterium and tritium fuelling of a PTE pulse, of the D-T reaction rate, of the fraction of tritium atomic flux at 56keV and of deuteron, triton, and noise count rates.

In preparation for the Preliminary Tritium Experiment (PTE), a neutron and γ-ray shield was installed around the instrument. This consisted of a ≈25cm thick layer of a water extended polythene (WEP) neutron moderator, and a 10cm thick layer of lead to suppress the γ-rays. The design value for neutron suppression for a fully enclosing shield such as this was 100. Due to penetrations in the shield for mechanical and vacuum connections, the measured suppression of neutrons was ≈ 60 for the low energy channels and only ≈15 for the more exposed high energy channels.

The shield enabled successful NPA measurements of deuterium and tritium during the PTE. Fig.66 shows D and T fuelling by NBI, evolution of D-T reaction rate R_{DT}, evolution of the ratio of tritium efflux F_T to total efflux ($F_D + F_T$) from which tritium concentration in the plasma may be inferred, and evolution of D and T count rates, R_D and R_T, measured by KR2. The spurious neutron count rate R_N is also shown. While R_D was well above the noise level, R_N throughout the pulse, R_T, being an order of magnitude smaller than R_D, was inseparable from R_N at the time of high fusion reactivity at t>12.5s. Fig.67 shows energy spectra of F_H, F_D, and F_T. These measurements enabled assessment and design of a neutron and γ-ray shield which will allow use of the instrument during full D-T operation, in future.

Far-Infrared Interferometer and Polarimeter

The interferometer has been in continuous use during 1991, but improvements have been carried out, as follows:

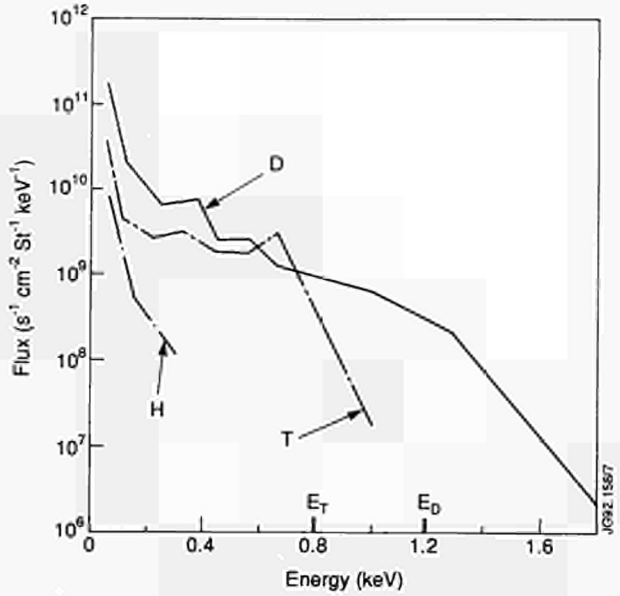

Fig.67: Energy spectra of the atomic flux of hydrogen, deuterium and tritium during the PTE. The deuterium and tritium injection energies ED and ET are shown. Deuterium and tritium slowing-down spectra are seen.

(i) The 0.119mm compensating interferometer, needed to correct for movement of mirrors in the interferometer arm of the lateral chords, has been upgraded with installation of InSb detectors with fifty-fold increase in sensitivity. This has increased reliability of the lateral chords. The pumped-divertor phase interferometry of the bulk plasma, for which the lateral chords are indispensable, will benefit greatly from this upgrade.

(ii) When the electron density changes too rapidly the interferometer loses count of fringes, such as in pellet injection experiments. This is an intrinsic limitation of existing electronic processing equipment. A new method has been developed and tested for real-time digital demodulation of interferometer signals using VME technology. This allows modulated signals to be digitized and their phase calculated in real time, even when the fringing rate approaches the modulation frequency (100kHz in JET). This facility is expected to make this system less susceptible to fringe loss due to rapid density changes.

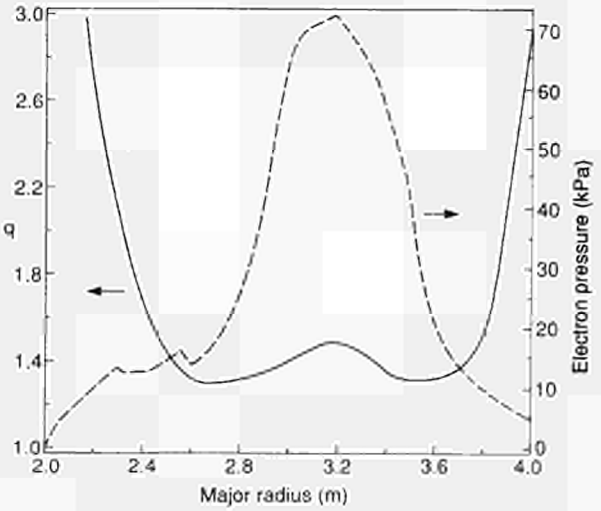

Fig.68: Measured radial q and electron pressure profiles during a PEP pulse.

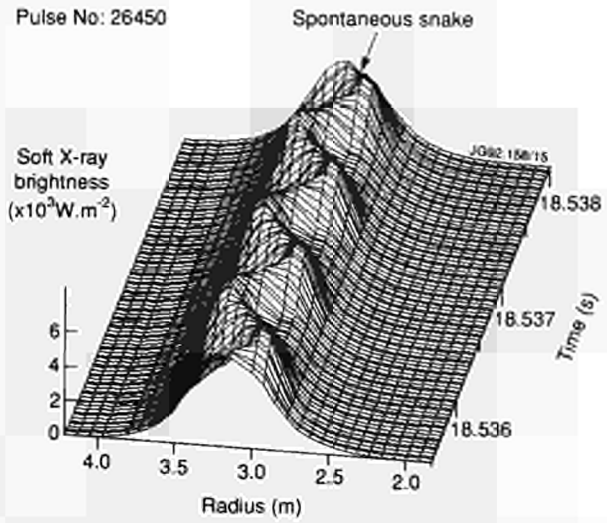

Fig.69: Giant snake observed by vertical soft X-ray camera.

Measurement of q-profile

Faraday rotation measurements using the far-infrared polarimeter have assumed greater importance in JET as attention has focussed on the role of current density distribution, $j_\phi(r)$, in energy transport, and on the origin of current scaling in L-mode confinement. Pellet Enhanced Performance (PEP) is also attributed to properties of $j_\phi(r)$, in particular the region of improved confinement in PEP discharges coincides approximately with the region of reversed shear, Fig.68. Faraday rotation measurements have played a key role in these investigations, since at present it gives the most direct access to temporal evolution of $j_\phi(r)$, and therefore, the q-profile and shear.

Soft X-Ray Measurements

The soft X-ray diode cameras have continued to function with a high level of reliability and have produced a wealth of new data. In particular, detailed MHD studies have been made in PEP mode discharges and β - collapses; the complex and varied phenomena are an on-going study. Novel MHD effects are frequently observed such as the giant snake-like mode which is found in the tail of high powered neutral beam heated discharges. This mode, Fig.69, has an amplitude on

the line-of-sight signals of up to 50%. This has been analysed with the recently installed rotational tomography code to show the spectacular nature of this mode which can not be regarded as a small perturbation of the main plasma. The real time tomography and trigger systems are now operated from the main Control Room.

New Compact Soft X-ray Cameras

Considerable progress has been made in the design of new compact cameras which will replace the existing vertical camera and toroidal detector systems and provide new views of the plasma in the poloidal plane. These new cameras will overcome many of the limitations inherent in the present systems. They will greatly improve our measurement capability on magnetic topology and MHD effects with improved spatial resolution which will improve the capability to separate mixed MHD modes in high b, monster sawteeth and PEP plasmas. Greatly improved poloidal MHD mode number resolution up to at least m = 4, should be achieved and this should allow much better tomography analysis of the data. The toroidal mode number determination should increase to at least n = 4 over all the plasma minor radius. In addition, the plasma shape determination in X-point and divertor plasmas should be improved.

The new system is based on the use of compact Si strip detectors mounted in cameras with a very short focal length (~5 cm) compared with existing systems (~80 cms). Tests have shown that these detectors work well in the JET machine and both the mechanical and electrical designs are proceeding well. The main mechanical features of a preliminary version of the poloidal detector array is shown in Fig.70. The entire system is enclosed in a metal pipe attached to the main diagnostic flange. The interior of the pipe forms a secondary vacuum and encloses the cabling and the Si detectors which view the plasma through pinholes and Be windows. The whole system is designed for easy installation into, and removal from, the machine. Although the detectors in the new system are much smaller than in existing cameras, because of the geometry the expected soft X-ray signals will be only slightly smaller but the signal to radiation induced noise in high neutron yields D-D shots should improve. The effects of radiation damage on the detectors should be considerably reduced by periodic detector annealing.

The electronic and data acquisition design is not as far advanced as the mechanical design. It has, however, been decided to place the detector pre-amplifiers outside the vacuum systems and to digitize the signals close to the machine with the digital signals being transmitted to the diagnostic hall along optical fibres. Many other combinations for the positions of the amplifiers and digitization system have been considered but the one chosen provides the simplest and least risky technical solution.

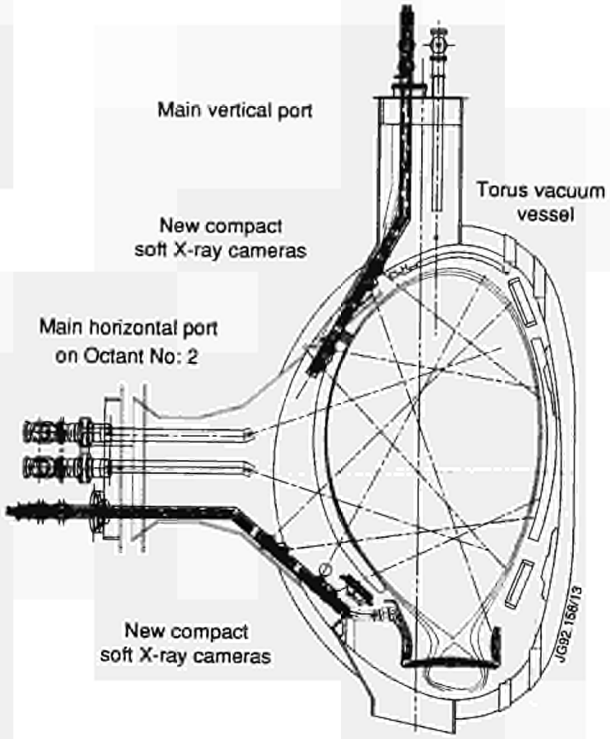

Fig.70: Disposition of proposed new compact soft X-ray cameras in relation to the pumped divertor plasma.

Z_{eff} Profiles using Soft X-ray Bremsstrahlung

As the signals from the soft X-ray cameras are absolutely calibrated, they may be used to determine the radial and time resolved values of Z_{eff}. In JET, the main impurities are the light elements Be, C and O which are fully ionised, with occasional small contributions from Ni and C, which generally only contribute a few % of the radiated power. To determine Z_{eff}, calculations are made of the radiated power observed through the Be filters which cover the detectors. An ionization equilibrium calculation is made both with and without transport effects. In addition, the relative contributions of the different low Z species in a particular plasma are required and these were determined from VUV spectroscopy and active charge exchange spectroscopy. The results of these calculations are compared with the tomographically inverted soft X-ray data and Z_{eff} is then found. Good agreement is found with existing methods, and a comparison is

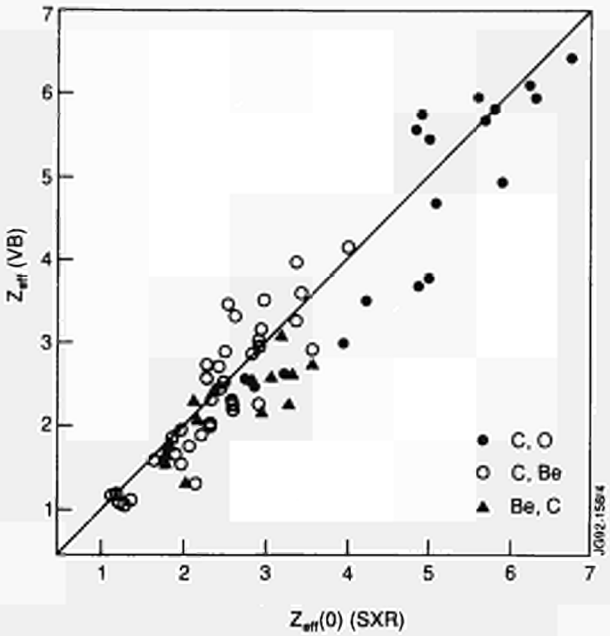

Fig.71: Comparison of Z_{eff} derived from analysis of the soft X-ray emissivity measurements and visible bremsstrahlung measurements.

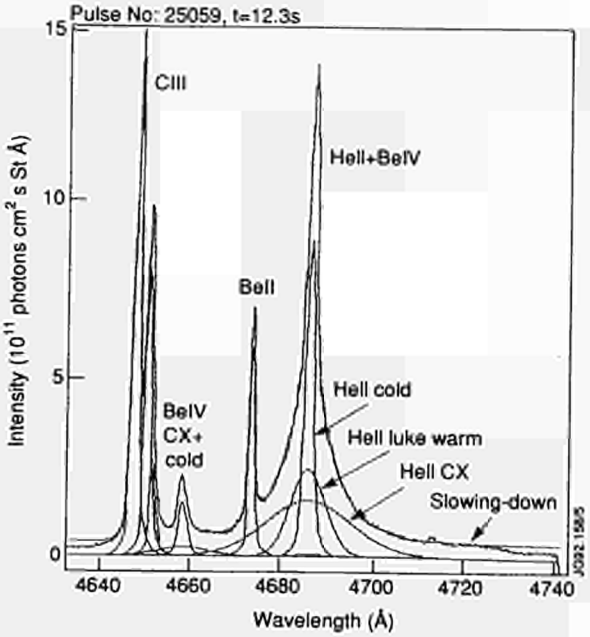

Fig.73 Complex structure of spectrum of charge-exchange emission.

shown in Fig.71 with the visible bremsstrahlung data for shots with flat Z_{eff} profiles. This method allows Z_{eff} measurement of on a rapid time-scale.

The pulse height analysis system has continued in reliable operation and has been used with a Ge detector to measure the line of sight integrated spectrum of low energy gamma rays (100 - 500 keV) caused by energetic plasma electrons produced in lower hybrid heating experiments and in plasma disruptions. In LH experiments, a clear high energy tail is seen extending up to 100s of keV (seeFig. 72).

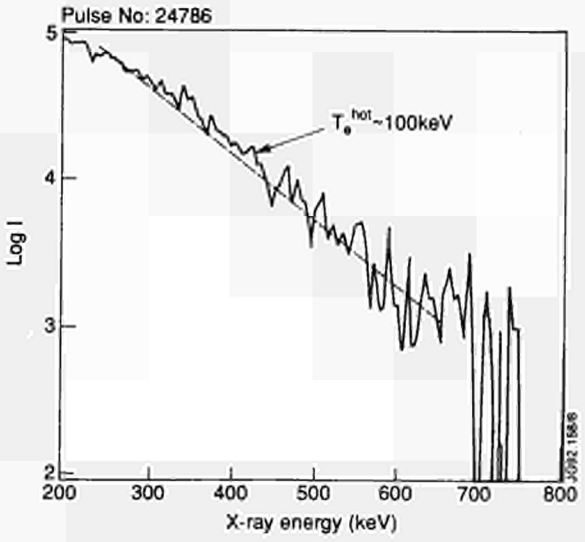

Fig.72: High energy tail to low energy gamma ray spectrum during lower hybrid experiment, measured with the pulse height analysis (PHA) system.

Charge Exchange Spectroscopy

Measurement of Light Impurity Densities and Temperature

Plasma heating by neutral helium beam injection during 1991 experimental campaign of JET has led to several new results which will be relevant for the diagnosis of thermo-nuclear alpha particles in next step devices. One aspect is the production of a significant amount of non-thermal alpha-particles whose distribution function can be investigated by means of charge exchange spectroscopy. For the first time, systematic studies could be carried out using ~ 5 MW of helium beam injection into deuterium plasmas. Peak fast helium ion densities between $2x10^{17}m^{-3}$ and $2x10^{18}m^{-3}$ have been measured. This is an order of magnitude higher than the α-particle density expected from thermo-nuclear reactions during the future full D-T operation of JET. The controlled fuelling of high energy helium neutrals represents a relevant test-bed for the capability of measuring absolute alpha-particle densities in the core of a confined plasma. Furthermore, transport studies are facilitated by switching on and off central sources and monitoring the temporal and radial redistribution.

The actual spectral analysis required for the deduction of a fast particle population is very complex, Fig.73, and can only be solved by a coupled-fit technique recently developed at JET. In particular, in the presence of high levels of alpha-particles, this new fit could be used routinely in an

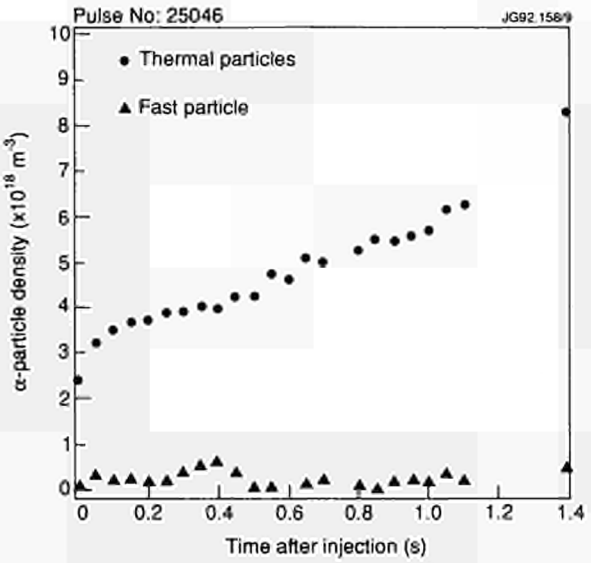

Fig.74: Evolution of density of fast (50-130 keV) and thermal (~ 10 keV) helium ions.

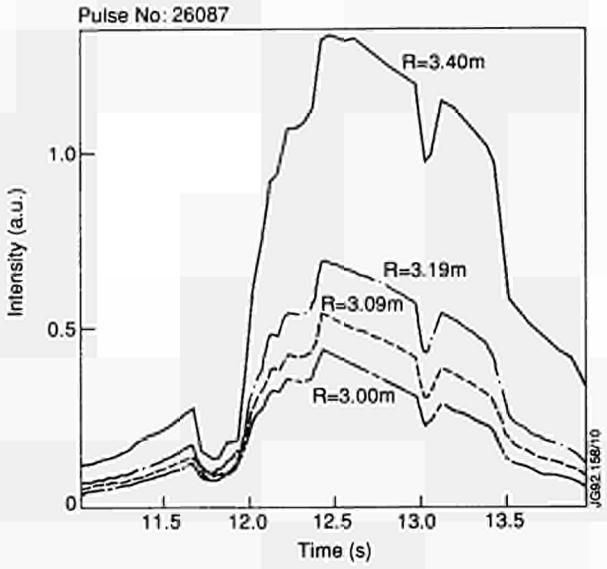

Fig.75 Evolution of the radial emission profile of the Octant No: 8 neutral beams.

automated inter-shot procedure for the simultaneous analysis of HeII and BeIV emission. There are however significant limitations at very low levels of impurity concentrations (i.e. n_{He}/n_e or $n_{Be}/n_e < 0.001$). One spin-off of the coupled fit technique is a very reliable determination of the He:Be ratio. Since the CX diagnostic employs the same central viewing chord for simultaneous monitoring of C^{6+}, H^{2+} and Be^{4+}, the ratio of light impurities can be derived to a high degree of reliability independent of external data input such as electron density and neutral beam power.

Fig.74 shows the temporal development of fast and thermalised alpha-particles in a helium beam fuelled plasma. The rate of increase for the thermal particles corresponds to the source rate for a neutral beam power of 5 MW. In the course of the fuelling the fast particle population remains nearly constant and the ratio of fast to thermalised particles therefore continuously decreases in time. The fast population is on average about one tenth of the thermal and thus only a minute fraction of the total plasma inventory.

The PTE experiment turned out to be one of the most challenging tasks for a quantitative spectroscopy analysis of temperature and density of the dominant light impurities. The main reason for this complexity was the mixture of three different types of neutral beams used for fuelling and heating the plasma and all beams acting as donor for the observed charge exchange process. At the same time, the presence of 80 keV tritium beams, and 80 and 140 keV deuterium beams respectively, have illustrated the potential of beam emission spectroscopy which was used to monitor the radial emission profile of the Octant No: 8 neutral beams (see Fig.75). Since each type of beam is characterised by different species mixture, beam divergence, energy and power the beam attenuation had to be calculated for each single species. The charge exchange analysis for deduction of light impurity densities was carried out in a self-consistent procedure which feeds back the derived impurity densities into the beam attenuation code which determines the locally derived densities.

Table X summarizes the type and quality of information deduced from charge-exchange spectroscopy data. The deuterium density is derived assuming charge neutrality and subtracting the contribution of each impurity from the independently measured electron density.

In a further consistency check the volume integrated thermo-nuclear neutron rate calculated from the CX profiles of deuteron density and ion temperature is compared to the rate derived by the JET TRANSP code. The onset of the carbon bloom phase was evidenced by the increasing hollowness of the carbon density profile, Fig.76, which led to reduced beam penetration, and thus to loss of central fuelling and heating.

Edge Ion Temperature and Rotation Measurements

During 1991, a new diagnostic was successfully installed with the main objective of measuring, with high temporal and spatial resolution, poloidal rotation velocity and ion temperature near the plasma boundary. The design, installation and scientific exploitation of the diagnostic were performed with cooperation of UKAEA-Culham Laboratory.

Table. X
Charge Exchange Measurements of PTE

Pulse No:		26147	26148	26095	26087
Time	(s)	13.12	13.21	13.7	13.4
$T_i(Y=0)$	(keV)	17.5±0.6	18.8±0.8	20.7±1.0	18.6±0.9
$T_i(Y=1)$	(keV)	3.3±0.1	5.2±0.1	3.1±0.1	3.9±0.1
$<T_i>_v$	(keV)	6.2±0.2	8.4±0.3	7.0±0.4	7.3±0.3
$n_D/n_e(0)$		0.75±0.05	0.76±0.05	0.83±0.05	0.84±0.06
$n_D(0)^*$	($10^{19}m^{-3}$)	2.30±0.15	2.10±0.15	4.30±0.20	3.90±0.18
$Z_{eff}(0)$		2.00±0.25	2.05±0.25	1.85±0.27	1.80±0.25
$<Z_{eff}>$		1.90±0.30	2.00±0.30	1.83±0.27	1.60±0.24
$<Z_{eff}>$		2.40±0.35	2.40±0.36	2.12±0.33	1.77±0.25
$<Z_{eff}>$		2.15±0.25	2.00±0.20	1.94±0.25	1.75±0.25
C:Be		2.30±0.40	2.40±0.40	3.00±0.50	2.50±0.40
C	(%)	2.70±0.40	3.00±0.35	2.10±0.35	1.90±0.30
Be	(%)	1.25±0.25	1.25±0.25	0.70±0.17	0.75±0.20
He	(%)	1.75±0.35	0.60±0.25	1.20±0.30	1.40±0.40
$N^{**}_{tot}(C^{6+})$	(10^{20})	0.90±0.20	1.00±0.20	1.10±0.20	1.35±0.25
$n\text{-}D\text{-}D_{th\text{-}th}$	($10^{16}s^{-1}$)	0.90±0.10	1.10±.15	2.10±0.40	2.30±0.30
$n\text{-}D\text{-}D_{th\text{-}th}$	($10^{16}s^{-1}$)	0.75	0.85	1.88	2.50

$^*n_D = n_D + n_T = n_e - 6\,n_C - 4\,n_{Be} - 2n_{He}$

$^{**}N_{tot}$ volume integrated impurity content in confined plasma

To increase the accuracy of measurement of low level velocity changes expected during the transition of L -to H-mode, two twin fans of lines-of-sight were implemented which view the same active volume from opposite ports. A tandem spectrometer system allows the simultaneous recording of spectra from the two opposing ports. The diagnostic has twenty chords aimed at the outer 13 cm of plasma, half the chords look from above and half from below. The view is predominantly poloidal with a small (15°) toroidal component, enabling measurement of both poloidal and toroidal components of plasma rotation. The achievable time resolution was limited by the intensity of CVI emission in the plasma boundary. At present, only tens of milliseconds resolution is feasible.

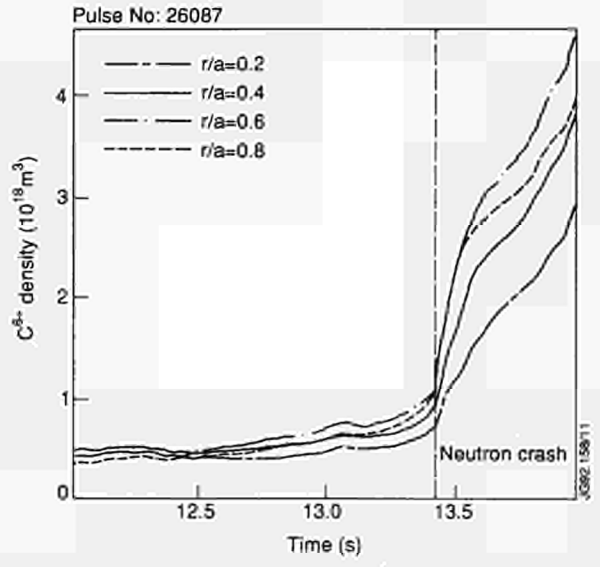

Fig.76: Evolution of radial carbon density profile near onset of a carbon bloom, showing increasing hollowness of the profile.

Measurements of toroidal rotation are also made at a single radius using a toroidal viewing array. This measurement can be used to cross check data from the poloidal view and to correct for line shape distortions arising from atomic physics effects rather than fluid motion. The diagnostic is designed to study charge exchange emission from interaction with the heating beams. Charge exchange transitions are excited along the length of the neutral heating beam, and therefore enable the only means of making measurements of visible light from plasmas with $T_c \geq 100$ eV.

Light from the plasma is imaged onto an array of discrete fibre optics and transmitted 100m to a remote spectrometer. The fibre array gives a spatial resolution of 1.5 cm, limited by the collection optics and fibre diameters. This resolution is degraded to 4cm due to intersection angle between viewing chords and magnetic flux surfaces at the region of neutral beam interaction. The spectrometer has, instead of a single entrance slit, twenty slits arranged in four rows of five. Light from each slit passes through a low dispersion spectrometer

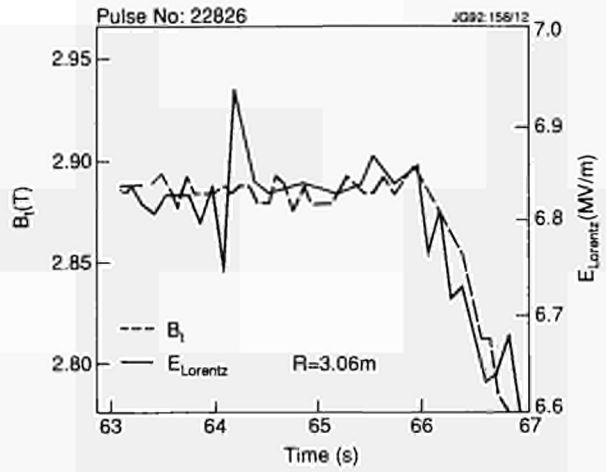

Fig.77: Variation of Stark electric field with applied toroidal magnetic field in a TF ramp experiment, showing capability for high resolution measurement of local magnetic field.

to limit the passband to ~15Å. A second spectrometer, with narrow entrance slits, disperses the light into non overlapping rows of spectra. These four rows of spectra are amplified in an image intensifier and recorded with four fast linescan cameras.

H-mode plasmas exhibiting gradual L-H transition with rapid ELMs persisting for more than 50ms have been studied, showing that development of poloidal rotation occurs during the ELM phase. The velocity is in the electron diagmagnetic direction. However, there is evidence of an additional sudden change in the poloidal velocity when H_α light first begins to show ELMs. Peak poloidal velocities observed are ~ 10-20km.s^{-1}, and limited in space to 5 cm or less. A typical value for the edge ion temperature at the beginning of the H-mode transitions is 200eV, rising to 600eV as the H-mode evolves.

Another important strength of the diagnostic is the capability for measuring ion temperatures in steep gradients near the separatrix, and for making local measurements of impurity density near the plasma edge. The latter will be important for investigating transport of impurities into magnetically confined plasma in the pumped-divertor operation.

Motional Stark Effect Polarimetry

The local measurement of magnetic field in a tokamak plasma by means of the motional Stark effect on fast injected neutrals can be divided in two parts: (i) measurement of Stark splitting of the beam-emission spectrum gives the magnitude of the Lorentz electric field $\mathbf{E} = \mathbf{v} \times \mathbf{B}$, (ii) polarimetry gives the direction of the electric field vector $\mathbf{E}$. The first is derived by using a multi-Gaussian fit which is capable of resolving the Doppler-shifted Stark spectrum to high accuracy, $\Delta|\mathbf{E}|/|\mathbf{E}| = 1\%$, (see Fig.77). The latter is calculated by taking the ratio of the linearly polarised Stark p-lines which can resolve changes in orientation of $\mathbf{E}$ of 0.3°.

The radial dependence of the magnetic field direction has been measured. Also a change in neutral beam velocity can be detected. Evidence of sawteeth is seen on the total beam emission, whereas a monster sawtooth crash causes a detectable change in polarisation angles derived from the different polarised p- and s-components of the Stark spectrum, indicating a fluctuation of the magnetic field direction. The sawteeth on the total beam emission signal can be attributed to a fluctuating excitation process, which depends on electron density, impurity concentration and ion temperature.

Measurement of H_α, Visible Bremsstrahlung and Impurity Influx

Several improvements have been made to the visible spectroscopy diagnostics throughout 1991. New lines-of-sight have been added to the multichannel OMA system, so that spectra can now be recorded on one of several chords giving

i) a view of the beryllium belt limiter;
ii) a view of the outer strike zone on the beryllium X-point target plates;
iii) a view of the outer strike zone on the carbon X-point target plates;
iv) a view of the inner strike zone on the carbon X-point target plates;
v) a vertical view of the reciprocating Langmuir probe.

In addition, the OMA spectra are analysed after each pulse to produce a pulse file (PPF) containing integrated line intensities as a function of time. This has allowed a comparison of fuel and impurity fluxes for beryllium and carbon outer strike zones, and for inner and outer X-point strike zones for carbon target plates. Data capacity has been upgraded by adding four new channels with 20kHz data acquisition for 6.5 s. This improved temporal resolution is essential for studying ELMs and other fast edge phenomena.

A PPF is now also generated from the KS3 photomultiplier signals. The nature of these signals means that each is the sum of some line radiation plus plasma bremsstrahlung at the same wavelength. One output corrects the raw signal for the bremsstrahlung, and then applies an absolute intensity calibration. The resultant calibrated impurity signals have proved useful for consistency checks for all visible diagnostics, and in particular, for validating the calibration of the charge-exchange spectroscopy diagnostics.

The system was used during the PTE to measure $<Z_{eff}>$ in the plasma, and influxes of D, Be and C at the plasma edge. The system performed reliably throughout the campaign. No serious adverse effects to the optical fibres were detected, arising from the high flux of neutrons and associated γ-rays. Measurements with fibres installed specially to detect effects produced by the 14 MeV neutrons showed that the irradiation induced a transmission loss in the optical fibres as well as generating optical signals in the fibres through luminescence. The level of irradiation produced during the PTE was not large enough to affect measurements of Z_{eff} and impurity influxes.

The induced transmission loss was measured by launching the output of a pulsed LED (wavelength at peak emission ~ 560 nm) into a fibre-optic loop which ran from the Diagnostic Wing to the torus, passing under a main vertical port, and back again. Monitoring the ratio of the transmitted to launched signals, as a function of time through the D-T discharges, yielded an induced loss of 0.03 dB in the loop for each of the two shots. The luminescence was detected by capping-off the remote end of an optical fibre at a main vertical port, so that it did not receive any plasma light, and measuring the signal passing through an interference filter of central wavelength 523,5 nm and band width 1 nm. A signal of ~ 1.5×10^{-10} W at the time of peak neutron emission was determined.

Estimates of the absorbed dose and dose rate at a main vertical port yield 50 - 100rads and 50 - 100rads.s^{-1}, respectively. The induced absorption in the fibre is in keeping with the results reported by other workers, but the luminescence signal is about two orders of magnitude higher than that expected. However, the reported luminescence measurements were performed using an electron or γ-ray source, of maximum energy 2MeV. Thus, the 14MeV neutrons will individually deposit considerably more energy in the fibres than the 2MeV electrons. In particular, there are several inelastic collision processes which exhibit sharp cutoffs at energies below about 5MeV, (e.g. the (n, p) reaction).

In conclusion, during the PTE, the effects of the absorbed dose on the diagnostic results could be neglected. However, during the full D-T phase of JET, doses per shot of up to two orders of magnitude greater may be anticipated, induced absorption and luminescence in the optical fibres will have to be taken into account. The methods employed during the PTE to quantify these effects offer a promising start to combatting the problems, but further refinement is needed.

Plasma Boundary Density Profile Measurement using a Lithium Beam

Density profile measurements in the ASDEX (Garching, Germany) scrape-off plasma have been made using an energetic neutral lithium beam. As the beam traverses the scrape-off layer, it is attenuated, mainly due to ionization by electron impact, and the neutral lithium atoms excited to higher energy states. The beam attenuation profile can be deduced from measurements of spatial profile of intensity of spectral emission, from which the electron density profile over the beam penetration distance may be obtained. Application of this technique in JET during the pumped divertor phase should be feasible. An appropriate system has been defined, and detailed design and procurement are in progress.

A neutral lithium beam source similar to that used in ASDEX is found to be most suitable for use in JET. To achieve good spatial resolution, it will be necessary to probe the plasma near the top of the torus at the stagnation point in the scrape-off layer, where the density scrape-off length should be 3-5 cm. It is feasible to make measurements with 5 mm spatial resolution over a path of 20cm, and time resolution of ~10 ms.

Spectroscopic Measurements in the VUV

Spatial Scan VUV Spectrometer

The radially scanning VUV spectroscopy instrument KT1, consisting of two dual chrome spectrometers [6, 7] has been operated throughout 1991. Emphasis has been to diagnose divertor plasmas and to measure the behaviour of carbon fluxes from the graphite target plates of the upper divertor.

When the ion $\nabla \mathbf{B}$ drift is directed towards the X-point, the carbon fluxes are typically greater on the inboard (ion drift) side up to moderate heating power P_{HEAT}, and remain approximately constant when P_{HEAT} is raised, while on the outboard (electron drift) side the carbon fluxes are initially lower, but show a stronger dependence on P_{HEAT}. Higher carbon flux on the inner X-point side is consistent with the observation that the electron density in the divertor is higher on this side. As sputtering is the prevailing carbon release process up to medium heating power, fluxes should be higher at higher densities. The sputtering coefficient of D^+ and C^+ ions on graphite does not vary significantly in the typical divertor temperature range. On the electron drift side, the electron density is lower and hence the electron temperature higher. The parallel thermal conductivity is therefore higher and so is the power load onto the

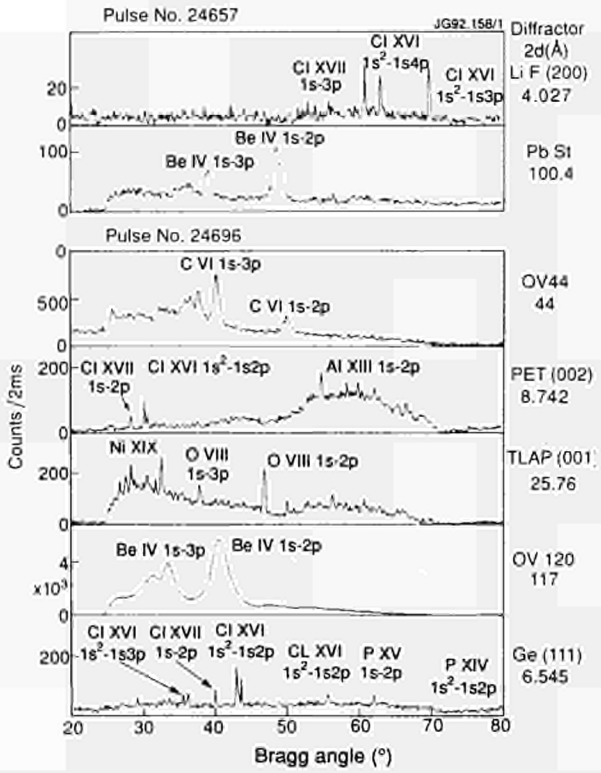

Fig.78: Survey spectra showing spectral coverage is almost complete between 2 Å and 100 Å, thus enabling measurement of all the important impurities.

target plate, favouring thermally induced carbon release. With the ion $\nabla \mathbf{B}$ drift away from the X-point the divertor density and the carbon fluxes are more balanced.

As the two spectrometers view the plasma cross section from two perpendicular directions, localised radiative events can be resolved spatially. When both spectrometers are set to the same pair of lines a rough estimate of the local electron temperature gradient near the divertor dump plates can be made. A typical value of $(\nabla T_e)_{pol} \simeq 500$eV/m was found using the carbon line pair CII (904Å)/CIV(312Å). Spatial location of MARFEs has been deduced by measuring the associated highly localised carbon line radiation, and thus the MARFE trajectory determined. MARFEs often form at the divertor, and via the inner scrape-off-layer, penetrate the bulk plasma.

X-ray Spectroscopy of Impurities

A new instrument, a Bragg rotor X-ray spectrometer was installed and operated during 1991. A wide range of crystal and multilayer diffractors is mounted on a hexagonal rotor to give almost complete coverage of the soft X-ray spectrum between 0.1 nm and 10 nm. This allows a single instrument to monitor K- L- or M-shell line radiation from highly ionised species of all plasma impurities (see Fig.78). This instrument is particularly useful for measurement of light impurities such as beryllium and carbon which usually contribute most to the radiated power and effective charge. The instrument shares the shielded, tritium-compatible beamline of the Active Phase Double-Crystal Monochromator, and both instruments were operated successfully to monitor all the main impurities throughout the PTE.

Impurity Transport Modelling

A time dependant predictive 1.5-D code, SANCO, for impurity transport simulations has been developed for solving the continuity equations for all ionisation stages of an element, properly averaged over each flux surface [8]. The geometric plasma configuration is reconstructed from JET equilibria. Implementation of plasma geometry makes it possible to simulate directly the data measured by different diagnostics, the multi-chord VUV spectroscopy, the bolometer and soft X-ray arrays. The code accesses directly the central atomic physics package being developed at JET in the structure of a look-up table, both temperature and density dependent, regularly kept up-to-date [9]. SANCO is a predictive code, i.e. the transport coefficients must be provided either heuristically or, in the case of neoclassical coefficients, calculated at each time step, and the results compared with measurements. The transport coefficients are iterated until a fit with measurement is obtained.

This code has been extensively used in the analysis of impurity transport. Simulations have been carried out to determine the transport parameters in cases of nickel injected into H-mode high density plasmas [10]. The formation of a convective layer, with a representative value v/D at the edge in excess of 100 m^{-1}, in the outer zone close to the edge has been confirmed, in good agreement with neoclassical behaviour.

Following Stringer [11], the neoclassical fluxes can be cast into a form explicitly retaining the radial electric field. A rough evaluation of the convection arising from this term seems to be in agreement with what is actually needed in the simulations. An experiment on TEXTOR, where a suitable diagnostic is available for measurement of an externally imposed electric field, has been proposed and will be performed during 1992, to check the relation of the strong peripheral convection to the radial electric field. It should be emphasized that the SANCO code can actually run with the TEXTOR circular geometry and preliminary simulations have already been carried out.

Neoclassical transport coefficients usually quoted in the literature for comparison with experimental results have been derived for particular asymptotic regimes and for circular geometry. The series of JET experiments aiming at the study of the transport of He from the plasma central region have stressed the need of reliable neoclassical transport coefficients valid more generally. To this end, a code has been developed for the calculation of the full set of neoclassical transport coefficients [12, 13]. Once the temperature and density profiles are given, this code calculates the classical and neoclassical transport coefficients (diffusion and convection for particle fluxes, thermal conductivity and pinch term for energy fluxes) for the plasma ions, all ionisation states of up to two impurities and, optionally, the electrons. When the electrons are included, also the Ware terms and the bootstrap current are calculated.

An important effect due to the geometry has come out, which particularly affects the Pfirsch-Schlüter terms dominant in the outer plasma region. In the case of the highly elongated JET X-point plasmas, this is the region where the departure from the circular approximation is most marked. In fact, the q^2 dependence virtually disappears, resulting in a very low diffusivity, as in Fig.79 consistent with analysis reported in [14].

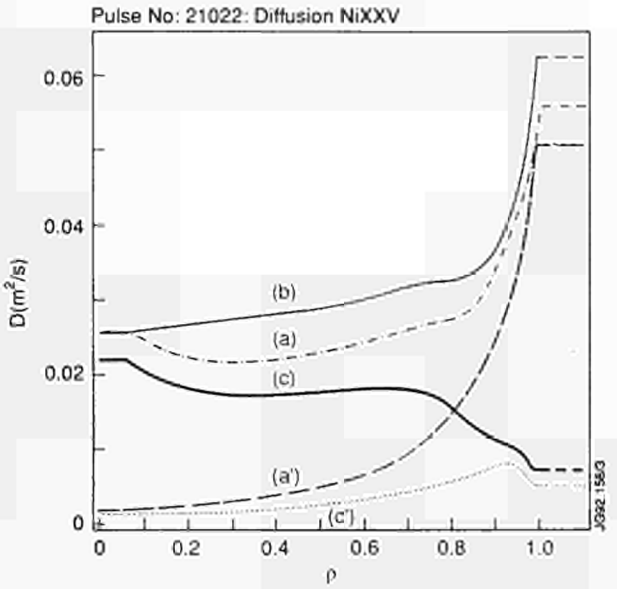

Fig.79: Neoclassical diffusion profile for Ni XXV, 0.6s into a H-mode discharge Pulse No: 21022:
(a) D_{NiXXV} total (circular cross-section approximation);
(a') D_{NiXXV} PS (circular cross-section approximation);
(b) D_{NiXXV} total (analytical approximation);
(c) D_{NiXXV} total (proper flux surfaces averages);
(c') D_{NiXXV} PS (proper flux surfaces averages).

Atomic Processes for Spectral Diagnostics and Plasma Modelling

Developments have been in three main areas, namely, neutral beam injection related spectroscopy, emission properties of species in edge and divertor conditions and finally in the general purpose 'Atomic Data and Analysis Structure' computation provision.

Charge exchange spectroscopy and beam emission spectroscopy, which depend upon fundamental collision data at the leading edge of the academic capability, are subject to steady improvement and revision [15]. With deuterium beams, Be^{+4}, B^{+5} and N^{+7} have been added to the analysable species, and an outstanding capability for He^{+2}, thermal and non-thermal [16] now exists. Deuterium beam emission modelling has been extended to very high plasma temperatures, high densities and arbitrary beam energies [17]. The most stimulating development has been the use of neutral helium beams. A moderate accuracy modelling capability has been developed, but the helium beam emission and charge exchange diagnostic potential is high and quite subtle. This is due partly to the presence of metastable states and the detailed energy level structure of He° [18]. A large effort has been expended throughout 1991 to develop these potentials for the future JET programme [19, 20].

Atomic studies for the edge and divertor regions have inevitably centered on beryllium, carbon and hydrogen. In particular, little fundamental cross-section data is available. This has been corrected with detailed studies for $e^{-}+Be^{\circ}$ [21] and $e^{-}+Be^{+1}$. Also the diagnostic impact of beryllium spectrum lines have been investigated in depth [22]. It is a helpful species for diagnostic spectroscopy. Photon efficiencies, effective emission coefficients and sensitive line ratios for beryllium and carbon atoms and ions and for hydrogen are in place and in use for interpretation of visible, quartz UV and VUV spectra. The capacity exists to model essentially all the spectral lines of species such as beryllium and carbon in arbitrary conditions and to synthesise complete spectral regions to compare with observations [23]. This is valuable for anticipatory studies of the planned pumped divertor.

The 'Atomic Data and Analysis Structure' (ADAS), is part of a concept for the diagnosis, modelling and control interface between spectral observations and key plasma parameters such as species densities, fluxes, radiated power etc. The computer package has been developed extensively in 1991 for interactive use and for embedding in applications [24]. Direct links have been established to key modelling codes such as EDGE2D, SANCO, DIVIMP as well as to most spectroscopic diagnostics.This has allowed

standardisation, centralised maintenance and quality control of the derived atomic data bases in use at JET. The recombination, ionisation, radiated power and line emissivity databases for lithium, beryllium, carbon, oxygen, fluorine and nickel have been targetted and revised together with a number of isoelectronic sequences. Development effort has also been placed into the more sophisticated model for recombination, ionisation and emission in plasmas known as generalised collisional radiative theory. This will support the expectations of spectroscopic diagnostics in the relatively dense, low temperature, dynamic conditions of the JET pumped divertor [25].

Pumped Divertor Diagnostics

Interferometry and Polarimetry of the Bulk Plasma

Design of modifications of the far-infrared interferometer/polarimeter has continued during 1991. Due to loss of some vertical chords, greater reliance will be put on the horizontal chords in the upgraded interferometer system. Optical design inside the interferometer frame is in progress. The most critical interface with other systems occurs at the main horizontal port of Octant No: 7, where waveguides for ECE measurements are located. A design of the main port flange has been completed. The finished interferometer system will be equipped with four vertical and four horizontal chords.

Calorimetry of Divertor Targets

Preparations for calorimetric measurements of pumped divertor targets are in hand, using thermocouples to measure temperature rise of target tiles. A design review has been completed, all interfaces with the torus defined, procurement is in hand and preparation for assembly has begun for the Mark I targets. Sixteen target tiles each on two radial divertor target support beams, located at Octant No: 4 and Octant No: 8 will be equipped with thermocouples. This will permit construction of a poloidal map of heat flux to the divertor, at two toroidal locations. This is envisaged as the main measurement of heat flux to the targets. Although rapid variations in heat flux can not be measured, this diagnostic is expected to provide essential validation of power balance in the divertor region.

Preparation for VUV Spectroscopy of the Divertor Plasma

A major aim of the pumped divertor is to study the dependence of impurity production and retention on edge and divertor plasma parameters. To achieve this, the spectroscopic capability will be extended in order to provide detailed measurements for comparison with edge and divertor plasma models. The location of the different ionisation stages along fieldlines as well as their poloidal density profiles in the divertor are of interest. This information should be available for several impurities and for several ionisation stages of each impurity at the same time. Therefore a spatial resolving VUV survey system with some tomographic capability is required. Consequently a new arrangement for VUV spectrometers on JET involving upgrading of existing systems as well as introduction of new spectrometers has been designed during 1991. A brief description of the two major groups of VUV instruments and their particular capabilities are given.

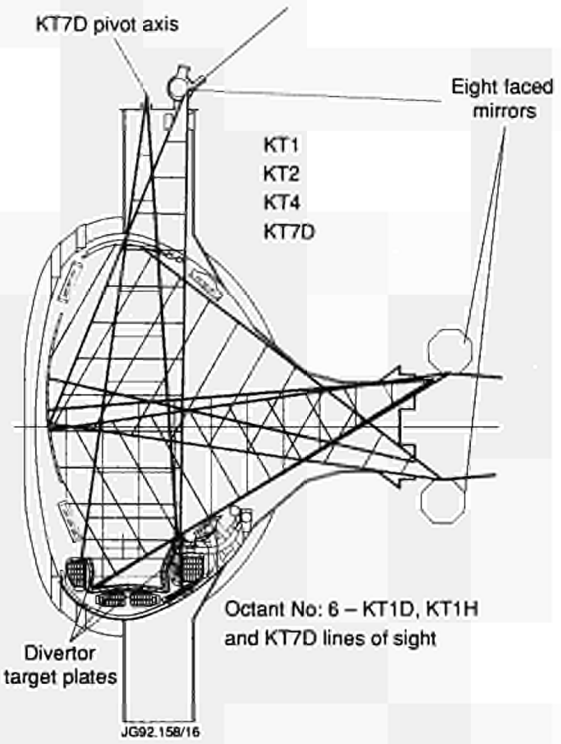

Fig.80: Poloidal cross-section of vessel showing the divertor design and spatial coverage of the different VUV systems.The eight faced mirrors and pivoting flange are also shown.

Spatial Scan System (KT1)

The existing system with two spectrometers will be upgraded to three spectrometers, one with a vertical view on top of the machine covering the divertor area and two at the midplane viewing the inner strike zone of the divertor and the upper target plates. Each spectrometer will be equipped with a new designed mirror chamber incorporating an eight face rotating mirror. The new mirror chamber allows four times better time resolution than existing two face

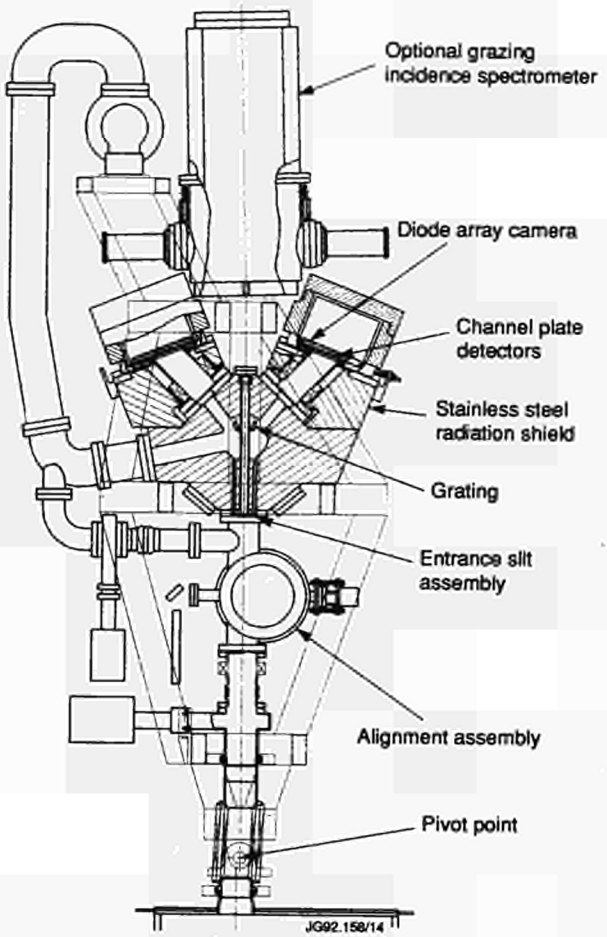

Fig.81: Cross-section through the new spectrometer. The optional grazing incidence on the back is also shown.

mirrors, 25 ms for a poloidal profile of 90 spatial points. The two different viewing angles towards the divertor, one vertical and one from the midplane, as shown in Fig.80, allowing localisation of the distribution of different ionisation stages along fieldlines. In addition, intensity (flux) profiles of the sputtered target plate material can be obtained. The system can provide this information with a high time resolution, 25ms. However, this system is limited to the observation of only two spectral lines at a time (two ionisation stages) in a limited wavelength range (25 nm to 250 nm). Due to these limitations a complementary group of spectroscopic instruments is required as described below).

Survey Systems (KT2, KT4, KT7D)

The KT4 grazing incidence spectrometer, covering two 6 nm wide wavelength bands between 1 nm and 30 nm, as well as the (SPRED) survey spectrometer covering the wavelength range from 10 nm to 110 nm continuously exist already. These systems, located at the midplane, will stay basically unchanged except for new diode array detectors. There will be a geometric rearrangement at the port, to make space for a third instrument. A spatial scanning capability (2Hz) has been commissioned during 1991. This will provide a similar spatial coverage of the new divertor as that provided by the spatial scan systems.

A new instrument, shown in Fig.81, is a double SPRED survey spectrometer located on top of the torus covering the wavelength range from 10 nm to 150 nm continuously. It is capable of scanning the divertor area with a frequency of 2Hz. Therefore it will measure poloidal profiles of emission from different impurity ionisation stages originating from the divertor area every 500ms. A third viewing channel through the middle of the instrument is foreseen for an optical grazing incidence spectrometer, to be mounted on the back of KT7D. This viewing channel can alternatively be used for a small Bragg spectrometer in order to observe C VI and Be IV lines below 10nm.

An additional new feature of the VUV and XUV instrument (KT7D) is its radiation shield, which should reduce the total radiation related background signal level by a factor of ten. It consists of a 10cm thick stainless steel structure protecting the detectors, channel plates and diode arrays, from X-ray and n-γ radiation, Fig.81. Fast neutrons, which are also present during high performance JET discharges, have a very small absorption cross section in the detector materials as well as in stainless steel. Therefore, the assumption is that fast neutrons pass through the shield and the detector without producing a considerable amount of radiation induced background.

KT7D together with the spatial resolving KT4 spectrometer at the midplane will be able to localise different impurity ions along fieldlines in the divertor area (inner strike zone, similar to KT1). In contrast to KT1, it covers the very important wavelength band between 10 nm and 30 nm and is furthermore capable of observing several impurity lines at the same time. The time resolution, however, is a factor of twenty lower than that for KT1.

As mentioned, the two viewing locations combined with the spatial resolution of the above described diagnostic systems will provide a new quality of VUV spectroscopy diagnostic. It will provide the capability of localising different ionisation stages along the field lines for the important impurities expected in the divertor area. This capability, is available for a wide wavelength range together with edge models will contribute to extending our understanding of impurity behaviour in the divertor region as well as in the scrape-off layer.

Visible Spectroscopy Divertor Plasma

There will be four visible spectroscopic systems capable of diagnosing the plasma in the pumped divertor. Two of these systems, KT5D and KT6D, are entirely new, whilst the other two, KS3 and KT3, already exist, but will require modification to a certain extent.

The existing multi-chord array on the Octant No:1 upper main vertical port will look straight into the divertor. Its lines-of-sight can be rearranged to give an improved coverage of the divertor plasma channel, but at the expense of reliable Z_{eff} profiles from the bulk plasma. However, the presence of the divertor plasma might preclude the latter possibility due to production of much extraneous light.

The existing Roof Laboratory link, system KY3, will be enhanced by the fitting of a new flange onto Octant No: 8B upper intermediate vertical port. This will provide a much wider field-of-view than at present, permitting observation of the outer half of the pumped divertor. The link will permit features down to ~200nm to be recorded, in contrast to the cut off at ~375nm using optical fibres. Several important Be lines should be observable.

The periscope viewing system, utilises either a coherent optical fibre bundle or a cluster of discrete fibres, to gain access through narrow tubes with re-entrant windows fitted to small circular ports located inboard and outboard of the divertor. By means of mirrors, a pair of periscopes in one octant is able to provide coverage of almost all of the divertor chamber in a radial direction. Periscopes can be fitted in six locations- Octant Nos:1B, 1C, 3D, 5B, 5C and 8B. Initially, three periscopes will be installed, two coherent bundles and one cluster of discrete fibres.

CCD cameras and filters, used in conjunction with the coherent fibre bundles, will provide 2-D pictures of the spatial distribution of spectral features from fuel, impurity and continuum emission. Using the discrete fibres, a spectral survey will be obtained using a grating spectrometer as analyser and a CCD camera as detector, at about ten different spatial positions in the divertor plasma channel.

The toroidal viewer, KT5D, will be located on Octant No: 7D near the midplane, viewing the divertor plasma in two toroidal directions, (co- and counter). Two bundles of ten discrete fibres will relay the light to grating spectrometers equipped with CCD cameras. The main purpose of the diagnostic is to measure flow velocities in the divertor plasma. By comparing opposing views of the same plasma, Doppler shifts should be identified without recourse to absolute wavelength calibration.

References

[1] S. Conroy, O.N. Jarvis, G. Sadler and G.B. Huxtable, Nuclear Fusion **28** (1988) 2127.

[2] G. Sadler, P. van Belle and O.N.Jarvis, Rev. Sci. Instrum. **61** (1990) 3175.

[3] M. Angelone, JET Report-IR(91)09

[4] O.N. Jarvis et al, Fusion Technology, **20** (1991) 265

[5] JET Progress Report, EUR 13493 EN (EUR-JET-PR8) (1990) p61

[6] P. Chabert et al., Proc 16th EPS Conf. on Contr. Fusion and Plasma Physics, Venice, Italy, (1989).

[7] JET Progress Report (1990), Vol.1 (1990) 71

[8] K Lackner et al, IPP Garching, Report IPP 1/195 (1981)

[9] H Summers et al, Atomic Data and Analyser Structure, in preparation

[10] D Pasini et al. Proc 18 EPS Conf. on Contr Fusion and Plasma Physics, Berlin (1991), also in Plasma Physics and Controlled Fusion

[11] TE Stringer, Neoclassical Transport in the Presence of Fluctuations, JET Report-P(91) 38 also published in Nuclear Fusion

[12] L Lauro Taroni et al., The Calculation of the Neoclassical Impurity Transport Coefficients, JET Report-R(91) 10

[13] S Hirshman, D Sigmar , Nucl. Fusion **21** (1981) 1089

[14] R Giannella et al., Proc 17th EPS Conf. on Contr Fusion and Plasma Physics, Amsterdam (1990).

[15] W. Fritsch, (1991), Private Communication.

[16] M. von Hellermann et al., Plasma Phys. Control Fusion. **33**, (1991) 1805.

[17] H.P. Summers et al. Z. Phy. D. Suppl 21 (1991) 517

[18] H.P. Summers, JET Report - P (91) 48.

[19] R. Hoekstra et al., (1992) Nucl. Fusion Suppl - submitted for publication.

[20] F de Heer et al. (1992) Nucl. Fusion Suppl - submitted for publication.

[21] Bartschat et al., JET Report - P (91) 09.

[22] H.P. Summers et al., Plasma Phys. Contro Fusion, 34, (1992) 325.

[23] Several contributions to Varenna Summer School (1991).

[24] H.P. Summers et al (1992) ADAS manual in preparation.

[25] H.P. Summers et al (1992) NATO Advanced Research Workshop on Recombination, JET Report P(91) 57.

Summary of Machine Operation

During 1991, JET operations were essentially made up of three main periods :

a) *The first period (Week 11 to Week 19)*

This period included the following activities :

- CODAS and power supplies commissioning in parallel with shutdown activities. Initially, this work was carried out in extended-day operation (Weeks 11 - 18), but as plasma operation approached, double-shift-day operation started in Week 19. Two separate incidents involving electric arcs on poloidal field coils (P3 Lower and P2 Upper) imposed breaks in the commissioning. The P3 lower coil was rapidly restored to operation (after 3 days) of the end of Week 19. However, the subsequent P2 upper coil incident resulted in a considerable delay (Week 20 to Week 23), before power supply commissioning could be restarted in Week 23. Significant time was required for the remedial work as an upper horizontal limb of the magnetic circuit had to be removed for access to the incident location. A further complication arose because of a vacuum leak associated with a diagnostic window, which required entry to the vessel for repair.

b) *The second period (Week 23 to Week 35)*

This period included the following activities :

- Power Supplies and plasma commissioning (Week 23 to Week 25). Plasma commissioning took some time as the vessel required reconditioning following the vessel entry;
- Execution of the experimental programme by the different task forces in 6-day working weeks, broken only by Public Holidays, JET Open Days (end of Week 26) and maintenance and remedial days (Monday and Tuesday of every third week);
- Plasma operation also involved the study of new in-vessel elements installed during the 1990/91 shutdown (e.g. lower and upper dump plates, a modified gas introduction system, new diagnostic systems and the NBI system in which all sources had been modified to operate at 140kV);
- Alternating current (AC) operation of the plasma for 4 days in Week 31. A plasma current pulse of 2 MA in one direction with a flat-top of 6s was reversed to achieve a current of 2 MA in the reverse direction for a flat-top of 6s. Additional heating in both phases of the current pulse was carried out.

c) *The third period (Week 39 to Week 51)*

This period followed a shutdown in which preparations for the Preliminary Tritium Experiment (PTE) were made. The time for the preparations was extended because of a rapid venting of the vessel caused by a vacuum leak of the in-vessel inspection system. A vessel entry was therefore arranged to effect the repair on a vacuum bellows and the opportunity taken to replace tiles on the upper X-point dump plates. These new carbon tiles were carefully machined and accurately installed to spread the plasma heat load more evenly.

This period included the following activities :

- Power Supply recommissioning and plasma commissioning which was slightly delayed as the torus had to be vented with nitrogen following the discovery of a vacuum leak on a diagnostic.
- Installation and commissioning of a uranium bed supplying deuterium to two sources of one of the neutral beam injectors (NBI). This was carried out to gain experience in operation of the NBI gas introduction system used in the PTE;
- Assessment of the heat loading characteristics of the carbon upper dump plate tiles;
- Execution of the experimental programme in 6-day working weeks broken only by maintenance and remedial days and a two-day period involving final preparations for the PTE;
- The Preliminary Tritium Experiment : this experiment (which is described in detail later in the report) involved tritium neutral beam injection and the operation of a gas collection system with tritium recovery. Special operational precautions were taken to ensure the success of this operation. During and following the actual experiment, machine operations were carried out in two-shift days and the gas collection system was also operated during the third shift;
- Lower Hybrid current drive system performance was improved to launch 3 MW power to the plasma;
- Neutron production was carefully restricted which meant that different gases for the plasma and neutral beam heating were used;
- Many magnetic configuration changes involving turn and polarity changes were made to enable the study of a wide range of plasmas.

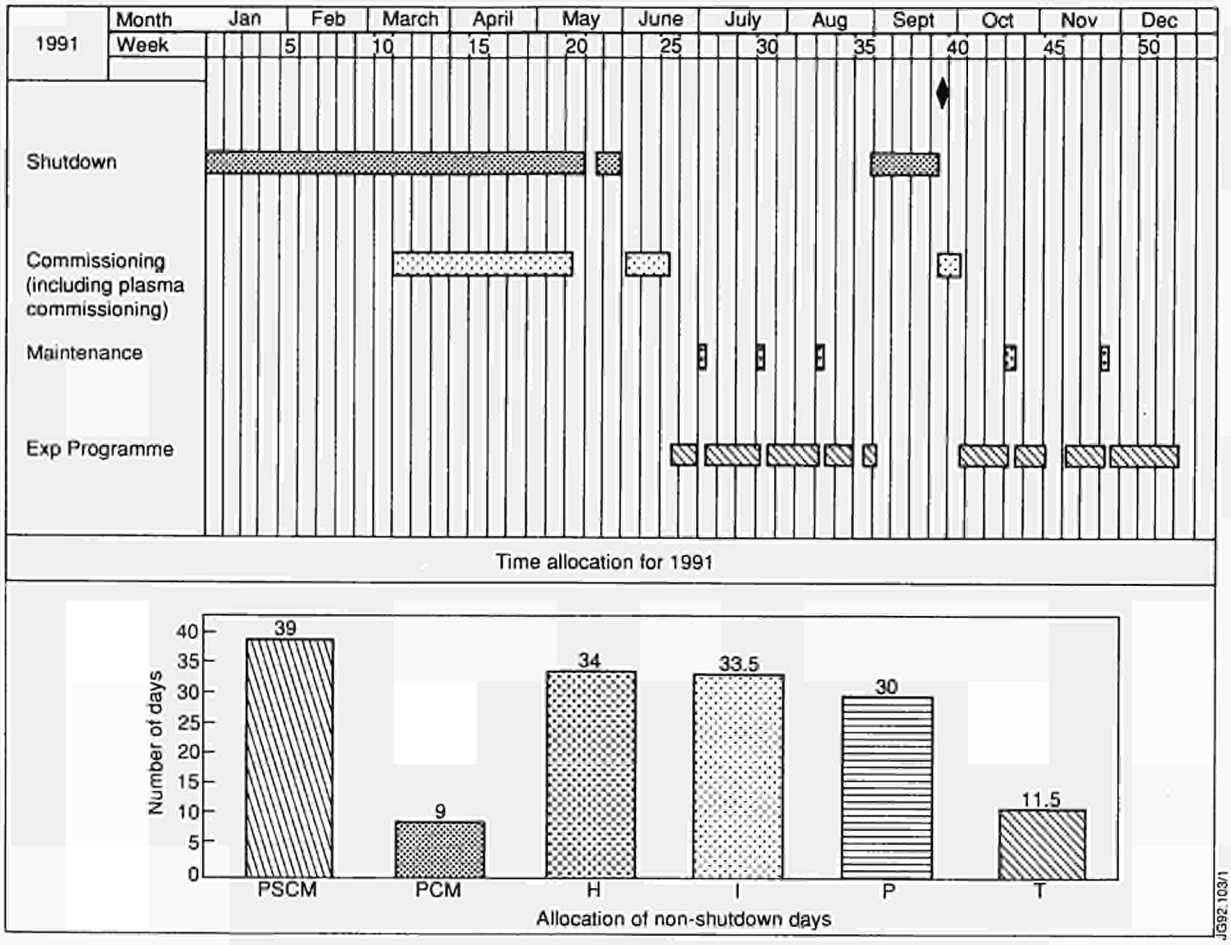

Fig 82: Allocation of days on which machine pulses were performed during 1991.

PSCM = Power Supplies and CODAS Commissioning
PCM = Plasma Commissioning
H = Task Force H
I = Task Force I
P = Task Force P
T = Tritium Task Force

In 1991 the machine was operated for 157 days, which was considerably more than in 1990. In fact, this time approached the total time of the 1989 and 1990 operation periods. The time for the experimental programme (109 double-shift days) was therefore greater than in 1990, even allowing for the increased time for commissioning required:

i) to restore plasma operation following the poloidal field coil incidents and vessel entries;
ii) to prepare for special experiments (e.g AC operation and the PTE).

The allocation of time to different activities is shown in Fig.82. The experimental programme was carried out by four Task Forces (and the Tritium Task Force for the PTE) and the double-shift days in which these were involved were distributed as follows :

Task Force H : High Performance	31.2%
Task Force I : Impurity Transport and Exhaust	30.7%
Task Force P : Physics Issues	27.5%
Tritium Task Force: PTE	10.6%

The number of pulses in 1991 was 3493, bringing the total number of JET pulses to 27023 (Fig.83). The percentage of commissioning pulses in 1991 (about 20%) was roughly the same as in 1990.

To avoid the possibility of damage to in-vessel components before the PTE, plasma currents were limited in 1991 to the smallest values compatible with programme requirements. This is shown in the plasma current distribution (Fig.84), where the higher plasma currents (>3 MA) make up only 51.0% of the total (c. f. 65.5% in 1990). Nevertheless, the percentage of low plasma current pulses (which

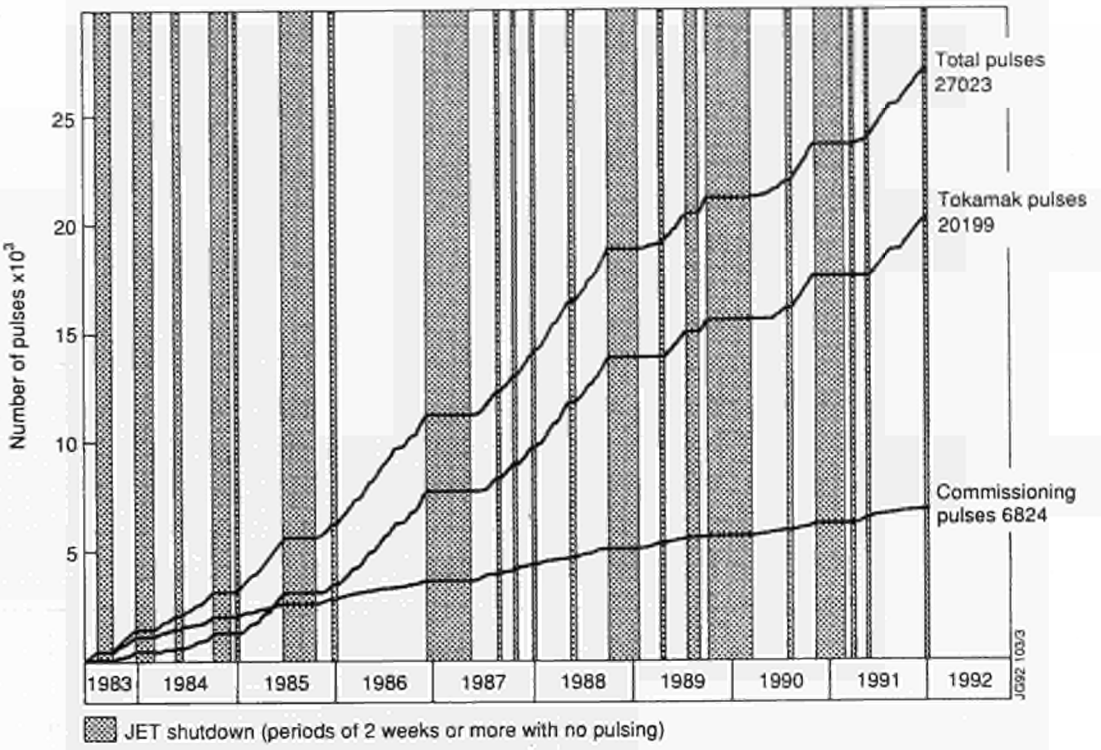

Fig.83: Cumulative totals of JET pulses 1983 to 1991

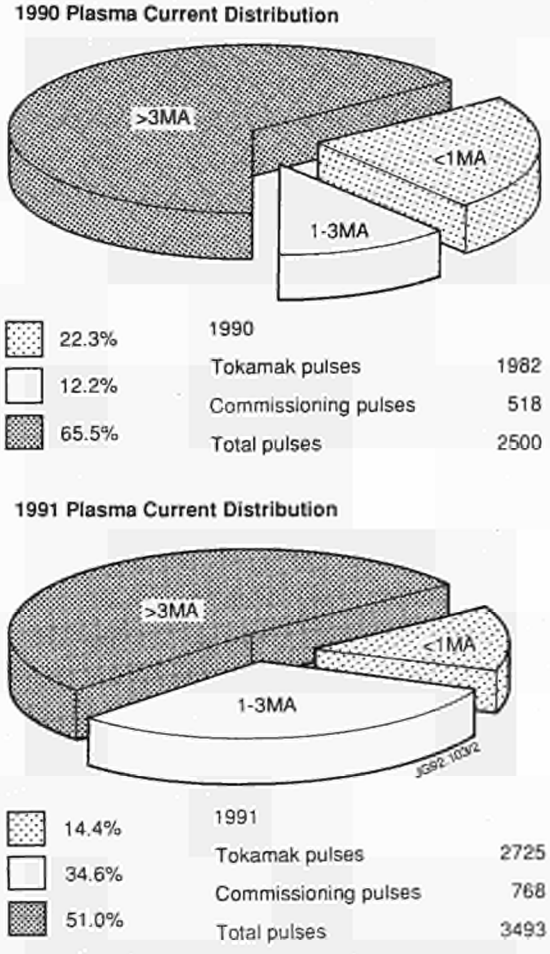

Fig.84: Comparison of numbers of pulses and distributions of plasma currents for 1990 and 1991. The plasma current distributions are for all tokamak pulses.

include plasma commissioning and "failed" discharges) is also much reduced.

1991 was an exciting year for machine operations, not only due to the success of the PTE but also due to :

- the long, unbroken runs of operation (representing improved reliability of performance of machine systems);
- novel operation of systems (AC performance);
- routine operation of the reactive power compensation for the high voltage, pulsed power supplies;
- introduction of mode-lock detection and pulse termination which greatly reduced the incidence of disruptions;
- upgrading of the shaping field circuit from 40 to 50kA current capability, improved current-drive performance (Lower Hybrid) and NB heating (high-energy deuterium, and tritium injection).

Technical Aspects of Preliminary Tritium Experiment (PTE)

To gain timely information on the introduction of tritium into JET, including retention of tritium in wall materials, operation of diagnostics, radiation monitoring and waste handling, it was decided in early 1991 to prepare for a limited tritium experiment which would involve only a few plasma

pulses. This would restrict the total amount of tritium used in the experiment so that the resulting activation of the vacuum vessel would not increase significantly above the level resulting from D-D operation during 1991 and early 1992. Therefore the impact of the first tritium experiment on the major shutdown planned to start in February 1992 would be minimised.

Preparations for the experiment included a physics programme to define the optimum plasma parameters, method of injection and diagnostics requirements, as well as a technical programme to design and install special equipment to inject tritium and recover tritiated exhaust gases. Safety aspects included the preparation of an overall probabilistic safety assessment and obtaining the requisite statutory and other approvals for the first tritium experiment. Further preparations included procurement of tritium, provision of a secure storage facility for tritium, training of staff, writing emergency procedures, and carrying out emergency exercises. In addition the tokamak, its diagnostic equipment and auxiliary systems had to be brought to a state of readiness for this experiment. Generally, only systems essential for the experiment were used. The pellet injectors and radio frequency handling systems and many diagnostics were not used and their vacuum systems communicating with the torus vacuum were isolated.

In parallel to preparations for the experiment, a waste sorting facility was designed and manufactured and arrangements were made for the intermediate storage of tritiated components. The waste sorting facility will receive components and secondary waste loaded in transport containers from the JET tokamak during the next shutdown in which all internal vacuum vessel components will be removed to allow the installation of the components of the pumped divertor.

Objectives

The main motive for carrying out the first tritium experiment was to gain important technical and physics information essential for the D-T phase. The principal objectives were:

(i) To produce in excess of 1MW of fusion power in a controlled way;

(ii) To validate transport codes and provide a basis for predicting accurately the performance of deuterium-tritium plasmas from measurements made in deuterium plasmas; to establish for these plasmas the consistency of different experimental measurements; and to calibrate diagnostics;

(iii) To determine trutium retention in the torus walls and the neutral beam (NB) injection system;

(iv) to demonstrate the technology related to tritium usage (tritium NB injection, cryopumping and tritium handling); and

(v) To establish safe procedures for handling tritium in compliance with the regulatory requirements.

Preparations for First Tritium Experiment

After an initial scoping study for the feasibility to carry out a limited D-T experiment, two Task Forces were formed to prepare for the experiment. One Task Force (P)was charged with studying the physics issues, including definition of optimum plasma parameters to be used, prediction of expected performances, as well as the selection of the actual tritium injection scenario. The other duties of Physics Task Force (P) included definition of the diagnostic systems, their testing and evaluation. A Technical Task Force was charged with the procurement of tritium, its safe and secure storage on the JET site, the design, testing and installation of tritium injection systems, and as an exhaust gas collection system. Further activities included the preparation of the safety analysis report, establishment of interfaces with the UK Authorities to obtain statutory and other approvals to allow the experiment to be conducted, the installation of radiological protection instrumentation and preparation of waste management facilities and procedures to deal effectively with the aftermath of the experiment.

Further tasks involved the training of staff, relating to operation of special equipment, and concerning the general handling of tritium. The latter involved a large number of JET staff. Other activities included the preparation of a measurement programme to assess tritium retention in the wall materials, during and after the experiment and the preparation of a site emergency plan as well as the installation of an emergency control desk in the JET Control Room.

Physics Issues and Experimental Plans

Extrapolation of the best results obtained in D-D discharges during earlier experimental campaigns in JET to D-T pulses predicted that fuelling with 14% gas mixtures (1 part tritium to 6 parts deuterium) would yield a total fusion power of 0.9 to 2.4 MW depending on which prediction model was used (provided that the wall recycled material would be of similar isotopic composition). This tritium concentration in the plasma was used as the basis for the first tritium experiment.

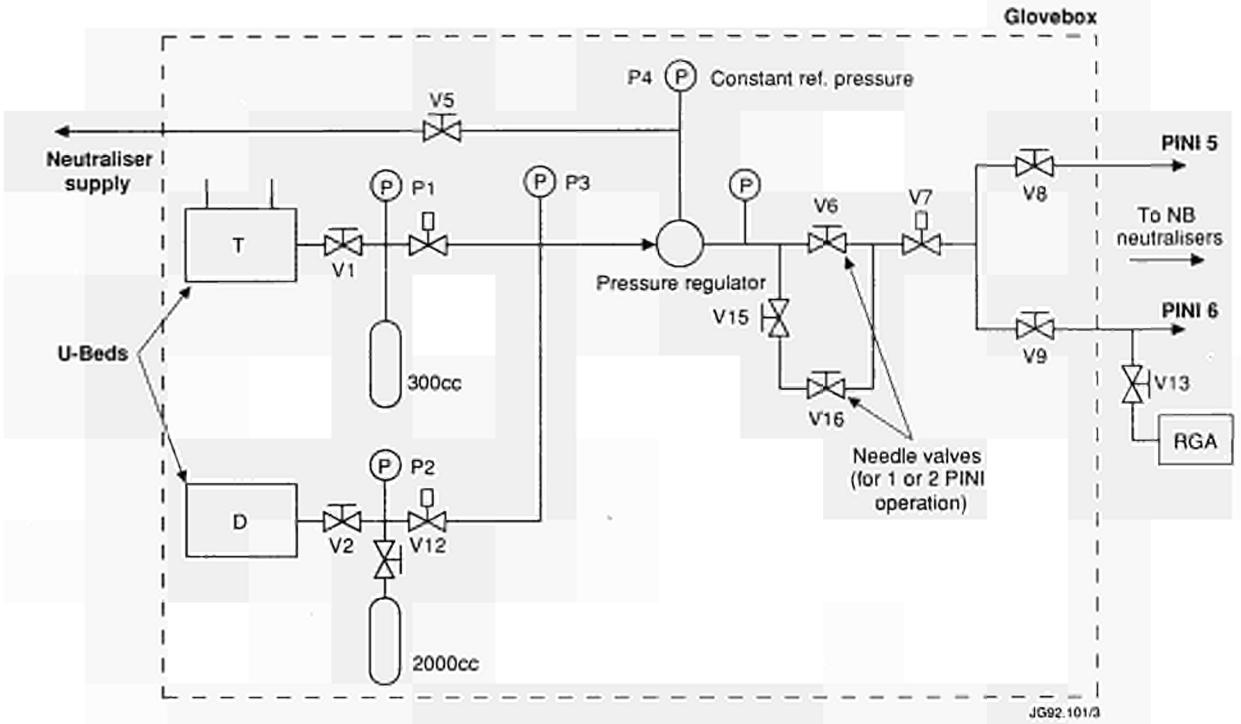

Fig. 85: Layout of tritium gas supply system

Two methods of tritium fuelling of the plasma were considered, namely gas puffing and neutral beam injection. Both methods required enhancement of existing hardware. Eventually, gas puffing was kept only as a fall-back solution and tritium introduction, using two neutral beamline sources (PINIs) and neutralisers allowing more defined deeper fuelling into the plasma, was developed for one of the two JET neutral injectors.

The experiment was split into two phases. The initial calibration phase used a very weak tritium-deuterium mixture (1% tritium in deuterium) for the 'tritium' PINIs and would include checking of diagnostics, especially neutron diagnostics. This phase involved 10 to 15 tokamak discharges. The second phase, the experiment proper, used pure tritium for the two 'tritium' PINIs and involved two useful tokamak discharges.

One of the main constraints on the experiment was to keep the activation resulting from D-T neutrons at a low enough level to allow a prolonged period of work inside the vacuum vessel during the shutdown planned to start in February 1992. The total production of D-T neutrons was therefore restricted to 1-2 x 10^{18} resulting in an in-vessel dose rate of 25-50 μSv/hour some twelve weeks after the experiment. This dose rate is lower or comparable to that expected from D-D neutron activation (~50 μSv/hr) from the 1991-1992 experimental campaign.

For this reason, the total amount of tritium to be used was limited to 74 TBq (2,000 Ci) which was sufficient for approximately 6 injection pulses of 2s duration with two beams. Two or three of these pulses would be used for injection into the plasma, the others would be used as commissioning pulses of the tritium beams which would not involve injection of tritium into the torus.

Description of Special Equipment

For the full D-T phase of JET an exhaust gas processing system, the JET Active Gas Handling System (AGHS) will be available to remove impurities from the hydrogen isotopes, to separate purified hydrogen into isotopic fractions and to re-supply the isotopic fractions to the tokamak subsystems. The installation of the AGHS is not yet complete and, therefore, for the first tritium experiment, special equipment had to be installed. This not only involved a gas collection system, but also modifications to the neutral injectors for tritium introduction.

Tritium Gas Introduction

Two PINIs of one JET neutral injector were modified for tritium service in the experiment. For these PINIs the gas was supplied from two uranium beds (U-beds), one loaded with deuterium (for commissioning) and the other with tritium (for fuelling) mounted close to the PINIs outside the

beamline magnetic shielding. The modifications to these PINIs did not involve the vacuum boundary but were concerned with the internal flow distribution so as to allow tritium introduction at ground potential. The remaining PINIs of the Octant No: 8 beamline were used for deuterium injection, both with and without concurrent tritium injection. The gas for the six deuterium PINIs was supplied from the neutral beam gas handling system, which is the existing arrangement.

The gas supply arrangements for the two tritium PINIs are shown schematically in Fig.85. The U-beds are the Mark 4 Amersham-type, all valves are JET standard as approved for tritium service in the AGHS with the exception of a few valves which are JET standard isolation valves. The pressure regulator is of the AGHS standard diaphragm-type, the reference pressure of which is set by the admission of a fixed quantity of deuterium from the existing neutraliser gas supply. An absolute manometer was used to measure the quantity of gas admitted to the PINIs.

All tritium primary containment and associated instrumentation were installed within a proprietary glass re-inforced plastic glove box. The glove box was connected by temporary ducting to an authorised discharge stack equipped with ionisation chamber and sampling system to monitor tritium releases. Ventilation was induced by a fan in a temporary ducting to maintain the enclosure at a slight underpressure with respect to the Torus Hall atmosphere. The glove box was provided with glove ports to allow operator manipulations and feedthroughs for service cables. The U-beds were installed in the glove box and the associated pipework, valving and instrumentation were leak tested just before the start of the experiment.

The essential features of the design of the overall system (Fig.85) include:

i) Provision of a deuterium loaded U-bed, in addition to that for tritium. This enabled the total system, including control and instrumentation, to be fully tested and used for deuterium injection experiments under identical conditions to those to be used with tritium.

ii) The combination of gas reservoirs, pressure regulating valve and needle valves provided constant gas flow for the envisaged pulse duration.

iii) Change from D to T and/or one or two PINI operation was accomplished by opening or closing the appropriate hand valves and did not entail any changes to pre-set calibrations of the needle valves.

iv) All internal pressures were sub-atmospheric.

The sizes of the various reservoirs, and the value of the reference pressure, were determined from the characteristics of the U-bed measured in the Testbed. The larger volume on the deuterium system was to allow full isotopic mixing of the total contents of the 1% T2, 99% D_2 U-bed mixture used in the first phase of the PTE and still maintained sub-atmospheric pressure. The size of the tritium reservoir was chosen to maximise the utilisation of the 1 barl of tritium available for the PTE.

The complete system was manufactured and assembled in the *"clean conditions"* area to UHV standards, using certified stainless steel and qualified welding procedures. Unavoidable demountable joints utilized nickel gaskets and were of the JET approved type. The pressure regulator used had been developed for the final D-T phase of JET.

Following construction, the complete system was fully commissioned prior to installation, close to the PINIs, in the Torus Hall where the glove box was connected to the dedicated ventilation system for the PTE which included radiological monitoring to detect any tritium release into the glove box.

In addition, the Octant No.8 Injector was prepared for the safe handling of tritiated water (in the event of a water leak during tritium operation) by fitting all the lower flanges with drainage connections.

Modification of PINIs for Tritium Injection

The standard PINI configuration utilizes two gas feeds; one at high potential for the plasma generator (ion source) plus one at ground potential for the neutralizer gas. For a number of technical reasons, it was decided to dispense with the gas feed at high potential and to introduce the source and neutralizer gas from a common feed at ground potential.

To maximise gas utilization and hence minimise the total tritium gas flow, the gas was introduced close to the final earth grid of the accelerator. For a given flow rate this maximises the gas target for neutralization and offers the maximum gas conductance into the plasma source to replace the gas which is removed in the form of the extracted ion beam.

The final optimised configuration is shown in Fig.86. The relatively thick walls of the final grid holder box (at earth potential) were deep-drilled to feed the gas into the gap between the grid holder box and the first stage neutraliser. A flexible metallic seal ensures the gas is directed into the first stage neutralizer close to the earth grid.

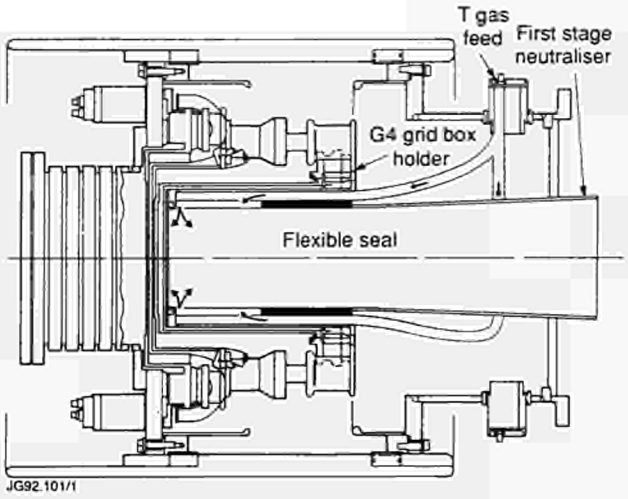

Fig.86: Modified JET PINI for use with tritium.

Detailed pressure measurements as a function of gas flow were carried out in order to fully characterise the system. Operational tests confirmed that this solution was not sensitive to Paschen breakdown in the accelerator structure. This configuration will now be used for all 140/160kV PINIs for the final D-T phase of JET operation. From beam neutralisation measurements in deuterium, the required optimum flow rate of tritium was predicted to be 17 mbℓs^{-1} per PINI.

Optimisation of arc and gas stabilisation times immediately prior to beam extraction enabled these to be reduced by a factor two or three to 0.5s which further reduces the overall tritium gas consumption. Two PINIs were modified for use as tritium injectors, both of which were conditioned and fully characterised at 80kV prior to installation on the tokamak.

Modification of 80kV D_2 PINIs for Higher Power

To maximise the performance of the "hot Ion" mode plasmas in the PTE, two 80kV tetrode PINIs were modified to deliver ~ 50% more power. In their standard configuration using deuterium, these PINIs deliver 40A of extracted ion beam at 80kV. By reducing the gaps in the ion extraction/acceleration system, the extracted current was increased to 60A at 80kV. Analytic calculations of the modified structure were confirmed by detailed computations of the ion optics.

As shown in Fig.87, the computations confirm that higher current beams can be produced without major beam aberrations or increase in beamlet divergence. Consequently, two PINIs were modified to this high current configuration and the increased performance was demonstrated prior to installation on the tokamak.

Isotope Exchange

As a consequence of the limited amount of tritium available for the PTE, it was essential to minimise the number of beam pulses required to change from deuterium to tritium operation. This was quantified by studying the change from deuterium to hydrogen operation using the neutron yield from beam-target reactions in the Testbed beam dump, to measure the deuterium contamination in hydrogen beams.

Following operation with deuterium beams during which the beam-target reactions achieved their equilibrium value, the operating gas was changed to hydrogen and the neutron yield was used to monitor the level of residual deuterium contamination of the hydrogen beam. Following a period of filament degassing shots, the isotopic exchange was ≥ 95% complete after 1 to 2s of PINI operation. The initial 5% contamination, measured in the first pulse, was subsequently observed to decay with successive pulses.

Analysis of the trajectories and power loadings in the injector due to the presence of ~ 5% D in a tritium ion beam, indicated that this would not present any difficulties and it was concluded that only two beam pulses would be required to change from deuterium to tritium operation. Finally, measurements were also made, using the same technique of exchange between isotopes implanted into beam line components which intercept the energetic beams. This data formed the basis for the removal of implanted tritium following the PTE.

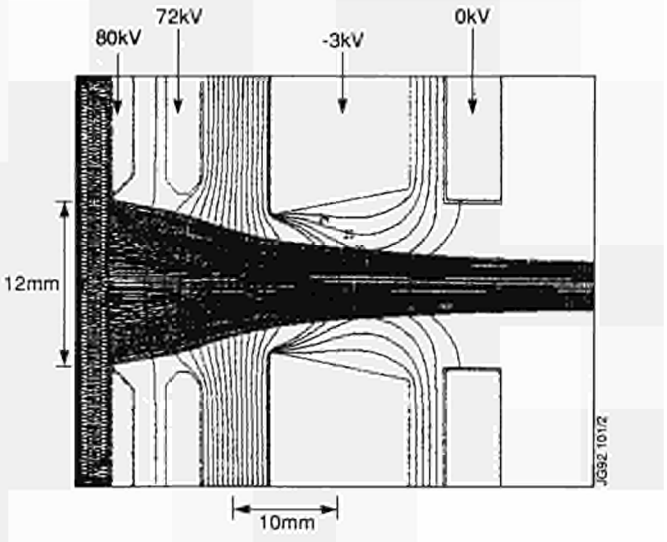

Fig.87: Computed particle trajectories for higher current version of the 80kV PINI.

Control of Gas Introduction System

The major preparatory work for the PTE related to the design and manufacture of the control and instrumentation for the Tritium Gas Introduction System (TGIS) and its integration into the operational software system which controls the injectors. Computational studies of the power and particle deposition profiles of tritium and deuterium in the envisaged target plasmas, were also carried out with a view to maximising deposition in the plasma centre.

A basic feature of the control system was the use of a single set of controls plus cables and pneumatics for operation of *either* the deuterium U-bed *or* the tritium U-bed. This ensures that there was no possibility of cross-contamination of the deuterium by tritium, or vice-versa. In addition, it enabled considerable operational experience and familiarity to be gained with the total system using deuterium prior to the PTE. The main disadvantages was the need to enter the Torus Hall to effect the change-over and the time taken to cool one U-bed and heat the other. However, this disadvantage was far outweighed by the simplicity and advantages discussed above. All operations relating to the TGIS (eg., installation and commissioning, change of D_2 and T_2 U-beds, operation of hand valves etc)., were governed by extensive strict written procedures.

The control system also incorporated fail-safe features with regard to over-pressure and over-temperature interlocks in addition to redundant temperature and pressure monitoring, plus a key-switch interlock to enable the use of the tritium U-bed. The output from all sensors and the status of all pneumatic valves of the TGIS were permanently displayed on a dedicated mimic in the JET Control Room.

Compatibility between the injector operating software (in particular the setting of the ion deflection magnet) and the use of deuterium or tritium, was ensured using a fail-safe interlock monitored by the software.

With respect to the studies of beam penetration, experiments using both injectors fully equipped with 140kV PINIs compared to operation with one injector at 140kV and one at 80kV, indicated that power and particle deposition in the central third of the plasma, may be an important prerequisite in obtaining the best performance hot-ion H-modes in JET. This led to the upgrade of the 80kV PINIs described above. The variation in central fuelling rate for the 140kV and upgraded high current 80kV PINIs (deuterium beams) over the density range applicable to the PTE are shown in Fig.88. Also shown is the computed deposition for the 80kV tritium beam.

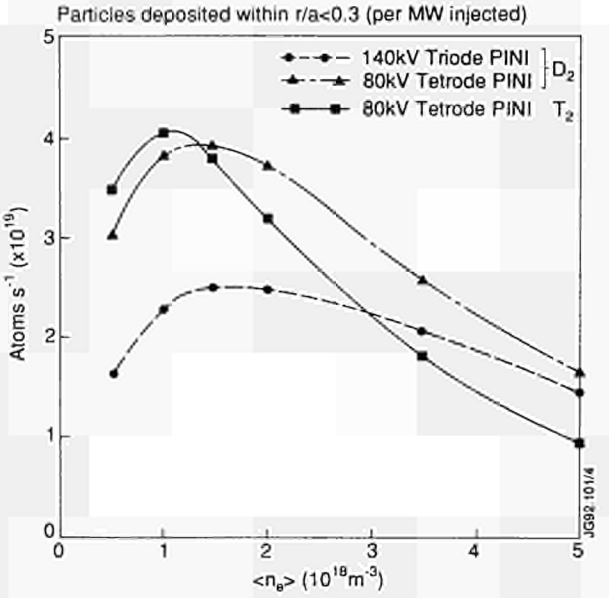

Fig.88: Computed particle deposition profiles for the configurations used in the PTE as a function of volume averaged density of the target plasma.

The PINI configuration of the two injectors for the PTE and subsequent experimental programme was, therefore, as follows:

- Octant No. 4: 8 x 140kV (D)
- Octant No. 8: 4 x 140kV (D)
  + 2 x modified 80kV (D)
  + 2 x 80kV (T)

The above configuration was employed to develop and optimise the hot Ion H-mode plasma using deuterium in the tritium PINIs. All PINIs were optimised using data from the Test Bed with respect to minimising the total gas consumption. This was in order to minimise the total gas load to be processed when tritium was introduced, by minimising arc and gas stabilization times and optimization of the total gas throughput.

Following this period of injector and plasma optimization, the deuterium U-bed was replaced by one containing 1% T and 99% D in order to carry out injection experiments which defined the fuelling requirements for the 100% T beams, and also to gain experience with the regeneration and recovery of tritiated gas using the dedicated tritium recovery system described elsewhere in this report. The 1% T U-bed was then replaced by a 100% D bed and the 100% T U-bed was installed in preparation for the PTE.

The following sequence of pulses was planned for the tritium PINIs during the one day execution of the PTE:

i) Final optimization of plasma with full NB power using D_2 in all PINIs;

ii) Change-over from D_2 to T_2 U-bed;

iii) Two filament degassing shots on T_2 PINIs;
iv) One beam pulse from both T_2 PINIs (0.7s arc + 0.1s beam) to confirm deflection magnet setting;
v) Two beam pulses from both T_2 PINIs (0.7s arc + 0.8s beam) to confirm perveance optimization and beam power;
vi) Injection into Tokamak of two T_2 PINIs + 14 D_2 PINIs.

This sequence was executed exactly as planned. The first tritium beams were produced at 78kV without any breakdowns and although measured perveance was some 10% less than predicted, no attempt was made to increase the voltage or the current to their maximum values, in order to maintain the reliability obtained in the first pulses.

The full power shot using all 16 PINIs was successfully repeated some hours after the first, in which 14.3MW was again delivered to the plasma with 1.5MW being from the tritium beams. Power waveforms for this pulse are shown in Fig.89.

Cryo Pumps

In order to minimise the time taken to regenerate the cryo-pumps when tritium had been used, a *"fast"* regeneration scenario was developed. This was accomplished by the injection of room temperature helium gas into the liquid helium circuit of the cryo-pump. In addition to giving an enhanced boil-off of the liquid helium and emptying the liquid helium in the pumps in ~ 15-20 minutes, this also served an additional and more important function. In view of the lower vapour pressure of T_2 compared to D_2, this *"warm"* gas ensured that the T_2 was not cryo-distilled onto well insulated cold spots, eg. the cryo-feed and internal manifolds, where it could remain condensed during the removal of D_2 gas. This mode of regeneration has proved so successful that it is now routinely employed in non-tritium operation.

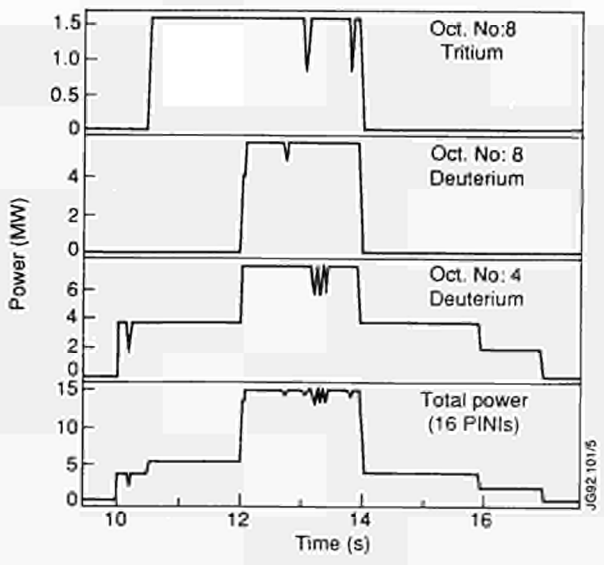

Fig.89: Injected power waveforms obtained during the PTE.

The Gas Collection System

The operational functions of the Gas Collection System (GCS) can be defined, as follows:

(i) To act as a temporary tritium-compatible primary pumping system, in place of the Roots blowers and rotary pumps, for the limited duration of the first tritium experiment;
(ii) To constitute a measuring unit to account for tritium exhausted from the torus and the two neutral beam injectors;
(iii) To separate hydrogen isotopes from the residual exhaust gases and safely store those isotopes by circulation through and hydriding of cold uranium beds;
(iv) To store tritiated residual gases (such as methane) for future reprocessing in the JET AGHS system or, following sentencing, discharging to stack if activity levels allow;
(v) To detect, safely handle and facilitate recovery from air inleakages into the torus, neutral injector, vacuum transfer lines or the GCS itself particularly with respect to the creation of hydrogen/air mixtures within the flammable range;
(vi) To assist the recovery from a water leak incident by providing a means of pumping and collecting water vapour from the torus or neutral injectors.

As shown in Fig.90, the GCS is connectable to the torus pumping duct or to the neutral injector pumping ducts. The valves connecting the ducts with their respective backing pumps were closed and blocked for the duration of the experiment. The tubular cryopump (Cold Finger) which replaced the backing pumps is constructed of a stainless steel flexible hose and filled with circa 100g of activated charcoal and is immersable in a 250ℓ liquid helium dewar. At the operating temperature of 4.2K all condensable gases including protium, deuterium and tritium are pumped by cryocondensation. The charcoal pumps helium by cryosorption. By warming up of the Cold Finger the gases can be collected in a 345ℓ reservoir. A scroll pump (Normetex) allows circulation of gases through the U-beds for hydrogen isotope abstraction. This pump is equipped with a non-return valve in a bypass line

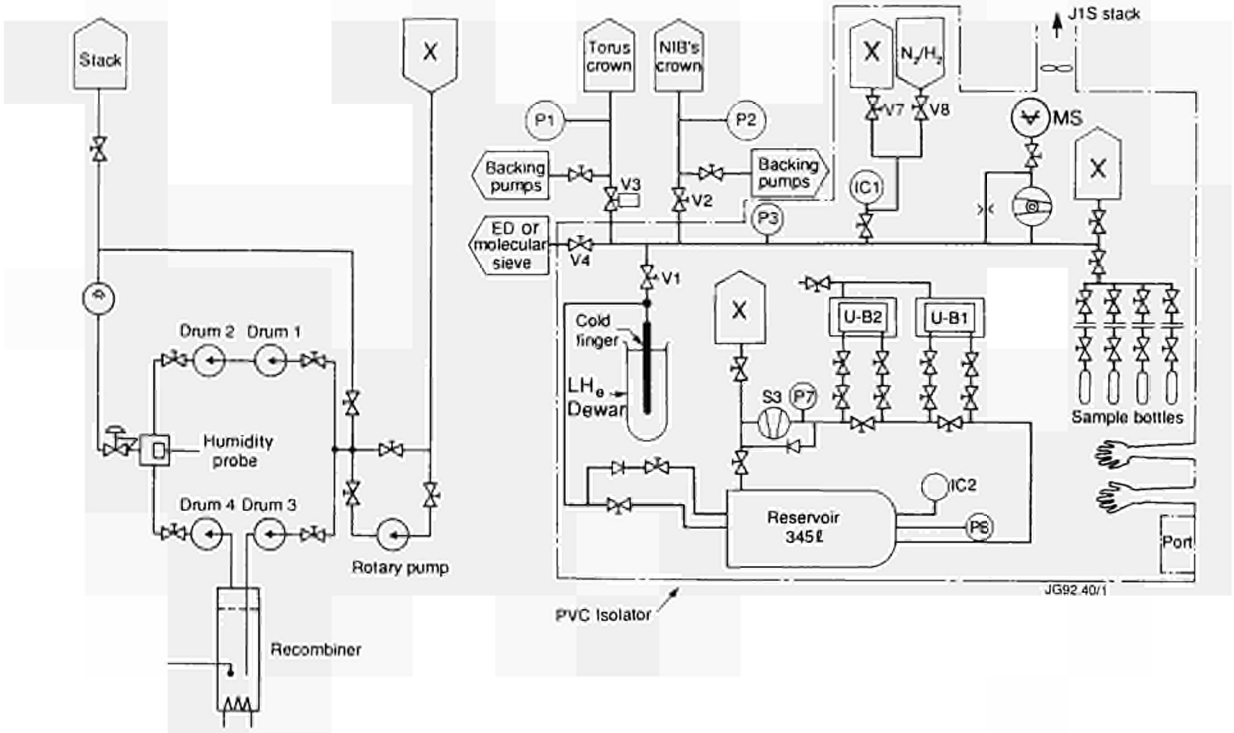

Fig. 90: Layout of gas collection system.

to protect against excessive discharge pressures. The U-beds (UB1 and UB2) are of JET design and each contains 4.3 kg depleted uranium. They have electrical bed heaters installed. In the event of bed de-activation due to accidental air inleakages, the U-beds can be re-activated by heating. All equipment required for re-activation was installed to the U-bed but with no external connections made.

The 345ℓ reservoir is instrumented with the JET standard AGHS ionisation gauge (IC2) and two pressure gauges (P7 and P8). On the torus/neutral injector side of the interface valve V1, there are facilities for gas sampling and composition and activity monitoring. Composition monitoring (principally to detect air inleakage) is done by a mass spectrometer (MS). Activity measurements are by a JET standard AGHS ionisation chamber (IC1) which allows the addition of nitrogen or protium to raise the gas pressure within the chamber to that corresponding to a calibration condition. This branch of the GCS also has a pressure gauge (P3) for real time measurement of the quantity of exhaust gas in the vacuum duct and a manual valve (V4) for connecting the branch to a molecular sieve drier to facilitate recovery in the event of air or water inleakages in the torus or neutral injectors.

In the event of an accidental torus air inleakage in the range that has historically occurred during JET operations, the torus would take days to vent to near atmospheric pressure. The humidity of the inleaked air and high temperature environment within the torus vacuum vessel would result in most of the tritium being in the oxide form in the latter stages of venting, thereby offering the possibility of removal from the exhaust stream by molecular sieving. To mitigate such an accident the molecular sieve drier was installed as shown in Fig.90. The drier consists of two parallel banks of zeolite granule filled 210ℓ drums with interconnecting pipework and valves. The torus exhaust (inleaked air and tritium) is drawn through the drums by an industrial vacuum cleaner with water breakthrough detection by a hygrometer. The discharge is subsequently routed directly to the monitored stack. The water capacity of each granule filled drum is circa 25ℓ. One row of molecular sieve drums includes a catalytic convertor which may be heated to 500°C allowing conversion of hydrogen isotopes and methane to water vapour which is subsequently absorbed in a molecular sieve drum.

The components of the GCS containing tritium during normal operation are enveloped within PVC isolators. The isolator is provided with glove ports to allow the operators to manipulate the appropriate valves. The isolators are ventilated by a fan and connected by leaktight temporary ducting to the monitored discharge stack.

Supply and Storage of Tritium

Five Amersham Mark 4 type U-beds filled each with 320g of uranium were activated at JET. These beds can store up to 18.7 bar.ℓ or 2 PBq (54,000 Ci) of tritium as uranium tritide and therefore measurements were carried out to define discharge characteristics of these beds with the very small quantities of gas used for the first tritium experiment. These experiments confirmed that more than 74 TBq (2000 Ci) can be recovered from a U-bed loaded with 88.8 TBq of tritium (2400 Ci, simulated with deuterium).

Tritium was loaded on the U-beds at the premises of a supplier of tritium. In the case of the 1% tritium mixture the bed was pre-loaded at JET with deuterium and 1.85 TBq of tritium with a certified purity of 99.4% was added at the tritium supplier. During loading, a small sample of the tritium was taken and analysed at the AEA Harwell Laboratory, UK. The analysis resulted in a much lower than certified tritium purity, ie approximately 94% tritium (in the form of T_2, HT, DT), the main impurity being approximately 5.1% protium (in the form of H_2 and HT). However, the mass spectrogram indicated background impurities and protium could therefore be largely the result of impurities in the mass spectrometer. To resolve this discrepancy, a sample was taken of the 1% tritium mixture before removing the U-bed from the neutral injector glove box. This sample was analysed using a mass spectrometer at the CEA Valduc Laboratory, France. The 1% tritium mixture yielded total contents of tritium, deuterium and protium of 0.97% (±0.05), 98.47% (±0.1) and 0.44% (±0.04) respectively. The amount of protium is lower than in the Harwell analysis and could have been introduced as an inherent impurity of deuterium, which according to the suppliers' brochure may contain up to 0.6% protium.

For the second phase of the first tritium experiment, an empty U-bed was charged at the supplier of tritium (from the same source as used for the 1% T in D mixture) with 88.8 TBq (2400 Ci) tritium. The Amersham U-beds were stored on the JET site inside a safe storage facility.

Existing control access arrangements to the JET Torus Hall were used to safeguard the U-beds whilst mounted near the neutral injector. The GCS area was made into an access controlled area using a computer controlled turnstile system. The area was monitored by television cameras with pictures relayed to and recorded in the JET Control Room. For the duration of the tritium experiments and for the week thereafter, access was further controlled by a permanently manned entrance post. Maintenance work in nearby áreas was controlled and restricted to an absolute minimum. Transfer of U-beds on the JET Site is controlled by formal procedures which involve Health Physics inspections.

Safety Analysis Report

A detailed probabalistic safety analysis report was prepared to appraise the radiological risks, principally those resulting from the introduction of tritium into the torus and subsequent collection in the first tritium experiment. Due to the fact that failure rate data on components used in the plasma environment are very limited, failure rates based on JET operating experience since 1983 were widely used in the report thereby taking account of factors intrinsic to JET design and operation. The safety analysis demonstrated that for all foreseeable worst cases of each category of accident, the estimated risks (based on conservative assumptions as to occurrence probability and release consequences) adequately satisfied the AEA standards for public and worker risk.

Radiological Protection Instrumentation

Glove Box Monitoring

The glove box for the neutral injector gas introduction and the isolators for the GCS were monitored for tritium leakage by connecting standard portable RPI type instruments with their own sampling pump into the exhaust ducting. The exhaust duct for the injection system joins the other ducts in the GCS. The gas sampling points to the ducts were made outside the JET biological shield thus avoiding the need for shielding of the instrument.

Working Area Monitoring

Fixed gamma and neutron monitoring instruments were installed early in the JET programme in the areas around the Torus Hall to which personnel have access. They are fully commissioned and operational. In addition, there are high level gamma and neutron monitors in the Torus Hall and two medium level instruments. One of these has remote electronics which may be used to monitor radiation levels prior to personnel entering the Torus Hall. Additional tritium area monitors were installed and commissioned prior to the first tritium experiment. The levels of radiation of all working area instruments are displayed on the JET computer data acquisition system (CODAS) and they also alarm locally. Their sensitivity is more than adequate to ensure that exposure of individuals is kept well below specified JET limits. A sufficient number of portable instruments and sampling

units was made available to carry out any ad-hoc monitoring required.

Stack Monitoring

The radiological protection instrumentation and monitors for the Torus Hall air conditioning stack and the basement air conditioning stack were installed prior to the first tritium experiment. The Torus Hall exhaust was connected to the air conditioning stack so that releases of activated air, particulate, and tritium could be monitored. The discharge stack for the glove box, isolators and backing pump exhaust ducts was instrumented with an ionisation chamber as well as a sampling system consisting of silica gel columns and a low temperature catalyst for conversion of hydrogen isotopes to water. Stack samples were scheduled to be analysed weekly.

Environmental Monitoring

A programme of air, rain water, ground water and river sampling has been in operation for a number of years. Tritium environmental monitoring equipment has been installed at several points within the Culham Laboratory Site boundary since mid 1990. This has enabled a level and variability of the background of tritium in the atmosphere around the JET buildings to be assessed. In addition, passive tritium, gamma and neutron monitoring devices have been installed around the site boundary for assessment of accidental doses. Crop sampling within the Culham Site was in operation before the experiment. The above programme will enable the Project to clearly demonstrate that no significant environmental effect has resulted from the first tritium experiment.

Training of Staff

Staff members were trained in the operation of the tritium injection systems as well as the GCS. The latter involved 24 hour operation, ie three-shift schedule. A large number of staff peripherally involved with the first tritium experiment attended training sessions on the general handling of tritium and in particular on the handling of tritium during the first tritium experiment. This included the detailed response to incidents which might occur.

Authorisations

The safety analysis report was reviewed by the UKAEA's Safety and Reliability Directorate (SRD) and endorsed by the JET Fusion Safety Committee at which SRD is represented. This formed the basis for the decision by the UKAEA to allow the experiment to proceed. The decision to carry out the experiment was taken by the JET Council.

All radioactive discharges and waste disposals must be made in accordance with an authorisation granted by Her Majesty's Inspectorate of Pollution (HMIP) and must be recorded. In good time before the experiment, JET lodged an application with HMIP for authorisations required for the full D-T Phase of JET. These were granted before the first tritium experiment. Furthermore, HMIP issued a Certificate of Registration for holding up to 33 PBq (900 000 Ci) tritium on site. In addition there is the overriding principle that Best Practical Means (BPM) must be used to limit discharges, even though they are within the authorised limit.

Emergency Plans

An emergency plan for the full D-T Phase had already been produced well ahead of the first tritium experiment and emergency instructions were specifically written for the experiment and endorsed by the JET Fusion Safety Committee. The JET Control Room was modified to include a separate Incident Desk and other modifications were made to enable the JET Control Room to function as an Emergency Control Centre. Site warning alarms and additional instrumentation such as wind monitoring equipment were installed. Two emergency exercises were held to test the response of the JET incident response team and the interaction between the various staff groups involved in an emergency.

Information to the Public

Two months before the tritium experiment, details were given to local organisations including the County Council, District and Parish Councils. Information was also given to local farmers to explain the use of tritium and seek their approval for crop and milk sampling for environmental monitoring analysis.

Waste Handling

Vessel Components

A survey of the waste arising during the 1992/1993 Shutdown has been carried out. Predictions made for the induced activity in components to be removed from the vacuum vessel during the 1992/1993 Shutdown together with the additional predicted activity due to tritium (after a 3 month clean-up phase) show typical levels for first wall components in excess of the conditions for acceptance as Low Level Waste (LLW) for the Drigg waste repository in the

UK. The waste components will therefore have to be classified as Medium Level Waste (MLW) unless the tritium levels can be reduced. JET aims to develop suitable decontamination techniques to reduce the levels to below the upper threshold for LLW at Drigg (12 kBq g^{-1}). This may include baking and surface treatment of components. To gain knowledge on the distribution of tritium hold-up inside the vacuum vessel, graphite tiles will be removed from various poloidal and toroidal positions and measured for tritium.

During the 1992/93 shutdown, all internal components will be removed from the vacuum vessel. Transport of the materials from the Torus Hall will be in sealed, standardized (ISO) freight containers to a waste sorting facility which is being constructed and will be commissioned before the start of the shutdown. Radwaste monitoring and determination of tritium levels of components will be carried out in this waste sorting facility as well as packing in waste containers. Many components will not be classified as waste but will require temporary storage until they are either re-used or declared waste. A number of freight containers will be prepared for interim storage of contaminated and activated components. Tritium levels will be continuously monitored.

Tritiated Water

A water leak incident in the neutral injector during the tritium experiment could have conceivably resulted in a few cubic metres of tritiated water. To facilitate recovery from such an incident, the injector box has been fitted with a drain valve and suitable storage drums, together with a local filling facility all of which has been designed and procured prior to the experiment. Drying out of the neutral injector box would be done by nitrogen gas purge which can be exhausted through the molecular sieve drums in the GCS.

Implementation of the First Tritium Experiment

Installation, commissioning and operation of the additional equipment was undertaken according to procedures established and approved within the Project. During the experiment, daily meetings were held between the two Task Forces, where all aspects of the experiment were discussed and the programme for the next day decided. Any changes of procedures that became necessary were fully discussed and decisions recorded. In one instance the changes required operation not covered by the existing Safety Analysis Report. In this case, the modifications were rigorously safety assessed and the analysis was submitted to SRD for review.

Plasma Discharges with 1% Tritium in Deuterium

This phase of the experiment was carried out over a two day period. In total, nine plasma discharges with tritium injection were carried out with a total tritium usage of 0.93 TBq (25 Ci) of which 0.05 TBq and 0.88 TBq are estimated to have been injected into the plasma and retained in the neutral injector box respectively. The amount of gas pumped by the cold finger was measured by expanding it into the 345l reservoir and its tritium content was measured with the ionisation chamber installed therein before absorption onto a U-bed.

After the two day experiment, the neutral injector was regenerated. The adopted procedure for this required many small batches to be taken onto the Cold Finger. The regenerated gas in the neutral injector was therefore transferred much more slowly than for routine regenerations. This resulted in a cooldown of the neutral injector box which may have been the cause of an air inleakage occurring during the processing of the last few batches. Several counter measures to avoid re-occurrence of such a leak were taken including a change of procedure enabling much larger batches of gas to be taken from the neutral injectors. A further regeneration was carried out prior to the 100% tritium injection experiment to prove these countermeasures. Inleakage did not reoccur and has not been detected since.

From the recovered quantities of tritium it may be deduced, that within the errors of measurement, nearly all tritium been utilised was recovered.

During transfer of the 1% T in D mixture from the U-bed to a 2l volume in the glove box, the hot U-bed walls permeated some tritium which, when extrapolated to the 100% tritium experiment, would indicate that this could constitute a substantial fraction of JET's own imposed daily discharge limit of 12 GBq. Following the 1% T in D experiment, two days were used to prepare for the 100% T in D experiment.

Plasma Discharges with 100% Tritium

The total amount of tritium used during the 100% T experiment has been measured and calculated to be 36.9 TBq (989 Ci). During injection the U-bed was open to a small pre-filled buffer volume and it is therefore difficult to

calculate accurately the amount of gas transferred from the U-bed during the pulse.

After two conditioning pulses were run for the two 'tritium' PINIs, two plasma discharges with two PINIs injecting tritium (and 14 PINIs injecting deuterium) were carried out. Both discharges achieved a peak D-T fusion power of approximately 1.7 MW. Of the total tritium used, 1.9 TBq has been estimated to have been injected into the plasma, 34.8 TBq remaining in the neutral injector box, and 0.17 TBq implanted in components in the duct between injector and torus. Following the two successful plasma discharges, 40 minutes was allowed for the torus to de-gas and the Cold Finger was warmed up $1^1/_2$ hours after the second plasma pulse. The collected tritium was measured prior to absorbing onto the U-beds. The total recovered tritium was 0.26TBq, ie 13.5% of the injected amount. The cryopump of the tritium neutral injector was regenerated (warmed up to LN_2 temperature) a few hours after the second tritium plasma discharge and 36.5TBq of tritium was recovered. The cryopump of the 'non-tritium' neutral injector was also regenerated and 14.8GBq of tritium was recovered. This small amount was higher than expected as a result of pumping by the neutral injector cryopumps from the vacuum vessel. The pumping speed is minimised by fast shutters, which limit the conductance of the interconnecting duct to nominally $100\ell^{-1}$s.

On the day of injection, the tritium supply U-bed was heated and remained hot during the PINI conditioning pulses and the tritium plasma discharges. This gave rise to permeation of 16GBq of tritium through the hot wall of the U-bed exceeding the JET imposed daily discharge limit (10GBq).

Clean-up Phase

One day of effort was required to bring back neutron diagnostics in a configuration suitable for deuterium operation. Other diagnostics and systems that had been isolated prior to the tritium experiment were individually assessed for risk of tritium contamination during the clean-up phase and re-connected progressively.

At the start of the clean-up phase, ~1.6 TBq of tritium was estimated left in the torus, whereas all tritium injected into the neutral injector had already been accounted for, within the accuracy of measurement. The subsequent tritium neutral injector regenerations delivered 1.85 TBq and 0.26 TBq, whereas the tritium recovery from the torus rapidly dropped from 16.6 GBq per discharge during the first operational day after injection to 0.93 GBq per discharge during the eighth operational day after the injection experiment. Several techniques, ie glow discharge cleaning, gas purging, etc, were tested. However, the rate of evolution continued to fall and allowed the torus to be reconnected to its normal backing pumps, exhausting directly into the monitored discharge stack three weeks after the start of the clean-up phase.

During the clean-up phase, two facts emerged that generated doubt as to the low conductance of the fast shutters which limit the conductance between torus and neutral injectors. Firstly some hydrocarbons were found in the neutral injectors and secondly subsequent regeneration of the 'non-tritium' neutral injector continued to show levels of tritium much higher than would be consistent with the conductance of $100\ell^{-1}$s. Therefore, the fast shutter conductances of the 'tritium' and 'non-tritium' injectors were measured again and showed levels similar to the conductance between the torus and the main turbomolecular pumps, ie 2000 and $3000\ell^{-1}$s, respectively. This much higher than expected conductance explains the activity found in the 'non-tritium' injector and the hydrocarbon content found during neutral injector regeneration. The accounting of the torus inventory can only be finalised when samples from vessel wall materials are removed at the start of the next shutdown and analysed for tritium.

After a few regenerations, the amount of tritium recovered from the 'non-tritium' injector fell below 3 GBq and as the storage capacity of the U-beds was limited, the regenerated gas was routed directly to the monitored stack. Whilst the amount of tritium recovered from the tritium injector decreased sharply after the first few regenerations, it then declined much more slowly. The amounts recovered remained about 0.1 TBq, which was considered too high to stack directly when applying BPM considerations. However, one month after the start of the clean-up phase, the storage capacity of the two U-beds had been exhausted. The introduction of two additional U-beds was therefore considered in detail. A safety assessment for the installation of new U-beds and transfer of the hydrogen isotopes to them from the existing U-beds was prepared and submitted for review to SRD. After endorsement of the safety assessment by SRD, the two new U-beds were activated (using protium) and then installed. The connection to the pipework of the existing system was made by removing a redundant pressure gauge whilst a small air inleak was established and maintained via a Cajon coupling into the GCS, thereby avoiding

the release of tritium into the isolator atmosphere. During and after installation, no tritium contamination was detected inside the isolator, either by ionisation chambers monitoring the atmosphere or on smear probes of internal surfaces.

During the transfer of gas between the U-beds, the amount of gas transferred was measured accurately using the 345ℓ reservoir with its pressure gauge and ionisation chamber. Transfer of gas occurred by direct absorption of gas from the reservoir by the new U-beds without having the facility to circulate gas through the U-beds by means of the scroll pump. Whilst the initial takeup of gas was very rapid, it showed that when the pressure decreases the absorption process slows down considerably without the use of the circulation pumps. This feature may lead to reconsideration of the U-bed designs in the AGHS where the intermediate storage system at present does not include circulation pumps. During gas transfer, cross calibrations were made between the ionisation chamber installed in the main manifold of the GCS and the ionisation chamber installed in the 345ℓ reservoir in order to improve the calibration accuracy. The total amount of tritium transferred to the newly installed U-beds was measured to be 42.8TBq (1158 Ci). This is 5% more than the accumulated measurements made during the gas collection of the exhaust gases from torus and neutral injector systems. Due to the better controlled conditions during transfer between U-beds and the additional benefit of improved calibration of the ionisation chamber, the higher value is assumed to be more accurate.

The assumed accuracy of the tritium amount used is ±7% and the assumed accuracy of measurement of transferred tritium is ±10%. This means that a maximum possible difference of 0.95 TBq (26 Ci) exists between used and recovered amount of tritium at the time when the transfer between the U-beds took place. Therefore, this is considered the upper limit of the amount of tritium still inside the system.

Following the transfer of gas to the new U-beds, two further regenerations of the 'tritium' injector yielded activities in excess of 1 Ci (27 GBq) each time. The recovered gas was therefore loaded on the U-beds. Over the 1991 Christmas period the cryopanels (liquid helium and liquid nitrogen) of the 'tritium' injector were warmed to room temperature and a small bleed of nitrogen gas was established into the injector box which was pumped by its mechanical backing pump into the monitored discharge stack, maintaining a pressure of approximately 1 mbar inside the injector box. The overall discharge was approximately 30 GBq during this period starting with a daily discharge of 9 GBq and finishing with 2 GBq. This was considered the appropriate procedure for starting decontamination of injector internal components in preparation for maintenance work during the 1992/93 shutdown period.

Stack Releases

Of the monitored stacks, only the discharge stack for the glove box, isolators and backing pump exhaust released tritium measurable by the on-line monitor. The quantity measured by the ionisation chamber as well as by the sampling system showed that the released activity amounted only to a very small fraction of the radioactive discharge authorisation which would indicate that BPM criteria were applied very successfully.

It was observed that the stack ionisation chamber readings were consistently higher than the sample analysis. This phenomenon has been investigated and will lead to some modifications to the sampling system.

Future Actions

The following must be carried out before this tritium experiment can be considered to be completed:

(i) Continue collecting gas from the tritium neutral injector until the regenerated tritium activity is insignificant and can be discharged directly through the stack;

(ii) Disconnect special equipment and decontaminate, possibly by purging with air (wet air preferably);

(iii) Prepare for removal of the special equipment . Decide whether the equipment can be scrapped or should be stored for re-use. Store tritium U-beds in safe store;

(iv) Take samples from torus wall for tritium analysis (during shutdown) to allow completion of accounting;

(v) Install waste sorting facility and develop detritiation procedures to allow first wall components to be classified as low level waste;

(vi) Carry out analysis of environmental samples taken during and after the tritium experiment.

Conclusions

The first JET tritium experiment has proven extremely valuable as preparation for the full D-T phase of JET. It required the preparation of a safety case and obtaining statutory and other approvals. It required establishing adequate communication and information channels with local authorities, organisations and residents in the vicinity

of the JET site. The experience thus gained will be essential when the same work has to be repeated for the use of much larger quantities of tritium.

A special programme management structure was set up to prepare the experiment, monitor its implementation and discuss, approve and record modifications to previously agreed plans. This structure worked well for the first experiment and will form the basis of a more formal organisation for the full D-T phase.

Up to the end of 1991, ie 10 weeks after the start of the clean-up phase, only ~ 0.2 TBq of tritium were discharged. This amounts to 0.25% of the total amount of tritium handled and represents a very small fraction of the radioactive discharge authorisation, indicating that the injection system and Gas Collection System operated very well and that BPM criteria were applied very successfully.

Special equipment which is based on components used in the JET Active Gas Handling System worked very well and according to specifications. The experience gained with some of the components may however lead to some modifications in the JET Active Gas Handling System, in particular with respect to U-beds for intermediate storage and stack sampling systems.

Valuable information has already been gathered on the torus decontamination and tritium retention of vacuum vessel walls and in-vessel components. However, due to error bars associated with measurement accuracy, the residual amount of tritium inside the tokamak can only be finally quantified when samples of first wall materials are analysed during the 1992-1993 shutdown.

Decontamination of the tritium neutral beam injector took longer than originally estimated. As a consequence, additional U-beds had to be installed to recover tritiated exhaust gases, which required the preparation of a special safety assessment. Preparations for the full D-T phase will have to take this situation into account.

The tritium experiment has initiated a study of the waste arising from tritium operation. The study revealed that detritiation of in-vessel components would be required. Decontamination techniques which may include baking and surface treatment are now under investigation. A waste handling facility to be used during the 1992-1993 shutdown and later during the full D-T phase is under construction.

During the two 100% tritium injection pulses, up to 1.7MW of D-T fusion energy was released for the first time in a controlled fusion experiment. This has strengthened the case for the development of fusion energy for peaceful uses.

Summary of Technical Achievements

During early 1991, the machine was already in a scheduled shutdown. This shutdown had started in November 1990, and the main tasks were to repair and strengthen the mechanical supports for in-vessel wall protection tiles and to install target plates at the top and bottom of the vessel, for use during single and double-null X-point configurations.

In 1990, operation had been disrupted and somewhat limited due to damage to wall protection tiles. The problem was attributed to the large forces generated by the so called "halo" currents, which flow during plasma vertical displacement events and disruptions. At the end of the 1990 experimental period, 49 wall tiles had been dislodged and had fallen or were projecting into the vessel thus restricting the size of the plasma that could be produced. During the shutdown from November 1990 to April 1991, remedial action was taken. Critical welds were systematically strengthened, cantilevered mountings were eliminated and weak mechanical supports were modified and stiffened. These actions which involved a considerable amount of work on a large number of components were remarkably successful insofar as no further damage to tile support mechanisms were observed for the rest of the 1991 campaign.

The values of "halo" currents could not be measured during the 1990 campaign. Installation of relevant current measuring devices was therefore one of the priority tasks of the shutdown. Some tiles were modified and electrically connected to the vessel wall through resistive elements, permitting measurement of the current flowing from the tile to the wall. These instrumented tiles allowed measurements at various poloidal and toroidal locations. These currents, up to 1kA per tile, together with measurements of the local values of the toroidal magnetic field and voltage drops along the vacuum vessel in the poloidal direction, confirmed that the total poloidal "halo" currents flowing in the vessel walls could reach about 20% of the total plasma current.

The main task of the shutdown was the installation of the X-point target plates. Each target plate consists of 48 inconel sectors firmly attached to the vacuum vessel. These sectors provide a dimensionally accurate base for fixing the tiles. Using specially designed assembly jigs and careful dimensional surveying techniques, it was possible to align the sectors with an absolute accuracy of ±1.5mm. In order to allow a comparative assessment of carbon and beryllium as a target plate material, carbon fibre composite (CFC) tiles

were installed at the top target plate, and beryllium tiles were installed at the bottom.

A disadvantage of beryllium as a target plate material is its low melting temperature making it prone to surface damage and irregularities, which can then lead to further damage. The beryllium target plate tiles were carefully machined to eliminate leading edges, which would be nearly normal to magnetic field lines and therefore receive a high power density. The machining involved relatively complicated profiles with chamferred edges and recessed fixing holes so that all leading edges and holes were shadowed by adjacent surfaces. This work was successful, as melting at leading edges was not observed during the 1991 campaign. However, this shaping of the tiles resulted in a considerable reduction in effective area of the target plates.

By the time machine operation resumed in June 1991, only the beryllium target plate tiles had been specially shaped as described. The carbon target plate tiles, although well aligned, had their leading edges and fixing holes edges exposed to high power fluxes. Operation with carbon target plates quickly revealed that carbon plate performance was indeed limited by local hot spots at leading edges. This was a phenomenon not observed with the specially shaped beryllium tiles. Therefore, a decision was taken in Summer 1991 to machine the carbon target plate tiles in a fashion similar to that of the beryllium tiles, to allow a meaningful comparison of the two materials. The design work was carried out in the summer and machining of the new tiles was completed by early September, allowing installation in a short shutdown during the first half of September.

The September 1991 shutdown coincided with an outage of the high voltage power grid for planned maintenance. A few days before the scheduled start of the shutdown, a leak occurred at a bellows of one of the lights associated with the in-vessel inspectrum system (IVIS). This lighting system had operated trouble-free for more than three years but failed when the light system jammed in one of the mechanical guides and caused undue stress on a bellows. The fault had serious consequences since the leak was large and occurred when the vessel was at 300°C. A large quantity of air and oxygen was introduced into the vessel and deconditioned the walls. The faulty system was quickly removed and replaced with a new design which had already been prepared and tested for installation in 1992. In particular, the new design included generous clearance in mechanical guides and was not be susceptible to a similar fault. When operation resumed in late September 1991, it took about two weeks to recondition the vessel walls by means of glow discharges, beryllium evaporation and tokamak cleaning discharges.

Operation of the machine and associated systems showed good reliability in 1991. The availability of systems was generally very high and fault finding and repairs were carried out speedily with a minimum of lost operation time. This was to be credited to ever improving fault reporting and maintenance organisation systems in the Divisions (particularly Magnet and Power Supplies Division and CODAS, which play a key role in the basic operation of the tokamak). Credit must also be given to the motivation and dedication of staff who had to carry out trouble shooting and repairs outside operation hours, which inevitably is carried out during nights or Sundays.

During 1991, a number of new systems were brought into operation and improved the performance of the machine. The Reactive Power Compensation system was commissioned smoothly and integrated rapidly into routine operation. It makes use of vacuum switches to switch capacitor banks and therefore reduce the reactive power consumption. The system operated very reliably and demonstrated its usefulness in keeping the JET power consumption within limits specified in contracts with the Electricity Companies. Electricity contracts were in the course of renegotiation with the new private electricity utilities, and it was expected that terms similar to those enjoyed with the former CEGB could be negotiated in the new contracts.

The poloidal field power supplies and, in particular, the vertical poloidal field system, were modified to allow the running of two successive plasma pulses with the plasma current flowing in opposite directions. This is the so-called AC (alternating current) operation. This mode of operation is relevant for future machines and reactor designs. The poloidal shaping circuit which controls the plasma elongation, was modified to increase its current capability from 40 to 50 kA. This allowed double null X-point operation with X-points well inside the vessel, and up to a plasma current of 4 MA. A disruption detector which monitors the amplitude of MHD modes and triggers a pulse termination at a defined threshold was implemented. With this system, the plasma elongation and current are ramped down in advance of the actual disruption, and the severity of the disruption, and in particular the intensity of forces acting on the vacuum vessel, is reduced.

In 1991, a serious fault recurred, which potentially could have had disastrous consequences. In May 1991, during the recommissioning of the poloidal shaping field, an electric

arc developed at a busbar link near the upper poloidal field coil No.2. Although spectacular, the damage due to the arc was limited to a local melting of the busbar and burn damage to cables and some nearby diagnostics. The poloidal field coil No.2 in particular was not affected. The fault was due to a flexible link where bolts were missing, thus allowing the link to open during operation. The repair of the damage required the removal of one of the upper limbs of the magnetic circuit, but was nevertheless completed in less than 3 weeks. The reason why bolts were missing at such a vital electrical connection was not elucidated but the accident showed the need for greater control of the work on the machine and tighter access control procedures in the Torus Hall. Such measures were implemented immediately after the incident.

The second half of 1991 was dominated by work relevant to the preparation, execution and aftermath of the Preliminary Tritium Experiment. The physics, technical and safety aspects of this experiment required a project wide effort and coordination involving all JET Divisions. In particular, Fusion Technology Division was heavily committed in operational aspects, as well as being responsible for technical and safety aspects of tritium handling.

Two Task Forces were set up for the experiment. The Physics Task Force was charged with the selection and optimisation of the type of tritium discharge, the choice of the method of tritium injection and, the preparation of simulation codes and diagnostics. The Technology Task Force was responsible for design, construction and commissioning of new systems for the introduction of tritium and recovery of tritiated exhaust gases; preparation of all safety reports and documentation to obtain the necessary authorisations from UK Safety Authorities, from the AEA and the JET Council; and for installation and commissioning of the necessary radiological protection instrumentation required for the experiment. Additional tasks included the procurement of tritium and provision for its safe storage on the JET site, the setting up of an emergency desk in the JET Control Room, the definition and execution of emergency exercises and extensive staff training in tritium hazards and the operation of tritium systems. Preparations were also being made for the safe handling of tritiated components and wastes during the shutdown planned to start early in 1992.

The preliminary tritium experiment was an outstanding success with a world wide impact on the fusion community and on the media. More importantly, it was also a faultless technical exercise from which a wealth of data was collected on various aspects of tritium handling and tritium safety. The results of the experiments are given in a separate section on this report.

Scientific Achievements during 1991

Introduction

For 1991, the system of operation of the scientific programme was the same as that in 1989 and 1990. The programme operated for a series of Campaign periods, the standard being of eight weeks duration (composed of six weeks tokamak operation and two weeks of maintenance/commissioning). Two Programme Leaders were appointed with responsibility for formulating near programme proposals (one campaign ahead) and outline plans (two campaign periods ahead). These proposals were within the broad outline of the JET Development Plan and subject to guide-lines provided by the Experiments Committee. These proposals were presented to the JET Experiments Committee for discussion and approval before implementation.

Programme Leaders for 1991 were:

D.J. Campbell and A. Tanga

Three Task Forces implemented the programme, as follows:

H) High Performance

(involving progression to full performance in material limiter and magnetic limiter configurations with currents up to 7MA, with high energy content and including progression to the highest fusion product, long pulse operation, steady state conditions and exploration of operation limits, etc.)

(Task Force Leader: P.J. Lomas)

I) Impurity Transport and Exhaust

(involving optimization of plasma purity and studying exhaust phenomena, and including studies of divertor physics and edge effects; impurity retention; erosion and redeposition; control of boundary instabilities, etc.)

(Task Force Leader: P.R. Thomas)

P) Physics Issues

(involving studies of control and optimization of plasma profile effects (using LHCD, RF, NB and high speed pellet injection, etc.) and optimization of heating effects, especially electron heating. This includes particle and energy transport studies in transient conditions; disruption and sawtooth stabilisation; high beta regimes; α-particle effects and fusion simulation studies; physics issues related to Next Step devices; etc.)

(Task Force Leader: D. Stork)

Task Force Leaders were appointed with responsibility for (i) interacting with and advising Programme Leaders on programme requirements within that task area; (ii) devising and setting out a detailed programme for allocated time within a campaign period; (iii) driving through that task programme (including acting as a Control Room representative); (iv) analysing data (in conjunction with Topic Leaders, if appropriate); (v) disseminating information in the task area through internal meetings and publications (in conjunction with Topic Leaders, if appropriate).

In addition, Topic Groups were formed, as follows:

Topic Group	*Topic Leader*
(a) Transport and Fluctuations;	J.G. Cordey
(b) MHD, Beta Limits and Topology;	J. Wesson
(c) Next-Step Related Issues (including α-particle heating effects)	B. Tubbing

Topic Group subjects are of longer term interest than the immediate tasks undertaken by the Task Force Groups. The Topic Groups are responsible for analysis of results within many areas across the Task Force spectrum, but

they also have responsibility for advising Programme Leaders on programme requirements which are topical and relevant to the Groups areas of activity. In addition, the Groups disseminate information through a number of internal meetings and in external publications.

Programme Objectives

JET operation during 1991 was mainly devoted to the introduction and exploitation of new facilities; on further improvements in plasma performance; and to the further assessment of beryllium and carbon as a first-wall materials. Impurity control in JET, as for other long-pulse high power tokamaks, is of fundamental importance and therefore significant effort has been devoted to this area of study.

The main themes for the 1991 Experimental Programme were:

- optimize plasma performance;
- exploit new facilities to the utmost;
- advance understanding in certain key areas of tokamak physics:
  - energy transport and confinement
  - transport of particles and impurities
  - magnetic topology of plasma
  - physics of the H-mode
- establish basis for Pumped Divertor and Next Step physics (including a Preliminary Tritium Experiment);
- complete certain experiments relevant to belt limiter configuration.

The scientific achievements for 1991 in these phases are described in the following sections, within the Task Force and Topic Group headings.

High Performance

The major goal of the Task Force on High Performance was to establish and develop regimes of high plasma performance in terms of high plasma temperature, high density, high plasma current and long pulse, concentrating in particular on the X-point configuration and H-mode regime. Double-null X-point configurations were developed and exploited up to plasma currents of 5MA and up to 4.2MA in the mode B (early X-point) scenario. High ion temperature regimes were explored in addition to high density regimes using gas and pellet refuelling. In particular, the additional heating power was increased to ~30MW, using combined NB and ICRF heating. High power beam injection was also exploited.

In the limiter configuration, the major performance parameter addressed was pulse length which was extended, together with additional heating, to current flat-top times of 1 minute. A programme of high power heating up to pulse lengths of 10s is planned for the 7MA configuration established in 1990, but this is presently scheduled for 1992.

In addition, experiments were carried out on the isotope effect on confinement, on the effect of error fields on the growth of stationary modes and on the suppression of disruptions with phased ICRF heating tuned to the $q_\psi = 2$ surface. These experiments were not directed at high performance as such but rather directed at specific physics issues.

One Minute Pulses and Lower Hybrid Current Drive

In previous JET operation, heating flat-tops up to 20s and plasma current flat-tops up to 30s were used, with shorter times at full heating powers and full plasma current. These durations are comparable with the current penetration times. In order to approach more closely steady state conditions, discharges have been developed up to 1 minute in duration at 2MA and 1.9T with additional heating powers up to 5MW, as shown in Fig.91. This example employed 2.5MW of ICRF heating together with 0.7MW of lower hybrid (LH) heating. The LH heating is capable of running such long pulses, albeit at reduced power. The ICRF generators and antennae are designed for 20s operation, and so in order to obtain the necessary heating duration, pairs of antennae were operated sequentially.

In these long pulses, there was a 30% change in internal inductance in the first 10s, but only a 5% change from 30 to 60s. The initial sawtooth frequency was about 4Hz rising to 6Hz at 30s and remaining constant thereafter. Clearly this plasma approaches magnetic steady state.

However, the particle behaviour did not approach steady state. The gas flow required to maintain a constant density fell gradually over the first 30s. This fall was consistent with the model of deuterium pumping by dynamic retention in material surfaces, the increasing deuterium inventory in the surfaces gave rise to a larger efflux back into the plasma. However, instead of falling assymptotically to a low value, the gas flow shown in Fig.91 reached zero at a finite time indicating an additional particle source, or a change in the dynamic retention. This particle source then contributed to the subsequent density rise, which was

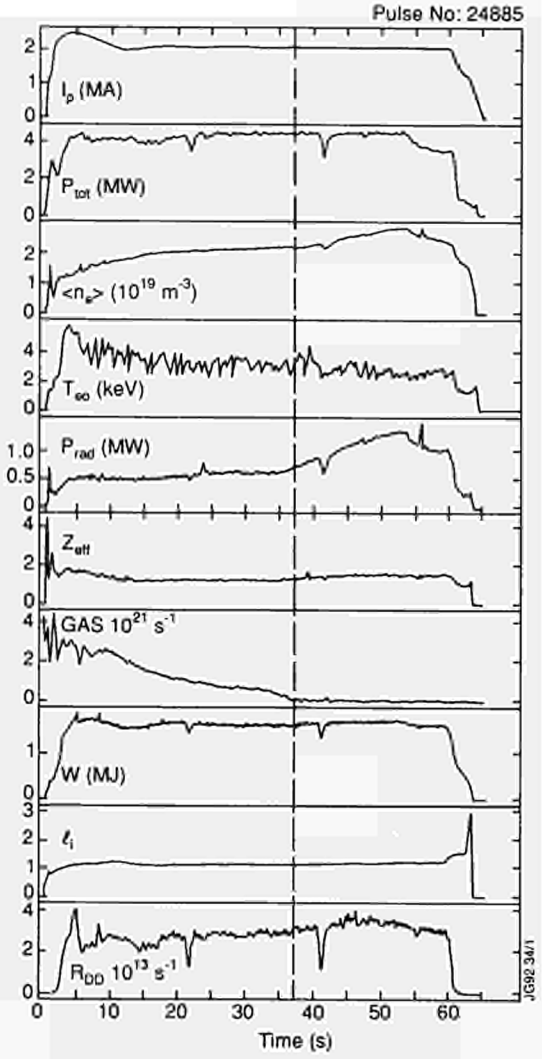

Fig.91: Various time traces for 1 minute Pulse No.24885 with ICRF and LHCD heating. The vertical line indicates the time at which the particle recycling coefficient approached unity.

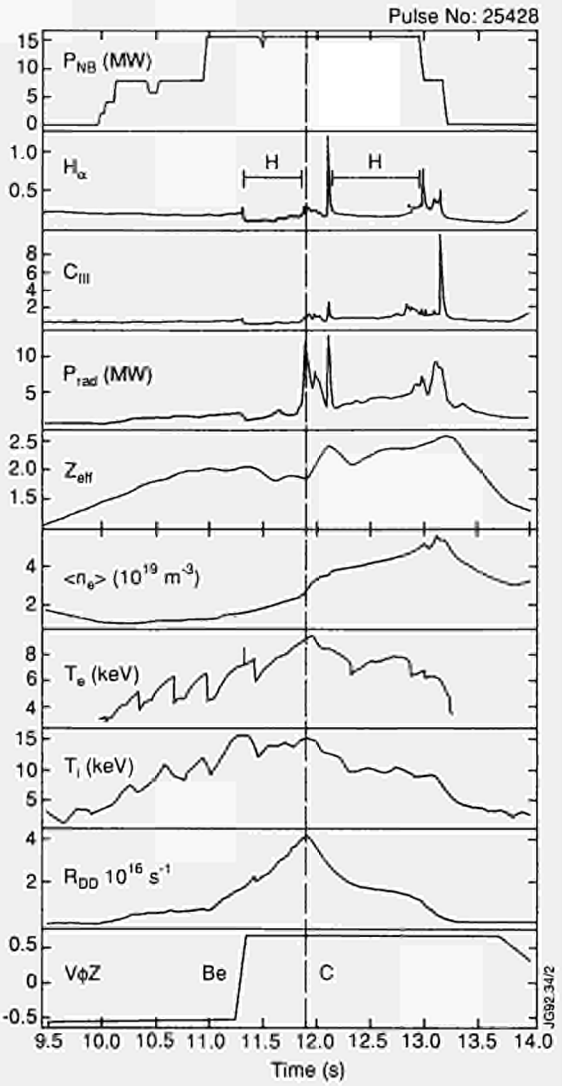

Fig.92: Time traces for 3MA DNX hot ion plasma (Pulse No.25428). The discharge steps from the beryllium tiles to the (unshaped) carbon tiles as shown by the lowest trace VØZ. The H mode phases are marked on the H_α trace. The vertical line marks the time when the CIII light increases, the radiated power (P_{rad}) increases and the density increases. Shortly afterwards, the D-D rate (R_{DD}), central electron temperature (T_e) and ion temperature (not shown) fall. Z_{eff} and the central carbon concentration increase dramatically at this time. There is no associated MHD event such as sawteeth or ELM's.

predominalty deuterium (small change in Z_{eff}, D-D reaction rate constant). A new density steady state was not reached before the end of the heating pulse, but density pump out occurred either if the heating power was stepped down or the plasma current was ramped down and so did not lead to a disruption in the termination.

The time into the pulse at which the gas flow became zero fell from 60s for about 2MW additional heating to 25s for 5MW of combined ICRF/LH power, as would be expected from an effect of limiter temperature. Multiple 2.7mm pellets (contributing <10% of the externally supplied particles) have been injected into such plasmas to probe the edge region. The pump-out time of the pellet supplied density was initially short but increased until after the gas flow had gone to zero, the density simply stepped up at each pellet and remained, suggesting complete recycling of the injected deuterium. Further analysis is underway, in order to understand these results which are important for density control in future devices.

The first demonstration of full current drive by LHCD in JET at 400kA current was made. The scenario involved the application of LHCD during the plasma current termination phase where the internal inductance rose to ~2. The constant 400kA plasma current was sustained for ~1s with constant inductance and zero loop voltage. This scenario was later exploited more systematically.

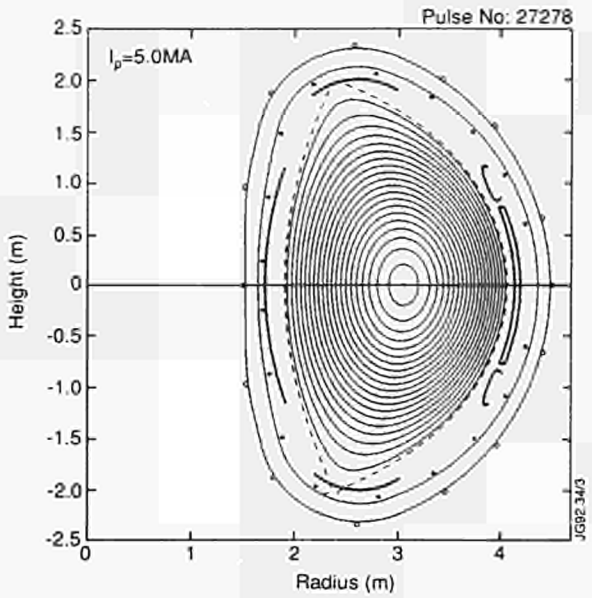

Fig.93: Equilibrium plot for the 5MA double-null X-point configuration of Pulse No.27278. Note that the X-points are outboard of the tiles in this "hybrid" configuration.

Development of X-point Scenarios

During the 1990/1 shutdown, new X-point dump plates were installed with unshaped carbon tiles on the upper dump plates and shaped beryllium tiles on the lower plates. The effect of these new tiles on high performance scenarios was studied. A range of conditions were explored: plasma currents 3-4MA, X-point - tile separation 10 cm inside to 10 cm outside, normal and reversed toroidal field (∇B up and ∇B down) with heating powers up to 16MW of D NBI and up to 12MW ^{3}He NBI (to minimise vessel activation). The performance of plasmas was limited by these tiles in a similar manner to previous tile configurations as shown by the Fig.92. In this example, the discharge was stepped upwards onto the carbon tiles after the start of the high power heating phase, but after only 0.5s on the carbon tiles at 15MW the fusion yield collapsed and the discharge became seriously contaminated with carbon. In this example, there is no MHD event (which might enhance the interaction with the tiles) and so it can be concluded that the carbon influx was a consequence of the high temperatures (~2400°C) on parts of the tiles. The energy load onto the tiles before this thermal carbon bloom was only ~5MJ indicating only a small improvement over the previous discrete rings of carbon tiles. In similar discharges, stepped downward onto the beryllium tiles, hot spots on the tiles reached 940°C after only ~5MJ energy exhaust. Broadly speaking similar performance was achieved with the X-point well inside or well outside the tile position, but a factor of ~2 deterioration in performance occurred with the X-point close to the tile surface. In a similar manner to 1990 results, a gain of factor ~2 was achieved with the ∇B direction away from the tiles, although this must be set against the higher H-mode threshold in this case. MHD events such as giant ELM's or sawteeth can "trigger" a similar collapse in the fusion performance. To improve the performance of the carbon tiles, these were replaced partway through the year by tiles shaped, in order to avoid tile edge loading at the plate-to-plate gap.

The new dump plate assemblies take up more space in the vacuum vessel than the discrete poloidal rings of tiles used previously. Therefore, it was necessary to increase the shaping currents to maintain a similar X-point to tile separation. This decreased the maximum current at which it was possible to make a marginal X-point in double-null configuration (i.e. X-point at the surface of the tiles) from about 4MA to about 3MA. This effect was offset by an enhancement to the capability of the shaping amplifier from 40kA to 50kA. With this enhancement, it was possible to develop scenarios at 3MA with the X-point 10cm inboard of the tiles. At 4MA, the X-point position was at best 2cm outboard of the tile surface and at 5MA the X-point was well outboard of the tiles by about 10 cm (see Fig.93).

Another problem with previously used double-null configurations was the curvature of the plasma on the large major radius side of the plasma in the region of RF antenna. Here, the radius of curvature was sufficiently large that the scrape-off plasma in front of the antenna was effectively shadowed by the belt limiters, reducing the RF coupling resistance to low values, and thereby making it difficult to couple high RF powers in high current X-point plasmas. This problem was solved by using only the turns in the P4 (vertical field) coils furthest from the midplane. As can be seen in Fig.92, the radius of curvature of the plasma boundary is sufficiently small (even at 5MA) that shadowing of the antenna by the belt limiter tiles is much reduced. Using similar configurations at 4MA with RF coupling position feedback made it possible to couple into H-modes up to 14MW of ICRF with dipole feed. The results of such experiments will be discussed later.

The mode-B start up scenarios were developed up to 4.2MA enabling early X-point formations even at high current. This made possible the high current X-point/H-mode studies in the absence of sawteeth as discussed later.

The forces on the vessel during high current X-point disruptions is a potential source of first wall component

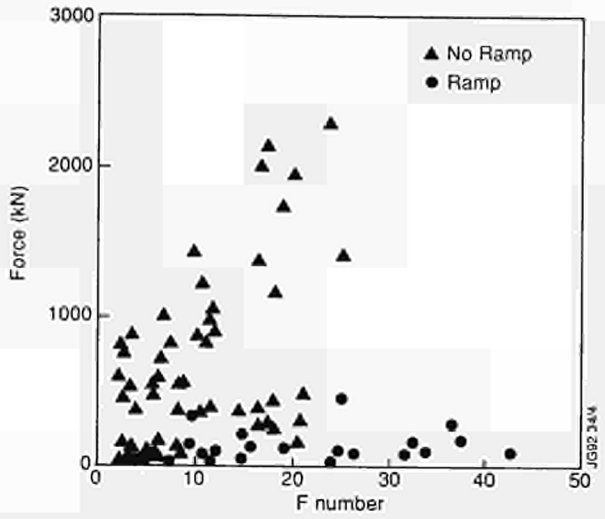

Fig.94: Vertical force on the vacuum vessel during disruptions versus a measure of the vertical destabilisation force on the plasma (F number). The triangles show the normal case whereas the circles show the effect of PFPS action on the PFX current following detection of the disruption precursor.

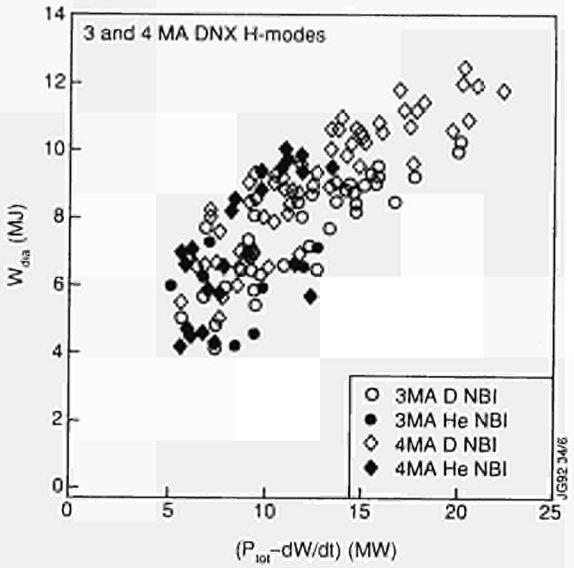

Fig.96: Diamagnetic stored energy, W_{dia}, versus loss power (P_{tot}-dW/dt) for 3MA and 4MA H-mode data in DNX. Most of the data is combined neutral beam and ICRF heating. The ICRF scheme is H minority. The NB species is either deuterium (open symbols) or He^3 (solid symbols).

damage, as shown by the 1990 results. In vessel components were strengthened during the 1990/1991 shutdown, but an attempt to ameliorate disruptions was an important safeguard for reliable high current X-point operation. A study of these disruptions was undertaken. The recent disruptions show a slow current quench (as slow as 1s) where a series of secondary disruptions follow the energy quench. Usually the vertical position is held during several of these secondary disruptions and then abruptly lost at a subsequent secondary disruption, whereupon the plasma moves vertically with an approximately constant velocity up to 80ms^{-1}. Large halo currents flow at the time of energy quench and at that time, the vertical position is lost. Although the gain of the vertical position feedback loop was optimised and a number of different signal combinations tried, these features remained. The most successful technique for ameliorating the effects of the disruption was to use the new Plasma Fault Protection System (PFPS) to detect the stationary mode disruption precursor and use this to force a rampdown of the PFX current (the major contributor to the vertical disabilisation force in double null plasmas) on the timescale of a few hundred milliseconds. This had the effect of postponing the loss in vertical position so that this occurred at lower plasma current. The halo currents were reduced, as were the forces on the vacuum vessel (see Fig.94).

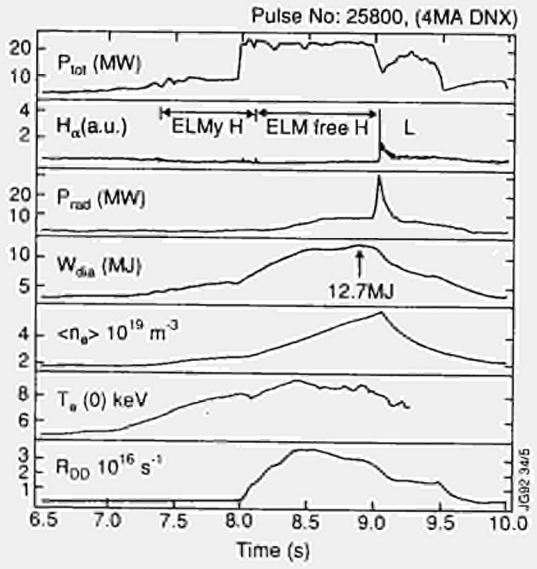

Fig.95: Various time traces for the 4MA double-null Pulse No.25800, where a record stored energy (W_{dia}) was achieved. The H-mode phases are indicated on the H_α trace.

High Performance at High Current in X-point

A range of experiments were carried out on 3-4MA double-null X-point configurations, with input powers up to 30MW. ICRF heating, NB injection and combined heating were used with both D and He^3 beams. Low and high density regimes were explored. Mode-D and mode-B operation were also compared.

Good confinement and high stored energy in ELM-free H mode regimes could be achieved despite the unfavourable location of the X-point as shown by the 4MA example of Fig.95. Here, a record 12.7MJ of stored plasma energy was achieved, and an electron temperature of ~10keV (sawteeth

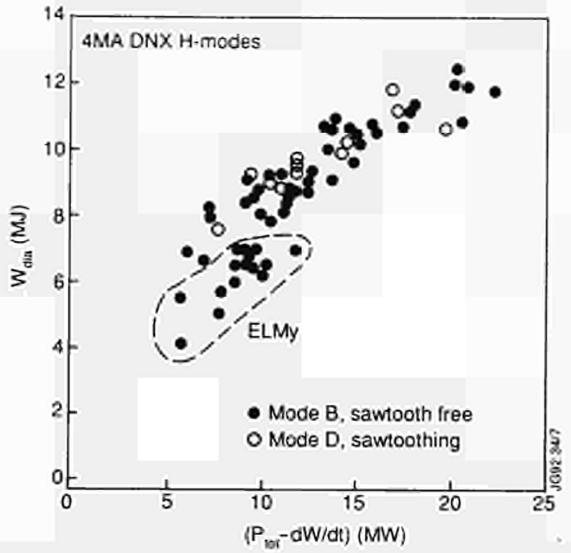

Fig.97: Diamagnetic stored energy W_{dia} versus loss power $(P_{tot}-dW/dt)$ for 4MA double-null X-point in H-mode. Data within the dashed boundary corresponds to ELMy H-modes, whereas the remainder of the data is ELM-free.

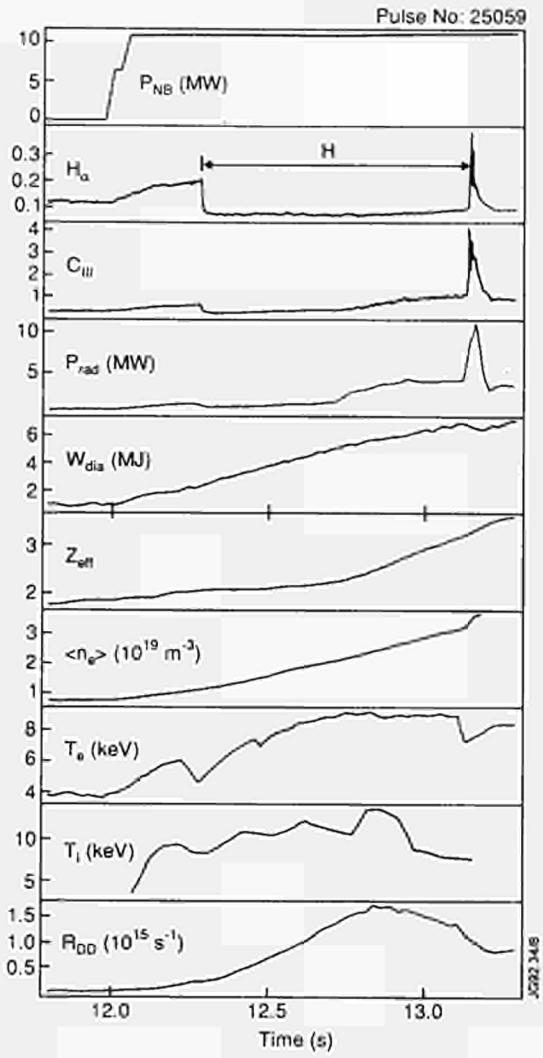

Fig.98: Various time traces for 3MA DNX plasma with ^{3}He neutral beam injection in the hot ion regime (T_i~14keV). The ELM-free H-mode phase is indicated on the H_α trace. The general behaviour of this discharge is similar to many cases with D NBI, except for the D-D yield. After the time marked by the vertical dashed line there is an increase in CIII light, radiated power (P_{rad}) and Z_{eff} (not shown).

suppressed by mode-B). In such discharges, the termination of the high confinement regime was associated with a transition back to the L-mode and not by the carbon bloom. The energy deposited on the carbon tiles was typically 20MJ. Similar discharges with lower density showed strong carbon influxes after 10-15MJ conducted to the tiles. The bloom could also be delayed at low density by careful gas puffing. Apart from this difference in the mechanism which terminated the H-mode there was no difference in confinement comparing low and high density. The confinement of such ELM-free H-modes does indeed improve with plasma current, but not quite linearly as shown by Fig.96, which compares 3 and 4MA H-mode data.

A comparison of mode-D and mode-B (early X-point) scenario, i.e. a comparison of sawtoothing and sawtooth-free H-modes, is made in Fig.97. There is essentially no change in either global confinement or central parameters when sawteeth are suppressed. Therefore, the pressure of sawteeth cannot account for the departure from linear current scaling. It is possible that this is a reflection of the unfavourable X-point location in the higher current discharges.

Fig.98 shows a typical H-mode obtained with He^3 NBI and deuterium plasma (in this case, at low density). Long ELM-free periods were obtained, and the ion temperature T_i ~14 keV is greater than the electron temperature (T_e ~ 9 keV) (i.e. the hot ion regime). The global confinement of such ELM-free H-modes is essentially identical to that of D beams, as can be seen from the global data of Fig.96.

High Q_{DD} regimes

In order to prepare for the preliminary tritium experiment (PTE), the high current double-null plasmas were extended into the low density hot ion regime. A 4MA example is shown in Fig.99 (using unshaped C tiles on the upper dump plate) which can be compared with the 1989 record Pulse No.20981 which was also a 4MA double-null configuration (but using the discrete poloidal rings). Despite similar ion temperatures (T_i ~ 20keV), the fusion performance of the recent pulse is poorer. There are a number of other differences between the two shots. Z_{eff} during the high power phase was high (~2.4), the ion temperature rolled over and the D-D reaction rate stopped rising at about the time of an

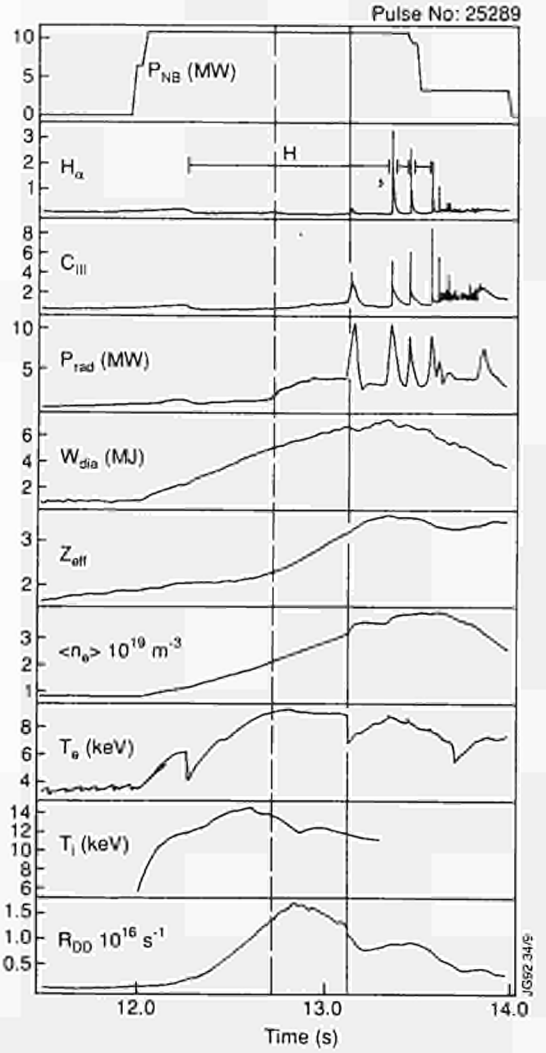

Fig.99: Time traces for 4MA DNX plasma with D beam injection in the hot ion regime. The H-mode phases are marked on the H_α trace. Note the increase in radiated power at a time marked by the vertical dashed line. There is a small increase in CIII light and Z_{eff} at this time and a little later the D-D reaction rate R_{DD} flattens out and T_i falls. At the time of the solid vertical line, there is a sawtooth and giant ELM which are followed by a decline in R_{DD} and a reduced slope on stored energy W_{dia}.

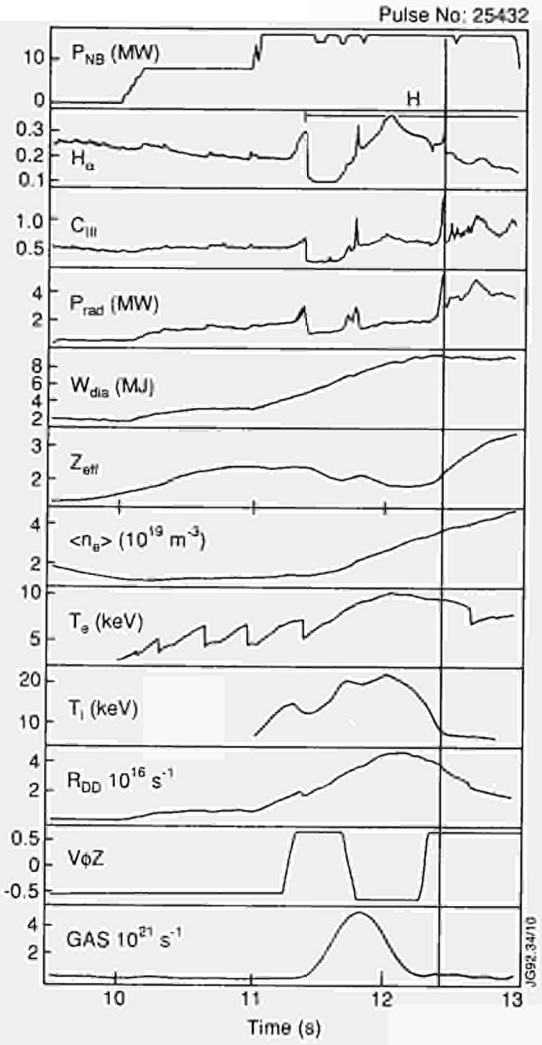

Fig.100: Time traces for the highest fusion performance plasma using both carbon (unshaped) and beryllium tiles (shaped). The slow stepping between upper and lower tiles is shown by the vertical position VØZ. A gas puff is applied whilst the discharge is on the beryllium tiles, shown on the lowest trace, which causes a rise in H_α which complicates the H-mode signature. An ELM occurs on the transition from upper carbon tiles to lower beryllium tiles but has little effect on the discharge. A second ELM just after the return to the carbon tiles at the time marked by the vertical line is followed by a degration in Z_{eff} and confinement.

increase in the carbon source and radiated power. In addition, the central particle fuelling from NBI gave a lower final central density. The high yield phase was terminated by a sawtooth crash rather than a catastrophic carbon influx (or bloom). Higher yields were obtained at lower plasma current (see for example Fig.92) which were terminated by a straightforward carbon influx. The best results in double null were obtained by stepping from the carbon to the Beryllium X-point tiles, so as to avoid the carbon influx as shown in Fig.100. In this case, gas puffing was used during the beryllium phase to avoid melting. The D-D yield obtained in this pulse is similar to the best previous results at beam powers of 15MW.

Analysis of these results suggested that improved carbon tile design, the use of some lower energy beams to aid central particle fuelling, an increase in beam power and the use of two tritium PINIS should improve the performance for the proposed PTE.

Isotope Scaling Experiments

A possible isotope effect on plasma confinement is an important question both for the extrapolation to Next Step devices and for underlying theory. A mass dependence $\tau_E \sim A^{1/2}$ (where A is the atomic mass) is indicated by data from

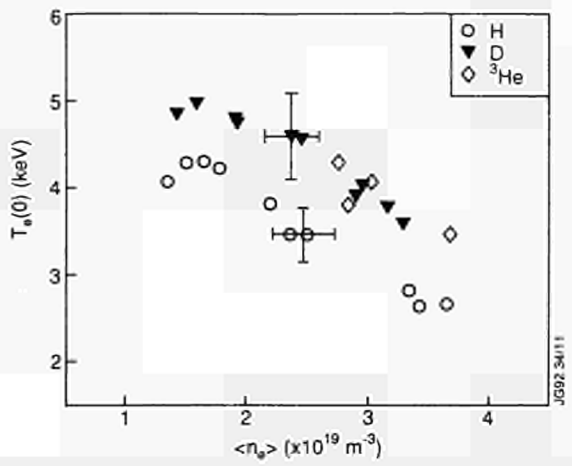

Fig.101: Central electron temperature versus volume average density for a series of 3MA/2.8T discharges with 5-6MW of neutral beam heating. The discharges differ only by the beam and plasma species.

small and medium tokamaks, but has never been systematically investigated on JET. With high power ^{3}He beam injection, it was possible to search for an isotope effect by using the same beam and plasma species and comparing D, H and ^{3}He. The available power with hydrogen beams was limited to about 6-7MW and at this power all three species can be compared. At higher powers up to 12MW, it was possible to compare ^{3}He and D. In each case, high and low density plasmas were run in order to separate out differences in beam penetration with the different species. Data was taken to make complete radial analysis of the transport and this is described in the section on Transport and Fluctuations. However, it can be seen from Fig.101, which shows the central electron temperature for beam powers 5-6MW as a function of plasma density, that the plasma species does indeed make a difference. Whereas the temperature for D and ^{3}He plasmas are similar, the temperature is lower for H plasmas.

Conclusions and Summary

Double-null X-point scenarios were established in the range 3-5MA using the new upper carbon tiles (both unshaped and shaped) together with the lower beryllium tiles (shaped). For plasma currents in the range 3-4MA, ELM-free H-modes were obtained with combined heating powers up to 28MW (input). At low powers up to 15MW input, this data overlapped previously obtained NB heating data and shows identical confinement. The higher power combined heating data shows similar confinement for various proportions of the two heating schemes and shows the expected $\tau_E \sim P^{-1/2}$ degradation in confinement (with power P) up to the highest powers used. The 5MA configurations show similar confinement to earlier single null H-modes at 5MA and will be developed to higher power in 1992. The scaling with plasma current is weaker than linear and this is not explained by sawteeth since similar behaviour is seen in mode-B scenarios (where the sawteeth are suppressed). ELM-free good H-mode confinement is obtained even with the X-point outboard of the tiles. For the higher plasma currents, limitations on shaping currents and elongation place the X-point outboard of the tiles and it is possible that this explains the departure from linear current scaling. In the course of the experiments, ion and electron temperatures $T_i \leq 20$ keV, $T_e \leq 12$keV have been achieved for central densities $n_{eo} \leq 4 \times 10^{19} m^{-3}$. At higher densities, obtained with gas fuelling or pellets, corresponding lower temperatures are seen. Whereas the high temperature regimes are terminated by carbon influx and/or internal MHD events after times ~1s (depending on detailed configuration), the higher density regimes show ELM-free H-modes for times as long as 3s limited by transition back to the L-mode or heating pulse or current flat-top.

In the limiter configuration, the major new development has been the demonstration of 1 minute heated plasma pulses. These discharges approach steady state magnetically (duration $\leq$ 3 skin times) but show that on these timescales the particle behaviour is not steady state. After times 30-60s (depending upon locating power), the recycling coefficient approached unity and the density rose without reaching a new steady state. The second major item in the programme on limiter operation was building up a database of shots for isotope scaling, including H beams into H plasmas, D beams into D plasmas and ^{3}He beams onto ^{3}He plasmas for the same 3MA target plasma. The global confinement of the D and ^{3}He cases is essentially identical, whereas the H case shows somewhat lower confinement. The remaining major item in the JET programme on limiter plasmas is the high power heating of 7MA plasmas. This is scheduled for the 1992 programme.

A number of experiments were started in 1991 which provided some interesting preliminary data but which require more experimental time in 1992 to bring to fruition. A particular example is the tuning of phased ICRF heating to the $q_\psi = 2$ surface, where both stabilisation and destabilisation of modes is observed, but where further experimentation is required to determine whether this is an effect of local current profile modification or local heating.

Impurity Transport and Exhaust

The objective of this Task Force was to optimise plasma purity and study exhaust phenomena. This included studies of divertor physics and edge effects; impurity retention; erosion and redeposition; and control of boundary instabilities. The planning, execution and interpretation of the experiments were divided into the following areas:-

- Assessment of Beryllium and Graphite X-point Targets
- Divertor Physics
- Particle Transport and Density Control
- Limiter experiments
- Physics of the H-mode.

The bulk of experimental time was devoted to the first two items. In the event, only a small period was devoted to limiter experiments, except for some measurements of impurity transport during heavy gas fuelling. The results of impurity transport in the core plasma are described in the Section on Transport and Fluctuations. Some experiments, most notably measurements of helium transport in a variety of plasma conditions, are not yet analysed.

Assessment of the Beryllium and Graphite X-Point Targets

Until October 1990, both upper and lower X-point target plates consisted of 32 poloidal bands of tiles, made of carbon

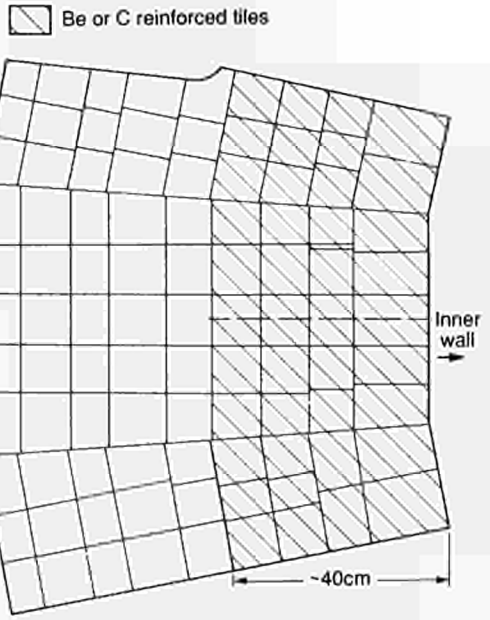

Fig.102: A plan view of the layout of the tiles on the new X-point dump plates. The region shown corresponds to half an octant, between the main vertical port and the Octant port. The unshaded tiles were made of fine grained graphite.

Fig.103: A schematic sectional view through the new beryllium X-point target tiles showing the contouring which shadows tile edges and bolt holes.

fibre composite (CFC) and beryllium (Be), respectively. Overheating of exposed tile edges limited the performance achievable with those targets. For the 1991 campaign the design of the target plates was modified. Inconel back plates were installed at the top and the bottom of the machine and Be and CFC tiles were attached, providing a toroidally continuous target. Fine grain graphite tiles were used outside the target zone. The X-point protection tiles are shown in Fig 102. The shadowed tiles represent the target region. The Be target tiles were specially machined to protect bolt holes and for mutual shadowing of edges (Fig. 103). In contrast, the CFC tiles used in the first part of the campaign (C I target) were simple flat tiles, providing a larger surface for power deposition at the target but no shadowing of exposed tile edges, caused by the unavoidable misalignment in the tile installation. In the second part of 1991 (September onwards), a new CFC target was installed (C II target), similar to the Be target tile design (Fig.104).

Carbon Target Assessment

The power handling capability of the carbon target was tested in a dedicated experimental series. The plasma configurations used were single-null with 3MA plasma current; the X-point to tile distance was varied from -10 to +6 cm, B_T from 2.1 to 3.2T, normal (+ ve) direction, varying the angle

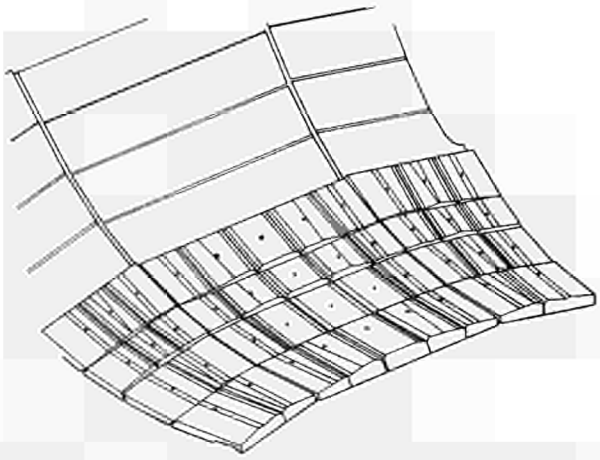

Fig.104: A view of the second set of CFC target tiles showing contouring similar to that of the beryllium tiles.

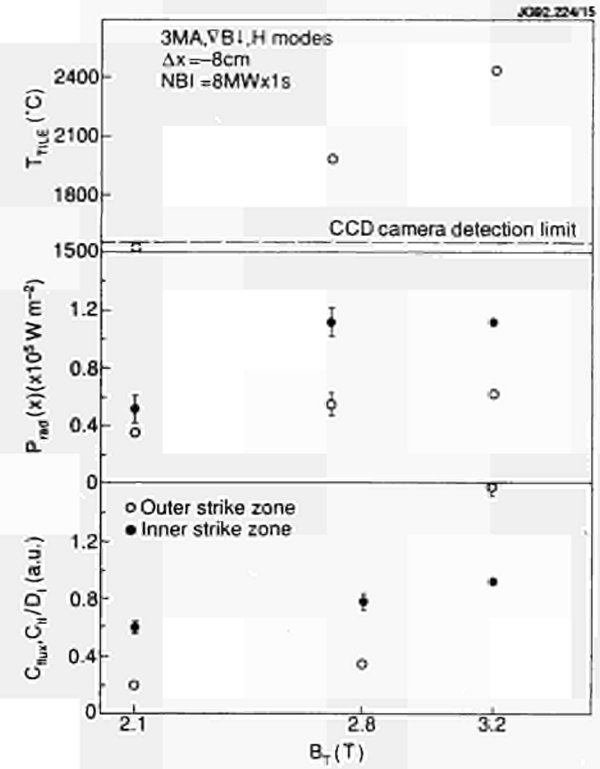

Fig.105: The peak target tile temperature (T_{tile}), radiated power (P_{rad}) and spectroscopically derived carbon yield for a toroidal field scan on the first unoptimised CFC target.

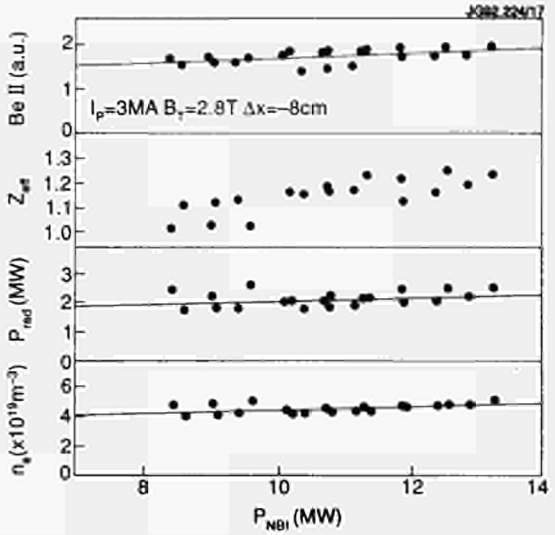

Fig.106: The beryllium influx signal (Be II), effective charge (Z_{eff}), radiated power (P_{rad}) and electron density (n_e) for a neutral beam power scan on the beryllium target. The gas fuelling rate was increased proportional to the input power.

of incidence of the magnetic field lines on the tile from 0° to 0.95° at the separatrix. The temperature of the observed hot spots on the tiles and the measured influxes increased with the toroidal field, in agreement with the expected behaviour of the parallel power flux (directly proportional to B_T) to which tile edges were exposed. The variation of the X-point to tile distance did not strongly affect the tile temperature or erosion as would be expected for a 'tile edge dominated' target. This behaviour (Fig.105), summarises the peak tile temperature, radiated power (P_{rad}) and carbon yield measured at the inner and outer strike zones for three plasma pulses having similar general parameters other than toroidal field. In particular, the temperature of the hottest spot in the CCD camera view increased linearly with the toroidal field, as did the carbon yield.

Beryllium Target Assessment

The power handling capability of the Be X-point target plates was tested at the beginning of the 1991 campaign and the discharges used were similar to those used for the C target assessment. These tests were carried out very carefully, since their aim was to establish the limits on the achievable power load on the target without generating gross melting with consequent loss of the geometry of the target. In particular, the total energy input during the X-point phase was limited to 15 MJ total; this limit remained in force for all but the last week of operations. In contrast to carbon, it was observed that the Be sputtering yield was constant for increasing B_T; the tile design was effective in accommodating tile misalignment by shadowing of the edges.

The use of gas puffing during the additional heating phase was effective in controlling the edge temperature, face temperature and Be influxes. A series of pulses were carried out at fixed I_p, B_T, X-point to tile distance and target density. All the pulses were similar H-modes to the C test series. The NBI power was increased in steps from 8 to 14 MW, with the gas puff rate during the heating phase increasing by a factor of two. As shown in Fig.106, the Z_{eff} and the radiated power were constant for all the pulses of the series.

Carbon versus Beryllium Power Handling Capability

The power handling capability tests were carried out in similar conditions for the carbon and the Be X-point targets. In the case of the C I target, the power handling was limited by overheating of exposed edges, while for Be the design of the tiles proved to be effective in accommodating misalignments of up to 0.5 mm. The tests were conducted with the constraint of a maximum of 15 MJ input energy during the X-point phase. As a consequence, the C I tiles were replaced with a new set (C II) whose design was very similar to those used for the Be target. In fact, the power handling capability of the new tiles was about a factor two

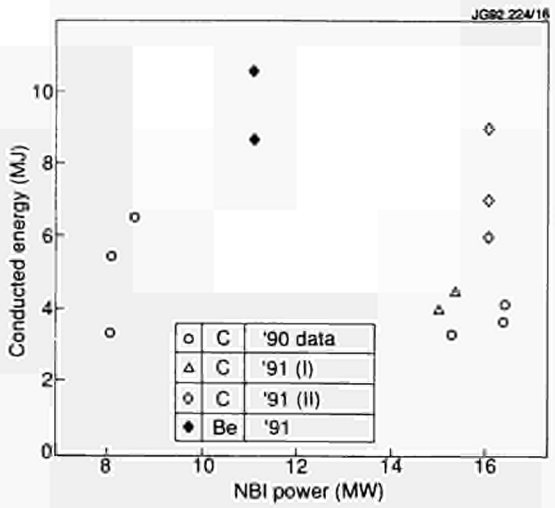

Fig.107: Energy conducted to the target tiles at the onset of a carbon bloom versus neutral beam power for different targets.

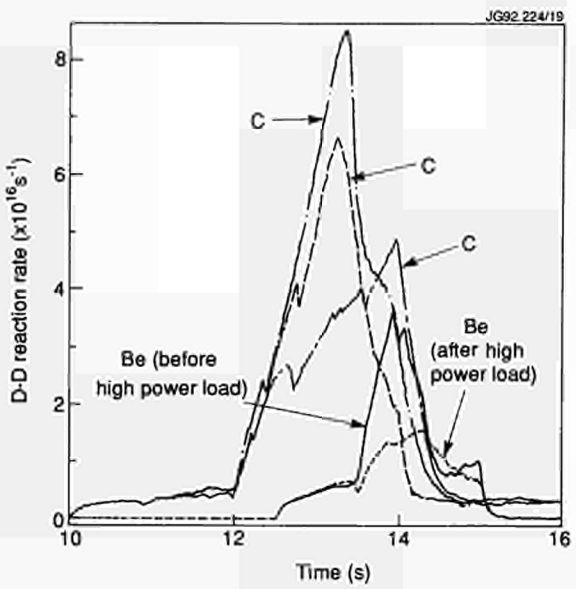

Fig.108: The fusion rate traces for hot-ion pulses conducted during high heat load tests on beryllium tiles, compared with similar pulses obtained on the graphite tiles during the PTE.

higher than those of the C I target. Fig.107 shows the maximum conducted energy to the target before the sudden increase in impurity influx (known as the 'bloom'), as function of the NBI power, for the 1990 carbon poloidal rings, and for CI, C II and Be 1991 target plates. The Be bloom threshold is ~ 10 MJ of conducted energy, at 11 MW of input power. For the C II target, the bloom threshold is 9 MJ at 16 MW of injected power, compared with 4 MJ observed for the C I target. Since the effective area of the C II target is reduced by a factor two compared with the C I target, the increase in the bloom threshold can be attributed mainly to shadowing of tile edges.

During the short shut-down for the installation of the C II target, an accurate photographic survey of the lower Be X-point target was carried out. At that time, the target had been used for three months, running single null X-point in normal and reversed toroidal field configuration and double nulls, mostly in the positive toroidal field configuration. The damage observed was confined to the sloping part of the tiles (the so called ski slopes), originally designed to intercept the power flux, and the tile edges and bolt holes did not show substantial signs of melting, as expected. The depth and poloidal extent of the damage in both strike zones was consistent with the history of operations up to that time.

High Heat Load Test of Beryllium X-point Tiles

In the last week of operation, the limit on the maximum energy to the plasma during lower X-point operation was increased to 70 MJ, the same as the limit in force for the C II target. An experiment was carried out to study the variation of plasma performance in lower X-point configuration, after the Be tiles were melted by running high power/high energy discharges on them. Two test discharges were selected: for the first test pulse the plasma configuration selected was similar to the one developed for the Preliminary Tritium Experiment (PTE), the second test pulse was a standard H-mode, with 12MW of NBI heating, and no gas puff during the additional heating phase. The two test pulses were run before starting the high power load series of pulses to establish a firm reference for the comparison. These two test discharges were then repeated after running several pulses characterised by conducted energy to the plates > 30 MJ, up to a 60 MJ maximum. This procedure was repeated twice. The results of these tests on the Be target were compared to the performance obtained in plasma pulses similar to the test discharges, but in the upper X-point configuration; i.e. using the C II target.

The PTE like discharges run on the Be target showed a marked degradation of performance, straight after the first group of high power load pulses. When compared to similar discharges run during the PTE preparation (Fig.108), it appeared quite clearly that this type of discharge performed far better on the CFC than the Be target.

In contrast, the performance of the standard H-mode was constant for all the test pulses. The neutron rate and the duration of the best performance phase of the H-mode were apparently not affected by the damage inflicted on the tiles. Interestingly, by comparison of the Be H-modes with analogous pulses run on the CFC target show that both the peak

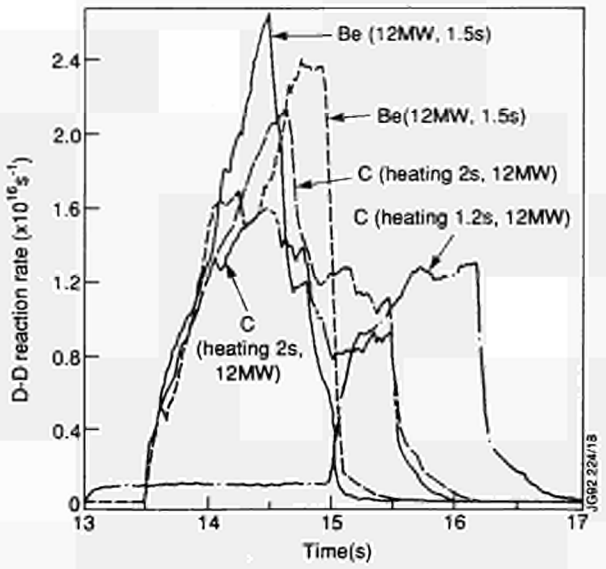

Fig.109: The fusion rate for moderate density beryllium and graphite targetted phases during high heat load tests.

performance and its duration are at least comparable for the two target materials (Fig.109).

Operation with Heavy X-point Gas Puffing

Plasma operation on the lower Be target has been performed at heating powers >20MW for 2s. By puffing deuterium into the X-point region, it was possible to keep the surface temperature of the Be tiles below 1030°C, and so prevent melting. The radiation from the bulk of the plasma was 6 MW, while from the target temperature rise only 2MW of power reached the target. The power deficit is in agreement, within uncertainty, with the estimate from the bolometer of radiation from the divertor region which accounts for 50% of the total radiation.

While H-mode operation has been demonstrated with the Be target, it was not achieved when operating in high gas puffing regime. When compared to Be limiter discharges with similar power and density, these plasmas had similar confinement and plasma purity.

Carbon Blooms and "X-events"

For some years, the performance of high temperature plasmas has been limited by a process known, as a 'carbon bloom'. This can be characterised as the result of regions of the target tiles overheating and the concomitant impurity influx overwhelming the plasma. An example of this process is shown in Fig.110. A delay is discernable between the onset of the bloom, as seen in the radiated power, and the fall-off in deuterium concentration, neutron rate and plasma energy content. Also, the roll over of all of these quantities is quite

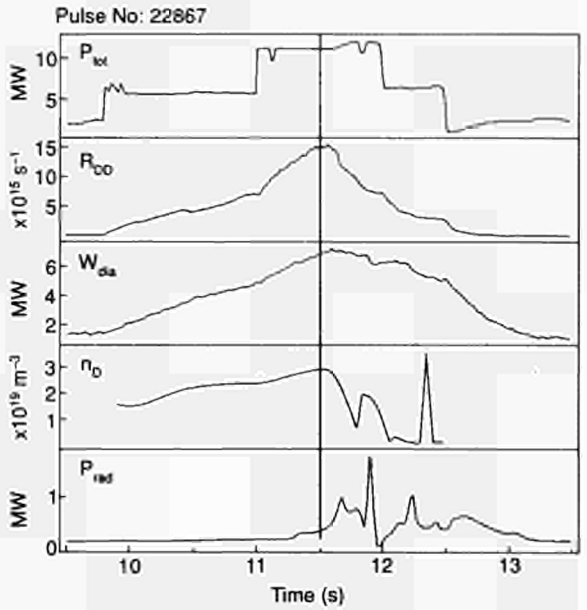

Fig.110: Total input power (P_{tot}), fusion rate (R_{DD}), plasma energy (W), deuteron density (n_D) and radiated power (P_{rad}) for a plasma displaying characteristics of the carbon bloom.

gentle. Behaviour of this kind might be anticipated, since the impurities which are produced at the boundary must be transported to the plasma core to effect performance.

In contrast, many of the 1991 hot ion H-mode plasmas have been terminated by a process which has similar features to the bloom observed previously but is surprisingly fast. In particular, the spike in the radiated power is approximately coincident with the collapse in the neutron yield. This would imply a communication of impurities between the edge and core on timescales which are

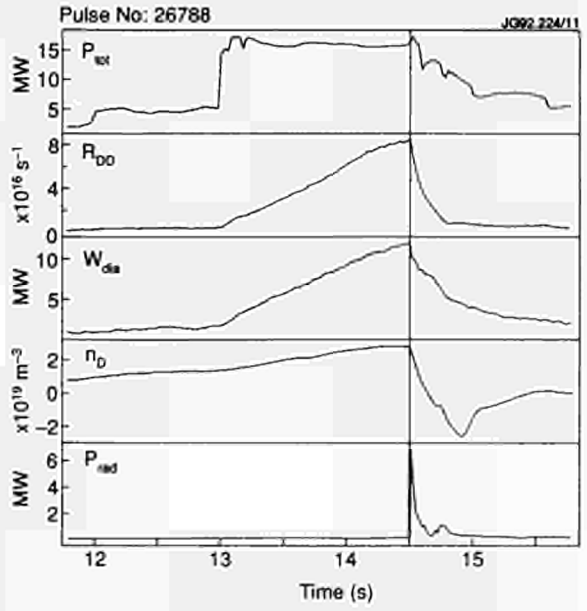

Fig.111: Total input power (P_{tot}), fusion rate (R_{DD}), plasma energy (W), deuteron density (n_D) and radiated power (P_{rad}) for a plasma displaying similar characteristics to the "X-event".

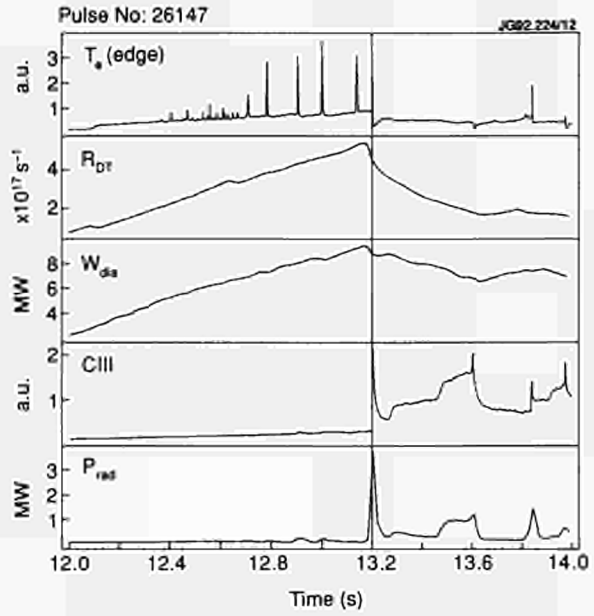

Fig.112: Boundary electron temperature (T_e (edge)), fusion rate (R_{DD}), plasma energy (W), carbon signal (C III) and radiated power (P_{rad}) for one of the plasmas displaying a correlation between the X-event and an ELM.

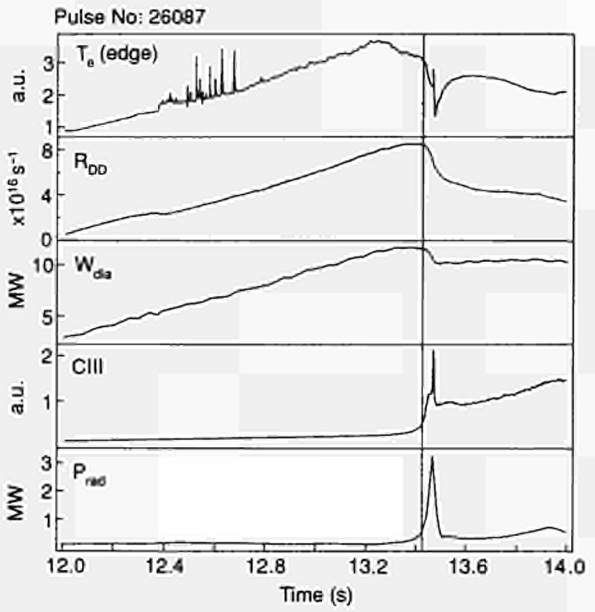

Fig.113: Similar traces to previous figure for a recent plasma showing behaviour more reminiscent of a carbon bloom than an X-event.

considerably shorter than the normal transport timescale. Such behaviour is exemplified by the beahviour in Fig.111. The radiation spike is clearly visible and the response in the core is more abrupt as shown by the neutron rate, energy content and deuterium concentration. To serve as a convenient distinguishing name and to emphasise the abruptness, this process was characterised the "X-event".

Several hypotheses were advanced to explain the differences:

- The X-event is often correlated with MHD instabilities such as ELM's and sawteeth or the H-mode termination, which all deposit extra energy on the target. It is supposed that the heating could release more impurities which are transported rapidly by the plasma turbulence, remaining after the initiating process. Such events are particularly rapid, as shown in Fig.112;
- The impurity influx could be a result of divertor impurity retention due to the increasing ion temperature there;
- The flattening of the density profile led to an increased transport coefficient for ions in the core. This would increase the heat flux to the target and so bring in more impurities. In fact, transport analyses of this phase does reveal an increase in the ion thermal conductivity. However, this could, be due to a collapse of the power input caused by impurities screening the neutral beams;
- These plasmas are typically at higher β and so could be prone to a pressure driven instability, of which there are signs in the limiting behaviour of the energy content.

The events which were not coincident with ELM's, sawteeth or the H-mode termination, although rather rapid, are reminiscent of 'blooms'. The increase in the impurity influx and the roll-over of the edge electron temperature occur 100-200ms before the effects are felt in the core shown (seeFig.113). Preliminary charge exchange recombination spectroscopy data indicates that there is an increasing impurity influx, seen in the main plasma, before the core collapse in these plasmas.

Understanding and mitigating these effects is of considerable importance to the JET programme. Analysis of data is underway and should provide information needed to determine whether X-events and blooms are basically the same process or entirely different.

Divertor Physics

The aim of the divertor physics programme was to establish an experimental data-base for the performance of the present JET X-point configuration on carbon and beryllium targets. This divertor performance can be split into the main sections: power handling of the target and, impurity production and retention and plasma density control. These areas have been addressed during the campaign in considerable detail by dedicated sets of experiments. This experimental effort was complemented by advances in modelling. As a part of the effort, a topical edge data-base was established, containing validated edge-specific data (Langmuir probes, spectroscopic data, etc.) for all the divertor experiment

discharges. The data set obtained from these investigations will be used to benchmark the EDGE codes of JET; as well as the DIVIMP Monte Carlo code. The bench marking and ultimate improvement of the edge codes will provide a better understanding of the divertor physics involved. In addition it should allow a more accurate prediction of the performance of the pumped divertor configuration in JET as well as of a conceptual ITER divertor.

Impurity Production and Retention Experiments

The various edge and divertor models predict a very sharp increase in impurity retention above a scrape-off (divertor) density [1,2]. The actual "threshold" density value depends on the power flow into the scrape-off layer, which together with the density yields a divertor ion temperature below which retention is achieved. This ion temperature is the dominant parameter in determining the retention of impurities in the divertor plasma due to the high power with which it enters the relevant equations. In particular the ratio of the friction force between impurities and the background plasma to the opposing ion thermal gradient force is proportional to $T_{i,Div}^{-7/2}$. All the other important scrape off plasma parameters such as the Mach number, the connection length and the ionisation stage of the impurities concerned are only of secondary importance. Thus a high divertor ion temperature cannot be easily compensated by an increased Mach number in the scrape-off plasma nor by an increased connection length. Therefore, the achievement of a high density in the divertor plasma and so a low divertor ion temperature is of utmost importance. Experiments on ASDEX [3] performed on Cu target plates, show a sharp improvement (up to a factor of 40) of the retention for target produced impurities above a certain density which was dependent on heating power, thus confirming the general features of the above models. The divertor experiments performed on JET in 1991 were designed to explore the above model predictions. In contrast to ASDEX, the JET divertor is much more an open configuration, and utilises low Z target materials (C, Be).

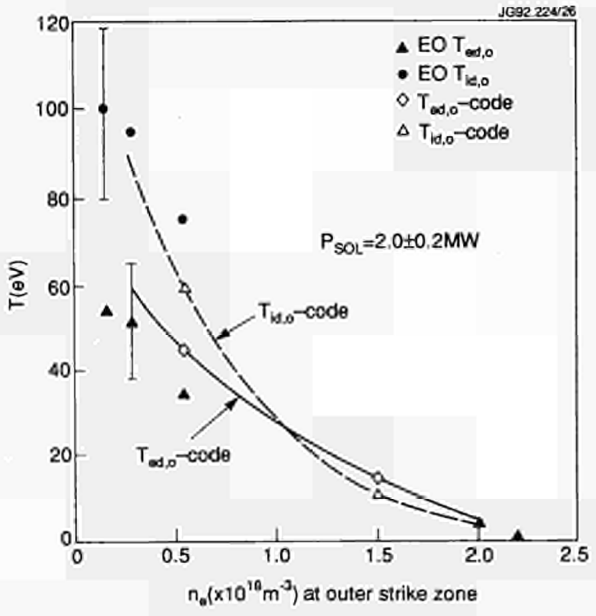

Fig.114: Experimental data for outer strike zone electron ($T_{ed,o}$) and ion ($T_{id,o}$) temperatures against outer strike zone electron density (n_e) compared with EDGE 1D code results. All points correspond to plasmas with ohmic heating only.

To enable experimental access to the impurity retention, a simple definition had to be found for this quantity. It can be expressed in the form of a global particle confinement time τ_p^{Div}, which compares the impurity content inside the closed flux surfaces with the impurity influx from the divertor target:

$$\tau_p^{Div} = \frac{N_z^{plas}}{\Phi_z^{Div}}$$

Small τ_p^{Div} thus implies good retention. A similar time can be defined for the limiter:

$$\tau_p^{Lim} = \frac{N_z^{plas}}{\Phi_z^{Lim}}$$

A dimensionless retention factor, R, can be defined:

$$R = \frac{\tau_p^{Lim}}{\tau_p^{Div}}$$

which represents the improvement of impurity screening for a divertor configuration compared to a limiter plasma. In JET experiments, this particle confinement time for limiter plasmas was not measured for all the different types of heating and density scenarios performed in the divertor physics experiments. Thus, to obtain a retention factor for all divertor discharges, the unmeasured τ_p^{Lim} were calculated by a one dimensional impurity transport code using measured limiter discharges to benchmark the code.

Divertor Physics Experiments on Carbon Tiles

Initial experiments were undertaken in single-null X-point plasmas on the carbon target tiles. A density scan was performed by varying the volume average density in the range 1.2 - 3.2x10^{19}m^{-3} by using a feedback system. Beside some problems with marfing, which increased the carbon content in the plasma in the higher density discharges, the scheme worked well in the ohmic phases. The predicted decrease of T_e and T_i with n_e in the divertor was verified experimentally (Fig.114).

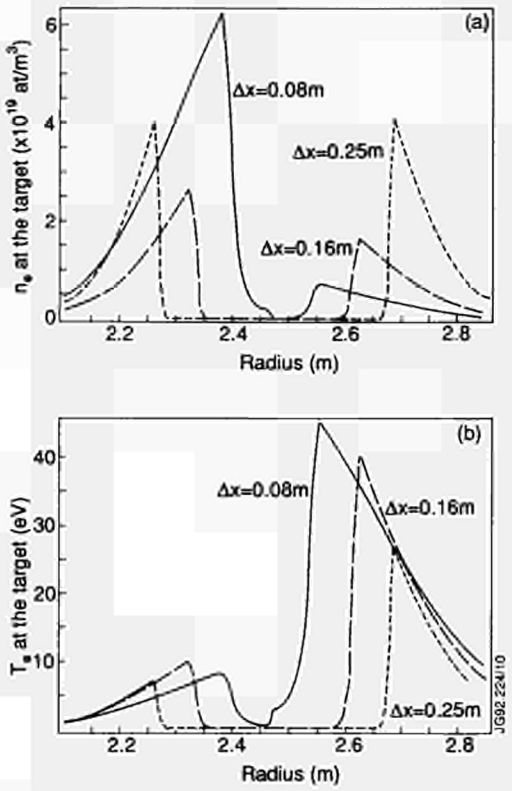

Fig.115: Target electron density (n_e) and temperature (T_e) profiles for an X-point-target distance (Δx) scan on graphite target.

During the 1s, 8MW NB heated phases, the plasma made a prompt transition into the H-mode. The ensuing increase in bulk plasma density caused the gas valves to be switched off completely by the feedback system. This lead to a depletion of particles from the scrape-off layer (SOL) and from the divertor, so that the density variation in the divertor plasma was very small during H-modes regardless of the different densities achieved before the heating was applied. The depletion of particles from the divertor was substantially helped by the fact that the JET X-point configuration has no baffling for neutrals. The neutrals originating from the target plates can therefore reach the main plasma SOL with a high probability either directly or by distant recycling. The leakage rate for neutrals depends strongly on the density in front of the target and reaches between 5% and 21% of the deuteron flux which impinges onto the target (results from code calculations). During the H-modes the ion temperatures were very high (100eV) and the densities low ($<10^{19}m^{-3}$), so that retention was poor.

The experience described above provoked a change in experimental set-up for all consequent divertor physics experiments, so that the divertor density was then varied over a wide parameter range by pre-programmed gas puffs. Two sets of divertor density scans were performed, one with the gas puffs applied in the mid plane and one with gas puffing into the X-point area. In addition, scans of X-point to target separation (Δx) as well as of the toroidal field were carried out to change the divertor volume and the connection length, respectively. The main density behaviour during H-modes was comparable to similar plasmas with density feedback. To avoid marfes during the low power phase (ohmic phase), 2 MW NB heating was applied for 2s before a 1s 12 MW heating pulse. This feed forward gas puffing scheme finally allowed higher edge and divertor densities to be sustained during H-modes. The reciprocating Langmuir probe was used successfully during most of these higher recycling C divertor experiments.

Although most of the carbon target data is still being evaluated, the results of the Δx scan are available. This scan varied the X-point to target separation in three steps; 0.08, 0.16 and 0.25m. Fig.115 shows electron density and temperature profiles obtained during high density L-mode discharges. When increasing Δx, the in-out asymmetry in the density profiles in front of the target vanishes, while T_e at the outer strike zone decreases. The consequent increase in n_e and, in particular, the decrease of the outer strike zone T_e suggest improved impurity retention of large values of Δx.

Fig.116(a) shows the carbon fluxes from the divertor target and the inner-wall of the main chamber. The latter increases with Dx and reaches 20% of the divertor flux. It is probably due to a higher back flux of neutrals from the target to the walls at large values of Δx and subsequent impurity sputtering. Taking account of the smaller screening of impurities from the wall, this influx of carbon from the wall, turns out to be as important as that from the divertor target as seen in Fig.116(b). Taking account of the carbon influx from the divertor alone, Fig.116(c) shows that the divertor retention factor does indeed increase with Δx as expected.

Divertor Physics Experiments on the Beryllium Target:

The feed-forward gas puffing scheme described above was used in all the Be target divertor experiments. In addition, the reciprocating Langmuir probe (RCP), which measures the density and temperature profiles in the main plasma SOL near the top of the machine (opposite to the target plates) was operational. Two density scans, with mid plane gas puffs and with X-point gas puffs, respectively, were performed with the full set of edge diagnostics. During the whole combined gas puff heating phases no marfing was observed.

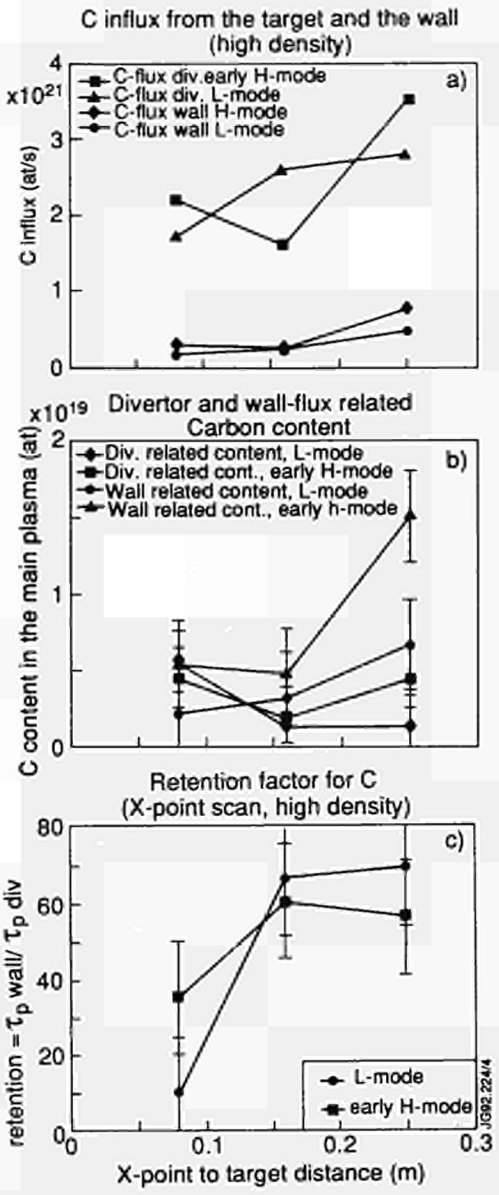

Fig.116: The carbon influx, main plasma carbon content and divertor retention for the X-point to target distance scan.

The most important information required for assessing the divertor performance were the parameters n_e and T_e in front of the target plates. These are required for transforming spectroscopic intensities into impurity influxes, and for measurements of the power flow, as well as for the edge modelling. These plasma parameters were measured by an array of Langmuir probes embedded in the target tiles. Due to the particular shape of the target tiles some of these probes were in the shadow of the edges of adjacent tiles, while others were in the private region between the strike zones. As a result only four probes were usable. One of these was located at the inner strike zone while the other three probes were located at the outer strike zone. To obtain density and temperature profiles in front of the target, the n_e and T_e profiles measured with the reciprocating Langmuir probe in the main plasma scrape-off layer were mapped onto the divertor target. This mapping procedure takes the magnetic flux topology, which is obtained from the equilibrium code (IDENTC) as well as pressure balance along field lines into account. The relatively accurate profile information from the RCP together with the four measurements obtained on the target have yielded the necessary spatial and time dependent density and temperature information.

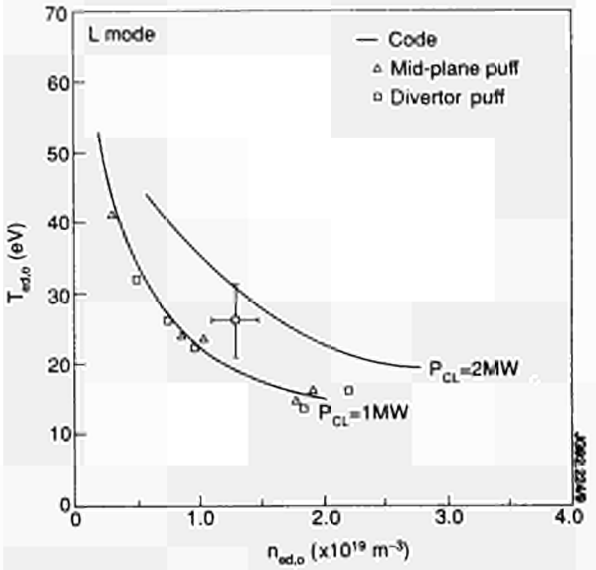

Fig.117: The peak, outer strike zone electron temperature against peak, outer strike zone electron density for a series of L-mode pulses with mid-plane or divertor gas fuelling compared with EDGE1D predictions.

The divertor density at the outer strike zone was scanned in the range 1 - 8x10^{19} m^{-3} and on the inner strike zone from 4 - 8x10^{19}m^{-3} by pre-programmed gas puffs from the mid-plane. T_e varied at the same time from 50 - 75 eV to 20 - 30 eV (outer strike zone) and from 10 - 25 eV to 5 - 20 eV (inner strike zone). The lower temperatures occurred during the low power heating phase (~ 4MW inclusive of OH). It should be noted that the plasma at the inner strike zone generally detached in the higher density regimes, in particular during the low power phase. Therefore, the temperatures and densities obtained from the target plate Langmuir probes have larger error bars in these cases. Fig.117 shows a comparison of the measured and predicted (EDGE1D) electron temperatures for the low power (L-mode) phase, for both mid-plane and X-point gas puffing discharges.

The X-point gas puff density scan revealed somewhat less impact on the outer strike zone (n(max) ≈ 6 x 10^{19} m^{-3}, T_e ≈ 40 eV) and greater impact (higher density) at the inner strike zone compared to the mid-plane puff. Differences were particularly evident in the high power phase.

The beryllium influx from the target was measured by a CCD camera using a filter for the Be II line at 313 nm. The Be influx was then obtained by folding the Be II intensity profile with the ratio of ionisation to excitation rates (S/X) for the 313 nm line taking the T_e profile at the target into account. The influx was also computed from the Langmuir probe measurements of the deuteron flux, coupled with a sputtering model. Comparison of the two results provided a check of the sputtering model. When comparing low divertor density (no gas puff) with high divertor density (strong mid plane or X-point gas puffs), it was noticed that in cases with gas puff the Be flux was up to a factor 4 larger than in cases with no gas puff. This observation can be explained by the weak dependence of the sputtering yield on the plasma temperature in front of the target when $T_e > 10$ eV. In these cases the amount of Be atoms released from the target depends only on the deuteron flux onto the target, which increases with density. This finding predicts a counteracting behaviour of improving retention and increasing impurity influx when raising the density in the divertor. However, at sufficiently high densities the divertor ion temperature decreases to the extent that the influx again decreases.

To deduce the global impurity confinement time (τ_p^{Div}) and the retention factor for these discharges, it was necessary to compare the Be content found inside the closed flux surfaces with the Be influx originating at the divertor target. The Be content inside the main plasma was measured by charge exchange (CX) spectroscopy, and can also be obtained from VUV spectroscopy, when making some assumptions (plasma transport, calibration with bolometer signals). The Be content from CX and from VUV spectroscopy differ by a factor 2, but display similar time behaviour. The VUV results were therefore calibrated by the CX measurement, which is quantitatively more accurate. With such a calibration the VUV measurements were used to extend retention studies into ohmic phases, or into discharges where the CX neutral beams tripped.

The impurity retention factor in the L-mode was nearly independent of density, whilst a strong improvement was apparent during H-modes. This behaviour was explained as follows: in high density L-mode discharges, the plasma is detached at the inner strike zone, which seems to lead to a low impurity retention in the divertor. In contrast, both strike zones are attached in the H-mode and the migration of impurities towards the main plasma is prevented. The divertor electron temperature decreases with increasing temperature which is indicative of the same behaviour in the ions. Thus, there are indications of the anticipated relationship between divertor impurity retention and ion temperature.

Particle Transport and Density Control

Isotope Exchange Experiments in Preparation for the PTE

The isotopic composition of a tokamak plasma depends not only on the composition of the gas input but also on that of the hydrogen which is retained in the first wall. From surface analyses first wall components, it is known that the near surface (few mm) wall reservoir of hydrogen and deuterium is $\sim 10^{24}$ atoms. This must be compared with about 10^{22} atoms that must be supplied to JET to sustain a total deuterium plasma inventory of $\sim 10^{21}$ atoms (equivalent to an average density of $10^{19} m^{-3}$) for about 10s. Plasma-wall interactions and fuel recycling cause particle exchange between the plasma and the wall, and a certain isotopic ratio in the plasma can only be kept constant if it is the same in both particle reservoirs. For this study, the retention mechanism in wall materials like carbon or beryllium can be assumed to be the same for the various hydrogenic isotopes, and in JET, the collective hydrogen retention in the low Z materials is at saturation [4,5].

The magnetic confinement of the plasma causes the plasma-wall interaction to be concentrated on limiters and divertor target plates. Therefore, the in-vessel wall will not be uniformly affected and the effective particle reservoir in the walls with which an exchange is possible is expected to be less than the figure given above.

A model which describes phenomenologically a change over from isotope 1 to isotope 2 in a tokamak plasma must take into account the magnitude of the plasma particle reservoir and of this effective wall particle reservoir. It has been shown [6], that equilibrium (i.e. equal isotopic ratios) between plasma and effective wall area, in direct contact with it (limiter, target plates), is reached on a time-scale of a global particle confinement time. By measuring the isotopic ratio (for example by measuring charge exchange fluxes leaving the plasma) and knowing the input of one isotope the quantity of the other isotope can be determined. If this change over experiment is carried out after many discharges with just one isotope, then the effective particle reservoir in the walls can be estimated. A series of such experiments were performed during 1991, with the aim of quantifying the number of particles in the wall, which

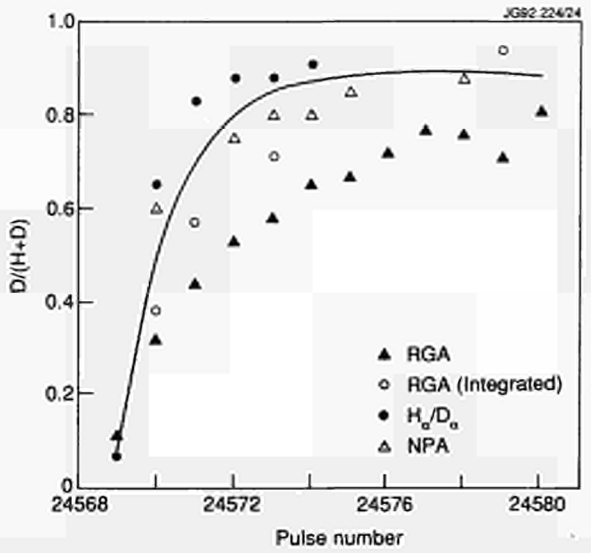

Fig.118: The fraction of helium in a deuterium discharge sequence following operation in hydrogen, showing the relative strengths of hydrogen and deuterium Balmer-a light; RGA measurements taken 10 minutes after the pulse; and neutral particle analyser measurements.

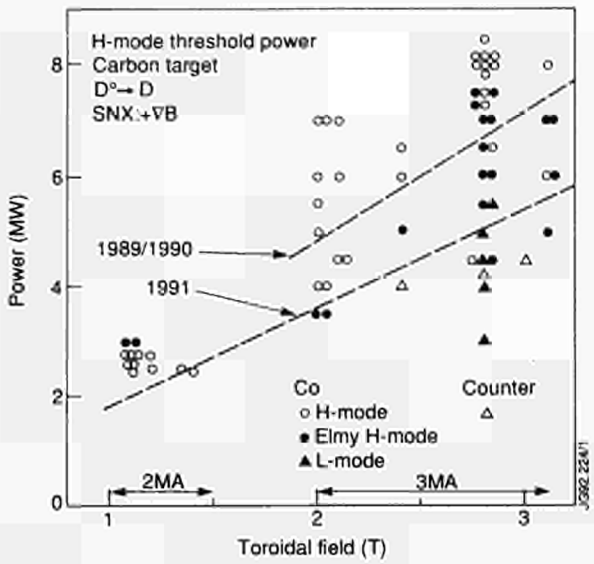

Fig.119: Fraction of tritium in a series of clean-up discharges after the PTE, showing the ratio of 14MeV to 2.5MeV neutrons produced during a neutral beam pulse, and RGA measurements integrated for 17 minutes after the discharge.

exchange with the plasma, and the rate at which these interactions take place. Besides being interesting from a particle recycling point-of-view, this information is important when considering in-vessel inventories of tritium for the preliminary tritium experiment (PTE) and the D-T phase.

Initial experiments were carried out in hydrogen/deuterium mixtures. Fig.118 shows the fraction of deuterium in a sequence of discharges during an exchange from hydrogen to deuterium. The initial exchange takes place in only about five pulses, at which time the plasma is ~80% pure. This rate of exchange implies that the divertor target plate contains 2×10^{22} accessible particles in the area 'wetted' by the plasma. Further purification of the plasma takes place on a much slower time scale since the exchange of particles with the rest of the first-wall maintains a background level of the minority isotope until this much larger reservoir has been exhausted. Thus, from the hydrogen/deuterium experiments, it is concluded that the recycling can be modelled by the 'three reservoir model'. Quantifying the size of the wall reservoir and the rate of particle exchange with this reservoir is difficult in hydrogen/deuterium experiments due to the detection thresholds of the various diagnostics.

The PTE provided an opportunity to improve knowledge of isotope exchange processes by using the increased measurement sensitivity for tritium. The fraction of tritium in the series of clean-up discharges after the PTE pulses is shown in Fig.119. The rate of decrease of this fraction after the initial fast drop, indicates a reservoir in the wall of $\sim 10^{24}$ interacting particles, as anticipated. The location and extent of any regions of longer term retention will only be quantified when the vessel is opened for the shut-down and the tritium content of the in-vessel components is measured.

Deuterium Outgassing Behaviour of the Walls

The outgassing of deuterium from the first wall after plasma discharges was investigated by measuring the total gas pressure and the partial pressures of the hydrogenic components (D_2, HD, H_2). Characteristically, after a discharge, the outgassing rate fell off with time closely following a power law, t^{-n}, with $0.5 < n < 0.8$. In the 1990 Progress Report, it was explained that no single mechanisim could be identified to cause such a time behaviour, but that outgassing from a surface layer with a thickness of several μm could produce the observed time dependence. The surface layer was needed to prevent particle losses into the bulk material causing too fast a fall off of the release rate. Further studies have employed a computer code simulating the particle balance between plasma and wall during a discharge and computing the particle loading of walls as well as the outgassing by solving the diffusion problem with the appropriate boundary conditions. This has shown that the experimentally time behaviour can almost naturally be a consequence of incomplete outgassing between consecutive discharges. The degree of particle accumulation in the first-wall determines the magnitude of the exponent 'n' in the

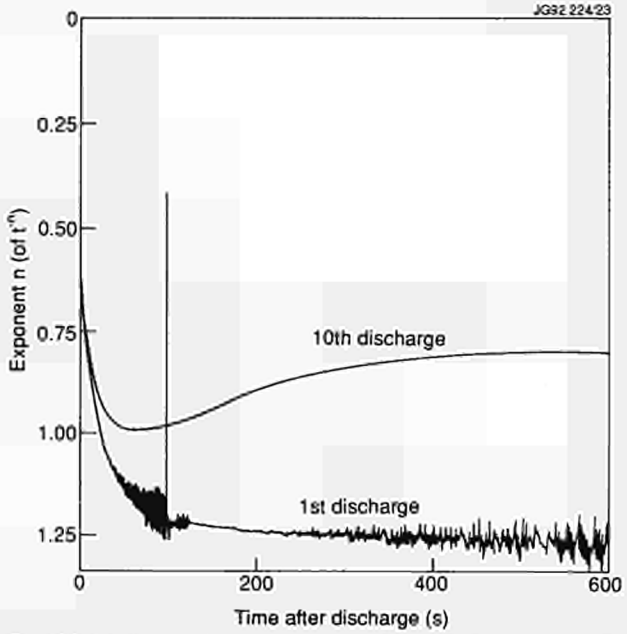

Fig.120: Variation of the exponent, n, where n is the exponent of the power law approximation to the dependence of the outgassing rate with time (t^n). Two cases are shown: after the first shot, n reaches values in excess of unity; and after the 10th shot, following particle accumulation during the previous shots, n remains at ~ 0.8.

power law approximation. h becomes smaller and smaller as the wall loading is larger and the deeper the deuterium distribution profile extends into the bulk material. It appears that n = 0.5 is the lower boundary value. A result of the change of the exponent with time and as well as with the accumulation of particles in walls is shown in Fig.120. The results are shown from the first and from the 10th discharge in a sequence of discharges. The fraction of outgassing over 10 minutes with regard to the particle input rises from initially 60% after the first discharge to about 80% after the 10th discharge. Continuation of the sequence would further decrease the exponent and increase the outgassing fraction until a steady state is reached when the outgassing fraction is unity.

This accumulation of particles occurs in all tokamaks (though to different degrees) and it is therefore not surprising that the temporal outgassing behaviour from different machines is very similar.

Helium Pumping by the Walls

The density of the fuelling gas component (deuterium, helium) in plasma discharges in JET is controlled by the external gas supply or neutral beams and by the pumping by the first wall materials (carbon, beryllium). It was shown in reference [7] that since beryllium was used, deuterium pumping was enhanced by a factor 10 compared to discharges with carbon first wall materials. A similar study was performed for helium discharges. It is important to know how helium recycles compared with deuterium, because: (a) even with an active pump installed in a tokamak as planned for the pumped divertor phase of JET, the material surfaces will still have an important if not dominating effect on the total pumping; and (b) it is necessary to know whether there might be any preferential pumping of deuterium over helium in a plasma burning machine with the effect that intolerably large helium accumulations might occur in the plasma. The experimental conditions for this study were simply that the plasma density was ramped up to a certain value and then the gas supply was interrupted. At that time, certain parameters were used to characterize the pumping behaviour :

1) The fuelling ratio $F(t) = N_p(t)/N_{gas}(t)$ where N_p is the deuteron or alpha-particle content of the plasma at time t and N_{gas} is the total deuterium or helium input until this time;
2) The pumping rate where $P = [(dN_p/dt) - F_{ex}]$ where F_{ex} is the external fuelling rate;
3) $[N_p/(dN_p/dt)]$, which is an effective time for particle removal from the plasma.

All data were taken at the time when the external flux was zero. The results are listed in Table XI. Also indicated are the electron and deuteron or alpha-particle contents of the plasma which could not be kept the same as the plasma conditions varied with fuel gas. For comparison, the deuterium pumping with a beryllium first wall is also indicated in Table XI. It is clear that with carbon, helium pumping is almost negligible. The typical duration of a discharge in JET is 20s and within this period almost no helium would be pumped resulting in a fuelling ratio of almost unity. With beryllium, helium is pumped much better, but less than deuterium. This underlines the need for additional active helium pumping in a deuterium/tritium burning tokamak using low Z wall materials.

Table XI

Gas - Wall	N_e [x 10^{21}]	N_i [x 10^{21}]	F	P [x 10^{19} s^{-1}]	τ^*[s]
He → C	4.2	1.3	0.9 -1	1.4	>50
He → Be	2.3	0.7	0.2 - 0.4	10	10
D → Be	2.3	2	0.1 - 0.2	90	1 - 4

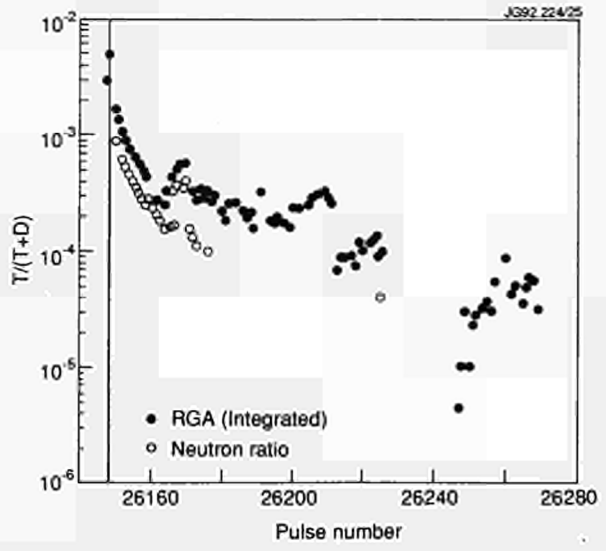

Fig.121: Plot of input power versus toroidal field for a range of plasma pulses.The symbols differentiate between the confinement regime attained by the pulses. The majority of the data is for co-injection, but the minimum power at which an ELM-free H-mode was attained with counter-injection is indicated at several values of toroidal field.

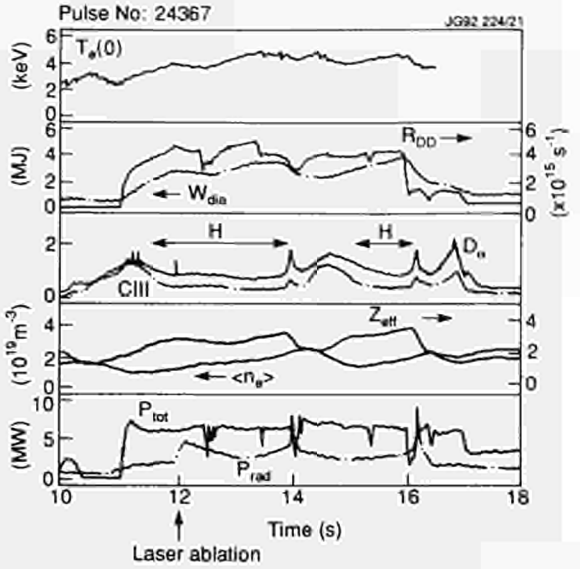

Fig.122: Evolution of main parameters during an H-mode with counter-injection. The rise in radiated power at 12s is due to injection of nickel by laser ablation. At 14s, the first H-mode period collapses due to edge radiation, but the fall in density and edge impurity content leads to a second H-mode at 14.5s.

Physics of the H-mode

As well as extending the range of H-mode operation in JET in several ways, H-mode studies during the 1991 campaign have sought to clarify the nature of changes in the plasma boundary associated with the H-mode transition and with edge localized modes (ELM's). This has been facilitated by the routine availability of diagnostics for measurement of edge electron temperature and density and by the commissioning of a new charge exchange (CX) diagnostic to measure edge ion temperatures and edge poloidal rotation.

H-modes with Counter - NB Injection

Studies of H-modes produced by counter-NBI on smaller tokamaks have generally yielded disappointing results. While the H-mode power threshold was found to be reduced relative to co-injection (by up to 30%), impurity accumulation in ELM-free H-modes generally caused the H-mode to collapse due to excessive radiation (eg. [8,9]). During the present campaign the first H-mode experiments with counter-injection were performed and the results differed in some respects from those previously reported.

As observed in smaller tokamaks, the threshold power for the H-mode transition is reduced relative to co-injection. However, the reduction factor is not as great as in smaller devices. Fig.121 shows an analysis of the H-mode power threshold for a range of data from the 1990 and 1991 campaigns. The data included is derived mainly from co-injection experiments and shows, that the H-mode power threshold during the 1991 was slightly reduced (~20%) relative to that observed in previous campaigns. This may be associated with the change from discrete (poloidal) target plates to a quasi-continuous toroidal X-point target. The lowest power at which an ELM-free H-mode was obtained at several toroidal fields in counter-injection is also shown. Even allowing for the scatter in the data and changes in vessel conditioning (the counter-injection experiments were carried out early in the campaign), the reduction in the H-mode power threshold is only ~10-20%.

Impurity transport also differed from that observed in other tokamaks. While there was some evidence of accumulation of metallic impurities (nickel) injected by laser ablation, this did not prove to be a significant problem as there was no indication of accumulation of low Z-impurities (such as carbon or beryllium) which were the dominant intrinsic impurities in JET. Thus, while ELM-free H-modes did collapse radiatively after several seconds, the radiation originated principally from the plasma edge. As a result, such an H-to-L transition was often followed by a rapid loss of edge density and impurities, due to the fall in edge confinement, leading to a further L-H transition once edge radiation had fallen sufficiently. Fig.122 illustrates such a case. One further, and unusual aspect of the impurity transport in counter-injection H-modes which is not understood is the development of a significant in-out asymmetry in the impurity profile. This was observed only for high Z-impurities and does not occur in L-mode plasmas.

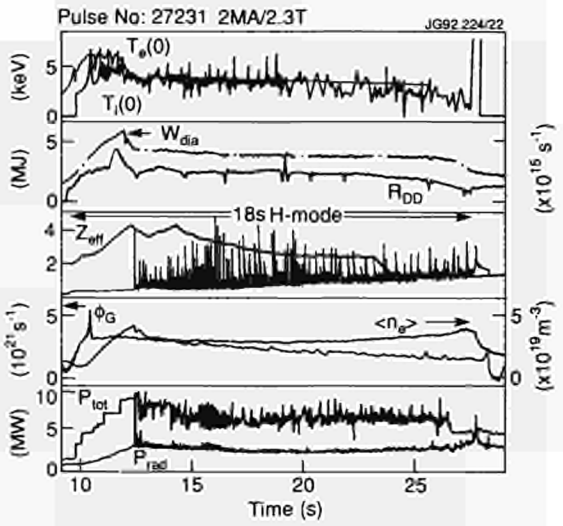

Fig.123: Behaviour of main plasma parameters during an 18s H-mode at 2MA/2.3T, held in a steady-state by ELM activity (visible on the D_α signal).

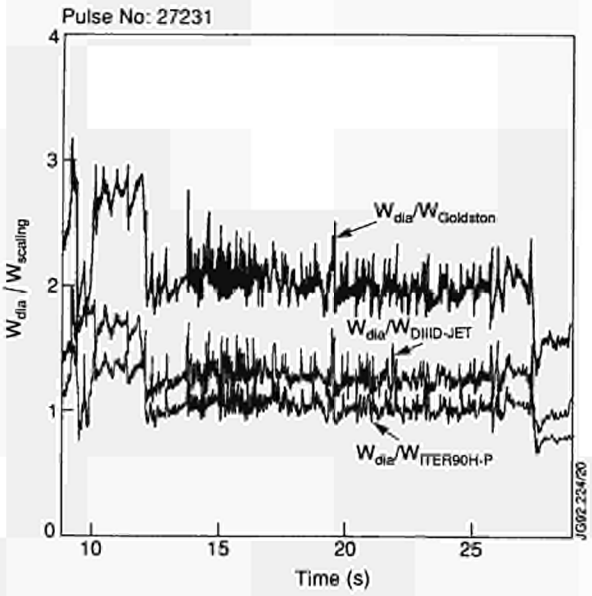

Fig.124: Stored plasma energy during an H-mode as a ratio that predicted by a number of confinement scaling laws, as a function of time.

Despite the similar behaviour of bulk plasma parameters in co- and counter-injection H-modes, plasma confinement was somewhat reduced in counter-injection plasmas. Only the best counter-injection H-modes achieved an energy confinement equivalent to twice the predicted by the Goldston L-mode scaling law, whereas co-injection H-modes generally reached or exceeded this level. This difference has been ascribed to a significant difference in central H-mode behaviour in the two cases. In co-injection H-modes, large amplitude, long-period (relative to ohmic plasmas) sawteeth were observed in the central temperatures. However, in counter-injection H-modes, small short period sawteeth were observed which flattened central temperature profiles and reduced central confinement and plasma performance.

ELM's and Steady-State H-modes

Edge localized modes (ELM's) are a characteristic instability of the H-mode, but as yet there is no understanding of the driving mechanism nor of the MHD modes involved. In addition, a reliable technique for the production of ELM's seems to be a prerequisite for attaining steady-state conditions in the H-mode. In smaller tokamaks ELM's occur naturally at high powers and steady-state H-mode conditions can be produced routinely. In JET, however, H-modes are generally ELM-free, and the density, and hence radiated power, rise throughout, leading to a termination of the H-mode after several seconds. Therefore, studies of ELM's during 1991 addressed both of these questions.

Several techniques were investigated for the production of ELM's: impurity injection (based on that plasma resistivity plays a key role [10]), current ramping and gas-puffing. All were successful to some extent, though current ramps were only advantageous under very limited conditions. In these studies, a scenario was developed in which long (up to 18s) H-modes were produced which exhibited high confinement and in which plasma parameters were held in steady-state by rapid ELM activity. The duration of these H-modes was limited by shear stresses induced in the shaping coils by electrical heating rather than intrinsic plasma behaviour.

The method used to achieve steady-state conditions was to combine NBI and off-axis ICRF heating with heavy gas fuelling (~50mbℓ s^{-1}). It was necessary to locate the ICRF resonance position ~ 50cm inboard of the magnetic axis to reduce the occurrence of large amplitude sawteeth which disturbed the plasma edge and generated large amplitude MHD modes. In addition, NB heating at 4MW was necessary to prevent persistent n=1 modes from locking and terminating the H-mode. The occurrence of these modes was sensitive to the level of both NBI and ICRF power.

In these experiments, the plasma current was restricted to 2-2.5MA, to obtain the longest possible H-modes, and the toroidal field was set 2.3T, partly by the necessity of locating the ICRF resonance off-axis and partly by the need to lower the H-mode threshold power to minimize power deposition on the X-point targets. The longest H-mode produced (at 2MA/2.3T) is shown in Fig.123. After an initial period of ~2s, when the H-mode was ELM-free, regular ELM activity started and maintained plasma parameters, (such as temperature, density, stored energy and neutron yield) constant.

A small rise in electron density towards the end of the H-mode may be due to saturation of the pumping capacity of the X-point target plates or may be the result of a gradual increase in impurity production from the target due to heating (during the H-mode 130MJ of energy was injected into the plasma, of which 75MJ was deposited on the target).

Fig.124 shows the confinement time for this discharge ratio versus that from several commonly used scaling laws: Goldston L-mode (without mass correction), D-IIID/JET H-mode [11], and ITERP-90H H-mode [12]. It is clear there is a loss of ~20% in confinement at the onset of ELM's. Nevertheless, confinement remains better than twice Goldston scaling, better than JET/D-IIID scaling and equal to ITERP-90H scaling throughout the ELMy H-mode. The results demonstrate the possibility of obtaining steady-state H-modes reproducibly, while maintaining high confinement.

In parallel, extensive measurements were made of temperature, density and magnetic fluctuations associated with ELM activity. ECE measurements of edge electron temperatures confirm previous observations of rapid sawtooth-like modulations of the electron temperature at each ELM [13]. However, interpretation of these results is complicated by the occurrence of non-thermal emission from the plasma edge, some of which is correlated with the ELM itself. Analysis of the density profile change at the ELM has not yet been possible due to the rapidity of the change, which is too fast for the microwave reflectometer to follow. Concentration has, therefore, focused on high frequency fluctuations associated with ELM's. Evidence has been obtained of narrow band fluctuations in both density and magnetic signals at frequencies in the range 50-100kHz during several ms preceding the ELM. The frequency drops during the period leading up to the ELM and the ELM appears as a short (~1ms) burst of broadband fluctuations. To date, no specific mode has been associated with the precursor activity.

Poloidal Rotation Measurements

Recent theories of the H-mode (eg [14]) propose that an edge confinement barrier arises from the growth of shear in the poloidal rotation of the edge plasma which suppresses the turbulence responsible for L-mode confinement. Using a multi-channel active charge exchange diagnostic, this question was addressed for the first time in JET. Analysis is at a preliminary stage, but evidence was obtained of a significant change in edge poloidal rotation at the L-to-H transition. In addition, the possibility that a threshold edge ion temperature exists for the L-to-H transition was investigated.

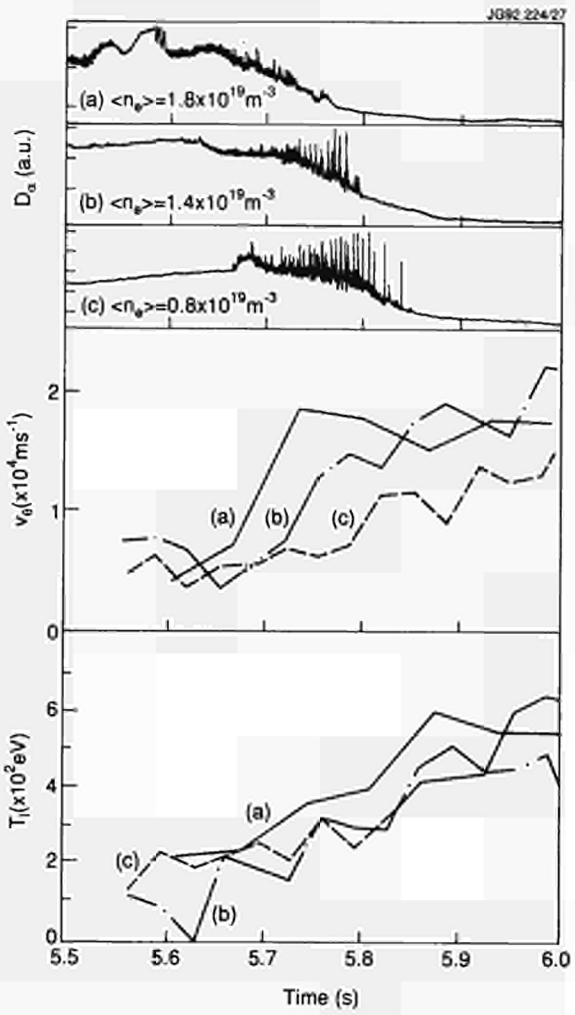

Fig.125: D_α signals from a sequence of three shots with different densities, showing the delay in the H-mode transition as the density decreases.

Fig.125 shows the results in which the average plasma density was varied on a shot-by shot basis in the range 0.7-1.9x10^{19}m^{-3}, while the input power was constant. The plot shows the time evolution of the D_α signal from three shots. Although the H-mode transition was rather slow, both the start and end of the transition phase (the 'dithering' phase) occured later in time at lower plasma density. The rapid increase in edge temperature during the 'dithering' phase was clear. However, at this stage of the analysis it is not possible to conclude whether the L-to-H transition can be associated with a specific ion temperature.

References

[1] M Keilhacker et al., Nuclear Fusion **31**, 535 (1991)

[2] G Vlases, R Simonini, 18th EPS Conf., Berlin 1991, Vol..3, p221

[3] G Janeschitz et al., Journ. of Nucl. Mat. **162-164** (1989) 624-628
[4] R Behrisch et al., J Nucl. Mat. **145-147** (1987) 723
[5] H Bergsaker et al., J. Nucl. Mat. **176 & 177** (1990) 941
[6] J Ehrenberg, J. Nucl. Mat. **145 - 147** (1987) 723
[7] P Thomas and the JET team, J Nucl. Mat. **176 & 177** (1990) 3
[8] The ASDEX Team, Nucl Fusion **29** (1989) 1959.
[9] D Schissel et al, Phys Fluids B **1** (1989) 1843.
[11] W Kerner et al, 33rd Annual Meeting of the Plasma Physics Division of the American Physical Society, Tampa, USA, 1991.
[12] D Schissel et al, Nucl Fusion **31** (1991) 73.
[13] J P Christiansen et al, JET Preprint JET-P(91)46 (to be published in Nucl Fusion).
[14] L Porte et al, Proc of the 18th European Conference on Controlled Fusion and Plasma Physics (Berlin, Germany, 1992) **4** 352.
[15] K Burrell et al, Phys Fluids B **2** (1990) 1405.

Physics Issues

A wide range of experimental topics were addressed during 1991, including studies of transport and confinement physics; high β regimes; sawtooth stabilisation and current profile measurement and modification; and issues related to particular aspects of Next Step devices.

The main experimental campaigns undertaken are summarised in the following sections:

MHD Related Experiments

MHD and Profile Effects in the Pellet Enhanced Performance (PEP) Mode

In the 1990 programe the Pellet-Enhanced Performance (PEP) mode and the H-mode were successfully combined to produce a new high performance regime in JET. The PEP H-mode [1], with its characteristic peaked density profile, underwent several rapid collapses both in the phase leading to peak performance and at the peak of the neutron yield. An investigation of the MHD phenomena associated with these collapses was started in 1990 and extended in the 1991 programme.

The 1991 programme aimed both to characterise the MHD associated with the collapses and also to improve the q-profile measurements in the PEP-H phase to confirm the existence of negative shear which had been postulated for the PEP plasma core. It was intended also to force a more radical change in the shear profile by injection of a pellet earlier in the discharge when the current profile was less well developed. This is described further in the section on MHD, Beta Limits and Topology.

β-limits in JET High Performance Plasmas

High β plasmas were studied in the 1991 campaign by pursuing two separate, but related, lines of attack. Firstly, H-mode plasmas were obtained with NB injection at low fields ($B_T \leq 1.2T$) and low safety factor ($q_{95} < 3.0$). In this way, it was intended to study plasmas with b values exceeding those predicted by the Troyon limit β_T, where $\beta_T(\%) = 2.8I(MA)/a(m)B(T)$. For Goldston scaling plasmas, the power to reach a β value scales as $P = 10a^{2.74}\ \kappa\beta^2 B_T^2/H^2R^{1.5}$, where, κ is the elongation and H is the scaling 'enhancement factor'. The NB power required is minimised by working at low toroidal field. Secondly, hot-ion H-mode discharges were generated using high NB power for a range of fields ($1.8T \leq B_T \leq 3.1T$). In these plasmas, it was intended to obtain pressures close to the high-n ballooning limit within the volume at the plasma center ($r/a \leq 0.4$) and hence study central β-limits under the highest performance conditions.

In the low field plasma experiments, all performed at 2MA and 1.5MA to keep q to reasonable values, several discharges were produced in which β-limiting behaviour was seen. Most of the discharges were strongly affected by ELMs, which set in ~300-400ms after the high NB power was applied. The onset of ELMs clipped the rise in stored energy and hence β. Fig.126(a) shows typical behaviour whereby at the energy 'clip' resulting from the first large ELM, the steadily growing n = 1 and n = 3 modes collapse and the n = 2 jumps suddenly to remain strong through the rest of the high power phase. Most of these discharges reached b values ~ 0.8-0.94 of the Troyon limit, a substantial improvement over previous results [2]. Some discharges reached even higher performance and exceeded the Troyon limit for periods of about an energy confinement time before a β collapse occurred. Such a discharge (Pulse No: 26236) is shown in Fig.126(b), where the ELM activity was held off long enough to reach a peak β value of 5.4% ($1.11 \times \beta_m$). It is clear that β rolls over about 200-300ms before the first small ELM then collapses with loss of about 0.5MJ stored energy with the second giant ELM. The n = 3 activity in this discharge does not grow as early as in the other ELM discharges and appears only at the sign of the β saturation.

The reasons for the superior performance of such discharges (i.e. Pulse No: 26236) are not clear but may be

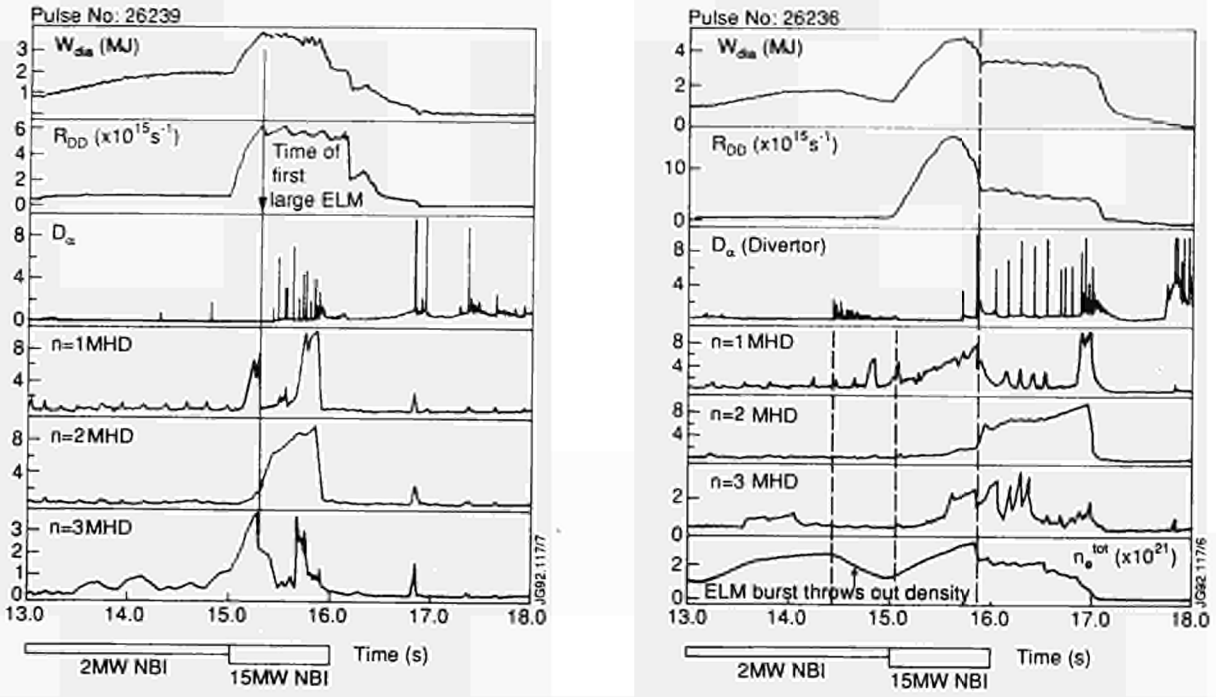

Fig.126: (a)Time development of a typical 2MA/1.1T double-null X-point plasma with high power NBI. The β values are clipped at ~90% of the Troyon value, coincident with the onset of the first large ELM at ~15.35 s. The time development of the low n MHD activity in this case was a frequently encountered phenomenon; (b) Time development of similar pulse, but where the Troyon limit is exceeded (peak β value ~5.4%) before a collapse of the plasma parameters occurs (at 15.58 s). Note the burst of ELMs which reduce the density before the high power phase.

related to the initial lower target density and consequent more centralised deposition of power. The stability analysis of these shots is at present under investigation.

In the second series of high-β experiments, the regime of the 'Hot Ion H -mode' was pushed to lower field values, extending the domain down to safety factor values (q_{95}) ~ 2.8. Experiments were performed in both the single -null and double -null X-point configurations. The aim was to investigate further the phenomena appearing in the 1990 pulses where the stored energy and neutron yield had shown limiting behaviour in advance of the occurrence of a carbon bloom. On a preliminary analysis, these discharges had central pressures (for r/a < 0.3) at or exceeded the high-n ballooning limit. The 1991 experiments were intended to push the high performance discharges closer to the β limit in the centre and to investigate the onset of MHD activity which might limit the performance.

The results obtained were complex and will not yield a clear pattern until in-depth analysis has been completed. It did prove possible to extend the Hot-Ion H-mode to 'low-q' and still maintain enhanced performance. All the Hot Ion H-modes have energy confinement times with enhancements significantly above 2 x L-mode confinement (often up to 50%). This has now been extended to Hot-Ion H-modes at 3.1 MA/1.8T with little sign of confinement degradation. The campaign also successfully created Hot-Ion H-modes early in the JET discharge, before the q = 1 surface entered the plasma. These H-modes should help to elucidate the role of MHD in the limiting of the Hot Ion regime's performance.

Fig.127(a) and (b) compare the behaviour of two Hot-Ion H-modes, one late in the discharge (t ~ 15 - 16 s) after the q = 1 surface entered the plasma, and the other early (t ~ 6 - 7 s) before the q = 1 surface was in the plasma. The late H-mode showed limiting behaviour at time t_L a few hundred milliseconds in advance of the collapse in the neutron yield and stored energy at a time t_C. This period t_L to t_C is associated with a rise in the low n MHD activity and also has the central pressure in the discharge close to the high-n ballooning limit. In this case, it seems that the MHD can be related to a limit in the performance. On the other hand, in the early H-mode discharge, there was little MHD activity and the central pressure was not close to the ballooning limit. A limit in stored energy and thermonuclear yield appeared nevertheless. The nature of the limit in these discharges is being investigated. It may be that impurity accumulation in the discharge centre caused deterioration performance. An early 'carbon-bloom' from the discharge edge did not seem to be the problem.

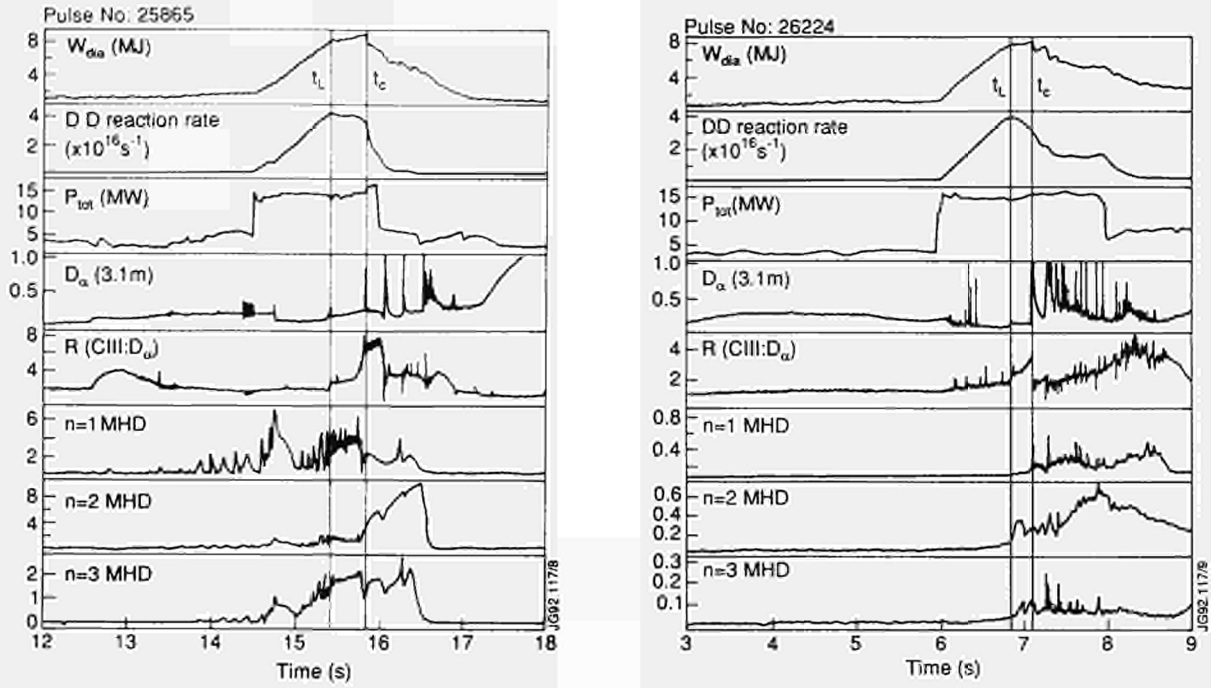

Fig.127: Comparison of the time development of two Hot-Ion H-mode pulses: (a) after the q = 1 surface has entered the plasma and (b) before the q = 1 surface has entered the plasma. The quantity R (CIII D_α) is the ratio of the CIII and D_α light signals seen along a vertical chord at R = 3.1m. This is sensitive to light from the edge of the plasma just outside the divertor region and a strong jump in R, has been used as an indication of carbon bloom, especially when the ratio increases out of control.

From the dataset, a β limit of the form $\beta(\%) - 2.0 I_p(MA)/B_T(T)$ emerged (Fig.128(a)), although a spread of peak β values existed at any particular value of I_p/B_T. The β peak value depended on purity of the target discharge as shown by consideration of the β value at which limiting behaviour occurs (β_{clip}), when plotted against volume averaged Z_{eff} for a set of 3.1 MA/2.8T Hot Ion H-modes, (as shown in Fig.128(b)).

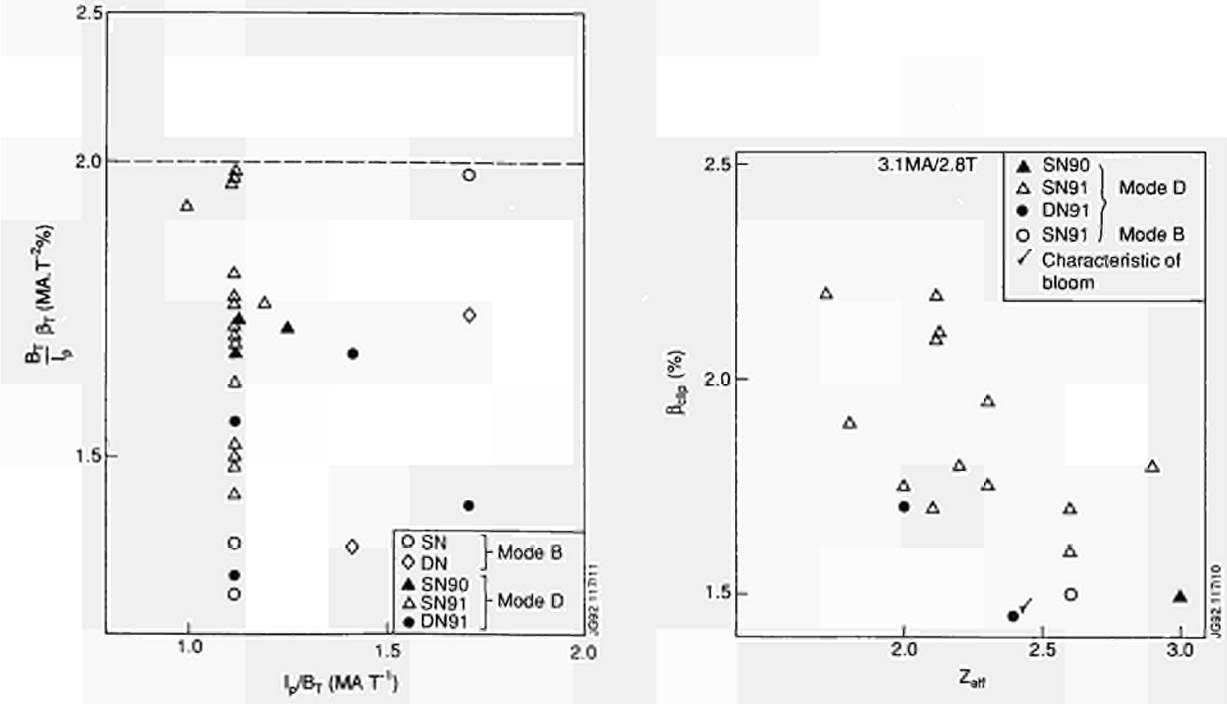

Fig.128: (a)Peak toroidal β (β_T) normalised by B_T/I_p, for a set of Hot Ion H-modes from the 1990 and 1991 campaigns; (b) β at which performance of the discharge begins to limit (β_{clip}) plotted against purity of the discharge during the first ~1 s of a Hot-Ion H-mode for a series of 3.1MA/2.8T discharges.

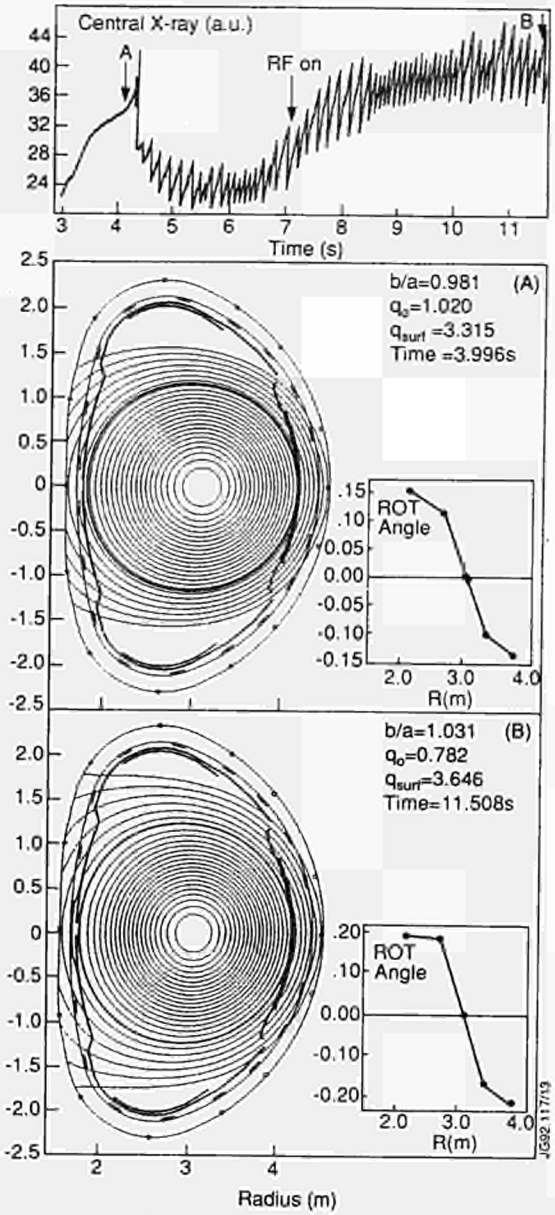

Fig.129: Behaviour of central soft X-ray signal during the evolution of a 2.5MA/2.8T circular cross section plasma (Pulse No: 27007), showing the onset of sawtoothing behaviour. (A) Equilibrium for Pulse No: 27007 together with fit to the polarimetry data and derived central safety factor (q_o). Data taken near to onset of sawteeth. (B) As in (A) but for a time several seconds after the onset of sawteeth.

Sawtooth Behaviour with Counter NB Injection

Sawtooth behaviour in plasmas with NB injection counter to the plasma current direction was studied during the 1991 campaign. This sawtooth behaviour sharply contrasts with that seen for co-NBI. Most obviously, in co-injection the sawtooth period was extended over that of the ohmic reference plasma, while for counter injection the sawtooth period was considerably shortened.

A more detailed comparison of the crash showed further differences. In the case of high power co-injection, a saturated m = n = 1 mode was normally seen before the crash, with a second m = n = 1 mode often seen at larger radius which survived the crash. During the early phase of the crash the hot core of the plasma was rigidly shifted off axis with a colder region growing behind. In the later phase of the collapse, the growth rate often abruptly increased. Subsequently, successor oscillations were seen which were the remnants of the hot core. The timescale of the crash was consistent with the Kadomtsev model as modified by Wesson to take account of electron inertia, that is 100-800 ms for sawteeth with periods of a few hundred milliseconds.

In the case of counter-injection, a small m = n = 1 mode was seen prior to the crash with a larger m = n = 2 modes further out. This indicates the presence of two q = 1 surfaces in the plasma, an observation which is consistent with the q-profile measured using Faraday rotation, which gives a broad and flat q profile with the central value of q_o, close to unity. At the time of the sawtooth crash, the m = n = 1 mode was observed to undergo a full 'Kadomtsev reconnection'. The outer m = n = 1 mode remained after the crash. After several milliseconds, the central m = n = 1 mode was again observed in the plasma centre. The timescale of the crash was consistent with the original Kadomtsev model, that is 3-5ms for sawteeth with periods of 30ms.

q-profile Measurements in Circular Plasma Configurations

Measurements of safety-factor (q) profiles were undertaken in circular plasma configurations. The programme had several aims:

- to minimise errors in the Faraday rotation (polarimetry) technique which occur in the inversion process before a q-profile can be obtained from raw data. The FIR Faraday rotation has been the mainstay of q profile measurements on JET and the errors in measurements on normal plasmas are associated with the elongation of the discharge;
- to compare the FIR Faraday rotation measurements with other diagnostic methods under these minimum error conditions; to compare q profile measurements with the newly commissioned Motional Stark Effect charge-exchange recombination spectroscopy (CXRS) diagnostic; and to compare Soft X-ray tomography measurements of the q = 1 surface with those of the Faraday Rotation.

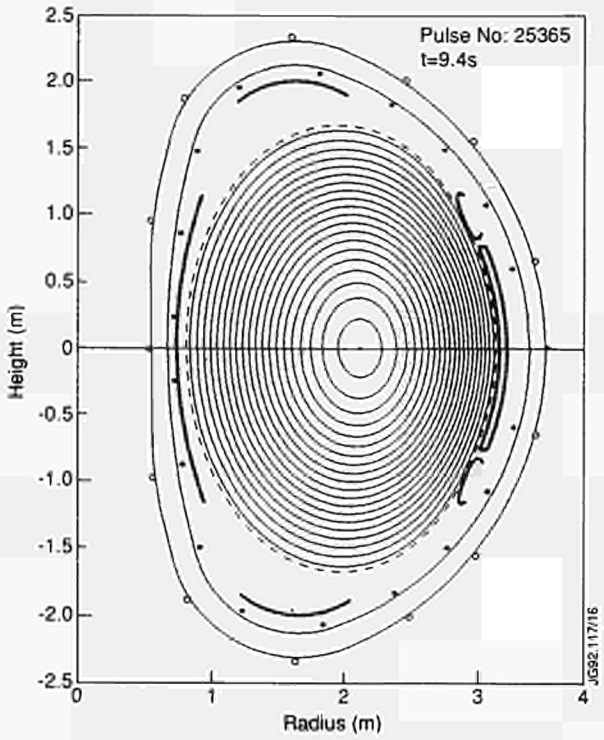

Fig.130: Inverse D plasma configuration during the current ramp experiments.

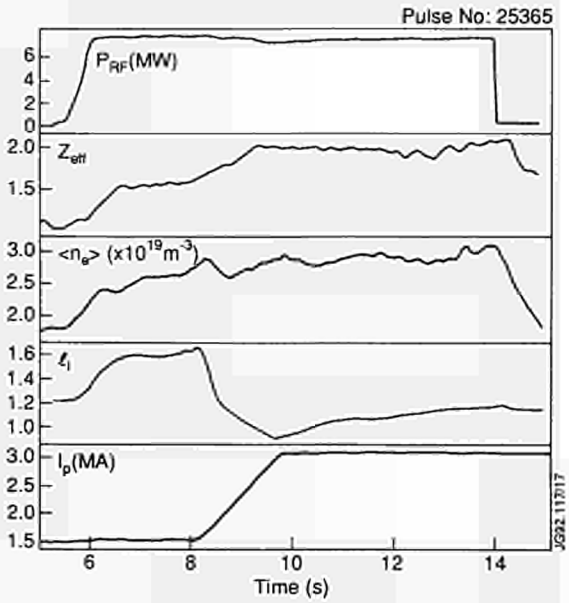

Fig.131: Time traces from Pulse No: 25365 with plasma configuration as in previous figure. The RF power, plasma density and Z_{eff} remain about constant through the current ramp from 8 - 10s in spite of a change in plasma inductance.

The special circular plasma configuration was established successfully. Ordinary sawtoothing discharges, and discharges with monster sawtooth, generated by the application of ICRF, were studied. The results obtain during a typical circular discharge are shown in Fig.129. This shows the sawtoothing behaviour of the discharge and the equilibria obtained with the IDENTD code fitted to the Faraday Rotation data are shown for two time points in Fig.129(A) and (B). The fits, obtained with smaller errors than usual, show that, q_o passes through unity as the sawtooth starts, and tends towards a value $q_o \sim 0.8$ at later times. This confirms the values indicated before in other JET discharges, but which were subject to greater errors.

For non-monster sawtooth cases, when the current profile has fully penetrated, q_o rose linearly with q_{surf} and the diameter of the q = 1 surface (D(q = 1)) was measured with reasonable agreement ($\pm$0.1m) between the Soft X-rays and the polarimeter.

Transport and Confinement Related Experiments

Experiments with Current-Ramp Plasmas

Experiments with current ramp plasmas were aimed at producing conditions under which the plasma shear (s) and poloidal field (B_{pol}) had been decorrelated for some time. This study aimed at establishing the variation of the local diffusivity (χ) in such plasmas (i.e. was the variation a function of B_{pol} only or B_{pol} and s?). All empirical tokamak scaling laws for global τ_e show pronounced current scaling and the origin of this could be either a local dependence on shear or B_{pol}. In steady-state plasmas, s and B_{pol} are correlated and so measurements on scaling in non-steady state plasmas are required for further understanding. The easiest way of decorrelating s and B_{pol} was via inducing a current ramp in the plasma.

There were technical difficulties to overcome in the setting-up of the experiment. During current ramps the inductance of the plasma changes transiently before the current profile was fully re-established. In this phase the plasma equilibrium was difficult to maintain and careful shaping current programming was necessary to avoid excursions of the plasma to hit the antennae protection screens and lead to a large influx of impurities. The plasma equilibrium chosen was an 'inverse-D' type shape shown in Fig.130. The plasma behaviour, the shaping current and the RF power coupled during a ramp from 3MA to 1.5MA is shown in Fig.131. It can be seen that good density and Z_{eff} control were maintained and the coupled RF power remained constant throughout the ramp. The ramp times were typically much less than the resistive times of the plasma ($\tau_{ramp} \sim 40\%\tau_h$; $\tau_h \sim a^2T^{3/2}$). Fig.132 shows the transient changes to the plasma inductance ℓ_i during upward and downward current ramps. (ℓ_i) moves in the opposite sense to the current ramp and, at the end of the ramps I and ℓ_i were effectively

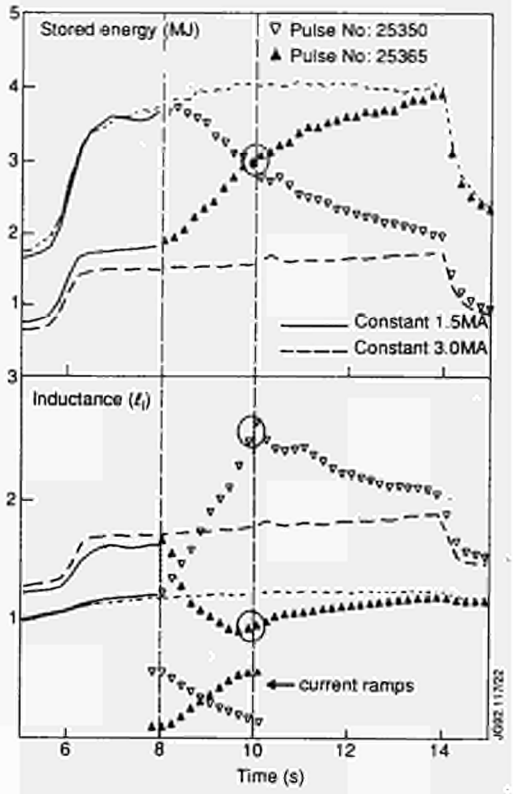

Fig.132: Behaviour of plasma inductance and stored energy during four pulses with identical RF power, where the plasma current was successively constant at 1.5MA; ramped up from 1.5MA to 3MA; constant at 3.0MA; ramped down from 3MA to 1.5MA. Note that in the current ramp pulses, I_p and l_i are effectively decorrelated at t = 10s.

decorrelated. Fig.132 also shows that the stored energy W did not follow the current I_p but lagged behind.

The results of these experiments show that scaling of stored energy should include the product of $\ell_i I$ rather than just I. These are discussed further in the Transport and Fluctuations section. However, the rapid control of thermonuclear burn by current ramps is precluded by these experiments since they demonstrate that at the 7-8keV temperatures achieved, control of the plasma stored energy could only be reached after ~15-25 confinement times. The situation would clearly be worse in a 15keV reactor plasma.

Transport and Confinement Studies in the PEP H-Mode

Transport and Confinement studies carried out with PEP H-mode discharges were aimed at:

- producing profile measurements, especially T_i and Z_{eff} profiles, to enable a full transport analysis on the PEP H-mode with the objective of clarifying the central improvement in the thermal diffusivity (χ), especially the possible scaling of χ with density gradient (∇n_e),

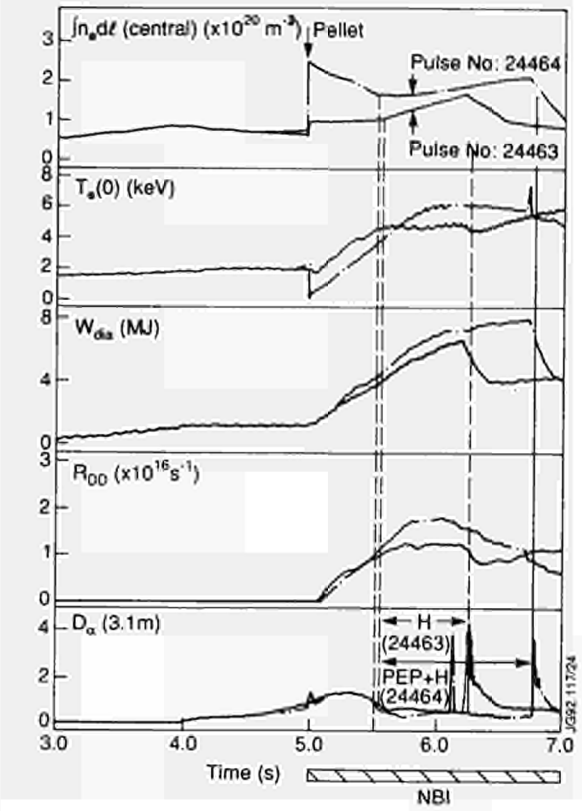

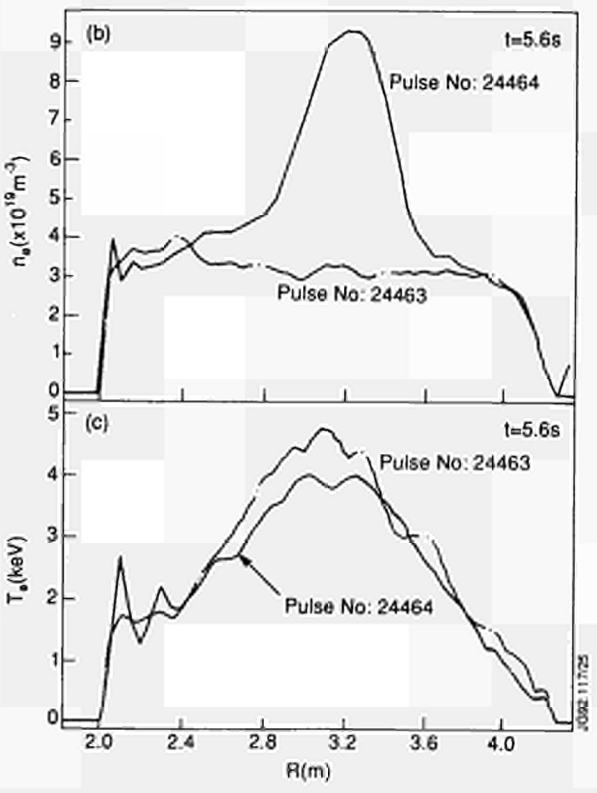

Fig.133: (a)Comparison of the development of an NBI heated H-mode with PEP density enhancement (Pulse No: 24464) and one without the density enhancement (Pulse No: 24463); (b) LIDAR derived density profiles for the two pulses in (a); (c) LIDAR derived temperature profiles for the two pulses.

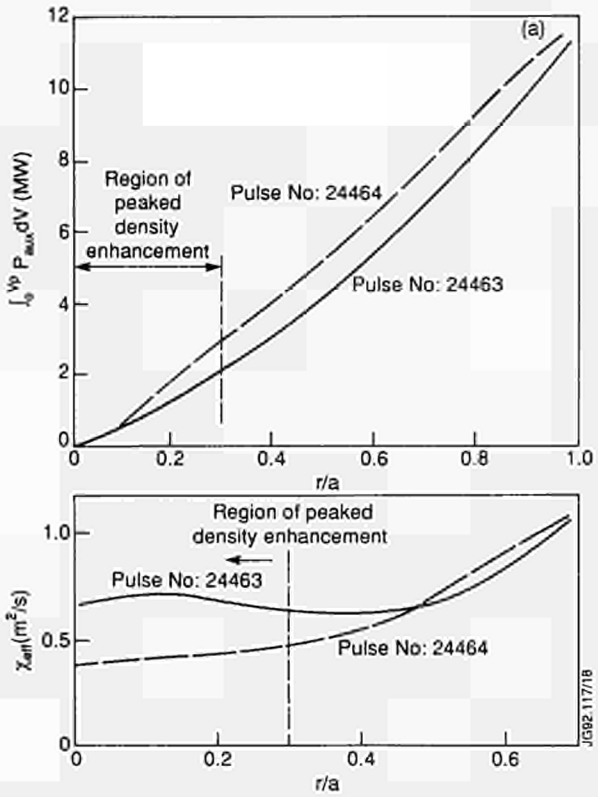

Fig.134: (a) Power deposition profiles for NBI H-modes with and without PEP density enhancement; (b) Effective thermal diffusivity (χ_{eff}) from local transport analysis for two NBI H-modes showing reduced central transport associated with the PEP phenomenon.

negative shear (q'/q) or power flow into the core of the PEP plasma;

- producing PEP H-modes generated by a single heating method e.g.: (ICRF alone or NBI alone)
- obtaining clear evidence of high ion heating using ICRF power alone.

Many ICRF-only and NBI-only PEPs were produced. The T_i profiles showed that, in the high density PEPs, the electron and ion temperature profiles were approximately equal (within ±1keV). The transport data have not yet been fully analysed, but earlier results, lend weight to the assertion that there is a significant confinement enhancement in the central region of the PEP discharge. Fig.133(a) shows the development of two NBI-heated discharges, one with a good pellet which displays the PEP density enhancement (Fig.133(b)), the other with a broken pellet which fails to show the enhancement. It can be seen in Fig.133(a) that the PEP discharge achieves superior stored energy and temperature values over the ordinary H-mode discharge, in spite of the same NBI input power. Thus, although the central density in the PEP H-mode just after the L-H transition is a factor 3 higher than the density in the ordinary H-mode, the temperatures achieved at 5.6 seconds are approximately the same in the two discharges (Fig.133(c)). An initial transport analysis, taking measured electron density and temperature profiles, and assuming $T_i(r) \sim T_e(r)$ shows that the absorbed NBI power within the region of the PEP density enhancement ($r = r/a \leq 0.4$) is only ~25% higher for the PEP H-mode shot than for the ordinary H-mode (Fig.134(a)) and that the effective diffusivity is reduced to about half of the ordinary H-mode value (Fig.134(b)). Work is in progress to quantify this improvement more exactly and relate its variation to the density gradient and negative shear parameters.

Ion heating by ICRF-alone has been maximized in the PEP H-mode plasmas by using two minority species, H and ^{3}He each at moderate concentrations (~ 10% n_{min}/n_D) and coupling RF power into each species. This minimises the temperature of the 'tail' of high energy minority ions accelerated by the RF ($T_{tail} \propto P_{RF}/n_{min}$) and hence maximises the ion heating from each of the accelerated minorities. This is inversely proportional to T_{tail}/E_{crit} with the critical energy (E_{crit}) dependent on the electron temperature (T_e). Using the mixed minority scheme and a low density PEP target plasma, obtained by allowing a pellet enhancement to decay before applying full heating, central ion temperatures of 14-16keV were obtained with about 9MW of ICRF coupled into the two minorities in an approximately 60:40 ratio (P(H):P(^{3}He)).

Scaling of H-Mode Confinement with Toroidal Field

The scaling of H-mode confinement with the toroidal magnetic field has been assessed. The strong scaling $\tau \propto B_T^{0.6\text{-}0.7}$ which emerged from a free fit to the ITER H-mode database is doubtful due to collinearity, especially between the parameters B_T and elongation. In 1990, a toroidal field scan experiment in sawtoothing discharges indicated a scaling $\tau \propto B_T^{0.3}$ but other parameters were varied as well. In 1991, a new toroidal field scan experiment was carried out in which as many parameters as possible were kept constant. In the new experiment, B_T was scanned from 1.5T to 2.8T in a series of 3MA DN-X-point 'Mode B' discharges (X-points formed early in the pulse before the full penetration of the current profile).

The H-mode was obtained by NB injection alone, the NB power was kept constant at 2-4MW for 2s and then increased to a constant 6-8MW for 3s. As expected, the L to H transition occurred already at the low power level for low field $B_T < 1.8$T. All shots had long duration (2.2s-4s) ELM-

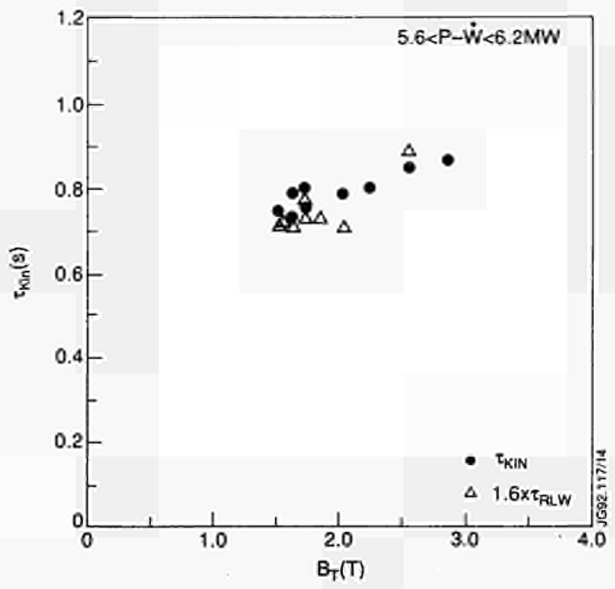

Fig.135: Energy confinement time from kinetic measurements (t_k) for a set of 3.0MA H-modes as a function of toroidal field (B_T). Also shown is the variation predicted from Rebut-Lallia-Watkins scaling (t_{RLW}) with an enhancement factor of 1.6.

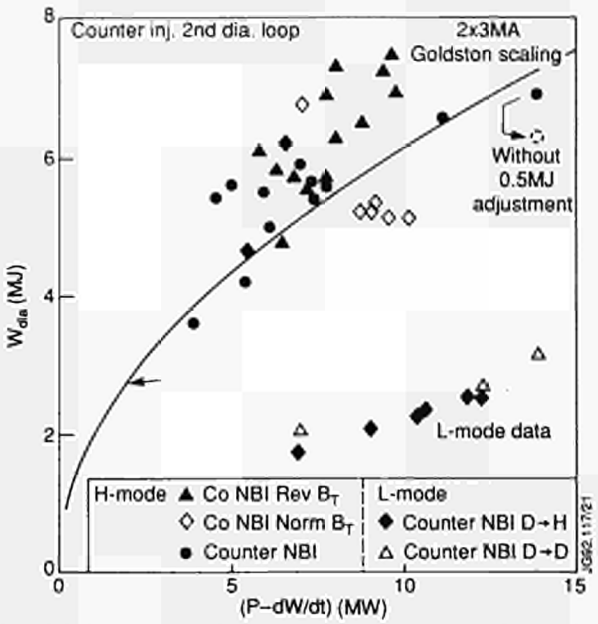

Fig.136: Comparison of counter-NBI H-mode data at 3MA/2.8T with the co-injection data set at 3MA and 2.2 < B_T < 3.2T. (The counter data set has been adjusted by +0.5MJ to account for known errors in the diamagnetic loop measurement)

free H-modes. The density and radiation was increasing throughout the H-mode period. It was observed that typically dW/dt ~ 0 for P_{rad}/P_{tot} ~ 40% and dW/dt<0 for P_{rad}/P_{tot} ~ 60% in all pulses. This meant that the energy W tended to decrease at the second power level in the longest H-modes (i.e. for B_T<1.8T). The time at which the first sawtooth appeared also varied from pulse to pulse. With B_T = 2.8T, the first sawtooth did not appear until just after the end of the second power step leaving the whole H-mode period sawtooth-free. The sawtooth started progressively earlier as the B_T was lowered. By comparing the data (W_{dia} and W_{kin}) at timepoints where P-dW/dt ~ 6MW; $\langle n_e \rangle \sim 4 \times 10^{19} m^{-3}$; $2.5 \leq Z_{eff} \leq 3.5$; P_{rad} ~ 2MW and $W_{fast} \leq 0.4$MJ, a variation of $\tau \propto B_T^{0.25}$ was obtained by regression analysis on all the data. In Fig.135, the kinetic confinement time is shown versus toroidal magnetic field. In these experiments, q_{cyl} = const x B_T, so that the observed B_T scaling could be interpreted as a q_{cyl} scaling. The increase of 20% is too small compared to the present uncertainties in local parameters to show a decrease in c with increased B_T, moreover the observed B_T dependence may be entirely due to sawtooth effects.

Confinement with Counter Injected NB Power

For the first time since 1986, the NB system was used to inject atoms counter to the direction of the plasma current. The aim was to compare the heating and confinement with counter NB power against the main JET L and H-mode datasets with co-injection. The campaign included the achievement of the first H-modes on JET with counter NB. The H-mode appeared to be relatively easy to achieve and a study of the H-mode threshold was undertaken. Impurity accumulation did not appear to be a problem in these H-modes (unlike reports from other tokamaks) and Z_{eff} and radiated power levels remained low throughout the H-mode phase. No evidence of peaked density profiles was seen in any of the counter-injection H-modes (although only a few attempts were made to run at low q where peaked profiles have been seen on other tokamaks).

The general L-mode and H-mode global confinement for counter NBI was compared with previous JET co-injection data at 3MA in Fig.136. The counter NBI H-modes had an enhancement factor ~ 2 over Goldston scaling which placed puts them on the lower side of the JET dataset. The slightly poorer confinement was related to the behaviour of the central T_i and T_e values with counter NBI. As already discussed, the sawteeth in counter-NBI heated discharges were small, irregular and high frequency. As a results the central ion and electron temperatures were not allowed to build up and a somewhat lower stored energy was achieved than in the co-injected case (where the sawteeth are often stabilised in the best performance shots). An example of the development of the electron temperature profile during a counter-NBI H-mode is shown in Fig.137.

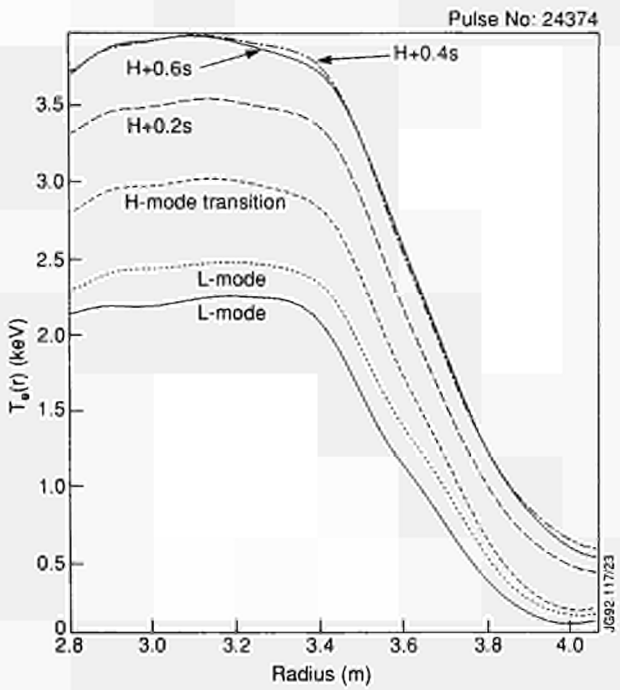

Fig.137: Development of the electron temperature profile in a 3MA/2.8T single-null X-point H-mode (8MW NBI).

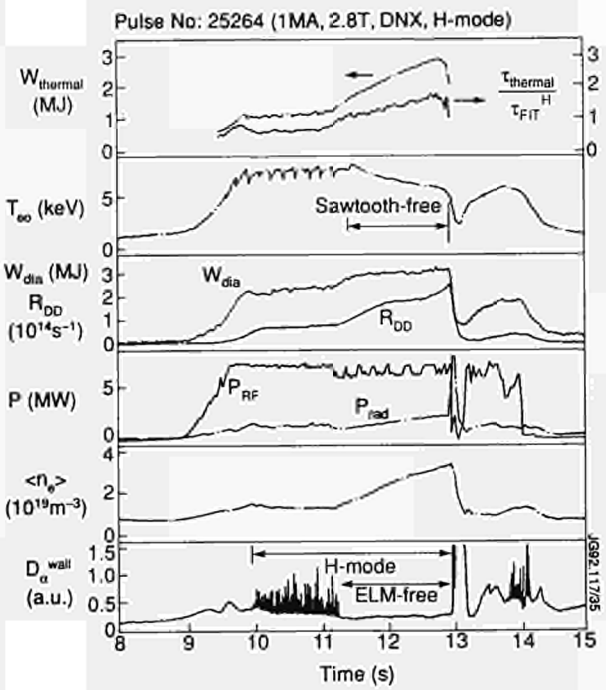

Fig.138: Time development of an H-mode with ICRF heating where the bootstrap mechanism dominated the current.

Next Step Issue Experiments

Operation of the JET Tokamak in the AC Mode

An important experiment was the demonstration of one full cycle of 2MA operation of the JET tokamak (viz counter plasma current followed by co-direction plasma current with a short dwell time 50ms - 5s. between half cycles). This experiment clearly opens up the prospect of an inductively-driven Next Step machine with obvious savings on non-inductive current drive schemes. This is described further in the section on Next Step related Issues.

Bootstrap Dominated Plasma Studies

Many studies for Next Step Tokamak designs (eg: the Japanese SSTR [3]) feature plasmas where a high fraction ($\geq^2/_3$) of the plasma current is sustained by the bootstrap mechanism, to improve the non-inductive current drive efficiency. In addition, the generation of the bootstrap current is controversial in a plasma without strong net particle fuelling from a source such as NBI, raising questions about the existence of such plasmas with ICRF heating schemes.

To address these questions, H-mode plasmas have been produced in which a large fraction of the plasma current (up to 70%) is driven by the bootstrap effect. The bootstrap current fraction is 2 - 3 times greater than in previous JET experiments [4] and comparable with values obtained at JT-60 [5]. These experiments provide an indication of the steady-state current profiles which can be expected in bootstrap current dominated plasmas. The discharges were obtained with low plasma currents, 1 - 1.5MA, with 5 - 10MW of D(H) dipole ICRF heating, in double-null X-point H-modes. This resulted in poloidal b values of ≈ 2.

Fig.138 shows a typical discharge at I = 1MA and B_T = 2.8T with $P_{RF} \approx 7$MW. ELMs were observed soon after the application of ICRF power resulting in a roughly constant, relatively peaked density profile. At t ≈11.2s, the ELMs ceased and the electron density rose rapidly while the profile flattens. The plasma stored energy rose at the cessation of the ELMs and the electron temperature sawteeth are suppressed. The thermal energy confinement time ($\tau_{thermal}$) was typically better than expected from the JET/DIII-D H-mode scaling [6]. In this case the enhancement factor rose to about 1.7 at the end of the H-mode phase (although it should be noted that these plasmas had high edge q_ψ compared with the data used for the scaling).

The combination of relatively high energy confinement and low plasma current allowed the production of high β_p plasmas expected to have a large bootstrap current. The theoretical value of the bootstrap current is calculated using measurements of density and temperature, and is shown in Fig.139. During the early phase of heating when ELMs were

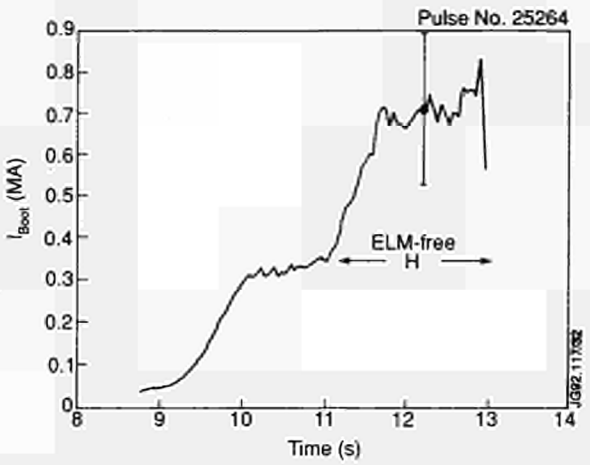

Fig.139: Modelled bootstrap current needed to simulate the loop voltage for the 1MA/2.8T DNX H-mode in previous figure.

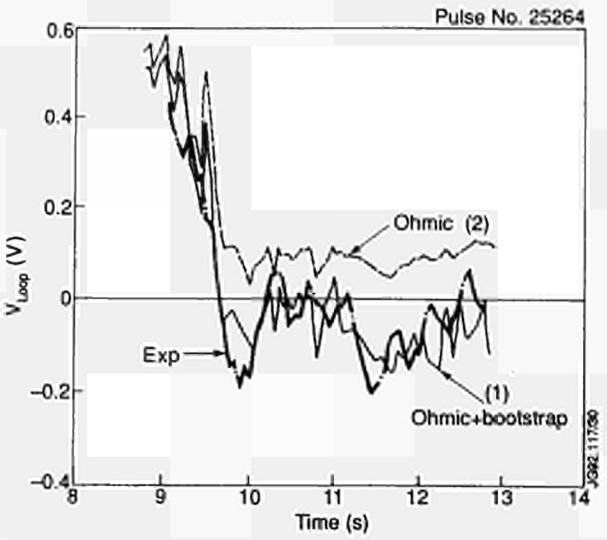

Fig.140: Measured behaviour of the surface loop voltage in the bootstrap dominated discharge of previous figure compared to predictions including (a) only ohmic current drive and (b) both ohmic and Bootstrap currents.

present, the calculated bootstrap current was about one third of the plasma current. During the ELM-free phase, this rose to ~ 70%. The effect of the calculated bootstrap current on the surface loop voltage is shown in Fig.140. Here the measured surface loop voltage is compared with a simulation using a time-dependant current diffusion code including (a) only Ohmic current drive and (b) both Ohmic and bootstrap currents. Good agreement is found only when the effect of the bootstrap current is included.

In these plasmas, as in typical ELM-free H-modes at JET, the relatively flat electron density profile has steep edge density gradients. These in turn result in a bootstrap current profile which is either flat or peaked near the plasma boundary. The duration of these H-modes is not sufficient to reach a steady-state, however they raise the question whether such a plasma would be stable or possess good confinement.

Profile Modification Experiments

ICRF Minority Current Drive Experiments

Although the efficiency predicted for current drive by RF minority ions is rather low, the effects of this form of current drive can be shown to have rather dramatic effects on plasma profiles. The resonant condition $\omega - \omega_{ci} = k_{\parallel} V_{\parallel i}$ suggests a sign change in the driven current on the two sides of the minority cyclotron layer provided the damping is not too strong.

The effect is local and can be used to modify the gradient of the plasma current. If the cyclotron layer is near the q=1 surface then sawteeth can be stablised or vice-versa [7]. The launched spectra of the antennae have to be asymmetric in $k_{\parallel}$ space to cause this effect. This has been achieved on JET by phasing the two halves of an antenna at values other than (0, 0) or (0, π).

In the convention adopted, positive phasing between antennae leads to minority current drive which adds to the plasma current (I_p) on the side of the resonance furthest from the magnetic axis and subtracts from I_p on the side of the resonance nearest the magnetic axis. Thus, if the ICRF resonance layer is located near to the q = 1 surface on the inboard side of the plasma centre, then the current profile near the q = 1 surface will be flattened and the sawtooth

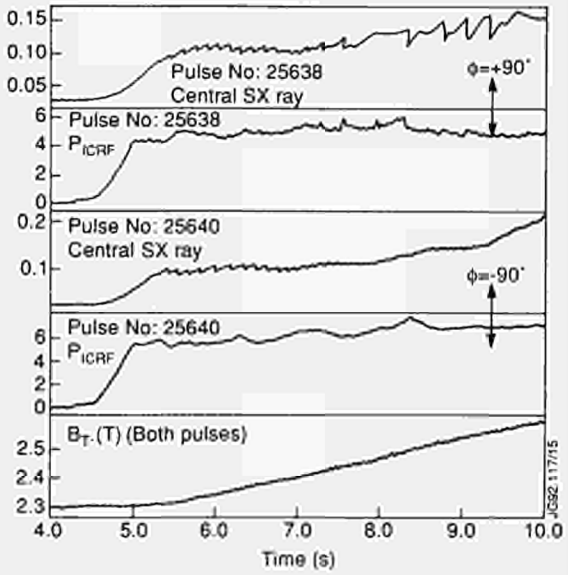

Fig.141: Sawtooth behaviour with phased ICRF minority heating located near the inboard q = 1 surface. As B_T (lower trace) is scanned (displacing the resonance), the stabilising effects of positive phasing (ϕ = +90°) and the destabilising effects of negative phasing (ϕ = -90°) can be clearly seen.

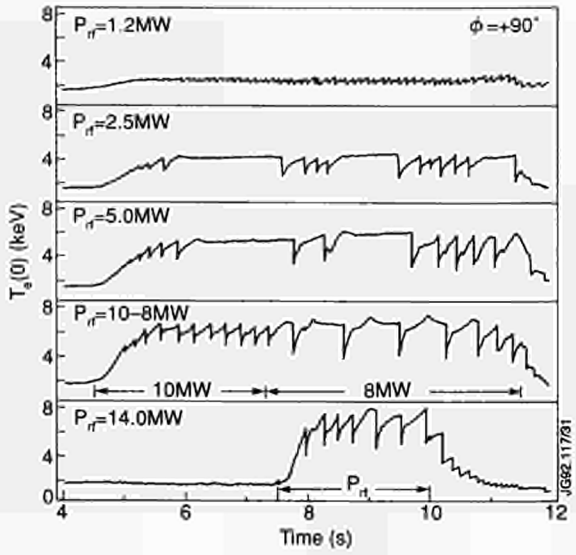

Fig.142: ICRF power scan with the resonance located at the inboard q = 1 location showing the appearance and disappearance of sawtooth stabilisation at powers which are either too low or too high.

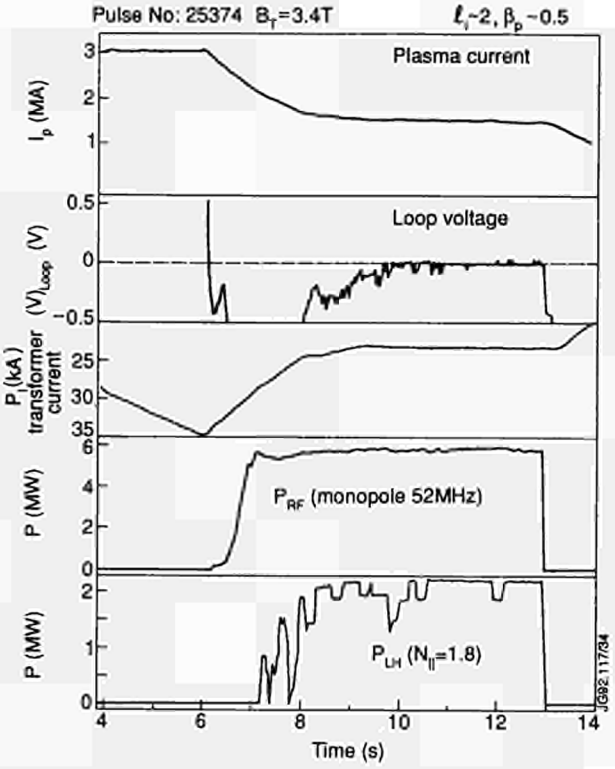

Fig.143: Full current drive at I_p = 1.5MA obtained with combined LHCD and ICRF.

instability will tend to be stabilised. With negative phasing, the sawteeth will tend to be destabilised. If the ICRF resonance layer is situated near the outboard q = 1 surface then the situation will be reversed with positive phasing causing destabilisation and negative phasing causing stabilisation.

Tests were performed and the theory was validated. Fig.141 shows two pulses each with ~6MW ICRF with the resonance layer on the inboard side. As the position of the layer was scanned (by scanning B_T) then as B_T passed a central value ~2.5T (at 8 s) the sawteeth were stabilised in the positive phasing ($+\pi/2$) case and destabilised in the negative phasing ($-\pi/2$) case, seen by the soft X-ray signals. This central value of B_T places the cyclotron resonance layer for 42MHz H minority (2.8T) at R_{CH} ~2.65m, within ~10cm of the inboard q = 1 surface, lending strong support to the theory. Data taken with the resonance located on the outboard q = 1 surface also supported the theory.

Experiments were also performed to establish how the effect varied according to the RF power coupled. A scan in RF power at fixed B_T (hence fixed R_{CH} location) are shown for R_{CH} close to the inboard q = 1 surface in Fig.142. There is a lower threshold for the appearance of the stabilisation effect (~1.5MW in this scan) but there is also an upper threshold, between 8-10MW, where the stabilisation effect disappears. This can be understood as a combination of effects, partly because of the 'overheating' of the minority ions and partly because of the increased perpendicular energy (W_p) given to the minority ions. The latter effect puts more ions into trapped orbits in which they can make no contribution to the current drive (and hence the sawtooth stabilisation). The overheating takes the minority ions which remain in passing orbits to energies where their characteristic tail temperature of their distribution ($T_t \propto P_{RF}/n_{min}$) is very much higher than 'critical energy' ($E_{crit} \sim 15T_e$). In the region where the Stix parameter, ξ (= T_t/E_{crit}), is ~ 1, the minority current drive efficiency should be at its highest [8] and thus the overheating effect leads to loss of efficiency and a weakened effect on the sawtooth. The minority current drive efficiency also falls off for $\xi<1$, which explains the lower threshold for the stabilisation effect in terms of insufficient tail temperature.

The validity of these qualitative explanations has been tested by performing experiments at fixed RF power and increasing the minority concentration, thereby reducing W_p and T_t. The sawtooth stabilisation can be pushed to higher RF powers as the $(n_{min}/n_{min}+n_D)$ ratio is raised, the low-power threshold for the effect being raised at the same time.

Experiments with Lower Hybrid Current Drive

Full sustainment of the plasma current up to 1.5MA was achieved with a combination of LHCD, (up to 2.3MW), and

ICRF on hydrogen minority heating in monopole configuration (3 to 5MW). Full current drive was observed when the LH induced fast electrons have a rather peaked profile which is achieved at high toroidal field: $B_T > 3T$, and low density: $n_{e0} < 3 \times 10^{19} m^{-3}$. An example of a discharge where the current of 1.5MA is sustained is shown in Fig.143).

Current drive efficiency can be deduced taking into account synergistic effects with the fast wave (10% ICRF power is estimated to be directly coupled to fast electrons) and an estimate of the bootstrap current generated. With full current drive, efficiencies increased with the electron temperature and reached: $n\ R\ I/P = 0.4 \times 10^{20}\ m^{-2}A/W$.

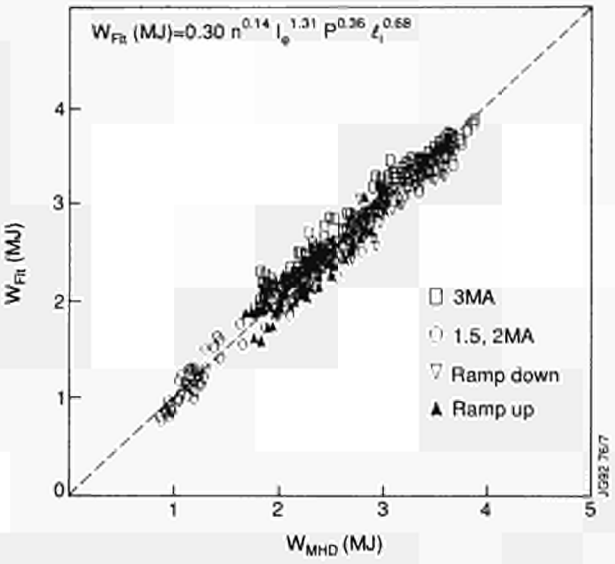

Fig. 144: Fit to stored energy $W_{fit} = 0.3\ n^{0.14} I_\varphi^{1.31} P^{0.36} \ell_i^{0.68}$ versus the measured stored energy for the current ramp pulses. I_φ is the toroidal current, n the average density, P the total power and ℓ_i the inductance.

References

[1] Tubbing B. J. D. et al, Nuclear Fusion **31** (5) 1991), 839.
[2] The JET Team (presented by P Smeulders) 13th Conference on Plasma Physics and Controlled Nuclear Fusion Research (Washington IAEA) (1990). Nuclear Fusion Supplement Vol. 1, p. 219, (1991).
[3] Kikuchi M., Nuclear Fusion **30** (2) (1990), 265.
[4] Challis C.D., et al, Nuclear Fusion **29** (4) (1989), 563.
[5] Kikuchi M. et al, Nuclear Fusion **30** (2) (1990), 343.
[6] Schissel D.P. et al, Nuclear Fusion **31** (1) (1991), 73.
[7] Cox. M. and Start D.F.H., Proc. Int. Conf. Plasma Phys. (Kiev, USSR) (1987), **1**, 232.
[8] Fisch. N. J., Nuclear Fusion **21** (1981), 15.

Transport and Fluctuations

A series of experiments and detailed analysis has been completed during the 1991 campaign, in an effort to improve understanding of the processes involved in heat and particle transport. One of the issues that has been studied in detail is the physical origin of the current scaling of energy confinement in both L-mode and H-mode discharges. This work is described in the first section. The main conclusion is that the source of the current scaling is through the poloidal field.

Experiments to determined the dependence of confinement upon isotopic mass have been carried out by the injection of hydrogen, deuterium and helium ions into plasmas of the same isotope. The analysis completed so far suggests that the energy confinement is only very weekly dependent on mass.

Studies of the mechanism responsible for the transport measurements have shown that suprathermal electrons have a faster diffusion time than thermal electrons suggesting that the micromagnetic fluctuations may be a key player in the anomalous transport of energy. Another controversial issue is the character of the heat pulse propagation in a tokamak and progress in this area is reported.

Progress in impurity and particle transport studies is also reported. An interesting observation is the marked reduction in particle transport in the plasma centre, a phenomena which is also apparent in energy transport. Finally, measurements of the density fluctuations in JET by correlation reflectometry are presented.

Current Scaling of Confinement by Current Ramping

A series of experiments were conducted in which the plasma current was ramped up or down from one flat-top value to another. The current ramp took place during an ICRF heating pulse at constant power and the density, field, plasma shape were also held constant. During the ramp and for some period after, the internal inductance, the safety factor and the shear profile were transiently decorrelated until a steady state was reached by resistive diffusion. The data from such experiments shows that global confinement depended on both the total plasma current I_φ and its distribution, e.g. the internal inductance ℓ_i. The scaling was found to fit the data, as shown in Fig.144. A local transport analysis, both interpretative (TRANSP code) and predictive (JETTO code), based on measured density and temperature profiles has been carried out. The resistive diffusion calculations

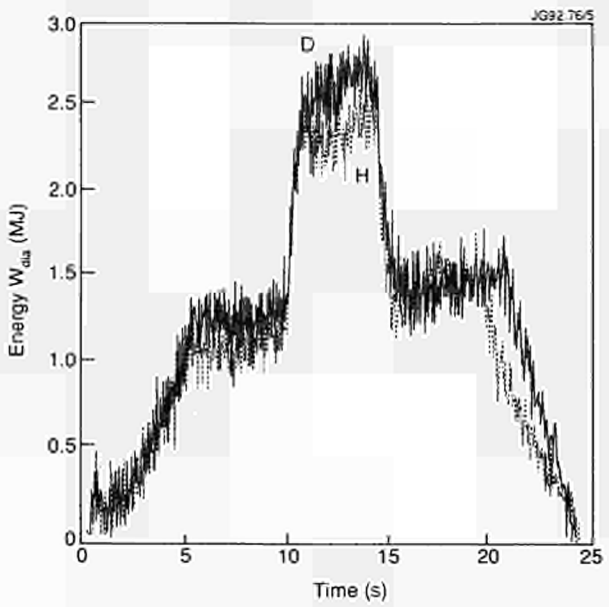

Fig. 145: Stored energy content from the diamagnetic loop for two pulses with identical geometry, current and field (one D→D and one H→H).

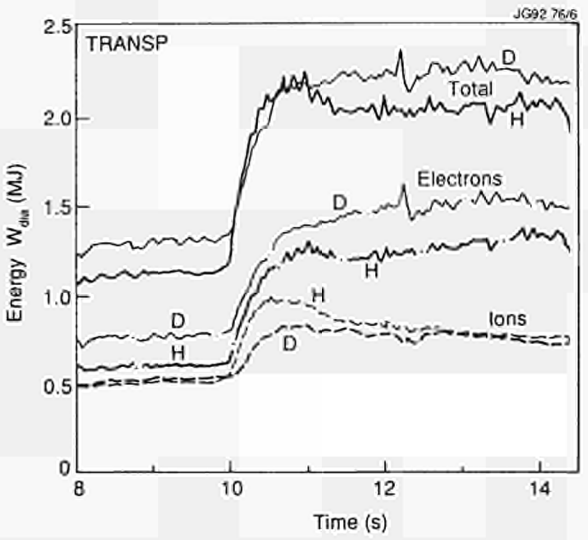

Fig. 146: Kinetic stored energies versus time for the same two pulses in the previous figure.

took into account the electron temperature dependence of resistivity and reproduced the data values from magnetic, soft X-ray and polarimeter measurements. The inferred effective diffusivity, χ, propagated inwards from the edge by resistive diffusion; this eliminates the need to invoke "action at a distance" principles for local confinement. The origin of the current scaling in global confinement was found to be mainly in a dependence of c upon the local poloidal field B_p while the shear dependence was weaker and present only in the outer half region. The scaling $\chi \sim B_p^{y} s^{\mu}$ with $-2 \le y \le -1$, $-1/2 < \mu < 0$ and y, μ varying with radius is consistent with the global scaling and is also well reproduced by the Rebut-Lallia-Watkins form for the thermal diffusivity.

Isotope Scaling Studies

Most scaling laws of energy confinement predict that the energy confinement time, τ_E, scales as A^{α} with $\alpha \approx 1/2$, A being the atomic mass of the plasma ion species. However, such a dependence is difficult to justify on theoretical grounds. In addition, a much weaker dependence was reported by the TFTR team.

To study the problem in JET, a series of well diagnosed discharges has been performed with different gas species, namely hydrogen (H), deuterium (D) and the helium isotope He^3. Care has been taken to avoid mixture of isotopes and to obtain discharges with the same plasma configuration, current, toroidal magnetic field, and similar density, power deposition profiles and impurity content. These aims have been achieved in ohmic and neutral beam heated discharges. The main limitation has been the maximum NBI power with hydrogen beams which could not exceed 7MW. This limitation has not allowed an extension of the study to comparisons of hydrogen and deuterium H-modes as the available power was not enough to achieve good H-modes in hydrogen. However, a complete set of reference discharges has been obtained for H, D and He^3 L-mode discharges in the limiter configuration. The main plasma parameters have been performed at $I_p = 3.1$MA, $B_T = 2.9$T, $P_{NBI} \approx 6$MW and a range of densities $\approx 2\text{-}3.3 \times 10^{19} m^{-3}$ has been covered. D and He^3 reference shots at $P_{NBI} \approx 12$MW and densities up to $4.5 \times 10^{19} m^{-3}$ have also been obtained.

The analysis of the results is still preliminary, the main limitation being that ion temperature profiles and Z_{eff} profiles from charge exchange recombination spectroscopy have not yet been taken into account in the analysis of local transport. Results of the analysis so far indicate that in JET L-mode discharges a dependence of the energy confinement time τ_E on the atomic mass A as strong as $A^{1/2}$ must to be ruled out. No difference in energy confinement has been observed between D and He^3, while for H and D cases, one has $0 \le (\tau_E^D - \tau_E^H)/\tau_E^D \le 20\%$.

Figures 145 and 146 illustrate the issue for typical reference discharges. These show that for H and D pusles, having the same configuration and the same plasma parameters, the time evolution of the energy content is the same for the same power input. Fig 145 shows the energy content from the diamagnetic loop measurements, and Fig 146 shows the thermal energy content evaluated by the interpretive code TRANSP.

Perturbative Measurement of Suprathermal Electron Diffusion

Rapid spatial diffusion has been deduced for suprathermal electrons of energy $200 \leq E(keV) \leq 250$, produced during Lower Hybrid Current Drive (LHCD) experiments. Thermal second harmonic and down-shifted non-thermal third harmonic electron cyclotron emission (ECE) produced during LHCD was measured using a fast twelve channel polychromator. Injection of a small deuterium pellet into the plasma to radius rp produced a sharp gradient in suprathermal electron density n_e^{ST} at $r=r_p$, causing a depletion front in n_e^{ST} to travel into the region $0 \leq r \leq r_p$, accompanied by a concomitant decay in non-thermal ECE. Measured characteristics of the ECE enabled definition of an energy band for electrons contributing most to the observed non-thermal ECE to $200 \leq E_e^{ST}(keV) \leq 255$, thus also fixing their radial position. During decay of ECE, energy of the suprathermal electrons can be assumed constant because their slowing down time is longer than the time of evolution for the non-thermal ECE. Then, emission was proportional to n_e^{ST}, and evolution of emission after the perturbation represents evolution of n_e^{ST}. Analysis of evolution of the non-thermal ECE yielded radial diffusivity of suprathermal electrons, $9 \leq D_e^{ST}(m^2/s) \leq 15$ at $0.4 \leq r/a \leq 0.6$. Effects of electron slowing down on the deduced value of D_e^{ST} were estimated to be small. Similar value for D_e^{ST} were deduced from LHCD modulation experiments in TORE SUPRA [1], and EC current drive in DIII-D[2]. Deductions of electron thermal diffusivity in JET in similar plasma conditions, using the same method, yield $\chi \approx 3m^2/s$, gave $D_e^{ST}/\chi_e = 3\text{-}5$.

That supra-thermal electrons diffuse faster than thermal ones (roughly as $v_e^{ST}/v_e^{thermal}$), reinforced previous deductions made from measurements of $\chi_e > D_e$[3], that micromagnetic fluctuation may be a key player in anomalous radial electron thermal transport in JET.

D_e^{ST} deduced from steady state LH power balance was much smaller than that deduced perturbatively. This discrepancy appears to be analogous to that observed in thermal transport measurements in steady state and in perturbation. The significance of this observation, and its consequences for steady-state LHCD schemes are under investigation.

Heat Pulse Propagation Studies

Ballistic or diffusive heat pulses?

Standard analysis treats the sawtooth induced heat pulse as a diffusive phenomenon by linearizing the diffusion equation around the unperturbed state of the plans. This implies that the heat pulse is governed by the *incremental* thermal diffusivity. This approach has been criticized [4], on the basis that turbulence associated with the sawtooth collapse affects the propagation of the heat pulse (ballistic heat pulse). However, this criticism is based on an incorrect application of the standard diffusive models. In the 'ballistic' modelling a time varying diffusivity is used with a strong enhancement just after the sawtooth collapse, relaxing to the steady state value after a few milliseconds. Modelling of the heat pulse data with this model is only possible with four or more dimensional parameters, which vary for different data. However, it has been shown that the measurements impose a temporary change of the effective thermal diffusivity during the heat pulse, which is similar to the implicitly imposed time behaviour by the linearised treatment. Furthermore, the analysis method at JET fits the heat pulse data of JET, TFTR and TEXT. The incremental heat pulse diffusivities agree with the incremental heat diffusivities derived from steady state diffusivities at different input powers to the plasma.

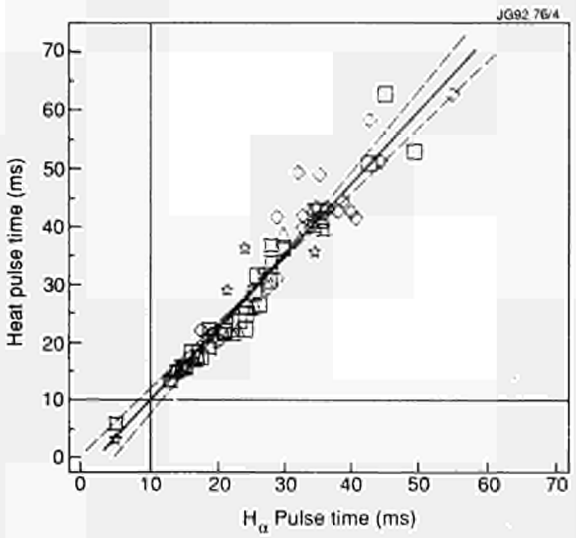

Fig. 147: The correlation between the arrival of the heat pulse and the maximum of the hydrogen emission at the edge of the plasma, after the sawtooth collapse. Short arrival times correspond to sawtooth collapses with a large mixing radius (>75% of the minor radius).

Heat Pulse at the Plasma Edge

The correlation of the arrival time of the heat pulse with the peak observed on the hydrogen emission at the plasma edge has been investigated. This study has been carried for sawteeth with varying mixing radii, including monster sawteeth. The results show that the maximum of the hydrogen emission at the edge, after the sawtooth collapse, correlates

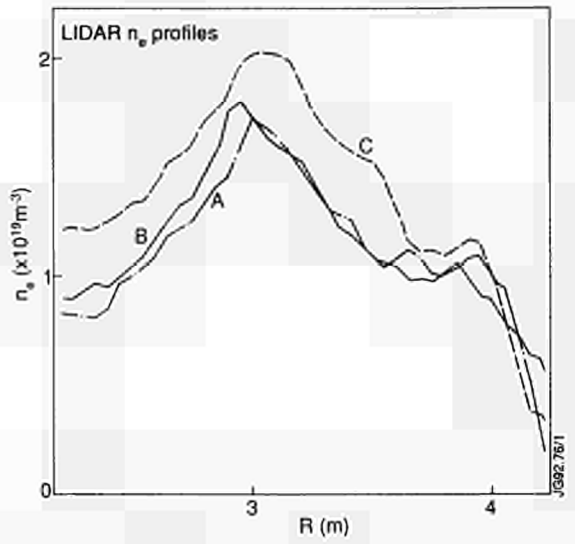

Fig.148: Typical LIDAR electron density profiles taken during the early ohmic phase of the discharge (t=2 s). A is Pulse No: 14815; B is Pulse No: 16009; and C is Pulse No: 18157.

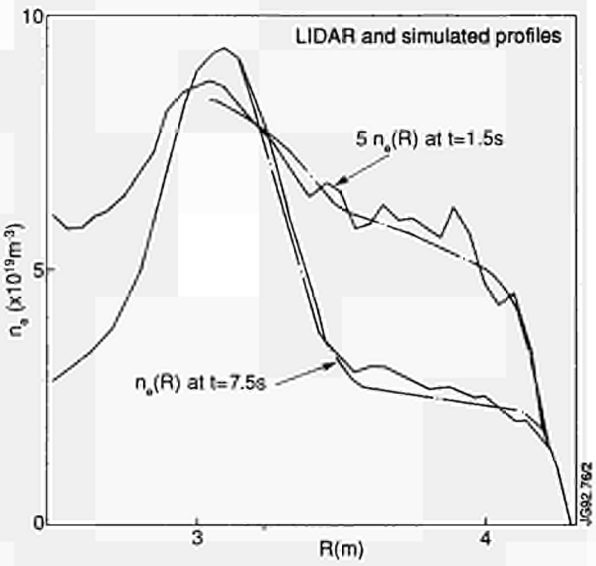

Fig.149: Experimental and simulated density profiles for a ohmic pulse (No: 13572) during the current ramp (t=1.5s) and 2s after injection of a large pellet into the discharge (t=7.5s).

with the arrival of the heat pulse. It has been demonstrated that a fast response of the hydrogen emission after the sawtooth collapse with a maximum of the emission a few milliseconds after the sawtooth, corresponds with a sawtooth collapse inside a mixing radius larger than 75% of the minor radius (see Fig.147).

Impurity and Particle Transport

The availability of space and time resolved information from a variety of diagnostics on transient phenomena is essential for an adequate analysis of the impurity transport in the bulk plasma. Furthermore, an extensive analysis with both predictive and interpretive techniques is necessary to assess the uncertainties on the derived transport parameters and the compatibility with different models. During 1991, progress has been made on both the production of new data, mainly by laser blow off injection of impurities, and their transport analysis. A wide variety of studied cases from the JET data-base is now available.

A zone of reduced anomalous impurity diffusivity in the central region, already reported from JET and several other tokamaks, appears to be a very general feature of the tokamak transport and not an occasional occurrence. In particular, as it has been observed in all the discharges that could be analyzed with adequate space resolution (including ohmic discharges in the current-ramp and the flat-top phases with and without pellets, additionally heated discharges with and without sawteeth activity as well as monster sawteeth cases), it appears to be largely independent of the value of the safety factor ($q < 1$ or $q > 1$) or the sign of the gradient in the central region, of the electron density and temperature or their gradients.

From the analysis of the LIDAR density profiles of sawteeth free plasmas (Figs 148 and 149), positive evidence has been found [5] of the systematic presence in ohmic pulses of a similar central marked reduction in the electron particle diffusion coefficient D_e for gas fuelled discharges as well as for pellet fuelled ones. As for the case of impurities the values of D_e appear to be close to the region of high anomalous transport is localized around one third of the minor radius in a narrow ($\Delta \leq 0.2$m) zone (see Fig 150).

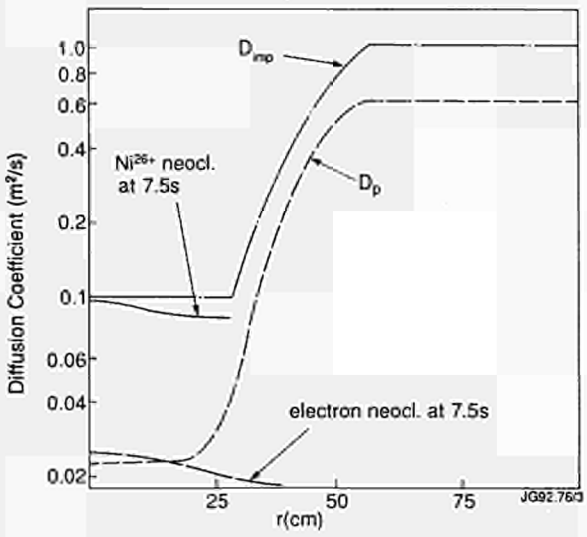

Fig.150: Radial profile of the electron and impurity diffusion coefficients for Pulse No: 13572. Neoclassical levels at the centre are also indicated for comparison.

Density Fluctuation Measurement using Correlation Reflectometry

Correlation reflectometry is a new diagnostic technique that was first developed at JET to investigate density fluctuations in the plasma. Using combinations of reflectometers, the scale lengths and dispersion relations of the density fluctuations is determined. Radial measurements may be made using reflectometers that operate along the same line-of-sight with different probing frequencies. Toroidal and/or poloidal measurements can be made using reflectometers with the same probing frequency, but which operate along different lines-of-sight.

On JET, both radial and toroidal correlation reflectometry has been carried out [6]. The radial results indicate that the density fluctuations do not propogate radially but move in a direction perpendicular to that of the probing beam. The scale lengths of the fluctuations is ≤ 5mm in both ohmic and H-mode plasmas but is ~ 10 - 30 mm in L-mode plasmas. Furthermore, it increases with increased additional heating power. The toroidal correlation reflectometer has been used to determine the toroidal rotation velocity of the density fluctuations. This has been compared with the rotation velocity of the bulk plasma as measured using charge exchange (CX) diagnostics, and in L-mode plasmas the two velocities are the same within uncertainties. This indicates that the density fluctuations have a significant velocity component in the poloidal direction. Although no poloidal velocity component can be determined, this observation is also consistent with CX observations.

These observations have led to the conclusion that density fluctuations on JET consist of fine scale density structures that are convected around the vessel with the bulk plasma. That is, the phase velocity of the structures is zero in the plasma rest frame.

References

[1] D. Moreau, 18th European Conference on Controlled Fusion and Plasma Physics, Berlin, June 3-7 1991.

[2] R.F. Ellis, private communiction, and S. Janz, et al, Bulletin of the American Physical Society, **36**(1991)2471.

[3] A. Gondhalekar, et al., Plasma Physics and Controll Fusion, **31**(1989)805.

[4] Fredrickson, et al, Phys. Rev. Lett. **65**, 2869 (1990)

[5] R. Gianella et al. Plasma Phys. Control Fusion (1992)

[6] P. Cripwell and A.E. Costley, Proc. 18th EPS Conference on Controlled Fusion and Plasma Physics, Berlin 1991, Vol 1, p17

MHD, Beta Limits and Topology

In 1991, studies of magneto-hydrodynamic (MHD) phenomena were undertaken in the following areas:

- ELM-related MHD;
- Error fields and locked modes;
- Fast disruptions:
- Fishbone activity;
- MARFES
- MHD activity in Pellet Enhanced Performance (PEP) plasmas;
- Sawtooth Phenomena.

The main advances are described in the following paragraphs.

ELM-related MHD

Edge Localised Modes (ELMs) of instability are frequently observed on JET during the H-mode, and at the transitions to and from the H-mode. They are characterised by a spike in the D_α light, with a rise-time of <250ms and duration of ~ 1ms. This is interpreted as a result of a transient reduction in particle confinement. Data from the reflectometer show that the event is localised at the edge ($r/a > 0.95$).

Recent observations on the magnetic diagnostic have shown a new high frequency (50-80kHz) coherent MHD precursor to the ELM event (Fig.151). The high mode frequency and relative phase of magnetic probes suggest high mode numbers (n>5). There is evidence of growth of this instability prior to the ELM, leading to a short period (<1ms) of strongly increased broad-band magnetic fluctuations, accompanied by a loop-voltage spike, at the time of the rise in the D_α light. Immediately after this event the mode is usually absent. It starts to grow again leading to the next ELM. The broad-band event is also observed on the reflectometer, Langmuir probes and D_α signals, and the pattern of turbulent particle flux to the edge is seen to be correlated with magnetic turbulence.

Before the main ELM spike, low level broad-band fluctuations are also seen on the D_α signal, with an envelope varying as the coherent MHD precursor, so that the presence of the MHD instability appears to be degrading confinement even before the strong magnetic turbulence is generated.

The sequence of events observed before the ELM suggests an edge-localised disruptive phenomenon. The development of steep profiles at the edge during the H-mode may be responsible for the appearance of the MHD instability.

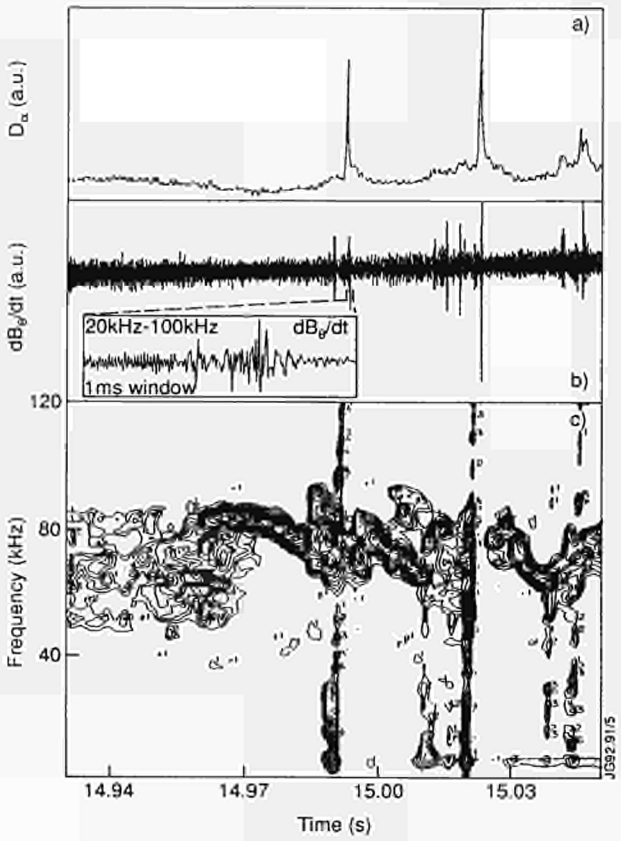

Fig.151: An MHD precursor to ELMs. The ELMs are seen on the D_α signal in (a) as spikes. A raw magnetic signal is shown in (b) indicating a sharp rise in activity when an ELM occurs. The Fourier spectrum, as a function of time, is given in (c), which shows a high frequency MHD precursor before each ELM, leading to broad-band activity at the time of the ELM.

The profiles would be expected to relax due to the loss of particles from the edge during an ELM, and this could remove the driving mechanism of the instability. Subsequent recovery of the profiles would then cause the process to repeat.

Error Fields and Locked Modes

Considerable progress has been made in understanding the growth of the type of locked mode which has no rotating phase. This helical perturbation grows on a long timescale (~100ms) and stationary with respect to the frame of the vessel. The condition for the growth of the perturbation defines a minimum density limit to stable plasma operation, unstable plasmas usually terminating disruptively.

The minimum density limit has a complex dependence on several plasma parameters. In particular the direction of the field line twist (left or right handed), the safety factor (Fig.152), Z_{eff}, and the amount of neutral beam injection all affect this 'low density limit'. The dependence on these parameters is such that the most unstable configuration is

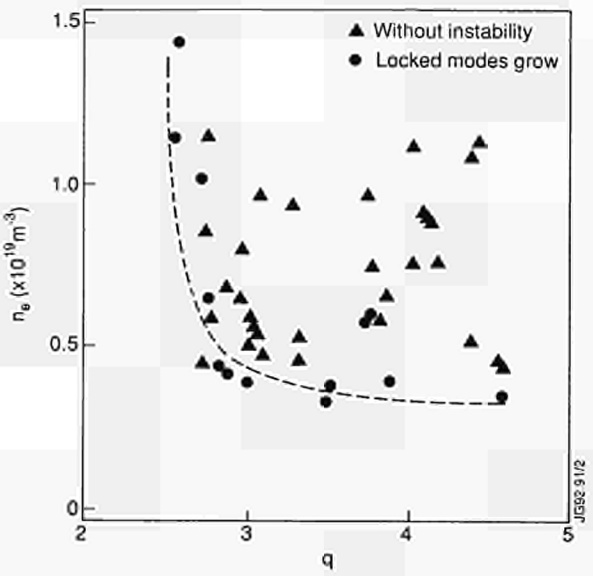

Fig.152: Data for the region close to the low density threshold for growth of a 'locked mode' plotted in $<n_e>/q$ space. The densities at which locked modes grow map out the stability boundary. The data is for ohmic, double null X-point plasmas in the configuration with the smallest known error field from the vertical field coils ($Z_{eff} > 1.8$).

that of an ohmically heated plasma, with a high purity, low safety factor and the plasma current in the direction of the toroidal magnetic field.

The characteristics of this low density threshold variation, combined with the entirely stationary nature of the perturbation, indicate that there is an error field problem in JET similar to that observed in DIII-D [1]. The high accuracy with which JET was constructed minimises the error field sources from the incorrect positioning of coils. However, the geometry of the coil and busbar design produces error fields with amplitudes of order 1G in the m=2, n=1 component on a typical q=2 surface.

The complications of the analysis have prevented a complete calculation of the total error field. However, the dependence of the minimum density threshold on the configuration of the vertical field coil provides strong evidence of a major source of field error, in good agreement (within 20°) with the phase of the perturbation, which is measured in conditions when the P4 coils are the dominant known source of error field.

Fast Disruptions

It has been suggested previously [2] that the very rapid current decays during fast disruptions in JET are due to an influx of impurities from the limiting surface. These are thought to quench the plasma, reducing the temperature to a very low value, ~ 5eV. A model has been developed to

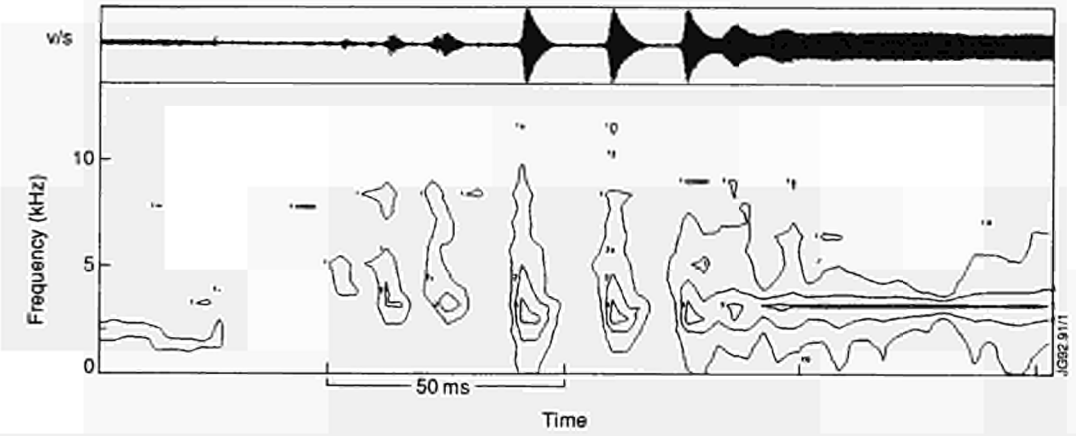

Fig.153: Magnetic pick-up coil signal showing a sequence of fishbone bursts which develop into a continuous oscillation. The evolution of frequency is shown in the contour plot of a time sequence of power spectra. As the amplitude of a burst decreases, the frequency typically decreases by a factor of 5. The continuous fishbone oscillation has constant amplitude and frequency.

explain how an impurity influx can penetrate to the plasma core on the required timescale (~1ms) without being ionised and trapped on the magnetic held lines. It is suggested that a localised region of the limiting surface is heated by a rapid MHD event which expels heat from the core. The resulting vaporisation of the surface is so strong that the pressure of the neutral gas exceeds the plasma pressure. The plasma is then forced aside along the magnetic field, remaining essentially separated from the expanding neutral gas cloud. The plasma is cooled by parallel thermal conduction. If the limiting material is carbon, the cloud of neutrals can penetrate to the core on a timescale of about 500ms.

The amount of impurity required for this process is large (1g) and is expected to lead to an order of magnitude increase in electron density. The temperature during the current decay is determined by a balance between ohmic heating and radiation from the almost pure carbon plasma. The temperature is expected to fall to ≤5eV.

Fishbone Activity

Fishbones are a common feature of JET discharges with auxiliary heating. They are seen either as repetitive bursts, lasting a few milliseconds, or as continuous oscillations. They are observed both in neutral beam heated and in ion cyclotron heated pulses, but their characteristics seem to be dependent on the heating system and the plasma conditions used. They occur in plasmas with sawtooth oscillations and, occasionally, in sawtooth-free regimes. They are very common at low values of the edge safety factor q, and there seems to be no low-β limit for their occurrence either in β_p or in β_T (see Fig.153).

In the low beta regimes, a high frequency oscillation of up to ten times that of the central plasma rotation frequency clearly distinguishes the bursts and the continuous oscillations from other observed m = 1, n = 1 oscillations. For ICRF heated discharges, the instability seems to be affected by the choice of minority gas. For 5MA discharges, the amplitude of the observed oscillations is larger for ^{3}He than for H minority. It is found also that for ^{3}He the instability appears mostly in the form of continuous oscillations.

As both the toroidal and the poloidal beta values are increased, larger amplitude oscillations are observed. For β approaching the Troyon limit, the amplitudes reach values comparable to those at which losses of fast ions became important in PDX. These large amplitude oscillations are seen during the saturation of β. Fast time-scale measurements indicate that the total neutron rate associated with the loss of fast particles may fall by 10-20% during a burst in the high beta regime. The distinction between fishbone oscillations and the oscillations around a sawtooth collapse becomes unclear in the high beta regime, since both oscillations have the same frequency.

The observed frequency in the rest frame varies between the ion diamagnetic frequency and the predicted fast ion precession frequency. The distinct high frequency of the oscillation together with the effect on the fast particle population observed in JET, although being smaller than in PDX, leads to the conclusion that the instabilities in JET are indeed similar to the PDX fishbones.

Marfes

A number of experiments have been carried out to clarify the physics of the localised radiation phenomenon called the

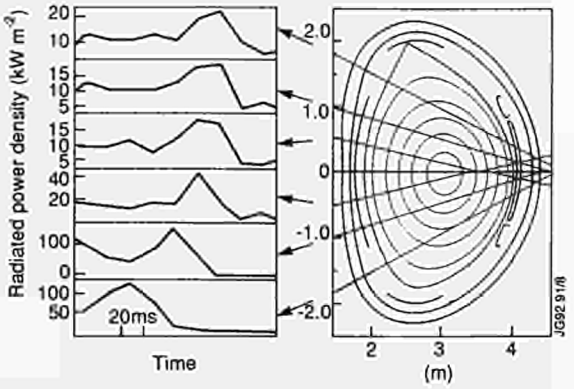

Fig.154: The geometry of the bolometers and the resulting time traces which give the movement of the Marfe.

marfe. These experiments had two aims, one to understand the dynamics of the marfe and the other to determine its composition.

Marfes form at the edge of the plasma and previous experiments indicated that marfes tend to be located on the high field side. This behaviour has been ascribed to poloidal flows or wall effects. To investigate the possible role of the wall, marfes were formed by gas puffing with the discharge being limited in some cases at the high field side and in other cases at the low field side. Marfes were initiated at the point of contact in both cases. The marfes formed on the high field side remained on that side but those formed on the low field side moved to the high field side. In X-point configurations, the marfe grew in the divertor where it could persist for several seconds. By puffing deuterium into the X-point, it was possible to generate a stable marfe in the divertor which almost perfectly shielded the target.

The movement of the marfe was tracked using a set of bolometers with lines-of-sight as illustrated in Fig.154. This figure also shows the resulting time traces which allow the movement of the marfe to be followed. This movement was exploited to make spectroscopic measurements of the impurity concentration. As the marfe passed through the line of sight the intensity of the carbon and helium line radiation were measured.

MHD Activity in Pellet Enhanced Performance Plasma

The pellet enhanced performance (PEP) mode is characterised by large neutron yield (about $10^{16}s^{-1}$) and very strong peaking of electron density and pressure.Soft X-ray data show (m,n) = (3,2) and (2,2) modes at r=12 and 28cm, respectively, indicating that the shear is negative in the plasma core [4]. An equilibrium code using the measured positions of the q=1 and 1.5 surfaces as input data, yields a

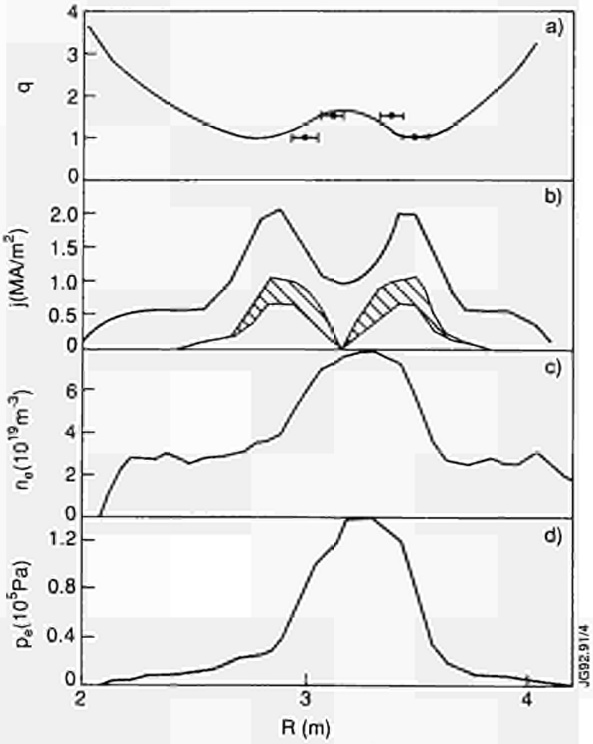

Fig.155: Profiles of safety factor, current density, electron density and electron pressure for a PEP plasma.

Shafranov shift of about 20cm in agreement with experiment, and a current profile with two large off-axis peaks matching the computed bootstrap current (as shown in Fig.155) and 1 1/2D transport simulations show that the shear reversal is maintained by a reduction of the transport to a value close to its neoclassical level in the central plasma region, in agreement with the critical temperature gradient model.

Collapses of the neutron rate are often correlated with fast (1, 1) MHD events, which are generally preceded by n=3 modes and followed by n=2 modes. Toroidal resistive linear MHD simulations, assuming a non-monotonic q-profile with an off-axis minimum decreasing from above to below unity, agree with this sequence of modes. However, the calculated n=1 mode is always dominant because of the high central poloidal beta, typically 1.5, observed during the PEP mode. A rotating (1,1) mode has been observed as a hot spot with a ballooning character on the low field side. This hot spot has some characteristics of a "hot" island consistent with the presence of negative shear in the plasma core.

More recent PEP-H modes exhibit too complex an MHD mode structure to be analysed accurately. However, polarimeter measurements confirm in some cases the observation of negative shear during the PEP mode. There is evidence of impurity accumulation in the plasma core during the PEP phase.

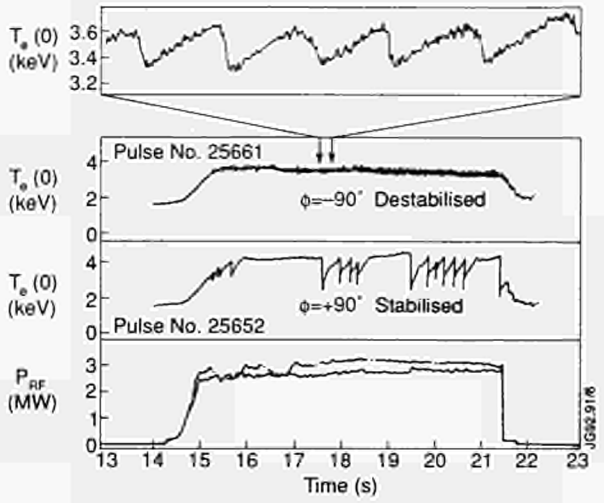

Fig.156: Electron temperature traces showing the fast sawteeth produced by - 90° phasing and sawtooth free periods produced by + 90° phasing during the application of R.F. power.

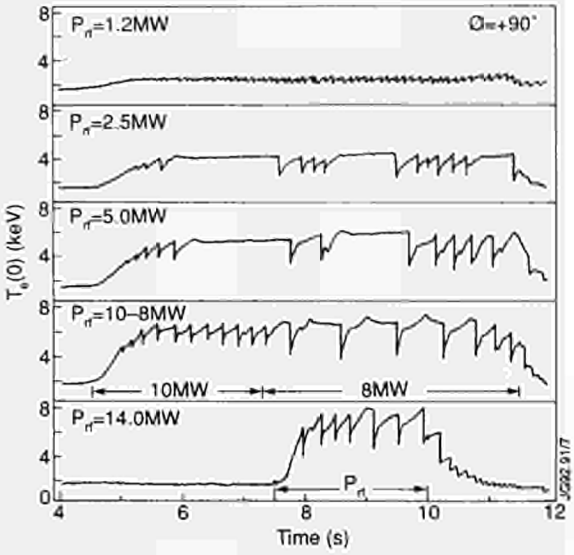

Fig.157: At higher power levels, the stabilising effect of R.F. stabilisation is diminished.

Sawtooth Phenomena

Sawtooth Oscillations

Detailed diagnosis of JET sawteeth indicates that local parameters play a crucial role in determining the type of sawtooth crash seen and the aim of much of the recent work has been to analyse this aspect of the behaviour and to identify the important local parameters.

Studies of the sawtooth collapse show a range of behaviour. In plasmas with neutral beams injected counter to the plasma current direction, the q profile is measured to be broad and flat with the central value, q_o, of the safety factor very close to unity. Indeed two q = 1 surfaces are observed in JET counter-NBI discharges. The central q = 1 volume appears to undergo a complete 'Kadomtsev reconnection', q_o rising above unity after the crash. The timescale of the crash, 3-5ms, is consistent with the original Kadomtsev model. For co-injection heated plasmas the sawtooth crash also involves a reconnection of the helical flux, although a second phase to the collapse, in which reconnection does not play an evident role, is also seen. In the case of co-injection, the timescale of the crash is much shorter, and the measured values of 300-800ms are more typical of the Kadomtsev model modified to take account of electron inertia. The q profile in these discharges is also inferred to be broad, with q_o close to unity. For ICRF heated discharges, the crash is faster still, the hot core being swept close to the q = 1 surface on a timescale of 100-300 ms, before energy is then lost. In this case Faraday rotation measurements show that q_o lies well below unity.

Nearly all observations point to the q-profile playing a vital role in defining the nature of a particular sawtooth collapse. The q-profile has been routinely measured on JET using Faraday rotation techniques. Much of the error on these measurements comes from the large elongation of most JET plasmas. In order to make improved measurements of the q-profile of JET, discharges with circular plasma have been used. These confirm the earlier JET results for ohmic plasma, giving a q_o value of 0.8 for discharges with an edge value of q of 3.5, rising to a value of q_o close to unity for plasma with an edge q of 8.5. Measurements of q_o during monster sawteeth also confirm earlier results, showing q on axis falling to values well below 0.8 before the crash. Further measurements of q are being made using measurements of the motional Stark effect with diagnostic neutral beams.

A good understanding of the experimental behaviour of the sawtooth collapse has been obtained over a wide range of parameters. The result suggests that full reconnection of the helical flux occurs in plasmas with centrally flat q-profiles in which q_o is closer to unity than is the case for ohmic discharges. Very fast sawtooth collapses which exhibit a convective flow occur in plasmas with peaked q-profiles in which q_o is well below unity. This is in direct conflict with the predictions established models.

Sawtooth Control using Phased ICRF Antennas

Recent technical improvements to the JET ICRH system have enabled the two striplines in each antenna to carry arbitrarily phased currents. As a result, travelling fast waves can be launched and have been used to perform minority ion

current drive experiments. In these experiments, the ICRF resonance layer was placed tangential to the q = 1 surface so that the current drive would act to change the local magnetic field and affect the stability of sawteeth. In a typical experiment with a resonance inboard of the plasma centre and a phase difference of +90° between antenna currents, the sawtooth period was increased by a factor of two over that produced by dipole phasing at the same power level. Reversing the direction of the waves had a dramatic destabilizing effects which produced very small sawteeth of extremely short period (see Fig.156). These results are consistent with the presence of minority ion current drive which, for +90° phasing, is expected to create a local flattening of the current density profile close to the q = 1 surface.

It is observed that the stabilisation effect is diminished at high power levels, as shown in Fig.157. Monster sawteeth were created at a power level of 2.8MW and were sustained for power levels up to 7MW. However, above 7MW, the sawtooth period decreased with increasing power. This loss of stabilising effect can be interpreted as a loss of current drive through enhanced trapping of the minority ions and through the increasing influence of electron collisions in the slowing down process as the tail energy increases.

Further experiments have been undertaken to investigate the effect of changing the minority ion density and of placing the resonance at the outboard q = 1 position. The minority density scan was performed with the resonance at the inboard q = 1 position. A gradual loss of sawtooth stabilisation was observed as the minority fraction was raised from 16% to 43% at a power level of 5MW. With 40% hydrogen fraction, stabilisation was restored by raising the power to 6.5MW. This compares with only 2.8MW at 3% minority concentration. The required higher power for stabilisation as the minority density is increased, as expected, since optimum current drive efficiency occurs at a minority tail energy close to the critical energy.

With the resonance located at the outboard q = 1 position, large sawteeth were obtained with +90° phasing and 4MW of RF power. With –90° phasing, a monster sawtooth was generated. Thus, – 90° phasing appeared to be slightly more stabilising than $\phi = +90°$, which is the reverse of the situation with the inboard resonance. Moreover, the effect was much reduced compared with the inboard case, where the destabilising phase (–90°) caused a dramatic reduction in sawtooth period and amplitude. Again, this result is consistent with current drive theory which predicts lower efficiency at the outboard side due to greater number of trapped ions.

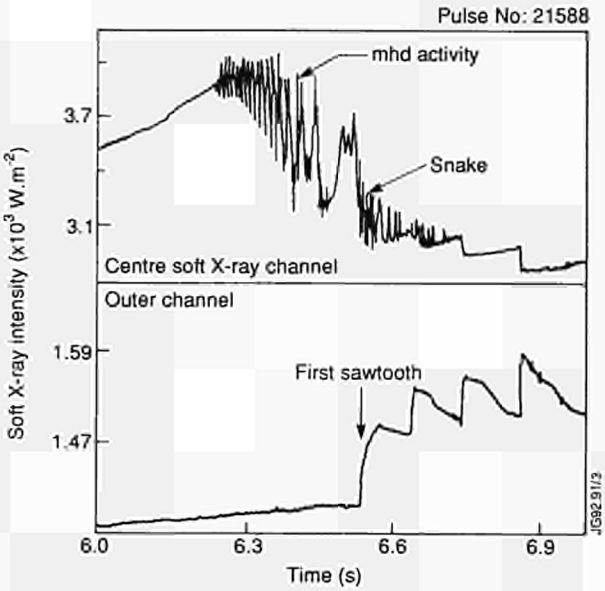

Fig.158: Soft X-ray traces showing the first sawtooth collapse on an outer channel, with the corresponding time development leading to the snake seen on the central channel.

Snake-like Sawtooth Collapse

Characteristic snake-like oscillations are sometimes seen with the soft X-ray cameras. These oscillations are due to a small region of enhanced X-ray emission rotating in front of the X-ray detectors. "Snakes" were first observed [5] following the injection of D_2 pellets into the plasma. These pellet-produced snakes have been studied with great interest because of their surprising persistence (several seconds) and because they acted as a diagnostic for the position of the q = 1 surface. The interest in snakes was revived this year following the observation that so called "impurity-snakes" sometimes appear at the onset of sawtoothing [6], the name arising from the role played by impurities in their formation.

In the snake region, the electron density was higher than the surrounding plasma. This was due to ablated deuterium particles in the pellet-snakes and to impurities in impurity-snakes. A pellet-snake is believed to be due to a magnetic island which forms as a result of cooling and increased resistivity when the pellet crosses the q = 1 surface, ablated deuterium particles being trapped in this island structure. Impurity snakes are formed following a phase of impurity accumulation and are terminated by MHD activity (predominantly m = n = 1) and the first sawtooth crash, which flattens the impurity profile (Fig.158). The impurity snake is a remnant of the hot core, where the impurities have accumulated, which persists following sawtooth crash. This remnant, surprisingly, survives the two or three following sawtooth crashes but gradually decays on a time scale of the order of 300ms,

consistent with neoclassical impurity diffusion. The development of the magnetic structure is not entirely clear, but will probably explain the essential difference between the longer lifetime of the pellet-snake as compared to that of the impurity snake.

References

[1] J. Scoville et al. Nuclear Fusion **31**, 875 (1991).

[2] D.J. Ward, R.D. Gill, P. Morgan, J.A. Wesson, Private Communication

[3] M.F.F. Nave, et al., Nuc. Fus. . (1991) 667.

[4] M. Hugon et al (1992) Nuc. Fus. **32**, to be published.

[5] A. Weller, et al., Phys. Rev. Lett. **59** (1987) 2303.

[6] R.D. Gill, et. al., EPS Conference, Berlin, Germany, Vol II (1991) 49, to be published in Nuclear Fusion (1992).

Physics Issues related to Next Step Devices

The objective of this Topic Group was to propose and carry out experiments on a number of issues of particular relevance to Next Step devices, that were not already represented in the JET programme. All this work was carried out in close cooperation with the Task Forces. The main areas of work were as follows.

AC Operation of JET

The toroidal plasma current, required in a tokamak for plasma confinement, can be driven either inductively, or by various means of non-inductive current drive. Inductively current-driven tokamaks reactors are necessarily pulsed devices, in which electricity production during the down-time must be maintained by means of an external energy storage. This down-time, and thus the demand for external storage, can be minimised by using AC operation, in which the current in the plasma current alternates in direction between subsequent burn phase. In AC operation, no re-charging of the central solenoid between burn-phases is necessary. In Fig.159, a full cycle of AC operation is shown. The first plasma is generated using low voltage breakdown with no bias current in the central solenoid; the loop voltage is applied directly by the solenoid power supply. The second plasma is generated by interrupting (at 13.0s) the current through the solenoid and redirecting the current through a resistor. The corresponding electric field is 0.75Vm^{-1}. Both breakdown scenarios are equivalent to those used in normal JET operation.

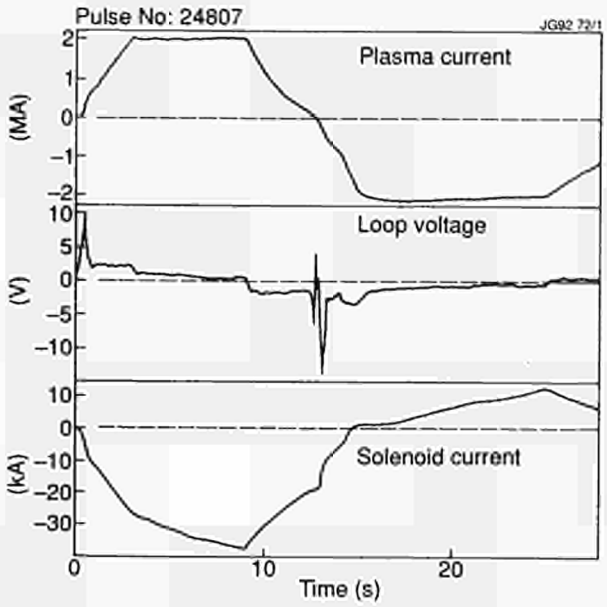

Fig.159: Parameters of a full cycle AC discharge (Pulse No.24807). Shown are plasma current, loop voltage and current in the central solenoid as a function of time. The slow increase in the solenoid current at the beginning of the second plasma (~15s) is due to non-saturation of the iron core.

The primary issue to be resolved is the one of the relative plasma performance and plasma purity of the successive cycles. In Fig.160, it is shown that there is no significant difference in these respects between the first and second phase of an AC discharge. The plasma density in both phases is the same, maintained by the density feedback system. The

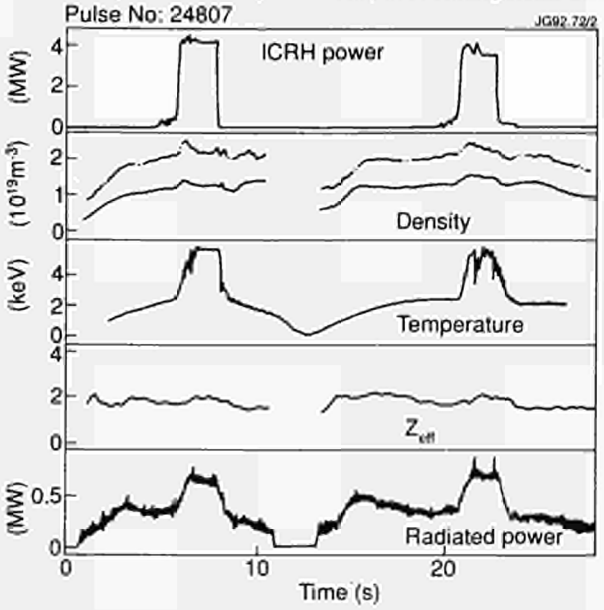

Fig.160:: Plasma purity of the two cycles (Pulse No.24807). Shown are ICRH input power, electron density (volume-average, solid trace and central, dashed trace), electron temperature, effective ion charge Z_{eff} and total radiated power as a function of time. Some of the traces are not available during part of the ramp-up and ramp-down.

transients in density are due to switching of the ICRF power. Then, the electron temperature, the effective ion charge, and the total radiated power are equal for both cycles.

All AC plasmas were obtained with a finite dwell time between first and second phase, i.e. a time in which there is no ionisation. The second plasma required a separate neutral prefill gas-puff. No indication was found that wall release of impurity gases after termination of the first plasma could affect the second breakdown. This was tested by extending the dwell time between the cycles up to 6s, which is a typical time for neutral pressure build-up after discharge termination.

The use of AC inductive current drive for a tokamak fusion reactor allows the reactor to operate with a minimum plant re-circulating power. It further allows more flexibility in the optimisation of the fusion power per unit capital investment. The machine parameters and the operating point are not restricted by the requirements posed by non-inductive current drive methods.

Toroidal Field Ripple

A detailed proposal was made for an experiment on toroidal field ripple. In this experiment, JET will be operated with 16 instead of the usual 32 toroidal field coils. A technical assessment was made, and the necessary hardware was acquired.

The primary purpose of the experiment is to study the effect of ripple on fast particles, both on tritons generated by D-D fusion reactions (triton burn-up method) and on fast minority particles generated by ion cyclotron resonance heating. It was predicted, on the basis of the theory of stochastic diffusion, that nearly all of the trapped triton population should be lose in the high ripple case.

Simulation of Fast Alpha Particles

The injection of high energy neutral helium beams produces a population of fast helium ions with energies from above thermal up to the injection energy. The distribution function of the fast particles is strongly anisotropic at the birth energy but subsequently isotropises in the course of the slowing down process. The first results at JET have given clear evidence of a broad high energy tail in the HeII spectrum observed perpendicular to the magnetic field. Assuming the excitation process to be dominated by the charge exchange interaction of neutral beam atoms and slowing down α-particles, we can calculate the expected spectral shape from a slowing-down distribution function and the cross-sections for charge-exchange excitation. As a slowing down test function we use a time-dependent analytical solution of the neutral Fokker- Planck equation. A comparison to the observed spectra shows that to first approximation the experimental shape can be described by the assumed test function and that a source rate can be deduced. For the case of a constant He^3 beam input (i.e. a constant source rate), the thermalised α-particle density rises linearly with time and is in excellent agreement with the total number deduced from the neutral beam current. The slowing down time and the predicted time for thermalisation can be confirmed by the time evolution of the observed thermal density.

The fast α-particle densities produced by the active fuelling are considerably higher than the densities expected for the D-T phase of JET and were almost a factor 20 above the density achieved in the preliminary tritium experiment in 1991. Active beam fuelling provides a precisely known source of fast particles and can be used as a test-bed for slowing-down studies and α-particle transport.

High-Minority ICRF Heating Experiments

In the active phase of JET and, to ease ignition in a reactor, it has been proposed to use ICRF heating with high concentration D-minority heating in a tritium plasma [1]. The aim is to reduce the minority tail energy such that it is optimum for the D-T fusion cross-section. This will produce significant levels of ICRF-driven D-T fusion reactivity [2]. Also, it will allow dominant background ion-heating from the minority as its tail would be below the critical energy. In a reactor, from penetration considerations, NB injection is planned with MeV range of energies which will lead to electron heating. However, transport calculations show that the most power-efficient route to ignition in a reactor will be via the heating of ions. Calculations for NET/ITER show that in the minority heating, for $n_d/n_T = 30\%$, at least 50% of the power will go to ions [3].

In the ICRF heating, as the minority ion concentration is increased, minority heating changes to mode conversion heating thus reducing the power damped on minority ions. A further increase in the minority concentration leads to the occurrence of radial eigenmodes, if the antenna is located on the low-field-side. Mode conversion at higher minority concentration can be avoided [4], if higher $k_{\parallel}$ refers to the wave parallel propagation constant. Hydrogen minority in He^3 majority plasma, (H)-He^3, offers the best combination to operate at higher minority concentration while remaining in the minority heating regime as shown in Fig.161. Therefore, this scenario can be used to show that indeed, one can

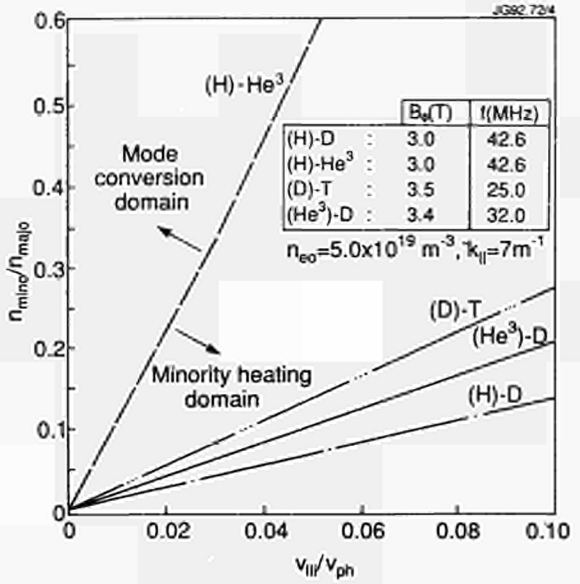

Fig.161: A theoretical prediction for the occurrence of mode conversion where minority to majority concentration is plotted versus minority ion $v_{\parallel}/v_{ph}$ for several JET scenarios, where v_{ph} is $w/k_{\parallel}$. Minority heating occurs below the curves as shown. For difference curves, the density is constant.

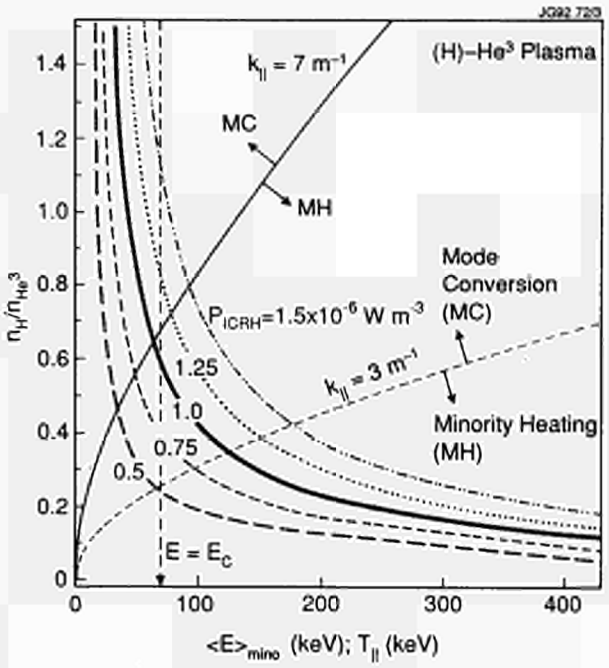

Fig.162: Time traces of a high concentration minority heating in a (H)-He³ plasma where n_H/n_e=0.3. T_{io} was measured by the Doppler broadening of the Ni^{27}-line. T_{io} is generally 30% higher than shown when corrections due to central burn out of He-like Ni-line and n_e profile effects are taken into account.

operate at higher minority concentrations and thus heat the plasma background ions. This scenario also simulates the plasma dispersion characteristics of the reactor (D)-T scenario (as the ratio of minority to majority charge-to-mass ration is identical), though themaximum D-minority concentration that can be used will be somewhat smaller than the maximum H-minority allowed in the He^3 case.

Typical time traces of a high concentration H-minority ($n_H/n_e \approx$ 30%) ICRF heating experiments carried out in a 3MA He^3 limiter plasma at about 10MW of RF power level are shown in Fig.162. The electron temperature T_{eo} (ECE) and the ion temperature T_{io} (Doppler broadening of Ni^{27}-line) are as shown in Fig.162. T_{io} is generally 30% higher than that shown, when corrections due to central burn out of He-like Ni-line and n_e profile effects are taken into account. It is noted that at high minority concentration $T_{io} \geq T_{eo}$, compared to a low minority concentration (~3%), where $T_{io} << T_{eo}$. In these high minority concentration experiments, the global energy confinement was similar to that in other L-mode ICRF heated discharges with $\tau_E \sim 1.3\tau_G$, where τ_G is the Goldston L-mode prediction for such discharges. The tail temperature as measured by a neutral particle analyser (NPA) plotted as a function of n_H/n_e is shown in Fig.163. The minority tail temperature decreased with increasing H-concentration and was near the critical energy when n_H/n_e = 0.3-0.4. In such a situation, the minmority gives about equal power to background electrons and ions. In these experiments, the minority concentration was determined by the 'density-rise method', when hydrogen was puffed. The concentration thus obtained were found to be consistent with a calculation based on a Stix model [5], using the measured fast-ion energy and the NPA measured tail temperature.

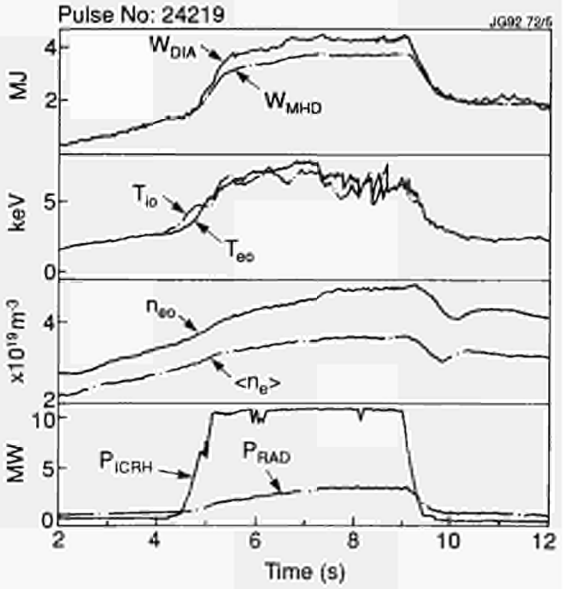

Fig.163: Neutral particle analyser measured minority tail temperature plotted versus minority concentration in the high minority (H)-He^3 scenario. For the lowest two points, minority/majority was strongly inverted.

Experiments described above were carried out in limiter configuration belonging to the L-mode regime of confinement. If such an experiment is carried out in a double-null X-point configuration and when ICRF heating makes a transition to the H-mode regime of confinement, higher values of ion temperatures are expected.

References

[1] Jacquinot, J., et al, (1988) Plasma Phys. and Contr. Fus. **30**, 1467;
[2] Cottrell, G.A., et al, (1989) Plasma Phys. and Contr. Fus., **31**, 1727;
[3] Koch, R., et al, (1990) IAEA Conf., Washington, U.S.A., Paper CN-53/G-2-9;
[4] Bhatnagar, V.P., Proc. 9th Topical Conf. on RF Power in Plasmas, (Charleston, U.S.A.), 1991;
[5] Stix, T.H., Nuclear Fusion, **15** (1975) 737.

Scientific Aspects of Preliminary Tritium Experiment (PTE)

Experimental Arrangement

Overall Limitations to Operation

In order to perform a deuterium-tritium experiment at this stage in the JET programme, it was necessary to limit the total neutron production to less than about 1.5×10^{18} neutrons so that the resulting vessel activation would be compatible with the pumped divertor modification work scheduled for 1992/1993. In addition, the total amount of tritium available was restricted to ≈0.2g (≈2000Ci) as the JET tritium processing plant is not scheduled to come into operation until 1993. Taken together, these limitations restricted, to a few, the total number of high performance discharges in this series of experiments.

First Wall Materials and Discharge Preparation

The interior of the JET vacuum vessel, consists of: a continuous top X-point target comprising plates clad with carbon fibre composite (CFC) tiles; a continuous bottom X-point target clad with beryllium tiles; a pair of outer wall toroidal belt limiters above and below the mid-plane, the upper of beryllium and the lower of carbon. All other plasma contacting surfaces, such as the inner wall, are of CFC, graphite or beryllium. The two target plates were carefully aligned to avoid discontinuities and in addition, individual tiles were carefully shaped to minimise the effect of residual protrusions and steps which were about 1 mm.

The plasma contacting surfaces were extensively conditioned by a combination of glow discharge cleaning and tokamak discharge operation. Prior to the introduction of tritium, all the plasma contacting components were coated with beryllium by periodically evaporating beryllium inside the vacuum vessel. A fresh layer was deposited about twelve hours before the deuterium-tritium experiment.

Discharge Type and Magnetic Configuration

A range of possible JET discharge types was, in principle, suitable for the deuterium-tritium experiment. However, pellet fuelling was excluded since the present pellet injector was not designed to operate with deuterium-tritium plasmas. Furthermore, ICRH, although available, was not used in order to avoid introducing tritium into the absorption pumps on the power feed lines. Consequently, attention concentrated on discharges heated by NB injection. Of these, the highest neutron emission rates were obtained in hot ion discharges (at low density with the ion temperature significantly higher than the electron temperature) in the H-mode regime (X-point discharges with improved confinement above an input power threshold). An attempt was made to identify such a discharge with good performance and reproducibility, and with relative insensitivity to small changes, for instance in the level of injected power.

During the series of experiments leading to the deuterium-tritium experiment, similar performance plasmas were achieved in both double-null X-point configurations (which took advantage of both the top and bottom X-point targets) and single-null X-point configurations (which used the top X-point target only). Ultimately, a single-null X-point discharge, diverted onto the upper carbon target, with reversed toroidal magnetic field, was chosen. In this configuration (shown in Fig.164), ions drift away from the target towards the plasma. This has been found to lead to more equal power loading between the inner and outer branches of the X-point [5]. Overall, this configuration allows consistently higher energy input and longer duration of the high performance phase of the discharge before the "carbon bloom".

Tritium Introduction by NB Injection

NB injection is an effective way of introducing tritium into the type of discharge selected for the deuterium-tritium experiment. It ensures that tritium reaches the hot, dense

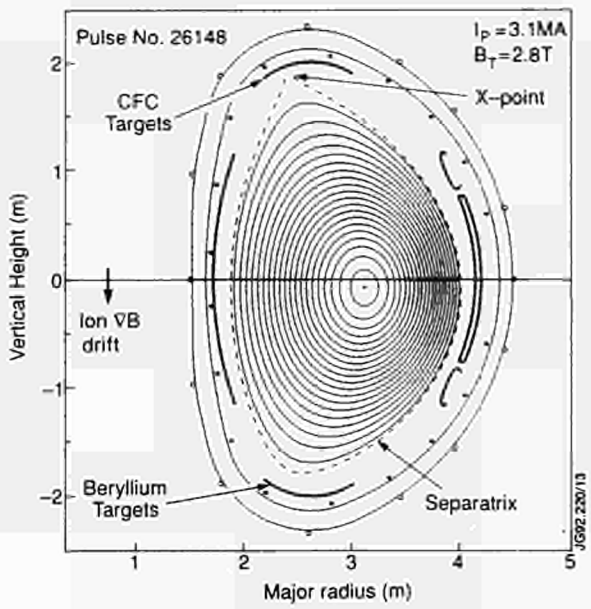

Fig.164: The magnetic configuration for Pulse No. 26148 in which the magnetic axis is at R_{axis}=3.15m, the horizontal minor radius, a=1.0m, the elongation, k=1.6 and the safety factor, q_ψ=3.8 (at the 95% flux surface) and q_{cyl}=2.8. Shown are the separatrix, X-point, the ion—B drift direction and the carbon fibre composite (CFC) and beryllium targets.

centre of the discharge where the reactivity is highest and minimises the amount of tritium injected into the torus. For the deuterium-tritium experiment, tritium gas was supplied from a uranium storage bed and buffer reservoir through a pressure regulator and needle valve and introduced into the neutralisers of two of the sixteen JET Positive Ion Neutral Injection sources, PINI's (as described in the section on Technical Aspects of the PTE).

The characteristics of each tritium PINI, given in Table XII, are those used in the deuterium-tritium experiment. These were deliberately operated below maximum performance to ensure high reliability. To conserve the limited amount of tritium available, the change from deuterium to tritium in these PINI's was simulated in the NB Test-bed using hydrogen and deuterium gas. Consequently, prior to the deuterium-tritium pulses, only two 1.5s tritium conditioning pulses were needed to change the beams from deuterium to tritium.

For the deuterium-tritium experiment, the remaining fourteen PINI's were operated in deuterium: twelve at 135kV delivering ≈10.5A each (total power ≈10.7MW with power fractions of 59%, 21% and 20%) and two at 75kV delivering ≈19A each (total power ≈2.1MW with power fractions of 73%, 17% and 10%); the total deuterium fuelling rate was 164A. The tritium fuelling relative to the total was ≈13% with two tritium PINI's.

Table XII: Tritium Neutral Beam Injection Characteristics for one PINI

Acceleration Voltage	78kV
Injected neutral species mix:	power fraction:
78kV	79%
39kV	12%
26kV	9%
Equivalent atomic current	12A
Power Injected	0.75MW
Tritium gas requirement for 2s injected pulse	45mbℓ(i.e. 120Ci or 0.012g)

Diagnostic Capability

Over thirty diagnostics were in operation for the deuterium-tritium experiment.

The time-dependent neutron emission rates were measured with silicon surface barrier diodes (which exploited the high threshold energy of (n,p) and (n,α) nuclear reactions in silicon to record 14MeV neutrons) and using ^{235}U and ^{238}U fission chambers (which were not capable of discriminating 2.5MeV and 14MeV neutrons). These detectors were calibrated by comparison with the total time-integrated neutron yield derived from the activation of two small samples of silicon, positioned in a vacuum vessel port with an unobstructed view of the plasma. Just before a discharge, the samples were put in place by a pneumatic system. Silicon was selected because of its short decay half-life (which allows the samples to be recycled between discharges) but, since the $^{28}Si(n,p)$ reaction cross-sections are not well known, it was necessary to cross-calibrate against the standard dosimetry reactions $^{63}Cu(n,2n)^{62}Cu$ and $^{56}Fe(n,p)^{56}Mn$ using samples at other positions. The neutron fluence at each measurement position was related to the total neutron yield from the plasma through extensive and detailed neutron transport calculations. The accuracy of the total neutron yield is estimated to be ±7%.

The neutron spectrum was measured with a liquid scintillator spectrometer. A flat pulse height distribution is obtained up to the maximum energy corresponding to the complete transfer of neutron energy to the recoiling proton. Neutron emission profile data can be obtained from 19 similar spectrometers arranged in two cameras with orthogonal views of a vertical section of plasma. 2.5MeV and 14MeV neutrons are distinguished, except when high fluxes of 14MeV neutrons inhibit the measurement of low fluxes of 2.5MeV neutrons.

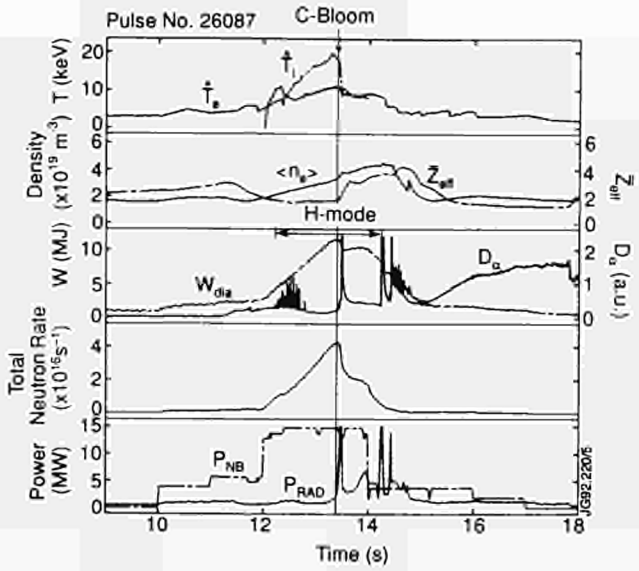

Fig.165: The time development of the central electron and ion temperatures, the volume-averaged electron density, the line-averaged Z_{eff}, the plasma diamagnetic energy, the D_α emission, the total neutron rate, and the NB and radiated powers for Pulse No. 26087.

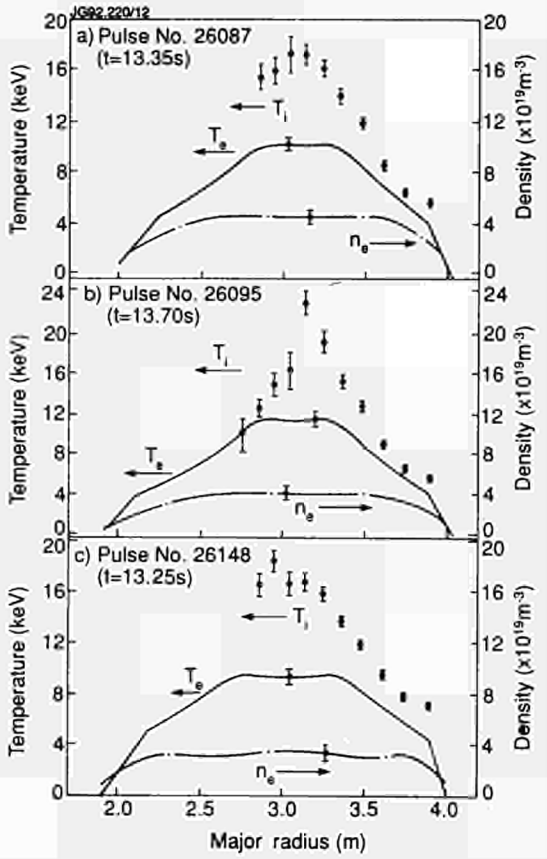

Fig.166: Radial profiles of the ion and electron temperatures and the electron density for (a) Pulse No. 26087, (b) Pulse No. 26095 and (c) Pulse No. 26148.

Other essential diagnostics included magnetic measurements (used to determine the equilibrium configuration and the plasma diamagnetic energy), electron cyclotron emission (for the electron temperature, T_e), an infrared interferometer (for the electron density, n_e), LIDAR Thomson scattering (for T_e and n_e), active charge exchange recombination spectroscopy (for the ion temperature, T_i and impurity concentrations) and visible bremsstrahlung (for the line-of-sight averaged effective ionic charge, Z_{eff}).

Data Consistency

In planning and executing the deuterium-tritium experiment, the TRANSP code [1] was used to check the internal consistency of the measured data and to estimate the fraction of neutrons which were produced by thermal-thermal, beam-thermal and beam-beam reactions on the basis of the measured profiles of n_e, T_e and T_i and the measured Z_{eff} with an assumed flat profile. In particular, the measurements and simulations were compared for the diamagnetic and MHD energies, the loop voltage and, most importantly, the neutron emission rates. An important advantage of the TRANSP code is its treatment of neutral injection physics using Monte Carlo techniques to determine, for example, the ion and electron heating and the neutron emission rates due to neutral beam (NB) injection.

Experimental Results

The results from three discharges in the series of experiments, culminating in the deuterium-tritium experiment, will be described. The first is the best of several similar high-performance pure deuterium discharges (Pulse No. 26087), the second is a deuterium-tritium discharge with a 1% mixture of tritium in deuterium introduced into one PINI (Pulse No. 26095 is one of three similar discharges) and the third is a deuterium-tritium discharge with a 100% mixture of tritium introduced into two PINI's (Pulse No. 26148 is one of two similar discharges). In all cases, the plasma current started to increase at a time, t=0, was maintained at a "flat-top" in excess of 3MA from 5s to 15s and then decreased towards zero, which was reached near 25s.

Pure Deuterium Discharge

Figure 165 shows the time development of a number of characteristic parameters during the current "flat-top" of Pulse No. 26087, and includes the central temperatures, average density, Z_{eff}, plasma diamagnetic energy and total neutron emission rates. The plasma target for NB injection

Table XIII: Main Plasma Parameters for Deuterium Pulse No: 26087 and Deuterium-Tritium Pulse Nos: 26095 and 26148

Parameter	Units	Pulse No:26087	Pulse No:26095	Pulse No:26148
Time (t)	s	13.35	13.7	13.25
Plasma Current (I_p)	MA	3.1	3.1	3.1
Toroidal Field (B_T)	T	2.8	2.8	2.8
NB Power (P_{NB})	MW	14.9	14.2	14.3
Volume averaged electron density ($\langle n_e \rangle$)	$10^{19}m^{-3}$	3.5	3.3	2.5
Central electron density ($\hat{n}_e$)	$10^{19}m^{-3}$	5.1	4.5	3.6
Volume averaged (D+T) density ($\langle n_D \rangle + \langle n_T \rangle$)	$10^{19}m^{-3}$	2.9	2.5	1.6
Central (D+T) density ($\hat{n}_D + \hat{n}_T$)	$10^{19}m^{-3}$	4.1	3.4	2.4
Line averaged effective charge ($\bar{Z}_{eff}$)		1.8	2.2	2.4
Average electron temperature ($\langle T_e \rangle$)	keV	5.6	6.1	6.0
Central electron temperature ($\hat{T}_e$)	keV	10.5	11.9	9.9
Average ion temperature ($\langle T_i \rangle$)	keV	6.7	7.4	8.0
Central ion temperature ($\hat{T}_i$)	keV	18.6	22.0	18.8
Plasma diamagnetic energy (W_{dia})	MJ	11.6	11.2	9.1
$(dW_{dia}/dt)^{(a)}$	MW	6.0	3.9	4.7
Plasma to toroidal field pressure ratio (β_T)	%	2.2	2.2	1.7
Plasma to poloidal field pressure ratio (β_p)		0.83	0.80	0.64
Ratio to Troyon Limit $(\beta_T/\beta_{Troy})^{(b)}$		0.8	0.8	0.6
Energy replacement time $(\tau_E)^{(a)(c)}$	s	1.2	1.0	0.9
Fusion triple product $\left((\hat{n}_D + \hat{n}_T)\hat{T}_i\tau_E\right)^{(a)}$	$10^{20}m^{-3}keVs$	9.0	7.5	3.8
Ratio of average T to D+T density $\left(\langle n_T \rangle / (\langle n_D \rangle + \langle n_T \rangle)\right)^{(d)}$	%	0	0.08	11
Ratio of central T to D+T density $(\hat{n}_T / (\hat{n}_D + \hat{n}_T))^{(d)}$	%	0	0.08	10
Maximum total neutron emission rate	$10^{17}s^{-1}$	0.43	0.49	6.0
Total neutron yield	10^{17}	0.55	0.70	7.2
$Q^{(c)}$		5.1×10^{-3}	6.5×10^{-3}	0.15

(a) Calculated from averages over previous 0.2s; (b) $\beta_{Troy}(\%) = g_x\mu_0 I_p(MA)/B_T(T)a(m)$: where a is the horizontal minor radius, g_x=2.2, and μ_0=0.4π in these units;
(c) $\tau_E = W_{dia}/(P_{ss} - dW_{dia}/dt)$; (d) From TRANSP simulation; (e) Similar definition to Q_{DT}

is formed by allowing the density to fall during the transition from a limiter to an X-point configuration. The result is a moderately peaked density profile. At 12s, the NB power increases to ≈15MW which leads, after 0.3s, to the transition to the H-mode phase of the discharge. During the subsequent 1s, sawteeth are stabilised and the centrally peaked NB heating produces peaked temperature profiles. The ion and electron temperatures rise continuously throughout this phase, reaching 18.6keV and 10.5keV, respectively. The plasma diamagnetic energy reaches 11.6MJ, corresponding to a ratio of plasma to magnetic pressure of 2.2%. The main plasma parameters at this time are listed in Table XIII and the plasma profiles are shown in Fig.166(a). As the central plasma pressure rises and energetic NB ions accumulate in the plasma centre, "fishbone"-like oscillations grow. However, these have no obvious effect on the energetic ions, neutrons or the discharge performance. The high performance phase is terminated at a time (13.4s) characterized by a rise in edge emission from CIII and D_α (the "carbon bloom"), followed by a sawtooth collapse of the central plasma temperatures. Nevertheless, the H-mode persists until the high power NB injection is switched off at 14s. The time development of these discharges is typical of hot-ion H-modes with their characteristically long sawtooth-free periods of up to 1.5s.

The consistency of the data is demonstrated by the good agreement obtained between the measured and simulated emission rates for 2.5MeV neutrons (see Fig.167). The simulation also showed that ≈60% of the neutrons were produced by thermal-thermal reactions, while the remainder were mostly by beam-thermal reactions with only a small fraction by beam-beam reactions.

Discharge with 1% Tritium in One PINI

Figure 168 shows the time development of the characteristic parameters for Pulse No. 26095. All of these increase throughout the H-mode phase of the discharge which starts at 12.3s and ends with a "carbon bloom" at 13.7s. The main plasma parameters at this time are listed in Table XIII and the plasma profiles are shown in Fig.166(b).

Again, the consistency of the data is demonstrated by the good agreement obtained between the measured and simu-

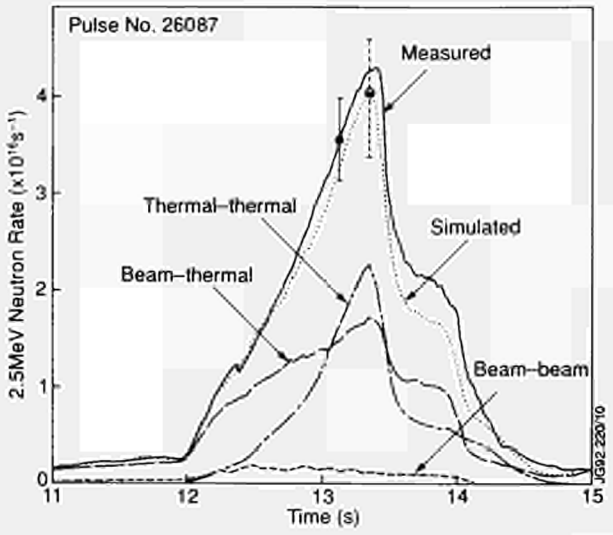

Fig.167: Fission chamber measurements and TRANSP simulations of 2.5MeV neutron rates for Pulse No. 26087.

lated neutron emission rates. In this case, the comparison is made for both 2.5MeV and 14MeV neutrons (see Fig.169) and indicates that the diagnostics and the TRANSP code are well-calibrated by these measurements. The simulations showed that ≈50% of the neutrons were produced by thermal-thermal reactions, while the remainder were mostly by beam-thermal reactions with only a small fraction by beam-beam reactions.

Specific experiments aimed at measuring the transport of thermalised tritium and deuterium were performed in discharges similar to Pulse No. 26095, but these experiments still require detailed analysis and will be reported in a subsequent publication.

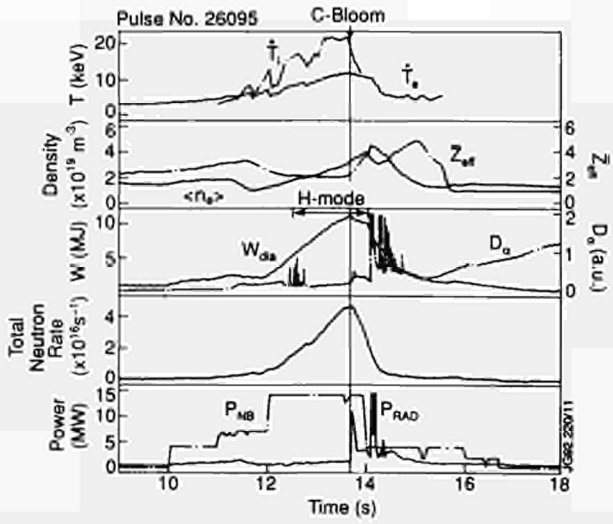

Fig.168: The time development of the central electron and ion temperatures, the volume-averaged electron density, the line-averaged, Z_{eff}, the plasma diamagnetic energy, the D_α emission, the total neutron rate, and the NB and radiated powers for Pulse No. 26095.

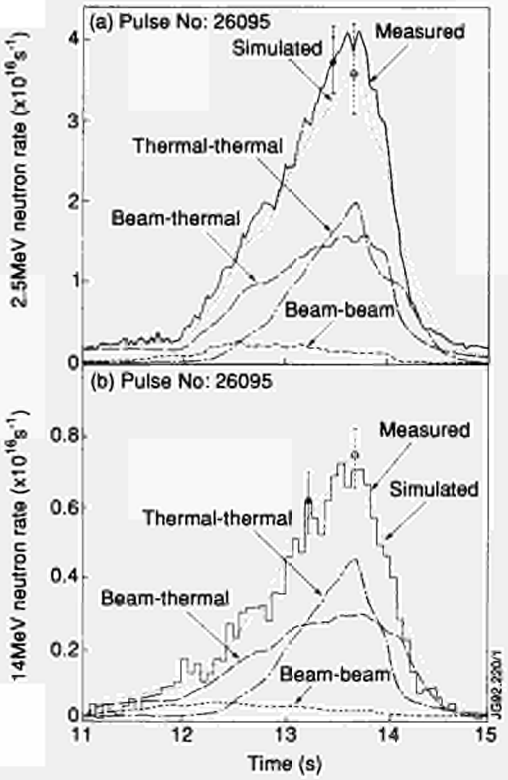

Fig.169: For Pulse No. 26095, (a) Fission chamber measurements and TRANSP simulations of 2.5MeV neutron rates, and (b) Silicon diode measurements and TRANSP simulations of 14MeV neutron rates.

Discharge with 100% Tritium in Two PINI's

To minimise activation levels and tritium usage, only two pulses of this type were attempted. Both were similar and each produced fusion power in excess of 1.5MW. The neutral beam power versus time (shown schematically in Fig.170) was chosen by selecting the switch-on time of pairs of PINI's. The full curve corresponded to Pulse No. 26148 (which had 1.5s tritium pre-fuelling) and the dashed curve to Pulse No. 26147 (which had 1s tritium pre-fuelling). These times were chosen to give effective fuelling, as predicted by the TRANSP code and confirmed by the results of discharges with 1% tritium in one PINI. These discharges were also heated by up to four deuterium PINI's, before and after high power heating. This suppressed MHD instabilities at early times and secured a disruption-free decay of the plasma current at late times. In Pulse No. 26147, two deuterium PINI's were switched-off at 13.2s.

Figure 171 shows the time development of the characteristic parameters for Pulse No. 26148. All of these increase

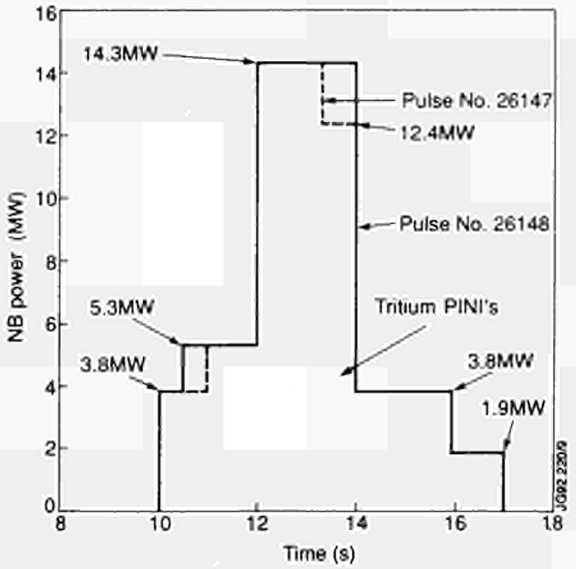

Fig.170: The NB power versus time for Pulse Nos. 26147 and 26148.

throughout the H-mode phase of the discharge which starts at 12.4s and ends with a "carbon bloom" at 13.3s. The main plasma parameters at this time are listed in Table XIII and the plasma profiles are shown in Fig.166(c).

Figure 172 compares the time development of the plasma diamagnetic energy in Pulse Nos. 26087, 26095 and 26148. For the two discharges with the same total input power (Pulse Nos. 26095 and 26148), the time development is very

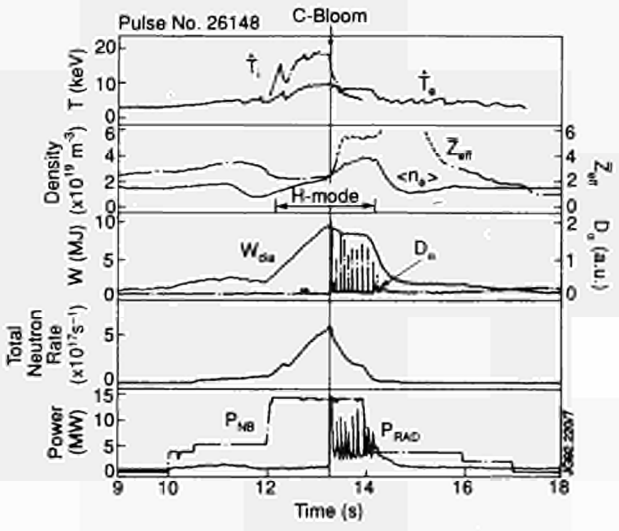

Fig.171: The time development of the central electron and ion temperatures, the volume-averaged electron density, the line-averaged , Z_{eff} , the plasma diamagnetic energy, the D_α emission, the total neutron rate, and the NB and radiated power for Pulse No. 26148. After the "carbon bloom". The Z_{eff} measurement is affected by black body radiation emanating from the targets.

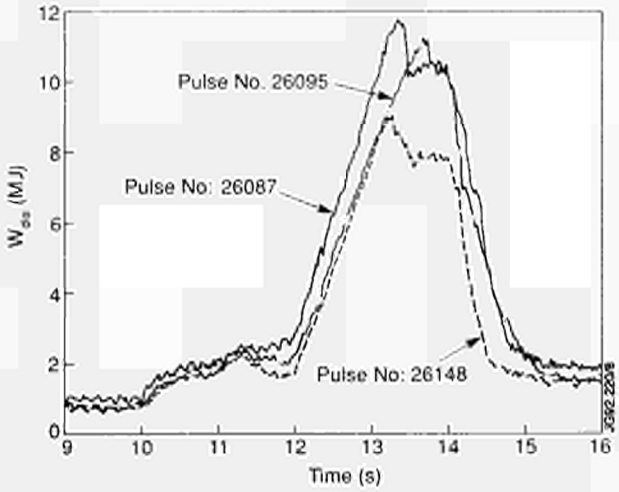

Fig.172: The time development of the diamagnetic energy, W_{dia}, for Pulse Nos. 26087, 26095 and 26148.

similar until the earlier onset of the "carbon bloom" at 13.3s in Pulse No. 26148, when the plasma energy was 9.1MJ. In Pulse No. 26095, the plasma energy increased to 11.2MJ at the time of the "carbon bloom" at 13.7s. The plasma diamagnetic energy was even higher in Pulse No. 26087, both at the start and termination of the H-mode. Furthermore, the fusion triple product for this pulse is about twice that for Pulse No. 26148 in which the hydrogen isotope density is lower due to the lower electron density and higher Z_{eff} (see Table XIII).

The proton recoil pulse height spectrum for Pulse No. 26147 (Fig.173) shows clearly the presence of 14MeV neutrons. The total emission is about forty times that obtained for 2.5MeV neutrons in a similar deuterium discharge

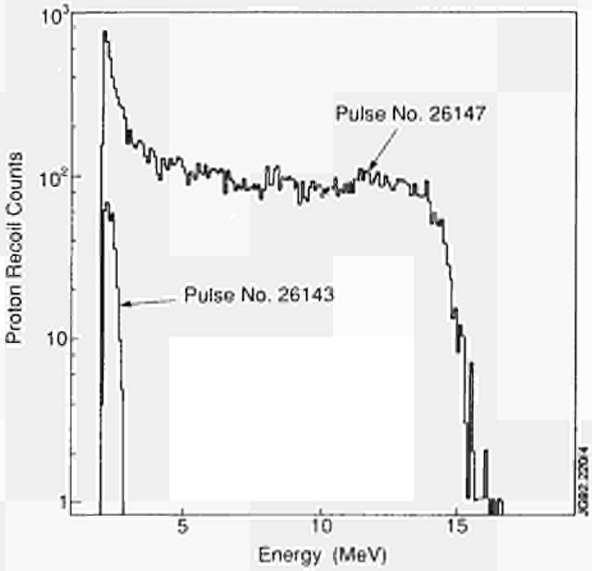

Fig.173: Proton recoil pulse height spectrum for deuterium-tritium Pulse No. 26147 (predominantly 14MeV neutrons) and deuterium Pulse No. 26143 (2.5MeV neutrons only).

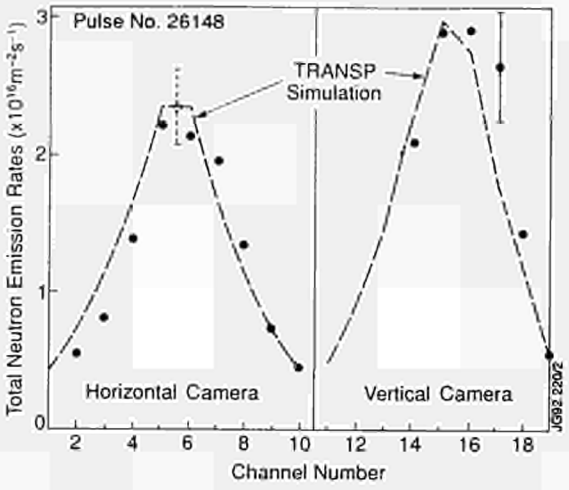

Fig.174: The measured and simulated line-integrated total neutron emission rates (predominantly 14MeV neutrons) as measured by the horizontal and vertical cameras of the neutron profile monitor, for Pulse No. 26148.

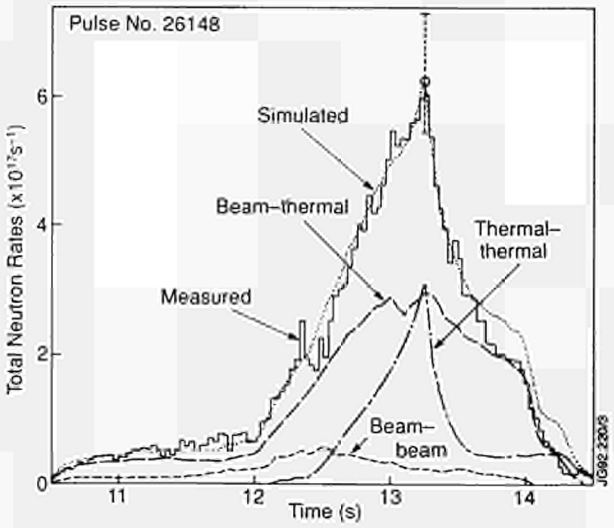

Fig.175: Silicon diode measurements and TRANSP simulations of the total neutron rates (predominantly 14MeV neutrons) for Pulse No. 26148.

(Pulse No. 26143). The 14MeV neutrons, which interact with carbon nuclei in the scintillator, also give rise to the high emission observed at a few MeV.

The line-integrated neutron emission rates, as measured by the horizontal and vertical cameras of the neutron profile monitor and normalised to the 14MeV neutron emission rates obtained from the fission chambers, show good agreement with the results of TRANSP simulations (Fig.174). The peaks are displaced by ≈0.1m, but this is well within the uncertainties of the simulation. More detailed studies, including improvements to the somewhat idealised geometries used, are in progress.

The consistency of the data is again demonstrated by the good agreement obtained between the measured and simulated emission of, predominantly, 14MeV neutrons (see Fig.175). Again, the simulations showed that ≈50% of the neutrons were produced by thermal-thermal reactions while the remainder were mostly by beam-thermal reactions with only a small fraction by beam-beam reactions. The peak total neutron emission rate was 6.0×10^{17} neutrons/s in an high power phase lasting about 2s. The integrated total neutron yield was 7.2×10^{17} neutrons with an accuracy of ±7%. The total fusion releases (α-particles and neutrons) were 1.7MW of peak power and 2MJ of energy.

The simulation also gave the α-particle statistics listed in Table XIV. Clearly, the level of α-particle heating was too low, in comparison with the NB power, to have a discernible effect on the electron temperature. Furthermore, the α-particle pressure and concentration were probably too low for the stimulation of collective effects, although these effects cannot be excluded entirely. However, the characteristics of the MHD activity observed in the two tritium discharges were very similar to those of pure deuterium discharges such as Pulse No. 26087.

Since the deuterium and tritium source rates were similarly peaked on axis, both mixing models described in [2] for deuterium and tritium (that is, identical radial profiles or

Table XIV: α-particle statistics from the TRANSP simulation of Pulse No. 26148 at 13.2s (instantaneous equilibration model for α-particles)

Overall power transfers		
From α-particles to electrons	:	260kW
From α-particles to ions	:	60kW
From NB to electrons	:	1.8MW
From NB to ions	:	9.4MW
NB loss by shine-through	:	0.4MW
NB loss by charge exchange	:	1.5MW
Equipartition ions to electrons	:	2MW
Central power transfers		
From α-particles to electrons	:	$13kWm^{-3}$
From α-particles to ions	:	$3.6kWm^{-3}$
From NB to electrons	:	$75kWm^{-3}$
From NB to ions	:	$610kWm^{-3}$
Central α-particle concentrations		
Ratio of α-particle to thermal plasma pressure	:	≈4%
Ratio of α-particle to total plasma pressure	:	≈2.5%
Ratio of α-particle to electron density	:	≈0.08%

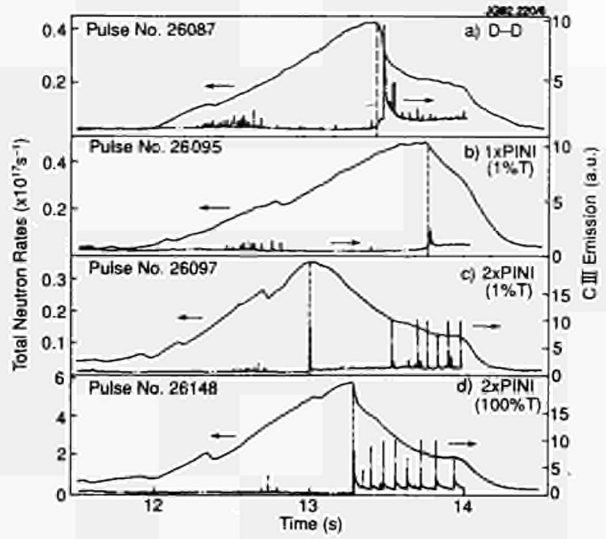

Fig.176: Variation in the time of termination of the high performance phase of a number of similar discharges as shown by the fall in the neutron emission rate. The dashed vertical lines show the time of the "carbon bloom" as characterized by increased emission of CIII light from the plasma edge. In (a) and (b) the bloom occurs "naturally"; in (c) it is triggered by an ELM; and in (d) by a sawtooth collapse coupled to an ELM.

equal velocities) resulted in similar deuterium and tritium profiles and gave an equally good fit to the neutron data.

Discharge Termination and Variability

The high performance discharges were limited by the "carbon bloom". The time at which this occurred affected the maximum neutron emission rates as shown in Fig.176 and, for a given magnetic configuration, was principally dependent on the level and duration of heating, characterised in by the total energy, E_c, conducted to the X-point targets:

$$E_c = \int_{t_{X\text{-}point}}^{t_{bloom}} \left(P_{tot} - P_{rad} - \frac{dW}{dt} \right)$$

where P_{tot} is the total input power, P_{rad} the radiated power and dW/dt the rate of change of plasma energy.

For the particular configuration, power and pulse duration in these experiments, the "carbon bloom" occurred when E_c was typically 11±3MJ. In some cases, this occurred "naturally", presumably due to the progressive rise of target temperature. In other cases, when the conducted energy was in this range, the "carbon bloom" could be triggered by a MHD event, such as a giant ELM (edge localised mode), or a sawtooth collapse which coupled to an ELM. The occurrence of these events appears to depend upon the precise time evolution of plasma density and additional heating and showed some variability in these experiments.

In comparison with other similar discharges in deuterium, the high performance phase of both deuterium-tritium Pulse Nos. 26147 and 26148 terminated as the result of a somewhat earlier sawtooth collapse, coupled to an ELM and leading to the "carbon bloom" (1.3s after the start of full NB power, see Fig.171 for Pulse No. 26148). Detailed analysis of the collapse shows that the inversion radius of such sawteeth was no larger than for normal sawteeth. However, a strong coupling between central and edge modes was observed and might have played a role in triggering the ELM, which occurred within 100μs of the sawtooth collapse.

Extrapolation to Full Performance Deuterium-Tritium Discharges

The fusion amplification factor, Q_{DT}, is defined in terms of the separate contributions from thermal-thermal, Q_{tt}, beam-thermal, Q_{bt}, and beam-beam, Q_{bb}, reactions:

$$Q_{DT} = Q_{tt} + Q_{bt} + Q_{bb}$$

where $Q_{tt} = P_{tt} / (P_{loss} - 0.2P_{tt})$, $Q_{bt} = P_{bt} / (P_b - P_{st})$,

and $Q_{bb} = P_{bb} / (P_b - P_{st})$

P_{tt}, P_{bt} and P_{bb} are the total fusion powers, respectively, from thermal-thermal, beam-thermal and beam-beam reactions, $P_{loss} = (P_b + P_W - P_{st} - dW/dt)$ is the total power lost from the plasma (including radiation and charge-exchange) and P_b, P_W, P_{st} and dW/dt are, respectively, the NB input power, the ohmic input power, the power lost by NB "shine-through", and the rate of change of plasma diamagnetic energy.

With this definition, it is easy to evaluate Q_{DT} for an actual plasma using the separation into thermal-thermal, beam-thermal and beam-beam powers given by the TRANSP code. At the time of peak neutron emission in Pulse No. 26148, Q_{DT} determined in this way is 0.15.

In order to estimate the Q_{DT} which would be obtained for a similar discharge but with a more optimum deuterium-tritium mixture, a nominal Q_{DT} is defined as the value that would be obtained if the hydrogen isotope content of the actual plasma were replaced instantaneously by the more optimum mixture with a tritium concentration, $c = \langle n_T \rangle / (\langle n_D \rangle + \langle n_T \rangle)$. At the times of peak neutron emission, and with c=0.6, nominal Q_{DT} is 0.46 in deuterium-tritium Pulse No. 26148, and 1.14 in deuterium Pulse No. 26087.

This nominal Q_{DT} is very similar to that which would have been obtained experimentally if eight of the sixteen PINI's (instead of two in Pulse No. 26148 and none in Pulse No.

26087) had been used to inject tritium into a 50:50 deuterium-tritium target plasma. TRANSP simulations of these two pulses, with the actual plasma conditions and NB power and acceleration voltages used in the experiment, then gives Q_{DT}=0.44 for Pulse No. 26148 and 1.07 for Pulse No. 26087 (in each case the value of c is determined by NB injection and is about 0.5). The total fusion power (neutrons and α-particles) and the fraction coming from thermal-thermal reactions for the two pulses would be 4.6MW(43%) and 9.6MW(57%), respectively.

In relating these extrapolations to what should be possible in JET in the future, it should be remembered that, for the main deuterium-tritium experiments foreseen for 1996, there will be 12.5MW of tritium NB injection at a principal energy of 160kV and 8MW of deuterium NB injection at a principal energy of 140kV. The higher power and better beam penetration should give higher values of Q_{DT}. It should also be possible to use up to 20MW of ICRH, either alone or in combination with NB heating, in which case the total fusion power should also increase, but with little increase in Q_{DT}. Experiments with the pumped divertor are expected to control impurities and give a cleaner plasma which should lead to a further increase in the Q_{DT} value.

Summary and Conclusions

In JET, high performance deuterium discharges with $Q_{DD}>2\times10^{-3}$ and nominal $Q_{DT}>0.5$ are obtained routinely and reliably. The best JET deuterium pulse gave $Q_{DD}\approx5\times10^{-3}$ and a nominal Q_{DT}=1.14, so that the total fusion power (neutrons and α-particles) would exceed the total losses in the equivalent deuterium-tritium discharge in these transient conditions.

For the first time, experiments on high fusion performance tokamak plasmas have been performed using a deuterium-tritium fuel mixture. An equivalent tritium neutral current of 24A was injected into a deuterium plasma, heated by deuterium neutral beams. The tritium concentration was ≈11% at the time of peak performance when the total neutron emission rate was 6.0×10^{17} neutrons/s. The integrated total neutron yield over the high power phase, which lasted about 2s, was 7.2×10^{17} neutrons, with an accuracy of ±7%. The total fusion releases were 1.7MW at peak power and 2MJ of energy. The amount of tritium injected and the number of discharges with tritium were deliberately restricted for operational convenience.

The consistency of the experimental data was established with simulations using the TRANSP code which showed, in particular, that thermal-thermal and beam-thermal reactions contributed about equally to the total neutron emission.

The good agreement obtained between measurement and simulation gave confidence in the accuracy of extrapolations from existing discharges. Assuming a tritium concentration, $c=\langle n_T\rangle/(\langle n_D\rangle+\langle n_T\rangle)$=0.6 (chosen near the optimum for fusion power output), the deuterium-tritium Pulse No. 26148 would have produced a fusion power of ≈5MW and a nominal $Q_{DT}\approx0.46$. The same extrapolation for the pure deuterium Pulse No. 26087 would have given ≈11MW and a nominal Q_{DT}=1.14. Use of the more optimum NB system intended for JET in 1996, together with control of the impurity influx as envisaged with the JET pumped divertor, should yield higher values of Q_{DT}.

The techniques used for introducing, tracking, monitoring and recovering tritium have been demonstrated to be highly effective. Essentially all of the tritium introduced into the NB system has been recovered and, so far, about two thirds that introduced into the torus. These levels are sufficiently low for the JET experimental programme in deuterium to continue normally. The wall tiles will be removed at the start of the next shutdown, and post-mortem analysis should provide important data for the choice of wall materials for a Next Step device.

The transient nature of the type of H-mode discharge used for the deuterium-tritium experiment emphasises the need to control the "carbon bloom" and to develop a viable mode of operation for a reactor. Controlling the plasma exhaust and the ingress of impurities released at the divertor plates will be the major theme of the JET Programme to 1995. These data, together with those on tritium retention, will allow the planning of an effective campaign of deuterium-tritium experiments in 1996. These should also permit accurate extrapolations to a Next Step device, one designed to operate routinely at a temperature sustained by its own fusion power.

References

[1] Goldston, R.J., McClune, D.C., Towner, H.H., et al., J. Comput. Phys. **43** (1981) 61.

[2] Stubberfield, P.M., Balet, B. and Cordey, J.G., Plasma Phys. and Control. Fusion **33(11)** (1991) 1255.

[3] Stork, D., Campbell, D.J., Clement, S., et al., Europhysics Conference Abstracts (Proc. 18th European Conference on Controlled Fusion and Plasma Physics), EPS, Berlin, Germany, **Vol. 15C(Part I)** (1991) 357.

Summary of Scientific Progress

In planning the 1991 experimental programme, the major considerations were:

(i) To exploit new facilities such as the continuous X-point targets, improvements in the poloidal field circuit, enhancements to heating systems and new diagnostics;

(ii) To advance our understanding in several key areas of tokamak physics such as energy and particle transport, impurity production and transport, magnetic topology and H-mode physics;

(iii)To improve fusion performance;

(iv)To address issues central to the Pumped Divertor and to Next Step devices;

(v) To complete certain experiments relevant to the belt limiter configuration.

Developing a programme strategy to incorporate these elements necessitated provision for a wide range of experimental scenarios. However, this had to be balanced against several constraints. The first of these was the need to provide experimental time for the commissioning of new facilities in advance of their exploitation in the programme. Fortunately, no major difficulties were encountered in this phase, and commissioning merged smoothly with the mainline experimental programme. A second major consideration was the prevention of damage to the torus and auxiliary systems as a result of disruptions. A successful strategy was adopted which limited the experimental scenarios which could be utilized while a parallel programme of research into the minimization of disruption effects was pursued. Substantial progress was made in this area and no significant damage to the torus occurred as a result of the experimental programme.

Finally, the necessity of limiting neutron production to minimize vessel activation inevitably restricted the number of pulses, though not the range of experiments, at the highest heating powers. An initial profile of neutron production was devised at the start of the programme to permit the range of experiments originally foreseen. However, this profile had to be adjusted several times in the course of the campaign as new elements were incorporated in the programme.

Exploitation of New Facilities

Investigation of the performance of diverted plasmas utilizing the newly installed toroidal X-point targets was a central activity throughout the campaign. The choice of beryllium tiles for the lower target and carbon fibre composite (CFC) tiles for the upper target permitted a careful study of the relative merits of the two materials in this role. In addition, in the course of these experiments, two designs of carbon fibre composite CFC tile were examined and this allowed the limitations arising from heating of tile edges to be studied. The principal aims of the target assessment were: to establish the power handling capabilities of different target materials and of different target designs; to investigate the causes of limitations in the power handling capabilities; and to study the influence of different target materials on bulk plasma performance.

The targets performed broadly as expected, though the power handling capability of the first design of CFC tiles, which was limited by power flux on tile edges, proved to be better than calculations had predicted. The improved design of target tile, which shielded the tile edges by appropriate machining, yielded about a factor 2 improvement in power handling capability. Comparisons of H-mode performance using CFC and Be targets showed that the two materials gave similar results at moderate to high densities, but that the CFC targets permitted considerably better fusion yield to be achieved in the relatively low density hot-ion H-modes used in the PTE. Significantly, it was found that reliable H-modes could be achieved using the Be targets even after extensive (deliberate) surface melting. While the performance in all H-mode plasmas was limited ultimately by impurity influxes, since neither target was actively cooled, a significant improvement in power handling capability was observed at high density. As a result, extensive gas puffing was used successfully to reduce power loading on the targets and thereby delay impurity influxes. Several other new facilities have been utilized extensively during the recent campaign. These include: improvements in the poloidal field circuit to permit X-point operation at higher current and to allow JET to be operated as an AC tokamak; upgrading of the energy of the second neutral injector box (NIB) to 140keV; use of the ICRF heating system as a phased array for fast wave current drive studies; an extended gas introduction system for radiative divertor studies; and an improved Plasma Fault Protection System which has allowed, in particular, softer termination of the plasma on indication of an approaching disruption. In addition, new diagnostics, such as a range of 14MeV neutron diagnostics, which played a key role in the preliminary tritium experiment (PTE), an edge charge exchange spectroscopy system for poloidal rotation and ion

temperature measurements, a motional Stark effect diagnostic for q-profile measurements, and an active neutral particle analyzer have yielded new insights into plasma behaviour.

Tokamak Physics Studies

Energy Transport and Confinement

Several specific experiments have been performed to elucidate the confinement properties of various plasma regimes. A series of standard discharges has been used during the experimental period to accumulate data on the influence of isotopic mass, A, and charge, Z, on confinement. Experiments using H, D and ^{3}He NB injection in L-mode plasmas have shown that the global energy confinement of D and ^{3}He plasmas is essentially the same, but that of H plasmas is slightly (-20%) lower. The JET data does not, therefore, support the $A^{0.5}$ dependence observed in smaller tokamaks.

To investigate the effects of poloidal field and magnetic shear on energy confinement, an experiment was performed in which the plasma current was ramped while other parameters, including input power were held constant. These studies suggest that the product of current and plasma inductance, rather than simply current, determines the scaling of global energy confinement. Local transport analysis indicates that the origin of the current scaling lies mainly in a dependence of the local thermal diffusivity, χ, on the poloidal field. Moreover, the data is well reproduced by the Rebut-Lallia-Watkins form for the thermal diffusivity. Studies of plasma behaviour at high toroidal beta, β_t, also allowed the scaling of confinement with toroidal field to be investigated, but in this case for H-mode plasmas. A variation of the kinetic energy confinement time, $\tau_{kin} \propto B_T^{0.25}$, was obtained, although this behaviour might equally well have been explained by a dependence on safety factor.

Investigation of the PEP H-mode constituted a further major area of study. In this regime, local transport, MHD stability and the evolution of the current profile appear to be inextricably linked, and the range of behaviour observed makes generalization difficult. Nevertheless, significant advances in understanding were made. In particular, unambiguous evidence of reversal of the shear in the plasma centre during the enhanced confinement phase was obtained from polarimetric measurements of the q-profile, supporting earlier deductions from observations of localized MHD modes. It is thought that this reversal of shear is fundamental to the enhanced central confinement observed in the PEP H-mode, but there is no complete understanding of the phenomenon. In the course of these experiments, exploitation of two-minority ICRF heating scenarios (H,He^3) produced ion and electron temperatures simultaneously in the region of 15keV.

A variety of studies of local transport properties were performed in the course of the campaign. Perturbative measurements of suprathermal electron diffusion showed that the suprathermal electrons accelerated by LHCD exhibited a radial diffusivity which was a factor of 3-5 greater than the electron thermal diffusivity (approximately equivalent to the ratio of thermal velocities involved) which lends support to the proposal that micromagnetic fluctuations are the source of anomalous electron thermal transport. Analysis of impurity transport using laser ablation of impurities has continued. The most remarkable result of these experiments is the existence of a region of reduced anomalous diffusivity in the central plasma. This region appears to be largely independent of whether q(0) is above or below unity, whether the plasma is ohmically or additionally heated and whether the central gradients of the plasma profiles are positive or negative.

H-Mode Studies

Exploitation and investigation of plasma behaviour in the H-mode is a major component of the JET experimental programme and several new areas of H-mode behaviour have been addressed for the first time in JET. NB counter-injection experiments established that the power threshold for the H-mode was perhaps 10-20% lower than for co-injection. Injection of high-Z impurities (Ni) by laser ablation showed some evidence of central impurity accumulation, as is observed in smaller devices, but this did not pose a significant problem as low-Z impurities (C, Be), which are dominant in JET, did not exhibit this behaviour. Overall, therefore, transport of intrinsic impurities and the resultant radiation losses were similar to co-injection H-modes and the time evolution and duration of ELM-free H-modes were similar in the two cases. The most significant difference in behaviour was, in fact, observed in central MHD behaviour. With counter injection, frequent, small-amplitude sawteeth were observed which maintained flattened central plasma profiles. As a result, the energy confinement of counter-injection H-modes was somewhat reduced relative to that obtained with co-injection, with only the best counter-injection cases exhibiting energy confinement times equal to twice those predicted by Goldston L-mode scaling.

Considerable efforts have been made to understand ELM behaviour and to investigate techniques for reliable ELM

production to permit steady-state H-modes to be established. Some evidence has been obtained of precursor activity to ELM's in both edge magnetic and density reflectometer signals. This activity consists of fluctuations with frequencies in the range 60-100kHz, implying that the mode numbers involved are rather high. Steady-state H-modes in which plasma parameters are held constant by ELM activity have been produced at 2MA/2.3T, with a maximum duration of 18s being achieved. At 2MA the duration limit of the H-mode was set by technical, rather than plasma-related, limitations. This regime was established by combining strong gas puffing (~50mbℓs^{-1}) using NB and off-axis ICRF heating. Energy confinement of these H-modes was high, typically corresponding to twice the Goldston L-mode prediction.

Recent theories of the H-mode postulate that the L-to-H transition is due to shear in the edge poloidal velocity driven by a radial electric field gradient. A new active charge exchange diagnostic for the measurement of edge ion temperatures and poloidal rotation has permitted this question to be investigated in JET for the first time. Initial measurements have shown that the poloidal rotation velocity in the plasma edge does increase gradually during the period of the H-mode transition, reaching values ~$2 \times 10^4 ms^{-1}$. However, there was no rapid jump as has been reported from other tokamaks.

MHD Stability

Experiments in JET have improved understanding of the conditions under which disruptions occur and of the evolution of the plasma towards a major disruption. Recently, greater emphasis has been given to the development of techniques for avoidance of disruptions, or for the minimization of their consequences. A substantial advance was made in this respect through improvements to the Plasma Fault Protection System (PFPS). Early detection of the the 'locked' (i.e. non-rotating) m=2, n=1 mode which is invariably a precursor to major disruptions has enabled measures to be taken (reduction of plasma current, plasma elongation and of heating power) to minimize the impact of the resultant disruption on the torus.

This has been of particular value in overcoming the problems resulting from vertical instabilities which follow major disruptions. Analysis has shown that these arise from loss of vertical stability in elongated plasmas at the energy quench and that their consequences are aggravated by the slow post-disruptive current decay observed since the introduction of beryllium into JET. Such instabilities lead to substantial forces on the vacuum vessel (several hundred tonnes) and have resulted in damage to internal components. By using detection of the occurrence of a 'locked' n=1 mode to trigger a rapid (few hundred milliseconds) reduction of the PFX amplifier current (the dominant source of the destabilizing force) to zero, it has been possible to postpone the loss of vertical stability until much later in the current decay with a consequent reduction in forces by an order of magnitude.

Although several aspects of major disruptions remain problematic, the causes of disruptions on JET have been well documented and are largely understood. One exception has been the disruption caused by the growth of a large amplitude n=1 'locked' mode as the internal separatrix (X-point) is formed. This mode becomes more persistent at low-q and appears to have a low-density threshold. More detailed experiments have now confirmed these observations and have identified the most likely cause of the growth of the mode as external error fields arising from details of the construction of the poloidal field coils. The principal source of these error fields appears to be the vertical field coils and it has been shown that the threshold density depends on the coil configuration, the helicity of the internal magnetic field (the pessimal arrangement occurs when the helicity of the tokamak magnetic field matches that of the calculated error field) and the edge safety factor. The occurrence of the mode as had previously been thought, does not, depend on the existence of an X-point, nor even of a plasma more elongated than the natural elongation in JET ($\kappa \sim 1.4$). In the worst cases, it is not possible to establish plasmas with $q_\psi < 3$ since the low density limit due to these 'error field' modes overlaps with the high density limit.

Studies of sawteeth oscillations have continued both to elucidate the nature of the instability and to investigate means of sawtooth stabilization. Measurements of q-profile in circular plasmas have been performed to minimize the systematic errors which increase the uncertainty of such polarimetric measurements in elongated plasmas. The results have confirmed earlier conclusions that q(0) remains below unity in sawtoothing discharges and that it decreases well below unity during 'monster' sawteeth. These experiments will also permit a comparison with measurements made by a new technique, the Motional Stark Effect (MSE) which makes use of spectral splitting of line emission from injected neutral beam atoms which arises from the Lorentz

electric field which the atomic electrons of the injected neutrals experience as they cross the magnetic field.

Evidence of the importance of local modifications of the current profile has been obtained from the first demonstration of fast wave current drive using the ICRF system antennas as a phased array. This technique yields little net current drive, but substantial anti-parallel currents on either side of the ICRF resonance are predicted. By varying the phase of the antenna array so as to reverse the relative directions of the predicted anti-parallel currents and by locating the resonance on the inboard and outboard q=1 radii in turn, it was possible to show that, when a flattening of the current profile about q=1 was predicted, sawteeth could be stabilized for periods of up to 2s. When an increase in the gradient of the current profile at q=1 was predicted, rapid small amplitude sawteeth were observed, indicating a destabilization of the sawtooth instability. Similar experiments were performed with the ICRF resonance located at the q=2 surface in an attempt to stabilize m=2 activity. Some evidence of stabilization of m=2 modes was observed, but further analysis is required to determine unambiguously whether the effect is due to local heating or local current drive.

Plasma Performance

High Performance Discharges

The performance of JET plasmas was extended in several ways. Uprating of the capability of the shaping amplifier from 40 to 50kA permitted improved X-point configurations to be established at 3 and 4MA and 5MA double null X-point plasmas to be established for the first time. Extensive experiments were performed at plasma currents in the range 3-4.5MA, in sawtoothing and sawtooth-free discharges, over a wide range of plasma densities and at combined heating powers of up to 25MW. In many cases, the performance of these discharges was limited by impurity influxes, though this could be influenced by varying the X-point to target distance, by judicious use of gas-puffing and by exploiting both X-point targets. The highest stored energy obtained to date, 12.7MJ, was obtained in a 4MA sawtooth-free plasma with 21MW of heating power. One of the most significant results was that, at high densities, fusion yield was independent of the type of heating used (NBI or ICRF). Furthermore, no significant difference in performance between sawtoothing and sawtooth-free discharges was observed, indicating that sawteeth do not play a major role in the confinement properties of these plasmas.

Considerable efforts were made to increase the fusion yield of plasmas in preparation for the PTE. Both single null (SNX) and double null (DNX) plasmas were investigated using NB heating and, for the first time, combined NB and ICRF heating. Studies focussed on hot-ion H-mode plasmas in the range 3-4MA as experience had shown that, in the present JET configuration, these plasmas produced the highest neutron yield and offered the best prospects for further development to higher performance.

Progress was made in several directions. In the DNX configuration, ICRF power in the range 3-5MW was successfully coupled into hot ion H-modes produced by NBI power in the range 12-16MW. The increased electron temperature resulting from ICRF heating led to a higher neutron yield for a given NB power, although no increase in total fusion yield was obtained. In the SNX configuration, the majority of experiments utilized the configuration in which the ∇B ion drift was away from the X-point, as previous experiments had shown that the more optimal power distribution between the inner and outer X-point strike zones yielded a longer delay until the impurity influx which terminates the high performance phase in this regime. Optimization of 3MA/2.8T discharges in this configuration yielded the highest neutron yield obtained to date, $4.3 \times 10^{16} s^{-1}$, which corresponded to a fusion product $n_D(0)\tau_E T_i(0) = 9.2 \times 10^{20} m^{-3} keVs$ and a $Q_{DT} = 1.1$.

Preliminary Tritium Experiment

The introduction of a significant fraction of tritium into a tokamak plasma for the first time is the most significant accomplishment of the recent experimental programme. This experiment was noteworthy not only for the production of over 1MW of fusion power, but for several substantial technical achievements: the establishment of procedures for the monitoring and tracking of tritium in a tokamak environment; the demonstration of reliable techniques for the handling of tritium and its introduction into the tokamak; and the first tritium neutral beam injection. Significant scientific information was also obtained in a number of areas: validation of simulation codes used to extrapolate from D-D to D-T performance; investigation of the transport of tritium in a tokamak plasma; the study of rates of removal of tritium from the tokamak first wall and ancillary systems.

The target plasma for this experiment was a hot ion H-mode in the SNX configuration at 3MA/2.8T such as that described above. To minimize activation of the vessel, optimization of this discharge was performed in deuterium,

followed by several shots at central tritium concentrations ~ 0.1% (obtained by the doping of two NBI sources with 1% tritium). In the two full power pulses to which the final experiment was limited, tritium was introduced into the plasma using tritium fuel in two of the sixteen NBI sources, resulting in a central tritium concentration of 10%. The performance of these discharges lay in the middle of the range of the hot ion modes produced during the optimization experiment, having an actual $Q_{DT} = 0.15$ and a projected $Q_{DT} = 0.5$ for an optimized deuterium/tritium mixture. The peak fusion power achieved was 1.7MW, with an integrated fusion energy of 2MJ. Analysis of these discharges is continuing to improve estimates of the tritium diffusion rate, to understand the MHD behaviour, and to evaluate transport and confinement. Overall, the experiment has produced invaluable scientific and technical data for the preparation of the full DT phase of JET which is planned for 1996.

High-β_t Experiments

Previous experiments in JET at high values of β_t have been rather limited, although values of $\beta_t \sim 5\%$ had been obtained. A more systematic investigation of the β-limit has been performed in which the performance of sawtoothing and sawtooth-free discharges has been compared to clarify the influence of the q=1 surface and its associated instabilities in determining the limiting β_t. In addition, hot ion H-modes have been established in sawtoothing and sawtooth-free plasmas to investigate the role played by β-limiting processes in limiting the performance of this regime.

The highest β_t values were obtained in 1.5-2MA DNX plasmas in which typical Troyon factors, $\beta_t/(I_p/aB_t)$, in the range 2.2-2.6 were obtained with a highest β_t value of 5.4%, corresponding to a Troyon factor of 3.1. As in earlier experiments, no evidence of a disruptive limit was observed, but several discharges exhibited b-limiting behaviour. In general, β_t was limited by ELM activity, often accompanied by large amplitude MHD modes with n=1, 2, 3. However, in a few cases, evidence of limiting behaviour was observed before ELM activity began. Further analysis is required to understand the cause of this behaviour.

Pumped Divertor and Next Step Physics

Pumped Divertor Studies

Control of the heat and particle flux to the the first wall and of the resultant impurity influxes to the plasma is perhaps the most important problem currently facing the development of fusion as a viable energy source. The new phase of the JET experiment, based on the installation of a Pumped Divertor, is designed to address this problem and to develop techniques for its satisfactory resolution. Therefore, a programme of research was undertaken to investigate the performance of the present divertor configuration in JET to obtain baseline data for comparison with the predictions of simulation code calculations.

From theoretical modelling of divertor behaviour, it is expected that divertor impurity retention should increase rapidly above a certain 'threshold' density which depends on the power flow into the scrape-off layer. This dependence arises from the strong variation of impurity retention with divertor ion temperature ($T_i^{-3.5}$). A series of experiments was carried out on both C and Be X-point targets to investigate how impurity retention varied with divertor density at fixed power, the divertor density being controlled by preprogrammed gas puffing into either the torus midplane or the X-point region. Measurements were obtained at high and low power levels. Experiments using the Be target showed that Be influxes increased with increasing gas puff rates (corresponding to increasing target density), an effect which counteracts the improved impurity retention observed at higher divertor densities. This behaviour is not unexpected as the sputtering yield for Be is insensitive to temperature for $T_e > 10$eV (which, therefore, necessitates the attainment of rather high densities to depress the ion temperature sufficiently to obtain high impurity retention). Similar measurements obtained on the C target are the subject of current analysis. In addition, detailed observations of divertor and scrape-off layer parameters are being used to validate numerical simulations of Pumped Divertor operation.

Current Drive Experiments

The design of Next Step devices in based upon the exploitation of a variety of current drive schemes. Two principal techniques for bulk current drive have been explored: lower hybrid current drive (LHCD) and bootstrap current. While the LHCD system has been employed in a variety of experiments, including a 1 minute duration limiter pulse, the emphasis in recent experiments has been the optimization of synergistic effects between ICRF and LHCD to optimize current drive efficiency and the demonstration of 100% current drive at the highest current. Studies have shown that synergistic effects are optimized

in plasmas with low electron density and peaked density and temperature profiles, which result in a large fast electron population in the inner half of the plasma. Under these conditions, overall current drive efficiencies (corrected downwards for direct current drive by TTMP damping of the ICRF waves) of up to $0.4 \times 10^{20} Am^{-2}W^{-1}$ have been achieved and 100% current drive has been attained at plasma currents up to 1.5MA. The enhanced current drive efficiency is thought to be due to TTMP damping of the fast waves on the fast electrons, resulting in their acceleration to energies of several hundred keV. This is supported by observations of bremsstrahlung spectra with characteristic energies above 100keV in LHCD experiments with ICRF heating, whereas the characteristic energy in full current drive plasmas without ICRF is ~40keV.

In many JET H-modes, bootstrap current fractions of 25% are typical. Previously no attempt had been made to optimize this figure nor to address the issue of whether significant bootstrap current can be obtained in ICRF heated plasmas with no central particle source. In low current (1-1.5MA) ICRF heated H-mode plasmas with $\beta_p \sim 2$, bootstrap current fractions of up to 70% were achieved and sawteeth were stabilized, presumably as a result of current profile broadening. In addition, these plasmas exhibited high thermal energy confinement, significantly (up to a factor of 1.7) above that predicted by the JET/DIII-D scaling.

AC Tokamak Operation

Operation of the tokamak as an AC device offers an alternative route to quasi-continuous operation without the overheads entailed in external current drive systems. The feasibility of such a scheme has previously been demonstrated on very small tokamaks at plasma currents of up to 4kA. Recent changes in the poloidal field circuit at JET have permitted this question to be investigated at significantly higher current, up to 2MA, and a systematic study of the parameters which determine the reliability of the second breakdown has been performed.

Reliable operation and additional heating of a two-cycle plasma was established at 2MA and plasma parameters were found to be very similar in the two cycles. Although it was not possible to demonstrate a smooth transition between the two cycles with zero dwell time, dwell times as small as 50ms and as long as 6s were achieved without difficulty. Indeed, the second plasma could be established following disruptions at up to 400kA in the tail of the first. Extensive studies were also made of the optimum control of the current ramp-down which has provided an understanding of the constraints on aperture and safety factor control necessary for successful termination of the first cycle, and initiation of the second.

Limiter Experiments

One Minute Pulse

The duration of JET limiter pulses is usually greater than that required to reach steady-state with respect to energy, and even particle, confinement, but it is generally short with respect to the resistive diffusion timescale and the timescale necessary for particle interactions with the limiter to approach steady-state. To explore the consequences of such long pulse operation, a one minute plasma at 2MA/1.9T was developed, utilizing ICRF heating and LHCD to minimize volt-second consumption.

While the plasma approached a quasi-steady-state with respect to magnetic diffusion (the central region being modulated by sawtooth activity) after ~ 10s, the plasma-wall interaction changed gradually throughout the pulse. It was found that the external gas requirements of the discharge fell to zero over a period of order 30s (which varied with the additional heating power), after which the density rose slowly. Z_{eff} measurements indicated that the rise in density was due primarily to increased deuterium recycling rather than increased impurity influxes. This behaviour was confirmed by observations of the decay of density following pellet injection and indicates a change in the recycling properties of the limiter with increasing temperature.

Conclusions

Experiments during the recent campaign have encompassed several objectives: demonstration of improved tokamak performance in several areas; enhancement of fusion yield; improvement of our understanding of the fundamental physics which determines plasma behaviour; and exploration of a number of issues central to the design of a Next Step tokamak. A wide range of experiments has been performed in addressing these issues and significant progress has been achieved. In addition, the foundation has been laid for a successful transition to the new phase of JET which will exploit the pumped divertor to address the key questions relating to the control of heat and particle exhaust and of impurity influxes.

Progress towards a Reactor

During 1991, significant progress was made in determining the conditions that will be required in a reactor. By using tritium, it has been possible to check predictions made in previous years concerning the power output and to assess whether the thermonuclear Q in JET with a D-T mixture were actually valid. In particular, the tritium experiments enabled detailed checks of the computer codes that have been used in predictions of the D-T performance. The outcome was that indeed the previous code predictions of Q_{DT} close to breakeven, have been fully justified. In Fig 175, a comparison is shown between the predicted 14MeV neutron yield and the measured yield, the very good agreement means that the code used for extrapolating to D-T conditions is accurately modelling the various physical processes such as the beam-thermal and thermal-thermal neutron emissions.

During the PTE series of experiments, discharges in deuterium were obtained in which the extrapolated Q_{DT} actually exceeded unity. The best discharge (Pulse No: 26087) had a D-D yield of 4.3×10^{16} neutrons and a Q_{DD} of 5×10^{-3}, the extrapolated Q_{DT} value was 1.14. The actual tritium pulses had a somewhat lower Q_{DT} value of 0.46. This was due to the reduced value of the fusion product $n_D T_i \tau_E$ in these particular pulses due to the early onset of the "carbon bloom". The $n_D T_i \tau_E$ values of the high performance JET pulses in both impure deuterium and in the D-T mixture pulses are compared in Fig.177 with data from other machines to illustrate the progress that has been made over the last 30 years.

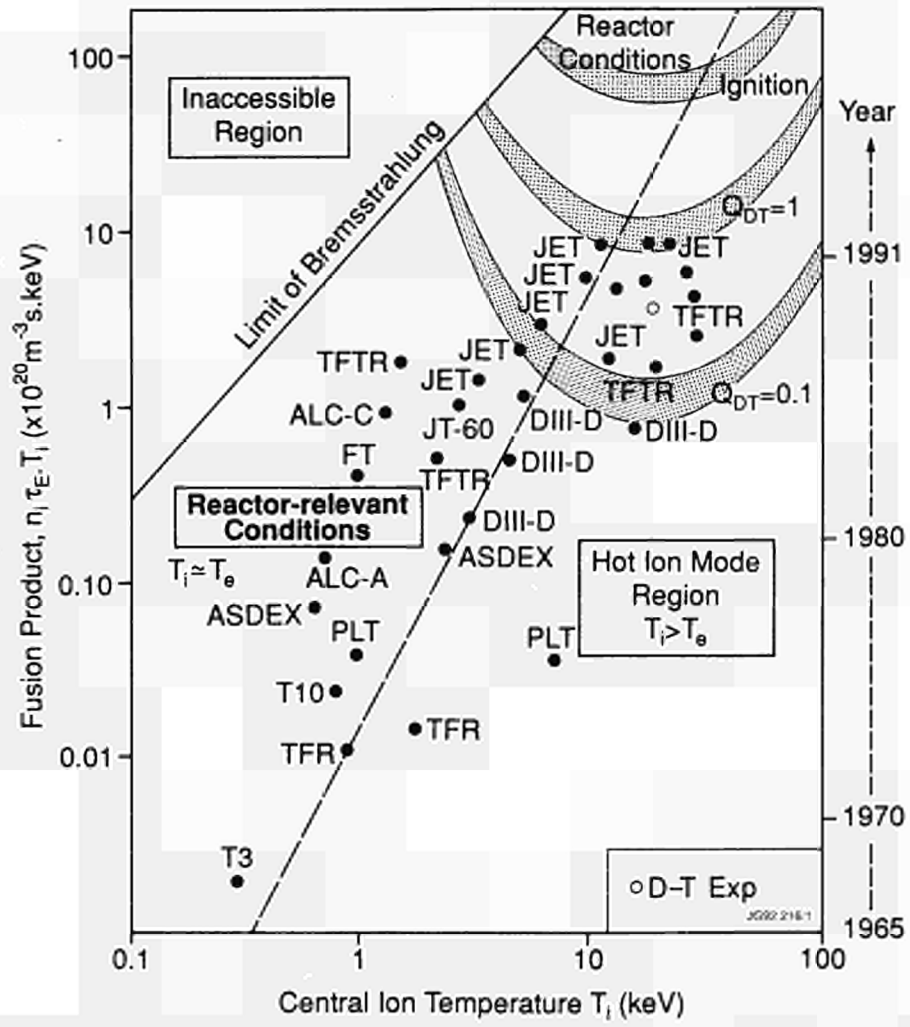

Fig 177: Triple fusion product ($n_D T_i \tau_E$) as a function of ion temperature, T_i, for a number of tokamaks worldwide.

Developments and Future Plans

In 1978, the original objectives of JET were set out in the JET Design Proposal, EUR-JET-R5, as follows:

'The essential objective of JET is to obtain and study a plasma in conditions and dimensions approaching those needed in a thermo-nuclear reactor. These studies will be aimed at defining the parameters, the size and the working conditions of a Tokamak reactor. The realisation of this objective involves four main areas of work:

i) the scaling of plasma behaviour as parameters approach the reactor range;

ii) the plasma-wall interaction in these conditions;

ii) the study of plasma heating; and

iv) the study of α-particle production, confinement and consequent plasma heating.

The problems of plasma-wall interaction and of heating the plasma must, in any case, be solved in order to approach the conditions of interest.

An important part of the experimental programme will be to use JET to extend to a reactor-like plasma, results obtained and innovations made in smaller apparatus as a part of the general tokamak programme. These would include: various additional heating methods, first wall materials, the control of the plasma profiles and plasma formation.'

At the start of 1991, the JET Project entered the last year of its planned Phase III - Full Power Optimization Studies. The general objectives of the experimental programme were to optimize performance and to explore the domain of high performance plasmas, studying aspects of plasma physics and engineering including: profile and heating effects; exhaust phenomena; and divertor edge physics. Priority was given to study of the power and energy handling capability of newly installed plasma facing components in regimes relevant to the Next Step and to the New Phase of JET.

Extensive studies had been made in the first and third areas of work of JET's objectives: reactor relevant temperatures (up to 30 keV), densities (up to $4 \times 10^{20} m^{-3}$) and energy confinement times (up to 1.7s) had been achieved in separate discharges. The second are of work had been well covered in the limiter configuration for which JET was originally designed. However, the highest performance JET discharges had been obtained with a 'magnetic limiter', (or X-point configuration). The duration of the high performance phase of these discharges exceeded 1.5s; this was achieved by careful design of the targets and specific operation techniques, but is limited, ultimately, by an unacceptably high influx of impurities, characterized by a rapid increase in electron density, effective ionic discharge and radiated power (referred to as the 'bloom').

The fourth area of work had been started by earlier studies of energetic particles produced as fusion products or by ion cyclotron resonance heating (ICRH). It was addressed further during 1991 by the first tokamak plasma experiments in deuterium-tritium mixtures. The high performance achieved in deuterium discharges, together with the experience gained in making substantial modifications to JET in a beryllium environment and with significant vessel activation, gave confidence that an experiment with about 10% tritium in the plasma could be performed and would provide data that could be used to plan an effective campaign of deuterium-tritium experiments in 1996.

Following extensive discussions during 1991, the JET Council approved the policy of a step-wise approach to the introduction of tritium in advance of the full D-T phase of JET operations. As a first such step, having obtained all necessary regulatory approvals, JET successfully carried out a preliminary tritium experiment in November 1991 (as already described). A release of fusion energy in the megawatt range in a controlled fusion device was achieved for the first time in the world.

The most recent experiments on JET achieved plasma parameters approaching breakeven values for about a second, resulting in large bursts of neutrons. However, in spite of the plasma pulse continuing for many seconds after reaching peak plasma values, the neutron count fell away rapidly as impurities entered the plasma and lowered its performance. This limitation on the time for which the near-breakeven conditions could be maintained is due to the poisoning of the plasma by impurities (the 'bloom'). This has further emphasised the need to provide a scheme of impurity control suitable for a Next Step device.

At its meeting on 19th December 1991, the Council of Ministers adopted Decisions concerning the Euratom Fusion Programme in the period to the end of 1994 and a modification to the Statutes of JET which prolongs its statutory lifetime by four years until 31st December 1996. The extension is to allow JET to implement the new Pumped Divertor Phase of operation, the objective of which is to establish the effective control of plasma impurities in operating conditions close to those of the Next Step. This programme of studies will be pursued before the final phase of full D-T operations in JET.

During 1991, a large proportion of JETs effort was devoted to preparation for the new pumped divertor phase of operations. Intensive design and procurement activities were continued to ensure timely delivery of the many components of the pumped divertor and related modifications to be installed during the 1992/93 shutdown.

Present achievements show that the main objectives of JET are being actively addressed and substantial progress is being made. The overall aim for JET can be summarised as a strategy "to optimise the fusion product ($n_i T_i \tau_E$). For the energy confinement time, τ_E, this involves maintaining, with full additional heating, the values that have already been reached. For the density and ion temperature, it means increasing their central values $n_i(0)$ and $T_i(0)$ to such an extent that D-T operation would produce alpha-particles in sufficient quantities to be able to analyse their effects on the plasma.

The enhancements to JET aim to build up a high density and high temperature plasma in the centre of the discharge (with minimum impurity levels) where alpha-particles could be observed, while maintaining an acceptably high global energy confinement time τ_E. The mechanisms involved are to decouple the temperature profile from the current density profile through the use of lower hybrid current drive and neutral beam injection to ensure that, at higher central temperatures, the current density in the centre does not reach the critical value that causes sawteeth oscillations.

This involves the following:

a) Increasing the Central Deuterium Density $n_D(0)$ by:
   - injecting deuterium pellets and high energy deuterium beams to fuel the plasma centre and dilute impurities;
   - injecting pellets to control the influx of edge material;
   - stabilising the m=2, n=1 magnetic oscillations present at the onset of a disruption with magnetic perturbations produced from a set of internal saddle coils which will be feedback controlled;

b) Increasing the Central Ion Temperature, $T_i(0)$ by:
   - trying to lengthen the sawtooth period;
   - controlling the current profile (by lower hybrid current drive in the outer region, and by counter neutral beam injection near the centre) to flatten the profile;
   - on-axis heating using the full NB and ICRF additional heating power (24MW, ICRH, and 20MW, NB)

c) Increasing the Energy Confinement time τ_E by:
   - increasing to 6MA the plasma current in full power, H-mode operation in the X-point configuration;

d) Reducing the impurity content, by:
   - using beryllium as a first-wall material to decrease the impurity content;
   - controlling new edge material by using the pumped divertor configuration.

In parallel, JET's preparations for the full D-T phase of operations have continued. In particular, JET has completed installation of all the main components of the active gas handling system in readiness for the system's commissioning programme. The JET Project is now in a position to enter the new phase of operations and next-step oriented studies in a pumped divertor configuration, leading to its final phase of full D-T operations. The following sections describe various developments which are underway on JET to implement these systems.

Current Drive and Profile Control

The main objectives of current drive and profile control remain :

- to suppress sawtooth activity and to benefit from higher core reactivity by sustaining peaked profiles of both density and temperature ;
- to modify local values of the current gradient and improve energy confinement in the plasma centre ;

- to assess the efficiency required for non-inductive operation of large tokamaks.

The main tool which is being prepared to control the plasma current profile in JET is the generation of non-inductive current by means of Lower Hybrid (LH) waves. First results with a prototype system (L0) have already been obtained. The full system (L1) will be installed during the 1992 shutdown. A high directivity ICRF antenna has also been prepared to drive a substantial amount of non-inductive current by means of either minority current drive or direct electron pumping. These antennae (A2) will be installed during the 1992 shutdown. Non-inductive current drive can also be produced by means of 140 keV neutral beams (NB) and by the bootstrap current.

A large quantity of data on current drive has been obtained during the 1991 campaign including the achievement of :

- 1.5 MA full current drive discharge with LHCD in combination with ICRH;
- discharges where the bootstrap current was up to 70 % of the total current in ICRF heated plasma. The corresponding energy confinement time was up to 1.7 times the H-mode scaling;
- good control of sawteeth by producing localised minority ion current drive near the q= 1 surface [1].

These data are encouraging for profile control and current drive application to future large experiments. In particular, it is proposed to drive the full current in a reactor with the following scenario:

- a seed current generated at the plasma centre by ICRF fast wave current drive (independent of density) or NBI current drive;
- large bootstrap current, in excess of 50% of the total required current, generated at approximately mid-radius;
- LH current drive generated in the outer plasma region.

The large systems which will be implemented on JET during the 1992-1993 shutdown should allow assessment of the proposed scenarios for a reactor.

Bootstrap Current

The difficulty in achieving the required non-inductive current drive efficiency for reactor grade plasmas has led to the proposal of bootstrap current dominated fusion plasmas. During previous JET experimental campaigns, bootstrap currents have been observed to constitute up to 35% of the total plasma current in NBI [2] or ICRF heated H-mode regimes. This current is located near the plasma boundary,

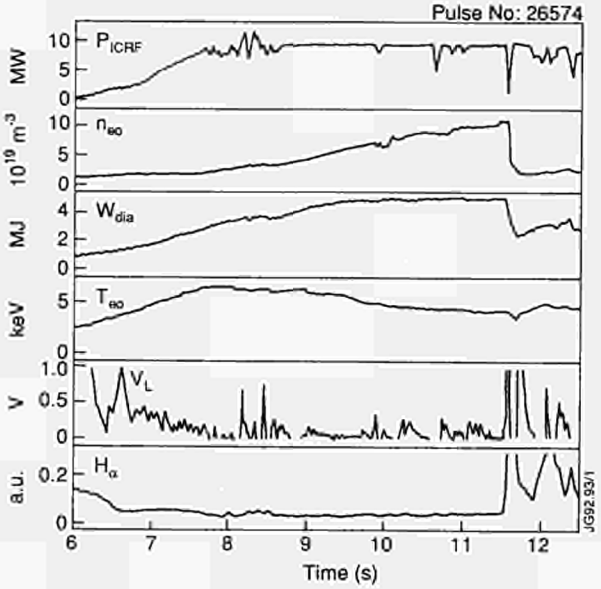

Fig. 178: Time history of a 1.5MA bootstrap dominated plasma discharge. Plasma energy reaches 5MJ and poloidal beta reaches 1.6 for 10MW ICRF input power ($B_T = 3.1T$). Estimated bootstrap current is 0.9 MA.

where the density gradient is steep, and the current profile seems to broaden significantly. However, the proposed scheme lacked, experimental demonstration of higher bootstrap current fraction without central particle fuelling, i.e without NBI and indications of the MHD stability of bootstrap dominated plasmas.

The use of high β poloidal plasmas (H-modes produced with ICRH only at low plasma current) has permitted generation of high fractions of bootstrap current and demonstrates a good MHD stability of such plasmas (up to $\beta \leq 2$).

For a total plasma current of 1 MA, with 6 MW of ICRF power of, about 75% of the plasma current was estimated to be driven by bootstrap current. In Fig 178, an example of such a discharge at $I_p = 1.5$ MA with 8 MW of ICRF power is shown. Data are still being analysed, but it is estimated that more than 60% of the total plasma current is driven by the bootstrap current with a broadening of the current profile and disappearance of sawtooth oscillations. It is to be noted that the energy stored in the plasmas reaches 5MJ which indicates good confinement, about 1.7 times above normal H-mode scaling.

ICRF Current Drive

Ion cyclotron waves can induce non-inductive current drive either by asymmetric heating of minority ions (minority current drive) or by direct interaction between the fast wave and electrons. The first scheme can produce very localised currents, although with a relatively low efficiency, and

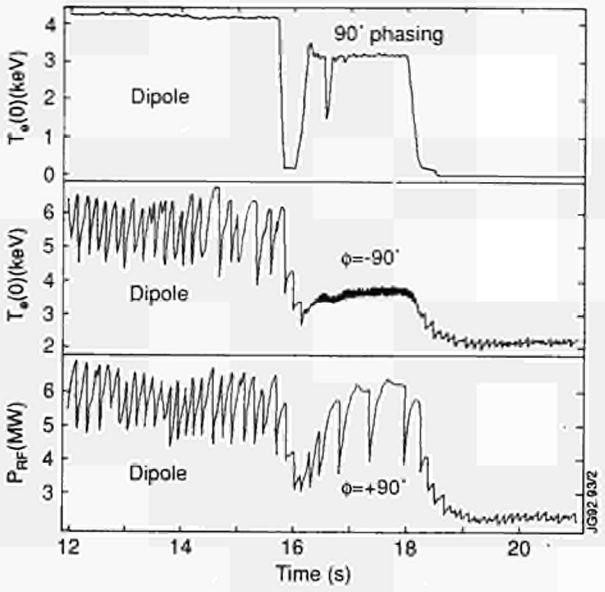

Fig. 179: Dependence of sawtooth behaviour with phasing of ICRF antennae. The large change in amplitude and frequency of sawteeth is attributed to ICRF minority current drive at q=1

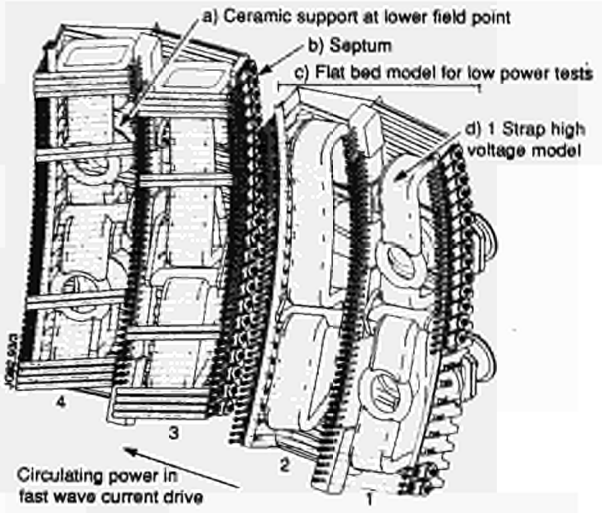

Fig. 180: Diagram of one of the A2 ICRF antennae

therefore can be very useful for local profile current control. The second scheme appears to be a promising current drive method for a reactor grade plasma namely due to its ability to drive central currents independent of the density value.

With the capability to control the phasing between the two striplines of an ICRF antenna significant results have been achieved with minority current drive. These experiments are of a preliminary nature, since the directivity of the two strap antennae is small. The theoretical estimate of this directivity is still under investigation and might vary between 25% and 60% depending upon the model of plasma coupling and damping mechanisms. By locating the minority ion fundamental resonance tangential to the q=1 surface, local plasma current gradients can be strongly modified. Since the current density gradient is the controlling element in sawteeth oscillations, minority current drive produces a dramatic effect on sawtooth oscillations. These results constitute the first practical demonstration of fast wave current drive.

An example of the effect of phasing the antenna with ± 90° on the sawtooth activity is shown in Fig 179. A systematic study of minority current drive is described elsewhere in this report. In particular, by comparing the behaviour of the sawteeth activity when the resonance is located on the inboard or on the outboard side of the plasma, it has been possible to assess that this effect was due to current drive effect and not to a localised heating effect. This minority current drive scheme can be used in a reactor grade plasma not only to stabilise the sawtooth activity, but also to achieve some burn control.

The interaction between the fast wave and electrons is a coherent combination of two forces parallel to the direction of the electric field :

- electron Landau damping (similar to LHCD);
- transit time magnetic pumping (TTMP), where the driving force is the product of the electron magnetic movement and of the magnetic field gradient.

Electron Landau damping and TTMP produce currents in the opposite direction. The TTMP component is dominant when the electron beta of the plasma is large or at low wave frequency; TTMP current drive will therefore occur at the plasma centre where the beta is a maximum. The advantage of TTMP current drive compared to other schemes is the absence of density limit. Direct electron absorption can be due to other processes such as torsional Alfvén wave and mode conversion of the ICRF fast wave [3, 4]. The importance of these different mechanisms for current drive remains to be investigated.

Some initial experiments have been carried out in 1991 with the new phasing facility. Unfortunately, with the existing system, it is not possible to phase the two strip-lines when the coupling is too low, such as in H-mode plasma operation which is required to achieve the necessary high beta. In limiter plasmas, the beta is much lower and, therefore, the damping is lower. Competing ion cyclotron damping mechanisms including second harmonic and third harmonic resonance (in particular, on the beams) have prevented the observation of net TTMP current drive.

Table XV: Antenna Parameters

		JET(A1)	JET(A2)	ITER
Antenna conductor to limiter distance	a(m)	0.06	0.12	0.2
Antenna conductor to backwall distance	d(m)	0.1	0.25	0.3
Antenna conductor screen distance	χ_{sc}(m)	0.012	0.012	0.3
Length of one antenna element	ω_y(m)	0.8	0.8	1
Half-width of the antenna element	ω_z(m)	0.055	0.105	0.125
Current propagation constant in y	$\beta(m^{-1})$	2	2	1.57
Number of boxes energized	N_{box}	8	4	30
Number of antennas per box	N_y, N_z	2.2	2.4	2.1
Mid-line distance between conductors	L_z(m)	0.31	0.4	0.55
Maximum directivity	D		0.85	0.9

However, the new antennae array which has been designed for the new phase of JET will not only significantly improve the directivity but will also allow operation at lower plasma impedance in the phasing mode [5]. The new antennae which are being built have four central conductors equally spaced in an integrated structure of two antenna boxes each with a septum that decouples adjacent conductors. The eight antennae will be rearranged around the torus in order to prevent intersepting the neutral beams. Their characteristics are given in Table.XV.

During 1991, the design of these antennae was completed and manufacture has started. A diagram of one antenna is given in Fig 180. A full scale quarter antenna prototype has been tested in vacuum for full current and voltage, in parallel with the production of series antennae (see Table XVI) [6]. A second full scale test at low power has enabled practical verification of the conductor current distribution and other RF parameters. In addition, this is also being used to design further developments of the ICRF plant control for handling the cross-coupled power associated with phased antenna currents for Fast Wave Current Drive experiments. A collaboration between JET and USDoE is being prepared, focussing on the subject of controlling the new four-strap ICRF antenna array, to be installed in the divertor phase.

Table XVI: Summary of A2 RF Testing

SHORT ASSEMBLY TESTS	
Ambient Temperature	200°C
Test Pressure measured in VTL	$<5.10^{-5}$ mbar
RF Pulse Length	20s
Test Frequencies	55, 42 and 24MHz
Duty Cycle	20:1
Test Parameter	**Performance achieved**
Measured Antenna Resonance Frequencies	$\lambda/4$ at 38.8MHz, $\lambda/2$ at 58MHz
Peak Line Voltage	45kV at all test frequencies
Peak Line Current	1.5kA at all test frequencies
Above RF tests repeated with Open Circuit Strap.	49kV standoff @28MHz.
ADDITIONAL TESTS	
	Performance achieved
Independent RF testing of A2 ceramic screen resistors	65A for 20s pulses at 48MHz with 10:1 duty cycle. Temp rise during pulse 300°C above ambient
Independent Disruption simulation testing of screen resistors	680A (peak) during quasi-sine wave pulses of 13ms duration (35kW total dissipation).

Due to coupling between conductors of the four-strap A2 antenna (Fig.180), the matching will have to be controlled by a new algorithm linking the control and protection system of four generator output instead of two as at present. This matching algorithm which is necessary for plasma heating, will be extended to include non-zero or π phasing of the antenna to optimise the directionality and the sharpness of the spectrum [7]. A two-strap algorithm was successfully tested on the A1 antennae and led to important minority current drive results.

In addition, a high power RF transmission line device, called a conjugate box, may be required to allow circulating RF power associated with the phased conductor operation. Without this, the power of the generators and the range of spectra available will be limited to high plasma coupling conditions (> 4W). JET has proposed a system using a 3 dB power combiner (see Fig.181) and the collaboration with

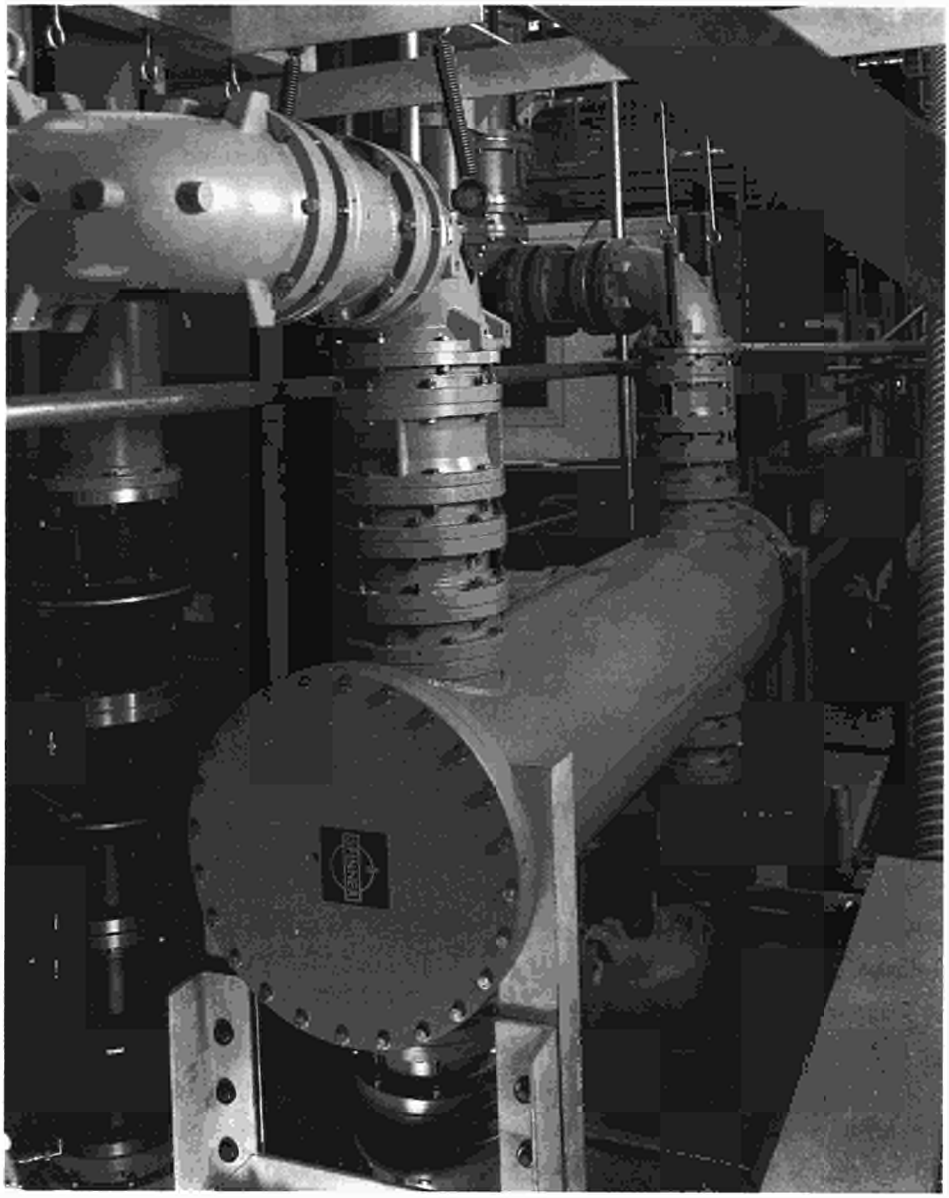

Fig. 181: View of a 3dB combiner proposed to recirculate cross-coupled ICRF power during phased experiments.

ORNL, US-DoE will be for the modelling, design and prototype manufacture of this conjugate box, together with participation in the FWCD experiments on JET. ORNL is responsible for the four-conductor (or strap) antenna in DIII-D. They already have a comprehensive calculation of the antenna electrical circuits and radiated spectrum.

Lower Hybrid Current Drive

The main characteristics of the JET LHCD system are shown in Table XVII. The programme is organised in two stages: the first consists of a prototype launcher installed during the 1989/1990 shutdown. This prototype has the main technical features of the complete system, which will be installed during the 1992 shutdown [8]. Slight modifications of the geometry of the multijunctions arrangement is required in order to fit the new magnetic geometry of the pump divertor phase.

To assess the radial profile of the LH induced fast electrons and to study the radial transport of the fast electrons, tomography of the fast electron bremmsthralung emission is being implemented using the general set-up of the neutron tomography system [9]. The vertical camera was installed during the 1990 shutdown and the horizontal camera was installed during the 1990/1991 shutdown. This diagnostic, together with the analysis of the non-thermal electron cyclotron emission, is the main tool for the interpretation of LHCD experiments [10].

Table XVII: The JET LHCD System

Generator	Prototype system
Frequency	3.7 GHz
No of klystrons	24
Power (launched)	10MW
Launcher	Multijunction type
Fixed phasing in the multijunction	90 degrees
Central $N_{\|\|}$	1.8
Range of $N_{\|\|}$	1.4 - 1.8
No of waveguides in horizontal row	32
Phase accuracy	10 degrees
Width of the $N_{\|\|}$ spectrum	0.2
Directivity	80 %
Density limit	8×10^{20} m^{-3}
Power handling	4-5kW cm^{-2}
Estimated drive current	
at $n_e = 2 \times 10^{19}$ m^{-3}	3.6MA
at $n_e = 5 \times 10^{19}$ m^{-3}	1.2MA

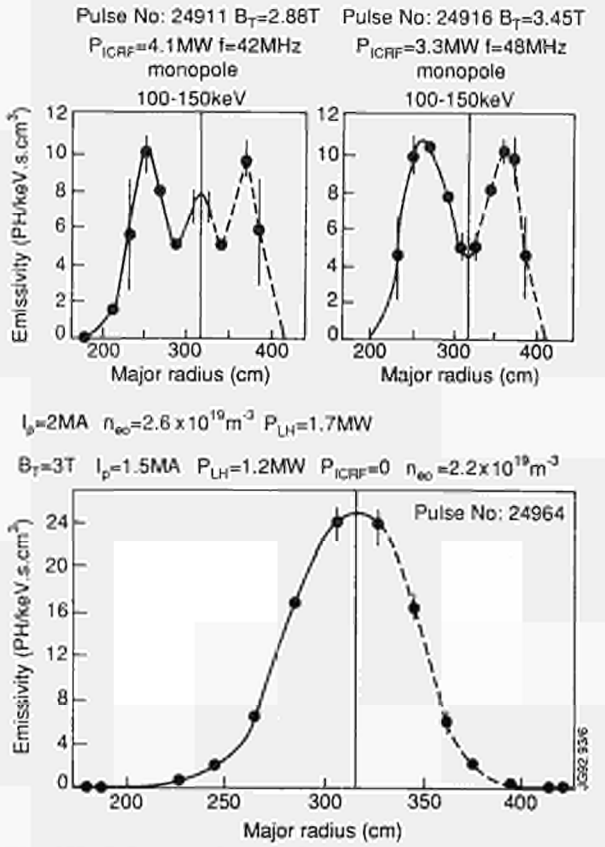

Fig. 182: Influence of some plasmas parameters upon radial profiles of photons emitted by LHCD induced fast electrons. Data are obtained from Abel inversion of signals from the Fast Electron Bremmsthralung (FEB) horizontal camera

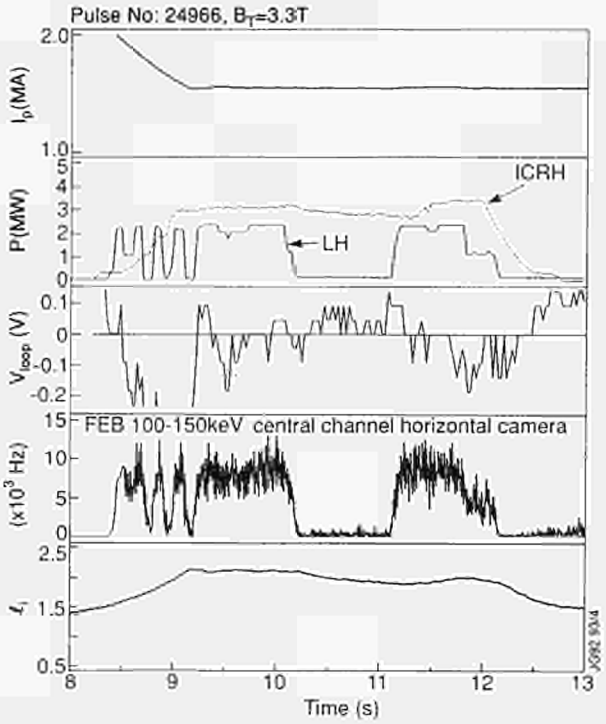

Fig. 183: Full current drive plasma discharge with combined LHCD and ICRF at 1.5 MA. During Lower Hybrid modulation, the loop voltage became negative while the plasma inductance was slightly increasing

The main results with the prototype launcher, related to current profile control, are the following:

- radial fast electron profiles can be either peaked or hollow depending upon plasma parameters such as density or magnetic field as shown in Fig.182. These dependences are in qualitative agreement with theoretical predictions [11];
- full current drive in almost steady-state conditions has been achieved with LHCD alone at plasma current of 0.4 MA and in combination with ICRF at plasma current up to 1.5 MA. An example of such a discharge is given in Fig.183 [12];
- synergistic effects between ICRF and LHCD have been observed. As shown in Fig.184, where the photon energy distribution, as observed with the horizontal FEB camera, is indicated for various plasma conditions, fast electrons created by LH waves are further accelerated by the ICRF fast wave;
- current drive efficiencies can be deduced taking into account synergisitic effects with the ICRF fast wave (10% of the ICRF power is estimated to be directly coupled to the fast electrons) and an estimate of the bootstrap current generated. Efficiencies increase with the electron temperature as indicated in Fig 185. Efficiencies up to $nRI/P = 0.4 \times 10^{20}$ m^{-2} MA/MW have

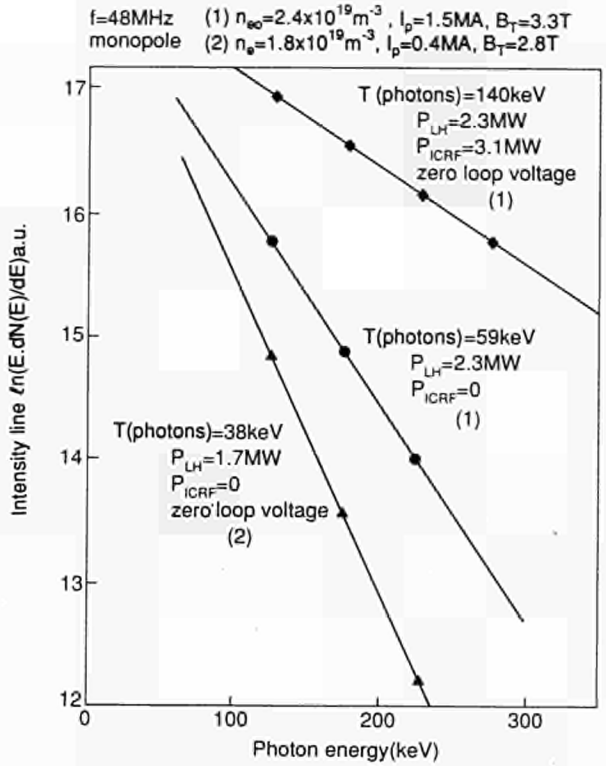

Fig. 184: Increase of X-ray energy spectra from the Fast Electron Bremmsthralung (FEB) horizontal camera due to synergy between LHCD and ICRF. The mechanism responsible for the acceleration of fast electrons created by LHCD is under investigation.

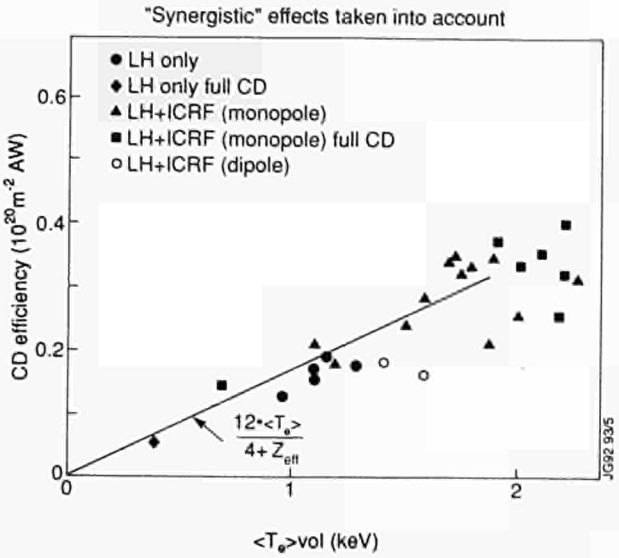

Fig. 185: Current drive efficiency versus volume averaged electron temperature taking into account bootstrap current and synergistic effects (assuming that 10% of the ICRF power is coupled to the fast electrons)

been obtained. Although these current drive efficiencies are the highest achieved, they are still lower than those required to fully drive the plasma current in a reactor, this is estimated to be between 0.4 and 0.8 x 10^{20} m^{-2}MA/MW at densities near 10^{20}m^{-3} depending upon the amount of bootstrap current which can be generated by other heating mechanisms.

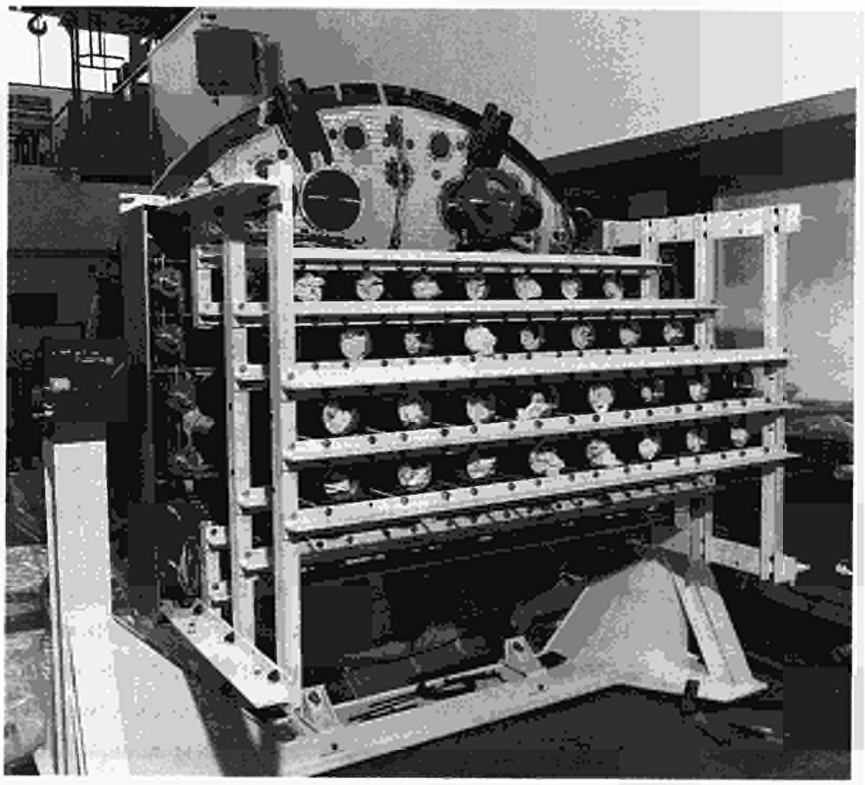

Fig. 186: View of the L1 launcher end plate in the JET Assembly Hall

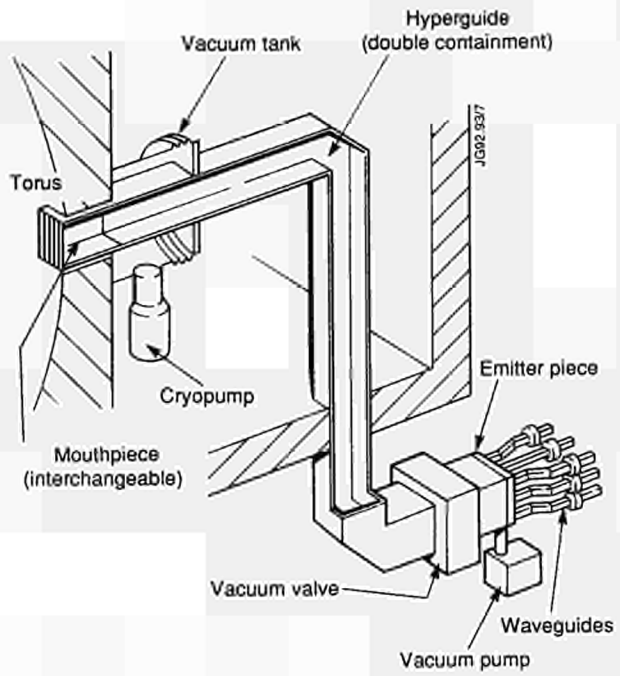

Fig. 187: Layout of a reactor relevant LHCD launcher using an hyperguide vacuum transmission line

The L1 launcher which has been modified to take into account the pumped divertor geometry is in the assembly phase. A view of the end plate where the forty-eight double vacuum windows will be welded is shown on Fig.186. This launcher will be able to match the so called "fat plasma" configuration, but it will not be possible to use the launcher with the alternative "thin" plasma configuration.

To overcome this problem, a conceptual solution has been studied which is based on a new concept: the "hyperguide". The hyperguide is a T_{E012}, large overmoded waveguide of ~5m long and may transmit large RF power with good vacuum conditions allowing avoidance of the electron resonance zones where breakdowns are likely to occur. Such a system can make use of the present vacuum vessel and of the L1 end plate. It will be less costly to build than the L1 launcher and might accommodate either a short conventional waveguide mouth or possibly a quasi-optical coupler. Studies are still continuing on this new development. A possible application to ITER type experiments is sketched in Fig.187.

References

[1] D. Start et al. in Proc. IAEA Tech. Comm. Meeting on Fast Wave Current Drive in Reactor Scale Tokamaks, Arles, France (1991), to be published.

[2] C. Challis et al. Nuclear Fusion **29** 4 (1989) 653

[3] J. Jacquinot and JET Team, in Controlled Fusion and Plasma Physics (Proc 18th Eur. Conf., Berlin, (1991) Vol 33, No. 13

[4] V.P. Bhatnagar et al. in Proc. 9th Topical Conf. on Radio Frequency Power in Plasmas, Charleston, USA (1991)

[5] V.P. Bhatnagar et al. in Proc. IAEA Tech. Comm. Meeting on Fast Wave Current Drive in Reactor Scale Tokamaks, Arles, France (1991), to be published.

[6] T. Wade et al. Proc. 14th Symp. IEEE Symp. on Fusion Eng. San Diego, USA (1991)

[7] G. Bosia, et al. Proc. IAEA Tech. Comm. Meeting on Fast Wave Current Drive in Reactor Scale Tokamaks, Arles, France (1991), to be published.

[8] M. Pain et al, Proc. 13th Symp. on Fusion Eng. Knoxville, USA (1989).

[9] C. Gormezano et al 32nd APS Meeting, Cincinatti, USA (1990) and (JET-IR(90)07).

[10]P. Froissard et al, in Proceedings 18th Eur. Conf. Cont. Fusion and Plasma Phys., Berlin, Germany (1991) III, 393.

[11]M. Brusati, in Proc. 8th Topical Conference on RF Power in Plasmas, Irvine, USA (1989) AIP (1990).

[12]C. Gormezano et al. Proc. IAEA Tech. Comm. Meeting on Fast Wave Current Drive in Reactor Scale Tokamaks, Arles, France (1991), to be published.

Pellet Injection

This section summarises the work on newer developments relating to pellet injectors for fuelling on JET. Until the latter part of the year, JET had planned to implement for the divertor and later phases of JET a repetitive high-speed pellet launcher system - the Advanced Pellet Launcher APL. This would have been alongside an intermediate-speed repetitive pneumatic launcher, JPL II, as a replacement for the present launcher (JPL I), built by Oak Ridge National Laboratory (ORNL). In addition, there would be a low-speed pellet centrifuge. Due to the budgetary situation at JET and in the USA, the APL will now not be pursued for financial reasons, and the negotiations on the supply of an upgraded ORNL Launcher JPL II were not fruitful. Although JET owns the rights to proceed with the conceptual design of the JPL II, jointly carried out by ORNL and JET, insufficient funds and manpower made it impossible to proceed. However, JET decided to follow up the work on the high-speed prototype launcher, which was not yet successfully completed, and on the centrifuge. Nevertheless,

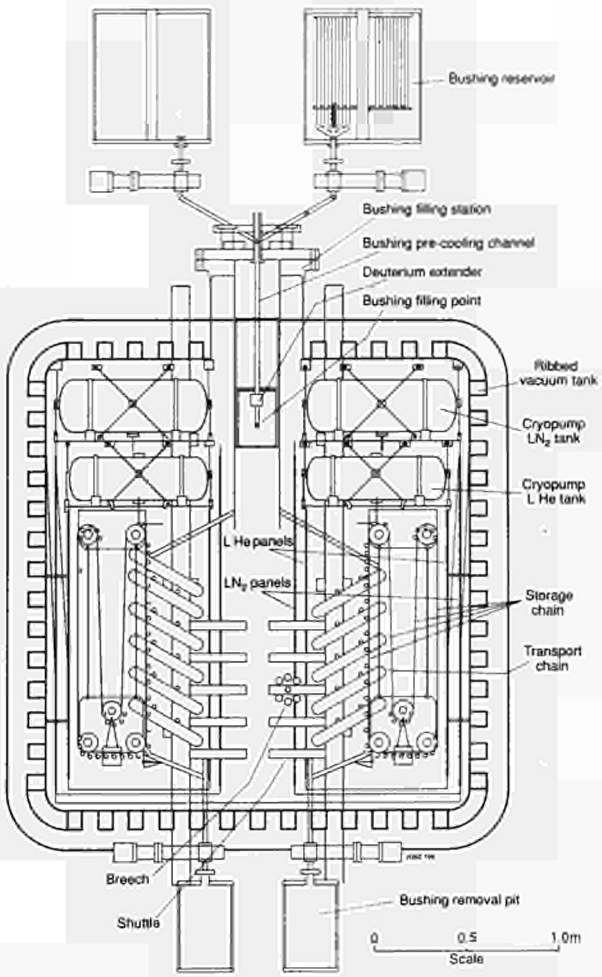

Fig. 188: Cross-section of the main Advanced Pellet Launcher (APL) cryostat

considerable efforts had been put into the APL design/ preparation and these are reported here, together with those on the centrifuge.

The Advanced Pellet Launcher (APL)

An attempt was made to design the APL from first principles rather than expanding a laboratory scheme, as in the case of the high-speed prototype pellet launcher. The basic design principles and design philosophy were outlined in the 1990 Progress Report. The two-stage gun system of up to 10 guns would use the successful two-stage gun of the prototype as start-up and upgrade the performance of this pneumatic driver at a later stage by lengthening the pump tube (from 3 to 5.5m, which would increase the compression ratio and therefore the adiabatic heating of the second stage driver gas). For higher performance, materials with higher figures of merit with respect to thermal resistance and mechanical stress than those for barrel/nozzle, compression head of pump tube and piston (now hardened austenitic, martensitic and titanium, respectively) will have to be employed. Therefore, the main emphasis was given to the design of the APL main cryostat. This unit comprises the breech region of the ten guns, the storage and transport of bushings (i.e. short, ~2cm sections of the barrel which contain bursting disc, sabot - a cartridge in support of the pellet during acceleration - and pellet which are prepared off-line before the operation) and the bushing filling station, which has the bushing reservoir and the bushing removal pot attached to it.

Fig.188 shows a diagram of the main cryostat as a cutaway almost perpendicular to the ten barrels which are focused under a shallow angle of a few degrees towards a point in a main horizontal torus port. The task of loading and firing the gun requires bushings at a temperature of less than 6°K to be brought into one of the breechs, to close the upstream and downstream barrel sections (which in repetitive action have to be regarded as warm) onto the bushing. This must cope, while the gun is firing, with leaking gas from the high-pressure surge (several 1000 bar for about a millisecond) into the pellet storage environment which is required to be at vacuum pressures of less than 10^{-6} mbar and at temperatures of less than 6°K. Experimental breech leak rate integrals - in the range of 1 to 10^2 mbarℓ - have been established at JET and under the supporting work at Centre d'Etudes Nucléaires de Grenoble (CENG), France. These assure that the open breech design is viable when the gas load is pumped by the cryopump (approaching $10^6 \ell s^{-1}$) pumping speed with a vacuum conductivity from the breech in the region of $10^3 \ell s^{-1}$ - surrounding the storage area for the bushings without leading to thermal loads to the stored bushings. The vacuum vessel - for reasons of the amount of hydrogen (from an accidental release of second and first stage gas of a gun) and deuterium from the pumping during pellet production and storage of up to 2500 barℓ - needs to be designed for a worst case scenario deflagration pressure surge of 23 bar absolute.

The bushings, already equipped with sabots and bursting discs, flow from a reservoir, containing sufficient bushings for about a week of operation and being exchanged by remote handling after that period, to the bushing filling station. The detailed design and first testing of a filling station cryostat for the APL is being carried out by CENG under an Article 14 contract. The test unit is now in the commissioning stage. It contains a channel to cool down bushings to 14°K (by gas contact with cryogenic heat exchanger walls), transfer mechanism to guide them one at a time to the filling point where deuterium is extruded from

a piston extruder into the bushing to form pellets at 14°K. At the filling station, the bushing is then cooled to less than 6°K and released into the transport chain of the APL. The entire filling cycle takes about two minutes excluding bushing cool-down. In the test unit, the bushing is released into an optical observation station to check the resulting ice quality. An additional LHe cryopump in the filling unit handles the gas loads of the various processes so that the bushing can be delivered smoothly into the main storage environment.

The latter is formed by two of the cryopumps, each serving the five guns on either side. The main storage support is a chain holding up to 200 filled bushings and allowing them to be handed over slowly to smaller transport chains serving individual barrels. Whereas the storage chain is not subjected to any timing specifications the transport chains are to permit advancing and releasing bushings to the shuttle at about one per second. So far, the bushings are in an environment in which they can safely remain for a day or so. After being loaded into the shuttle to bring them into the breech, time is important because they have to leave the cryopump to be handed over to a warm breech, which is designed for cooling to LN_2 temperatures, but certainly not lower. Therefore, the shuttle was conceived to be a magnetically levitated transport system using new high-temperature superconductors and propelled into the breech by linear electrical motor action. Over most of the time, the shuttle will rest in the LHe cryopump; once the bushing is trapped by closing the breech the shuttle returns to a safe environment. The bushing transfer time is thought to be ~15ms, and the breech closure time ~5ms. The breech is opened (slowly) by pneumatic high-pressure helium actuators, counteracted by 30 kN spring stacks and closes on quick release of the helium. The principle design strength of the breech is aimed at 300 kN breech closure, most of it assumed to be generated by the action of the two-stage gun itself, since the pressure surge of the compression head is acting on the upstream barrel. After opening the barrel, the bushing drops out and is guided to a collection pot at the bottom of the tank, which finally also has to be removed by remote handling in an action similar to the system on top for bringing-in new bushings.

The design had concentrated on the vacuum vessel, cryopump and breech section. When the work on the APL was stopped, the vacuum tank had been subjected to finite element analysis and was ready to go to tender, the LHe and LN_2 panels for the cryopump had actually gone to tender and the remainder of the cryopump was ready to do so. The breech was being detailed and the storage chain, transport chain and shuttle were being worked on. Also part of the gun system for the first generation of guns (identical to the prototype launcher guns but equipped with fast first-stage gas release for repetivity) and the related high-pressure gas introduction and exhaust services were in preparation for tender action. Non-procurement of a vacuum vessel, half the size of the APL main cryostat tank for the pellet testbed, will not now permit early testing of the centrifuge extruders.

The Pellet Centrifuge

The pellet centrifuge is to provide a source of deuterium particles at varying depths beyond the recycling layer and with it a minimum recycling flow into the divertor, which is sufficiently strong to sweep impurities into the divertor and hinder impurities to flow back from it. The injection parameters chosen are pellet sizes of 1.5 - 3mm at repetition frequencies up to $40s^{-1}$ at speeds in the range of 50-600ms^{-1} for long pulses approaching 1 minute. At the upper end, this provides up to 1000mbarℓs^{-1} of gas flow regardless of pellet speed and the penetration depth variation is over a factor 12 (neutral gas shielding model assumed).

An outline of the first conceptual design as well as the plan for positioning the centrifuge at Octant No: 2 midplane, alongside the pneumatic pellet injector, was given in the 1990 Progress Report. The detailed design (see Fig.189) of the vacuum vessel, the centrifuge and the cryopump, needed to absorb the gas load evaporated from the pellets during acceleration and guidance, has been finalised. Vessel and internal cryopump may be subjected to a hydrogen-air deflagration pressure surge in the event of an undetected air leak, with arbitrary amounts of air drawn onto the cryopump which may have a monitored accumulated deuterium ice quantity as high as 2500 barℓ. The worst case scenario in this ~ $5m^3$ vessel would then lead to a 23bar absolute deflagration pressure peak, and the design does take this condition into account. This is a necessity, since in the D-T Phase of JET, the deuterium returning from the recovery plant will still be slightly tritiated.

Contracts for the centrifuge on the basis of a Pfeiffer TPH 5000 turbopump and attached rotor arm (the same as employed for the ASDEX Upgrade pellet centrifuge) and for the cryopump LHe panels have been placed. The vacuum vessel and the internal cryogenic vessels are out to tender and contracts will be placed at the beginning of 1992. JET will carry out the assembly work, which integrates the

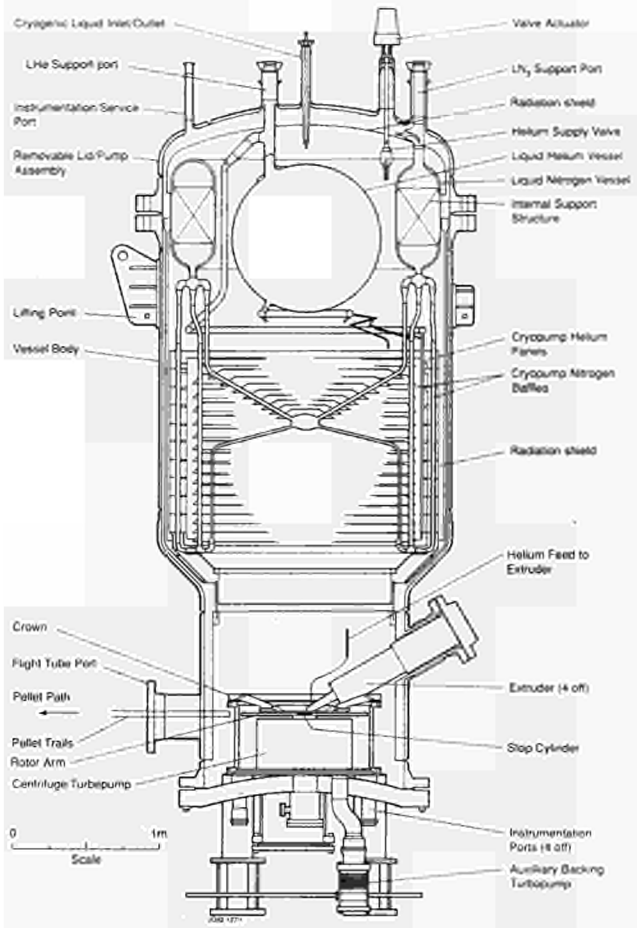

Fig. 189: The Pellet Centrifuge.

cryopump into the vacuum vessel; the cold valves for the distribution of LHe and LN_2 will be mounted from the upper lid of the vessel. Tenders are in preparation for the cryopump, LN_2 baffles and the vessel support steelwork. Design work is in progress concerning the pellet guide track to the torus, the control cubicles (a local one employing an Allen Bradley PLC 5/15 and interfacing to the new CODAS work station), the cabling as well as gas, vacuum and helium piping and related services.

The most demanding technical problem is the design of the extruder units which must provide the pellets of specific size to the rotor arm. Up to four can launch pellets into the acceptance angle of the "stop cylinder", a stationary cylindrical diaphragm with a window in the correct starting position for the pellet on the rotor arm; a blade attached to and running around with the rotor hub directs the pellets to the window. The pellets are to be formed by extrusion from a deuterium ice reservoir of ~ 150 cm^3, held at about 14°K, into a nozzle of pellet dimension cross-section and have to be cooled dynamically during extrusion (over a nozzle length of about 180 mm at a maximum extrusion speed of 160 mm/s) to about 7°K. At the end of the extrusion process, pellets are chopped off at required lengths by an electromagnetic punch. The extruder unit, which is about 1 m long, has been conceptually designed from the hydraulic actuator for the extrusion to the deuterium reservoir and nozzle, and, in particular, the coolant flow/heat transfer calculations for helium two-phase flow have been carried out. The detailed design is now being started. The dynamic cooling of the deuterium, needed for the huge quantities of quasi-continuous injection, has so far never been attempted and bears some risk 'in principle' as to the achievement of the correct ice quality, although it seems a natural extension of the isothermal extrusion used so far (e.g. at IPP Garching, Germany). In the first instance, the extruder in an isothermal mode will be commissioned, in which case, the total number of pellets for a tokamak pulse will be limited to about 40 and then expand the operational parameter space to the long-pulse operation. Experiments with early commissioning of the extruder in an APL test bed tank will not now be possible and will have to await the centrifuge main vessel and cryopump completion.

The New Phase of JET: The Pumped Divertor

In 1991, there was no major changes to the pumped divertor concept or components, as described in the 1990 JET Progress Report. Detailed design of all major components proceeded and procurement contracts were placed for all long delivery items. In addition a large effort was made to study the assembly procedures and design of the related assembly jigs and tools.

Magnetic Configuration and Plasma Control

Configuration Studies

The current requirements for sweeping the diverted plasma across the target plates have been established using the PROTEUS code with the objective of maintaining a good match of plasma to the shape of the ICRF antennae and of avoiding excessive currents in the poloidal field (PF) coils. The effects of changing the current profile were also examined. It was possible to obtain 6 MA FAT and 5 MA SLIM configurations without the need for shaping currents (P2/P3 coils in series) exceeding 40 kA. The improved 6 MA FAT

configuration was obtained by the use of small reversed current of -4 kA in the outer divertor coils, D4. In the original FAT configuration the inner and outer coils D1 and D4 were currentless.

Preliminary studies were performed relating to the current rise phase of the plasma. From these it appears possible to establish the divertor configuration already at an early phase when the plasma current is still below 1 MA. This possibility relies however on the requirement that the current rise is performed at full plasma size. The ramp rate may have to be limited to avoid MHD instability which could arise from a hollow current profile.

The magnetic field topology in the vicinity of the target plates was examined in some detail. These studies provided necessary information for the design of the target plates, for example to define the tilt angles of the plates at the inner and outer strike zones of the separatrix.

Magnetic Measurements for Plasma Control

The present magnetic measurement system must be enhanced to obtain the desired control parameters in the presence of the divertor coil current, namely: the plasma current, the current moment with respect to the mid-plane, the location of the X-point, and the gaps between the plasma boundary (separatrix) and in-vessel structures (poloidal limiter, disruptions feedback coils, inner wall protection tiles). The studies performed so far indicate that the plasma current and the current moment can be obtained with sufficient accuracy using the existing set of 18 internal pick-up coils and 14 external saddle loops, combined with measurements of the divertor coil currents. There is no need to employ signals from new pick up coils which will be located near the target plates and which may therefore have a higher risk of damage. It is of particular importance to ensure a high reliability of the current moment measurement which is vital for the vertical stabilisation.

Eddy Current Effects in JET Structures

The eddy currents and forces expected during disruptions at JET elements such as divertor target plates and the lower hybrid launcher have been further studied by several analytic and computational means. The assessment of divertor elements will continue to ensure that any design modification is compatible with the expected forces. The estimated forces at the present lower hybrid launcher are within acceptable limits.

Divertor Coils

The divertor coils will be mounted inside the JET vacuum vessel and the magnetic field is designed to enable the creation of various divertor plasmas.

There was no significant change to the coil design in 1991. The coils are of conventional construction (water cooled copper, epoxy glass insulation [1]) and are contained in thin Inconel cases. The coils are supported from the vacuum vessel by hinged links, which allow the vessel to expand independently of the coils. The links are joined to the coils by Inconel 625 clamps and to the vacuum vessel by welded on blocks. These blocks are the first components to be welded onto the vessel and are designed to form a well aligned ring of supports.

The coils are manufactured in two stages, first at the coil contractor's factory and finally in the JET vacuum vessel. The work at the factory includes:

a) forming the conductors to the correct radius to make half or third turns;
b) pre-assembly of coils to check conductor size and shape;
c) application of dry glass and Kapton insulation to conductors.

A problem which was examined in 1991, is that of the behaviour of the coil insulation when subjected to radiation doses. Development work carried out by NET has shown that boron free glass fibre (R-glass) has a much greater radiation resistance than E-glass which contains typically 6-9% of boron oxide. It was decided to use boron free glass fibre for the JET divertor coils. Another aspect is that of the gas evolution from the epoxy resin under neutron and gamma irradiation. Tests have been organised to verify data from the literature and provisions were made in the design to pump out any gas evolving inside the coil case.

The coil cases are made by another contractor. They are pressed out of 1.2mm thick Inconel sheets to make curved channels and then welded together to make quarter circumferential channels. (Thus four quarter sections make a lower case and another four make an upper case or lid.

A new feature of the design of the coil cases is a thermal shield consisting of a pack of 10 layers of thin Inconel sheets which will surround the coil cases. This was found necessary, following detailed stress analysis of the coil cases, in order to cut down the radiative heat load and reduce thermal stress to a safe level.

The coils are finally assembled in the JET vacuum vessel. In-vessel operations included:

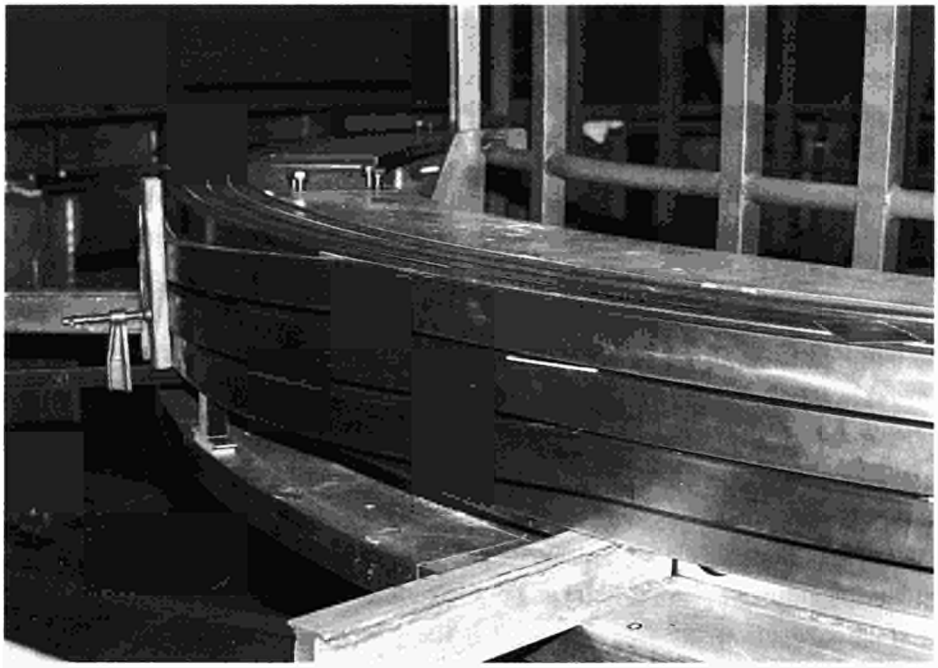

Fig 190: Pre-assembled divertor coil at Contractor's factory.

a) welding of a case quarter sections to make lower cases and lids;
b) welding of coil mounting blocks to vacuum vessel;
c) assembly of winding tables;
d) assembly of conductors on winding table and brazing together to form coils;
e) application of glass and Kapton ground insulation to assembled coils;
f) assembly of coils in cases and welding of upper and lower halves of case together. These final welds will be performed in the vessel. The high dimensional precision required of these casings mean that extensive jigging and very careful welding is an integral part of the manufacturing process;
g) evacuation and impregnation of coils with epoxy resin and heating to cure,

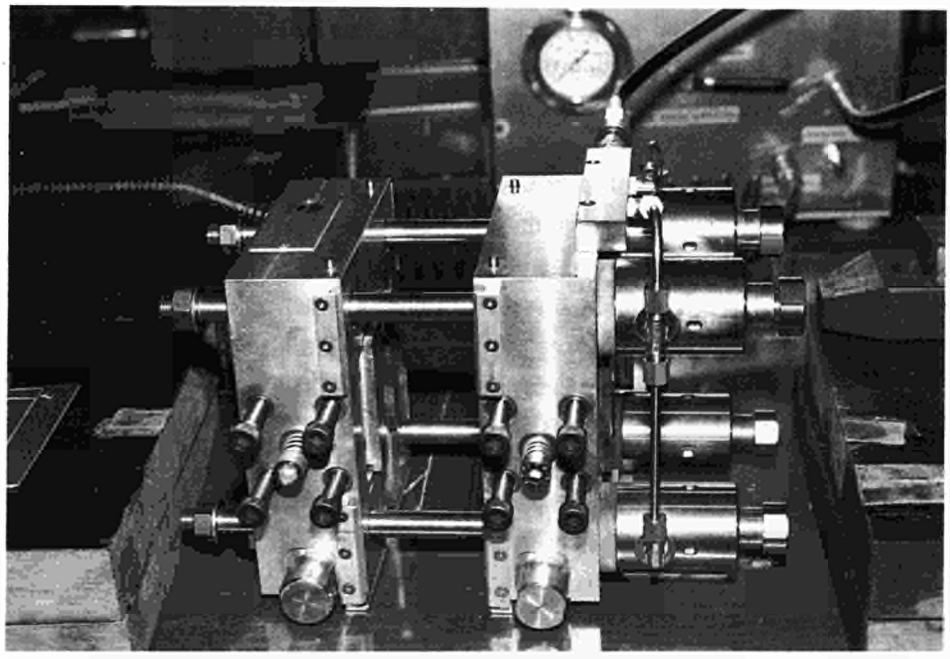

Fig 191: Tool for clamping joints during brazing

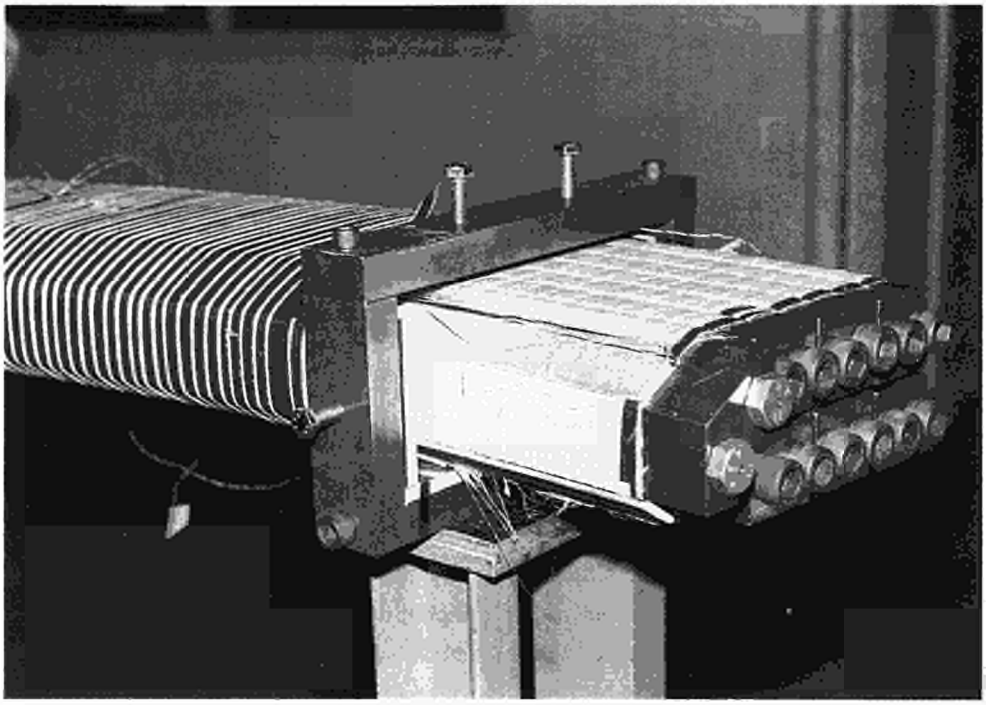

Fig 192: Divertor coil impregnation test model ready for insertion into case.

h) assembly of mounting clamps on coils and lower into final position on supports.

During 1991, the conductors for the first two coils have been formed and pre-assembled (see Fig 190). The press tools for the cases have been made and tested and the supports were almost completed.

Considerable effort has been devoted to studying and planning the in-vessel assembly operations. Problems of in-vessel work include restricted space, restricted size of access port and restricted choice of materials. Lifting operations require special equipment, as no in-vessel crane is available. A number of solutions to this problem were still being examined at the end of 1991.

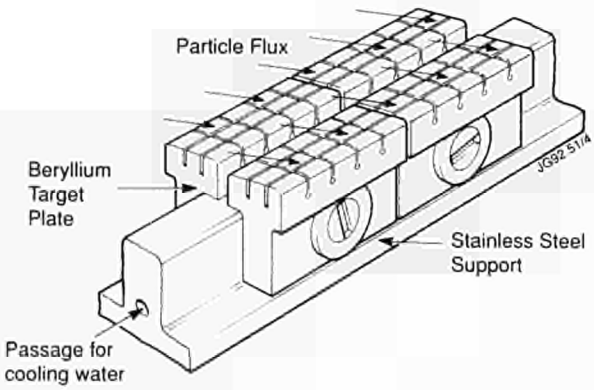

Fig 193: Beryllium tiles for target plate (Mark I)

The topology of the coils and their terminals strongly affects the assembly sequence for the coils and cases. This sequence has been studied in detail using CAD models to check feasibility and determine the optimum.

All in-vessel operations must be thoroughly pre-tested to ensure the reliability of the coils and to avoid delays or problems during assembly. For example tools for conductor brazing (see Fig.191) have been designed and tested during 1991 and an epoxy resin impregnation test model is nearing completion (see Fig.192). This model will also be used to check the case welding process.

Radiatively Cooled Target Plates (Mark I)

Installation of the target plates will proceed in two steps. Step I will use radiatively-cooled tiles as target plates, while Step II will use water-cooled beryllium clad hypervapotrons. Step I provides a simple and robust design which will allow the early exploration of the pumped divertor operation parameter space. Step II will be used for impurity control studies at high power and long pulse duration.

Thermo-mechanical Evaluation of Mark I (Solid Be) Target Plate Tiles

The conceptual design of the solid beryllium target plates is shown in Fig.193. Solid beryllium tiles are clamped onto water cooled stainless steel support beams. The front face of the tiles is castellated to reduce the intensity of thermal and

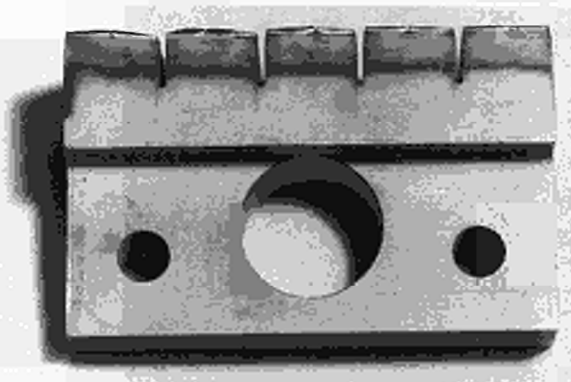

Fig 194: Tests of Solid Beryllium Mark I Target Plates

limit the propagation of surface cracks. Preliminary stress analysis indicated that the size of castellations and the type of root of the castellation played a large role in the fatigue life of a solid target plate. First tests were carried out with a strongly cooled beryllium tile (start temperature before irradiation 70°C) and castellations 12 x 15 mm by 10 mm deep subjected to a train of heat flux pulses (14 MW/m^2 for 0.1s then 0.145s without flux) during 6s. After 50 pulses (about 10^3 stress reversals), the irradiated surface had broken up in an unacceptable manner. After a further 2000 pulses, the test was stopped as the surface deteriorated as seen in Fig.194. There were no visible cracks emanating from the root of the castellations, and this result was the same for all of the castellation shapes under test.

A second series of tests was carried out with flux densities 14 MWm^{-2} to 25 MWm^{-2} onto tiles with finer castellations; 6 x 7.5 mm x 6 mm deep, 6 x 7.5 mm x 12 mm deep. No fatigue cracking of the loaded surface was observed after 5 x 10^3 stress reversals. No cracks were seen to emanate from the root of the castellations. The surface was deliberately overloaded to produce localised melting; the resultant resolidified surface showed some cracks due to melting but no fatigue cracks of the kind seen in Fig.194 were observed. Detailed metallographical studies are to be made.

A final series of tests is planned for 1992 to study the effect of start temperature on the fatigue life of Mark I solid beryllium tiles. By varying the extent of cooling in the test piece start temperatures of 70 - 350°C can be achieved. It is now planned to use the fine castellations = 6 x 7.5mm x 6mm deep in the final design.

Beryllium Tiles and Mechanisms

The divertor target plates carry 7296 beryllium tiles. The tiles are attached in pairs to the beams and the pairs have been designed to be fully compatible with remote handling requirements. A spring washer arrangement allows the tiles to be attached or dismantled easily whilst maintaining a precise location. The surface of the tiles is saw-toothed, each tile surface being at an angle of 5° to the horizontal. This design ensures that the tile edges are shadowed as well as making allowances for possible misalignments in the system due to installation and manufacturing tolerances, as well as those caused by thermal displacements. Procurement of the beryllium tiles is making good progress. The material was being delivered from a US supplier and the contract for machining was let in November 1991.

Beam Modules

The beam modules are the support structure for the divertor target plate files. There are 48 beam modules each consisting of 6 radial stainless steel support beams. The beams form the strong back for the tiles taking up the eddy and halo current forces. Each beam is water cooled via deep drilled holes and, in turn, cools the attached tiles mainly by radiation. The modules are positioned on rails which are welded onto the divertor coil casings. Care is being taken to allow for the difference in thermal expansion between the beam modules, which may become hot and reach 350°C during bake out, and the coil casings which are always cooled by the coil. The contract for the beam modules was let in October 1991.

Cooling Pipework

New feedthroughs are required for the increased water flow. These are required early on in the shutdown and are planned to be delivered in April 1992. The internal pipework also includes bellows and water manifolds for which a manufacturing contract has been let. The cooling pipe manifold design is completed. It takes into account eddy current forces which necessitate substantial supports for the pipes on the vessel wall. The supports allow for the differential expansion between the vessel and the cooling pipes and ensure that the stress on the feedthrough is minimised.

An insulated electrical break for the water cooling pipes has been designed and a prototype has been manufactured and successfully tested. The break allows for the electrical insulation of two pipe sections in which high pressure water (10atm) is flowing whilst permitting substantial mechanical stresses. The breaks will be installed at the entrance and exit pipes of each divertor module. In particular these will protect the flexible pipe sections, the

flexibles, from high currents and forces induced eg. by the plasma halo. The manufacturing contract for the breaks was let in November 1991.

Water Cooled Target Plates (Mark II)

All the copper chromium Zirconium alloy (CuCrZr) for the target plates has been procured, and machining of the hypervapotron internal structure is well advanced. Final machining of the surface interfacing with beryllium tiles will be performed with the target plates attached to their rigid stainless steel support structures. This approach enables the overall dimensional accuracy of the divertor to be maintained within acceptable limits.

The design of the assembly of individual target plates into modules has been completed. Prior to assembly into modules, it is intended to test the completed elements by subjecting them to ~10MW m^{-2} in the NB Testbed and a suitable test rig has been designed to accept batches of eighteen target plates.

During 1991 investigations have continued into the bonding of beryllium to CuCrZr with the aim of achieving routine high strength bonding. Efforts have concentrated on minimising the build-up of brittle intermetallics at the beryllium-braze interface and improving the bond to the beryllium surface. These have been demonstrated to be the limiting factors in achieving adequate bond strength by means of operational tests of prototype elements and mechanical tests on small samples. The three major lines which have been pursued are:

Vacuum Oven Brazing

InCuSil ABA (which contains titanium as an oxygen getter) has achieved higher bond strengths than BAg 18, but both brazes show considerable scatter in the bond strength results.

A silver-germanium braze alloy was also tried (germanium is one of the few elements which does not form intermetallics with beryllium). The first attempt suffered from the poor wetting and a high oxygen content in the joint. Further trials using a low oxygen content foil will be carried out.

Induction Brazing

This was carried out in an attempt to minimise the formation of intermetallics by minimising the time duration of the braze cycle. Both BAg 18 and InCuSil ABA brazes were used. However in all cases the 10-60s dwell time required for wetting to occur resulted in the formation of brittle intermetallic layers. Fig.195 illustrates the range of shear strengths obtained from 15 test samples brazed with InCuSil ABA using a 60s dwell time.

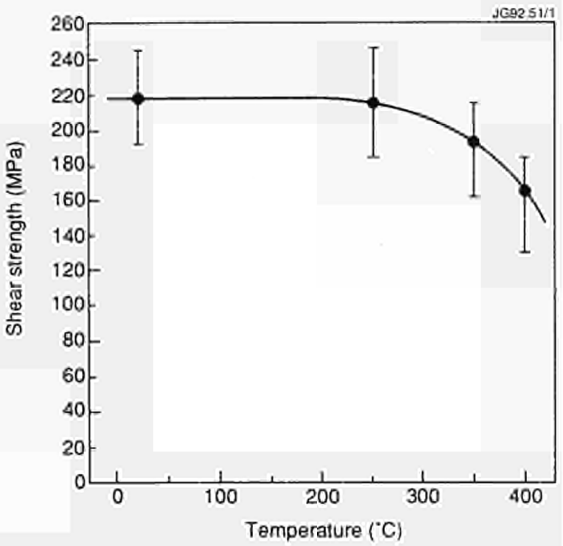

Fig 195: Shear strength versus temperature for induction brazed joint (brazed alloy InCuSil ABA)

Diffusion Bonding using an Intermediate Layer of Silver

The formation of intermetallics is avoided by the use of lower temperatures (250°-450°C) than required for brazing with bonding being promoted by the application of high pressures (80-140 MPa).

The common factor necessary for successful application of all of these methods is the ability to obtain a high strength bond between beryllium and an intermediate layer of silver. Various methods are being evaluated and the most successful will be applied to the above techniques.

The Cryopump and Water Cooled Baffles

Further progress has been made with the procurement of the cryopump and the water cooled baffle. In particular, a series of major technical problems to cope with the harsh environment for this equipment could be solved. A suitable copper alloy for the chevron structure was required to provide the required mechanical strength necessary to cope with the extreme forces by the eddy currents. At the same time, the material needs provide good thermal conductivity and also high electrical resistivity. All these requirements are basically contradictory and only by using a precipitation hardening copper alloy and by optimising the precipitation hardening process can a satisfactory solution could be found. However, the precipitation cycle had to match the required thermal cycle for the brazing of the chevrons onto the stainless steel cooling pipes.

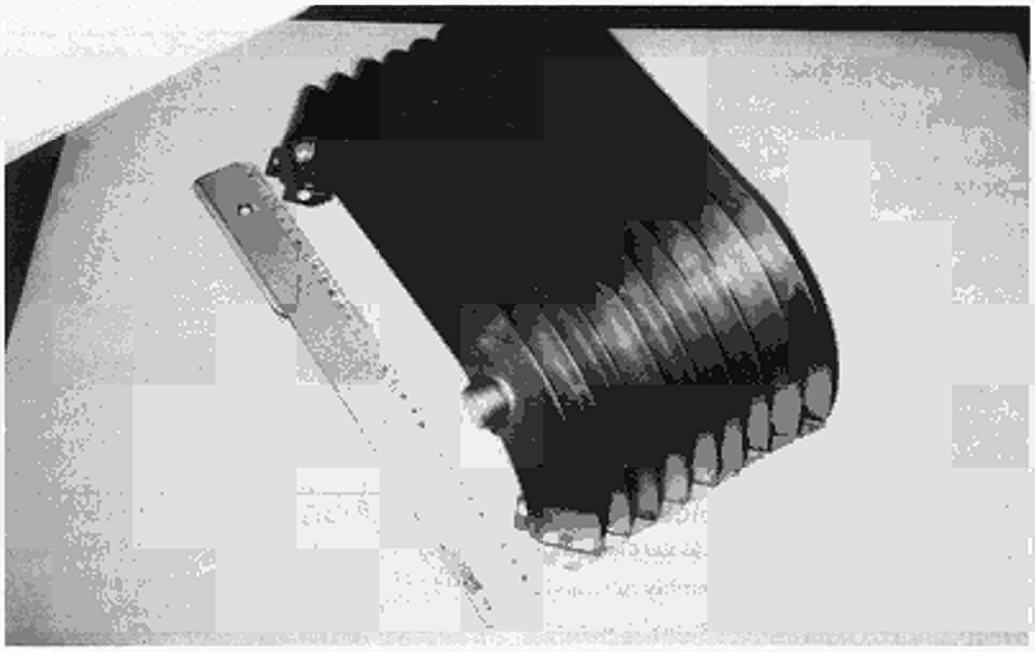

Fig 196: Cryopump chevron test assembly

A special blackening process for the chevrons could be developed and qualified by using a plasma sprayed coat of Al_2O_3 and TiO_2. The main achievement was to find a suitable intermediate coat in order to make the coat compatible with both copper and the high temperature cycle for the combined precipitation hardening and brazing process of the chevrons. (In contrast to stainless steel for which this coat has been used at JET on the belt limiter, copper shows at high temperatures a loss of adhesion, probably due to formation of copper oxide).

The first manufacturing prototypes for the cold formed chevrons have been successfully produced and assembled for brazing trials (Fig.196). The detailed drawings for manufacturing are mostly completed and all materials have been ordered. Further studies on the transient flow conditions such as cool down, warm up and accidental break of the torus vacuum have been done and implemented in the design.

High Frequency Systems

ICRF System for the Pumped Divertor

The design of the A2 antennae was described in the 1990 Progress Report. During 1991, the design has been largely completed and manufacturing drawings approved. Many tests have been carried out to qualify manufacturing procedures, notably on the corrugated plates forming the side and back panels of the housing, and the septum which forms the main structural element of the antenna. Manufacture is proceeding and the first unit will be at JET in mid 1992. Forming of the central conductor tubes is now complete.

All beryllium screen elements and the mounting assemblies for these antennae have been delivered. Manufacture of four new vacuum transmission lines is well advanced and a contract has been placed for modification of the existing lines after removal from the torus. This contract provides for limited levels of radioactivity on the lines, and provision is also being made for de-tritiation by baking if necessary.

The antennae rely on distributed support from the torus to survive disruptions. The design of these supports, which must allow thermal expansion, is also complete. With four of the antennae relocated in the torus, the corresponding main transmission lines need to be modified. The design of these is complete and the contract placed.

High power tests on the model antenna have been largely completed. After refinement of the design following initial tests, the full required performance (45 kV for 20s) has been achieved.

LHCD Developments

The design of the L1 LHCD launcher has been modified to position the grill mouth at the large plasma boundary and to match the profile of the adjacent A2 ICRF antenna. It is not possible to reach the small plasma boundary due to the tight fit of the launcher in the port. These changes have required some minor re-working of the external dimensions of the multijunctions, which is now complete. Preparation of the multijunction/waveguide assemblies is well advanced and assembly of the launcher is proceeding. A view of the launcher grill mouth is shown in Fig.197.

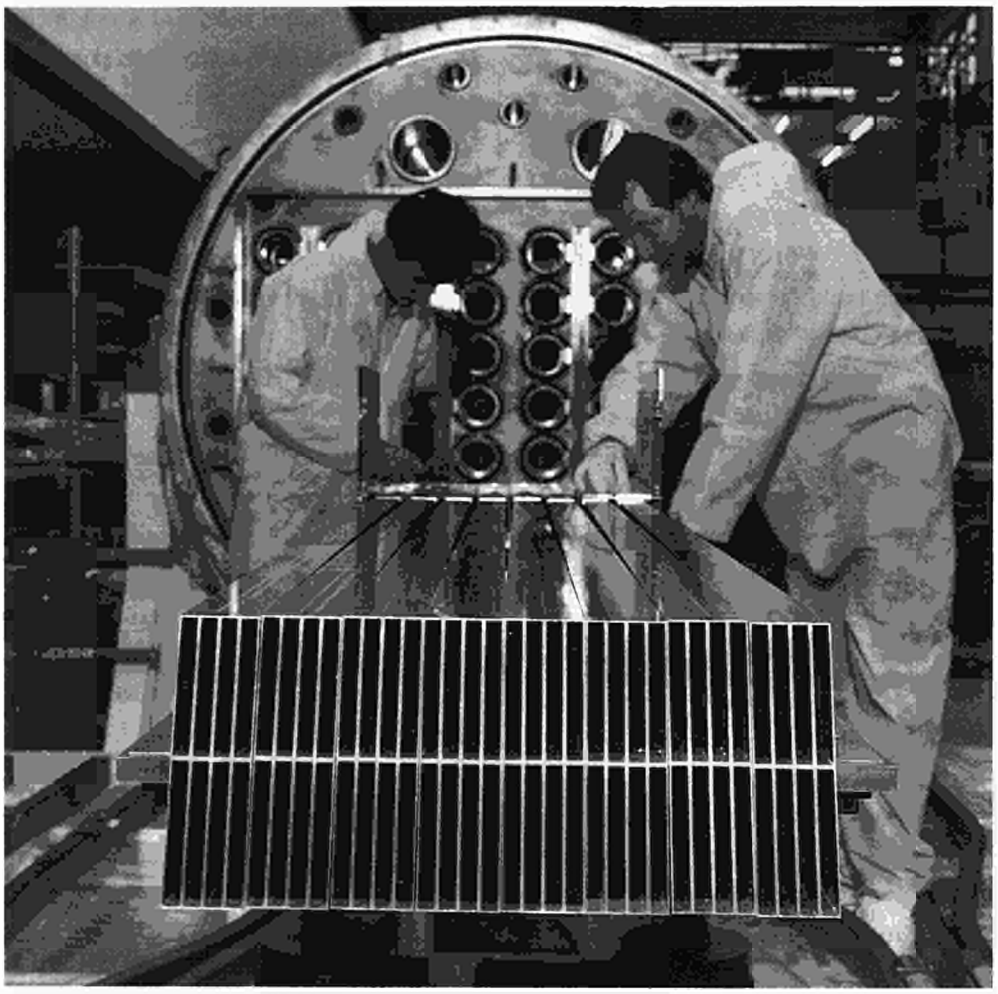

Fig 197: View of the LHCD Launcher (L1)

The side protection and its support also require modification to match the new profile. The design work is complete and modification of the components can start after removal from the torus and decontamination. New remote handling tools are being prepared for these items.

About 50 microwave windows have been received and each tested to full power. Waveguides for use in the launcher have also been tested and show losses typically a factor 1.3 above theoretical for silver. Return loss is typically -30dB.

Other Components of the Pumped Divertor Configuration

New Saddle Coil Components, Supports and Protection Tiles

The saddle coils are being modified so that the lower coils can be installed at a higher position than originally planned. The new position of the lower coils ensures an optimal penetration of the saddle coil field into the plasma. The modifications include new supports, additional coil clamps insulated with ceramic balls, lengthening of the crossover bars, etc. In addition the coils must be re-arranged to take account of the changes in the position of the feedthroughs for power input.

Poloidal Limiters

The existing belt limiters will be replaced by a series of poloidal limiters the main task of which will be to protect the new antennae. A belt limiter system cannot protect the antennae for all possible plasma configurations. These poloidal limiters have been designed to use the tiles, either Be or carbon, which have been used for the belt limiter. The tiles are to be reshaped and installed horizontally into the structure of the poloidal limiters. The eddy currents induced, in particular when Be tiles are inserted, will be substantially higher than in the present limiter configuration. Additional high forces can be expected from halo currents. The result is that strong supports are required which because they span the bellows, must be insulated. Successful prototypes of insulated pins have been tested. Additional requirements for the poloidal limiter system which have been met in the

design are: the ability to move the limiters radially to a different position when operating with slim plasmas and antennae which have been moved (which requires the lower section of the limiters to be hinged and moveable); the capability to finely adjust the position after installation to ensure a precise positional accuracy of the limiters in radial direction relative to the antennae and the magnetic centre of the machine; to accommodate the needs of numerous diagnostics which require opening, holes and cut-outs in the limiter structures, as well as to allow the remote handling boom to enter the vessel unhindered. The latter requirements necessitated the design of two basic widths for the limiters and additional individual variations between them. Careful consideration has been made in the design concerning the appearance of halo currents and the grounding cables have been included at strategic locations. The manufacturing contract was awarded by the end of 1991.

Poloidal Limiter Tiles

The shape of the poloidal limiter tiles has not been finalised. The aim is to shape them in such a way as to maximise the power handling capability of the limiters for use as limiters as opposed to solely a protection of the antennae. The basic shape of the tiles has been optimised but work is proceeding on the design of the tiles in the areas of the diagnostic holes and cut-outs which could limit the power handling capability. A complication for the subsequent machining of these tiles is that they contain an amount of tritium which, although small, is not negligible and requires that firms be able to handle the radioactive gas emitted and the active swarf as well as the ability to machine beryllium or beryllium covered graphite. Companies able to machine the tritium containing Be tiles have been identified and test machining runs have been performed by several companies to the satisfaction of JET.

Inner Wall Guard Limiter Beams and Supports

The inner wall of JET needs to be re-shaped as a consequence of the new plasma configurations in the divertor phase together with the need to protect the lower saddle coils from disruptions and halo currents. A major concern for the new design was reliability as the previous tile, tile backplate, carrier rail and associated bellows protection plate system proved to be one of the weakest parts of the in-vessel configuration susceptible to the effects of halo currents. The chosen solution is a set of eighteen poloidal guard limiters. These guard limiters consist of strong Inconel beams attached to the inner wall at three positions and able to withstand the expected maximum forces caused by halo currents. In addition, as with the poloidal limiters on the outer wall, careful consideration has been given to locating earthing straps a strategic locations so as to minimise the currents which will flow through the new components. The contract for the inner wall guard limiters was awarded in October 1991.

Guard Limiter Tiles

The contract to manufacture the new fibre reinforced graphite tiles was placed, in December 1991. Although the guard limiters are basically intended to protect the inner wall, the saddle coils and divertor coil 1, the tiles will be shaped to maximise the power handling capability of the guard limiter system.

First-Wall Protection

A general refurbishment of all first wall protection is planned for the divertor shutdown. The position and design of bellows protection plates and octant joint protection has been defined after a detailed analysis. Mushroom shaped tiles will be installed in the area between the dump plates and saddle coils at the top of the machine. These tiles protect the adjacent components whilst minimising the attenuation of the saddle coil field. Areas exposed to the neutral beam shine through on the inner wall between the guard limiters as well as on the outer wall are to be protected by specially designed tiles and plates.

In-vessel Instrumentation

Instrumentation will be installed in the vessel on specific components aimed at monitoring their performance and to ensure that the conditions remain within the operational limits prescribed. Planned instrumentation includes thermocouples at various positions on the coil casings and divertor rails. These positions will be chosen to provide information on the temperature distribution and thereby allow estimates to be made on the existing stresses in the casings. Current shunts will be attached to earthing straps of both the poloidal limiters and the inner wall guard limiters. Current shunts will also be attached to a number of the mushroom tiles. These measurements allow the analysis of the position and magnitude of halo currents. Similarly voltage shunts across the ceramic breaks of the water cooling system will help determine whether large currents

Table XVIII
Additional Diagnostics for the Divertor Phase of JET

System	Diagnostic	Function	Status
KE9D	LIDAR Thomson scattering	T_e and n_e profiles in divertor plasma	In-vessel design complete, procurement in progress.
KG6D	Microwave interferometer	$\int n_e dl$ along many chords in divertor plasma	In-vessel waveguide design complete, procurement in progress
KG7D	Microwave reflectometer	Peak n_e along many chords in divertor plasma	In-vessel waveguide design complete, ex-vessel microwave design and mockup experiments in progress
KK4D	Electron cyclotron absorption	$n_e T_e$ profile along many chords in divertor plasma	In-vessel waveguide design complete, ex-vessel microwave design and mockup experiments in progress
KD1D	Calorimetry of Mark1 divertor targets	Power balance of divertor plasma	Thermocouple installation awaiting delivery of target tiles
KC1D	Magnetic pickup coils	Plasma geometry in divertor region	Manufacture in progress
KY4D	Langmuir probes in divertor target tiles	n_e and T_e in the divertor plasma	Design completed
KY5D	Fast pressure gauges	Neutral flow in divertor region	Manufacture in progress
KT6D	Poloidal view visible spectroscopy of divertor plasma using a periscope	Impurity influx, 2-D emissivity profile of lines	Periscope and in-vessel components in manufacture. Design of other components and optics in progress
KT5D	Toroidal view visible spectroscopy of divertor plasma from Octant No:7 mid-plane	T_i and V_i, ion temperature and toroidal velocity of impurities	Design in progress. Optics components defined and procurement in progress
KT7D	VUV and XUV spectroscopy of divertor plasma	Impurity influx, ionization dynamics	Spectrometer in manufacture, mechanical design in hand, procurement of electronics and data acquisition in hand
KB3D	Bolometry of divertor region	Power balance of divertor plasma	Design of mechanical interface being finalized. Final tests of detector element in progress. Procurement of electronics and data acquisition in hand.
KY6	50kV lithium atom beam	Parameters of the scrape-off-layer plasma	Concept approved, detailed design in progress

must be expected to flow in these pipes if the breaks were to be removed.

Evaporator Extensions

The beneficial effects of beryllium evaporation will be retained in the divertor phase. The evaporators have operated reliably at and beyond their maximum operating conditions. Therefore the evaporators are to remain unchanged but need to be lengthened by approximately 30cm.

Gas Introduction System

A new gas introduction system will be installed for the divertor phase. A system has been designed which will permit gas, including tritium, to be puffed directly into the X-point region of the plasma. This will be accomplished by a series of 24 toroidally spaced small injector pipes localised just beneath the X-point between the target plate tiles. A similar but somewhat less elaborate system is planned for the upper X-point region.

Divertor Diagnostics

Development of divertor diagnostics is well advanced. Design integration and procurement of hardware with interfaces in the divertor region have received priority as these will be required first for installation. Scientific details of the diagnostic concepts and applications have been presented earlier in the report in the section on diagnostic Systems. Current status in respect of design, procurement and installation is given in Table XVIII.

Preparation for the Assembly of the Pumped Divertor Configuration

A new group, First Wall Installation Group has been set up with the task of preparing the pumped divertor installation. To minimise the installation time and to optimise the working conditions inside the vessel (beryllium, tritium radiation and limited space) special procedures, jigs and equipment have been developed and suitable working methods and organisation has been set up.

Handling of components, through the ports and inside the vessel, has required a great deal of effort. In addition to the articulated boom and the TARM a special designed toroidal travelling crane will be installed. A series of permanent bosses will be welded to the roof of the vessel. These will support the temporary lifting features (arched beams) required during the manufacturing of the divertor coils and subsequently a toroidal travelling crane and a mobile platform for installation of the other components (see Fig.198).

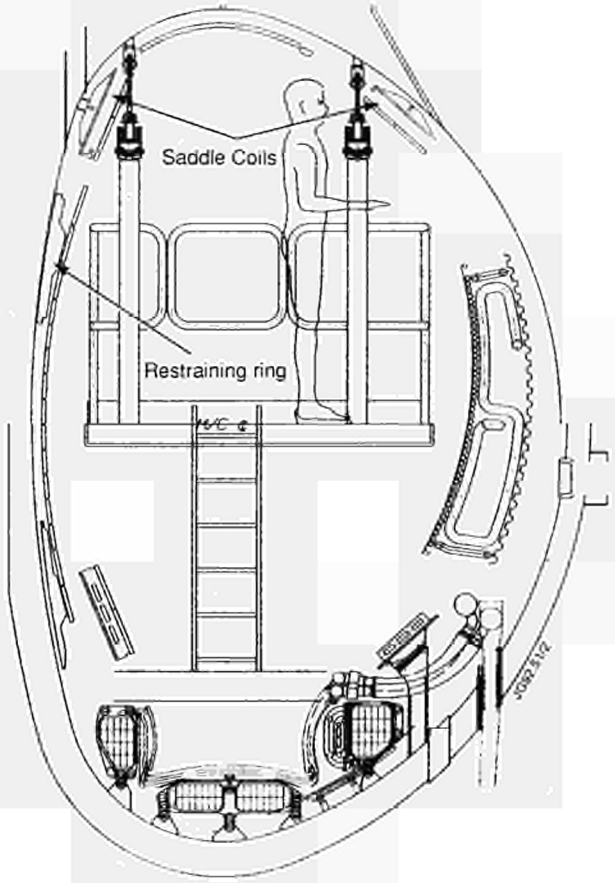

Fig 198: Divertor Assembly arrangement

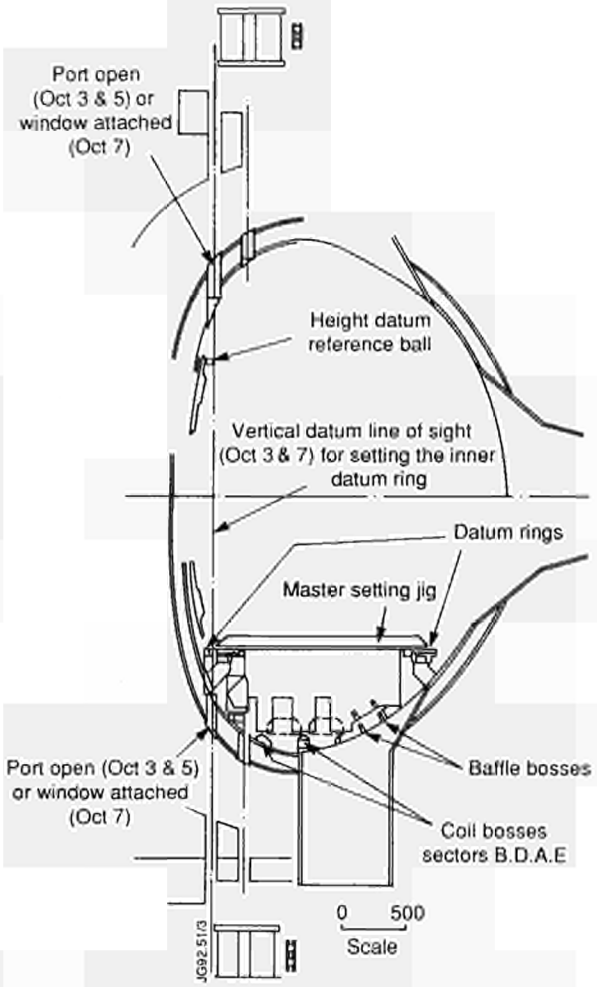

Fig 199: Schematic loss setting arrangement

The geometry and construction of the vacuum vessel does not lend itself to the installation of the divertor system to the level of accuracy required. Therefore special fixtures and jig will be used to set the position of each component as closely as possible to the magnetic configuration of the machine using external datum. Fig.199 shows the mounted reference rings.

All inner wall components of the vacuum vessel will be stripped at the earliest stage possible in order to achieve decontamination of the vessel and, therefore, to require only minimal personal protection for the installation of the divertor. This enhancing as well as the number of people working in the vessel to improve their efficiency. Decontamination methods are still under investigation at the moment.

Divertor Power Supplies

The magnetic configuration (X-point) for the new pumped divertor will be achieved by circulation of DC currents in the four discrete coils to be installed inside the vacuum vessel. The accurate control of the magnetic configuration (X-point position) and the sweeping requirements will be achieved by supplying the divertor coils from individual thyristor controlled power supplies (PDFA). The contract (Stage I for the first three PDFA units) was placed in July 1991 and Stage II for the supply of the fourth PDFA unit was released in December 1991.

Stage I involves two phases: Phase 1 for the design of the complete PDFA system and Phase 2 for the manufacture, installation and testing of the first three PDFA units. The time schedules are respectively 20 months for the completion (including commissioning tests on JET site) of Stage I and 21 months for the completion of Stage II, both counted from the release of the Stage I.

A report for the power system design as well as a final quality plan and draft quality schedules have been submitted. Specifications for the supply of equipment have been drafted and sub-contracts have been placed (transformer) or are in the process of being placed (shelter and enclosure, thyristors, DC choke, etc).

Fast Radial Field Amplifier

A fast radial field amplifier is essential to control the plasma vertical position with the elongated configurations of the

pumped divertor. The amplifier has been conceived in a modular way, each module based on a H-bridge in which each arm consists of two Gate Turn Off (GTO) thyristors, connected in parallel. The contract for the fast radial field amplifier was placed in 1990.

The first design report, received in February, dealt with the power components; after its approval the construction started followed by the factory tests. The majority of the components of all four amplifiers have been delivered to the factory where installation is in progress; the first shelter and the transformer are already in the position where the integrated factor tests will take place. Installation of the power components inside the shelter started in October.

References

[1] Bertolini, E, et al, The JET Divertor Coils, 12th Int. Conf. on Magnetic Tech. (Lenningrad, USSR, 1991)

Tritium Handling

Following the extension of the Project to the end of 1996, the Active Gas Handling System (AGHS) will be required to be fully operational before the start of the full D-T phase of JET scheduled for 1996. As a result of the planning for and implementation of the preliminary tritium experiment during 1991, essentially all manpower of the Tritium Safety Group and a large proportion of the manpower of the Active Gas Handling Construction Group were required to work on the experiment during the second half of 1991. As a consequence, work on the preparation for the full D-T phase, including preparation of the Final Safety Analysis Reports and the installation of the AGHS was slowed down.

Active Gas Handling System (AGHS)

At the end of 1991, mechanical plant installation was nearing completion with the exception of the gas transfer connections from the AGHS to the tokamak and auxilliary systems which can only be installed during the 1992/93 shutdown. Electrical connections were well advanced, commissioning of subsystems, including cryodistillation system and exhaust detritiation system and active drainage system were underway. Major installation activities during 1991 included the five modules of the cryogenic forevacuum system, the impurity processing system, the U-beds for intermediate storage, gas chromatography and product storage systems. The control system is operational with software tests in progress.

Fig.200 shows the five modules of the cryogenic forevacuum system with in the background buffer tanks and the liquid helium and liquid nitrogen distribution system.

Safety Assessments

The safety assessments for the main process systems were completed in 1990. Effort in 1991 has concentrated on assessment of the common systems such as building ventilation, services, valve box over/under pressure protection systems forming part of the Final Safety Analysis Report. The final design of the hard-wired protection system has been established and will be reviewed to demonstrate compliance with the reliability assumptions made in the plant Design Safety Reviews. A fire hazard assessment has been completed for the AGHS building which has concluded that the overall hazard is low.

A number of design changes have been made since some systems were assessed. In particular, the mode of operation of the Impurity Processing System has changed radically. This has required a full revision of the Impurity Processing Design Safety Review to be carried out, as some of the new modes of operation in which residual gas from many sub-systems is collected, negated the original safety case.

Commissioning Procedures

Progress has been made on preparing the commissioning procedures for the plant. In order to speed up the approval process, a distinction has been made between process commissioning and safety-related commissioning. A schedule of safety-related tests has been issued to the Fusion Safety Committee and endorsed.

Radiation Dose Assessments

Radiation Dose Assessments for releases of tritium and activation products to the atmosphere and River Thames have been carried out in connection with the application to HMIP for discharge authorisations. In addition a new study has been initiated with the Canadian Fusion Fuel Technology Project (CFFTP, Canada) to use the Ontario Hydro (Canada) code ETMOD to assess doses from tritium both in the form of HT and HTO. The original studies for JET assumed tritium was in the form of HTO as little information was available at that time on the

Fig.200: View of the Active Gas Handling System showing the five cryogenic forevacuum modules with buffer tanks and cryodistribution system in the background.

conversion in the environment of HT to the more hazardous form of HTO.

Aspects of the ETMOD code have been validated against field studies on tritium releases carried out in Canada and France. The results of the analysis have confirmed the calculations carried out for the earlier submissions and have shown that releases in the form of HT (or T_2) rather than HTO result in significantly lower doses.

U-beds

The safety case for air and nitrogen ingress into the JET design of U-beds has been accepted by SRD. This is based on the results of air ingress tests carried out at JET in 1990 supported by the results of a series of tests carried out by Ontario Hydro, Canada.

Calibration of Ionisation Chambers

The JET design of ionisation chamber used for monitoring of tritium in process lines and valve box atmospheres in the AGHS is novel. It was an open helical bias electrode which may be heated to desorb layers of tritiated water or other impurities giving a high background signal (memory effect).

Tests were carried out at TSTA (USA) to determine the calibration, the effect of contamination and heating the bias electrode and the response to gamma exposure. The tests showed that the use of heated bias electrode enabled memory effects to be minimised and provided sufficient range for use in AGHS process control applications.

This design of chamber was successfully used in the preliminary tritium experiment both in its normal mode and in a novel "ion-collector" mode at low pressures in which the current arising from tritium decay, rather than from ionisation created by the beta particles is measured. Several calibration runs were carried out during processing of tritiated gas after the PTE to establish the relative sensitivity of the two modes and the effect of differing pressures and gas compositions.

Future Plans

The JET Programme is divided into phases governed by the availability of new equipment and fitting within the accepted life time of the Project. The programme to 1996 is shown in Table XIX. Phase I (Ohmic Heating Studies) was completed in September 1984, and Phase II (Additional Heating Studies) in October 1988. Phase III (Full Power Optimization Studies) will end in February 1992. The scientific aims of Phase III were to obtain maximum performance in (belt) limiter configuration (currents up to 7MA) and to optimize X-Point Operation (currents up to 6MA) including a comparison of H-modes in X-point configuration using beryllium (lower X-point) with carbon (upper X-point) dump plates.

JET future plans are dominated by the insertion of a new phase of the Project (Phase IV Pumped Divertor Configuration and Next-Step Oriented Studies), before the final full Tritium Phase, which is now scheduled to start in December 1995. This new phase has now been formally approved and has extended the lifetime of the Project by four years up to the end of 1996.

The aim of the new phase is to demonstrate, prior to the introduction of tritium, effective methods of impurity control in operating conditions close to those of a Next-Step Tokamak with a stationary plasma (10s-1m) of 'thermonuclear grade' in a single-null axisymmetric pumped divertor configuration. This configuration can only be achieved in JET by using divertor coils internal to the vessel.

Following the approval by the JET Council of the stepwise approach to the introduction of tritium in advance of the full Tritium Phase, a first preliminary tritium experiment (PTX1) was carried out and successfully completed in November 1991. A second tritium experiment (PTX2) is scheduled for the first half of 1994 at a point, yet to be determined, when divertor operation has been well established, but in time to allow the necessary period of radioactive decay before the following shutdown. The information derived from these preliminary tritium experiments will provide a safer approach to the full tritium phase and will help to optimize the active handling and waste management arrangements.

More information on the future phases of the Project are provided below.

New Phase (first part): Pumped Divertor Configuration and Next Step Oriented Studies - Phase IVA (March 1992 - October 1994)

In March 1992, the Project will enter an extended shutdown, which will last until Summer 1993, in order to install the components relevant to the new pumped divertor phase. This will involve intensive in-vessel work to install the following equipment:

- lower divertor structure with Mark 1 beryllium target plates (inertially cooled Be blocks)
- pumping chamber and cryopump;
- internal divertor coils and necessary power supplies;
- poloidal limiters;
- new ICRF heating antennae (A2);
- full lower hybrid current drive (LHCD) system with its modified launcher;

Table XIX
JET Programme to 1996

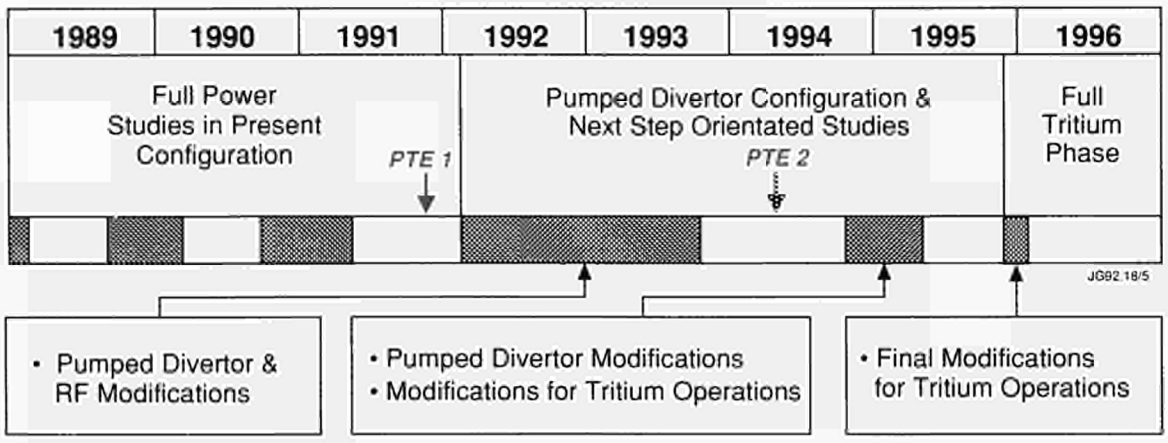

PTE: Preliminary Tritium Experiment

- divertor diagnostics;
- high-speed pellet launcher (for plasma core injection);
- centrifuge pellet launcher (for plasma edge injection);
- disruption control system using internal saddle coils.

The single-null X-point pumped divertor configuration should enable JET to progress towards extended high power operation with 40MW additional heating using neutral beam and ICRF power (e.g. plasma currents of 6MA for up to 3s, 3MA for up to 5s). The control of disruptions using saddle coils system and the control of sawteeth using the full power LHCD systems should also be studied.

The first operating period should focus initially on establishing reliable operation in this new configuration. Subsequently, attention should be devoted to the study of performance and effects of the pumped divertor in controlling impurities, plasma density and exhaust, and power loading on the target plates.

Preparations for D-T operations will also continue during this period, including finalisation of Remote Handling tests and commissioning of the Active Gas Handling System (AGHS) with tritium gas (subject to consent by the approving bodies).

New Phase (Second Part): Pumped Divertor Configuration and Next Step Oriented Studies - Phase IVB (Nov. 1994 - Nov. 1995)

The proposed shutdown (~6 months) in late 1994 would be used to replace the Mark 1 Be target plates by the Mark 2 version (water cooled Be clad hypervapotrons) and to provide an opportunity, depending on information from the experimental programme and elsewhere, to implement other modifications to the pumped divertor. In addition, it should be possible to install other enhancements aimed at improving performance in the new configuration or for the D-T Phase (e.g. enhanced pellet injection or fuelling system, modifications to LHCD or additional heating systems, etc.).

The primary objective of this period of the new phase (to end 1995) would be to provide information needed to demonstrate steady divertor operation with 40MW power and to establish with confidence the key design features of the Next Step in relation to:

- impurity control;
- fuelling;
- helium transport and exhaust of ashes.

Another objective would be to optimise reliability and plasma performance in the divertor configuration in preparation for D-T operations.

In parallel, the tritium commissioning of the Active Gas Handling System would be completed and the main tritium modifications to the machine and its associated systems (including remote maintenance and waste handling) would be implemented.

Full Tritium (D-T) Operation - Phase V (Dec. 1995 - Dec. 1996)

Subject to the approval of the JET Council and to necessary official consents and when general levels of system reliability justify it, the D-T phase would start in Dec. 1995, after a short shutdown to complete final adjustments required for active operations.

During D-T operations, it would be possible to undertake in-depth studies of the physics of α-particle production, confinement and heating and thermal excursions. In addition, the real experience of tritium operation in a relevant scale tokamak (i.e. tritium handling and recovery, fuel mixture control, confinement properties of D-T plasmas, and remote maintenance and plasma diagnostic with large neutron and gamma backgrounds) should provide essential information for a Next Step device.

Appendix I

JET Task Agreements 1991

Title	*Associations (JET Responsible Officer)*	*Duration of Agreement*
RF HEATING DIVISION		
LOWER HYBRID CURRENT DRIVE ON JET • Exchange of knowledge • Design and construction of special item • High power tests	EUR-CEA CADARACHE (CEA/TA4) (J. Jacquinot)	Completed The prototype launcher built by CEA has been installed and operated successfully
LH AND ICRF EFFECTS ON JET • CD efficiency including transport • Synergistic effects between FWCD and LHCD • Modulated heating modelling • Minority CD experiments • Effect of RF CD on MHD stability	EUR-UKAEA CULHAM, UK (J. Jacquinot)	In progress: detailed comparison with JET experiments on LH and FW synergy, fast electron transport and minority CD
EXPERIMENTAL DIVISION I		
EDGE PLASMAS & PLASMA SURFACE INTERACTIONS	CULHAM, UK (CUL/TA2) (P.E. Stott)	Started June 1983
PLASMA WALL INTERACTIONS	GARCHING, FRG (CUL/TA2) (P.E. Stott)	Started Jan. 1984
NEUTRON PRODUCTION RELATED PHYSICS AND ASSOCIATED DIAGNOSTICS	SWEDEN (NFR/TA1) (P.E. Stott)	Started Jan. 1984
PLASMA SURFACE INTERACTIONS	SWEDEN (NFR/TA2) (P.E. Stott)	Started July 1987
NEUTRON PRODUCTION RELATED PHYSICS	HARWELL, UK (HAR/TA1) (P.E. Stott)	Started Jan. 1984

Title	*Associations (JET Responsible Officer)*	*Duration of Agreement*
NEUTRON PRODUCTION RELATED PHYSICS AND ASSOCIATED DIAGNOSTICS	FRASCATI, ITALY (ENEA/TA3) (P.E. Stott)	Started Jan 1986
PHYSICS OF TURBULENT AND CONVECTIVE TRANSPORT, MHD AND RELATED DIAGNOSTICS	FOM NETHERLANDS (FOM/TA2) (P.E. Stott)	Started Nov. 1987
EXPERIMENTAL DIVISION II		
BULK IMPURITY PHYSICS AND IMPURITY RELATED DIAGNOSTICS	EUR-IPP FRG (P.R. Thomas)	Started Feb. 1983
SPECTROSCOPIC MEASUREMENTS: INTERPRETATION AND IMPURITY ANALYSIS	EUR-CEA CADARACHE, FRANCE (P.R.Thomas)	Started July 1984
IMPURITY ANALYSIS AND PLASMA DIAGNOSTICS USING SPECTROSCOPIC MEASUREMENTS	EUR-NFR SWEDEN (P.R. Thomas)	Started Jan. 1988
IMPURITIES AND OTHER TOPICS	EUR-AEA CULHAM,UK (P.R. Thomas)	Started June 1987
THEORY		
ANALYSIS OF LOCAL TRANSPORT IN JET AND COMPARISON WITH THEORETICAL MODELS	EUR-UKAEA CULHAM, UK (F. Tibone)	Started Jan 1991
THE PHYSICS OF SHAPED CROSS-SECTIONS	EUR-UKAEA CULHAM, UK (CUL/TA4) (W. Kerner)	Started July 1991

Appendix II

List of Articles, Reports and Conference Papers Published in 1991

1. Studies of D-D fusion reactivity in high temperature JET plasma.
   Adams J M Balet B Boyd D A Campbell D J Challis C D Christiansen J P Cordey J G Core W G F Costley A E Cottrell G A Edwards A W Elevant T Eriksson L-G Hellsten T Jarvis O N Lallia P P Lawson K Lowry C Nielsen P Sadler G Start D F H Thomas P R von Hellermann M Weisen H
   Nuclear Fusion, vol.31 no.5 May 1991, pp.891-905.

2. A parameter study of mode conversion at ion-ion hybrid resonances for ICRF-heating schemes in JET.
   Alava M J Heikkinen J A
   Joint European Torus (JET), July 1991. 45p. Report JET-P(91)31. Submitted to Physica Scripta.

3. Interpretation of deuterium pumping by plasma-facing beryllium surfaces.
   Andrew P L Peacock A T Pick M A
   Joint European Torus (JET), July 1991. 14p. Report JET-P(91)18. Submitted for publication in Journal of Nuclear Materials.

4. Confinement of high performance JET plasmas.
   Balet B Cordey J Stubberfield P M Thomsen K
   JET papers to 18th EPS Conference on Controlled Fusion and Plasma Physics, Berlin, 3-7 June 1991. Joint European Torus (JET), April 1991. Report JET-P(91)08, pp.29-32.

5. Double-crystal X-ray spectroscopy at JET.
   Barnsley R Schumacher U Kallne E Morsi H W Rupprecht G
   Review of Scientific Instruments, vol.62 no.4 April 1991, pp.889-898. (Report JET-P(90)39).

6. Atomic data for spectroscopic studies on JET. (Second report).
   Bartschat K Berrington K A Burke P G Burke V M Fon W C Hibbert A Kingston A E Reid R Tait J H
   Joint European Torus (JET), June 1991. 37p. Report JET-R(91)09.

7. Particle transport in pellet fuelled JET plasmas.
   Baylor L R Houlberg W A Milora S L Schmidt G l Kupschus P
   Nuclear Fusion, vol.31 no.7 July 1991, pp.1249-1259.

8. Pellet deposition and penetration in JET and TFTR.
   Baylor L R Schmidt G L Houlberg W A Milora S L Kupschus P Gowers C
   American Physical Society Bulletin, vol.36 no.9 1991 (Program of 33rd Annual Meeting of the Division of Plasma Physics, Tampa, Florida, 4-8 November 1991) Abstract 4S 4, p.2366.

9. Risk assessment methodology for the JET Active Gas Handling System (AGHS) and the significance of the exhaust detritiation system in meeting design safety targets.
   Bell A C Ballantyne P R
   Fusion Technology 1990. Procs. 16th Symp., London, 3-7 September 1990. Amsterdam, North-Holland, 1991. Vol.2, pp.1457-1461. (Report JET-P(90)56 vol.II pp.151-156).

10. The JET divertor coils.
    Bertolini E Celentano G Last J R Tait J Tesini A Dal Mut G D'Urzo C Ghirlanda L Laurenti A Maragliano A Veardo A
    Joint European Torus (JET), September 1991. 4p. Report JET-P(91)26. Presented to 12th Int. Conf. on Magnet Technology, Leningrad, USSR, 24-28 June 1991.

11. Supplying JET from the UK 400kV supergrid: A major engineering achievement relevant to the 'Next Step'.
    Bertolini E Cleobury E Dwek M Jervis B Marchese V Mondino P L Murphy G
    Fusion Technology 1990. Procs. 16th Symp., London, 3-7 September 1990. Amsterdam, North-Holland, 1991. Vol.1, pp.233-237. (Report JET-P(90)56 vol.I pp.1-6).

12. Fast wave current drive in the ion cyclotron range of frequencies.
    Bhatnagar V P Jacquinot J Moreau D Rimini F Start D F H
    Theory of Fusion Plasmas. Procs. of Joint Varenna-Lausanne Int. Workshop, Varenna, 27-31 August 1990. Bologna, Editrice Compositori for Societa Italiana di Fisica, 1990. pp.243-262. (Report JET-P(90)22).

13. Fast-wave current-drive efficiency calculations for JET A2-antennas.

Bhatnagar V P Jacquinot J Start D F H
Joint European Torus (JET), September 1991. 13p. Report JET-P(91)41. Presented at IAEA Technical Committee Meeting on FWCD in Reactor Scale Tokamaks, Arles, France, 23-25 September 1991.

14. ICRF heating and synergistic LH and fast-wave current drive in JET.
Bhatnagar V P Jacquinot J Gormezano C Start D F H and the JET Team
Joint European Torus (JET), September 1991. 14p. Report JET-P(91)44. Invited paper presented to 9th Topical Conf. on Radio Frequency Power in Plasmas, Charleston, USA, 19-21 August 1991.

15. ICRH H-modes produced with Be-screen antennas and coupling-resistance position feedback control.
Bhatnagar V P Bosia G Bures M Campbell D Fessey J Gottardi N Jacquinot J de Kock L Lowry C Morgan P Thomsen K Tubbing B J D Vlases G Ward D
JET papers to 18th EPS Conference on Controlled Fusion and Plasma Physics, Berlin, 3-7 June 1991. Joint European Torus (JET), April 1991. Report JET-P(91)08, pp.125-128.

16. ICRH-produced H-modes in the JET tokamak.
Bhatnagar V P Jacquinot J Tubbing B J Stork D Tanga A Balet B Bosia A Bures M Campbell D Clement S Hatayama A Lawson K Tibone F Start D F H
Plasma Physics and Controlled Fusion, vol.33 no.2 March 1991, pp.99-121. (Report JET-P(90)44).

17. An optical scanning diagnostic for neutral beam alignment on JET.
Bickley A J Jones T T C Norman T Stork D Wight J
Fusion Technology 1990. Procs. 16th Symp., London, 3-7 September 1990. Amsterdam, North-Holland, 1991. Vol.1, pp.607-611. (Report JET-P(90)56 vol.I pp.55-60).

18. Collective Thomson scattering in a relativistic magnetized plasma.
Bindslev H
JET papers to 18th EPS Conference on Controlled Fusion and Plasma Physics, Berlin, 3-7 June 1991. Joint European Torus (JET), April 1991. Report JET-P(91)08, pp.9-12.

19. Dielectric effects on Thomson scattering in a relativistic magnetized plasma.
Bindslev H
Joint European Torus (JET), 1991. Report JET-P(91)14. Submitted to Plasma Physics and Controlled Fusion.

20. An analytic procedure for currents and forces calculation in JET.
Bobbio S Bertolini E Garribba M Miano G Noll P Senatore E
Fusion Technology 1990. Procs. 16th Symp., London, 3-7 September 1990. Amsterdam, North-Holland, 1991. Vol.2, pp.1114-1118. (Report JET-P(90)56 vol.I pp.85-90).

21. MHD modelling of density limit disruptions in tokamaks.
Bondeson A Parker R D Hugon M Smeulders P
Nuclear Fusion, vol.31 no.9 September 1991, pp.1695-1716. (Report JET-P(90)73).

22. Beryllium related maintenance on JET.
Booth S J Celentano G Newbert G Pick M Tesini A
Fusion Technology 1990. Procs. 16th Symp., London, 3-7 September 1990. Amsterdam, North-Holland, 1991. Vol.2, pp.1383-1387. (Report JET-P(90)56 vol.II pp.133-138).

23. Automatic VSWR control in JET ICRH transmitters.
Bosia G Lamont B Sibley A Schmid M Wade T
Fusion Technology 1990. Procs. 16th Symp., London, 3-7 September 1990. Amsterdam, North-Holland, 1991. Vol.2, pp.1099-1103. (Report JET-P(90)56 vol.I pp.67-72).

24. The simulation of energy and particle transport, heat and density pulse propagation and H-mode confinement in JET and a reactor.
Boucher D Rebut P-H Watkins M L
JET papers to 18th EPS Conference on Controlled Fusion and Plasma Physics, Berlin, 3-7 June 1991. Joint European Torus (JET), April 1991. Report JET-P(91)08, pp.193-196.

25. First results from the JET time of flight neutral particle analyser.
Bracco G Bonnerue J L Corti S Clarke H Moleti A Tilia B Zanza V
Joint European Torus (JET), April 1991. 26p. Report JET-R(91)02.

26. High power tests of the JET prototype LHCD launcher.
Brinkschulte H Rey G Brusati M Ekedahl A Gormezano C Kaye A Lennholm M Pain M Panissie H Plancoulaine J Schild P
Fusion Technology 1990. Procs. 16th Symp., London, 3-7 September 1990. Amsterdam, North-Holland, 1991. Vol.2, pp.1166-1170. (Report JET-P(90)56 vol.I pp.91-96).

27. Lower hybrid current drive experiments in JET.
Brusati M Bartlett D Bosia G Dobbing J Ekedahl A Froissard P Gormezano C Gowers C Jacquinot J Jarvis N Kaye A Lennholm M Naito O Pain M Paoletti F Pasini D Ramos de Andrade M C Rey G Rimini F Sadler G Schild P Wade T
Joint European Torus (JET), September 1991. 44p. Report JET-P(91)45. Submitted to Nuclear Fusion.

28. Recent results from the lower hybrid current drive experiment on JET.
Brusati M Ekedahl A Froissard P Gormezano C Jacquinot J Lennholm M Lomas P J Pain M de Andrade M C R Rimini F Schild P Start D
Joint European Torus (JET), September 1991. 10p. Report JET-P(91)42. Invited paper presented to RF Topical Conference, Charleston, USA, 19-21 August 1991.

29. Assessment of beryllium Faraday screens of the JET ICRF antennas.
Bures M Jacquinot J Stamp M Summers D Start D F H Wade T D'Ippolito D Myra J
Joint European Torus (JET), July 1991. 15p. Report JET-P(91)37. Submitted for publication in Nuclear Fusion.

30. High performance H-modes with ICRF and NBI heating in JET.
Bures M Campbell D Jacquinot J Lomas P Pasini D Start D Thomas P and the JET Team
American Physical Society Bulletin, vol.36 no.9 October 1991 (Program of 33rd Annual Meeting of the Division of Plasma Physics, Tampa, Florida, 4-8 November 1991) Abstract 4S 7, p.2366.

31. Impurity release from the ICRF antenna screens in JET.
Bures M Jacquinot J Lawson K Stamp M Summers H P D'Ippolito D A Myra J R
Plasma Physics and Controlled Fusion, vol.33 no.8 July 1991, pp.937-967. (Report JET-P(90)49).

32. Low Particle Confinement H-Mode observed during ICRF Heating on JET.
M. Bures, D. Campbell, N. Gottardi, J. Jacquinot, M. Mattioli, P. Morgan, D. Pasini, D.F.H. Start
Nuclear Fusion. Report JET-P(91)61

33. The JET in-vessel inspection man-machine interface.
Businaro T Junger J F
Fusion Technology 1990. Procs. 16th Symp., London, 3-7 September 1990. Amsterdam, North-Holland, 1991. Vol.2, pp.1254-1258. (Report JET-P(90)56 vol.II pp.109-114).

34. Methodology of tritium and radiation compatibility assessments for JET diagnostic and other systems and the preliminary results.
Caldwell-Nichols C J
Fusion Technology 1990. Procs. 16th Symp., London, 3-7 September 1990. Amsterdam, North-Holland, 1991. Vol.2, pp.1452-1456. (Report JET-P(90)56 vol.II pp.145-150).

35. Characteristics and control of disruptions.
Campbell D J
JET papers presented at European Tokamak Programme Workshop, Arles, France, 5-7 December 1990. Joint European Torus (JET), March 1991. Report JET-P(91)05, pp.27-36.

36. H-mode studies in JET.
Campbell D J Giannella R Janeschitz G Lowry C G Thomas P R
American Physical Society Bulletin, vol.36 no.9 October 1991 (Program of 33rd Annual Meeting of the Division of Plasma Physics, Tampa, Florida, 4-8 November 1991) Abstract 4S 6, p.2366.

37. Overview of recent H-mode studies in JET.
Campbell D J
Contributions to 3rd Workshop on H-mode Physics, JET Joint Undertaking, Abingdon, June 1991. Joint European Torus (JET), 1991. Volume 1, pp.99-139.

38. Sawteeth and their stabilization in JET.
Campbell D J (presenter) and the JET Team
Plasma Physics and Controlled Nuclear Fusion Research. 13th Int. Conf., Washington, DC, 1-6 October 1990. Vienna, IAEA, 1991. Volume 1, pp.437-451. (Report JET-P(90)62 pp.119-131).

39. The installation of the JET pumped divertor systems inside the vacuum vessel.
Celentano G Macklin B Scott S Tait J
JET papers presented to 14th Symposium on Fusion Engineering, San Diego, USA, 30 September - 3rd October 1991. Joint European Torus (JET), October 1991. Report JET-P(91)51, pp.17-22.

40. Octant removal at JET for a toroidal field coil exchange.
Celentano G Macklin B Booth S Last J R Papstergiou S Pick M A Presle P Scott S Tesini A
Fusion Technology 1990. Procs. 16th Symp., London, 1990. Amsterdam, North-Holland, 1991.Vol.2, pp.1604-1608. (JET-P(90)56 vol.II pp.169-174).

41. Magnetic field measurements at JET based on the Faraday and motional Stark effects.
Challis C von Hellermann M Keegan B Konig R Mandl W O'Rourke J Wolf R Zwingmann W
JET papers to 18th EPS Conference on Controlled Fusion and Plasma Physics, Berlin, 3-7 June 1991. Joint European Torus (JET), April 1991. Report JET-P(91)08, pp.73-76.

42. Reliability study of the JET neutral injection system.
Challis C D Bickley A J Browne A de Esch H P L Fogg M Jones T T C Stork D Svensson L
JET papers presented to 14th Symposium on Fusion Engineering, San Diego, USA, 30 September - 3rd October 1991. Joint European Torus (JET), October 1991. Report JET-P(91)51, pp.73-78.

43. Theoretical analysis of the role of the infernal mode in the stability of peaked pressure profiles in pellet fuelled JET discharges.
Charlton L A Baylor L R Edwards A W Hammett G W Houlberg W A Kupschus P Lynch V E Milora S L O'Rourke J Schmidt G L
Nuclear Fusion, vol.31 no.10 1991, pp.1835-1842.

44. Power supplies for the stabilisation of plasma vertical position: recent upgrades and future developments.
Chiron D Bonicelli T Huart M Garribba M Mondino P L Noll P
JET papers presented to 14th Symposium on Fusion Engineering, San Diego, USA, 30 September - 3rd October 1991. Joint European Torus (JET), October 1991. Report JET-P(91)51, pp.55-60.

45. Application of plasma physics constraints to confinement data.
Christiansen J P Cordey J G Kardaun O J W F Thomsen K
Nuclear Fusion, vol.31 no.11 November 1991, pp.2117-2129. (Report JET-P(91)03).

46. A global energy confinement H-mode database for ITER.
Christiansen J P Cordey J G Thomsen K Tanga A, and teams from DIII-D, ASDEX, PDX, PBX-M, JAERI and NIFS.
Joint European Torus (JET), September 1991. 110p. Report JET-P(91)46. Submitted to Nuclear Fusion.

47. Papers to 4th Topical Meeting on Tritium Technology in Fission, Fusion and Isotopic Applications, Albuquerque, N. Mexico, Fusion Technology.
P. Chuilon et al
Conf. Proceedings. Report JET-P(91)25

48. The conversion and operation of the JET neutral beam power supplies up to 160kV.
Claesen R Mondino P L Baigger P Bertoldi P Binder D Jensen F Rushton R
Fusion Technology 1990. Procs. 16th Symp., London, 3-7 September 1990. Amsterdam, North-Holland, 1991. Vol.2, pp.1619-1623. (Report JET-P(90)56 vol.II pp.187-192).

49. Thermal instabilities in the divertor plasma during density limit discharges at JET.
Clement S Erents S K Gottardi N Harbour P J de Kock L Loarte A Lowry C L Summers D Tagle J A
American Physical Society Bulletin, vol.36 no.9 October 1991 (Program of 33rd Annual Meeting of the Division of Plasma Physics, Tampa, Florida, 4-8 November 1991) Abstract 4S 12, p.2367.

50. Deuterium and tritium release on venting the JET torus to air after the beryllium phase.
J P Gibson A Haigh A D Kaveney G Orchard J
JET papers to 18th EPS Conference on Controlled Fusion and Plasma Physics, Berlin, 3-7 June 1991. Joint European Torus (JET), April 1991. Report JET-P(91)08, pp.49-52.

51. Fusion Division of IUUSTA - Triennial Report.
J.P. Coad, S.A. Cohen, W. Poschenreider L:
IUUSTA News Bulletin and Vacuum TAIP. Report JET-P(91)56

52. Electron temperature and density sensitive X-ray emission line ratios for Cl XVI.
Coffey I H Keenan F P McAdam C Barnsley R Dickson W J Lawson K D
Peacock N J
Joint European Torus (JET), September 1991. 14p. Report JET-P(91)49. Submitted for publication in Physica Scripta.

53. Alpha-particle diagnostics for the D-T phase.
Conroy S W Bergsaker H Coad J P Jarvis O N Marcus F B McCracken G M Pitts R A Sadler G van Belle P Zhu J
JET papers to 18th EPS Conference on Controlled Fusion and Plasma Physics, Berlin, 3-7 June 1991. Joint European Torus (JET), April 1991. Report JET-P(91)08, pp.81-84.

54. Triton burnup for high neutron yield JET discharges.
Conroy S W Adams J M Jarvis O N Loughlin M J Sadler G Watkins N
American Physical Society Bulletin, vol.36 no.9 October 1991 (Program of 33rd Annual Meeting of the Division of Plasma Physics, Tampa, Florida, 4-8 November 1991) Abstract 4S 10, p.2367.

55. Tokamak stray field compensation system for JET neutral beams.
Cooper D Altmann H Carwardine J Challis C De Esch H P L Stork D
Fusion Technology 1990. Procs. 16th Symp., London, 3-7 September 1990. Amsterdam, North-Holland, 1991. Vol.2, pp.1109-1113. (Report JET-P(90)56 vol.I pp.79-84).

56. Suppression of sawtooth oscillations: Improvements to the theory.
Coppi B Migliuolo S Pegoraro F Porcelli F Schep T
American Physical Society Bulletin, vol.36 no.9 October 1991 (Program of 33rd Annual Meeting of the Division of Plasma Physics, Tampa, Florida, 4-8 November 1991) Abstract 9T 7, p.2503.

57. Electron heating in JET by ICRH.
Cordey J G Christiansen J P Core W G F Cottrell G A Eriksson L G Kovanen M A Lomas P Start D F H Taroni A Tibone F

JET papers to 18th EPS Conference on Controlled Fusion and Plasma Physics, Berlin, 3-7 June 1991. Joint European Torus (JET), April 1991. Report JET-P(91)08, pp.37-40.

58. The deposition of energy in the X-point region of a tokamak plasma.
Core W G F
Theory of Fusion Plasmas. Procs. of Joint Varenna-Lausanne Int. Workshop, Varenna, 27-31 August 1990. Bologna, Editrice Compositori for Societa Italiana di Fisica, 1990. pp.171-178.

59. Orbit effects on the particles and energy flow in the poloidal null region of a tokamak axisymmetric divertor.
Core W G F Lazzaro E
Joint European Torus (JET), April 1991. 10p. Report JET-R(91)01.

60. Neutral Beam - Plasma Interaction in JET: Comparison of PENCIL and TRANSP Modelling Results.
G. Corrigan, D.G. Muir and F. Tibone.
Report JET-R(91)14

61. First results from the JET time-of-flight neutral particle analyser.
Corti S Bracco G Moleti A Zanza V
JET papers to 18th EPS Conference on Controlled Fusion and Plasma Physics, Berlin, 3-7 June 1991. Joint European Torus (JET), April 1991. Report JET-P(91)08, pp.5-8.

62. JET Papers presented to Diagnostics for Contemporary Fusion Experiments Course and Workshop, Varenna, Italy, 27th August - 6 September 1991.
A.E. Costley et al.
Report JET-P(91)55

63. A large-orbit model of fast ion slowing down during ICRH: Comparison with JET data.
Cottrell G A Start D F H
Nuclear Fusion, vol.31 no.1 January 1991, pp.61-71. (Report JET-P(90)17).

64. Evidence for fine scale density structures on JET under additional heated conditions.
Cripwell P Costley A
JET papers to 18th EPS Conference on Controlled Fusion and Plasma Physics, Berlin, 3-7 June 1991. Joint European Torus (JET), 1991. 53-56. JET-P(91)08.

65. On comparison of spectroscopically deduced central ion temperatures and plasma rotation at JET.
Danielsson M von Hellermann M G Kallne E Mandl W Morsi H W Summers H P Zastrow K-D
Joint European Torus (JET), June 1991. 19p. Report JET-P(91)19. Submitted to Rev .Scientific Instruments.

66. Experience with helium neutral beam systems.
De Esch H P L Massmann P Bickley A Challis C D Deschamps G H Falter H D Hemsworth R S Jones T T C Stork D Svensson L Young D
JET papers presented to 14th Symposium on Fusion Engineering, San Diego, USA, 30 September - 3rd October 1991. Joint European Torus (JET), October 1991. Report JET-P(91)51, pp.35-40.

67. Local confinement in neutral beam heated JET discharges.
de Esch H P Tibone F Balet B Bickley A Challis C D Cordey J G Jones T T C Stork D von Hellermann M
JET papers to 18th EPS Conference on Controlled Fusion and Plasma Physics, Berlin, 3-7 June 1991. Joint European Torus (JET), April 1991. Report JET-P(91)08, pp.137-140.

68. Reionised power deposition in the JET neutral beam duct and plasma facing components.
De Esch H P L Jones T T C Stork D
Fusion Technology 1990. Procs. 16th Symp., London, 3-7 September 1990. Amsterdam, North-Holland, 1991. Vol.1, pp.493-497. (Report JET-P(90)56 vol.I pp.49-54).

69. Interpretation of heat and density pulse measurements in JET in terms of coupled transport.
De Haas J C M O'Rourke J Sips A C C Lopes Cardozo N J
Nuclear Fusion, vol.31 no.7 July 1991, pp.1261-1274. (Report JET-R(90)04).

70. Design of high heat flux components for the JET pumped divertor.
Deksnis E Garribba M Martin D Sborchia C Tivey R
Fusion Technology 1990. Procs. 16th Symp., London, 3-7 September 1990. Amsterdam, North-Holland, 1991. Vol.1, pp.478-482. (Report JET-P(90)56 vol.I pp.31-36).

71. Experience with high heat flux components in large tokamaks.
Dietz K J Chappuis P Horiike H Jackson G L Ulrickson M
Joint European Torus (JET), June 1991. 42p. Report JET-P(91)11. Presented at ISFNT 2, Karlsruhe.

72. Properties and performance of beryllium and carbon for plasma-facing components.
Dietz K J and the JET Team
Fusion Technology, vol.19 no.4 July 1991 (Special Issue on Carbon Materials), pp.2031-2034.

73. Edge convection driven by ICRF.
D'Ippolito D A Myra J R Jacquinot J Bures M
American Physical Society Bulletin, vol.36 no.9 October 1991 (Program of 33rd Annual Meeting of the

Division of Plasma Physics, Tampa, Florida, 4-8 November 1991) Abstract 3S 20, p.2341.

74. A model of sheath-driven impurity production by ICRF antennas.
D'Ippolito D A Myra J R Bures M Jacquinot J
Plasma Physics and Controlled Fusion, vol.33 no.6 June 1991, pp.607-642.

75. On diffusion of magnetic field lines.
Duchs D F Montvai A Sack C
Plasma Physics and Controlled Fusion, vol.33 no.8 July 1991, pp.919-935.

76. Global Sawtooth Instability Measured by Magnetic Coils in the JET Tokamak.
P.A. Duperrex, A. Pochelon, A. Edwards, J. Snipes
Nuclear Fusion. Report JET-P(91)43

77. Enhanced wall pumping in JET.
Ehrenberg J Harbour P J
Nuclear Fusion, vol.31 no.2 1991, pp.287-307.

78. The JET neutron time-of-flight spectrometer.
Elevant T Aronsson D van Belle P Grosshoeg G Hoek M Olsson M Sadler G
Nuclear Instruments & Methods in Physics Research A: Accelerators, Spectrometers, Detectors and Associated Equipment, vol.A306 nos.1,2 1991, pp.331-342.

79. Calculations of ICRF driven current profiles caused by TTMP and ELD.
Eriksson L-G Hellsten T
Theory of Fusion Plasmas. Procs. of Joint Varenna-Lausanne Int. Workshop, Varenna, 27-31 August 1990. Bologna, Editrice Compositori for Societa Italiana di Fisica, 1990. pp.347-354. (Report JET-P(90)50).

80. Time dependent self-consistent calculations of ICRH-power deposition and ion velocity distributions.
Eriksson L-G Willen U Hellsten T
Theory of Fusion Plasmas. Procs. of Joint Varenna-Lausanne Int. Workshop, Varenna, 27-31 August 1990. Bologna, Editrice Compositori for Societa Italiana di Fisica, 1990. pp.421-428. (Report JET-P(90)42).

81. $T_i(r)$ profiles from the JET neutron profile monitor for Ohmic discharges.
Esposito B Marcus F B Adams J M Conroy S Jarvis O N Loughlin M J Sadler G van Belle P Watkins N
JET papers to 18th EPS Conference on Controlled Fusion and Plasma Physics, Berlin, 3-7 June 1991. Joint European Torus (JET), April 1991. Report JET-P(91)08, pp.145-148.

82. High Resolution LIDAR Thomson Scattering at JET.
H. Fajemirokun, C. Gowers, K. Hirsch, T. Kajiwara, P. Nielsen, H. Salzmann
Proc. Laser-Aided Plasma Diagnostics Conference. Report JET-P(91)52

83. Power loading tests of the JET pumped divertor plates.
H D Martin D Massmann P Altmann H Deschamps G H Deksnis Hemsworth R S Tivey R Thompson E
Fusion Technology 1990. Procs. 16th Symp., London, 3-7 September 1990. Amsterdam, North-Holland, 1991. Vol.1, pp.483-487. (Report JET-P(90)56 vol.I pp.37-42).

84. Low density locked modes in large tokamaks.
Fitzpatrick R Hender T C Morris A W Fishpool G M Campbell D J
American Physical Society Bulletin, vol.36 no.9 October 1991 (Program of 33rd Annual Meeting of the Division of Plasma Physics, Tampa, Florida, 4-8 November 1991) Abstract 4Q 3, p.2357.

85. Fast electron dynamics during LHCD on JET.
Froissard P Brusati M Adams J M Ekedahl A Gormezano C Jarvis O N Pasini D Peysson Y Ramos de Andrade M C Rimini F Sadler G
JET papers to 18th EPS Conference on Controlled Fusion and Plasma Physics, Berlin, 3-7 June 1991. Joint European Torus (JET), April 1991. Report JET-P(91)08, pp.117-120.

86. Specific features of the control and data acquisition for the JET pellet injector.
Gadeberg M Krom J G Kupschus P Parker S B
Fusion Technology 1990. Procs. 16th Symp., London, 3-7 September 1990. Amsterdam, North-Holland, 1991. Vol.2, pp.1249-1253. (Report JET-P(90)56 vol.II pp.103-108).

87. Control and operational aspects of the MASCOT 4 force feedback servomanipulator of JET.
Galbiati L Raimondi T Garetti P Costi G
JET papers presented to 14th Symposium on Fusion Engineering, San Diego, USA, 30 September - 3rd October 1991. Joint European Torus (JET), October 1991. Report JET-P(91)51, pp.29-34.

88. Comparison of impurity and electron particle transport in JET discharges.
Giannella R Hawkes N C Lauro Taroni L Mattioli M O'Rourke J Pasini D
JET papers to 18th EPS Conference on Controlled Fusion and Plasma Physics, Berlin, 3-7 June 1991. Joint European Torus (JET), April 1991. Report JET-P(91)08, pp.185-188. Also issued as report JET-P(91)33, 1991. 16p.

89. Particle transport in JET H-modes.
Giannella R
Contributions to 3rd Workshop on H-mode Physics, JET Joint Undertaking, Abingdon, 10-12 June 1991.

Joint European Torus (JET), 1991. Volume 3, pp.677-691.

90. Spontaneous appearance of snakes in JET.
Gill R D Edwards A W Pasini D Wolfe S W
JET papers to 18th EPS Conference on Controlled Fusion and Plasma Physics, Berlin, 3-7 June 1991. Joint European Torus (JET), April 1991. Report JET-P(91)08, pp.153-156.

91. Snake-Like Density Perturbations in JET.
R.D. Gill, A.W. Edwards, D. Pasini, A. Weller
Nuclear Fusion. Report JET-P(91)54

92. Highlights of recent JET operation.
Gondhalekar A and the JET Team
JET papers presented at European Tokamak Programme Workshop, Arles, France, 5-7 December 1990. Joint European Torus (JET), March 1991. Report JET-P(91)05, pp.1-

93. Long pulse high power heating of JET plasmas.
Gondhalekar G Barnsley R Jones T T C Morgan P Lomas P Pasini D Stamp M F Stangeby P C Summers D Tagle J A Tanga A
JET papers to 18th EPS Conference on Controlled Fusion and Plasma Physics, Berlin, 3-7 June 1991. Joint European Torus (JET), April 1991. Report JET-P(91)08, pp.85-88.

94. Measurement of radial diffusion of suprathermal electrons in JET.
Gondhalekar A Martin-Solis R Bartlett D Brusati M Froissard P Hugon M Rimini F Tanzi C
American Physical Society Bulletin, vol.36 no.9 October 1991 (Program of 33rd Annual Meeting of the Division of Plasma Physics, Tampa, Florida, 4-8 November 1991) Abstract 4S 9, p.2367.

95. Determination of the deuterium temperature profile in magnetic fusion plasmas.
Gorini G Gottardi N
Nuovo Cimento, vol.13D no.3 March 1991, pp.319-336.

96. Lower hybrid current drive experiments on JET.
Gormezano C Bosia G Brusati M Dobbing J Ekedahl A Froissard P Jacquinot J Kaye A Lennholm M Naito O Pain M Paoletti F Pasini D Ramos de Andrade C Rey G Rimini F Schild P
JET papers to 18th EPS Conference on Controlled Fusion and Plasma Physics, Berlin, 3-7 June 1991. Joint European Torus (JET), April 1991. Report JET-P(91)08, pp.133-136.

97. Radio frequency heating and current drive -Status and prospects for the Next Step.
Gormezano C
Fusion Engineering and Design, vol.14 nos.1&2 April (I) 1991 (Invited papers of 16th Symp. on Fusion Technology, London, 3-7 September 1990) pp.99-110. (Report JET-P(90)64).

98. Synergistic Effects Between Lower Hybrid and Fast Magnetosonic Waves in JET.
C. Gormezano, M. Brusati, A. Ekedahl, P. Froissard, J. Jacquinot, F. Rimini
Proc. IAEA Tech. Comm. on Fast Wave Current Drive in Reactor. Report JET-P(91)53

99. LIDAR Thomson Scattering (Report on the IAEA Technical Committee Meeting, JET Joint Undertaking, Abingdon, Oxfordshire, UK, 8-10 April 1991).
Gowers C W
Nuclear Fusion, vol.31 no.11 November 1991, pp.2173-2180. (Report JET-P(91)27).

100. Experiments with high-voltage insulators in the presence of tritium.
Grisham L R Falter H Stevenson T Wright K Causey R Christman W
Review of Scientific Instruments, vol.62 no.2 February 1991, pp.376-380. (Report JET-P(90)07).

101. The behaviour of neutral particles in the private region of X-point discharges in JET.
Haas G Duchs D Ehrenberg J Lesourd M Montvai A Reichle R Summers D
JET papers to 18th EPS Conference on Controlled Fusion and Plasma Physics, Berlin, 3-7 June 1991. Joint European Torus (JET), April 1991. Report JET-P(91)08, pp.89-92.

102. SOL parameters and profiles in JET H-modes and their relation to transport.
Harbour P J
Contributions to 3rd Workshop on H-mode Physics, JET Joint Undertaking, Abingdon, 1991. Joint European Torus (JET), 1991. Volume 1, pp.185-201.

103. Intensity calibrations of the broadband VUV impurity survey spectrometer - KT2.
Hawkes N Peacock N J Lawson K D
Joint European Torus (JET), August 1991. 24p. Report JET-R(91)07.

104. Fast wave absorption at the Alfven resonance during ion cyclotron resonance heating.
Heikkinen J A Hellsten T Alava M J
Nuclear Fusion, vol.31 no.3 March 1991, pp.417-429.

105. Fusion technology (Report on the 16th Symp. on Fusion Technology (SOFT), London, UK, 1990).
Hemsworth R S
Nuclear Fusion, vol.31 no.1 January 1991, pp.199-205. (Report JET-P(90)61).

106. Some key technical developments for the fast ion and alpha particle diagnostic system on JET.
Hoekzema J A Hammond N Taylor E F Stevens A L
Fusion Technology 1990. Procs. 16th Symp., London, 3-7 September 1990. Amsterdam, North-Holland, 1991. Vol.1, pp.627-631. (Report JET-P(90)56 vol.I pp.61-66).

107. Evidence of coupling of thermal and particle transport from heat and density pulse measurements in JET.
Hogeweij G M D O'Rourke J Sips A C C
Plasma Physics and Controlled Fusion, vol.33 no.3 March 1991, pp.189-198. (Report JET-P(90)45).

108. JET gas economy with C and Be first wall and implications for the gas introduction system.
How J Usselmann E Saibene G Sartori R Green B J Brelen H Rainford M Gondhalekar A
Fusion Technology 1990. Procs. 16th Symp., London, 3-7 September 1990. Amsterdam, North-Holland, 1991. Vol.1, pp.728-732. (Report JET-P(90)56 vol.II pp.115-120).

109. AC operation of JET tokamak: modification of the JET poloidal field system.
Huart M Benfatto I Chiron D Dolgetta N Garribba M Noll P Tubbing B
JET papers presented to 14th Symposium on Fusion Engineering, San Diego, USA, 1991. Joint European Torus (JET), 1991. Report JET-P(91)51, pp.47-54.

110. Current rise studies.
Hugon M Balet B Christiansen J P Edwards A Fishpool G Gimblett C G Gottardi N Hastie R J Lomas P Milligen B Neill G O'Rourke J Sips G Smeulders P Stubberfield P M Tagle T Wolfe S
JET papers to 18th EPS Conference on Controlled Fusion and Plasma Physics, Berlin, 3-7 June 1991. Joint European Torus (JET), April 1991. Report JET-P(91)08, pp.141-144.

111. Self-consistent magnetic chaos induced by electron temperature gradient.
Hugon M Rebut P H
Plasma Physics and Controlled Nuclear Fusion Research. 13th Int. Conf., Washington, DC, 1-6 October 1990. Vienna, IAEA, 1991. Vol.2, pp.45-57. (Report JET-P(90)62 pp.132-144).

112. Shear reversal and MHD activity during pellet enhanced performance plasmas in JET.
Hugon M van Milligen B Ph Smeulders P Appel L Bartlett D Boucher D Edwards A Eriksson L Gowers C Hender T C Huysmans G Jacquinot J Kupschus P Porte L Rebut P H Start D Tibone F Tubbing B J D Watkins M Zwingmann W
Joint European Torus (JET), July 1991. 25p. Report JET-P(91)29. Submitted to Nuclear Fusion.

113. Shear reversal and MHD behaviour during PEP-mode in JET.
Hugon M Appel L Bartlett D Boucher D Edwards A Eriksson L Gowers C Hender T C Huysmans G Jacquinot J Kupschus P Milligen B V Porte L Rebut P H Sack C Start D Smeulders P Taroni A Tibone F Tubbing B Watkins M Zwingmann W
American Physical Society Bulletin, vol.36 no.9 1991 (33rd Annual Meeting of the Division of Plasma Physics, Tampa, Florida, 1991) Abstract 4S 1, p.2365.

114. Design of the JET pumped divertor.
Huguet M Altmann H Barabaschi P Bertolini E Deitz K Deksnis E Falter H Froger C Garribba M Kaye A Last J R Lobel R Martin E Massmann P Noll P Obert W Papastergiou S Peacock A Pick M Rebut P-H Rossi L Sborchia C Sannazzaro G Tesini A Tivey R
JET papers presented to 14th Symposium on Fusion Engineering, San Diego, USA, 30 September - 3rd October 1991. Joint European Torus (JET), October 1991. Report JET-P(91)51, pp.91-96.

115. JET status and prospects.
Huguet M presenter, and the JET Team
JET papers presented to 14th Symposium on Fusion Engineering, San Diego, USA, 30 September - 3rd October 1991. Joint European Torus (JET), October 1991. Report JET-P(91)51, pp.11-16.

116. Technical aspects of impurity control at JET: status and future plans.
Huguet M and the JET Team
Fusion Technology, vol.19 no.3 May 1991 (Procs. 9th Topical Meeting on the Technology of Fusion Energy, Oak Brook, Illinois, 7-11 October 1990), pp.1237-1246. (Report JET-P(90)70).

117. The sputtering yields and impurity spatial distributions at the beryllium belt limiters in JET.
Hwang A Stamp M F Summers D D R Elder D Forrest M J McCracken G M Morgan P D Stangeby P C Summers H P
Plasma-Surface Interactions in Controlled Fusion Devices. 9th Int. Conf., Bournemouth, 21-25 May 1990. Journal of Nuclear Materials, vols.176-177, 1990, pp.588-592.

118. Charge-Exchange Diagnostic of Fusion Alpha Particles and ICRF Driven Minority Ions in MeV Energy Range in JET Plasma.
A.B. Izvozchikov, A.V. Khudoleev, M.P. Petrov, S. Ya Petrov, S.S. Kozlovskij, S. Corti, A. Gondhalekar.
Report JET-R(91)12

119. D - ^{3}He fusion in the JET tokamak: Recent experimental results.
Jacquinot J Sadler G and the JET Team
Joint European Torus (JET), 1991. Report JET-P(91)07.

120. Heating, current drive and confinement regimes with the JET ICRH and LHCD system.
Jacquinot J presenter and the JET Team
Plasma Physics and Controlled Fusion, vol.33 no.13 November 1991, (Controlled Fusion and Plasma Physics: 18th Euro. Physical Society, Plasma Physics Division Conf., Berlin, Germany, 3-7 June 1991. Invited Papers) pp.1657-1675. (Report JET-P(91)20).

121. JET results with both fast and lower hybrid waves. Consequences for future devices.
Jacquinot J presenter and the JET Team
American Physical Society Bulletin, vol.36 no.9 1991 (Program of 33rd Annual Meeting of the Division of Plasma Physics, Tampa, Florida, 4-8 November 1991) Abstract 2I 1, p.2295.

122. JET Results with Both Fast and Lower Hybrid Waves Consequences for Future Devices.
J. Jacquinot, M. Bures, JET Team
Physics of Fluids. Report JET-P(91)58

123. Power dissipation and impurity dynamics in the divertor region in JET.
Jaeckel H J Giannella R Gottardi N Harbour P J Janeschitz G Reichle R Summers D D R Tagle T
American Physical Society Bulletin, vol.36 no.9 October 1991 (Programme of 33rd Annual Meeting of the Division of Plasma Physics, Tampa, Florida, 4-8 November 1991) Abstract 4S 13, p.2367.

124. Dependence of He retention on X-point plasma parameters in JET.
Janeschitz G Gottardi N Jaeckel H Coulon J P Denne B Gianella R Haas G Lawson K Tagle T
JET papers to 18th EPS Conference on Controlled Fusion and Plasma Physics, Berlin, 3-7 June 1991. Joint European Torus (JET), April 1991. Report JET-P(91)08, pp.77-80.

25. Neutron diagnostics for tokamak experiments.
Jarvis O N
Joint European Torus (JET), April 1991. 6p. Report JET-P(91)13. Presented to the International Conference on Nuclear Data for Science and Technology, Julich, 1991.

126. Triton burnup in JET - Profile effects.
Jarvis O N Adams J M Conroy S W Marcus F B Sadler G J Watkins N van Belle P
JET papers to 18th EPS Conference on Controlled Fusion and Plasma Physics, Berlin, 3-7 June 1991. Joint European Torus (JET), April 1991. 57-60. JET-P(91)08, pp.

127. Use of activation techniques for the measurement of neutron yields from deuterium plasmas at the Joint European Torus.
Jarvis O N Clipsham E W Hone M A Laundy B J Pillon M Rapisarda M Sadler G J Van Belle P Verschuur K A
Fusion Technology, vol.20 no.3 November 1991, pp.265-284. (Report JET-P(90)46).

128. The design and construction of the TARM - a crane-mounted remotely-controlled transporter for JET.
Jones L P D F Galbiati L Gredel M Neddermeyer W
Fusion Technology 1990. Procs. 16th Symp., London, 3-7 September 1990. Amsterdam, North-Holland, 1991. Vol.2, pp.1378-1382. (Report JET-P(90)56 vol.II pp.127-132).

129. Simulated ash transport experiments in JET using helium neutral beams and charge exchange spectroscopy.
Jones T T C von Hellermann M G Bickley A J Boucher D Breger P Challis C D Christiansen J P Cottrell G A Davies J F de Esch H PL Fogg M Frieling J Gianella R Gondhalekar A Koenig R W T Lomas P J Magyar G Mandl W Marcus F B Morgan P D Morsi H Prentice R Sadler G Stamp M F Stork D Summers H P Svensson L Tanga A Taroni A Thomas P R Thompson E Wolf R
JET papers to 18th EPS Conference on Controlled Fusion and Plasma Physics, Berlin, 3-7 June 1991. Joint European Torus (JET), April 1991. Report JET-P(91)08, pp.121-124.

130. New classifications in Si-like Kr XXIII and Mo XXIX.
Jupen C Martinson I Denne-Hinnov B
Joint European Torus (JET), June 1991. 19p. Report JET-P(91)21. Preprint of paper to be submitted for publication in Physica Scripta.

131. JET: Progress in performance and understanding.
Keilhacker M presenter and the JET Team
Plasma Physics and Controlled Fusion, vol.33 no.13 November 1991 (Controlled Fusion and Plasma Physics: 18th Euro. Physical Society, Plasma Physics Division Conf., Berlin, Germany, 3-7 June 1991 Invited Papers) pp.1453-1477. (Report JET-P(91)30).

132. Modelling impurity control by plasma flows in the JET pumped divertor.
Keilhacker M Deksnis E Harbour P Rebut P-H Simonini R Taroni A Vlases G C Watkins M L
Plasma Physics and Controlled Nuclear Fusion Research. 13th Int. Conf., Washington, DC, 1-6 October 1990. Vienna, IAEA, 1991. Volume 1, pp.345-364. (Report JET-P(90)62 pp.79-96).

133. Scrape-off layer model for the study of impurity retention in the pumped divertor planned for JET.
Keilhacker M Simonini R Taroni A Watkins M L
Nuclear Fusion, vol.31 no.3 1991, pp.535-545. (Report JET-P(90)37).

134. Computing the damping and destabilization of global Alfven waves in tokamaks.
Kerner W Poedts S Goedbloed J P Huysmans G T A Keegan B Schwarz E
JET papers to 18th EPS Conference on Controlled Fusion and Plasma Physics, Berlin, 3-7 June 1991. Joint European Torus (JET), April 1991. Report JET-P(91)08, pp.97-100.

135. MHD model of ELM's in JET.
Kerner W Campbell D Janeschitz G Zwingmann W Huysmans G Goedbloed J P
American Physical Society Bulletin, vol.36 no.9 October 1991 (Program of 33rd Annual Meeting of the Division of Plasma Physics, Tampa, Florida, 4-8 November 1991) Abstract 2R 13, p.2310.

136. Modelling of the observed particle and heat fluxes in the X-point region at JET.
Kovanen M A Reichle R Lazzaro E Summers D D R Taylor T
Joint European Torus (JET), March 1991. 21p. Report JET-P(91)06. Submitted for publication in Nuclear Fusion.

137. Monte-Carlo study of high power (D)T ICRF heating in JET.
Kovanen M A J
Joint European Torus Report JET-P(91)24.

138. High thermonuclear yield on JET by combining enhanced plasma performance of ICRH-heated, pellet-peaked density profiles with H-mode confinement.
Kupschus P Balet B Bartlett D Boucher D Challis C Corrigan G Corti S Edwards A Eriksson L G Gill R Gormezano C Gowers C Holm H Hugon M Jacquinot J Lawson K Morsi H Neill G Oosterbeek H O'Rourke J Pasini D Porte L Rimini F Sadler G Schmidt G Sips G Smeulders P Start D Stubberfield P Taroni A Tibone F Tubbing B von Hellermann M van Milligen B Zwingmann W
JET papers to 18th EPS Conference on Controlled Fusion and Plasma Physics, Berlin, 1991.
Joint European Torus (JET), April 1991. Report JET-P(91)08, pp.17-20.

139. The JET high-speed pellet launcher prototype -Development, implementation and operational experience.
Kupschus P Sonnenberg K Bailey W Flory D Gadeberg M Ge X Hedley L Helm J Novak A Romain R Twynam P Szabo T Watson M Willis B Zheng Z
Fusion Technology 1990. Procs. 16th Symp., London, 3-7 September 1990. Amsterdam, North-Holland, 1991. Vol.1, pp.268-272. (Report JET-P(90)56 vol.I pp.7-12).

140. Development of a high-speed repetitive pellet launcher for JET.
Lafferanderie J Claudet G Disdier F Gagne M Jacquemet M Kupschus P Sonnenberg K
Fusion Technology 1990. Procs. 16th Symp., London, 3-7 September 1990. Amsterdam, North-Holland, 1991. Vol.1, pp.742-746.

141. JET TF coil fault-detection, diagnosis and prevention.
Last J R Bonicelli T Cooke M Dolgetta N Huguet M Lanza R Noll P Presle P
Sborchia C
Fusion Technology 1990. Procs. 16th Symp., London, 3-7 September 1990. Amsterdam, North-Holland, 1991. Vol.2, pp.1609-1613. (Report JET-P(90)56 vol.II pp.175-181).

142. The JET divertor magnetic configuration and coil design.
Last J R Barabaschi P Bertolini E Garribba M Huguet M Noll P Rebut P H Sborchia C
Fusion Technology 1990. Procs. 16th Symp., London, 3-7 September 1990. Amsterdam, North-Holland, 1991. Vol.2, pp.1614-1618. (Report JET-P(90)56 vol.II pp.181-186).

143. The calculation of the neoclassical impurity transport coefficients.
Lauro Taroni L Bittoni E Giannella R Springmann E Taroni A
Joint European Torus (JET), October 1991. 25p. Report JET-R(91)10.

144. Results from edge spectroscopy in JET.
Lawson K D Barnsley R Denne-Hinnov B Gianella R Gottardi N Hawkes N C Morgan P D Patel T K Peacock N J Stamp M F
JET papers to 18th EPS Conference on Controlled Fusion and Plasma Physics, Berlin, 3-7 June 1991. Joint European Torus (JET), April 1991. Report JET-P(91)08, pp.173-176.

145. An investigation of the power balance associated with recycling in JET ohmic limiter discharges.
Loarte A Harbour P J Summers H P Tagle J A Dickson W J
Joint European Torus (JET), June 1991. 4p. Report JET-P(91)22. Submitted for publication in procs. of 18th Annual Conf. on Plasma Physics, University of Essex, 3-5 July 1991.

146. The Effect of the Magnetic Flux Geometry of a Poloidal Divertor on the Profiles and Parameters at the Target.
A. Loarte, P.J. Harbour
Nuclear Fusion Letters. Report JET-P(91)60

147. ICRF antennae for the JET pumped divertor configuration.
Lobel R Bhatnagar V Jacquinot J Kaye A Panissie H Rebut P-H

Fusion Technology 1990. Procs. 16th Symp., London, 3-7 September 1990. Amsterdam, North-Holland, 1991. Vol.2, pp.1104-1108. (Report JET-P(90)56 vol.I pp.73-78).

148. Ion temperature and fuel dilution measurements using neutron spectrometry.
Loughlin M J Adams J M Conroy S Elevant T Hawkes N Jarvis O N Marcus F B Morsi H Olsson M Sadler G van Belle P von Hellermann M
JET papers to 18th EPS Conference on Controlled Fusion and Plasma Physics, Berlin, 3-7 June 1991. Joint European Torus (JET), April 1991. Report JET-P(91)08, pp.109-112.

149. Optimisation of performance in JET limiter plasmas.
Lomas P J (presenter) and the JET Team
Plasma Physics and Controlled Nuclear Fusion Research. 13th Int. Conf., Washington, DC, 1-6 October 1990. Vienna, IAEA, 1991. Volume 1, pp.425-435. (Report JET-P(90)62 pp.27-40).

150. The performance of high current belt limiter plasmas in JET.
Lomas P J Bartlett D Brusati M Cottrell G Christiansen J P de Esch H Fishpool G Gianella R Gondhalekar A Hugon M Jones T T C Magyar G Marcus F Prentice R Sadler G Sartori R Stamp M Tanga A Taroni A Tibone F
JET papers to 18th EPS Conference on Controlled Fusion and Plasma Physics, Berlin, 3-7 June 1991. Joint European Torus (JET), April 1991. Report JET-P(91)08, pp.45-48.

151. Sawtooth heat pulse propagation in tokamaks.
Lopes Cardozo N J Sips A C C
Plasma Physics and Controlled Fusion, vol.33 no.11 September 1991, pp.1337-1345. (Report JET-P(91)17).

152. Sawtooth heat and density pulse propagation in tokamaks.
Lopes Cardozo N J Sips A C C
American Physical Society Bulletin, vol.36 no.9 October 1991 (Program of 33rd Annual Meeting of the Division of Plasma Physics, Tampa, Florida, 4-8 November 1991) Abstract 9S 23, p.2500.

153. JET experiments with 120 keV 3He and 4He neutral beam injector.
Marcus F B Adams J M Bartlett D V Bhatnagar V Bickley A J Bures M Campbell D J Challis C D Christiansen J P Conroy S Cordey J G Core W Corti S Cottrell G de Esch H de Kock L Elevant T Eriksson L G Falter H Giannella R Gill R D Gondhalekar A Gottardi N Hemsworth R Jacquinot J Jarvis O N Jones T T C Konig R Lomas P Loughlin M Lowry C Magyar G Mandl W Massmann P Morgan P Morsi H Nielsen P Obert W O'Rourke J Prentice R Sadler G Smeulders P Stamp M Start D F Stork D Summers D Summers H Svensson L Tanga A Taroni A Thomas P R Thompson E Tubbing B Tibone F van Belle P von Hellermann M Watkins N
JET papers to 18th EPS Conference on Controlled Fusion and Plasma Physics, Berlin, 3-7 June 1991. Joint European Torus (JET), April 1991. Report JET-P(91)08, pp.149-152.

154. JET neutron emission profiles and fast ion redistribution during sawtooth crashes.
Marcus F B Adams J M Cheetham A D Conroy S Core W G F Jarvis O N Loughlin M J Olsson M Sadler G Smeulders P van Belle P Watkins N
Plasma Physics and Controlled Fusion, vol.33 no.4 April 1991, pp.277-287. (Report JET-P(90)55).

155. Pumping of ^{3}He and ^{4}He gas using argon frosted liquid helium cryo-pumps at sub-condensation temperatures.
Massmann P Bickley A J Davies J F Deschamps G H De Esch H P Falter H D Hemsworth R S Jones T T C
Fusion Technology 1990. Procs. 16th Symp., London, 3-7 September 1990. Amsterdam, North-Holland, 1991. Vol.1, pp.463-467. (Report JET-P(90)56 vol.I pp.13-18).

156. Global modelling of impurities in JET belt limiter discharges.
McCracken G M Matthews G F De Kock L Erents S K Gottardi N A Lowry C Morgan P D Stamp M F Stangeby P C
Plasma-Surface Interactions in Controlled Fusion Devices. 9th Int. Conf., Bournemouth, 1990. Journal of Nuclear Materials, vols.176-177 1990, pp.392-397.

157. The JET quality assurance programme and its associated system of technical documents.
Meriguet P Evans C Green B Horn G Hurd F Rebut P H Sigournay D
Fusion Technology 1990. Procs. 16th Symp., London, 1990. Amsterdam, North-Holland, 1991 Vol.2, pp.1462-1466. (Report JET-P(90)56 vol.II pp.157-162).

158. Impurities and Ion Temperature Gradient Modes.
S. Migliuolo.
Report JET-R(91)13

159. Ion temperature gradient driven impurity modes.
Migliuolo S
Joint European Torus (JET), July 1991. 17p. Report JET-P(91)34.

160. Stabilization of collisional drift-tearing modes at the breakdown of the constant-y approximation.
Migliuolo S Pegoraro F Porcelli F
Physics of Fluids B: Plasma Physics, vol.3 no.6 June 1991, pp.1338-1345.

161. The design, development and use of pipe cutting tools for remote handling in JET.
Mills S F Loving A Irving M
JET papers presented to 14th Symposium on Fusion Engineering, San Diego, USA, 30 September - 3rd October 1991. Joint European Torus (JET), October 1991. Report JET-P(91)51, pp.61-66.

162. The Thermodynamics of the Vlasov Equilibria.
E. Minardi
Journal of Plasma Physics. Report JET-P(91)62

163. The high power, wide bandwidth disruption feedback amplifiers for JET.
Mondino P L Tenconi S M Boselli A Carpita M Dolgetta N Gallandt C Marchese V Odone A Pittera L Rizzo E Santagiustina A
Fusion Technology 1990. Procs. 16th Symp., London, 1990. Amsterdam, North-Holland, 1991. Vol.2, p.1624. (Report JET-P(90)56 vol.II pp.193-198).

164. Magnetohydrodynamic Stability Thresholds as a Function of Hartmann Number and Pinch Ratio.
D. Montgomery
Plasma. Phys. & Contr. Fusion. Report JET-P(91)64

165. Lower hybrid current drive in TORE SUPRA and JET.
Moreau D Gormezano G
Plasma Physics and Controlled Fusion, vol.33 no.13 November 1991 (Controlled Fusion and Plasma Physics: 18th Euro. Physical Society, Plasma Physics Division Conf., Berlin, Germany, 1991 Invited Papers), pp.1621-1638.

166. The evolution of Z_{eff} during H-mode operation in JET.
Morgan P D Ellis J J Morsi H W Oord E Oster J Stamp M F Thomsen K von Hellerman M Zastrow K D
JET papers to 18th EPS Conference on Controlled Fusion and Plasma Physics, Berlin, 1991. Joint European Torus, 1991. Report JET-P(91)08, pp.69-72.

167. A new diagnostic for the tritium phase of JET covering the visible and UV wavelength range.
Morsi H W Hatzky R von Hellermann M Mandl W McKillen R R Mijnarends M Millward P Nielsen P Reid J Roberts P Ryan J Thomas P Viaccoz B
JET papers to 18th EPS Conference on Controlled Fusion and Plasma Physics, Berlin, 3-7 June 1991. Joint European Torus (JET) 1991. Report JET-P(91)08, pp.65-68.

168. Power threshold for L-H mode transition in JET.
Nardone C Bhatnagar V P Campbell D Gottardi N Lazzaro E O'Brien D Tanga A Weisen H
JET papers to 18th EPS Conference on Controlled Fusion and Plasma Physics, Berlin, 3-7 June 1991. Joint European Torus (JET), 1991. Report JET-P(91)08, pp.169-172.

169. Fishbone activity in JET.
Nave M F F Campbell D J Joffrin E Marcus F B Sadler G Smeulders P Thomsen K
Nuclear Fusion, vol.31 no.4 April 1991, pp.697-710.

170. JET pumped divertor cryo-pump.
Obert W Papastergiou S Rebut P H Barabaschi P Deschamps G Deksnis E Garribba M Mayaux Ch Perinic G Sannazarro G
Fusion Technology 1990. Procs. 16th Symp., London, 3-7 September 1990. Amsterdam, North-Holland, 1991. Vol.1, pp.488-492. (Report JET-P(90)56 vol.I pp.43-48).

171. Edge current density in H-mode discharges at JET.
O'Brien D P Challis C D Cordey J G Ellis J J Jackson G Lao L L Stubberfield P M Taylor T S
JET papers to 18th EPS Conference on Controlled Fusion and Plasma Physics, Berlin, 3-7 June 1991. Joint European Torus (JET), April 1991. Report JET-P(91)08, pp.157-160.

172. Equilibrium analysis of iron-core tokamaks using a full-domain method.
O'Brien D P Lao L L Solano E R Garribba M Taylor T S Cordey G Ellis J J
Joint European Torus (JET), October 1991. 23p. Report JET-P(91)50. Submitted for publication in Nuclear Fusion.

173. Energy Resolution Optimization of a Two-Detector Time-of-Flight Spectrometer for D-D Neutrons.
M. Olsson
Nucl. Instrum. and Methods. Report JET-P(91)65

174. The change in the safety factor profile at a sawtooth collapse.
O'Rourke J
Plasma Physics and Controlled Fusion, vol.33 no.4 April 1991, pp.289-296. (Report JET-P(90)43).

175. Perturbative measurements of the electron transport matrix using ICRF power modulation.
O'Rourke J Rimini F Start D H F
Joint European Torus (JET), September 1991. 11p. Report JET-P(91)47. Submitted to Nuclear Fusion.

176. The role of the plasma current distribution in L-mode confinement.
O'Rourke J Balet B Challis C Cordey J G Gowers C Jacquinot J Kramer G Tibone F Stubberfield P
JET papers to 18th EPS Conference on Controlled Fusion and Plasma Physics, Berlin, 1991. Joint European Torus, 1991. Report JET-P(91)08, pp.129-132.

177. Impurity transport in JET.
Pasini D
Joint European Torus, 1991. 14p. Report JET-P(91)36.

178. Impurity transport in JET.
Pasini D Denne-Hinnov B Gianella R Hawkes N Lauro Taroni L Magyar G
Mattioli M
Weisen H JET papers to 18th EPS Conference on Controlled Fusion and Plasma Physics, Berlin, 3-7 June 1991. Joint European Torus (JET), April 1991. Report JET-P(91)08, pp.105-108.

179. Operational experience with the JET beryllium evaporators.
Peacock A T Coad J P Dietz K J Israel G Jensen H S Pick M A Saibene G Bergsaker H
Fusion Technology 1990. Procs. 16th Symp., London, 1990. Amsterdam, North-Holland, 1991. Vol.1, pp.468-472. (Report JET-P(90)56 vol.I pp.19-24).

180. Latest JET experimental results on the sawtooth.
Pearson D Campbell D J Edwards A W O'Rourke J
JET papers to 18th EPS Conference on Controlled Fusion and Plasma Physics, Berlin, 3-7 June 1991. Joint European Torus (JET), April 1991. Report JET-P(91)08, pp.1-4.

181. Internal m=1 modes and large ion-gyroradius effects.
Pegoraro F Porcelli F Schep T J
Theory of Fusion Plasmas. Procs. of Joint Varenna-Lausanne Int. Workshop, Varenna, 27-31 August 1990. Bologna, Editrice Compositori for Societa Italiana di Fisica, 1990. pp.539-556.

182. Large gyroradius m=1 Alfven modes and energetic particles.
Pegoraro F Porcelli F Schep T J
Physics of Fluids B: Plasma Physics, vol.3 no.6 June 1991, pp.1319-1325.

183. Evidence of halo currents in JET.
Pick M A Noll P Barabaschi P Marcus F B Rossi L
JET papers presented to 14th Symposium on Fusion Engineering, San Diego, USA, 30 September - 3rd October 1991. Joint European Torus (JET), October 1991. Report JET-P(91)51, pp.85-90.

184. Superconductors and superconducting magnets. Part I.
Pohlchen R
Joint European Torus (JET), May 1991. 9p. Report JET-R(91)04.

185. Collisionless m=1 tearing mode.
Porcelli F
Physical Review Letters, vol.66 no.4 28 January 1991, pp.425-428. (Report JET-P(90)23).

186. Fast particle stabilisation.
Porcelli F
Plasma Physics and Controlled Fusion, vol.33 no.13 November 1991 (Controlled Fusion and Plasma Physics: 18th Euro. Physical Society, Plasma Physics Division Conf., Berlin, Germany, 3-7 June 1991. Edited by D C Robinson. Invited Papers), pp.1601-1620. (Report JET-P(91)32).

187. Internal kink stabilization by high energy ions with non-standard orbits.
Porcelli F Berk H L Zhang Y Z
Joint European Torus (JET), September 1991. 13p. Report JET-P(91)35. Submitted for publication in Physics of Fluids B.

188. First results with the upgraded ECE heterodyne radiometer on JET.
Porte L Bartlett D V Campbell D J Costley A C
JET papers to 18th EPS Conference on Controlled Fusion and Plasma Physics, Berlin, 3-7 June 1991. Joint European Torus (JET), April 1991. Report JET-P(91)08, pp.189-192.

189. Fusion Energy Production from a Deuterium-Tritium Plasma in the JET Tokamak.
P-H. Rebut, A. Gibson, M. Huguet et al (JET Team)
Nuclear Fusion Journal. JET-P(91)66

190. Future prospects for JET and Next Step tokamaks.
Rebut P-H
Fusion Engineering and Design, vol.14 nos.1&2 April (I) 1991 (Invited papers of 16th Symp. on Fusion Technology, London, 3-7 September 1990), pp.171-182. (Report JET-P(90)66).

191. Impact of JET results on the concept of a fusion reactor.
Rebut P-H
Joint European Torus (JET), May 1991. 20p. Report JET-P(91)23. Talk at AD Sakharov Int. Conf. on Physics, Moscow, USSR, 27-31 May 1991.

192. The JET results and the scientific feasibility of thermonuclear fusion.
Rebut P-H
Revue Generale Nucleaire, no.1 1991, pp.30-40.

193. Magnetic turbulence self-sustainment by finite Larmor radius effect.
Rebut P-H Hugon M
Plasma Physics and Controlled Fusion, vol.33 no.9 August 1991, pp.1085-1101. (Report JET-P(90)58).

194. A programme towards a fusion reactor.
Rebut P-H
JET papers presented at European Tokamak Programme Workshop, Arles, France, 5-7 December 1990. Joint European Torus (JET), March 1991. Report JET-P(91)05, pp.17-22.

195. A program toward a fusion reactor.
Rebut P-H Watkins M L Gambier D J Boucher D

Physics of Fluids B: Plasma Physics, vol.3 no.8 pt.2 August 1991 (Special Issue: Invited and Review Papers from the 32nd Annual Meeting of the Division of Plasma Physics of the American Physical Society, Cincinnati, Ohio, 12-16 November 1990), pp.2209-2219. (Report JET-P(90)75).

196. Recent JET results and future prospects.
Rebut P-H presenter and the JET Team
Plasma Physics and Controlled Nuclear Fusion Research. 13th Int. Conf., Washington, DC, 1-6 October 1990. Vienna, IAEA, 1991. Volume 1, pp.27-52. (Report JET-P(90)62 pp.1-26).

197. Power loading and radiation distribution at the X-point target in JET for normal and reversed toroidal field.
Reichle R Clement S Gottardi N Jaeckel H J Lesourd M Summers D D R
JET papers to 18th EPS Conference on Controlled Fusion and Plasma Physics, Berlin, 3-7 June 1991. Joint European Torus (JET), April 1991. Report JET-P(91)08, pp.101-104.

198. Synergistic effects between lower hybrid and fast magnetosonic waves in JET.
Rimini F Brusati M Ekedahl A Froissard P Gormezano C Jacquinot J Paoletti F
American Physical Society Bulletin, vol.36 no.9 October 1991 (Program of 33rd Annual Meeting of the Division of Plasma Physics, Tampa, Florida, 4-8 November 1991) Abstract 7R 3, p.2440.

199. Remote handling mock-up trials of replacement of a JET neutral beam ion source.
Rolfe A C Burgess T Removille J
JET papers presented to 14th Symposium on Fusion Engineering, San Diego, USA, 30 September - 3rd October 1991. Joint European Torus (JET), October 1991. Report JET-P(91)51, pp.23-28.

200. Beryllium safety at JET.
Russ R M Haigh A D Booth S J
JET papers presented to 14th Symposium on Fusion Engineering, San Diego, USA, 30 September - 3rd October 1991. Joint European Torus (JET), October 1991. Report JET-P(91)51, pp.41-46.

201. ^{3}He-D fusion yield studies in JET.
Sadler G Christiansen J P Cottrell G A de Esch H P L Eriksson L Gianella R Gondhalekar A Jacquinot J Jarvis O N Jones T T C Lomas P J Loughlin M J Magyar G Marcus F B Prentice R Stamp M Start D F H Tanga A Taroni A van Belle P Willen U
JET papers to 18th EPS Conference on Controlled Fusion and Plasma Physics, Berlin, 3-7 June 1991. Joint European Torus (JET), April 1991. Report JET-P(91)08, pp.93-96.

202. Experimental determination of the helium pumping by beryllium.
Saibene G Clement S Ehrenberg J Peacock A Phillips V Sartori R
JET papers to 18th EPS Conference on Controlled Fusion and Plasma Physics, Berlin, 3-7 June 1991. Joint European Torus (JET), April 1991. 41-44. JET-P(91)08, pp.

203. Power handling capability of C and Be X-point target plates in JET.
Saibene G Clement S Deksnis E Israel G Loarte A Lowry C Pick M Reichle R Rossi L Summers D Stork D Thomas P
American Physical Society Bulletin, vol.36 no.9 October 1991 (Program of 33rd Annual Meeting of the Division of Plasma Physics, Tampa, Florida, 4-8 November 1991) Abstract 4S 11, p.2367.

204. Low cycle fatigue testing of Inconel 600 and life assessment of JET vacuum vessel.
Sannazzaro G Sborchia C Sonnerup L Huguet M
JET papers presented to 14th Symposium on Fusion Engineering, San Diego, USA, 30 September - 3rd October 1991. Joint European Torus (JET), October 1991. Report JET-P(91)51, pp.79-83.

205. H-mode energy confinement scaling from the DIII-D and JET tokamaks.
Schissel D P DeBoo J C Burrell K H Ferron J R Groebner R J St. John H Stambaugh R D Tubbing B J D Thomsen K Cordey J G Keilhacker M Stork D Stott P E Tanga A
Nuclear Fusion, vol.31 no.1 January 1991, pp.73-81.

206. Fuelling of JET limiter and X-point plasmas by multiple deuterium pellet injection.
Schmidt G L Kupschus P and the JET Team
American Physical Society Bulletin, vol.36 no.9 October 1991 (Program of 33rd Annual Meeting of the Division of Plasma Physics, Tampa, Florida, 4-8 November 1991) Abstract 4S 3, p.2366.

207. Monte Carlo modelling of edge re-cycle fuelling on JET.
Simonini R Spence J Stangeby
P C Plasma Physics and Controlled Fusion, vol.33 no.6 June 1991, pp.653-675.

208. Interpretation of heat and density pulse propagation in tokamaks.
Sips A C C Lopes Cardozo N J Costley A E Hogeweij G M D O'Rourke J
JET papers to 18th EPS Conference on Controlled Fusion and Plasma Physics, Berlin, 3-7 June 1991. Joint European Torus (JET), April 1991. Report JET-P(91)08, pp.161-164.

209. Reflectometry and transport in thermonuclear plasmas in the Joint European Torus.
Sips A C C
Euratom-FOM Institute for Plasma Physics, Rijnhuizen, November 1990. 118p. Report Rijnhuizen Report 91-200. Doctoral thesis.

210. Resolving apparent differences between heat and density pulse propagation in JET and TEXT.
Sips A C C Hogeweij G M D Costley A E O'Rourke J Lopes Cardozo N J
de Haas J C M
Nuclear Fusion, vol.31 no.8 August 1991, pp.1545-1550. (Report JET-P(91)01).

211. High density regimes and beta limits in JET.
Smeulders P (presenter) and the JET Team
Plasma Physics and Controlled Nuclear Fusion Research. 13th Int. Conf., Washington, DC, 1-6 October 1990. Vienna, IAEA, 1991. Volume 1, pp.219-227. (Report JET-P(90)62 pp.70-78).

212. MHD studies in JET.
Smeulders P Edwards A Fishpool G Hender T C Hugon M van Milligen B Nardone C Neill G Porte L Wolfe S Zwingman W
JET papers to 18th EPS Conference on Controlled Fusion and Plasma Physics, Berlin, 3-7 June 1991. Joint European Torus (JET), April 1991. Report JET-P(91)08, pp.181-184.

213. Impurity transport at the plasma edge.
Stangeby P C
Plasma-Surface Interactions in Controlled Fusion Devices. 9th Int. Conf., Bournemouth, 21-25 May 1990. Journal of Nuclear Materials, vols.176-177, 1990, pp.51-64.

214. Some possibilities for measuring local plasma parameters in the edge plasma by impurity injection.
Stangeby P C Elder J D
Joint European Torus (JET), April 1991. 28p. Report JET-P(91)09. Submitted for publication in Plasma Physics and Controlled Fusion.

215. Subsonic and supersonic divertor solutions.
Stangeby P C
Plasma Physics and Controlled Fusion, vol.33 no.6 June 1991, pp.677-683. (Report JET-P(90)60).

216. Fast Wave Heating and Current Drive in JET: Present Results and Future Plans.
D.F.H. Start, V. Bhatnagar, G. Bosia, M. Brusati, M. Bures, D. Campbell, C. Challis, G. Cottrell, M. Cox A. Edwards, L-G. Eriksson, P. Froissard, C. Gormezano, C. Gowers, S. Hugonard, J. Jaquinot, P. Kupschus, N. Gottardi, M.R. O'Brien, D. Pasini, F. Porcelli, E. Righi, F. Rimini, G. Sadler, D. Stork, A. Tanga, K. Thomsen, F. Tibone, B. Tubbing, M. von Hellermann
Proc. IAEA Tech. Comm. Mtg. on FWCD Scale Tokamaks in Reactor, Arles, 1991. Report JET-P(91)63

217. ICRF heating in reactor grade plasmas.
Start D F H presenter and the JET Team
Plasma Physics and Controlled Nuclear Fusion Research. 13th Int. Conf., Washington, DC, 1-6 October 1990. Vienna, IAEA, 1991. Volume 1, pp.679-687. (Report JET-P(90)62 pp.107-118).

218. Ion heating in minority ICRH experiments on JET.
Start D F H Bhatnagar V Bures M Challis C Eriksson L-G Gowers C Hugonard S Jacquinot J Kupschus P Tubbing B
Joint European Torus (JET), June 1991. 4p. Report JET-R(91)06. Lecture presented to Institute of Physics Plasma Physics Conference, University of Essex, 1991.

219. Control of carbon blooms and the subsequent effects on the H to L mode transition in JET X-point plasmas.
Stork D Campbell D J Clement S Gottardi N de Kock L Lowry C Morgan P Reichle R Saibene G Smeulders P Summers D D R Thomas P
JET papers to 18th EPS Conference on Controlled Fusion and Plasma Physics, Berlin, 1991. Joint European Torus, 1991. Report JET-P(91)08, pp.61-64.

220. Neutral beam heating and current drive systems.
Stork D
Fusion Engineering and Design, vol.14 nos.1&2 (I) 1991 (Invited papers of 16th Symp. on Fusion Technology, London, 1990), pp.111-134. (Report JET-P(90)63).

221. Recent results from JET.
Stott P E (presenter) and the JET Team
Plasma Physics and Controlled Fusion, vol.33 no.10 September 1991, pp.1213-1224.

222. Recent results from JET.
P E Stott (presenter) and the JET Team
Joint European Torus (JET),. February 1991. 16p. Report JET-P(90)74. Iinvited paper presented to 32nd Meeting of the Division of Plasma Physics of the American Physical Society, Cincinnati, Ohio, 1990.

223. Different forms of the plasma energy conservation equation.
Stringer T E
Plasma Physics and Controlled Fusion, vol.33 no.14 November 1991, pp.1715-1722. (Report JET-P(91)04).

224. Inclusion of poloidal potential variation in neoclassical transport.
Stringer T E

Physics of Fluids B, vol.3 no.4 April 1991, pp.981-988. (Report JET-P(90)29).

225. Inclusion of poloidal potential variation in neoclassical transport.
Stringer T E
Theory of Fusion Plasmas. Procs. of Joint Varenna-Lausanne Int. Workshop, Varenna, 27-31 August 1990. Bologna, Editrice Compositori for Societa Italiana di Fisica, 1990. pp.99-106.

226. Neoclassical transport in the presence of fluctuations.
Stringer T E
Joint European Torus (JET), September 1991. 18p. Report JET-P(91)38. Submitted for publication in Nuclear Fusion.

227. Extrapolation of the high-performance JET plasmas to D-T operation.
Stubberfield P M Balet B Cordey J G
Plasma Physics and Controlled Fusion, vol.33 no.11 September 1991, pp.1255-1287. (Report JET-P(90)47).

228. The effects of particle drift orbits on flux deposition profiles at the JET X-point target.
Summers D D R Lesourd M Reichle R Schulz J P Zhu Y
JET papers to 18th EPS Conference on Controlled Fusion and Plasma Physics, Berlin, 3-7 June 1991. Joint European Torus (JET), April 1991. Report JET-P(91)08, pp.21-24.

229. Applications of Recombination.
H.P. Summers, W.J. Dickson
Proc. NATO Advanced Research W/S on Recombination, 7-9 Oct. 1991. Report JET-P(91)57

230. Atomic data for fusion.
Summers H P Thomas P Giannella R Von Hellermann M
Journal de Physique, vol.1 March 1991, pp.C1-191 - C1-195. (Report JET-P(90)54).

231. Atomic processes relevant to neutral beam based tokamak diagnostics.
Summers H P von Hellermann M Breger P Frieling J Horton L D Konig R Mandl W Morsi H Wolf R de Heer F Hoekstra R Fritsch W
Joint European Torus (JET), September 1991. 10p. Report JET-P(91)48. Invited paper presented at APS Topical Meeting on Atomic Processes in Plasmas, Portland, Maine, USA, 26 August 1991.

232. On spectral emission from beryllium in plasmas.
Summers H P Dickson W J Boileau A Burke P G Denne-Hinnov B Fritsch W Giannella R Hawkes N C von Hellermann M Mandl W Peacock N J Reid R Stamp M F Thomas P R
Joint European Torus (JET), April 1991. 36p. Report JET-P(91)12. Submitted for publication in Plasma Physics and Controlled Fusion.

233. Edge radial profiles and transport in JET X-point plasmas.
Tagle J A Bures M Campbell D Clement S de Kock L Erents S K Harbour P J Loarte A Lowry C
JET papers to 18th EPS Conference on Controlled Fusion and Plasma Physics, Berlin, 3-7 June 1991. Joint European Torus (JET), April 1991. Report JET-P(91)08, pp.177-180.

234. Power flow thickness and edge temperature and density scaling in the scrape-off layer of JET with Be limiters.
Tagle J A Clement S Erents S K Harbour P J de Kock L Loarte A Richards S D
JET papers to 18th EPS Conference on Controlled Fusion and Plasma Physics, Berlin, 3-7 June 1991. Joint European Torus (JET), April 1991. Report JET-P(91)08, pp.165-168.

235. High performance H modes in JET.
Tanga A (presenter) and the JET Team
Plasma Physics and Controlled Nuclear Fusion Research. 13th Int. Conf., Washington, DC, 1-6 October 1990. Vienna, IAEA, 1991. Volume 1, pp.261-276. (Report JET-P(90)62 pp.41-58).

236. Hot-ion and H-mode plasmas in limiter configuration in JET.
Tanga A Jones T T C Lomas P J Nardone C Sartori R Tibone F von Hellermann M Watkins M L
JET papers to 18th EPS Conference on Controlled Fusion and Plasma Physics, Berlin, 3-7 June 1991. Joint European Torus (JET), April 1991. Report JET-P(91)08, pp.113-116.

237. Operational aspects.
Tanga A
Contributions to 3rd Workshop on H-mode Physics, JET Joint Undertaking, Abingdon, 10-12 June 1991. Joint European Torus (JET), 1991. Volume 3, pp.917-951.

238. Statistical analysis of JET disruptions.
Tanga A Johnson M F
Joint European Torus (JET), July 1991, 38p. Report JET-R(91)08.

239. Study of plasma disruptions in JET and its implications on engineering requirements.
Tanga A Garribba M Hugon M Johnson M F Lowry C Nardone C Noll P Pick M Saibene G Sannazzaro G
JET papers presented to 14th Symposium on Fusion Engineering, San Diego, USA, 30 September - 3rd

October 1991. Joint European Torus (JET), October 1991. Report JET-P(91)51, pp.67-72.

240. Interpretation and modelling of energy and particle transport in JET.
Taroni A Tibone F Balet B Boucher D Christiansen J P Cordey J G Corrigan G C Duchs D F Giannella R Gondhalekar A Gottardi N Hogeweij G M D Lauro-Taroni L Lawson K Mattioli M Muir D O'Rourke J Pasini D Rebut P H Sack C Sips G Springmann E Stringer T E Stubberfield P Thomsen K Watkins M L Weisen H
Plasma Physics and Controlled Nuclear Fusion Research. 13th Int. Conf., Washington, DC, 1-6 October 1990. Vienna, IAEA, 1991. Volume 1, pp.93-107. (Report JET-P(90)62 pp.59-68).

241. Local transport analysis in L and H regimes.
Taroni A Sack Ch Springmann E Tibone F
JET papers to 18th EPS Conference on Controlled Fusion and Plasma Physics, Berlin, 3-7 June 1991. Joint European Torus (JET), April 1991. Report JET-P(91)08, pp.13-16.

242. Contributions to 4th European Fusion Theory Conference, Aspenäs, Sweden, 17th-19th June 1991
Many Authors
(Theory Division). Report JET-R(91)11

243. Comparison of beryllium and graphite first walls in JET.
Thomas P R (presenter) and the JET Team
Plasma Physics and Controlled Nuclear Fusion Research. 13th Int. Conf., Washington, DC, 1-6 October 1990. Vienna, IAEA, 1991. Volume 1, pp.375-384. (Report JET-P(90)62 pp.97-106).

244. Edge plasma measurements in JET H-modes.
Thomas P R
Contributions to 3rd Workshop on H-mode Physics, JET Joint Undertaking, Abingdon, 10-12 June 1991. Joint European Torus (JET), 1991. Volume 2, pp.389-407.

245. The scaling of global H-mode confinement using the ITER H-mode database.
Thomsen K
Contributions to 3rd Workshop on H-mode Physics, JET Joint Undertaking, Abingdon, 10-12 June 1991. Joint European Torus (JET), 1991. Volume 3, pp.737-748.

246. Local energy transport in the H-mode regimes of JET.
Tibone F
Contributions to 3rd Workshop on H-mode Physics, JET Joint Undertaking, Abingdon, 10-12 June 1991. Joint European Torus (JET), 1991. Volume 3, pp.661-675.

247. Local energy transport in JET H-modes.
Tibone F Balet B Cordey J G Corrigan G Sack C Stringer T E Taroni A
American Physical Society Bulletin, vol.36 no.9 October 1991 (Program of 33rd Annual Meeting of the Division of Plasma Physics, Tampa, Florida, 4-8 November 1991) Abstract 4S 5, p.2366.

248. Transition to a regime of improved confinement in JET limiter discharges.
Tibone F
Joint European Torus (JET), September 1991. 9p. Report JET-P(91)40. Submitted for publication in Nuclear Fusion.

249. AC operation and fast current rampdown studies in JET.
Tubbing B J D Green B How J Huart M Kupschus P Lallia P Lomas P Lowry C Noll P Rebut P-H Stork D Tanga A Taroni A Wijnands T
American Physical Society Bulletin, vol.36 no.9 October 1991 (Programme of 33rd Annual Meeting of the Division of Plasma Physics, Tampa, Florida, 4-8 November 1991) Abstract 4S 2, p.2365.

250. AC Plasma Current Operation in the JET Tokamak.
B. Tubbing, B. Green, H. How, M. Huart, R. Konig, C. Lowry, P. Lomas, P. Noll, P.H. Rebut, J. O'Rourke, D. Stork, A. Tanga, A. Taroni, D. Ward
Nucl Fusion. Report JET-P(91)59

251. Combination of pellet-peaked density profiles with H-mode confinement.
Tubbing B J D
Contributions to 3rd Workshop on H-mode Physics, JET Joint Undertaking, Abingdon, 10-12 June 1991. Joint European Torus (JET), 1991. Volume 3, pp.749-765.

252. A fast predictive calculation of the magnetic configuration in air-core tokamaks.
Tubbing B J D Gaze P Q F
Joint European Torus (JET), April 1991. 14p. Report JET-R(91)03.

253. H-mode confinement in JET with enhanced performance by pellet peaked density profiles.
Tubbing B J D Balet B Bartlett D V Challis C D Corti S Gill R D Gormezano C Gowers C W von Hellermann M Hugon M Jacquinot J J Jaeckel H Kupschus P Lawson K Morsi H O'Rourke J Pasini D Rimini F G Sadler G Schmidt G L Start D F H Stubberfield P M Tanga A Tibone F
Nuclear Fusion, vol.31 no.5 May 1991, pp.839-850. (Report JET-P(90)67).

254. A review of carbon blooms on JET and TFTR.
Ulrickson M, the JET Team, and the TFTR Team.

Plasma-Surface Interactions in Controlled Fusion Devices. 9th Int. Conf., Bournemouth, 21-25 May 1990. Journal of Nuclear Materials, vols.176-177, 1990, pp.44-50.

255. JET - a large physics experiment.
van der Beken H
Europhysics News, vol.22 no.2 1991, (Special Issue on Controls in Experimental Physics) pp.26-28.

256. Real time diagnostic data acquisition and plasma control using transputers.
van der Goot E Edwards A W Ellis J O'Brien D
Fusion Technology 1990. Procs. 16th Symp., London, 1990. Amsterdam, North-Holland, 1991. Vol.2, pp.1244-1248. (Report JET-P(90)56 vol.I pp.97-102).

257. Software for the real time X-ray tomography system at JET.
van der Goot E
Joint European Torus (JET), July 1991. 10p. Report JET-P(91)28. Presented at Real Time '91, Julich, FRG, 25-28 June 1991.

258. High current ($I_p \geq 5$ MA) disruptive pulses in JET.
Vannucci A Gill R D
Nuclear Fusion, vol.31 no.6 June 1991, pp.1127-1133. (Report JET-P(90)30).

259. Mode-coupling triggering mechanism in tokamak major disruptions.
Vannucci A Nascimento I C Caldas I L Gill R D
Research using Small Tokamaks. Procs. of Technical Committee Meeting, Arlington, 1990. Vienna, International Atomic Energy Agency, 1991. p.35.

260. An analytical model for retention of divertor impurities by forced flows.
Vlases G C Simonini R
JET papers to 18th EPS Conference on Controlled Fusion and Plasma Physics, Berlin, 1991. Joint European Torus, 1991. Report JET-P(91)08, pp.33-36.

261. Investigation of thermal and slowing-down alpha particles on JET using charge-exchange spectroscopy.
von Hellermann M Mandl W Summers H P Boileau A Hoekstra R de Heer F J Frieling J
Plasma Physics and Controlled Fusion, vol.33 no.14 November 1991, pp.1805-1824. (Report JET-P(90)59).

262. Measurement of thermal and non-thermal alpha particles in the JET tokamak.
von Hellermann M Frieling J Koenig R Mandl W Summers H P
American Physical Society Bulletin, vol.36 no.9 October 1991 (Program of 33rd Annual Meeting of the Division of Plasma Physics, Tampa, Florida, 4-8 November 1991) Abstract 4S 8, p.2366.

263. High power (22MW) ICRH at JET and developments for Next Step devices.
Wade T J Jacquinot J Bosia G Sibley A Schmid M
JET papers presented to 14th Symposium on Fusion Engineering, San Diego, USA, 1991. Joint European Torus (JET), 1991. Report JET-P(91)51, pp.3-8.

264. Impurity influx model of fast tokamak disruptions.
Ward D J Wesson J A
Joint European Torus (JET), April 1991. 17p. Report JET-P(91)10. Submitted to Nuclear Fusion.

265. Influence of grad-B drift direction on H-modes in JET.
Ward D Bhatnagar V Bures M Campbell D Clement S Fessey J Gottardi N Harbour P de Kock L Lowry C Morgan P Nardone C Reichle R Saibene G Smeulders P Stork D Summers D Thomas P Thomsen K Vlases G
JET papers to 18th EPS Conference on Controlled Fusion and Plasma Physics, Berlin, 1991. Joint European Torus, 1991. Report JET-P(91)08, pp.25-28.

266. Modelling JET plasmas.
Watkins M L
JET papers presented at European Tokamak Programme Workshop, Arles, France, 1990. Joint European Torus (JET), 1991. Report JET-P(91)05, pp.11-15.

267. Boundary ion temperatures in JET.
Weisen H Bergsaker H Campbell D Erents S K de Kock L McCracken G M Stamp M Summers D Thomas P von Hellermann M Zhu J
Joint European Torus (JET), June 1991. 46p. Report JET-P(91)16. Submitted to Nuclear Fusion.

268 Measurement of light impurity densities and Z_{eff} in JET using X-ray tomography.
Weisen H Pasini D Weller A Edwards A W
Review of Scientific Instruments, vol.62 no.6 June 1991, pp.1531-1538.

269. Density limit in tokamaks.
Wesson J A
JET papers presented at European Tokamak Programme Workshop, Arles, France, 5-7 December 1990. Joint European Torus (JET), March 1991. Report JET-P(91)05, pp.23-25.

270. Energy balance in tearing modes.
Wesson J A
Joint European Torus, 1991. 20p. Report JET-P(91)39. Submitted to Plasma Physics and Controlled Fusion.

271. Non-linear behaviour in tokamaks.
Wesson J A
Procs. 2nd Int. Toki Conf. on Plasma Physics and Controlled Nuclear Fusion, (Nonlinear Phenomena in Fusion Plasmas - Theory and Computer Simulation),

Toki City, Japan. National Institute for Fusion Science, Nagoya. 1991. pp.187-193. (Report JET-P(91)02).

272. Sawtooth reconnection.
Wesson J A
Plasma Physics and Controlled Nuclear Fusion Research. 13th Int. Conf., Washington, DC, 1-6 October 1990. Vienna, IAEA. 1991. Vol.2, pp.79-85. (Report JET-P(90)62 pp.145-152).

273. Spontaneous m = 1 instability in the JET sawtooth collapse.
Wesson J A Edwards A W Granetz R S
Nuclear Fusion, vol.31 no.1 January 1991, p.111-116.

274. Development of interface for remote mass spectrometer.
Winkel T Usselmann E Steed A
Fusion Technology 1990. Procs. 16th Symp., London, 1990. Amsterdam, North-Holland, 1991. Vol.1, pp.473-477. (Report JET-P(90)56 vol.I pp.25-30).

275. Neutron rate interpretation for neutral-beam-heated tokamaks.
Wolle B Eriksson L-G Hubner K Morgan P D Morsi H W Sadler G
von Hellermann M G
Plasma Physics and Controlled Fusion, vol.33 no.14 November 1991, pp.1863-1870. (Report JET-P(91)15).

276. Safety analysis of potential graphite oxidation effects in JET.
Wykes M E P Deksnis E B Caldwell-Nichols C J
Fusion Technology 1990. Procs. 16th Symp., London, 1990. Amsterdam, North-Holland, 1991. Vol.2, pp.1447-1451. (JET-P(90)56 vol.II pp.139-144).

277. Spectroscopic measurement of electron temperature and electron density at the Extrap-T1 experiment.
Zastrow K Brzozowski J H Kallne E Summers H P
Royal Institute of Technology Stockholm, 1991. Report TRITA-PFU-91-09. 8p.

278. Plasma equilibria and stationary flows in axisymmetric systems. Part III.
Zelazny R Stankiewicz R Galkowski A Potempski S Pietak R
Joint European Torus (JET), August 1990. 110p. Report JET-R(91)05.

279. Experimental investigations of helium ion implantation in the first wall of JET.
Zhu J McCracken G M Coad J P
Nuclear Instruments and Methods in Physics Research B: Beam Interactions with Materials and Atoms, vol.B59-60 pt.I 1991 (Procs. 7th Int. Conf. on Ion Beam Modification of Materials, Knoxville, TN, 1990) pp.168-172.

280. ECE correlation radiometry as a diagnostic for MHD ballooning modes on JET and PBX-M.
Zolfaghari A Luckhardt S Woskov P Kesner J Ramos J Barlett D Costley A E Cripwell P Porte L Kaita R
American Physical Society Bulletin, vol.36 1991 (Programme of 33rd Annual Meeting of Division of Plasma Physics, Tampa, Florida, 1991) Abstract 2S 37, p.2317.

281. JET Annual Report 1990. JET Joint Undertaking, 1991.
Edited by B.E.Keen and G.W.O'Hara.
EUR-13492 EN-C (EUR-JET-AR13).

282. JET Progress Report 1990. JET Joint Undertaking, March 1991. 2 vols.
Edited and compiled by B.E.Keen.
EUR-13493 EN (EUR-JET-PR8).

283. Plasma-Surface Interactions in Controlled Fusion Devices
Edited by Keen BE McCracken GM and Stott PE.
Proceedings of Ninth International Conference on Plasma-Surface Interactions in Controlled Fusion Devices (Bournemouth, UK, 1990) (North Holland Publishers, Amsterdam) (also in J. Nucl. Mat. Vols 176 and 177, 1990).

284. Fusion Technology 1990, Volumes 1 and 2
Edited by Keen BE Huguet M and Hemsworth R.
Proceedings of the 16th Symposium on Fusion Technology (SOFT) (London, UK, 1990) (North Holland Publishers, Amsterdam).